TECHNISCHE UNIVERSITÄT DARMSTADT

Paleogeographic and tectonic evolution of the western branch of the East African Rift System using multiple provenance methods (Albertine Rift, Uganda)

vom Fachbereich Material- und Geowissenschaften der Technischen Universität Darmstadt

zur Erlangung des akademischen Grades
Doctor rerum naturalium
(Dr. rer. nat.)

Dissertation
von Sandra Schneider

Erstgutachter : Prof. Dr. Matthias Hinderer
Zweitgutachter: Prof. Dr. Christoph Schüth

Darmstadt 2019

Eidesstattliche Erklärung (Declaration of authorship)

Ich erkläre hiermit, die vorliegende Dissertation ohne Hilfe Dritter und nur mit den angegebenen Quellen und Hilfsmitteln angefertigt zu haben. Alle Stellen, die aus Quellen übernommen wurden, sind als solche kenntlich gemacht worden. Diese Arbeit hat in dieser oder ähnlicher Form noch keiner Prüfungsbehörde vorgelegen. Die schriftliche Fassung stimmt mit der elektronischen Fassung überein.

I hereby certify that the complete work to this PhD thesis was done by myself and only with the use of the referenced literature and the described methods.

Darmstadt, den 04.07.2018

Sandra Schneider

Acknowledgements

First of all, I would like to thank my family, especially my parents, who supported me in every possible way throughout writing this thesis and my life in general. I am grateful for having a person in my life that constantly backs me up. Thank you, Christopher.

I would like to express my sincere gratitude to my advisor Prof. Dr. Matthias Hinderer for giving me the opportunity to join his research group at the Technical University Darmstadt, and to perform my PhD studies in such a fascinating research project. I am grateful for his continuous support, patience, motivation, and immense help during the preparation of the manuscripts. His persistent guidance helped me in all the time of research and writing of this thesis. Without him this dissertation would not have been possible.

My sincere thanks go to Dr. Jens Hornung, especially for the excellent introduction into the topic and, particularly, into the field work in Uganda.

I owe special thanks to my colleague Dennis Brüsch for his cooperation and for keeping me company during many weeks of field work in Uganda. Dennis largely contributed to this thesis by sediment logging in the field, drawing of sedimentary logs, and by his interpretations concerning sedimentology, facies and depositional environments of the studied sediment. His work largely provided the base of my thesis.

I thank the Ugandan National Council for Science and Technology (UNCST) for permitting the research work in Uganda and the Uganda Wildlife Authority (UWA) for their support and permission to work in the national parks. Many thanks to our Ugandan research partners from Makerere University for cooperation, in particular Andreas Schumann for his on-site guidance and Dr. John Tiberindwa for his support and for providing us with equipment. Special thanks go to our driver Kitam Ali for his profound help, field endurance, and pleasant company.

I am grateful to the staff from the department of geoscience at the Johannes Gutenberg University of Mainz, who assisted me during various analytic measurements. Dr. Stephan Buhre helped me with EMP analyses; Dr. Regina Mertz supported me during the LA-ICP-MS measurements; Klemens Link introduced me into zircon geochronology and helped with the evaluation of the final data set, and Dr. Tobias Häger aided me during Raman spectroscopy of heavy mineral sections. Furthermore, I want to thank all student assistants, who prepared the samples for the several methods. Moreover, I would like to thank Dr. Friederike Bauer (now Department of Earth Science, University of Bergen) for her help with the magnetic separation of heavy mineral fractions at the University of Heidelberg.

I would like to express my gratitude to Prof. Dr. Eduardo Garzanti from the Laboratory for Provenance Studies, Department of Earth and Environmental Sciences, Università di Milano-Bicocca, for being my co-author on my very first article. His exceptional knowledge about sediments in general, and provenance analysis in particular, certainly helped to greatly improve the manuscript on modern river sediments. Furthermore, Alberto Resentini and Mara Limonta kindly analyzed selected Rwenzori sands for petrography and heavy minerals. Prof. Garzanti and his working group are furtherly thanked for inviting Prof. Hinderer and me to Milano, where we could learn much about provenance studies.

There are many people at the department for Applied Geoscience at the TU Darmstadt that supported me in one way or another. Prof. Dr. Christoph Schüth gave me access to the laboratory and research facilities. Dr. Thomas Schiedeck, Holger Scheibner, Gabriela Schubert, Claudia Cosma, Zahra Neumann, Bernd Dreieicher, and Rainer Seehaus always supported me during laboratory work. I thank Jacintha Nayebare for sample preparation.

I would particularly like to thank my colleagues from the working group of Applied Sedimentology, who gave me such a good time in Darmstadt. Lots of thanks go to PD Dr. habil. Olaf Lenz for all the pleasant conversations during countless hours of microscoping.

Last but not the least, the German Research Foundation (DFG) is thanked for funding this project as part of the interdisciplinary research group *RiftLink – Rift Dynamics, Uplift and Climate Changes in Equatorial Africa* (H1643-7/1).

Preface

The Albertine Rift represents the northern termination of the western branch of the East African Rift System. Since the Miocene, uplift of rift walls led to the creation of a remarkable topography that influenced local and global climate pattern, which in turn, had a strong impact on the development of early hominids from other primates. As part of the DFG-funded, interdisciplinary research program *RiftLink – Rift Dynamics, Uplift and Climate Changes in Equatorial Africa* (H1643-7/1), which seeks to investigate the connection between tectonic uplift and atmospheric/climatic changes in Equatorial Africa, this study focuses on the erosional history of the rift flanks by studying the composition and provenance of rift sediments and modern river sands in and around the Albertine Rift. The analytical approach integrates framework and heavy mineral petrography, bulk rock geochemistry, garnet and rutile mineral chemistry, and U-Pb dating of detrital zircon. The results are presented in five manuscripts of which three articles have been published in international research journals. Two further manuscripts are under consideration to be prepared for publication in the near future.

The opening chapter of this thesis (Chapter 1) gives an overview of the research aims, the study area, and the *RiftLink* project, followed by an overview about classical and modern provenance methods. The following two chapters of this thesis are dedicated to modern stream sediments collected along the rift flanks of the Albertine Rift, including the Rwenzori horst block, to study modern processes and products in that particular rift setting. Based on petrographic and geochemical analyses, Chapter 2 mainly investigates to what extent extreme weathering in hot humid equatorial climate modifies the composition of sediments and whether provenance signatures are preserved in extremely weathered sands. Chapter 3 aims at identifying the characteristics of a variety of Ugandan basement rocks by the application of varietal studies on garnet, rutile and zircon. The goal of this chapter is to define potential source rocks for the Neogene rift sediment within the Albertine Graben, which is important for provenance determinations. In the third part of this thesis (Chapter 4–6), the provenance and depositional setting of Miocene to Pleistocene rift sediments from two key areas (Kisegi-Nyabusosi and Nkondo-Kaiso) in the Albertine Rift are examined. The detailed description of the temporal and spatial evolution of sediment compositions and textures provides insights into source rocks/areas, dispersal pathways, and uplift pattern of rift shoulders, which in turn, is of fundamental importance for paleotectonic and -geographic interpretations. The multi-proxy data of this thesis are summarized and statistically analyzed in the final chapter (Chapter 7). On basis of the synthesis, existing tectono-sedimentary models of the Albertine Rift are evaluated and partly revised. Furthermore, this chapter assesses the usefulness of multi-proxy sedimentary provenance analysis for reconstructing rift evolution in tropical basement areas.

Chapter 1 (Introduction) introduces this thesis by giving an overview of the study aims, the *RiftLink* project, the geological setting, and about sedimentary provenance analysis (SPA), including the analytical tools applied during this thesis.

Chapter 2 (published article) investigates the effects of chemical weathering on sands and muds generated in equatorial Africa, the factors controlling weathering rates, and the extent and conditions under which original provenance signatures are preserved. In the extreme case of the rift-related Rwenzori basement uplift, this study documents how daughter sediments may faithfully reflect parent lithologies even in wet equatorial climate. This chapter is largely analogue to the article 'Petrography and geochemistry of modern river sediments in an equatorial environment (Rwenzori Mountains and Albertine Rift, Uganda) - Implications for weathering and provenance', which was published in the special issue of *Sedimentary Geology* 'Sediment generation and provenance: processes and pathways' in May 2016. Co-authors are J. Hornung, M. Hinderer (both Institute of Applied Geoscience, TU

Darmstadt) and E. Garzanti (Laboratory for Provenance Studies, Department of Earth and Environmental Sciences, Università di Milano-Bicocca). Sampling, sample preparation, data evaluation and interpretation as well as manuscript preparation were done by S. Schneider. Some data were kindly provided by E. Garzanti. The manuscript largely benefited from discussion with the co-authors.

Schneider, S., Hornung, J., Hinderer, M., Garzanti, E., 2016. Petrography and geochemistry of modern river sediments in an equatorial environment (Rwenzori Mountains and Albertine Rift, Uganda) - Implications for weathering and provenance. Sedimentary Geology, 336, 106–119.

Chapter 3 (unpublished manuscript) presents geochemical compositions of detrital garnet and rutile, and U-Pb ages of detrital zircon of recent stream sediments from the eastern rift shoulder of the Albertine Rift in western and southwestern Uganda to provide constraints about the nature of Ugandan basement terrains and to test whether the provenance signals provided by these minerals are also representative in highly weathered equatorial sands. The results of this study underline the great potential of garnet, rutile and zircon in reconstructing sediment provenance, but also show that they reach limitations when derived from polycyclic sediments, in which they are witness of former transportation and depositional cycles. This chapter is considered to be prepared for publication in the near future. The manuscript is completely autonomously written and not overhauled by the potential co-authors M. Hinderer and J. Hornung.

Chapter 4 (published article) focuses on the provenance of Miocene to Pleistocene synrift sediments that were deposited in the southern Lake Albert sub-basin (Kisegi-Nyabusosi area) during multiphase rifting. The aim of this study is to identify sediment sources and supply paths with the ultimate goal to reconstruct the exhumation history of different tectonic blocks during prolonged rifting, with specific focus on the uplift of the > 5000 meter above sea level high Rwenzori Mountains. The multi-proxy approach of this study includes petrographic data, heavy mineral spectra, and chemical analyses on detrital garnet and rutile. This chapter is mostly identical to the manuscript ‘Evolution of the western East African Rift System reflected in provenance changes of Miocene to Pleistocene synrift sediments (Albertine Rift, Uganda)’ that was published in *Sedimentary Geology*. Co-authors are J. Hornung and M. Hinderer (both Institute of Applied Geoscience, TU Darmstadt). Sampling, sample preparation, data evaluation and interpretation as well as manuscript preparation were done by S. Schneider. J. Hornung and D. Brüsch accompanied the field work. The manuscript benefited from discussion with the co-authors.

Schneider, S., Hornung, J., Hinderer, M., 2016. Evolution of the western East African Rift System reflected in provenance changes of synrift sediments (Albertine Rift, Uganda). Sedimentary Geology, 343, 190–205.

Chapter 5 (published article) investigates possible sources and the depositional history of the rift infill in the northern Lake Albert sub-basin (Nkondo-Kaiso area) by combining petrographic and single grain geochemical data. This study complements to the previous chapter by providing further constraints on the chronology of uplift and rifting events in the Albertine Rift. This chapter is largely similar to the article ‘Provenance evolution of synrift sediments in the northern Albertine Rift, Uganda: constraints from framework petrography, heavy mineral composition and mineral chemistry’ that was published in the *Journal of African Earth Science*. Co-authors are J. Hornung and M. Hinderer (both Institute of Applied Geoscience, TU Darmstadt). Sampling, sample preparation, data evaluation and interpretation as well as manuscript preparation were done by S. Schneider. J. Hornung

and D. Brüsch accompanied the field work. The manuscript benefited from discussion with the co-authors.

Schneider, S., Hornung, J., Hinderer, M., 2017. Evolution of the northern Albertine Rift reflected in the provenance of synrift sediments (Nkondo-Kaiso area, Uganda). Journal of African Earth Sciences, 131, 183–197.

Chapter 6 (unpublished manuscript) discusses the maturity, weathering degree, and source rocks of the Miocene-Pleistocene rift sediment in the Albertine Rift (Kisegi-Nyabusosi and Nkondo-Kaiso areas), based on whole rock geochemistry and U-Pb zircon ages. This additional study on the rift infill contributes to the previous chapters 4 and 5 with the aim to obtain further constraints on the provenance of the sediment in the Kisegi-Nyabusosi area and Nkondo-Kaiso area. The new data set supports recently proposed paleodrainage directions, and refines interpretations deduced from petrographic and single grain chemical studies. This chapter is considered to be prepared for publication in the near future. The manuscript is completely autonomously written and not overhauled by the potential co-authors M. Hinderer and J. Hornung.

Chapter 7 (Synthesis) presents a final discussion and summary of the results obtained during this study. This section includes statistical treatment (PCA) of the multivariate data set applied to identify the most powerful provenance indicators for discriminating the rift sediment and to link them to specific source regions. The results are integrated into a sedimento-tectonic model of rift evolution which is compared to existing models. This chapter further discusses the usefulness of multi-proxy provenance approaches, as well as the potential of provenance studies in reconstructing the evolutionary history of rift basins in tropical basement areas.

Summary

As part of the DFG-funded interdisciplinary research project *703 RiftLink – Rift Dynamics, Uplift and Climate Changes in Equatorial Africa (H1643-7/1)*, this presented PhD thesis aims at reconstructing the evolutionary history of the Albertine Rift in the western branch of the East African Rift System by combined studies on ancient rift sediments and modern stream sediments.

The major part of this thesis is dedicated to the Miocene-Pleistocene rift infill that has been studied for its provenance and depositional history in order to gain a broader understanding of rift dynamics and the tectono-sedimentary history of the Albertine Rift since its initiation in the early Miocene. Sedimentary successions of rift sediment studied in the Albertine Rift are exposed in two key areas on the Ugandan side of Lake Albert, the Kisegi-Nyabusosi area and Nkondo-Kaiso area. Both areas represent a distal and proximal setting with respect to the extremely upthrusted > 5000 m high Rwenzori Mountains, which form a promontory of the eastern rift flank of the Albertine Rift. The rift sediment mainly comprises unconsolidated siliciclastics from clay to coarse gravel deposited in a fluvial-deltaic to lacustrine setting during multiphase rifting. Based on systematic logging and sampling of sedimentary outcrops, this study presents a multi-proxy methodological approach that combines framework and heavy mineral petrography, bulk sediment geochemistry, varietal studies of detrital garnet and rutile, as well as U-Pb zircon geochronology. The outcome of this thesis is a paleotectonic model of erosion, sediment transport, and basin evolution that presents a more detailed picture of the spatial-temporal history of the northern western branch of the East African Rift System.

The second part of this doctoral thesis focuses on modern river sediment collected in the Rwenzori Mountains and adjacent rift flanks. This additional study complements this thesis by providing profound insights into present-day sediment generation and erosional processes in this particular rift setting. By using the same analytical approach as for the rift fill, the modern stream sediment helps to identify the characteristics of a variety of Ugandan basement rocks and to define potential source rocks for the Neogene successions. Furthermore, this study aims at quantifying the effects of chemical weathering on the composition of modern sediment generated under extreme equatorial climatic conditions.

The synthesis of available information collected during this provenance study allows to modify and refine existing evolutionary models for the Albertine Rift. Three major rifting stages were identified that may be interpreted in terms of rifting activity:

- Early Miocene to early Pliocene (~17.0 –5.0 Ma)

Exposures of the earliest rift sediment are only known from the southern Lake Albert sub-basin (Kisegi-Nyabusosi area). Provenance data imply that sediment transport was dominated by a westward directed large-scale river system and flowed from Kenya westwards through Uganda and probably further towards the Congo Basin and to the Atlantic Ocean. Sediment sources extend towards the at least 400 km away located East African Orogen as demonstrated by the occurrence of Pan-African zircon ages. The dominant source represents gneissic-granulitic rocks of the Neoarchean North Uganda Terrane that occupies major parts of the Ugandan basement proved by a high amount of Neoarchean zircon as well as amphibolite- to granulite-facies garnet and rutile.

- Early Pliocene to late Pliocene (~5.0–2.6 Ma)

A major provenance shift occurred during the Miocene-Pliocene boundary, interpreted to mark the transition from the pre-rift into the syn-rift stage with enhanced subsidence and uplift of rift flanks and the Ugandan plateau. Sediment transport from distal sources was largely disrupted, likely due to a phase of first major rifting affecting the Albertine Rift. This can mainly be concluded from a change in

the heavy mineral composition and missing of Neoproterozoic zircon ages. Provenance data indicate proximal sediment sources for both the southern and northern study areas, probably from the adjacent rift margin with major derivation from the North Uganda Terrane as indicated by a majority of Neoarchean zircon, epidote-amphibolite-dominated heavy mineral assemblages, as well as high-grade metamorphic garnet and rutile (amphibolite- to granulite-facies).

- Early Pleistocene (since ~2.6 Ma)

A further provenance shift around the Pliocene-Pleistocene transition is concurrent with the beginning of the extreme uplift of the Rwenzori fault block and the initiation of inversion tectonics in the Albertine Rift. In the southern Albertine Rift, sediment supply from mainly southern sources with major supply from the Rwenzori Fold Belt in the Rwenzori Mountains is indicated by less mature sediment accompanied by the occurrence of lower-grade metamorphic garnet and rutile (amphibolite-facies), as well as pinkish zircon grains. On the contrary, additional input from the Neoproterozoic Bunyoro Group overlying the local basement along the rift shoulder leads to a higher maturity of the sediment in the further to the north located Nkondo-Kaiso region with higher abundances of more resistant minerals, like quartz, zircon and tourmaline. In both areas, sediment sources changed only slightly compared to the Pliocene and sediment transport is still from the adjacent rift flank.

The proposed provenance changes are coincident in both study areas and largely coincide in timing with major faulting episodes in other parts of the EARS, suggesting that tectonic movements in eastern Africa act at a global scale.

Present-day sediment generation in the Albertine Rift takes mainly place under hot-humid climate conditions and in contrasting geomorphological settings, including poorly-drained lowlands of the rift plateau and the high-altitude Rwenzori horst, in which two fundamental types of sediment is created. In the extremely uplifted and young Rwenzori horst, where high topography promotes rapid physical degradation, sediment is rich in feldspar and rock fragments with very rich heavy-mineral assemblages controlled by amphibole and epidote. Sediment created in the low-relief rift plateau, widely covered by thick lateritic soils, is highly quartzose due to intense weathering prolonged over millions of years. The study of modern sediment in the Albertine Rift clearly demonstrates that identification of original provenance signatures is still possible even in areas characterized by extreme climatic conditions such as those of equatorial latitudes. Heavy mineral spectra, zircon geochronology, garnet and rutile chemistry, and geochemical parameters, especially non-mobile elements and element ratios, best preserve the imprint of the source-rock lithology.

Altogether, this study highlights the high potential of sedimentary provenance analysis (SPA) in reconstructing the sedimento-tectonic history of rift basins in tropical regions, and also underlines the importance of multi-proxy approaches to fully understand sediment supply into depositional systems. The research on the Albertine Rift exemplifies that the application of SPA is most successful by using a combination of ‘traditional’ petrographic-mineralogical methods with ‘innovative’ geochemical and geochronological methods. Single-grain varietal studies on zircon, garnet and rutile are the most powerful applications to constrain specific sources. While age populations obtained from zircon U-Pb geochronology can be directly linked to the age of a certain tectono-thermal terrane, chemical compositions of garnet of rutile allow distinguishing lithologies characterized by different metamorphic overprint, e.g., amphibolite-facies vs. granulite-facies rocks. However, varietal studies fail for recovering sediment input from recycled sedimentary rocks. Because of the durability of zircon, garnet and rutile during the sedimentary cycle, polycycle sedimentation is masked, which might lead to an incorrect interpretation of exclusively primary sources. For reconstructing provenance from sedimentary (recycled) lithologies or for revealing the weathering degree of sediments, bulk-rock petrographic and geochemical methods proofed to be the most suitable applications.

Zusammenfassung

Die vorliegende Doktorarbeit ist Bestandteil der DFG-geförderten Forschergruppe *703 RiftLink – Rift Dynamik, Hebung und Klimawandel in Äquatorialafrika (H1643-7/1)*. Das Ziel der Studie war die Rekonstruktion der Entwicklungsgeschichte des Albertrifts im westlichen Riftarm des Ostafrikanischen Grabensystems mittels kombinierter Untersuchungen an neogenen Riftsedimenten und rezenten Flusssanden.

Im ersten Teil der Doktorarbeit wurden miozäne bis pleistozäne Riftsedimente hinsichtlich ihrer Provenienz und Ablagerungsgeschichte untersucht, um ein umfassenderes Verständnis für die dynamische und tektonisch-sedimentäre Entwicklung des Albertrifts seit dessen Initiierung im frühen Miozän zu erlangen. Die untersuchten sedimentären Riftsequenzen sind in zwei Gebieten in Uganda in unmittelbare Nähe des Albertsees aufgeschlossen (Kisegi-Nyabusosi Region und Kaiso-Nkondo Region). Diese Gebiete repräsentieren einen distalen und proximalen Ablagerungsraum zum extrem herausgehobenen > 5000 m hohen Rwenzori Gebirge, welches einen Teilbereich der östlichen Riftflanke des Albertrifts bildet. Bei den sedimentären Ablagerungen handelt es sich vorwiegend um unverfestigte, tonige bis grobkiesige Siliziklastika, die während mehreren Riftphasen in einem fluviatil-deltaischen bis lakustrinen Milieu abgelagert wurden. Basierend auf hochauflösenden sedimentfaziellen und geophysikalischen Profilaufnahmen und Beprobungskampangen, wurden die Riftsedimente mit einer multi-proxy Analyse untersucht, welche petrographische (Leicht- und Schwerminerale), geochemische (Granat- und Rutilchemie, Gesamtgesteinsgeochemie) und geochronologische (U-Pb Zirkonalter) Untersuchungsmethoden integriert. Die Ergebnisse dieser Arbeit sind in einem paläotektonischen Modell der Erosion, des Sedimenttransfers und der Riftbeckenbildung zusammengefasst, welches ein detaillierteres Bild der zeitlich-räumlichen Entwicklung des nördlichsten Sektors des westlichen Ostafrikanischen Grabensystems darstellt.

Der Fokus im zweiten Teil dieser Arbeit lag auf der Untersuchung rezenter Flusssande, welche im Rwenzori Gebirge und der angrenzenden Riftschulter genommen wurden. Diese weitere Studie komplettiert die Dissertation indem sie wichtige Einblicke in gegenwärtige Sedimentations- und Erosionsprozesse im Albertrift liefert. Durch die Analyse der modernen Flusssande mit einem identischen methodischen Ansatz wie für die Riftsedimente, konnten Provenienzsignaturen für verschiedene geologische Einheiten in der Umgebung des Albertrifts definiert und anschließend in den neogenen Riftsedimenten sicher identifiziert werden. Darüber hinaus wurde anhand der Flusssande untersucht, inwieweit sich die chemische Verwitterung auf die Komposition von Sedimenten unter extremen äquatorialen Klimabedingungen auswirkt.

Die Synthese aller während dieser Studie zusammengetragenen Informationen ermöglichte die Weiterentwicklung bzw. Modifizierung des bestehenden Evolutionsmodells des Albertrifts. Insgesamt konnten drei Riftentwicklungsphasen identifiziert werden, welche mit tektonischer Aktivität des Riftsektors in Verbindung gebracht werden können:

- Unteres Miozän bis Unteres Pliozän (~17,0–5,0 Ma)

Aufschlüsse der ältesten Riftsedimente sind nur im südlichen Teilbecken des Albertsees (Kisegi-Nyabusosi Region) bekannt. Die Daten dieser Provenanzstudie implizieren, dass der Sedimenttransport über ein westwärts gerichtetes, großskaliges Entwässerungsnetz erfolge, das über das Kongobecken in den Atlantik entwässerte. Das Liefergebiet der Sedimente erstreckt sich dabei bis zum mindestens 400 km vom Ablagerungsort entfernten neoproterozoischen Ostafrikanischen Orogen, was anhand des Vorkommens von panafrikanischen Zirkonaltern in den Sedimenten abgeleitet werden kann. Ein hoher Anteil an neoarchaischen Zirkonen zusammen mit Granat und Rutil typisch für amphibolit- bis granulitfazielle Bildungsbedingungen lassen auf den neoarchaischen Norduganda-

Terran (Uganda-Kraton), welcher große Bereiche des Grundgebirges von Uganda einnimmt, als Hauptschüttungsgebiet schließen.

- Unteres Pliozän bis Oberes Pliozän (~5,0–2,6 Ma)

An der Grenze Miozän/Pliozän kommt es zu einer Fragmentierung des bestehenden Entwässerungsnetzes und das Albertrift geht in die Synriftphase mit verstärkter Subsidenz und verstärkter Hebung der Riftschultern und des westugandischen Plateaus über. Der Sedimenttransport erfolgt jetzt aus proximalen Liefergebieten, was hauptsächlich aus einem Wechsel in den Schwermineralspektren und dem Fehlen von neoproterozoischen Zirkonen abgeleitet werden kann. Im Süden ist dies die östliche und südliche Riftschulter mit dem Rwenzori-Gebiet, im Norden die östliche Riftschulter. In beiden Fällen wird durch ein Vorherrschen von neoarchaischen Zirkonen in Kombination mit Epidot-Amphibol-dominierten Schwermineralspektren und hochgradig metamorphem Granat und Rutil (amphibolit- bis granulitfaziell) das Norduganda-Terran als das Haupterosionsgebiet impliziert.

- Unteres Pleistozän (seit ~2,6 Ma)

An der Grenze Pliozän/Pleistozän um 2,6 Ma erfolgt eine weitere Phase der Riftentwicklung, welche mit der beschleunigten Heraushebung des Rwenzori-Horstes und der Riftschultern sowie zurückgehenden Subsidenzraten und sogar teilweiser Inversion einhergeht. Im Süden ist die Abkopplung und forcierte Hebung des Rwenzori-Blockes an einer geringeren Maturität der Sedimente zusammen mit einer Modifikation des Schwermineralspektrums, insbesondere durch das Fehlen granulitfazieller Granate und Rutile, zu erkennen. Umgekehrt führt im Norden Recycling aus neoproterozoischen (Meta-) Sedimenten zu reiferen Quarzsanden mit höheren Anteilen an widerstandsfähigeren Schwermineralen (Zirkon, Turmalin). Die Liefergebiete verändern sich in beiden Fällen gegenüber dem Pliozän nur wenig und der Sedimenttransport erfolgt weiterhin von der nahegelegenen Riftschulter.

Die aus der Provenienz ableitbaren Phasen einschließlich deren zeitlicher Korrelation korrespondieren sehr gut mit den großen Ablagerungszyklen der Sedimentfüllung im Albertbecken sowie den Entwicklungsphasen anderer Riftsegmente des Ostafrikanischen Rifts. Dies impliziert, dass tektonische Aktivität in Ostafrika im globalen Maßstab erfolgt.

Gegenwärtig finden Sedimentbildungsprozesse im Albertrift unter tropischem Äquatorialklima in unterschiedlichen geomorphologischen Räumen, einschließlich schlecht entwässerter Ebenen des ugandischen Plateaus sowie dem stark herausgehobenen Rwenzori Gebirge, statt. In diesen werden zwei fundamentale Sedimenttypen erzeugt. Im Falle des geologisch jungen Rwenzori Gebirges herrscht aufgrund des starken Reliefs vor allem die physische Degradation vor. Die abgetragenen Sedimente sind gekennzeichnet durch einen hohen Anteil an Feldspäten und Gesteinsfragmenten sowie einer Epidot-Amphibol-betonten Schwermineralzusammensetzung. Im Gegensatz dazu sind Sedimente der mit mächtigen Lateritböden überdeckten Plateauebenen durch viele Millionen Jahre anhaltende intensive Verwitterung stark an Quarz angereichert. Die Studie an modernen Flusssedimenten demonstriert einschlägig, dass die vom Ausgangsgestein vorgegebenen Provenienzsignaturen auch in Gebieten mit extremen Klimabedingungen noch in den Sedimenten wiedergefunden werden können. Die Charakteristika des Liefergebietes werden am besten von Schwermineralspektren, Zirkonaltern, Granat- und Rutilchemie sowie geochemischen Parametern, insbesondere immobilen Elementen und Elementverhältnissen, bewahrt.

Zusammenfassend verdeutlich die vorliegende Doktorarbeit das große Potential von Provenienzstudien zur Rekonstruktion der tektonisch-sedimentären Entwicklungsgeschichte von Riftbecken in tropischen Klimaregionen und untermauert zudem die Bedeutung eines Multi-Proxy-

Methodenansatzes für ein umfassendes Verständnis von Sedimentationsprozessen und -produkten sowie deren Liefergebieten und Ablagerungsräumen. Die Studie an den Sedimenten im Albertrift demonstriert deutlich die Notwendigkeit einer Kombination von „traditionellen“ petrograhisch-mineralogischen Analysen mit „innovativen” geochemischen und geochronologischen Methoden für eine erfolgreiche Durchführung von Provenienzstudien. Es hat sich erwiesen, dass Varietätsstudien an Zirkon, Granat und Rutil am vielversprechendsten sind, um bestimmte Liefergebiete einzugrenzen. Während die ermittelten U-Pb Alter von Zirkonen direkt den Altern bestimmter Grundgebirgsterrane zugeordnet werden können, erlauben chemische Analysen von Granat und Rutil Rückschlüsse auf Metamorphosebedingungen während der Gesteinsbildung, sodass eine Unterscheidung von amphibolitfaziellen und granulitfaziellen Lithologien ermöglicht wird. Es hat sich jedoch gezeigt, dass diese drei Mineraltypen aufgrund ihrer hohen Beständigkeit innerhalb des sedimentären Zyklus nicht geeignet sind, um eine Sedimentanlieferung aus rezyklierten Sedimenten zu erkennen, da diese hier ausschließlich die Bildungsbedingungen ihrer ursprünglichen Lithologien reflektieren. Zur Bestimmung eines polyrezyklierten Liefergebietes sowie auch zur Ableitung von Verwitterungsszenarien eignen sich am besten Analysen des Modalbestands (Leicht- und Schwerminerale) und der Gesamtgesteinsgeochemie.

Contents

List of figures

List of tables

Abbreviations

Afsp – alkali feldspar
Alm – almandine
a.s.l. – above sea level
bt – biotite
BG – Bunyoro Group
CA – Cluster analysis
CIA – chemical index of alteration
CIW – chemical index of weathering
CL – cathodoluminescence
CR – Central Rwenzori Mountains
DF – discriminant function
EAO – East African Orogen
EARS – East African Rift System
EMP – electron microprobe
F / Fsp – feldspar
FeC – lateritic fragment
Gro – grossular
Grt – garnet
GZi – garnet:zircon index
HFSE – high field strength elements
HM – heavy mineral
HMA – heavy mineral analysis
HMC – heavy mineral concentration
ICP-OES/AES – inductively coupled plasma optical emission spectrometry
ICP-MS – inductively coupled plasma mass spectrometry
L – lithic fragments
LAB – Lake Albert basin
LA-ICP-MS – laser ablation inductively coupled plasma mass spectrometry
LGB – Lake George basin
LILE – large-ion lithophile elements
Lmb – metabasite grain
Lmf – metafelsite grain
Lms – metasedimentary grain
Lt – total lithic fragments including Qp
LVT – Lake Victoria Terrane
MDS – Multidimensional scaling
MER – Main Ethiopian Rift
Mu – muscovite (white mica)
NR – Northern Rwenzori Mountains
NUT – North Uganda Terrane
PAAS – Post-Archean Australian Shale
PC – principal component
PCA – principal component analysis
PIA – plagioclase index of alteration
Pl / Plag – plagioclase feldspar
Pyr – pyrope

Q% – relative abundance of quartz
Qm – monocrystalline quartz
Qp – polycrystalline quartz
Q / Qtot – total quartz (mono- and polycrystalline quartz + chert)
R – rock fragments
REE – rare earth element (HREE – heavy REE; LREE – light REE)
RFB – Rwenzori Fold Belt
RuZi – rutile:zircon index
Sp – spessartine
THMC – transparent heavy mineral concentration
TTE – transition trace elements
TTG – Tonalite–trondhjemite–granodiorite
UCC – Upper Continental Crust
WIP – Weathering Index of Parker
WNB – West Nile Block
WTT – West Tanzania Terrane
ZTR – zircon-tourmaline-rutile index

Chapter 1

1 Introduction

1.1 The 'RiftLink'-Project

The interdisciplinary research program *RiftLink – Rift Dynamics, Uplift and Climate Changes in Equatorial Africa* (H1643-7/1) was implemented by the German Research Foundation (Deutsche Forschungsgemeinschaft, DFG) in the year 2006 to provide a significant contribution towards a fundamental understanding of rift dynamics in eastern Africa. The *Riftlink* team is a consortium of scientists from thirteen national and international universities and research organizations, and more than twenty collaborative institutions (Fig. 1-1). The integrated research includes a combination of multiple geoscientific disciplines and methods, such as geophysics, petrology, low-temperature thermochronology, structural geology, geomorphology, sedimentology, paleontology, isotope geochemistry, climatology and numerical modeling. The major aim of *RiftLink* is to provide a full-scale process understanding of uplift pattern in rift settings, which is poorly constraint and therefore remains an important geological issue. Moreover, special emphasis is on the causal link between crustal uplift and atmospheric, biogeographical, and climatic processes, which is widely accepted, but has not been addressed in detail, before.

The study area of *RiftLink* represents the Albertine Rift in the equatorial part of the western branch of the East African Rift System (EARS). In this setting, rift topography reaches altitudes up to 3ooo meter above sea level. The Rwenzori Mountains, which form a promontory on the rift shoulder of the Albertine Rift, reach altitudes of > 5000 meter above sea level and represent an extreme example of basement uplift that has no counterpart on Earth (Ring, 2008, 2014; Sachau et al., 2013). The exceptional position of the Rwenzori horst block in extensional crust leads to a fundamental geodynamic questions and one of the central issues of the *RifLink* research group: Why are the Rwenzori Mountains so high? The rise of this unique horst block might have also substantially contributed to the aridification of eastern Africa by forming a new rain shadow.

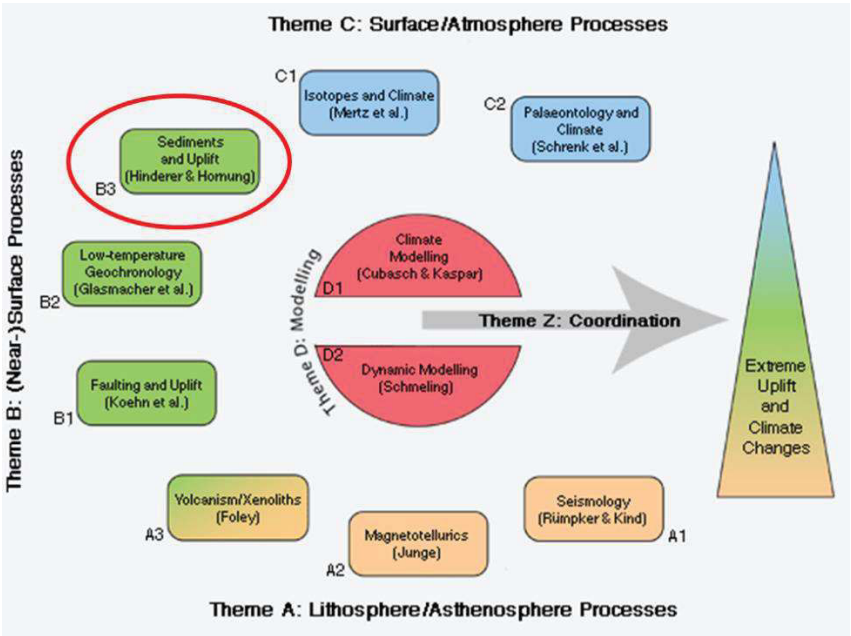

Figure 1-1. Organigram of the 'RiftLink' research group.

The results of the *Riftlink* research group are published in multitude research articles, partly compiled in two special issues of the *International Journal of Earth Science*:

- Bauer et al. (Eds.), 2010a. *Long-term rift evolution.* Volume 99(7),
- Rümpker and Mertz (Eds.), 2016. *With contributions to: The Albertine Rift (East Africa): mantle-crust interaction, surface processes, and impact on climate*. Volume 105(6).

This PhD thesis is integrated in the subproject B3 − *Linking Source and Sink in the Rwenzori Mountains and adjacent areas – Uganda: landscape evolution and the sedimentary record of extreme uplift,* which aims to reconstruct the erosional evolution of the Rwenzori Mountains and adjacent rift shoulders since their extreme uplift. The primary focus is placed on source-sink relationships in and around the Rwenzori block to better understand the interplay between rift dynamics and its impact on regional events. During two work periods, the project contributes to the uplift history and tectonic evolution of the Albertine Rift by carrying out studies on basin evolution, landscape evolution, paleoaltimetry, and neotectonics in cooperation within and outside the *Riftlink* research group.

During the first project period (2008–2011), which was mainly carried out by postdoc Dr. Sybille Roller (now Senckenberg Research Institute and Natural History Museum), detailed logging of Middle Miocene to Pleistocene sediment sections (including gamma-ray and magnetic susceptibility) was performed in two areas around Lake Albert (Kisegi-Nyabusosi and Nkondo-Kaiso). The results of logging and sedimentary facies analysis of 380 m sediments in the Kisegi-Nyabusosi area are published by Roller et al. (2010). Furthermore, erosion and denudation rates from ^{10}Be concentrations in quartz of river sands were calculated to receive information about erosion processes in the Rwenzori Mountains (Roller et al., 2012; Hinderer et al., 2013).

In the second work period (2011–2015), the postdoc position was split into two PhD studies. Further sedimentological logging and sampling was carried out in Uganda to fill remaining gaps in the sedimentary record. Additional samples from river sediments were collected. In the first PhD study, logged outcrop sections and collected samples have been analyzed with respect to stratigraphy, sedimentary cycles and paleoclimate reconstructions (D. Brüsch, dissertation in prep.). The second PhD study (this thesis) focuses on the erosional evolution of the Albertine Rift by studying the provenance of the rift infill and modern river sediments by using bulk rock petrography and geochemistry, heavy mineral analysis, chemical studies of single grains (garnet and rutile), as well as zircon U-Pb geochronology.

1.2 Study Aims

Based on an integrated multi-proxy provenance analysis that includes detailed petrographic-mineralogical and geochemical compositional descriptions of rift sediments and modern river sands in and around the Albertine Rift, this study intents to address following key issues:

- Create the first comprehensive petrographic, geochemical and geochronological data set for the entire rift succession in two areas around Lake Albert (Kisegi-Nyabusosi and Nkondo-Kaiso), and modern river sands along the rift shoulder/plateau and Rwenzori Mountains,
- Test the usefulness of multi-proxy provenance approaches in tropical basement areas,
- Evaluate the validity of sedimentary provenance studies for reconstructing the evolutionary history of rift settings,

Rift sediments:

- Identify, characterize and separate potential source rocks/areas and determine the timing of their sediment supply,
- Reconstruct the palaeogeographic and tectonic evolution of sediment supply paths and depocenters, which includes the coupling and exhumation history of different tectonic blocks with special focus on the uplift of the Rwenzori Mountains (= sedimento-tectonic model),
- Describe and compare the spatial (Kisegi-Nyabusosi vs. Kaiso-Nkondo) and temporal (Miocene to Pleistocene) evolution of the rift infill,
- Compare the timing of tectonic events in the Albertine Rift with those of other parts of the East African Rift System,

Modern stream sediments:

- Quantify the effects of chemical weathering on the composition of modern sediments that derive from a variety of basement rocks in areas characterized by different climate and relief,
- Ascertain whether the initial lithological signature is preserved in clastic sediments even under extreme climatic conditions, and
- Identify the characteristics of different rock lithologies of the Ugandan basement to provide the base for provenance reconstructions of the Neogene rift succession.

1.3 Study area

1.3.1 The East African Rift System

The East African Rift System (EARS), the most prominent tectonic and geomorphological feature in Africa, is the classical example for an active continental rift (Chorowicz, 2005). The rift valley developed successively during the Cenozoic and has been most probably induced by the impingement of a mantle plume below eastern Africa (Morley, 1995; Sepulchre et al., 2006). The EARS is several thousand kilometers long and forms two main branches; an older, volcanically active eastern branch and a younger, less volcanically active western branch (Ebinger, 1989; Morley, 2002) (Fig. 1-2B). Both rift arms follow Proterozoic mobile belts that enclose the mechanically stronger Archean Tanzanian Craton (Calais et al., 2006). The eastern branch of the EARS has its origin in the Afar depression that marks the triple junction between the Arabian, Somalian and Nubian shield. From Afar, the rift spreads over a distance of ~2200 km through the Main Ethiopian Rift (MER), the Omo-Turkana lows, the Kenyan Rift into the North-Tanzanian Divergence (Fig. 1-2A). At the Mbeya triple junction located north of Lake Malawi (Macheyeki et al., 2008), the eastern rift reemerges and converges with the western rift arm. The western branch of the EARS extends over a distance of ~2100 km. It consists of at least 32 individual tectonic basins distributed over three main segments (Chorowicz, 2005), and is bordered by ca. 100 km long border fault systems (Ebinger, 1989). The northern segment spreads from Lake Albert in the north to Lake Kivu in the Virunga province with turning trend from NE-SW to N-S, corresponding with Kibaran basement structures (1.4–0.9 Ga; Albaric et al., 2009) (Fig. 1-4). The central segment spreads from Lake Kivu further to Lake Tanganyika, mainly trending N-S, and controlled by reactivated, 1.11 Ga old Ubendian fault systems (Ring, 1994). The southern segment straddles towards Lake Rukwa and further to Lake Malawi, with changing orientation from NE-SW to N-S. Some literature refers the Mozambique Channel as a third, less developed, southeastern rift branch (Chorowicz, 2005).

Each rift branch consists of several individual, narrow, roughly N-S aligned tectonic half basins of thinned continental lithosphere, which are bounded by a border fault on one side and a flexural warp or faulted monocline on the other (Ebinger, 1989; Foster et al., 1997). While crustal thicknesses beyond the rift range between 30 and 35 km, and are less than the average of the African continent (Stamps et al., 2010), the border faults are flanked by broad uplifted shoulders that may be elevated several thousand meters above surrounding areas (Ring, 2014). In the extreme case of the Rwenzori Mountains within the Albertine Graben in the western rift, basement uplift accounts for more than 4 km (Ring, 2008; Bauer et al., 2010b). The uplift of topography is contemptuous to subsidence of surrounding areas, like the Congo Basin and the northern Arabian plate, as result of convective drawdown in the mantle (Moucha and Forte, 2011). The rift valleys themselves are linked and segmented by intracontinental transform faults, transfer fault zones and accommodation zones, and are mostly filled with sediment or volcanic material (Chorowicz, 2005).

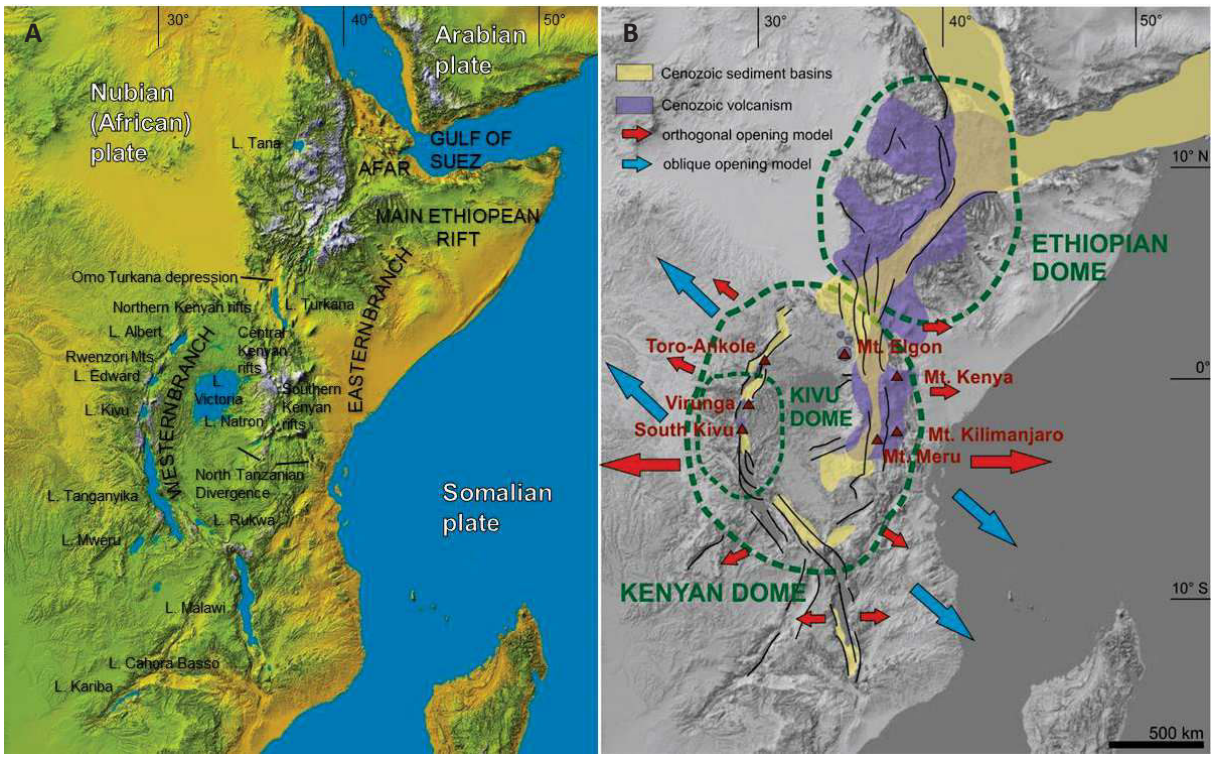

Figure 1-2. (A) Morphological overview of the East Africa Rift System. The basemap (Digital Elevation Model) is a SSRT image provided by the NASA. (B) Distribution of Cenozoic sedimentary basins and volcanism in eastern Africa (e.g., Ebinger, 1989; Rosendahl et al., 1992; Chorowicz, 2005; Schlüter, 2008) and orthogonal vs. oblique extension models for the formation of the EARS (e.g., Morley, 1988; Tiercelin et al., 1988; Ebinger, 1989; Versfelt and Rosendahl, 1989; Bosworth et al., 1992; Ring et al., 1992; Chorowicz et al., 1994; Stamps et al., 2008).

Initiation of the EARS is believed to have started in the eastern rift branch with first fracturing in the Afar and Ethiopian plateau regions caused by mantle plume activity at ~30 Ma (Chorowicz, 2005). This was accompanied by emission of large amounts of trap lava flows (Hofman et al., 1997). As is known from global seismic tomography and geodynamic modeling, eastern Africa rests above a major mantle upwelling (‘African Superswell’), driven by buoyancy forces of ascending hot and relatively fertile asthenosphere material in the deep-seated African Superplume. The plume is believed to rest in the lower mantle underneath Zambia from where it flows to the NE beneath East Africa (Bagley and

Nyblade, 2013). However, there is still debate about whether there is more than one plume underlying East Africa, as well as about their depths and extend (Pik et al., 2006).

After the opening of first graben structures, rifting in the eastern branch shows a southward propagation along suture zones, accompanied by further volcanism, particularly in the Kenyan Rift region. The coeval southward propagation of volcanism and rifting is supposed to be the response to southward migration of the mantle plume or the development of other plumes that weakened the crust and prepared further failures along suture or transform zones (Ebinger, 1989), together with the northward motion of the African tectonic plate over it (Ebinger, 2005; Moucha and Forte, 2011). The Tanzania Rift represents the southernmost and most juvenile segment in the eastern branch (Ring, 2014).

The onset of rifting in the western branch is still under debate, but magmatic evidence account for a diachronous opening during the Mid-Miocene that started in the Virunga and central Tanganyika regions probably initiated by stress transmission (Nyblade and Brazier, 2002). Initial fracturing and subsidence of the continental crust probably nucleated locally at pre-existing weak zones, which might be suture zones between old cratonic crust and younger thinner lithosphere (e.g., Foster et al., 1997). From there, the rift propagates to the north (~12 Ma) and to the south (~7 Ma) to link former isolated basins (Ebinger, 1989; Kampunzu et al., 1998; Morley, 1999; Ebinger and Furman, 2003). A much earlier initiation of rifting in the western rift (~25 Ma), largely contemptuous to the eastern branch, was insinuated by Roberts et al. (2012).

The eastern and western rift branches are characterized by marked differences concerning magmatic activity and morphology, most probably as result of the location and movement of the mantle plume below Africa (Ring, 2014). According to White et al. (1987), the temperatures may be 100–150 °C higher underneath the eastern branch than the western branch. A significant role in rifting processes plays the composition of the lithosphere through which the rift spreads. While the eastern rift arm mainly runs through the Cambrian Pan-African Orogenic Mozambique Belt, the western branch developed in older, relatively stiff Proterozoic belts or partly in Archean cratons (Ring, 2014). It seems plausible that the younger lithospheric material was rather vulnerable to crustal thinning, deformation and fragmentation than the old lithosphere that experienced repeated high-grade metamorphism making it relative strong and rigid (Ring, 2014). Heterogeneities in the rheology in the crust also affect the depths of earthquake hypocenters that deepen from north to south in the eastern rift (10 to 20 km), and are deeper in the western rift (up to 35 km) (Albaric et al., 2009). Intensive volcanic activity with distinctly greater volumes of magma is restricted to the eastern rift arm. Prior to initial rifting, the emplacement of flood basalts affected the region around southern Ethiopia at 45–35 Ma (Ebinger et al., 1993), probable caused by heating and mantle metasomatism along the asthenosphere-lithosphere boundary (Ring, 2014). Rift-related productive magmatism, usually of alkaline to hyperalkaline type, began at ~30 Ma in northern Kenya and Ethiopia, at ~20 Ma in central Kenya, and at ~12 Ma in southern Kenya (George et al., 1998), followed by a further period of significant magmatic activity at 5–2 Ma (Chorowicz, 2005). Most eruptive centers are located on or near fault systems or at intersections of border faults (Ebinger, 2005), and are surrounded by a broad regional culmination, particularly developed in the Kenyan and Ethiopian Dome (Fig. 1-2B).

In the western branch, rift related volcanism is less common and restricted to four isolated provinces − Virunga, South Kivu, Rungwe, and Toro-Ankole (Chorowicz, 2005). First volcanic activity took place in the Virunga region at ~12.6 Ma either prior or concurrent to initial faulting and subsidence (Bellon and Pouclet, 1980) and propagated southwards, causing volcanism in South Kivu at ~10 Ma, and Rungwe at ~7 Ma (Ebinger, 1989). In the northern Toro-Ankole field, volcanism started much later during the Quaternary. Magmatism in the western branch occurs periodically (Delvaux et al., 1992; Ebinger et al., 1993; Ring and Betzler, 1995), and produces strongly silica-undersaturated and potash-rich magmas (Rogers, 2006). In contrast to the eastern branch, regional doming and uplift is much less

developed. However, some of the basins in the western branch show the greatest absolute subsidence on Earth, with the bottom of the deep rift lakes lying at or below sea level (Ring, 2014). An exception are the Rwenzori Mountains between Uganda and the Democratic Republic of Congo, which form a promontory of the eastern rift shoulder and rise to more than 5 km above sea level (Pickford et al., 1993; Ring, 2008, 2014; Bauer et al., 2010b, 2013). The Rwenzori Mountains are the most extreme expression of rift-mountain uplift on Earth (Ring, 2008, 2014).

It is widely accepted that the remarkable topographic growth of the East African Plateau due to rift-related uplift and doming had strong influence on the regional and global climate during the past million years (Pik, 2011). High topographic ridges along the EARS serve as rain shadow that forms an effective barrier to moisture-bearing winds, thus regulating the distribution and the amount of rainfall in east Africa. The result is climate changes during the past 8 Ma from moist and warm to arid and perhaps slightly cooler resulting in a decrease of tropical rainforest and expansion of savannah landscapes (deMenocal, 2004; Spiegel et al., 2007; Rasmussen et al., 2015). The interplay between the long-term aridification trend and landscape fragmentation due to the multi-stage and mainly nonsynchronous evolution of the EARS is believed to have triggered human evolution (Denton, 1995; Coppens, 1999; Maslin and Trauth, 2009), and to have largely controlled hominid speciation, extinction and dispersal out of Africa (Sepulchre et al., 2006). Today, eastern Africa is known as the 'Cradle of Mankind' (Leakey, 1973) because most early hominid fossils have been encountered in the basins of the eastern EARS.

As indicated by the distribution of seismicity in eastern Africa, rifting processes are known to be still active in most sectors of the EARS (Nusbaum et al., 1993). Nowadays, the EARS propagates southwards at a rate between 2.5 cm/year (Oxburgh and Turcotte, 1974) and 5 cm/year (Kampunzu and Lubala, 1991; Kampunzu et al., 1998). The overall direction of extension of the EARS has long been under debate (Acocella and Korme, 2002; Chorowicz, 2005) with suggested movement direction either roughly NW-SE (Tiercelin et al., 1988; Versfelt and Rosendahl, 1989; Ring et al., 1992; Chorowicz et al., 1994), E-W (Morley, 1988; Ebinger, 1989; Bosworth et al., 1992; Stamps et al., 2008) or combination of both directions (Boccaletti et al., 1998). Nevertheless, spatial variations due to local-scale differences in the movement direction of single rift segments occur. Surrounded on three sides by divergent plate boundaries (Somalian, African, Arabian plates), east Africa is beginning to break apart along the EARS with relative velocity of the Somalian plate with respect to the Nubian plate of 6 mm/year (Stamps et al., 2008).

1.3.2 The Albertine Rift and Rwenzori Mountains

The ~500 km long and ~45 km-wide, NE-SW trending Albertine Rift represents the northernmost part of the western branch of the EARS. It stretches from the Kivu volcanic province in the south to the Aswa shear zone at the border between Uganda and South Sudan in the north straddling the Equator and covering parts of Uganda, Rwanda and the Democratic Republic of the Congo (DRC) (Fig. 1-3). The rift valley is located at the northwestern flank of the East African Dome adjacent to the watershed of Africa's two largest river systems, the Nile River and the Congo River, where it marks the climatic boundary between the tropical rainforest to the west and the arid savannah landscape to the east (Pickford et al., 1993). Tectonically, the Albertine Rift represents a transtensional pull-apart depression composed of several highly asymmetrical sub-basins (e.g., the Lake Albert Basin, Lake Edward-George Basin), some of them filled with the lakes Albert (Mobutu), Edward (Idi Amin) and George. The sub-basins are bounded by large border faults on one side and sets of smaller step faults on the other side and mainly linked to each other by 'Accomodation Zones' (Ebinger, 1989). Because of rift-related doming, the region is characterized by considerable relief. The lowest point of Lake Albert is at elevations of 618 m and rift shoulders are uplifted > 2200 m (west) and > 1300 m (east).

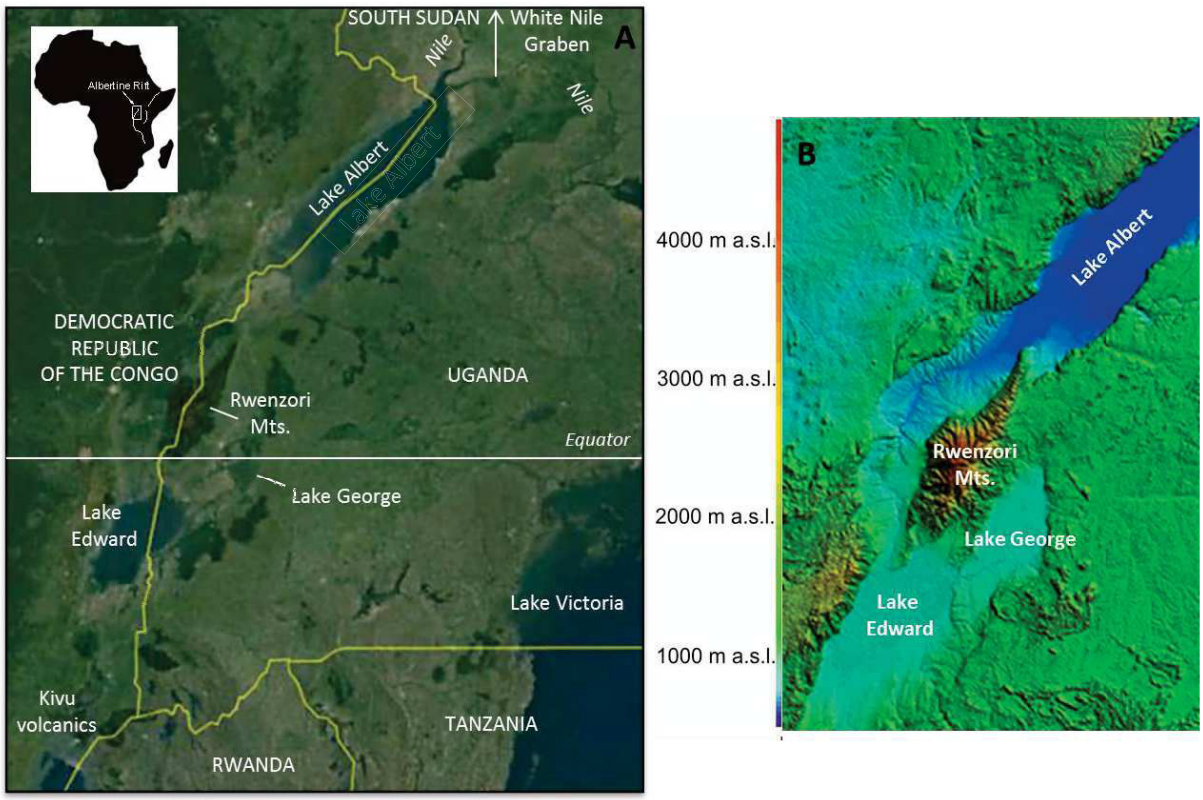

Figure 1-3. (A) Satellite image of the Albertine Rift (Source: Google Earth). (B) Digital Elevation Model of the Rwenzori region.

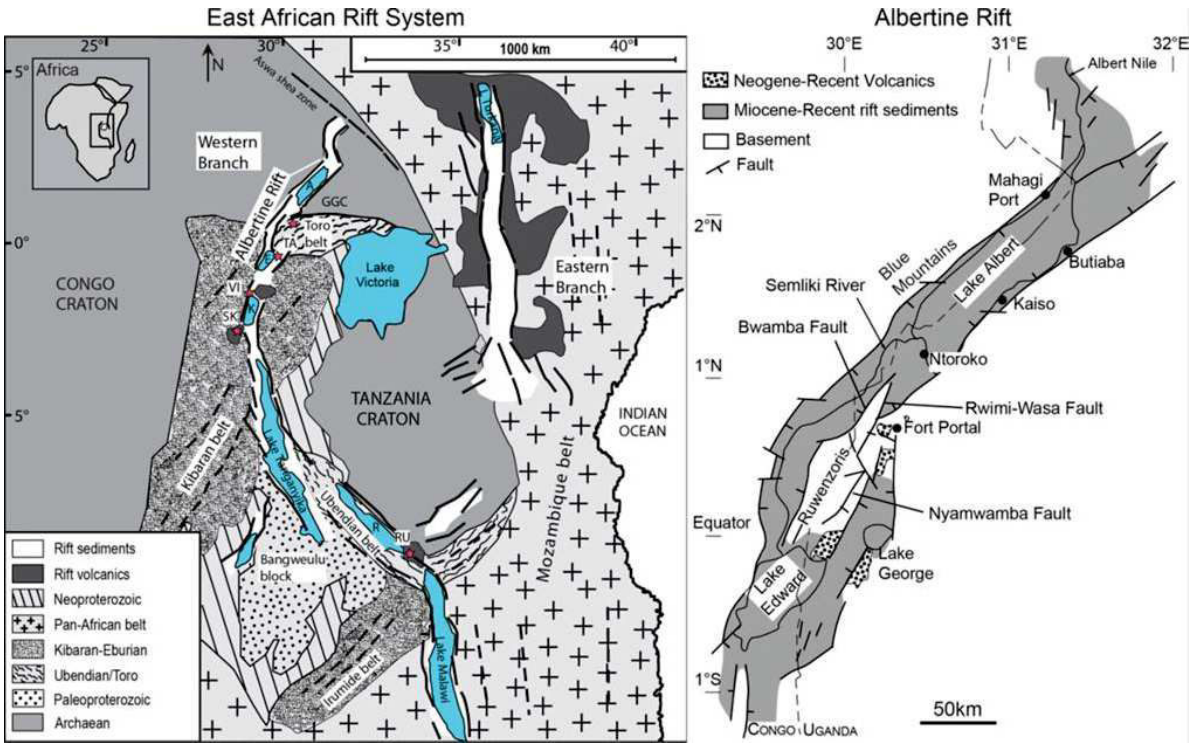

Figure 1-4. (left) Simplified structural and geological map of the western EARS with location of the Albertine Rift. *A* Lake Albert, *E* Lake Edward, *K* Lake Kivu, *R* Lake Rukwa, *TA* Toro-Ankole, *VI* Virunga, *SK* south Kivu, *RU* Rungwe volcanic provinces. (*right)* Outline of the Albertine Rift with main localities. (adopted from Bauer et al., 2016).

The rift floor of Lake Edward is at 200 m with rift shoulders rising up to 2300 m in the west and 1600 m in the east (Chorowicz, 2005). The northern continuation of Lake Albert forms the Neogene White Nile Graben. The Rwenzori Mountains situated between Lake Albert and Lake Edward roughly at 0.5°N and 30°E rise to more than 5 km above sea level and represent the highest example of basement uplift on Earth. With the Margherita Peak having an altitude of 5109 m above sea level the Rwenzoris are the third highest mountain range in Africa, and the highest without volcanic origin. Both, the Kilimanjaro (5893 m a.s.l.) and Mt. Kenya (5199 m a.s.l.) which rest on the eastern flanks of the eastern rift branch represent volcanic massifs. The Rwenzori Mountains are the wettest mountains on the African continent with 300 days of rainfall per year. The landscape was shaped by rivers and, above 2500 m a.s.l., large ice sheets that covered the mountains during several glaciation cycles in the Pleistocene and Holocene (Kaufmann et al., 2016). The three highest summits are still capped by glaciers (Fig. 1-5). Tectonically, the 50 km wide and 120 km long Rwenzori horst, which is sometimes referred to as the Rwenzori micro-plate, forms an active transfer-zone at the intersection of two rift segments (Koehn et al., 2008). The mountain range is dissected into several tectonic blocks by N-S, NW-SE, NE-SW and E-W trending normal faults that locally have a significant strike-slip component (Koehn et al., 2010). Major faults that bound the Rwenzori horst are the large-displacement Bwamba border fault on the western flank, the Rwimi-Wasa fault in the north of the eastern side as well as the Nyamwamba fault in the south of the eastern flank (Fig. 1-4). The Rwenzori Mountains are surrounded by deep rift valleys, including Semliki Valley to the north and west and the Lake Edward Rift with Lake George to the south and to the east. An exception is the north-eastern end that is still connected to the basement of the Tanzanian Craton (Koehn et al., 2010). Tilting of the Rwenzori Mountains along a NNE-SSW trending axis has been described by Osmaston (1989) and Taylor and Howard (1998), but may not account for the southern part of the Rwenzori block (Koehn et al., 2010; Bauer et al., 2013).

Figure 1-5 (previous page). Impressions of the > 5000 m high Rwenzori horst block. The mountain range is characterized by steep and rugged relief, bare rock faces and unique exotic vegetation that ranges from tropical rainforest to alpine meadows and gets scarce close to the mountain tops. The highest summits are still capped by glaciers all around the year. Photo courtesy S. Roller, J. Hornung, M. Hinderer.

The Rwenzori Mountains are situated at the transition between the 1.2 Ga old Kibaran belt (or Burundian-Karagwe-Ankole belt), the 2.5–1.85 Ga old Rwenzori belt (or Buganda-Toro belt) and the Archean Congo Craton. Unlike most other parts of the EARS, the Albertine Rift does not follow mobile belts, but runs into Archean basement and branches exactly at the position where the Rwenzori horst is located (Koehn et al., 2008). Straight rift propagation is hindered by the ENE-WSW striking Buganda-Toro belt (Link et al., 2010). The highest seismic activity is monitored NE of the Rwenzori block between Lake Albert and Lake George and is probably triggered by melt intrusions in the crust (Lindenfeld et al., 2012). The observed earthquake swarms go along with significant variations in the local stress field (Sachau et al., 2016). The extraordinary position of the Rwenzori Mountains in the middle of a system that is characterized by extension and that disclaims all features of a passive rift leads to a fundamental geodynamic questions: Why are the Rwenzoris so high? One hypothesis by Wallner and Schmeling (2010) favors rift-induced delamination of mantle lithosphere (termed RID) which causes fast isostatic pop-up of the Rwenzori horst due to reduction of viscosity and strength of the lowest part of the lower crust (Fig. 1-7). Their theory is supported by a detailed mapping study on the crust-mantle boundary in the region around the Rwenzori Mountains performed by Wölbern et al. (2010). According to their findings, the eastern rift flank of the Albertine Rift has a simple crustal structure and thicknesses of ~30 km. The crust beyond the Rwenzori horst is much more complex and also thinner than the crust of the rift shoulder with depths of the Moho ranging between 24 km in the northern Rwenzoris, 21 km in the eastern central Rwenzoris and 28 km in the southern tip of the mountain ridge. The lithosphere-asthenosphere boundary is at depth of 135–210 km, whereas the boundary between pristine and altered lithosphere is located at depths 54–104 km with the shallowest depths underneath the rift segments and the deepest underneath the cratonic crust (Wölbern et al., 2012). Gummert et al. (2016) who consider a missing crustal root beneath the Rwenzori horst also support the delamination theory. Another concept for the uplift of the Rwenzori Mountains was introduced by Koehn et al. (2010) and is based on fieldwork and seismological data. A numerical model proposes three evolutionary stages for the Albertine Rift (Fig. 1-6). The initial stage, which began at approximately ~14 Ma and lasted for about 2 Ma years, is characterized by the generation of the two rift segments, which are nowadays occupied by Lake Albert and Lake George. In the second stage (~10–12 Ma) the Rwenzori basement was trapped between the two segments and rotates clockwise, what leads to disruption of the former stress field and to transection faults that dissect the basement block. During the third step (~8 Ma to present), the rift segments propagate further towards each other and finally merge. According to Koehn et al. (2010), significant uplift and tilt is only achieved after the two rift segments are entirely merged. Detachment of the Rwenzori horst from the Victoria plate is still ongoing (Sachau et al., 2016). At present, the Albertine Rift extents with a velocity rate of 2.1 mm/year in ESE direction with the Victorian plate rotating anticlockwise with respect to the Nubian plate (Calais et al., 2006; Stamps et al., 2008; Saria et al., 2014). Link et al. (2010) argue that also the pre-rift geology may have played an important role on the height and position of the Rwenzori horst, e.g., the relative stiffness of the Paleoproterozoic Buganda-Toro mobile belt.

Bauer et al. (2010b, 2013) tried to reconstruct the uplift and denudation history of the Rwenzori Mountains by using low temperature geochronology and concurrent thermal modelling. Their studies indicate that the exhumation history of the Rwenzori Mountains is likely to be dated back to Paleozoic times and includes three major evolutionary stages: (1) long-term landscape evolution since the

Paleozoic includes several cooling events; distinct decoupled tectonic blocks of the Rwenzoris horst were exhumed at different times, (2) medium-term landscape evolution since the Miocene led to the high topography and asymmetry as erosion could not compensate for rock uplift, and (3) short-term landscape evolution in the near past (Pliocene-Pleistocene); fast uplift together with glacial erosion led to the creation of the present topography.

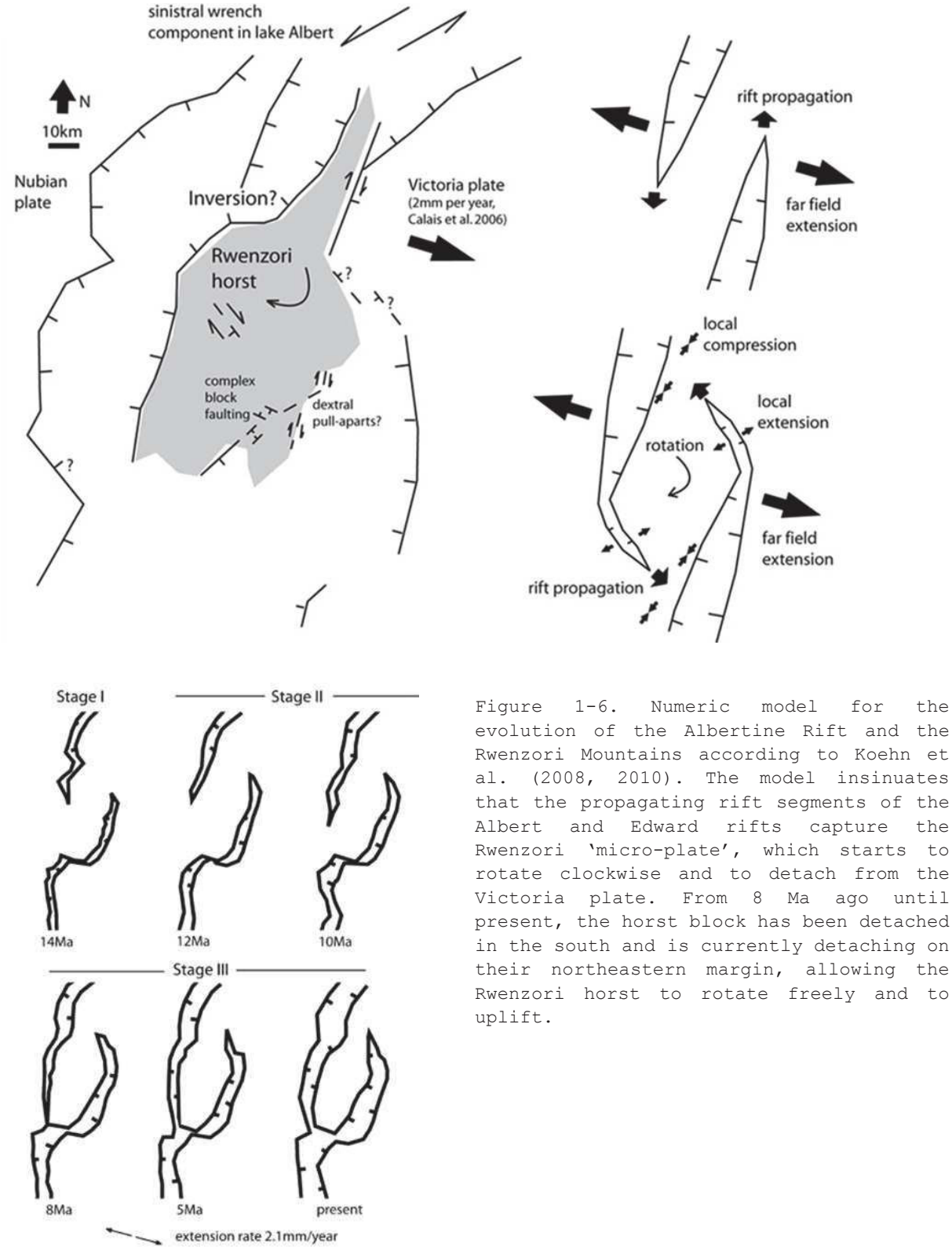

Figure 1-6. Numeric model for the evolution of the Albertine Rift and the Rwenzori Mountains according to Koehn et al. (2008, 2010). The model insinuates that the propagating rift segments of the Albert and Edward rifts capture the Rwenzori 'micro-plate', which starts to rotate clockwise and to detach from the Victoria plate. From 8 Ma ago until present, the horst block has been detached in the south and is currently detaching on their northeastern margin, allowing the Rwenzori horst to rotate freely and to uplift.

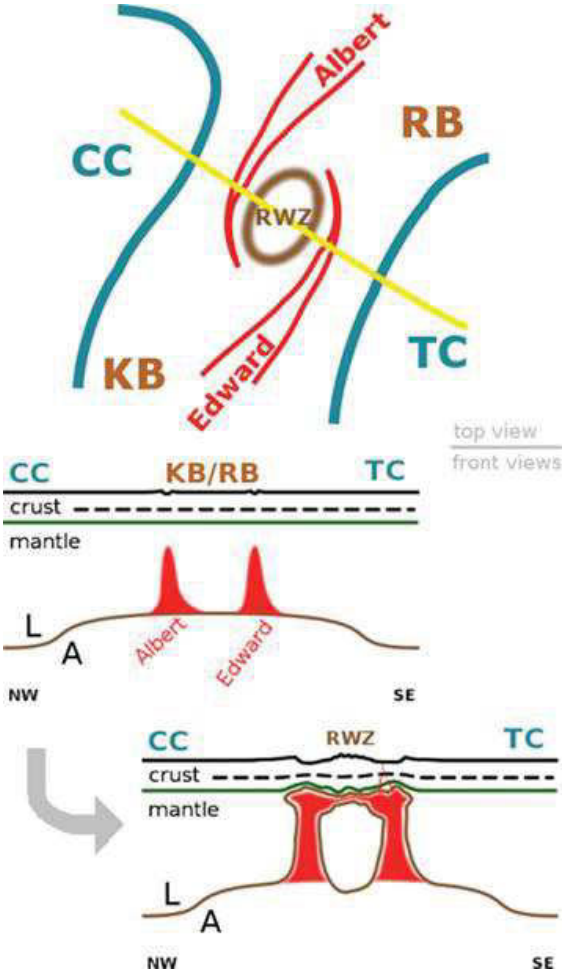

Figure 1-7. Sketch of the 'rift induced delamination of mantle lithosphere (RID) and uplift of crust' model after Wallner and Schmeling (2010) showing initial temperature anomalies (in red) from the Albert and Edward rift tips (middle) and the later upwelling of asthenospheric material(bottom). CC Congo Craton, TC Tanzania Craton, KB: Kibaran Belt, RB: Rwenzori Belt, RWZ: Rwenzori Mountains. Albert, Edward: Cenozoic rifts, A: Asthenosphere, L: Lithosphere.

As most basins in the EARS, the Albertine Rift is also filled with sediment (Fig. 1-8). Surface and subsurface observations indicate that the northern Albertine Rift occupies a pile of ~5 km thick sedimentary deposits (Karp et al., 2012) that mainly consist of fluvial-deltaic sediments in the bottom and top, and lacustrine sediments in between. The sedimentary detritus includes conglomerate, sand, silt, clay, chert, shale, oil shale and coal-bearing horizons (Westerhof et al., 2014). Based on structural, sedimentological and paleontological studies, rifting in the northern Albertine Rift is believed to have started in the early Miocene, at approximately 18–20 Ma with early faulting and subsidence (de Heinzelin, 1963; Lepersonne, 1970; Pouclet, 1975; Delvaux and Barth, 2010). Some younger age of 15–16 Ma was assumed by Pickford et al. (1993). Whatever the correct age might be, the Albertine Rift is older than the other basins along the western rift branch (Westerhof et al., 2014). Initial volcanism in the Virunga Province is reported at ~12 Ma, prior or concurrent to faulting and subsidence in the Albertine Rift (Ebinger, 1989). The earliest fluvial rift sediments were deposited in a shallow downwarp around 17 Ma (Simon, 2015), whereas first lacustrine deposits probably accumulated around 8 Ma. At this time, the Albertine Rift experience a first major period of rifting associated with uplift of rift flanks (Ring et al., 1992; Ebinger et al., 1993; Ring and Betzler, 1995). From ~7.5 Ma, the area of the Albertine Rift was covered by a huge paleo-lake (Lake Obweruka) that lasted until 2.5 Ma, when it was separated into Lake Albert and Lake Edward during another major tectonic pulse at ~2.5 Ma (cp. Pickford et al., 1993; Ring, 2008). It is assumed that this tectonic event was associated with extensive rifting, surface uplift and exhumation of the Rwenzori Mountains (Ebinger, 1989; Pickford et al., 1993; Taylor and Howard, 1998) (Fig. 1-8).

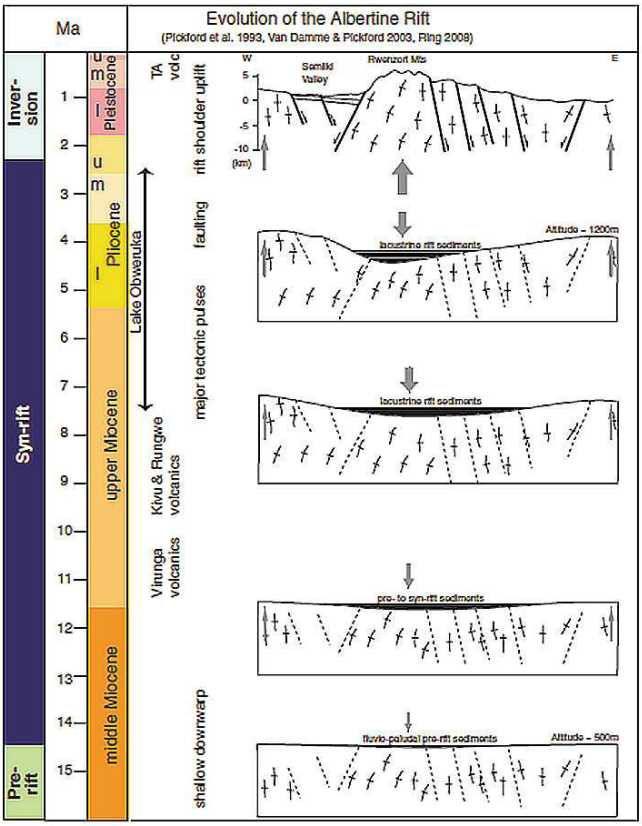

Figure 1-8. Scheme of the structural and sedimentary evolution of the Albertine Rift with phases of major tectonic and volcanic events (adopted from Bauer et al., 2010).

1.4 Sediments in the EARS – International state of research

The continental basins in East Africa are important sediment storage systems that have long been of interest to sedimentologists. The architecture of the basin and rift infill is a complex composite of several factors, e.g., sediment-supply rates, accommodation space, regional drainage and climate pattern, most of them determined by the displacement geometry along the border fault system. The long-term record of the numerous rift sectors represent excellent natural archives documenting the climatic, environmental and tectonic history of eastern Africa during the past million years (e.g., deMenocal, 2004; Pickford, 1990).

Numerous investigations of the sedimentary record exposed in the EARS have been carried out during the last decades, whereas in the beginning of East African research more attention was paid to the eastern branch of the EARS. For one thing, this is because the structure and location of the older rift branch allows to study all aspects concerning rifting, including the transition from continental to oceanic rifting (Logatchev et al., 1972), and secondly, because of spectacular fossil remains that have been found within the valleys of the eastern rift branch. A large amount of studies have been published that deal with late Pleistocene to Holocene global and local climate changes (e.g., Hecky and Kilham, 1973; Richardson and Dussinger, 1986; Gasse, 2000; Verschuren et al., 2000; Gasse et al., 2008; Scholz et al., 2007, 2011), and its possible connection with tectonically driven uplift of rift shoulders (e.g., Sepulchre et al., 2006), orbital forcing (Olsen, 1986; Johnson and Odada, 1996; Trauth et al., 2003; Maslin and Christensen, 2007), and/or human evolution (e.g., Trauth et al., 2005, 2007; Holmes, 2007; Maslin et al., 2014, 2015). As in the ongoing ‘Hominin Sites and Paleolakes Drilling Project’,

which addresses the causal link between geohistorical processes, especially climatic and environmental ones, with events in hominin evolution (Campisano et al., 2017), most of these studies have been applied on Pliocene-Holocene fluvio-lacustrine marine sediments deposited in the numerous rift lakes. The high resolution marine records in the shallow rift lakes of the EARS are sensitive environments for quantifying paleoprecipitation, water balance and paleotemperature changes, including seasonality (Trauth et al., 2007). Few authors also considered terrestrial outcrop-based studies for addressing the linkage between paleoclimate/-environmental changes and hominin evolution (Stollhofen et al., 2008; Simon, 2015; Mtelela et al., 2016). Besides for paleoenvironmental archives, several of the rift basins bear important hydrocarbon resources and are thus attractive targets for petroleum exploration (e.g., Robbins, 1983; Katz, 1990; Lambiase, 1995; Lambiase and Morley, 1999). To better understand the basin geometry and its sedimentary infill, many exploratory drilling campaigns were initiated and a variety of investigations, including magneto telluric, gravity surveys and geophysical modelling (e.g. Ebinger et al., 1989) have been conducted. Moreover, intensive seismic subsurface mapping has been carried out in many of the rift sections, e.g., Lake Tanganyika (Rosendahl, 1988), Lake Malawi (Scholz et al., 1989), Lake Turkana (Dunkelman et al., 1989) and in the Rukwa Basin (Morley et al., 2000), many of them sponsored by the oil companies. Further published data include conceptual models for the evolution of syntectonic sedimentary architecture of rift basins (Gawthorpe and Leeder, 2000), volcanic dating (e.g. Wichura et al., 2011) and lakebed lithological studies (e.g., Tiercelin et al., 1992). So far, two special papers on African Rift sedimentation were edited by Frostick et al. (1986) and Renault and Ashley (2002), in which results and the progress in rift tectonics, volcanism, and fluvial-lacustrine depositional systems are compiled in several articles.

Despite the relatively large volume of literature on rift sediments, information about the onset and long-term evolution of the rift is rare. Sedimentary provenance studies, which provide a perfect tool for addressing uncertainties concerning the detailed chronology of uplift, volcanism and rifting in eastern Africa, remain insufficient in the EARS. Until now, only few compositional studies on the rift deposits have been undertaken. Mathisen and Vondra (1983) studied heavy-mineral associations of Plio-Pleistocene fluvio-lacustrine sediments in the East Turkana Basin to unravel the timing of rifting, magmatism and drainage development. Roberts et al. (2012) studied the paleoenvironmental and paleoclimatic history of the Rukwa Basin by using sedimentological, paleontological and geochronological approaches. Multi-proxy provenance studies are completely absent for most rift basins and are also lacking in the northern section of the western branch of the EARS (Albertine Rift).

Although the Albertine Rift is a key region for understanding the evolutionary history of eastern Africa and preserves some of the oldest and most complete sedimentary successions in the EARS, research activity remained relatively poor during the last century. Existing sedimentological studies date back to the early 20th century (Wayland, 1926; Solomon, 1939; Lepersonne, 1949; Bishop and Trendall, 1966; Bishop, 1969; overview in Pickford et al., 1993). The first deep well was drilled in the Kaiso area (WAKI) in 1938; however, well data were not published (Davies, 1951). More systematic paleontological and biostratigraphical studies, as well as mapping were carried out since the 1960th by various authors, including De Heinzelin (1963), Gautier (1970), Pickford (1986), Senut et al. (1987), Pickford et al. (1993), and VanDamme and Pickford (1995, 1998, 2003). Major parts of the present knowledge about the geological and paleontological evolution of the rift valley bases on fossil founds gathered during several expeditions, such as the Uganda Paleontological Expedition (Pickford et al., 1993). Pickford et al. (1993) and Senut and Pickford (1994) especially reviewed the molluscan and mammalian biostratigraphy and introduced most of the formations in the Albertine Rift, which are still of fundamental relevance and provide the base for this thesis. Based on their studies, same authors also provided a more detailed overview about tectonic events affecting that particular rift sector.

Figure 1-9. (A) Rift valley in the Nkondo-Kaiso region east of Lake Albert (619 m a.s.l.) with the uplifted rift shoulder (in the back), reaching altitudes of ~ 1300 m a.s.l. (B) Road cut unveiling Miocene sediment successions in the southern Lake Albert sub-basin (Kisegi-Nyabusosi area; photo courtesy D. Brüsch). (C) Rift sediment exposed at the Warwire Cliff near the Lake Albert Safari Lodge east of Lake Albert (Nkondo-Kaiso area; photo courtesy S. Roller).

The relative little research activity on the rift sediments in the Albertine Rift during the last century has several reasons: (i) sedimentary outcrops are rare and only exposed in few scattered patches around Lake Albert, (ii) outcrops are often of poor quality (e.g., dense vegetation), (iii) no possibility of high-resolution tephrochronology especially in lower parts of the stratigraphy because of only sporadically occurring tephra layers, (iv) no spectacular fossil finds, (iv) poor infrastructure and accessibility of the area, (v) the region has been of great political conflict throughout the past decades with civil wars in Uganda, Rwanda, and the Democratic Republic of Congo and is now and then still affected by political instabilities in some parts.

Sedimentological studies in the Albertine Rift were only intensified in the recent years in the course of the interdisciplinary *RiftLink* research program (Bauer et al., 2010a, Rümpker and Mertz, 2016), established to address rifting dynamics, uplift, and climate change in Equatorial Africa with special focus on the Rwenzori Mountains and surrounding rift sectors. In this context, Roller et al. (2010) developed a depositional model for the southern Albertine Rift (Kisegi-Nyabusosi area) based on logged sedimentary sequences on the northern side of the Rwenzori Mountains. Moreover, much attention has been paid to the Albertine Rift lately, because of its large volumes on hydrocarbon resources that can be found at the margin of the basin. Since the Albertine Rift represents one of the most petroliferous onshore rifts in Africa, oil companies and the Uganda government have put much effort in sedimentary research. Intensive seismic profiling was conducted that covers the entire lake area by a grid of transversal and longitudinal lines to better understand the overall morphology of the basin. In 2002, a deep well (Turaco-1) was drilled to depths of almost 2500 m, but without significant hydrocarbon discoveries (Logan et al., 2009). This was followed by several successful deep wells drilled in and around Lake Albert (Kingfisher 1-3, Ngassa 2, Waki-1). Research data from the wells are only sparsely available; some of them only presented at conferences and investors presentations (Macgregor, 2015). Published studies attempt to provide a broader understanding of the structure and stratigraphy of the basin by integrating seismic reflection and gravity data. Palynological studies were applied to better understand the climate and environmental conditions of the basin through time (Lukaye, 2009; Shaw et al., 2009). Simon (2015) and Lukaye et al. (2016) attempted to refine the existing stratigraphic scheme for the Albertine Rift by integrating surface data and subsurface data. However, the time of onset of the rift valley is still controversially discussed between industry and academics with proposed ages ranging from early Miocene (Lepersonne, 1949; Lukaye, 2009), mid-Miocene (Abeinomugisha and Kasande, 2012; Lukaye et al., 2016) to late Miocene (Pickford and Senut, 1994; Yasui et al., 1992). Information about sediment sources is rare. Authors consider that most of the sediment was delivered into the valley by fluvial means (Pickford et al., 1993). Several attempts have been carried out to reconstruct the Miocene to recent drainage network of east Africa (Cooke, 1958; de Heinzelin, 1962). Authors suggest that before the mid-Pleistocene, the hydrological system of Uganda was dominated by westward directed rivers that flowed from Kenya to join the great Congo system (Wayland, 1929; de Heinzelin, 1962; Bishop, 1965; Taylor and Howard, 1999). Thermally induced uplift of continental crust caused disruption of this surface drainage, by the so-called ‘axis of upwarping’ located 13–32 km east of the western rift, leading to river reversal (Doornkamp, 1968) and formation of Lake Victoria some 400.000 years ago (Johnson et al., 2000). Provenance studies are completely absent for the sedimentary infill of the Albertine Rift, but have recently been applied to modern river sediments along the western rift branch of the EARS, including the Albertine Rift, and the River Nile system to study modern erosional processes and products (Garzanti, 2013a, 2013b, 2015). Despite the fact that research activity has been strongly enhanced during the last couple of years and new well data provide a broader insight into the evolution of the Albertine Rift, the data acquisition remains still insufficient to develop a profound understanding of the regional and local tectonic, climatic and sedimentary history of the northern part of the western rift branch.

1.5 Introduction to Sedimentary Provenance Analysis and Applied Methods

1.5.1 Sedimentary Provenance Analysis (SPA)

The term *provenance* derives from the Latin word ‘provenire’, meaning as much as ‘to originate’. Broadly defined, provenance analysis serves as a tool to reconstruct all aspects under which sediment forms, including the parent rock lithology, as well as the tectonic, paleoclimatic and paleogeographic conditions of the source area and the final depositional basin. Inferring the entire history of sediment generation from the erosion of the source rock towards the burial of the siliciclastic detritus is anything but a simple task, taking into account that the sedimentary detritus does not remain static, but constantly evolves during the sedimentary cycle. In first place, sediment composition is the result of the composition of the weathered parent rock from which it originates. The initial signature imparted by source-rock lithology is however modified by several physical and chemical processes that operate before and after deposition (e.g., Morton and Hallsworth, 1994, 1999; Weltje and von Eynatten, 2004). As soon as a rock is exposed to the surface, it is subject to erosion and weathering, both processes mainly determined by the interplay of lithology, relief, climate and vegetation (Johnsson, 1993). Weathering results in depletion of instable components, such as mafic minerals (e.g., pyroxene, amphibole, biotite) and feldspar, whereas stable constituents, like zircon and quartz, are continually enriched (e.g., Nesbitt et al., 1997; Van Loon and Mange, 2007). During transport away from its place of origin, compositional and textural modifications of the detritus are mainly governed by abrasion and breakage of grains, mixing of detritus from various source rocks/areas, as well as sorting of grains due to their different hydraulic properties (Fig. 1-10). Intermittent storage of the detritus in floodplains results in chemical modifications of the sediment composition. Here, the intensity of alteration generally depends on the overall intensity of weathering and its duration (Johnsson and Meade, 1990). After final deposition, the detritus is prone to the environmental conditions of the depocenter. Sediment that experiences (deep) burial is affected by diagenetic processes fostered by increasing pressure and temperature conditions. The main diagenetic processes include mineral intrastratal dissolution, recrystallization, compaction, grain deformation and precipitation of new mineral phases (Blatt, 1979, Worden and Burley, 2003, Morton and Hallsworth, 2007).

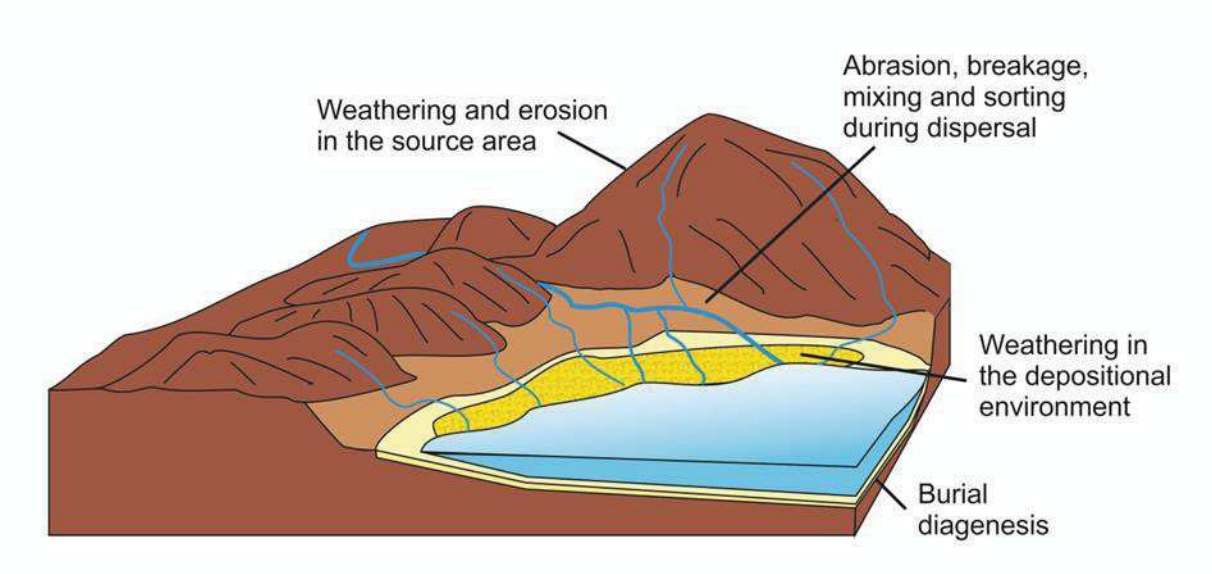

Figure 1-10. Major processes that can modify sediment composition from source to sink (modified after Morton and Hallsworth, 1994).

Provenance analysis requires that compositional and textural modifications of the detritus are adequately recognized, and that, ideally, all individual processes affecting the sediment along the sediment pathway are singled out. However, in reality, a full reconstruction of all weathering, transport and postdepositional processes is hardly to achieve, because much information is lost from source to sink. The challenging task to gain as much information as possible might be tackled best by using a combination of interdisciplinary approaches. Modern provenance reconstructions are commonly based on the application of compositional analysis, and largely benefit from continuing technological advances. Applied techniques commonly include petrographic, isotopic and geochemical approaches, and concentrate on three main categories: (1) Petrographic-mineralogical and chemical analysis of the bulk composition, (2) analysis of a specific mineral group (e.g., heavy minerals), and (3) analysis of specific minerals from a certain mineral group (Weltje and von Eynatten, 2004). This thesis covers a variety of techniques that proved to be reliable methods in unraveling sediment provenance, including bulk rock petrography and geochemistry, heavy mineral analysis, chemical studies of single grains (garnet and rutile) radiometric dating of zircon (Fig. 1-11).

1.5.2 Methodological approach

The subsequent section presents a general overview of the methods applied during this study. Detailed descriptions of analytical procedures are given in the following chapters (2−6) of this thesis.

Framework petrography (‘Light mineral’ analysis)

Petrographic investigations of thin sections have a long tradition and are a basic tool in sedimentary research (Weltje and von Eynatten, 2004). By definition, framework grains (‘light minerals’) have a specific density < 2.89 g/cm^3 (Boenigk, 1983), and commonly represent more than 90% of the total content of sands and sandstones. Even though the examination of framework components is rather time-consuming and results often less informative compared to other methods, e.g., heavy mineral or single grain analysis, the qualitative and quantitative analysis of framework grains can give important information on the origin and history of clastic sediments. Common applications include the classification of sediments in ternary diagrams (QFL, QmFLt, e.g., McBride, 1963, Garzanti, 2016), determination of the tectonic setting (arc, orogeny, craton, recycled) of the sediment source (e.g., Dickinson, 1985; Dickinson and Suczek, 1979), and reconstruction of the diagenetic history (Gaupp, 1996). Detailed investigations of the lithic grains allow more specific characterization of the provenance. Ideally, the texture and mineral parageneses of rock fragments give first-hand information on the source rock (low-grade metamorphic, high-grade metamorphic, sedimentary) and might even allow reconstruction of e.g., metamorphic temperature-pressure-time paths. Due to the decomposition of rock fragments in finer grain size fractions, this, of course, requires grain sizes big enough to still carry the full suite of coexisting minerals, which usually is not the case in grain size fractions normally used for microscopic investigations. Quantification of the modal composition is routinely achieved by counting a representative amount of grains per thin section, usually performed by using an electronic point-counter with mechanical stage.

Heavy mineral studies

Heavy minerals are useful indicators for source rock determination, because, unlike quartz and feldspar, their composition and parageneses strongly depends on the chemistry and tectono-stratigraphic level of their protosource. Per definition, heavy minerals have a specific density of > 2.85 g/cm^3 (Boenigk, 1983). Although some heavy minerals (e.g., amphibole, pyroxene) are rock-forming

in magmatic or metamorphic rocks, in clastic sediments they usually occur as accessories with proportions less than 1%. In many cases, the heavy mineral association in sediments does not simply reflect the original assemblage of the provenance, but might be modified during several external processes, described in the section above (1.5.1), whereas hydraulics and burial diagenesis are believed to be the most crucial controlling factors (Morton and Hallsworth, 1999, 2007). Chemical dissolution during weathering or diagenesis may lead to loss of instable minerals (e.g., olivine, pyroxene) and enrichment of chemically and mechanically (ultra)stable components, such as zircon, tourmaline and rutile, during the sedimentary cycle (Morton, 1985; Velbel, 2007). Mineral sorting during transport and dispersal may lead to segregation of different mineral types or even within the same mineral group due to a different hydraulic behavior. Generally, changes in the provenance signal in overprinted sediments can be obtained by: (i) following the occurrence of diagnostic stable minerals (e.g., spinel, e.g., von Eynatten and Gaupp, 1999), (ii) comparing the ratio of two stable minerals (e.g., apatite/tourmaline or garnet/zircon; Morton and Hallsworth, 1994), and (iii) examining changes in the chemistry of single grains of a certain mineral group (= varietal studies; e.g., garnet, rutile; e.g., Morton, 1985; Zack et al., 2004 a, b). The effect of physical sorting that causes deposition of minerals with the same size and shape in different size fractions due to differences in their hydraulic behavior can be minimized by analyzing a specific grain size interval (Morton and Hallsworth, 1994).

Chemical analysis of heavy minerals (garnet and rutile)

Single-grain chemical analysis by microbeam techniques allows investigating the major and trace element composition of minerals from a certain mineral group and the variability among these grains (Mange and Morton, 2007). Because every rock suite has specific elemental characteristics that are also inherited by the minerals that originate from this source, distinct elemental signatures or variations within the group can be used to trace back their protosource. Chemical analysis can be applied to a variety of minerals, such as feldspar (e.g., Trevena and Nash, 1981), pyroxene (e.g., Krawinkel et al., 1999; Pinto et al., 2004), tourmaline (e.g., Henry and Guidotti, 1985; Morton et al., 2005), or opaque minerals (e.g., Basu and Molinaroli, 1989, 1991; Amini and Anketell, 2015). The most often used constituents are those that occur in a variety of rock suites and are widespread in siliciclastic rocks. In this thesis, garnet and rutile are chosen for microprobe investigations; both minerals have been proven as reliable index minerals in multiple provenance studies.

Garnet

Due to its many compositional variations with six principal end-member compositions (pyrope, almandine, spessartine, grossular, andradite, uvarovite), garnet is a widely used indicator mineral in provenance studies, that can give distinct information about the source area of siliciclastic rocks (e.g., Morton, 1985, 1987; Aubrecht et al. 2009). The chemistry of garnet depends both on the composition of the parental rock and on the P-T conditions during formation. Besides its chemical variability, other advantages that make garnet a suitable fingerprinting mineral is its relative stability during long distance fluvial-deltaic transport and its resistance against chemical modification during diagenesis or low-grade metamorphism (Morton, 1984; Hutchison and Oliver, 1998). However, garnet responds sensitive to acidic environments, in which it might undergo secondary alteration processes, like chemical modification until total dissolution (Morton, 1984). Dissolution of garnet in East African modern river sands has been described by Andò et al. (2012) and Garzanti et al. (2013), who found that garnet weathers out much faster than hornblende in wet and humid equatorial environments. The stability of garnet depends on the chemical composition with the most Ca-rich species becoming instable first (Morton, 1987).

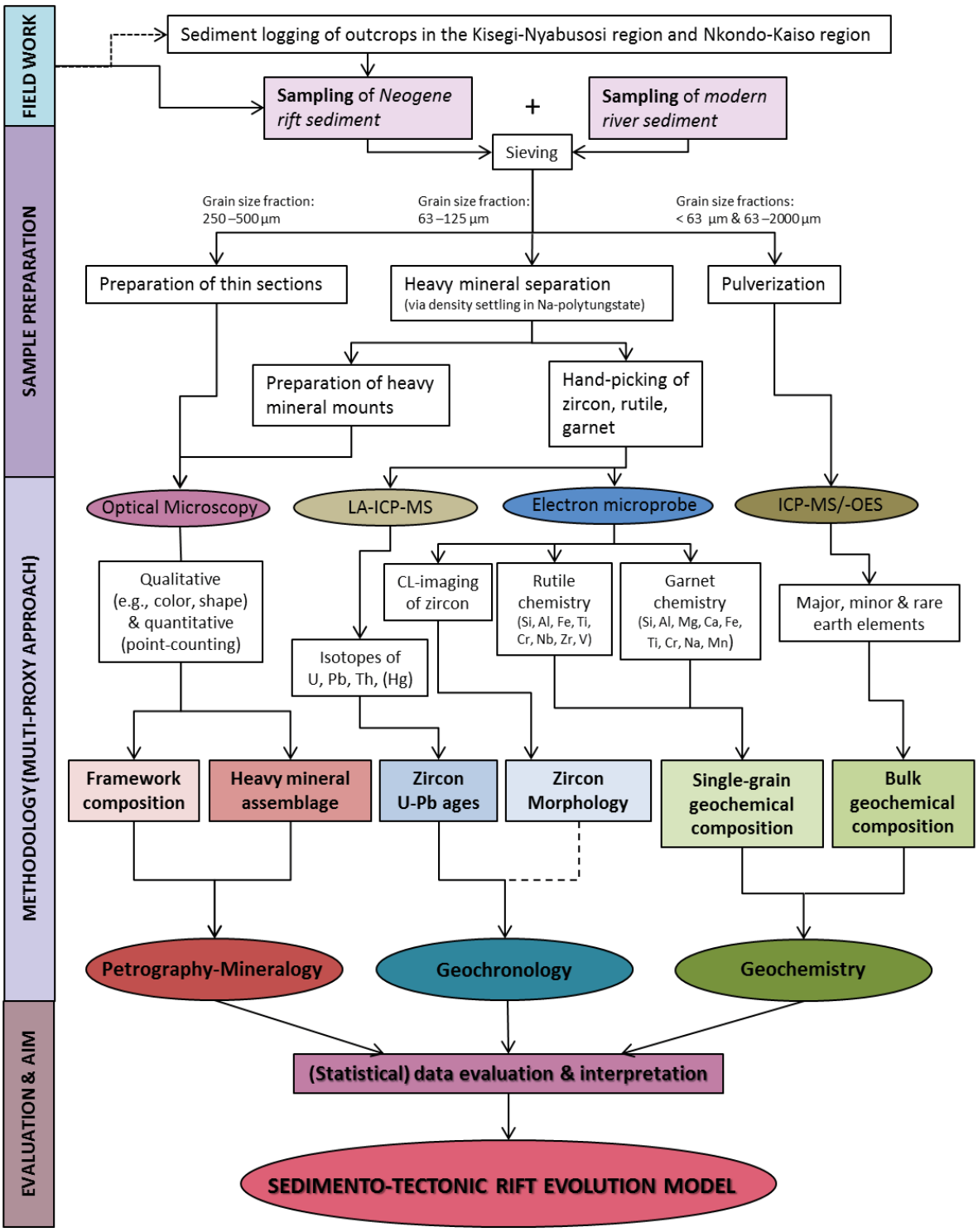

Figure 1-11. Schematized work flow of this thesis.

The general chemical formula of the garnet group is $X_3Y_2Si_3O_{12}$. Possible substitutions for X are Fe^{2+}, Ca^{2+}, Mg^{2+}, and Mn^{2+}, and the Y position can be occupied by either Al^{3+}, Fe^{3+}, and Cr^{3+}. The most common garnet species are almandine ($Fe_3Al_2Si_3O_{12}$), pyrope ($Mg_3Al_2Si_3O_{12}$), spessartine ($Mn_3Al_2Si_3O_{12}$), grossular ($Ca_3Al_2Si_3O_{12}$), andradite ($Ca_3(Fe,Ti)_2Si_3O_{12}$), and uvarovite ($Ca_3Cr_2Si_3O_{12}$). In nature, garnet with a chemical composition corresponding to any end-member is rare. They are usually a solid solution of these principal end-member compositions in highly diverse proportions (Deer et al. 1992). Garnet is characteristic for a wide range of metamorphic rocks, but may also originate from granites, pegmatites, acid volcanic rocks, skarns and mantle rocks (Mange and Maurer, 1992).

Rutile chemistry and thermometry

For many reasons rutile became an important indicator mineral in sedimentary provenance studies (summary in Meinhold, 2010). Rutile crystallizes in a wide range of rock suites (predominantly in greenschist- to granulite-facies metamorphic rocks) and, because of its chemical and mechanical stability during weathering, transport and burial diagenesis (e.g. Morton and Hallsworth, 1999), rutile is a common accessory mineral even in very mature clastic sediments and sedimentary rocks, in which many diagnostic, but unstable minerals, are already lost.

Rutile is the high temperature polymorph of TiO_2. It is not only a major source for titanium dioxide, but it also incorporates a large variety of trace elements, such as Al, Cr, Fe, Hf, Mo, Nb, Sb, Sn, Ta, Th, U, V, W, Zr, which substitute for Ti in the crystal lattice (e.g., Deer et al., 1992; Zack et al., 2002). Variations in trace elements are dependent on the composition of the source lithology and might therefore be used as fingerprint of chemical and physical conditions in the host rock during rutile formation. Previous studies on the application of detrital rutile geochemistry by, e.g., Zack et al. (2002), Zack et al. (2004a, b), Watson et al. (2006), Tomkins et al. (2007), Triebold et al. (2007, 2012), Meinhold et al. (2008) led to two principal conclusions: (1) the content of Nb and Cr allows to differentiate between the two main sources for rutile - metapelitic and metamafic rocks, and (2) the incorporation of zircon in the rutile lattice gives information about the maximum metamorphic temperatures during rutile crystallization, i.e., rutile serves as a geothermometer.

Cr-Nb chemistry of rutile

On the basis of Cr and Nb contents, the two major host lithologies for rutile, metamafic (e.g., mafic granulite, eclogite) and metapelitic (e.g., felsic granulite, paragneiss, mica-shist) rocks, can be distinguished (Zack et al., 2002; Zack et al., 2004b; Triebold et al., 2007, 2012; Meinhold et al., 2008). Zack et al. (2002) were the first to describe that the Ti/Cr and Ti/Nb ratio in the source rock is also mirrored by associated rutile. Based on their studies, metapelitic rocks contain high Nb, but low Cr contents, while, both, low Cr and low Nb values or low Nb, but high Cr concentrations, respectively, are characteristic for metamafic rocks. Discrimination fields using the minimum and maximum Nb and Cr values were introduced. In recent studies, several modifications of the discrimination line between the fields for metapelitic and metamafic rutile have been proposed (Triebold et al., 2007; Meinhold et al., 2008). The latest known refinement was presented by Triebold et al. (2012).

Zr-in-rutile thermometry

Zr-in-rutile thermometry bases on the assumption that the incorporation of zirconium (Zr) into rutile is temperature dependent (Zack et al., 2004b; Watson et al., 2006; Tomkins et al., 2007), with the requirement that zircon and quartz were coexisting phases during rutile formation (Zack et al., 2004b). The first to introduce rutile as a geothermometer were Zack et al. (2004b), who proposed a temperature calculation that bases on the empirical study of rutile from 31 natural metamorphic rock samples covering a wide range of temperature conditions. Further studies on Zr-in-rutile thermometry (Watson et al., 2006; Ferry and Watson, 2007; Tomkins et al., 2007) are based on experimental data. Watson et al. (2006) suggested that pressure conditions during metamorphosis play a key role on the Zr content of rutile, and Ferry and Watson (2007) emphasize the importance of SiO_2 activity. The latest refinement of the thermometer calculation was given by Tomkins et al. (2007), who introduced three equations that do not only take pressure, but also the polymorph type of coexisting quartz into account. However, when dealing with detrital rutile, pressure conditions during metamorphosis of the source rock are commonly unknown. Therefore, in studies lacking any information about pressure, a default setting (10 kbar, α-quartz) should be applied (Triebold et al., 2012).

Bulk rock geochemistry

Geochemical analyses of the whole rock composition serve as a tool to discriminate, classify and categorize rocks according to their major and trace element inventory. In contrast to other methods, e.g., petrographic investigations, whole rock geochemistry has the advantage that it can be applied to all grain sizes and that a large number of variables can be processed within a relatively short period of time (Weltje and von Eynatten, 2004). However, geochemical analyses do not distinguish between detrital and authigenic minerals, nor do they give any information about mineral parageneses or textures of grains, which might be relevant for the interpretation of the source rock/area. Nevertheless, when combined with other techniques, particularly optical observations, bulk rock geochemistry can give important insights into the evolution of sediments.

The main controlling factor on the geochemical composition of sediments is the geochemical character of the parental rock. Different lithologies and tectonic settings show systematic mineralogical and thus chemical compositional variations, e.g., some elements are sensitive indicators of either felsic (e.g., Th, U, Zr, Hf, Nb, Ta, Y) or mafic rocks (e.g., Ni, Co, Cr, V, Cu; Bhatia and Crook, 1986; Cullers, 2000; Lee, 2002). However, secondary processes, like weathering, diagenesis, sorting and metamorphism, can affect and modify the initial chemical signature. Chemical weathering results in selective mobilization and leaching of elements, leading to either a loss or enrichment of certain elements in the sediment. Especially, alkaline and alkaline-earth elements might be highly fractionated due to their mobility during weathering and diagenesis. Mobile elements with small ionic radii (Ca, Na, Sr) are selectively removed from the weathered system, while elements with large ionic radii, like Cs, Ba and Rb, are assumed to remain within the sediment as they are adsorbed to secondary (clay) minerals (Nesbitt et al., 1980). Fractionation of sedimentary grains by means of their size, shape, density, mechanic stability etc. leads to enrichment of certain elements in different grain size fractions. Coarser grain size classes are characterized by increased Si due to a higher content of quartz, whereas other major elements, such as Al, Mg and Fe remain more abundant in the mud fraction, because of their affiliation to clay minerals, phyllosilicates and oxyhydroxides (Garzanti et al., 2011). The highest concentration of trace elements and REE is present in clay minerals and heavy minerals and therefore depends on their distribution (Rollinson, 1993). Zr and Hf which are both highly associated with zircon are enriched in the finest tail of the sand mode, where ultradense zircon usually accumulates (Garzanti et al., 2011). After deposition, chemical modifications are mostly dependent on the pH value

and the redox potential of the depositional environment. Some element ratios, like Fe^{2+}/Fe^{3+}, V/Cr and Ni/Co can provide information about oxidative or reductive conditions (Mingram, 1995). Generally, elements, such as La, Ce, Nd, Y, Th, Zr, Hf, Nb, Ti and Sc are described to be most suitable for provenance reconstruction (Bathia and Crook, 1986), because they are relatively immobile within the sedimentary cycle and are directly transported into the sediment (McLennan et al., 1983). According to McLennan and Taylor (1991), the most reliable constituents are the REE, Th and Sc, because they are not influenced by any modification processes, whereas Zr, Hf and Ti are stronger influenced by heavy mineral fractionation.

Zircon U-Pb geochronology

In the last decades, rapid isotope geochronology by laser ablation inductively coupled plasma mass spectrometry (LA-ICP-MS) became one of the principle tools in unravelling the geological history of sediments and their source regions. This is because this method provides precise age determinations of large populations from a single sediment sample in a relatively short time period. High-U minerals that can be utilized for this method include zircon, monazite, apatite, xenotime, titanite, rutile, baddeleyite, allanite, and perovskite. Of all of these geochronometers, *in situ* U-Pb dating of zircon is, however, widely applied as the method of choice, likely due to its many advantages (Corfu et al., 2003). Zircon is present in a variety of lithologies, and is ubiquitous in sediments, because of its high resistance to physical and chemical weathering, and metamorphic processes. Due to its robustness against external factors, zircon crystals behave like timecapsules carrying the history of their proto-sources. Furthermore, zircon has a high closure temperature of approximately 900 °C (Pilot et al., 1998), presenting a valuable measure for the timing of magma crystallization. Thus, the age information obtained for a single grain can be linked to a certain crystallization event in the source area, i.e., the age directly reflects the age of a sediment's protosource. Besides provenance and palaeogeographic reconstructions, most common applications of geochronological methods are stratigraphic correlations, to assess the timing of magmatic and metamorphic events, and to infer the maximal age of sediment deposition (summarized in Gehrels, 2014). Sedimentary rocks usually contain several components from multiple crystallization cycles as result of (1) various magmatic cycles within the same locality, (2) the adjacent occurrence of rocks with different ages as consequence of tectonic processes, (3) the mixing of detritus from various localities during transport, and/or (4) the mixing of detritus from primary source(s) with older recycled sedimentary rocks (Thomas, 2011). Especially, the latter process provides a challenge in provenance studies, because zircon can be reworked during multiple sedimentary cycles due to its durability.

U-Th-Pb geochronology bases on the fact that multiple parent isotopes decay to different stable isotopes of Pb, each with a different half-life (Fig. 1-12). The element lead has four naturally occurring stable isotopes, ^{204}Pb, ^{206}Pb, ^{207}Pb, and ^{208}Pb, of which the latter three are produced through the independent radiogenic decay of ^{238}U, ^{235}U, and ^{232}Th, respectively. The isotopic decay does not lead directly to Pb, but traverses several alpha and beta decays during which a series of intermediate daughter isotopes are created before reaching the stable isotope of Pb.

The age of a zircon crystal is calculated by the ratio of the initial isotopes and their daughter products. For each of the three independent decay systems, an isochron equation is expressed:

$$\left(\frac{^{206}Pb}{^{204}Pb}\right) = \left(\frac{^{206}Pb}{^{204}Pb}\right)_0 + \left(\frac{^{238}U}{^{204}Pb}\right)\left(e^{\lambda_{238}t} - 1\right)$$

$$\left(\frac{^{207}Pb}{^{204}Pb}\right) = \left(\frac{^{207}Pb}{^{204}Pb}\right)_0 + \left(\frac{^{235}U}{^{204}Pb}\right)\left(e^{\lambda_{235}t} - 1\right)$$

$$\left(\frac{^{208}Pb}{^{204}Pb}\right) = \left(\frac{^{208}Pb}{^{204}Pb}\right)_0 + \left(\frac{^{232}Th}{^{204}Pb}\right)\left(e^{\lambda_{232}t} - 1\right)$$

Ideally, all three equations result in similar ages. In this case, the obtained age data are concordant, and data interpretation can be seen as reliable. In reality, however, the three independent decay systems usually show deviation between calculated ages, i.e., the obtained ages are discordant. Commonly, discordancy of zircon ages results from two main processes: (1) the impact of inheritance, i.e., complex zircon grains have several age domains due to multiple individual growth phases, and (2) disturbance of the U-Pb system after crystallization that leads to loss of the relatively mobile Pb when in contact with hydrothermal fluids (Gehrels, 2014). The decision whether to include or exclude discordant analyses for data interpretation is still controversially discussed between geochronologists and largely depends on the aim of the study (Gehrels, 2014).

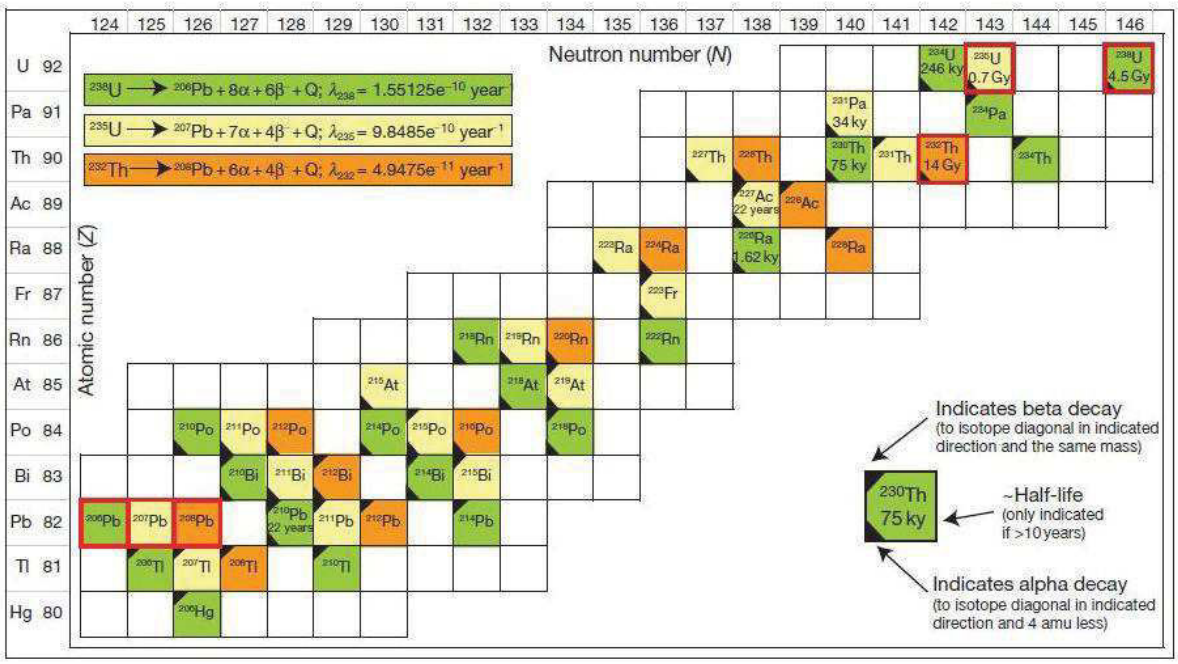

Figure 1-12. Radioactive decay chain of the U-Th-Pb system. Parent isotopes and stable daughter isotopes of Pb are outlined in red. α = alpha particle, β = beta particle, Q = energy released during the decay (after Schoene, 2013).

1.6 References

Abeinomugisha, D., Kasande, R., 2012. Tectonic control on hydrocarbon accumulation in the intracontinental Albertine Graben of the East African rift system, In: Gao, D. (Ed.), Tectonics and sedimentation: Implications for petroleum systems. AAPG Memoir, 100, pp. 209–228.

Acocella, V., Korme, T., 2002. Holocene extension direction along the main Ethiopian Rift, East Africa. Terra Nova, 14, 191–197.

Albaric, J., Déverchère, J., Petit, C., Perrot, J., Le Gall, B., 2009. Crustal rheology and depth distribution of earthquakes: Insights from the central and southern East African Rift System. Tectonophysics, 468, 28–41.

Amini, A., Anketell, J. M., 2015. Textural and geochemical studies of detrital Fe–Ti oxides and test of their validity in provenance determination, a case study from Central Iran. Journal of African Earth Sciences, 103, 140–152.

Andò, S., Garzanti, E., Padoan, M., Limonta, M., 2012. Corrosion of heavy minerals during weathering and diagenesis: a catalogue for optical analysis. In: von Eynatten, H., Critelli, S., Ingersoll, R. V., Weltje, G. J., (Eds.), Actualistic models of sediment generation. Sedimentary Geology, 280, pp. 165–178.

Aubrecht, R., Méres, Š., Sýkora, M., Mikus, T., 2009. Provenance of the detrital garnets and spinels from the Albian sediments of the Czorsztyn Unit (Pieniny Klippen Belt, Western Carpathians, Slovakia). Geologica Carpathica, 60, 463–483.

Bagley, B., Nyblade, A. A., 2013. Seismic anisotropy in eastern Africa, mantle flow, and the African superplume. Geophysical Research Letters, 40, 1500–1505.

Basu, A., Molinaroli, E., 1989. Provenance characteristics of detrital opaque Fe-Ti oxide minerals. Journal of Sedimentary Research, 59, 922–934.

Basu, A., Molinaroli, E., 1991. Reliability and application of detrital opaque Fe-Ti oxide minerals in provenance determination. Geological Society of London, Special Publications, 57, 55–65.

Bauer, F. U., Koehn, D., Glasmacher, U. A., 2010a. Long-term rift evolution. International Journal of Earth Sciences, 99, 1483–1485.

Bauer, F. U., Glasmacher U. A., Ring U., Schumann A., Nagudi B., 2010b. Thermal and exhumation history of the central Rwenzori Mountains, Western Rift of the East African Rift System, Uganda. International Journal of Earth Sciences, 99, 1575–1597.

Bauer, F. U., Glasmacher, U. A., Ring, U., Karl, M., Schumann, A., Nagudi, B., 2013. Tracing the exhumation history of the Rwenzori Mountains, Albertine Rift, Uganda, using low-temperature thermochronology. Tectonophysics, 599, 8–28.

Bauer, F. U., Glasmacher, U. A., Ring, U., Grobe, R. W., Mambo, V. S., Starz, M., 2016. Long-term cooling history of the Albertine Rift: new evidence from the western rift shoulder, DR Congo. International Journal of Earth Sciences, 105, 1707–1728.

Bellon, H., Pouclet, A., 1980, Datations K-Ar de quelques laves du Riftouest de l'Afrique Centrale: Implications sur l'évolution magmatique et structural. Geologische Rundschau, 69, 49–62.

Bhatia, M. R., Crook, K. A., 1986. Trace element characteristics of graywackes and tectonic setting discrimination of sedimentary basins. Contributions to mineralogy and petrology, 92, 181–193.

Bishop, W. W., 1965. Quaternary geology and geomorphology in the Albertine Rift Valley, Uganda. In: Wright Jr., H. E., Frey, D. G. (Eds.), International studies on the Quaternary, pp. 293–321.

Bishop, W. W., 1969. Pleistocene stratigraphy in Uganda. Geological survey of Uganda, Memoir, 10, Government Printer, Entebbe.

Bishop, W. W., Trendall, A. F., 1966. Erosion-surfaces, tectonics and volcanic activity in Uganda. Quarterly Journal of the Geological Society, 122, 385–420.

Blatt, H. 1979. Diagenetic processes in sandstones. SEPM Special Publication, 26, 141–157.

Boccaletti, M., Bonini, M., Mazzuoli, R., Abebe, B., Piccardi, L., Tortorici, L., 1998. Quaternary oblique extensional tectonics in the Ethiopian Rift (Horn of Africa). Tectonophysics, 287, 97–116.

Boenigk, W., 1983. Schwermineralanalyse. Ferdinand Enke Publishers, Stuttgart, 158 S., 77 Abb., 4 Tafeln, 8 Tab.

Bosworth, W., Strecker, M. R., Bliniuk, P. M., 1992. Integration of East African paleostress and present-day stress data: implications for continental stress field dynamics. Journal of Geophysical Research, 97, 11851–11865.

Calais, E., Ebinger, C., Hartnady, C., Nocquet, J. M., 2006. Kinematics of the East African Rift from GPS and earthquake slip vector data. In: Yirgu, G., Ebinger, C. J., Maguire, P. K. H. (Eds.),

Structure and evolution of the rifts systems within the Afar volcanic province, Northeast Africa. Geological Society of London, Special Publications, 259, pp. 9–22.

Campisano, C. J., Cohen, A. S., Arrowsmith, J. R., Asrat, A., Behrensmeyer, A. K., Brown, E. T., Deino, A. L., Deocampo, D. M., Feibel, C.S., Kingston, J. D., Lamb, H. F., Lowenstein, T. K., Noren, A., Olago, D. O., Owen, R. B., Pelletier, J. D., Potts, R., Reed, K. E., Renaut, R. W., Russell, J. M., Russell, J. L., Schäbitz, F., Stone, J. R., Trauth, M. H., Wynn, J. G., 2017. The Hominin Sites and Paleolakes Drilling Project: High-Resolution Paleoclimate Records from the East African Rift System and Their Implications for Understanding the Environmental Context of Hominin Evolution. PaleoAnthropology, 1–43.

Chorowicz, J., 2005. The East African rift system. Journal of African Earth Sciences 43, 379–410.

Chorowicz, J., Collet, B., Bonavia, F., Korme, T., 1994. NW to NNW extension direction in the Ethiopian Rift deduced from the orientation of tension fractures and fault slip analysis. Geological Society of America Bulletin, 105, 1560–1570.

Coppens, Y., 1999. Introduction. In: Bromage, T. G., Schrenk, F. (Eds.), African biogeography, climate change and human evolution. Oxford University Press, pp. 13–18.

Cooke, H. B. S., 1958. Observations relating to the Quaternary environments in East and Southern Africa. Transactions of the Geological Society of South Africa, 60, 1–74.

Corfu, F., Hanchar, J. M., Hoskin, P. W., Kinny, P., 2003. Atlas of zircon textures. Reviews in mineralogy and geochemistry, 53, 469–500.

Cullers, R. L., 2000. The geochemistry of shales, siltstones and sandstones of Pennsylvanian–Permian age, Colorado, USA: implications for provenance and metamorphic studies. Lithos, 51, 181–203.

Davies, K. A., 1951. The Uganda section of the western rift. Geological Magazine, 88, 377–385.

Deer, W. A., Howie, R. A., Zussman, J., 1992. An Introduction to the Rock-Forming Minerals (2nd edition). Longman, Harlow.

De Heinzelin, J., 1962. Les formations du Western Rift et de la cuvette congolaise. Annales du Musée Royal de L'afrique Centrale, 40, 219–243.

De Heinzelin, J., 1963. Palaeoecological conditions of the Lake Albert-Lake Edward Rift. In: Howell, F. C., Bourliere, F. (Eds.), African ecology and human evolution. Chicago, Chicago University Press, pp. 276–284.

Delvaux, D., Barth, A., 2010. African Stress Pattern from formal inversion of focal mechanism data. Implications for rifting dynamics. Tectonophysics 482, 105–128.

Delvaux, D., Levi, K., Kajara, R., Sarota, J., 1992. Cenozoic paleostress and kinematic evolution of the Rukwa–North Malawi rift valley (East African Rift System). Bulletin des Centres de Recherche Exploration-Production ElfAquitaine, 16, 383–406.

DeMenocal, P., 2004. African climate change and faunal evolution during the Pliocene-Pleistocene. Earth and Planetary Science Letters, 220, 3–24.

Denton, G. H., 1995. The problem of Pliocene paleoclimate and ice-sheet evolution in Antarctica. In: Paleoclimate and Evolution. Yale University Press, 213-229.

Dickinson, W. R., 1985. Interpreting provenance relations from detrital modes of sandstones. In: Zuffa, G.G. (Ed.), Provenance of arenites. Dordrecht, Reidel, NATO ASI Series 148, pp. 333–361, Springer Netherlands.

Dickinson, W. R., Suczek, C. A., 1979. Plate tectonics and sandstone compositions. AAPG Bulletin, 63, 2164–2182.

Doornkamp, J. C., 1968. The role of inselbergs in the geomorphology of Southern Uganda. Transactions of the Institute of British Geographers, 44, 151–162.

Dunkelman, T. J., Rosendahl, B. R., Karson, J. A., 1989. Structure and stratigraphy of the Turkana rift from seismic reflection data. Journal of African Earth Sciences (and the Middle East), 8, 489–510.

Ebinger, C. J., 1989. Tectonic development on the western branch of the East African rift system. Geological Society of America Bulletin, 101, 885–903.

Ebinger, C., 2005. Continental break-up: the East African perspective. Astronomy & Geophysics, 46, 2–16.

Ebinger, C. J., Yemane, T., Woldegabriel, G., Aronson, J. L., Walter, R. C., 1993. Late Eocene–Recent volcanism and faulting in the southern main Ethiopian rift. Journal of the Geological Society, 150, 99–108.

Ebinger, C., Furman, T., 2003. Geodynamical setting of the Virunga volcanic province, East Africa. Acta Vulcanologica, 15, 9–16.

Ferry, J. M., Watson, E. B., 2007. New thermodynamic models and revised calibrations for the Ti-in-zircon and Zr-in-rutile thermometers. Contributions to Mineralogy and Petrology, 154, 429–437.

Foster, A., Ebinger, C., Mbede, E., Rex, D., 1997. Tectonic development of the northern Tanzanian sector of the East African Rift System. Journal of the Geological Society, 154, 689–700.

Frostick, L. E., Renaut, R. W., Reid, I., Tiercelin, J. J. (Eds.), 1986. Sedimentation in the African rifts. Geological Society of London, Special Publication 25, Oxford, Blackwell Scientific.

Garzanti, E., 2016. From static to dynamic provenance analysis–Sedimentary petrology upgraded. Sedimentary Geology, 336, 3–13.

Garzanti, E., Andò, S., France-Lanord, C., Galy, V., Censi, P., Vignola, P., 2011. Mineralogical and chemical variability of fluvial sediments. 2. Suspended-load silt (Ganga-Brahmaputra, Bangladesh). Earth and Planetary Science Letters, 302, 107–120.

Garzanti, E., Padoan, M., Andò, S., Resentini, A., Vezzoli, G., Lustrino, M., 2013a. Weathering and relative durability of detrital minerals in equatorial climate: sand petrology and geochemistry in the East African Rift. The Journal of Geology, 121, 547–580.

Garzanti, E., Padoan, M., Peruta, L., Setti, M., Najman, Y.; Villa, I.M., 2013b. Weathering geochemistry and Sr-Nd fingerprints of equatorial upper Nile and Congo muds. Geochemistry, Geophysics, Geosystems, 14, 292–316.

Garzanti, E., Andò, S., Padoan, M., Vezzoli, G., El Kammar, A., 2015. The modern Nile sediment system: Processes and products. Quaternary Science Reviews, 130, 9–56.

Gasse, F., 2000. Hydrological changes in the African tropics since the Last Glacial Maximum. Quaternary Science Reviews, 19, 189–211.

Gasse, F., Chalié, F., Vincens, A., Williams, M. A., Williamson, D., 2008. Climatic patterns in equatorial and southern Africa from 30,000 to 10,000 years ago reconstructed from terrestrial and near-shore proxy data. Quaternary Science Reviews, 27, 2316–2340.

Gaupp, R., 1996. Diagenesis types and their application in diagenesis mapping. Zentralblatt für Geologie und Paläontologie, 11, 1183–1199.

Gautier, A., 1970. Fossil freshwater mollusca of the Lake Edward–Lake Albert Rift. Annual Reports of the Royal Museum of Central Africa, Tervuren, 67, 1–144.

Gawthorpe, R. L., Leeder, M. R., 2000. Tectono-sedimentary evolution of active extensional basins. Basin Research, 12, 195–218.

Gehrels, G., 2014. Detrital zircon U-Pb geochronology applied to tectonics. Annual Review of Earth and Planetary Sciences, 42, 127–149.

George, R., Rogers, N., Kelley, S., 1998. Earliest magmatism in Ethiopia: evidence for two mantle plumes in one flood basalt province. Geology, 26, 923–926.

Gummert, M., Lindenfeld, M., Wölbern, I., Rümpker, G., Celestin, K., Batte, A., 2016. Crustal structure and high-resolution Moho topography across the Rwenzori region (Albertine rift) from P-receiver functions. Geological Society of London, Special Publications, 420, 69–82.

Hecky, R. E., Kilham, P., 1973. Diatoms in alkaline, saline lakes: ecology and geochemical implications. Limnology and Oceanography, 18, 53–71.

Henry, D. J., Guidotti, C. V., 1985. Tourmaline as a petrogenetic indicator mineral- An example from the staurolite-grade metapelites of NW Maine. American mineralogist, 70, 1–15.

Hinderer, M., Pflanz, D., Schneider, S., 2013. Chemical denudation rates in the humid tropics of East Africa and comparison with ^{10}Be-derived erosion rates. Procedia Earth and Planetary Science, 7, 360–364.

Hofmann, C., Courtillot, V., Feraud, G., Rochette, P., Yirgu, G., Ketefo, E., Pik, R., 1997. Timing of the Ethiopian flood basalt event and implications for plume birth and global change. Nature, 389, 838–841.

Holmes, K. M., 2007. Using Pliocene palaeoclimatic data to postulate dispersal pathways of early hominins. Palaeogeography, Palaeoclimatology, Palaeoecology, 248, 96–108.

Hutchison, A. R., Oliver, G. J. H., 1998. Garnet provenance studies, juxtaposition of Laurentian marginal terranes and timing of the Grampian Orogeny in Scotland. Journal of the Geological Society, 155, 541–550.

Johnson, T. C., Odada, E. O. (Eds.), 1996. The Limnology, Climatology and Paleoclimatology of the East African Lakes. Gordon and Breach Publishing, Amsterdam, 664 pp.

Johnson, T. C., Kelts, K., Odada, E., 2000. The holocene history of Lake Victoria. AMBIO: A Journal of the Human Environment, 29, 2–11.

Johnsson, M. J., 1993. The system controlling the composition of clastic sediments. In: Johnsson, M. J., Basu, A. (Eds.), Processes controlling the composition of clastic sediments. Geological Society of America Special Papers, 284, pp. 1–19.

Johnsson, M. J., Meade, R. H., 1990. Chemical weathering of fluvial sediments during alluvial storage: the Macuapanim Island point bar, Solimões River, Brasil. Journal of Sedimentary Petrology, 60, 827–842.

Kampunzu, A. B., Lubala, R. T., 1991. Magmatic evolution and petrogenesis in the East African rift system. In: Kampunzu, A. B., Lubala, R. T. (Eds.), Magmatism in Extensional Structural Settings. Springer-Verlag, Berlin, pp. 131–135.

Kampunzu, A. B., Bonhomme, M. G., Kanika, M., 1998. Geochronology of volcanic rocks and evolution of the Cenozoic Western Branch of the East African Rift System. Journal of African Earth Sciences, 26, 441–461.

Karp, T., Scholz, C. A., McGlue, M. M., 2012. Structure and stratigraphy of the Lake Albert Rift, East Africa: Observations from seismic reflection and gravity data. In: Baganz, O. W., Bartov, Y., Bohacs, K., and Nummendal (Eds.), Lacustrine Sandstone Reservoirs and Hydrocarbon Systems, AAPB Memoir, 95, pp. 299–318.

Katz, B. J., 1990. Lacustrine basin exploration–Case Studies and Modern Analogs. American Association of Petroleum Geologists Memoir, 50, 340 pp.

Kaufmann, G., Hinderer, M., Romanov, D., 2016. Shaping the Rwenzoris: balancing uplift, erosion, and glaciation. International Journal of Earth Sciences, 105, 1761–1778.

Koehn, D., Aanyu, K., Haines, S., Sachau, T., 2008. Rift nucleation, rift propagation and the creation of basement micro-plates within active rifts. Tectonophysics, 458, 105–116.

Koehn, D., Lindenfeld, M., Rümpker, G., Aanyu, K., Haines, S., Passchier, C. W., Sachau, T., 2010. Active transsection faults in rift transfer zones: evidence for complex stress fields and implications for crustal fragmentation processes in the western branch of the East African Rift. International Journal of Earth Sciences, 99, 1633–1642.

Krawinkel, H., Wozazek, S., Krawinkel, J., Hellmann, W., 1999. Heavy-mineral analysis and clinopyroxene geochemistry applied to provenance analysis of lithic sandstones from the Azuero–Soná Complex (NW Panama). Sedimentary Geology, 124, 149–168.

Lambiase, J. J., 1995. Hydrocarbon Habitat in Rift Basins. Geological Society Special Publication, 80, 370 pp.

Lambiase, J. J., Morley, C. K., 1999. Hydrocarbons in rift basins: the role of stratigraphy. Philosophical Transactions of the Royal Society of London A: Mathematical, Physical and Engineering Sciences, 357, 877–900.

Leakey, R. E. F., 1973. Evidence for an advanced plio-pleistocene hominid from East Rudolf, Kenya. Nature, 242, 447–450.

Lee, Y. I., 2002. Provenance derived from the geochemistry of late Paleozoic–early Mesozoic mudrocks of the Pyeongan Supergroup, Korea. Sedimentary Geology, 149, 219–235.

Lepersonne, J., 1949. Le fossé tectonique Lac Albert–Semliki–Lac Edouard. Annales de la Société Géologique de Belgique, 62, 1–92.

Lepersonne, J., 1970. Revision of the fauna and the stratigraphy of the fossiliferous localities of the Lake Albert-Lake Edward rift (Congo). Annalen-Koninklijk Museum voor Midden-Afrika. Geologische wetenschappen, 67, 171–207.

Lindenfeld, M., Rümpker, G., Link, K., Koehn, D., Batte, A., 2012. Fluid-triggered earthquake swarms in the Rwenzori region, East African Rift - Evidence for rift initiation. Tectonophysics, 566, 95–104.

Link, K., Koehn, D., Barth, M. G., Tiberindwa, J. V., Barifaijo, E., Aanyu, K., Foley, S. F., 2010. Continuous cratonic crust between the Congo and Tanzania blocks in western Uganda. International Journal of Earth Sciences, 99, 1559–1573.

Logan, P., Curd, S., Downie, B., Weston, J., Shaw, D., 2009. Exploration on the frontier: towards an understanding of the Albert Basin. American Association of Petroleum Geologists, Search & Discovery Article, 10192.

Logatchev, N. A., Beloussov, V. V., Milanovsky, E. E., 1972. East African rift development. Tectonophysics, 15, 71–81.

Lukaye, J. M., 2009. Biostratigraphy and Palynofacies of Four Exploration Wells from the Albertine Graben, Uganda. American Association of Petroleum Geologists, Search & Discovery Article, 50169.

Lukaye, J., Worsley, D., Kiconco, L., Nabbanja, P., Abeinomugisha, D., Amusugut, C., Njabire, N., Nuwagaba, R., Mugisha, F., Ddungu, T., Sserubiri, T., Sserubiri, T., 2016. Developing a Coherent Stratigraphic Scheme of the Albertine Graben-East, Africa. Journal of Earth Science and Engineering, 6, 264–294.

Macgregor, D., 2015. History of the development of the East African Rift System: a series of interpreted maps through time. Journal of African Earth Sciences, 101, 232–252.

Macheyeki, A. S., Delvaux, D., De Batist, M., Mruma, A., 2008. Fault kinematics and tectonic stress in the seismically active Manyara–Dodoma Rift segment in Central Tanzania–Implications for the East African Rift. Journal of African Earth Sciences, 51, 163–188.

Mange, M. A., Maurer, H. F. W., 1992. Heavy minerals in colour. Chapman and Hall, London.

Mange, M. A., Morton, A. C., 2007. Geochemistry of heavy minerals. In: Mange, M. A., Wright, D. T. (Eds.), Heavy Minerals in Use. Developments in Sedimentology, 58. Elsevier, Amsterdam, pp. 345–391.

Maslin, M. A., Christensen, B., 2007. Tectonics, orbital forcing, global climate change, and human evolution in Africa: introduction to the African paleoclimate special volume. Journal of human evolution, 53, 443–464.

Maslin, M. A., Trauth, M. H., 2009. Plio-Pleistocene East African pulsed climate variability and its influence on early human evolution. In: Grine, F. E., Fleagle, J. G., Leakey, R. E. (Eds.), The First Humans–Origin and Early Evolution of the Genus Homo, Springer Netherlands, pp. 151–158.

Maslin, M. A., Brierley, C. M., Milner, A. M., Shultz, S., Trauth, M. H., Wilson, K. E., 2014. East African climate pulses and early human evolution. Quaternary Science Reviews, 101, 1–17.

Maslin, M. A., Shultz, S., Trauth, M. H., 2015. A synthesis of the theories and concepts of early human evolution. Philosophical Transactions of the Royal Society B., 370, 20140064.

Mathisen, M. E., Vondra, C. F., 1983. Provenance of the Plio-Pleistocene sediments in the east Turkana basin, northern Kenya. Palaeogeography, palaeoclimatology, palaeoecology, 44, 141–168.

McBride, E. F., 1963. A classification of common sandstones. Journal of Sedimentary Research, 33, 664–669.

McLennan, S. M., Taylor, S. R., 1991. Sedimentary rocks and crustal evolution: tectonic setting and secular trends. The Journal of Geology, 99, 1–21.

McLennan, S. M., Taylor, S. R., Eriksson, K. A., 1983. Geochemistry of Archean shales from the Pilbara Supergroup, western Australia. Geochimica et Cosmochimica Acta, 47, 1211–1222.

Meinhold, G., 2010. Rutile and its applications in earth sciences. Earth-Science Reviews, 102, 1–28.

Meinhold, G., Anders, B., Kostopoulos, D., Reischmann, T., 2008. Rutile chemistry and thermometry as provenance indicator: an example from Chios Island, Greece. Sedimentary Geology, 203, 98–111.

Mingram, B., 1995. Geochemische Signaturen der Metasedimente des erzgebirgischen Krustenstapels, Scientific Technical Report STR 9604, GFZ Potsdam.

Morley, C.K., 1988. Variable extension in lake Tanganyika. Tectonics, 7, 785–801.

Morley, C. K., 1995. Developments in the structural geology of rifts over the last decade and their impact on hydrocarbon exploration. Geological Society of London, Special Publications, 80, 1–32.

Morley, C. K., 1999. Geoscience of rift systems-evolution of East Africa. American Association of Petroleum Geologists Studies in Geology, 44, 242 pp.

Morley, C. K., 2002. Tectonic settings of continental extensional provinces and their impact on sedimentation and hydrocarbon prospectivity. In: Renault, R. W., Ashley, G. M. (Eds.), Sedimentation in continental rifts, SEPM Special Publication, 73, pp. 25–55.

Morley, C. K., Vanhauwaert, P., De Batist, M., 2000. Evidence for high-frequency cyclic fault activity from high-resolution seismic reflection survey, Rukwa Rift, Tanzania. Journal of the Geological Society, 157, 983–994.

Morton, A. C., 1984. Stability of detrital heavy tertiary sandstones from sea basin. Clay minerals, 19, 287–308.

Morton, A. C., 1985. Heavy minerals in provenance studies. In: Zuffa, G. G. (Ed.), Provenance of arenites. Dordrecht, Reidel, NATO ASI Ser. 148, pp. 249–277.

Morton, A. C., 1987. Influences of provenance and diagenesis on detrital garnet suites in the Paleocene Forties Sandstone, central North Sea. Journal of Sedimentary Research, 57, 1027–1032.

Morton, A. C., Hallsworth, C. R., 1994. Identifying provenance-specific features of detrital heavy mineral assemblages in sandstones. Sedimentary Geology, 90, 241–256.

Morton, A. C., Hallsworth, C. R., 1999. Processes controlling the composition of heavy mineral assemblages in sandstones. Sedimentary Geology, 124, 3–29.

Morton, A. C., Hallsworth, C., 2007. Stability of detrital heavy minerals during burial diagenesis. Developments in Sedimentology, 58, 215–245.

Morton, A. C., Whitham, A. G., Fanning, C. M., 2005. Provenance of Late Cretaceous to Paleocene submarine fan sandstones in the Norwegian Sea: integration of heavy mineral, mineral chemical and zircon age data. Sedimentary Geology, 182, 3–28.

Moucha, R., Forte, A. M., 2011. Changes in African topography driven by mantle convection. Nature Geoscience, 4, 707–712.

Mtelela, C., Roberts, E. M., Downie, R., Hendrix, M. S., 2016. Interplay of Structural, Climatic, and Volcanic Controls on Late Quaternary Lacustrine–Deltaic Sedimentation Patterns In the Western Branch of the East African Rift System, Rukwa Rift Basin, Tanzania. Journal of Sedimentary Research, 86, 1179–1207.

Nesbitt, H. W., Markowics, G., Price, R. C., 1980. Chemical processes affecting alkalis and alkaline earths during continental weathering. Geochimica et Cosmochimica Acta, 44, 1659–1666.

Nesbitt, H. W., Fedo, C. M., Young, G. M., 1997. Quartz and feldspar stability, steady and non-steady-state weathering, and petrogenesis of siliciclastic sands and muds. Journal of Geology, 105, 173–191.

Nusbaum, R. L., Girdler, R. W., Heirtzler, J. R., Hutt, D. J., Green, D., Millings, V. E., Schmoll, B. S., Shapiro, J., 1993. The distribution of earthquakes and volcanoes along the East African rift system. Episodes, 16, 427–432.

Nyblade, A. A., Brazier, R. A., 2002. Precambrian lithospheric controls on the development of the East African rift system. Geology, 30, 755–758.

Olsen, P. E., 1986. A 40-million-year lake record of early Mesozoic orbital climatic forcing. Science, 234, 842–848.

Osmaston, H. A., 1989. Glaciers, glaciations and equilibrium line altitude on the Rwenzori. In: Mahaney, W. C. (Ed.), Quaternary and Environmental Research on East African Mountains. Balkema, Rotterdam/Brookfield, pp. 31–104.

Oxburgh, E. R., Turcotte, D. L., 1974. Membrane tectonics and the East African rift. Earth and Planetary Science Letters, 22, 133–140.

Pickford, M., 1986. Sedimentation and fossil preservation in the Nyanza Rift system, Kenya. Geological Society of London, Special Publications, 25, 345–362.

Pickford, M., Senut, B., Hadoto, D., 1993. Geology and Palaeobiology of the Albertine Rift Valley, Uganda-Zaire. Vol. I: Geology. International Centre for Training and Exchanges in Geosciences, Occasional Publications, 24, 1–190.

Pik, R., 2011. Geodynamics: east Africa on the rise. Nature Geoscience, 4, 660–661.

Pik, R., Marty, B., Hilton, D. R., 2006. How many mantle plumes in Africa? The geochemical point of view. Chemical Geology, 226, 100–114.

Pilot, J., Werner, C. D., Haubrich, F., Baumann, N., 1998. Palaeozoic and proterozoic zircons from the Mid-Atlantic ridge. Nature, 393, 676–679.

Pinto, L., Hérail, G., Moine, B., Fontan, F., Charrier, R., Dupré, B., 2004. Using geochemistry to establish the igneous provenances of the Neogene continental sedimentary rocks in the Central Depression and Altiplano, Central Andes. Sedimentary Geology, 166, 157–183.

Pouclet, A., 1975, Histoire des grands lacs de l'Afrique centrale: Mise au point des connaissances actuelles. Revues Géographie Physique Géologie Dynamique, 17, 475–482.

Rasmussen, C., Reichenbacher, B., Lenz, O., Altner, M., Penk, S. B., Prieto, J., Brüsch, D., 2015. Middle–late Miocene palaeoenvironments, palynological data and a fossil fish Lagerstätte from the Central Kenya Rift (East Africa). Geological Magazine, 154, 24–56.

Renault, R. W., Ashley, G. M., 2002. Sedimentation in continental rifts. SEPM Special Publication, 73, 329 pp.

Richardson, J. L., Dussinger, R. A., 1986. Paleolimnology of mid-elevation lakes in the Kenya Rift Valley. Hydrobiologia, 143, 167–174.

Ring, U., 1994. The influence of preexisting structure on the evolution of the Cenozoic Malawi rift (East African rift system). Tectonics, 13, 313–326.

Ring, U., 2008. Extreme uplift of the Rwenzori Mountains in the East African Rift, Uganda: Structural framework and possible role of glaciations. Tectonics, 27, 1–19.

Ring, U., 2014. The East African Rift System. Australian Journal of Earth Sciences, 107, 132–146.

Ring, U., Betzler, C., 1995. Geology of the Malawi Rift: kinematic and tectonosedimentary background to the Chiwondo Beds, northern Malawi. Journal of Human Evolution, 28, 7–21.

Ring, U., Betzler, C., Delvaux, D., 1992. Normal vs. strike-slip faulting during rift development in East Africa: the Malawi rift. Geology, 20, 1015–1018.

Robbins, E. I., 1983. Accumulation of fossil fuels and metallic minerals in active and ancient rift lakes. Tectonophysics, 94, 633–658.

Roberts, E. M., Stevens, N. J., O'connor, P. M., Dirks, P. H. G. M., Gottfried, M. D., Clyde, W. C., Clyde, R. A., Armstrong, A. I. S, Hemming, S., 2012. Initiation of the western branch of the East African Rift coeval with the eastern branch. Nature Geoscience, 5, 289–294.

Rogers, N. W., 2006. Basaltic magmatism and the geodynamics of the East African Rift System. Geological Society of London, Special Publications, 259, 77–93.

Roller, S., Hornung, J., Hinderer, M., Ssemmanda, I., 2010. Middle Miocene to Pleistocene sedimentary record of rift evolution in the southern Albertine Graben (Uganda). International Journal of Earth Sciences, 99, 1643–1661.

Roller, S., Wittmann, H., Kastowski, M., Hinderer, M., 2012. Erosion of the Rwenzori Mountains, East African Rift, from in situ-produced cosmogenic ^{10}Be. Journal of Geophysical Research: Earth Surface, 117, F03003, 20 p.

Rollinson, H. R., 1993. Using Geochemical Data: Evaluation, Presentation, Interpretation. Longman Scientific & Technical, Essex, UK, 352 pp.

Rosendahl, B. R., 1988. Seismic atlas of Lake Tanganyika. East Africa: PROBE project: Durham, North Carolina, Duke University.

Rosendahl, B. R., Kilembe, E., Kaczmarick, K., 1992. Comparison of the Tanganyika, Malawi, Rukwa and Turkana Rift zones from analyses of seismic reflection data. Tectonophysics, 213, 235–256.

Rümpker, G., Mertz, D. (Eds.), 2016: With contributions to: The Albertine rift (East Africa): mantle-crust interaction, surface processes, and impact on climate. International Journal of Earth Sciences, 105, Springer.

Sachau, T., Koehn, D., Passchier, C., 2013. Mountain-building under extension. American Journal of Science, 313, 326–344.

Sachau, T., Koehn, D., Stamps, D. S., Lindenfeld, M., 2016. Fault kinematics and stress fields in the Rwenzori Mountains, Uganda. International Journal of Earth Sciences, 105, 1729–1740.

Saria, E., Calais, E., Stamps, D. S., Delvaux, D., Hartnady, C. J. H., 2014. Present-day kinematics of the East African Rift. Journal of Geophysical Research: Solid Earth, 119, 3584–3600.

Schlüter, T., 2008. Geological Atlas of Africa, 2nd edition, Springer Verlag, Berlin, 307 pp.

Schoene B. 2013. U-Th-Pb geochronology. In: Rudnick, R. L. (Ed.), The Crust. Treatise on Geochemistry, 2nd ed., 4, pp. 341–378, Amsterdam, Elsevier.

Scholz, C. A., Rosendahl, B. R., Versfelt, J. W., Kaczmarick, K. J., Woods, L. D., 1989. Seismic atlas of Lake Malawi (Nyasa). East Africa: PROBE project: Durham, North Carolina, Duke University.

Scholz, C. A., Johnson, T. C., Cohen, A. S., King, J. W., Peck, J. A., Overpeck, J. T., Talbot, M. R., Brown, E. T., Kalindekafe, L., Amoako, P. Y., Lyons, R. P., Shanahan, T. M., Castañeda, I. S., Heil, C. W., Forman, S. L., McHargue, L. R., Beuning, K. R., Gomez, J., and Pierson, J. 2007. East African megadroughts between 135 and 75 thousand years ago and bearing on early-modern human origins. Proceedings of the National Academy of Sciences USA, 104, 16416–16421.

Scholz, C. A., Cohen, A. S., Johnson, T. C., King, J., Talbot, M. R., and Brown, E. T. 2011. Scientific drilling in the Great Rift Valley: the 2005 Lake Malawi Scientific Drilling Project — An overview of the past 145,000 years of climate variability in Southern Hemisphere East Africa. Palaeogeography, Palaeoclimatology, Palaeoecology, 303, 3–19.

Senut, B., Pickford, M., 1994. Geology and Palaeobiology of the Albertine Rift Valley, Uganda-Zaire. Vol. I: Palaeobiology. International Centre for Training and Exchanges in Geosciences, Occasional Publications, 29, 1–423.

Senut, B., Pickford; M., Ssemmanda, L., Elupu, D., Obwona, P., 1987. Découverte du premier Homininae (Homo sp.) dans le Pléistocene de Nyabusosi (Ouganda Occidental). Comptes rendus de l'Académie des Sciences, Paris, 305, 819–822.

Sepulchre, P., Ramstein, G., Fluteau, F., Schuster, M., Tiercelin, J. J., Brunet, M., 2006. Tectonic uplift and Eastern Africa aridification. Science, 313, 1419–1423.

Shaw, D., Logan, P. C., Weston, J., 2009. A Palynological Study of Neogene and Holocene Sediments from Lake Albert, Uganda, with Implications for vegetation and climatic changes in East Africa, American Association of Petroleum Geologists, Search and Discovery Article #50180. <http://www. searchanddiscovery.com/documents/2009/50180shaw/index.htm>.

Simon, B. 2015. Rift du Lac Albert, Ouganda, Rift Est Africain : Déformation, érosion, sédimentation et bilan de matière depuis 17 Ma, Université de Rennes 1, Rennes, 403 pp.

Solomon, J. D., 1939. The Pleistocene succession in Uganda. In: O'Brien, T. P. (Ed.). The Prehistory of Uganda Protectorate, Cambridge, Cambridge University Press, pp. 15–50.

Spiegel, C., Kohn, B. P., Belton, D. X., Gleadow, A. J., 2007. Morphotectonic evolution of the central Kenya rift flanks: Implications for late Cenozoic environmental change in East Africa. Geology, 35, 427–430.

Stamps, D. S., Calais, E., Saria, E., Hartnady, C., Nocquet, J. M., Ebinger, C. J., Fernandes, R. M., 2008. A kinematic model for the East African Rift. Geophysical Research Letters, 35, L05304, doi:10.1029/2007GL032781.

Stamps, D. S., Flesch, L. M., Calais, E., 2010. Lithospheric buoyancy forces in Africa from a thin sheet approach. International Journal of Earth Sciences, 99, 1525–1533.

Stollhofen, H., Stanistreet, I. G., McHenry, L. J., Mollel, G. F., Blumenschine, R. J., Masao, F. T., 2008. Fingerprinting facies of the Tuff IF marker, with implications for early hominin palaeoecology, Olduvai Gorge, Tanzania. Palaeogeography, Palaeoclimatology, Palaeoecology, 259, 382–409.

Taylor, R. G., Howard, K. W. F., 1998. Post-paleozoic evolution of weathered landsurfaces in Uganda by tectonically controlled deep weathering and stripping. Geomorphology, 25, 173–192.

Taylor, R. G., Howard, K. W. F., 1999. The influence of tectonic setting on the hydrological characteristics of deeply weathered terrains: evidence from Uganda. Journal of Hydrology, 218, 44–71.

Thomas, W. A., 2011. Detrital-zircon geochronology and sedimentary provenance. Lithosphere, 3, 304–308.

Tiercelin, J.-J., Chorowicz, J., Bellon, H., Richert, J. P., Mwanbene, J. T., Walgenwitz, F., 1988. East African Rift System: offset, age and tectonic significance of the Tanganyika–Rukwa–Malawi intracontinental transcurrent fault zone. Tectonophysics, 148, 241–252.

Tiercelin, J. J., Soreghan, M., Cohen, A. S., Lezzar, K. E., Bouroullec, J. L., 1992. Sedimentation in large rift lakes: example from the Middle Pleistocene—Modern deposits of the Tanganyika Trough, East African Rift System. Bull. Bulletin du Centre de recherches Elf Exploration Production Elf Aquitaine, 16, 83–111.

Tomkins, H. S., Powell, R., Ellis, D. J., 2007. The pressure dependence of the zirconium-inrutile thermometer. Journal of Metamorphic Geology, 25, 703–713.

Trauth, M. H., Deino, A. L., Bergner, A. G., Strecker, M. R., 2003. East African climate change and orbital forcing during the last 175 kyr BP. Earth and Planetary Science Letters, 206, 297–313.

Trauth, M. H., Maslin, M. A., Deino, A., Strecker, M. R., 2005. Late cenozoic moisture history of East Africa. Science, 309, 2051–2053.

Trauth, M. H., Maslin, M. A., Deino, A. L., Strecker, M. R., Bergner, A. G., Dühnforth, M., 2007. High-and low-latitude forcing of Plio-Pleistocene East African climate and human evolution. Journal of Human Evolution, 53, 475–486.

Trevena, A. S., Nash, W. P., 1981. An electron microprobe study of detrital feldspar. Journal of Sedimentary Research, 51, 137–150.

Triebold, S., von Eynatten, H., Luvizotto, G. L., Zack, T., 2007. Deducing source rock lithology from detrital rutile geochemistry: an example from the Erzgebirge, Germany. Chemical Geology, 244, 421–436.

Triebold, S., von Eynatten, H., Zack, T., 2012. A recipe for the use of rutile in sedimentary provenance analysis. Sedimentary Geology, 282, 268–275.

Van Damme, D., Pickford, M., 1995. The late Cenozoic Ampullariidae (Mollusca, Gastropoda) of the Albertine Rift Valley (Uganda-Zaire). Hydrobiologia, 316, 1–32.

Van Damme, D., Pickford, M., 1998. The late Cenozoic Viviparidae (Mollusca, Gastropoda) of the Albertine Rift Valley (Uganda—Congo). Hydrobiologia, 390, 171–217.

Van Damme, D., Pickford, M., 2003. The late Cenozoic Thiaridae (Mollusca, Gastropoda, Cerithioidea) of the Albertine Rift Valley (Uganda-Congo) and their bearing on the origin and evolution of the Tanganyikan thalassoid malacofauna. Hydrobiologia, 498, 1–83.

Van Loon, A. J., Mange, A. M. 2007. “In situ” dissolution of heavy minerals through extreme weathering, and the application of the surviving assemblages and their dissolution characteristics to correlation of Dutch and German silver sands. In: Mange, M. A., and Wright, D. T. (Eds.), Heavy minerals in use. Amsterdam, Elsevier, Developments in Sedimentology Series, 58, pp. 189–213.

Velbel, M. A., 2007. Surface textures and dissolution processes of heavy minerals in the sedimentary cycle: examples from pyroxenes and amphiboles. Developments in Sedimentology, 58, 113–150.

Verschuren, D., Laird, K. R., Cumming, B. F., 2000. Rainfall and drought in equatorial east Africa during the past 1,100 years. Nature, 403, 410–414.

Versfelt, J., Rosendahl, B. R., 1989. Relationships between pre-rift structure and rift architecture in Lakes Tanganyika and Malawi, East Africa. Nature, 337, 354–355.

Von Eynatten, H., Gaupp, R., 1999. Provenance of Cretaceous synorogenic sandstones in the Eastern Alps: constraints from framework petrography, heavy mineral analysis and mineral chemistry. Sedimentary Geology, 124, 81–111.

Wallner, H., Schmeling, H., 2010. Rift induced delamination of mantle lithosphere and crustal uplift: a new mechanism for explaining Rwenzori Mountains' extreme elevation?. International Journal of Earth Sciences, 99, 1511–1524.

Watson, E. B., Wark, D. A., Thomas, J. B., 2006. Crystallization thermometers for zircon and rutile. Contributions to Mineralogy and Petrology, 151, 413–433.

Wayland, E. J., 1926. The Geology and Palaeontology of the Kaiso Bone-beds. Geological Survey of Uganda, 2, 1–70.

Wayland, E. J., 1929. Rift valleys and Lake Victoria. Compte Rendu, XVth Session, International Geological Congress (Pretoria), 11, 323–353.

Weltje, G. J., von Eynatten, H., 2004. Quantitative provenance analysis of sediments: review and outlook. Sedimentary Geology, 171, 1–11.

Westerhof, A. B. P., Härmä, P., Isabirye, E., Katto, E., Koistinen, T., Kuosmanen, E., Lehto, T., Lehtonen, M. I., Mäkitie, H., Manninen, T., Mänttäri, I., Pekkala, Y., Pokki, J., Saalmann, K., Virransalo, P., 2014. Geology and Geodynamic Development of Uganda with Explanation of the 1:1,000,000-Scale Geological Map. Geological Survey of Finland, Special Paper, 55, 387 pp., 329 figures, 29 tables and 2 appendices.

White, R. S, Spence, G. D., Fowler, S. R., McKenzie, D. P., Westbrook, G. K., Bowen, A. N., 1987. Magmatism at a rifted continental Margin. Nature, 330, 439–444.

Wichura, H., Bousquet, R., Oberhänsli, R., Strecker, M. R., Trauth, M. H., 2011. The Mid-Miocene East African Plateau: a pre-rift topographic model inferred from the emplacement of the phonolitic Yatta lava flow, Kenya. Geological Society of London, Special Publications, 357, 285–300.

Wölbern, I., Rümpker, G., Schumann, A., Muwanga, A., 2010. Crustal thinning beneath the Rwenzori region, Albertine rift, Uganda, from receiver-function analysis. International Journal of Earth Sciences, 99, 1545–1557.

Wölbern, I., Rümpker, G., Link, K., Sodoudi, F., 2012. Melt infiltration of the lower lithosphere beneath the Tanzania craton and the Albertine rift inferred from S receiver functions. Geochemistry, Geophysics, Geosystems (G3), 13, Q0AK08.

Worden, R. H., Burley, S. D., 2003. Sandstone diagenesis: the evolution of sand to stone. Sandstone Diagenesis: Recent and Ancient, 4, 3–44.

Yasui, K., Kunimatsu, Y., Kuga, N., Bajope, B., Ishida, H., 1992. Fossil mammals from the Neogene strata in the Sinda Basin, Eastern Zaire. African Study Monographs Supplementary Issue, 17, 87–107.

Zack, T., Kronz, A., Foley, S. F., Rivers, T., 2002. Trace element abundances in rutiles from eclogites and associated garnet mica schists. Chemical Geology, 184, 97–122.

Zack, T., Von Eynatten, H., Kronz, A. 2004a. Rutile geochemistry and its potential use in quantitative provenance studies. Sedimentary Geology, 171, 37–58.

Zack, T., Moraes, R., Kronz, A., 2004b. Temperature dependence of Zr in rutile: empirical calibration of a rutile thermometer. Contributions to Mineralogy and Petrology, 148, 471–488.

Chapter 2

2 Petrography and Geochemistry of Modern River Sediments in an Equatorial Environment (Rwenzori Mountains and Albertine Rift, Uganda) – Implications for Weathering and Provenance

Sandra Schneider[1], Jens Hornung[1], Matthias Hinderer[1], Eduardo Garzanti[2]

[1] Institute of Applied Geosciences, TU Darmstadt, Schnittspahnstrasse 9, D-64287 Darmstadt

[2] Laboratory for Provenance Studies, Department of Earth and Environmental Sciences, Università di Milano-Bicocca, 20126 Milano, Italy

2.1 Abstract

In hot-humid equatorial climate chemical weathering may be so strong that provenance signatures may be largely lost and even detritus derived from crystalline basement rocks reduced to quartzose sand. We tested this hypothesis in western Uganda, where stable plateau areas contrast with the active tectonic setting of the Albertine Rift (western branch of the East African Rift System, EARS), culminating in the strongly exhumed fault block of the > 5000 m high Rwenzori Mountains. In this setting, sediments derived from similar types of basement rocks including gneiss, schist, amphibolite, metasediment and granite can be traced from rapidly eroding high-altitude areas to low-altitude areas undergoing prolonged weathering. Sand and mud carried by 51 rivers overall in these two contrasting landscapes were sampled to study how and to what extent detrital modes are modified by the selective loss of unstable detrital minerals.

Sediments generated in the high-relief Rwenzori Mountains show abundant feldspar (up to 32%) and rock fragments (up to 52%), which together with low SiO_2/Al_2O_3 ratio and composition close to the Upper Continental Crust (UCC standard) reflect erosion in weathering-limited conditions. In the central Rwenzori Mountains, low Th/Sc and Zr/Sc ratios, weak negative Eu anomaly, lower La_N/Yb_N values, and heavy-mineral assemblages with hornblende and epidote reflect the lithology of source rocks in the Buganda-Toro-Greenstone Belt. In contrast, sediments produced on the low-relief plateau have quartz content up to 98% and higher SiO_2/Al_2O_3 ratio. Systematic loss of mobile elements is indicated by high chemical weathering indices CIA, PIA and WIP. However, provenance from metamorphic basement rocks is still indicated by heavy-mineral assemblages dominated by epidote and amphibole, whereas provenance from granitic rocks is revealed by high Th/Sc and Zr/Sc ratio, negative Eu anomaly and higher La_N/Yb_N values. We conclude that first-cycle sediments generated in high-relief areas preserve the original imprint of parent lithologies even in very humid equatorial climate. In low-relief areas, although weathering processes have proceeded over millions of years turning basement-derived detritus into an almost pure quartzose resistate, provenance signals are not erased entirely, and can be still retrieved from the residual heavy-mineral suite and relative abundance of high-field-strength trace elements.

2.2 Introduction

The mineralogical and geochemical composition of clastic sediments is a complex function of its source-rock lithology, topography/relief, climatic conditions in the source area and hydraulic processes in the depositional environment (Weltje and von Eynatten, 2004). In order to obtain

information on the provenance of clastic sediments and to fully reconstruct their history univocally, it is necessary to quantify the contribution of each single controlling factor that influences sediment composition on the way from the source to the depositional basin.

Many authors maintain that chemical weathering exerts a major control on sediment composition (Johnsson and Meade, 1990; Liu et al., 2007; van Loon and Mange, 2007). Extreme chemical alteration of rocks takes place in equatorial regions, because intensified bacterial degradation of organic material leads to acidic soil water that promotes leaching not only of unstable constituents (e.g., ferromagnesian minerals), but even of the most resistant minerals, such as tourmaline, zircon or quartz (Stallard, 1985; Morton and Hallsworth, 1999; White and Brantley, 2003; van Loon and Mange, 2007). Because of prolonged weathering over geological time, sands generated from feldspar-bearing basement rocks are enriched in quartz in hot-humid climates (Suttner et al., 1981; Nesbitt and Young, 1982; Basu, 1985; Johnsson et al., 1988; Nesbitt et al., 1996, 1997; Fedo et al., 1997; van de Kamp, 2010; Garzanti et al., 2013a). Furthermore, weathering intensity is influenced by the composition of the parent rock assemblage, because silicate minerals have different stabilities on the Earth's surface and weather incongruently. Relief determines erosion rates and transport capacity and consequently the time during which a rock is exposed to alteration (Johnsson et al., 1988, Taylor and Howard, 1999b; Dixon et al., 2009a).

The Albertine Rift in the western branch of the East African Rift System (EARS) provides an excellent natural laboratory to study the diverse processes that influence sediment composition, and specifically the contrasting effects of weathering and topographic relief. In the vicinity of the Equator, the climate is generally warm and humid, with seasonal monsoonal rainfall. Besides extreme weathering conditions, the Albertine Rift also represents a tectonically active rift setting, where thermal-induced rift-flank uplift results in contrasting topography between low-relief rift plateaus and adjacent high-altitude horsts such as the Rwenzori massif (Ebinger, 1989; Chorowicz, 2005). Exposed basement rocks include Archean and Proterozoic cratonic crust punctuated locally by small rift-related volcanic fields. Soils are mainly yellowish to reddish ferrallitic sandy (clay) loams (Uganda. Soils, 1967). The removal of mobile alkali and alkaline-earth metals from crystalline bedrock occurs in situ, with different weathering intensity below and above the water table (Taylor and Howard, 1999a). In this active rift setting sediments derived from various bedrock types including metamorphic, plutonic, volcanic and metasedimentary units can be studied.

Even though the EARS provides an excellent place to study processes that control modern sand composition in a humid subequatorial setting, only a few articles have dealt with sediment composition so far (Andò et al., 2012; Garzanti et al., 2013a, b; Garzanti et al., 2015a). Recent studies by Garzanti et al. (2013a, b) give a geochemical and petrographic overview on modern river muds and sands along the western branch of the EARS. In comparison to our study, sampling sites cover a large area which spreads from Tanzania to Sudan. Furthermore, Andò et al. (2012) provide an optical catalogue of corrosion features studied on mineral grains of modern equatorial sands. This article complements these larger-scale studies by a detailed case study of the equatorial part of the western branch of the EARS. Most sampled river sites are new, but some replicate samples are also considered for cross checking data and results.

In the present study, petrographic and heavy-mineral analyses have been combined with the analysis of major and trace chemical elements. Our principal aim is to quantify the effects of chemical weathering on the composition of sediments that derive from a variety of basement rocks in areas characterized by different climate and relief, and to ascertain whether the initial lithological signatures are preserved in clastic sediments even under extreme climatic conditions.

2.3 Study area

The Cenozoic East African Rift System, one of the most prominent tectonic features on Earth, ruptures the African continent over 4000 km, from the Afar region in Ethiopia to the Okavango Delta in Botswana (Ebinger and Scholz, 2012). It is characterized by a series of mainly N-S trending individual tectonic basins that host most of the Great Lakes of Africa (with exception of Lake Victoria). The EARS can be divided into an eastern (Gregory) and western branch, which differ by their uplift rate, volcanic activity, depth of rift basins, and gradient of surrounding fault scarps (Chorowicz, 2005). Both rift arms formed in the Neogene and follow Proterozoic mobile belts that wrap around the mechanically stronger Archean Tanzanian Craton (Albaric et al., 2009).

Our study area is located on the Ugandan side of the 500 km long Albertine Rift, that forms the northernmost part of the western branch of the EARS and is referred to as the part of the rift that stretches from the Virunga volcanic province in the south to the border between Uganda and South Sudan in the north. Initiated in the middle Miocene, rifting processes led to the formation of a series of asymmetrical rift basins bordered along both sides by steep faulted escarpments that rise up thousands of meters adjacent to the rift floor (Koehn et al., 2010). Today the formerly isolated rift segments are mainly linked to each other and occupied by the three lakes Albert, Edward and George, joined by the Semliki River. A special case of basement uplift is represented by the Rwenzori Mountains, a horst block of Paleoproterozoic crustal rocks located at the intersection of graben segments which reaches an altitude of 5109 m a.s.l. (Bauer et al., 2010), and is thus the highest non-volcanic mountain range in Africa.

2.3.1 Climate, relief and vegetation

In the equatorial part of the western branch of the EARS climate is warm and humid. On the low relief rift plateau the median daily air temperatures vary between 17 and 26 °C, depending on elevation and landscape, but are relatively constant throughout the year. The average rainfall of ~1500 mm/year is distributed over two rainy seasons with two peaks in March-May and September-November related to the migration of the Intertropical Convergence Zone (ITCZ). Vegetation is mainly dominated by tropical rainforest together with woodland or wooded savannah. Basement rocks on the plateau are typically highly weathered, indicating prolonged pedogenic processes leading to the formation of widespread, reddish-brown lateritic ferralsols several meters-thick. The plateau in western Uganda corresponds to the so-called African surface held to have formed in the Late Cretaceous (Burke and Gunnell, 2008) and partly dissected during Neogene rifting to form inselbergs and a duricrust-capped plateau (Taylor and Howard, 1998).

In contrast to the plateau, the > 5000 m high Rwenzori Mountains are characterized by a rugged relief. The mountains are cloud covered over more than 300 days per year, and experience a precipitation and moisture rate among the highest on Earth. Depending on altitude, annual rainfall varies from 2000−3000 mm and occurs throughout the year (Osmaston, 1989). Rainfall is heaviest on the eastern side of the mountains, where strong winds prevail (Eggermont et al., 2009). Daily temperatures vary between -5 and 20 °C. Freezing occurs during night time at altitudes > 3000 m a. s. l. Vegetation ranges from tropical rainforest to alpine meadows and becomes scarce close to the mountain tops, which are glaciated and capped by snow all around the year (Osmaston, 1989).

2.3.2 Regional geology

The crystalline basement of Uganda comprises three principal suites of rocks, including the Archean Gneiss-Granulite Complex, Paleoproterozoic mobile belts and rift-related Neogene magmatic

provinces. The basement rocks are covered locally by syn-rift sediments and alluvial deposits (Fig. 2-1).

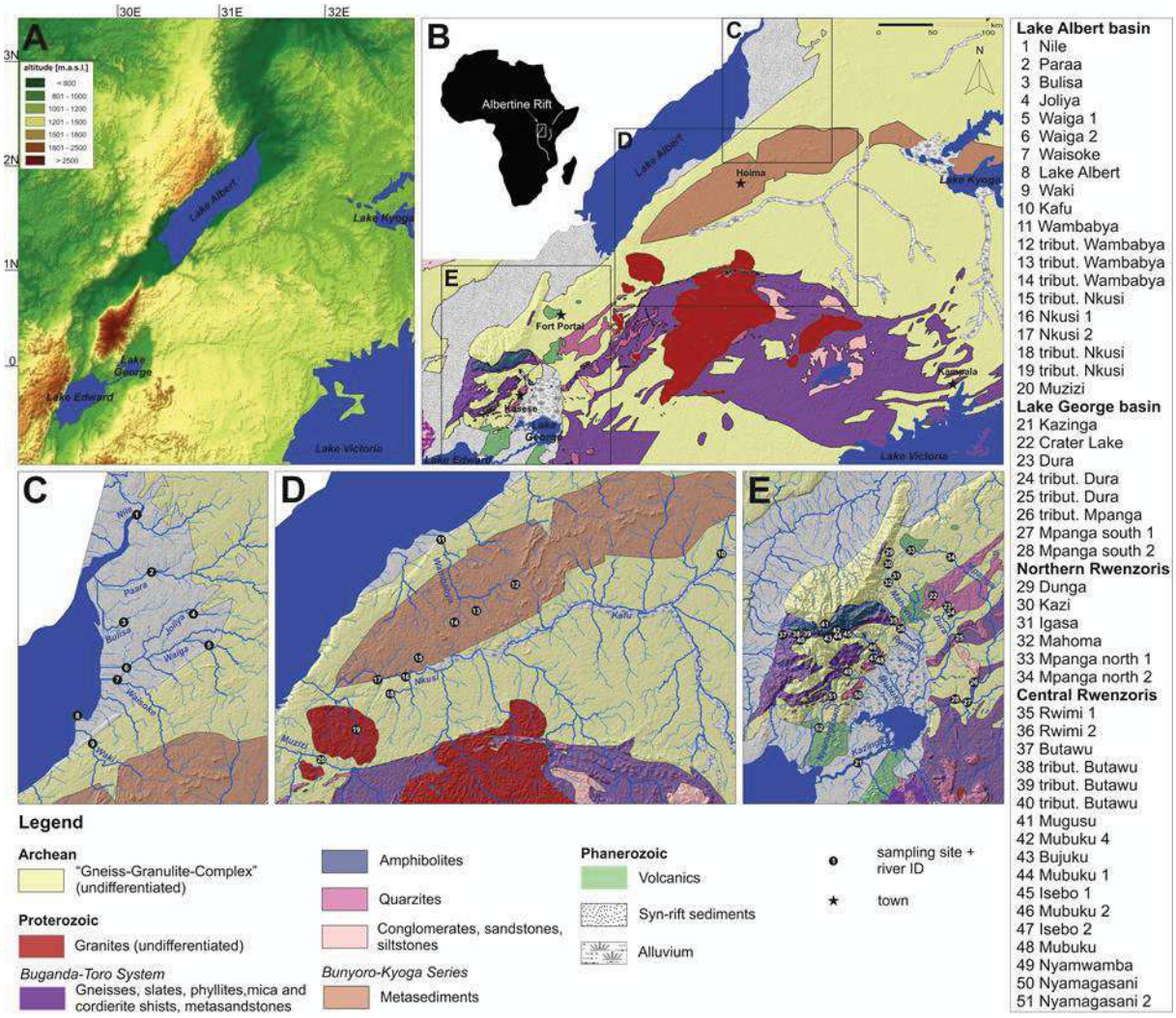

Figure 2-1. Study area. A: Topographic relief in western Uganda, B: Geology of western Uganda (modified after Schlüter, 2008). C, D and E: Sampling sites of modern river sediments.

Archean basement

The oldest exposures in the study area are high-grade metamorphic rocks of the Archean Gneiss-Granulite Complex, also termed the 'Ugandan Basement Complex' (MacDonald, 1966). It occupies ca. 60% of rocks exposed in Uganda (Schlüter, 2008) and is supposed to represent the eastern end of the Congo Craton as well as the northern continuation of the Tanzania Craton (Leggo, 1974). According to lithology, age of structural overprint and P-T conditions during metamorphic events, four gneissic units ('Watian', 'Aruan', 'Nyanzian', 'undifferentiated') have been distinguished by Hepworth and MacDonald (1966). Exposed in the central part of Uganda are undifferentiated, mainly granitoid gneisses yielding U-Pb zircon ages of 2637–2584 Ma (Link et al., 2010), corresponding to those of Neoarchean Aruan and Watian units (Taylor and Howard, 1998).

Proterozoic basement

Paleoproterozoic rocks of the Buganda-Toro System (or Rwenzori Fold Belt) occupy large parts of southwestern Uganda, where they overlie the northern continuation of the Tanzania Craton (Gabert, 1990). The mobile belt, stretching from the northern shores of Lake Victoria to the Rwenzori horst, is composed of low- to medium-grade gneiss, amphibolite, quarzite, slate, phyllite and cordierite schist. In the central part of Uganda, these rocks are intruded by Paleoproterozoic granites. All granitic bodies were believed to be broadly coeval (MacDonald, 1966), but U-Pb zircon ages of 1615 ± 19 Ma were subsequently obtained for the Singo granite (Nagudi et al., 2001), whereas controversial Rb-Sr biotite ages around 1800 Ma were suggested for the Mubende granite (in Nagudi et al., 2003). In a belt parallel to the eastern shore of Lake Albert and along the northern side of Lake Kyoga, low-grade Neoproterozoic slate and metasandstone supposed to overlie a basal tillite are exposed (Bunyoro-Kyoga Group; Schlüter, 2008).

Phanerozoic rocks

In western Uganda, rift-related Neogene volcanic and sedimentary rocks occur, as well as recent alluvial deposits. Several Quaternary volcanic fields bordered by the Rwenzori horst to the west (e.g., Fort Portal) are characterized by strongly silica-undersaturated lavas including kamafugites and carbonatites (Barker and Nixon, 1989; Foley et al., 2012). Since the middle Miocene, rifting processes caused uplift of rift flanks and initiated erosion and sedimentation in the graben, where up to 4 km thick fluvio-lacustrine sediments accumulated (Pickford et al., 1993; Roller et al., 2010). The record mainly comprises unconsolidated siliciclastic sediments deposited in fluvio-deltaic to lacustrine settings. Sediments are poorly lithified, and include frequent intercalations of highly ferruginous (‘iron crusts’) or calcareous paleosols, and several tephra layers (Pickford et al., 1991).

2.3.3 Hydrology

Before the mid-Pleistocene, the hydrological system of Uganda was dominated by westward directed river basins that drained the Ugandan hinterland towards the Albertine Graben and further west to the Congo Basin (de Heinzelin, 1962; Bishop, 1965; Taylor and Howard, 1999b). Thermally induced uplift of continental crust caused disruption of this surface drainage, including the major catchments of the paleo-Kagera, paleo-Kafu and paleo-Katonga rivers, by the so-called ‘axis of upwarping’ located 13–32 km east of the western rift (Doornkamp, 1968). Reversed flow directions and downwarping of the country east of the axis led to the creation of Lake Kyoga and Lake Victoria by either flooding of former headwaters or pooling of waters (Doornkamp, 1968; Ollier, 1990; Taylor and Howard, 1999b). As a result of increased gradients and flow reversal, several valleys were deepened below their former stream levels (Doornkamp, 1968); the Nkusi and Mpanga Rivers draining the rift flanks towards Lake Albert and Lake George formed deeply incised narrow valleys cutting into the basement. In contrast, river discharge along the western side of the ‘uplift axis’ was strongly reduced.

Streams draining the eastern flank of the Rwenzori Mountains (e.g., Bujuku, Mubuku, Mahoma and Nyamwamba) represent a significant source for the water supply of western Uganda. Rwenzori rivers, initially steep and flowing rapidly, get flatter and slower as they reach the lowland plains and swamps within the graben (Eggermont et al., 2009). Because of higher precipitation and frequent recharge by rainfall and melting of mountain glaciers, they show higher runoffs than rivers on the rift plateau (Eggermont et al., 2009; Taylor et al., 2009).

2.4 Sampling and methods

2.4.1 Sampling and sample grouping

To characterize the modern drainage system in the Albertine Rift, a total of 67 sediment samples (39 sands and 28 muds) from 51 rivers were collected from the Rwenzori mountain area and the rift flanks, along with one sediment sample each from Lake Albert and Crater Lake (Fig. 2-1; Table A2-1, Appendix). Seventeen of these samples have been analyzed by Garzanti et al. (2013a). Sediments were collected from the active bed of major rivers, as well as from lower-order tributaries. Sampling sites were chosen to be representative of every bedrock lithology exposed into the four 'tectonic provinces' identified (Lake Albert basin, Lake George basin, Northern Rwenzoris and Central Rwenzoris) and of different climatic and topographic conditions (e.g., high relief Rwenzori vs. low relief rift plateau).

Lake Albert basin (LAB; 20 samples; low relief). This province comprises the northern and eastern sides of Lake Albert, including the Victoria Nile, Paara, Bulisa, Joliya, Waiga, Waisoke, Waki, Kafu, Wambabya, Nkusi and Muzizi Rivers. Samples represent either low-grade metasediments of the Bunyoro-Kyoga Group, undifferentiated Archean basement gneiss, granitic intrusions ('Singo granite') or recycled sediments of the Albertine Graben.

Lake George basin (LGB; 8 samples; low relief). Rivers of southern Uganda, including the Kazinga, Dura and lower section of the Mpanga, mainly drain metamorphic basement of the Buganda-Toro system. The Crater Lake sample receives some input also from Miocene ultramafic volcanic rocks, and samples collected in the Kazinga Channel additionally receive detritus from the Archean Gneiss-Granulite Complex and recycled from syn-rift sediments of the George Basin.

Northern Rwenzoris (NR; 6 samples; high relief). This province includes the northern tip of the Rwenzori Mountains near Fort Portal, where sediments originate from undifferentiated gneiss of the Archean basement complex with minor influence of Miocene volcanic rocks. Major rivers are the Dunga, Kazi, Igasa, Mahoma and northern section of the Mpanga.

Central Rwenzoris (CR; 17 samples; high relief). Basement rocks exposed in this province comprise Archean gneiss and medium- to high-grade metamorphic rocks of the Buganda-Toro belt, including amphibolite. Samples were taken from the Rwimi, Butawu, Mugusu, Mubuku, Bujuku, Isebo, Nyamwamba, Nyamagasani and smaller streams.

2.4.2 Framework petrography

A total of 42 samples (27 low-relief, 15 high-relief), separated into several grain-size fractions by dry sieving were analyzed. The 250–500 μm class was chosen for petrographic investigations to avoid grain size effects (Johnsson et al., 1988). Grains were embedded in epoxy resin and cut into standard thin sections. At least 300 grains were counted in each section using an automatic point-counter. In contrast to the Gazzi-Dickinson method (Ingersoll et al., 1984; Zuffa, 1985), all polymineralic grains were counted as rock fragments. Modal analyses for 17 additional samples were carried out on the 250–1000 μm class according to the Gazzi-Dickinson method (Garzanti et al. 2013a).

2.4.3 Heavy minerals

For heavy-mineral analysis (40 samples; 25 low-relief, 15 high-relief), the grain size class 63–125 μm (Morton, 1985) was chosen in this study. The wider size-window 63–250 μm was preferred in the analysis of 14 additional samples by Garzanti et al. (2013a). Heavy minerals were separated via density settling using sodium polytungstate (ρ = 2.855 g/cm^3) and grain mounts were impregnated

with epoxy resin (n = 1.54). In each separate, preferentially 200–250 non-opaque and non-micaceous grains (Mange and Maurer, 1992) were counted using an automatic point counter.

2.4.4 Major and trace element geochemistry

Thirty samples were analysed. To remove organic material, the sediments were first washed and then dissolved in hydrogen peroxide (H_2O_2). The organic-free samples were split by wet sieving into mud (< 63 μm) and sand fractions (0.063–2 mm), and analyzed for their major and trace element concentrations at the laboratories Actlabs (Canada; mud fraction) and ALS minerals (Spain; sand fraction). Nine samples from Garzanti et al. (2013a) were analyzed at Acme Laboratories (Canada). Major elements and a few trace elements were quantified using ICP-OES/-AES, whereas the majority of minor elements was determined by ICP-MS. Prior to analysis, the samples were treated with three different digestions: a lithium metaborate/tetraborate fusion for the resistate elements (Si, Al, Fe, Ti, Ca, Na, K, Mn, P, Mg, Ba, Ce, Cr, Cs, Ga, Ge, Nb, Rb, REE, Sn, Sr, Ta, Th, U, V, W, Y, Zr), an acid solution for the base metals (Ag, Ca, Co, Cu, Li, Mo, Ni, Pb, Sc, Zn), and aqua regia for As, Bi, Hg, In, Re, Sb, Se, Te and Tl. Table A2-2 (Appendix) gives a summary of the analyzed elements, detection limit of each element, and adopted method. For more detailed information concerning the analytical procedures visit www.actlabs.com and www.alsglobal.com.

For the evaluation and interpretation of the geochemical dataset, element concentrations were normalized to the Upper Continental Crust (UCC; Rudnick and Gao, 2003). REE are discussed with reference to CI Carbonaceous Chondrites (McDonough and Sun, 1995) as well as to Post-Archean Australian Shale (PAAS; Nance and Taylor, 1976). Diverse chemical weathering indices have been calculated to assess the degree of (paleo-)weathering of sediments and sedimentary rocks (e.g., WIP of Parker, 1970; CIA of Nesbitt and Young, 1982; CIW of Harnois, 1988; PIA of Fedo et al., 1995; CIX of Garzanti et al., 2014a, 2014b). Formulas for the CIA, PIA and WIP are:

$$CIA = [Al_2O_3) / (Al_2O_3 + CaO^* + Na_2O + K_2O] \bullet 100 \quad [1]$$

$$WIP = [(Ca) / 0.7) + (2\ Na / 0.35\ ) + (2\ K / 0.25) + (Mg / 0.9)] \bullet 100 \quad [2]$$

$$PIA = [(Al_2O_3 - K_2O)/(Al_2O_3 + CaO^* + Na_2O - K_2O)] \bullet 100 \quad [3]$$

* CaO in silicate-bearing minerals only

No correction for CaO incorporated in carbonates and phosphates was done, because such phases were never observed in the samples analyzed. Whereas the CIA and PIA are calculated by using molecular proportions of Al, Na, Ca, Mg and K, Parker (1970) used the ratio of cations, because these are the constituents dissolved during the alteration process. With increasing weathering intensity, the values of the CIA and PIA increase, whereas the WIP decreases. Al-rich phyllosilicates have high CIA values (kaolinite and chlorite ~100, illite and smectite ~80 and muscovite ~75), unweathered feldspars values of ~50, and biotite, hornblende and pyroxene of 50–55, 10–30, and 0–10, respectively (Nesbitt and Young, 1982).

Weathering intensities may be quantified also by comparing the concentration of each mobile element in the sediment sample and in the UCC. To avoid effects of generalized element depletion (e.g., caused by quartz dilution), and to prevent uncertainties caused by the determination of the UCC standard and by the variability of bedrock lithologies in the source areas, each mobile element needs to be normalized to an immobile element (e.g., Al, Ti, Nd, Sm, Th; Gaillardet et al., 1999). However, Ti, Nd, Sm, and Th chosen as references are preferentially hosted in ultradense minerals that can be

markedly concentrated locally by hydraulic processes, causing very strong bias. Much more reliable and consistent results are obtained by choosing non-mobile Al as normalizing factor for all elements (Garzanti et al., 2013a, 2013b). For each mobile element (*E*) we thus calculated normalized values as:

$$\alpha^{Al}_{E} = (Al/E)_{sample}/(Al/E)_{UCC} \quad [4]$$

Furthermore, Principal Component Analysis (PCA) was performed using: 1) framework petrographic composition, and 2) the values of weathering-sensitive major and trace elements K, Na, Ca, Rb, Sr, Ba as well as immobile Al and Si (Belov and Belova, 1979). Calculation was performed using the free software package PAST – PAlaeontological Statistics (Hammer et al., 2001). In order to treat the data set systematically, all variables were normalized by dividing their standard deviations with the correlation matrix function (normalized var-covar) and transformed into centered log-ratio coordinates (Aitchison and Egozcue, 2005). Data points were illustrated in a scatter plot (biplot) showing the first two principal components.

The tectonic setting of sediments has been inferred by two discriminant function-based major element diagrams introduced by Verma and Armstrong-Altrin (2013) and recently tested by Armstrong-Altrin (2015), which distinguish between sediments from three main tectonic settings: island or continental arc, continental rift, and collision. Two diagrams for the tectonic discrimination of high-silica [$(SiO_2)_{adj}$ = 63%–95%] and low-silica rocks [$(SiO_2)_{adj}$ = 35%–63%] were proposed. The discriminant function equations for high-silica clastic sediments are:

$$DF1_{(Arc\text{-}Rift\text{-}Col)m1} = (-0.263 \times In(TiO_2/SiO_2)_{adj}) + (0.604 \times In(Al_2O_3/SiO_2)_{adj}) + (-1.725 \times In(Fe_2O_{3t}/SiO_2)_{adj}) + (0.660 \times In(MnO/SiO_2)_{adj}) + (2.191 \times In(MgO/SiO_2)_{adj}) + (0.144 \times In(CaO/SiO_2)_{adj}) + (-1.304 \times In(Na_2O/SiO_2)_{adj}) + (0.054 \times In(K_2O/SiO_2)_{adj}) + (-0.330 \times In(P_2O_5/SiO_2)_{adj}) + 1.588. \quad [5]$$

$$DF2_{(Arc\text{-}Rift\text{-}Col)m1} = (-1.196 \times In(TiO_2/SiO_2)_{adj}) + (1.604 \times In(Al_2O_3/SiO_2)_{adj}) + (0.303 \times In(Fe_2O_{3t}/SiO_2)_{adj}) + (0.436 \times In(MnO/SiO_2)_{adj}) + (0.838 \times In(MgO/SiO_2)_{adj}) + (-0.407 \times In(CaO/SiO_2)_{adj}) + (1.021 \times In(Na2O/SiO_2)_{adj}) + (-1.706 \times In(K2O/SiO_2)_{adj}) + (-0.126 \times In(P_2O_5/SiO_2)_{adj}) - 1.068. \quad [6]$$

Discriminant function equations for low-silica clastic sediments are:

$$DF1_{(Arc\text{-}Rift\text{-}Col)m2} = (0.608 \times In(TiO_2/SiO_2)_{adj}) + (-1.854 \times In(Al_2O_3/SiO_2)_{adj}) + (0.299 \times In(Fe_2O_{3t}/SiO_2)_{adj}) + (-0.550 \times In(MnO/SiO_2)adj) + (0.120 \times In(MgO/SiO_2)_{adj}) + (0.194 \times In(CaO/SiO_2)_{adj}) + (-1.510 \times In(Na_2O/SiO_2)_{adj}) + (1.941 \times In(K_2O/SiO_2)_{adj}) + (0.003 \times In(P_2O_5/SiO_2)_{adj}) - 0.294. \quad [7]$$

$$DF2_{(Arc\text{-}Rift\text{-}Col)m2} = (-0.554 \times In(TiO_2/SiO_2)_{adj}) + (-0.995 \times In\ (Al_2O_3/SiO_2)_{adj}) + (1.765 \times In(Fe_2O_{3t}/SiO_2)_{adj}) + (-1.391 \times In(MnO/SiO_2)_{adj}) + (-1.034 \times In(MgO/SiO_2)_{adj}) + (0.225 \times In(CaO/SiO_2)_{adj}) + (0.713 \times In(Na_2O/SiO_2)_{adj}) + (0.330 \times In(K_2O/SiO_2)_{adj}) + (0.637 \times In(P_2O_5/SiO_2)_{adj}) - 3.631. \quad [8]$$

2.5 Results

2.5.1 Lake Albert Basin (LAB)

The sands consist of rounded to angular quartz grains, with up to 98% quartz and low feldspar (1–19%) and rock fragments (0–18%; Fig. 2-2A; Table A2-3, Appendix). Plagioclase is rare. Rock fragments include low-rank metapsammite, gneiss and some granitoid grains in the Waiga, Joliya and Nkusi Rivers. Lateritic fragments are widespread, reaching 36% in rivers draining the metasedimentary Bunyoro-Kyoga Group (Fig. 2-3A). These fragments exhibit Fe-oxide groundmass frequently with layered texture (Fig. 2-3A1–A3), inclusions of detrital quartz and clay minerals, and occasionally idiomorphic quartz crystals with straight extinction filling small intragranular pore spaces. Abraded overgrowths around quartz grains may be present, indicating recycling of older sandstones (Fig. 2-3A). Quartz grains commonly show etch pits, indicating dissolution in soils (Crook, 1968; Cleary and Conolly, 1971). Heavy-mineral assemblages include amphibole (mainly green hornblende), epidote, zircon, rutile, tourmaline, Ti-oxides, garnet, kyanite, sillimanite, apatite and titanite (Table A2-4, Appendix; Fig. 2-4). Rivers draining low-grade metasediments or rift sediments are rich in chemically more durable zircon, rutile and tourmaline. Sands collected at the Lake Albert shoreline include pyroxene.

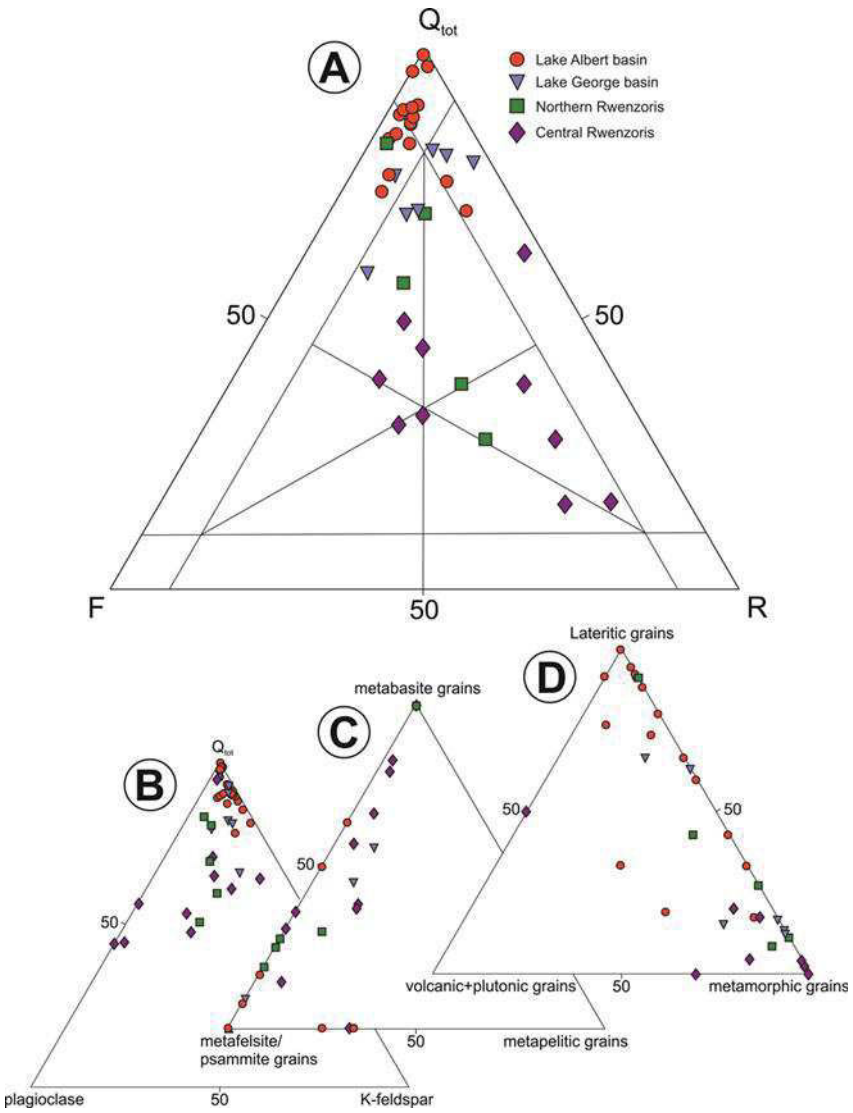

Figure 2-2. Framework petrography of the sand mode. Q_{tot} = mono- and polycrystalline quartz, F = feldspar, R = rock fragments.

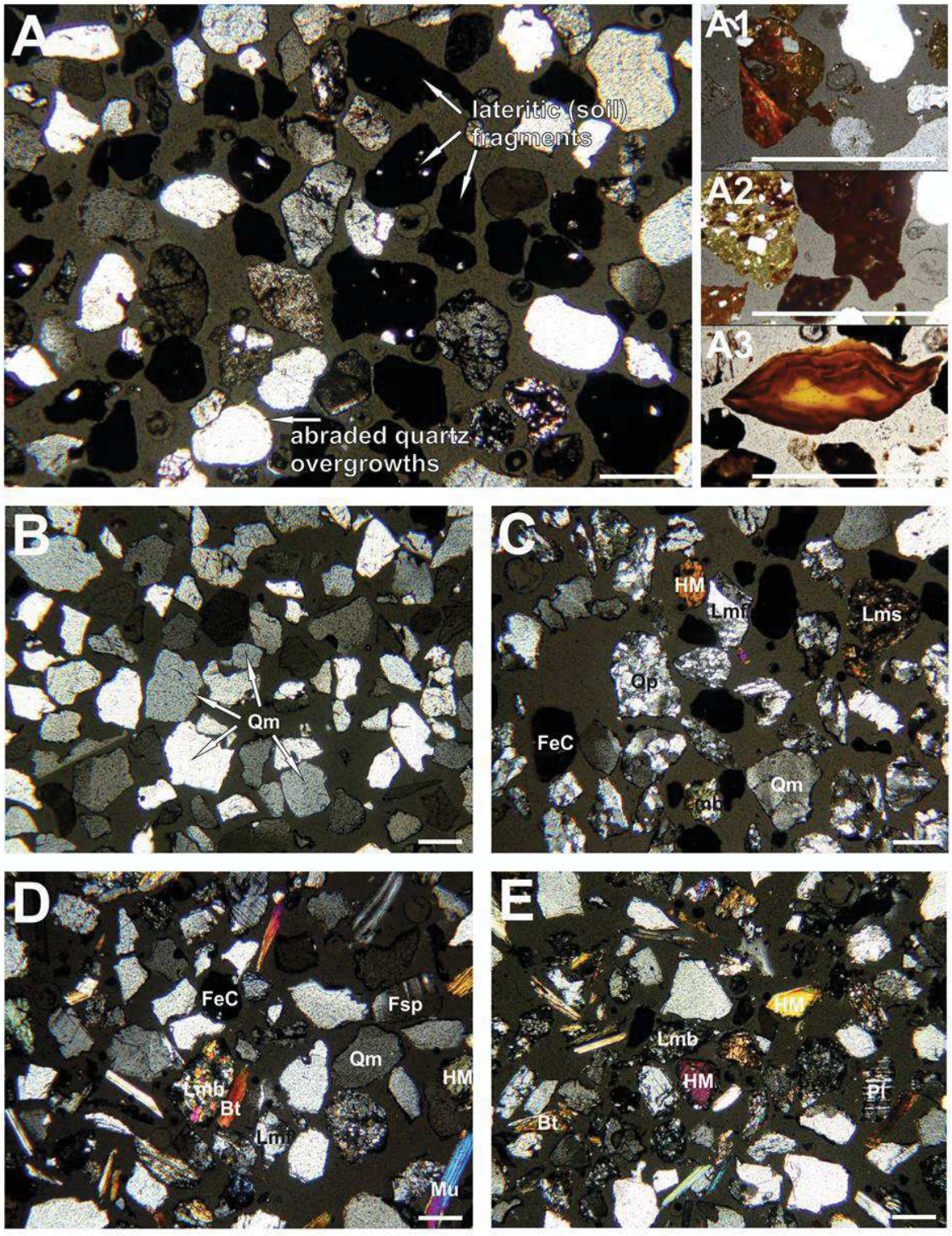

Figure 2-3. Sand composition in the Albertine Rift. Note the contrast between quartzose sands of the rift shoulder/plateau (A, B, C) and sands of the Rwenzori mountains rich in feldspars and rock fragments. A) Abundant laterite fragments (A1–A3) associated with recycled quartz grains with abraded overgrowths B) Quartz sand with angular grains showing solution pits. C) Sand rich in polycrystalline quartz. D+E) Sands rich in feldspars, rock fragments, mica and heavy minerals. All photos with crossed polars, scale bar = 300 µm. Bt = biotite, FeC = lateritic fragment, Fsp = feldspar, HM = heavy mineral, Lmb = metabasite grain, Lmf = metafelsite grain, Lms = metasedimentary grain, Mu = white mica; Pl = plagioclase, Qm = monocrystalline quartz, Qp = polycrystalline quartz.

The quartzose composition of the LAB sediments is reflected by low relative abundances of the mobile elements K, Cs, Mg, Sr, Ba, and especially Na and Ca (Table A2-5, Appendix; Fig. 2-5). Besides Si and Cr, all elements exhibit higher concentrations in the mud fraction, in particular Zr and Hf. A distinct enrichment in Cr is shown by sand fraction, whereas metals such as Sc, Mn, Co, Ni and Zn are slightly depleted in both sand and mud fractions. Sediments originating from granitic rocks are rich in Th, Ti and LREE, but strongly depleted in Eu (Fig. 2-11). Because of different provenances chondrite-normalized REE patterns for both sand and mud fractions are variable (especially for HREE in sand fraction) with La_N/Yb_N values ranging between 4.8 and 36.7 ($\tilde{x}$ ~ 10.1; sand) and 6.6 and 18.3 ($\tilde{x}$ ~ 9.5; mud). All samples show negative Eu-anomaly (with Eu/Eu* = 0.1–0.7 for sand and 0.2–0.6 for mud), which is, as mentioned above, most pronounced in sediments draining granitic terrane. In comparison to PAAS, all samples show flat patterns, depleted for sand and enriched for mud (Fig. 2-5).

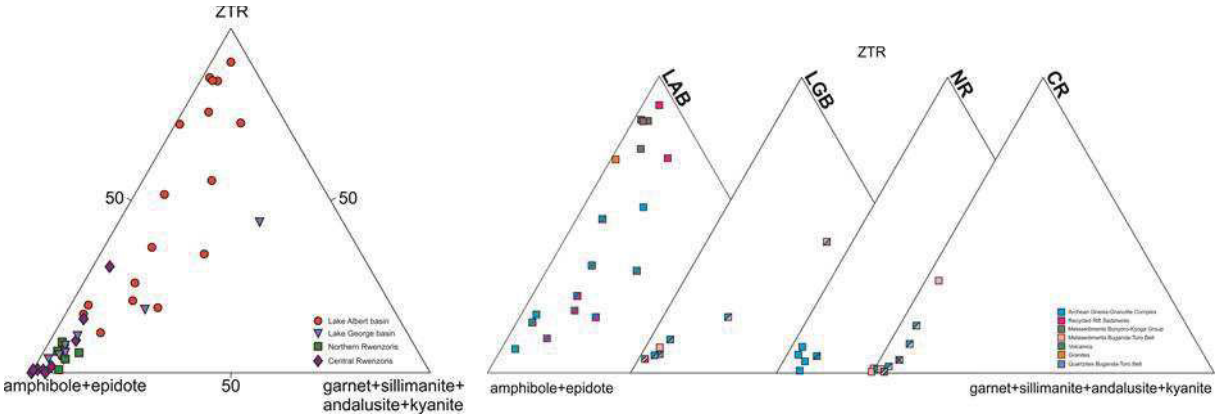

Figure 2-4. Heavy-mineral composition of the sand fraction. Most sediments in the Albertine Rift are rich in amphibole and epidote. Samples from the LAB show higher contents of zircon, tourmaline and rutile, reflecting extensive recycling of syn-rift sands and low-grade metasediments of the Bunyoro-Kyoga Group.

2.5.2 Lake George Basin (LGB)

These sands are quartz-rich (average quartz/feldspar ratio 5). Rock fragments (7–13%) include slate, phyllite, mica-sillimanite schist and gneiss. Lateritic clasts are widespread but generally minor (1–3%), except Crater Lake and Dura River samples where they exceed 25%. River sands derived from quartzitic sources are dominated by polycrystalline quartz, making up to half of the framework (Fig. 2-3C). Volcanic rock fragments are not abundant and include lathwork lithics. This holds true also for sands directly taken from a crater lake close to Fort Portal (sample ID 22), where polycrystalline quartz dominates. Heavy minerals include zircon, amphibole, epidote and sillimanite in varying proportions; only Crater Lake sand includes significant amount of pyroxene (10%).

LGB sediments are depleted in the mobile elements Na, Mg, Cs, Ca and Sr, and in the transition trace elements (TTE) Sc, Fe, Co, Ni, Cu, Zn, Al and Ga. Very low values for the TTE are observed in river sediments representing quartzitic terrains, but they are markedly enriched in catchments draining volcanic centres. All analyzed elements but Cr and Si show higher concentrations in the mud fraction, which shows the highest concentration in Zr, Hf, Nb and Ta. REE patterns are enriched in LREE when normalized to chondrite with La_N/Yb_N values varying between 3.9 and 20.6 ($\tilde{x}$ 8.7) for sand and 5.7 and 56.3 ($\tilde{x}$ 12.2) for mud. PAAS-normalized REE patterns show strong depletion in total REE for sand, but strong enrichment for mud (Fig. 2-5). HREE are more homogenous in sand than in mud.

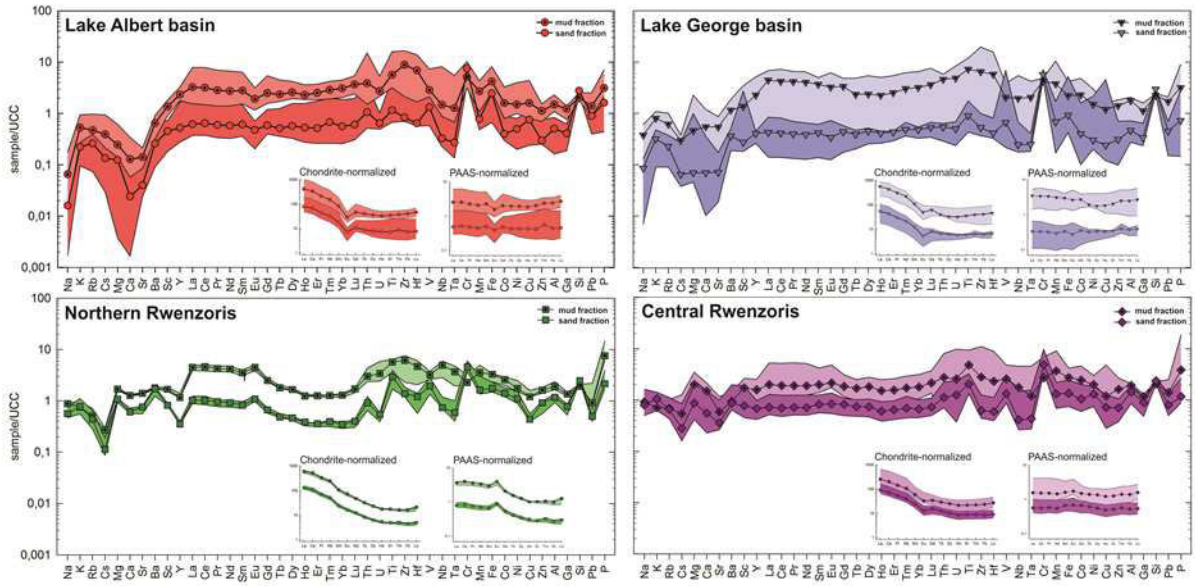

Figure 2-5. Geochemistry of sand and mud fractions in river sediments of Uganda. UCC-normalized elements (Rudnick and Gao, 2003) are arranged following the periodic table group by group (after Garzanti et al., 2013a); REE are also normalized to CI carbonaceous chondrites (McDonough and Sun, 1995) and to PAAS (Nance and Taylor, 1976). Dotted lines represent median values for sand and mud of each 'tectonic province', whereas colored areas depict the total range of element concentrations. Most elements (but Cr and Si) show higher concentrations in the mud fraction than in the sand fraction. Sediments draining the Rwenzori Mountains (NR and CR) display element concentrations close to UCC. Sands in the LAB and LGB are depleted in most elements, reflecting quartz dilution.

2.5.3 Northern Rwenzoris (NR)

These river sediments have a homogeneous petrographic and geochemical composition, which reflects their common source from Archean basement gneiss. They include subequal K-feldspar ($\tilde{x}$ ~ 9%) and plagioclase ($\tilde{x}$ ~ 12%). Rock fragments (2–40%) are mainly high-rank gneiss, schist and amphibolite. Muscovite and biotite occur. Grains are more angular than in sands from the LAB and LGB. Lateritic clasts are minor ($\tilde{x}$ 6). The heavy-mineral assemblages are dominated by amphibole and epidote, and include abundant brown hornblende. Opaque grains are common. Only one sample collected in a volcanic-dominated region near Fort Portal (Mpanga n1) contains significant clinopyroxene (30%).

Geochemical composition is similar to the UCC, but for Cs which is depleted up to a factor of twelve. Most elements, including mobile ones, show similar concentrations in sand and mud fractions; REE, Th, Zr, Hf, U, Ti, Nb, Ta and P exhibit higher values in mud. Chondrite- and PAAS-normalized REE patterns show strong LREE enrichment and relatively high La_N/Yb_N ratio ranging between 23.6–34.5 (sand) and 34.5–42.2 (mud). All sediments lack a Eu-anomaly (median Eu/Eu* = 0.95 for sand and 0.97 for mud).

2.5.4 Central Rwenzoris (CR)

The CR province is characterized by angular sands with low quartz/feldspar ratio ($\tilde{x}$ 1.5) and abundant feldspars (3–36%) and medium- to high-rank metamorphic rock fragments (18–52%) including gneiss, schist, granitoid, amphibolite and prasinite (Fig. 2-3D+E). Lateritic fragments are rare or absent. Abundant white mica invariably prevails over biotite. The heavy-mineral fraction is commonly rich in opaque grains including rutile needles, which partly represent altered phyllosilicates. Transparent

heavy minerals are dominated by epidote and amphibole with subordinate tourmaline, rutile, garnet, and rare zircon, apatite, titanite, andalusite, pyroxene, kyanite and sillimanite. Both sand and mud fractions have geochemical composition similar to the UCC (besides Cs); Zr and Hf are relatively enriched in mud, but depleted in sand fraction. Chondrite-normalized REE-patterns show a slight depletion in Eu (median Eu/Eu* 0.8 for sand and 0.75 for mud) and La_N/Yb_N values of 7.8–19.7 (x̃ 11.5) for sand and 4.7–18.1 (x̃ 9.9) for mud. Compared to PAAS, REE are depleted in sands, but enriched in muds. All patterns are flat, with very slightly positive Eu anomaly.

2.6 Discussion

Detrital minerals show different mechanical durabilities in the sedimentary environment. Most, including those generally held to be chemically unstable such as olivine or pyroxene, resist high-energy mechanical transport over thousands of kilometers (Garzanti et al., 2015a, 2015b). Conversely, all are variously affected by chemical weathering; with quartz, zircon, tourmaline and rutile generally held to be the most resistant. The relative abundance of quartz in first-cycle sediments derived from plutonic and metamorphic basement rocks can thus be used as an indicator of weathering.

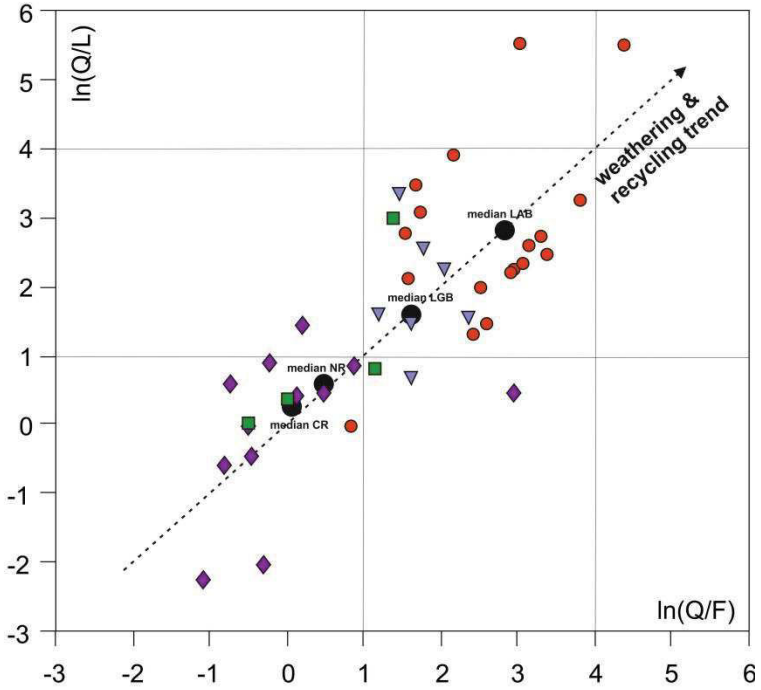

Figure 2-6. Log-ratio diagram discriminating the samples of the four provinces by their quartz/feldspar [ln(Q/F)] and quartz/rock fragment [ln(Q/R)] ratios.

In this study, median ln(Q/F) and ln(Q/L) ratios range between 2.22–3.10 in the LAB, 1.53–1.74 in the LGB, 0.82–1.14 in the NR and -0.03–0.37 in the CR, indicating that weathering progressively increases northward from the CR to the NR, LGB and LAB provinces (Fig. 2-6). These results are confirmed by geochemical data. The SiO_2/Al_2O_3 ratio shows median ratios of 25.1 (sand) and 5.2 (mud) for LAB, 23.2 (sand) and 5.3 (mud) for LGB, 8.9 (sand) and 3.4 (mud) for NR and 6.2 (sand) and 4.1 (mud) for CR, reflecting higher abundance of quartz in sediments generated in low-relief regions (LAB and LGB) than in the NR and CR. The increase of SiO_2/Al_2O_3 ratio from mud to sand is a classical grain-size effect reflecting increasing quartz dilution in coarser fractions. THMC

(transparent Heavy Mineral Concentration; Garzanti and Andò, 2007) and ZTR (Zircon-Tourmaline-Rutile; Hubert, 1962) indices are widely used indicators of the mineralogical stability of transparent heavy-mineral suites. HMC (wt%) are higher in the NR and CR (x̃ 28) than in the LAB and LGB (x̃ 9), suggesting preservation of most detrital minerals including unstable ferromagnesian ones in the former and some degree of depletion in the latter. Median ZTR values are 41 (LAB), 8 (LGB), 4 (NR), 1 (CR), correlating well with the quartz content. The highest concentration of zircon, tourmaline and rutile is present in sands derived from granites and low-grade metasediments of the Bunyoro-Kyoga Group or recycled within the Lake Albert rift basin (Fig. 2-4).

2.6.1 Weathering and recycling

Chemical weathering indices measure the degree of depletion in mobile alkali and alkaline earth metals and enrichment in non-mobile Al_2O_3 during weathering of rocks (Nesbitt and Young, 1982, 1984; Velbel, 1992). Weathering indices (Table A2-6, Appendix) in our samples vary widely between 49–92 (CIA), 49–100 (PIA) and 4–64 (WIP) for sand and 56–92 (CIA), 58–98 (PIA) and 6–44 (WIP) for mud. For both sand and mud, a clear northward trend of progressively increasing weathering intensity from CR to NR, LGB and LAB provinces is documented. WIP indices tend to be lower for sand in the LAB and LGB, because this index strongly reflects quartz dilution (Garzanti et al. 2013a; Fig. 2-7). Because lithology has a major control on the composition of sediments (Johnsson, 1993), chemical indices of weathering can be markedly affected by provenance from different source rocks (Fedo et al., 1995, Garzanti and Resentini, 2015).

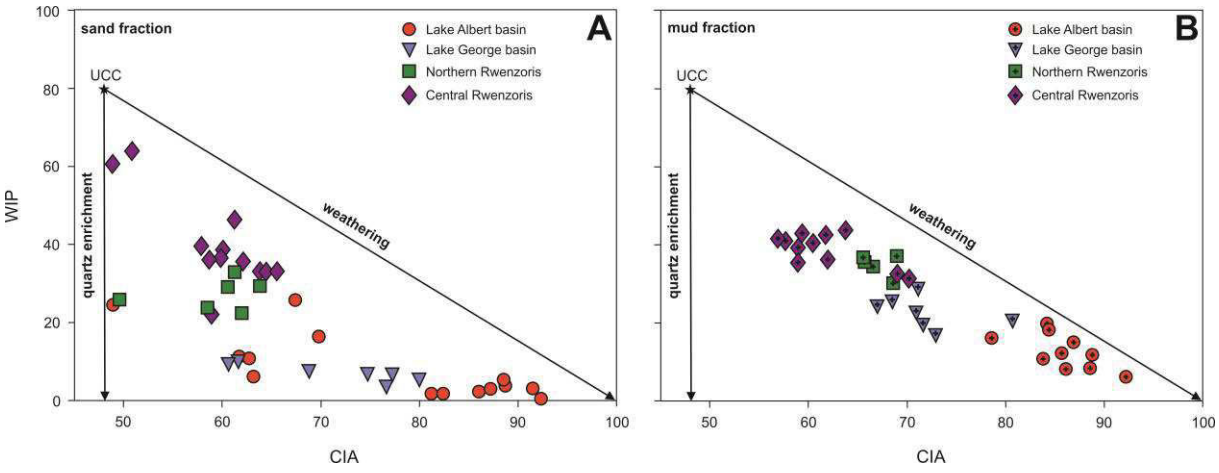

Figure 2-7. The CIA/WIP diagram (after Garzanti et al., 2013a) shows that all sediments are enriched in quartz to some extent, the sand fraction (A) more than the mud fraction (B). Quartz dilution, affecting the WIP but not the CIA, is most evident for sands draining the LAB and LGB, were WIP values remain low even where CIA values are low.

Comparison of calculated αAl values reveals different mobility sequences among 'tectonic provinces' (Fig. 2-8; Table A2-6, Appendix). Notably stronger depletion of mobile elements for LAB and LGB sediments is indicated by high αAl for Na, Ca and Sr. In the LAB province both sand and mud fractions show typical element mobility sequences, with higher loss for small cations (Ca, Na, Sr) and lower loss for cations with larger ionic radius (K, Rb, Ba) (Nesbitt et al., 1980). Sediments collected in the LGB exhibit similar values as the LAB, but slightly lower concentration of Mg, which may be a provenance effect. In general, NR and CR sands reveal only minor depletion of mobile elements, confirming limited weathering. The same mobility sequence obtained for the LAB and LGB have also

been observed in muds generated in hyper-humid rift highlands to the south (Garzanti et al., 2013b). The depletion of mobile elements with small ionic radii (Ca, Na, Sr) is inferred to be largely a consequence of selective plagioclase weathering in first-cycle sediments derived from igneous or metamorphic rocks, but can result also from recycling of siliciclastic or low-grade metasedimentary source rocks initially poor in plagioclase (e.g., Bunyoro-Kyoga Group). Elements with large ionic radii (especially Cs) are less mobile as they are adsorbed to secondary clay minerals (Kronberg et al., 1987).

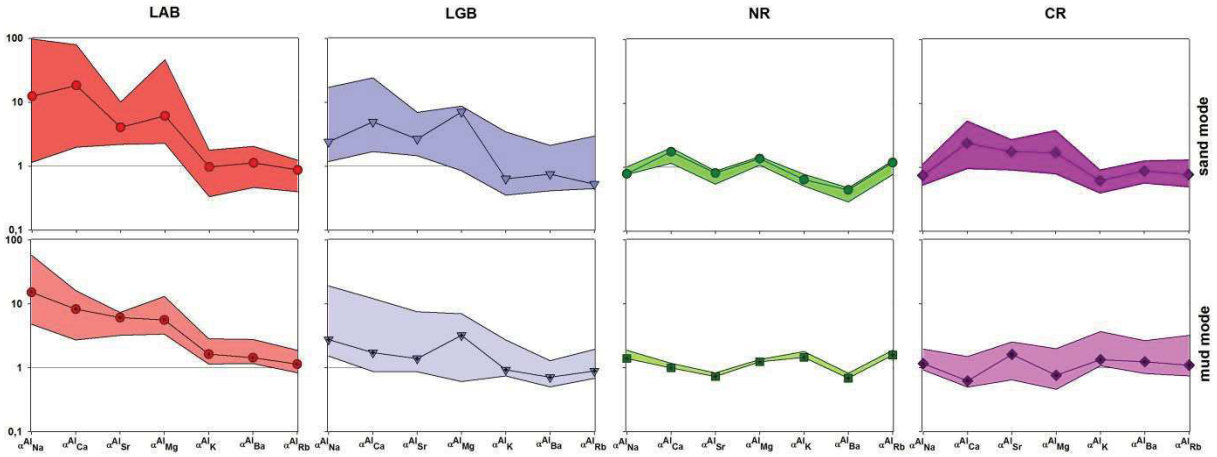

Figure 2-8. Systematic depletion in mobile elements relative to non-mobile Al. LAB and LGB sediments are most strongly depleted in the small cations Ca, Na and Sr. Sediments draining the Rwenzori mountains have mostly αAl values ~ 1, indicating limited chemical weathering.

A PCA carried out for both sand and mud using the mobile elements K, Na, Ca, Sr, Ba, Rb and Eu (which can substitute for Ca, McLennan and Taylor, 1991), as well as non-mobile Al and less mobile Si (Belov and Belova, 1979), clearly distinguishes LAB and LGB sediments from those of the NR and CR provinces (Fig. 2-9). For the sand fraction three groups of major elements are observed in the biplots: 1) Si, reflecting accumulation of more weathering-resistant minerals (i.e., quartz); 2) K and Rb, associated with K-feldspar and phyllosilicates; 3) Al, Na, Ba, Ca, Sr and Eu mainly associated with plagioclase. Overall, LAB/LGB and NR/CR are discriminated by their Si concentration, reflecting different weathering intensities and/or degree of recycling and quartz dilution.

These conclusions are supported by petrographic observations. The majority of LAB and LGB sands contain abundant monocrystalline quartz and lateritic fragments, whereas most NR and CR sands contain more rock fragments, feldspar, mica and heavy minerals (Fig. 2-2). Feldspars in sediments of the LAB and LGB are mostly K-feldspar, whereas sands derived from the NR and CR include abundant plagioclase (Fig. 2-2B). Because mobile elements are mainly hosted in feldspars, which is the most common silicate mineral group in the continental crust, the destruction of plagioclase and K-feldspar is the leading weathering process. Dominance of K-feldspar over plagioclase in LAB and LGB sands thus supports an advanced weathering state in these provinces (Nesbitt et al., 1997). Depletion of rock fragments in LAB and LGB sands may be ascribed to: 1) mechanical disintegration into individual mineral grains in high-energy environments (Garzanti et al., 2012), or 2) in situ destruction due to progressive weathering (Grantham and Velbel, 1988; Nesbitt et al., 1997). The former process has long been demonstrated to be scarcely effective (e.g., Russell and Taylor, 1937; Kuenen, 1959; Garzanti et al., 2015b), whereas in situ decomposition is widely documented in weathering profiles of Uganda (McFarlane, 1991; Taylor and Howard, 1999b). Extensive input of

highly weathered regolith into rivers is documented by the abundance of lateritic fragments in many samples and by common solution pits in quartz grains.

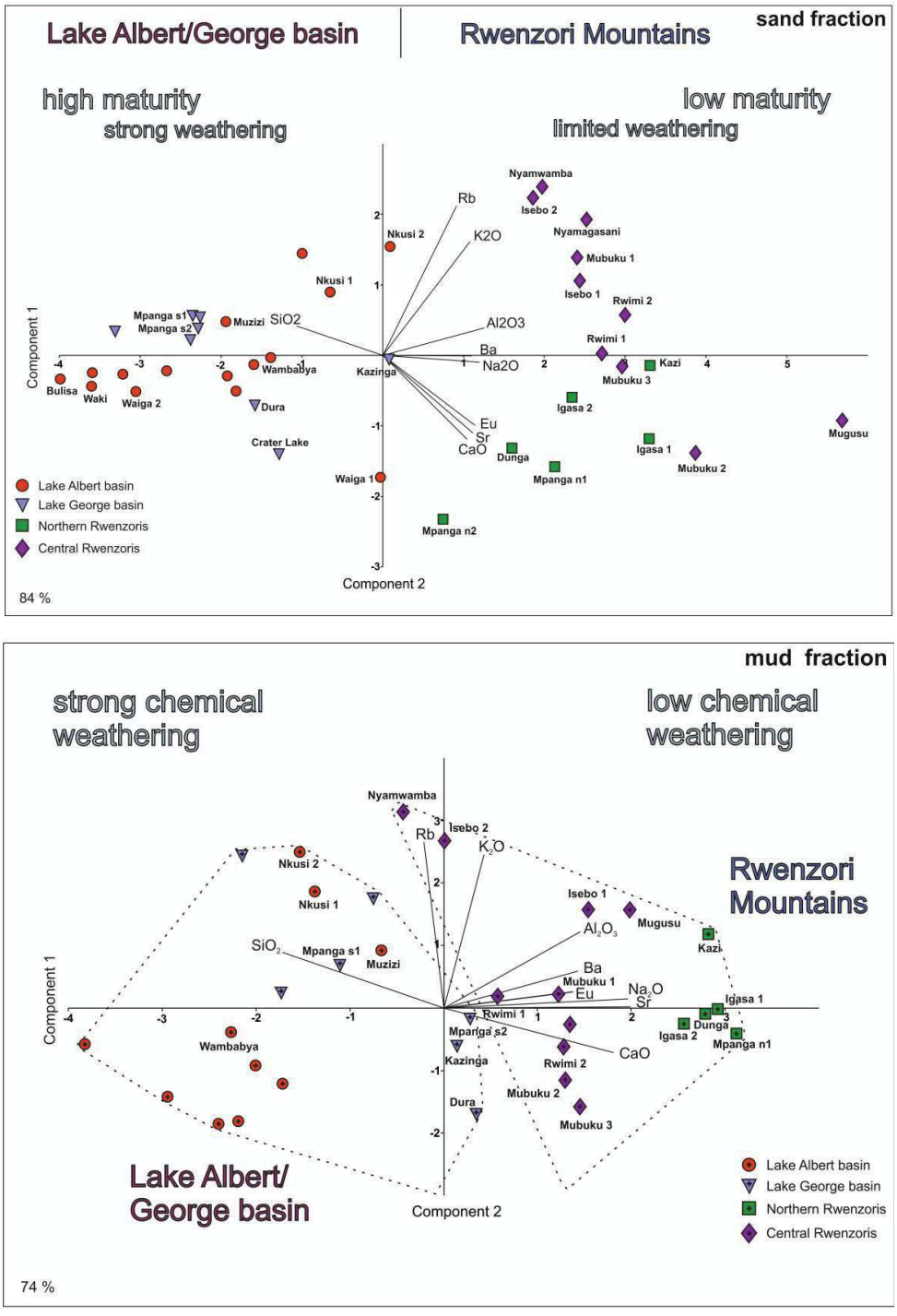

Figure 2-9. Biplots for the sand (above) and mud fractions (below) discriminate strongly weathered sediments generated in the low relief LAB and LGB from less altered sediments of the rugged Rwenzori Mountains.

In contrast to low-relief regions, abundant plagioclase, rock fragments, mica and heavy minerals indicate that sediments generated in the Rwenzori Mountains are much less modified by chemical alteration. This is confirmed by the scarcity of lateritic clasts, reflecting the steep morphology of the

Rwenzori horst where extensive soil forming processes are suppressed and rivers mainly drain bare rock faces (Eggermont et al., 2009).

2.6.2 Provenance

The geochemical composition of sediments is widely used to infer sediment provenance, trace elements being diagnostic of either felsic (e.g., Th, U, Zr, Hf, Nb, Ta, Y) or mafic rocks (e.g., Ni, Co, Cr, V, Cu) (Bhatia and Crook, 1986; Cullers, 2000; Lee, 2002; Armstrong-Altrin et al., 2015). According to McLennan and Taylor (1991), REE, Th and Sc are not significantly influenced by weathering, diagenesis or metamorphism, whereas Zr, Hf and Ti are strongly affected by hydraulic sorting and heavy-mineral fractionation. In the Zr/Sc vs. Th/Sc provenance diagram (McLennan et al. 1993), sand and mud samples indicate different provenances (Fig. 2-10). The highest Th/Sc ratios characterize most sands and muds from the LAB and LGB, whereas NR and CR plot close to the UCC. One sand sample from the LGB and mud sample from the CR show very low Th/Sc and Zr/Sc values, suggesting mafic source rocks. Some sand samples, mostly from the LAB and LGB, show slightly higher Zr/Sc ratio thus weakly following the sediment recycling trend. The Zr/Sc ratio is higher for mud, which may suggest enrichment of zircon in finer grain size fractions.

Chondrite-normalized REE patterns may also be diagnostic (Girty et al. 1994; Cullers, 2000; Yang et al. 2003; Singh, 2009). In general, mafic rocks tend to have low LREE/HREE ratio and no Eu anomaly, whereas felsic rocks show high LREE/HREE ratio and negative Eu anomaly because of their equilibrium with plagioclase-rich residuum (rich in Eu^{2+}; Gao and Wedepohl, 1995).

In general, the ∑REE is higher for mud than for sand (Fig. 2-11). The ∑REE of sand samples increases roughly from the LAB/LGB to the CR and NR, whereas the opposite is true for mud samples (excepting NR and some LGB samples). The majority of sand and mud samples from the LAB, LGB and CR show similar LREE/HREE ratio, but more negative Eu anomaly for most LAB and LGB sediments than for CR sediments, indicating more mafic provenance for the latter. Sands and muds from the NR exhibit highest LREE/HREE ratio and no Eu anomaly. Few samples from the LAB depict very negative Eu anomaly but relatively high LREE/HREE ratio, suggesting provenance from felsic rocks. Some sediments from the NR province show peculiar REE patterns with highest ∑REE values and LREE/HREE ratio but no Eu anomaly, which may point to provenance from Archean rocks due to high fractionation ratios (McLennan et al., 1993).

As a complement to geochemical data, heavy minerals are widely used to infer provenance of clastic sediments, because they are more source rock specific than quartz or feldspar (Morton, 1985; Morton and Hallsworth, 1994; Garzanti and Andò, 2007). Widespread amphibole and epidote reflect the preponderance of greenschist- to amphibolite-facies rocks in the study area. Amphibole-epidote suites are not restricted to the Rwenzori Mountains, but occur as well in LAB and LGB sediments, where these minerals partly resisted more extensive weathering.

2.6.3 Tectonic setting

The Albertine Rift, where sediments are derived from actively uplifted basement rocks, is an excellent natural laboratory in which to test whether the discriminant function-based major element diagrams recently introduced by Verma and Armstrong-Altrin (2013) can succesfully identify a rift-related setting. In these diagrams high-silica (SiO_2 = 63%–95%) and low-silica (SiO_2 = 35%–63%) sedimentary rocks are discriminated into three tectonic settings (island or continental arc, continental rift, and collision).

Because of SiO_2 concentration > 63%, some mud samples from the LAB and LGB plot in the high-silica diagram (Fig. 2-12A). Here, all LAB sediments and the majority of LGB samples plot in the expected field for a rift setting, whereas samples from the NR and CR plot in the arc field, close to the boundary between the arc and the rift field. In the low-silica diagram (Fig. 2-12B) all samples plot in the collision field near the boundary of the rift field. The conclusions drawn by the use of the high-silica and low-silica diagrams thus result to be inconsistent and misleading.

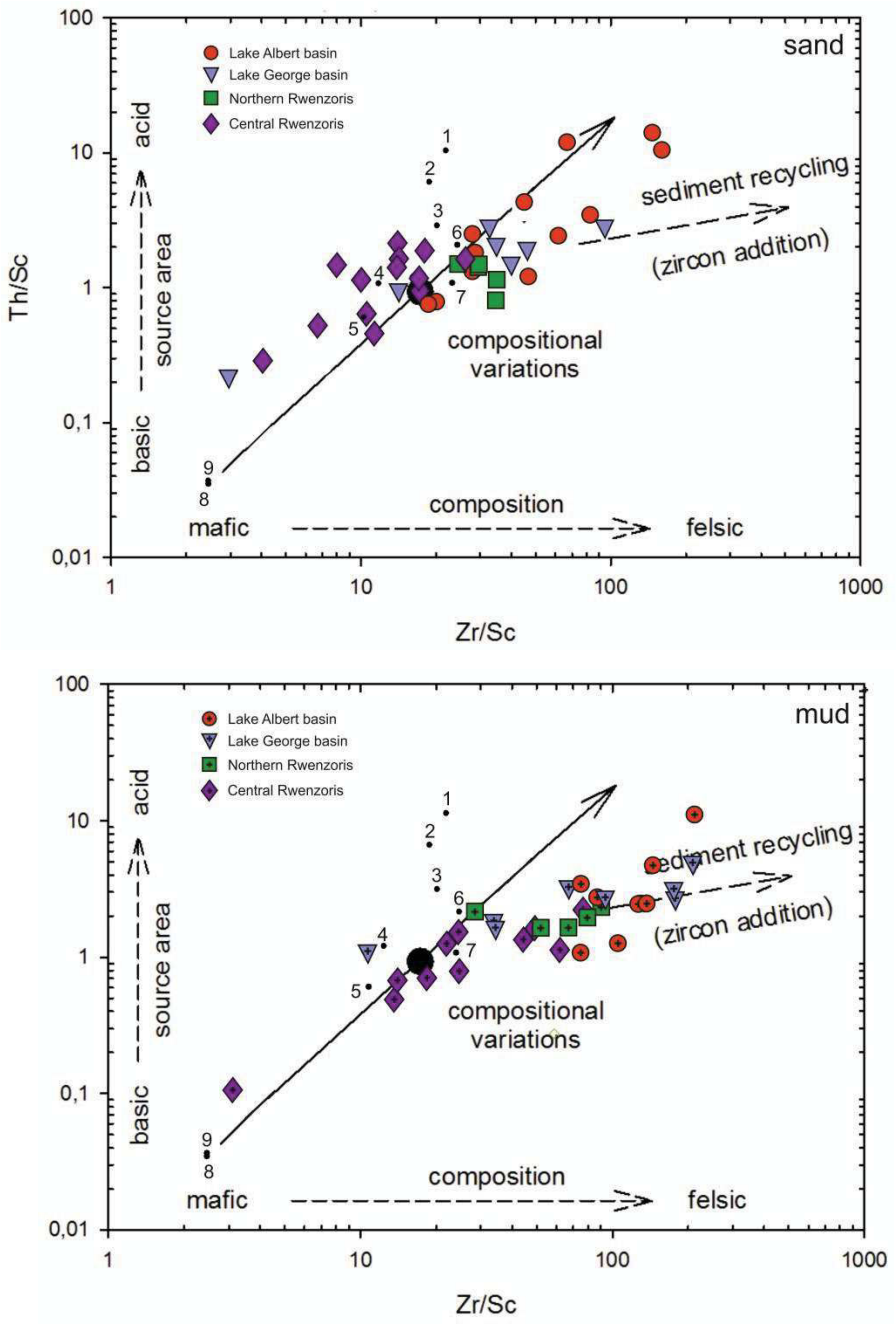

Figure 2-10. Discrimination diagram after McLennan et al. (1993) for sand (left) and mud (right) illustrating compositional variations (Th/Sc) and sediment recycling (Zr/Sc). Data from various Ugandan basement rocks are plotted for comparison with (1+2) granite (Singo, unpublished), (3) granite (Singo; Nagudi et al., 2003), (4) schist (Karl, 2008), (5) gneiss (Karl, 2008), (6+7) gneiss (Link, unpublished), (8) amphibolite (Karl, 2008), and (9) meta-dolerite (Link, unpublished).

2.6.4. The grain size effect

Fractionation of detrital grains because of their different hydraulic behavior is a process that invariably occurs during transport and deposition, thus distorting the original provenance signature. Sorting of sedimentary grains by their size, density or shape leads to concentration of different minerals in different grain size fractions. For example, ultradense minerals such as zircon, rutile or monazite that are the major carriers of REE and HFSE (U, Th, Zr, Hf, Y) elements (Deer et al., 1992) are markedly enriched in the fine tail of the size distribution of all sediments deposited from tractive currents (Garzanti et al., 2008), but may also result from their originally smaller size within parent rocks (Morton and Hallsworth, 1994). Quartz is concentrated in sand which implies a higher Si content, whereas most other elements are enriched in mud because of their affiliation to phyllosilicates and oxy-hydroxides (Garzanti et al. 2011). A decrease in SiO_2/Al_2O_3 ratio from sand to mud is thus the rule, as observed also in sediments of the Albertine Rift.

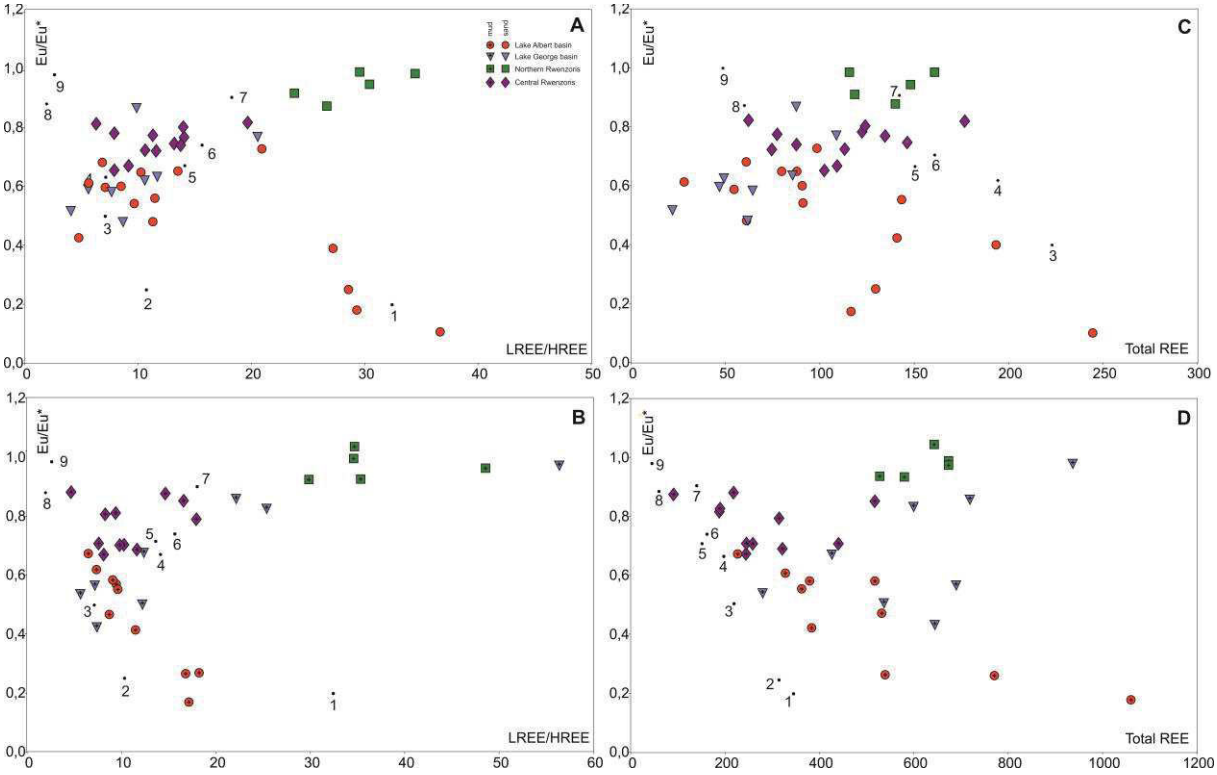

Figure 2-11. Fractionation of LREE and HREE (La_N/Yb_N) in relation to the Eu anomaly (Eu/Eu*) for (A) sand and (B) mud. Total REE content in relation to Eu/Eu* for (C) sand and (D) mud. Data of Ugandan basement rocks are given for comparison with (1+2) granite (Singo, unpublished), (3) granite (Singo; Nagudi et al., 2003), (4) schist (Karl, 2008), (5) gneiss (Karl, 2008), (6+7) gneiss (Link, unpublished), (8) amphibolite (Karl, 2008), and (9) meta-dolerite (Link, unpublished).

In the low-relief LAB and LGB provinces, all elements besides Si and Cr are markedly enriched in the mud fraction, whereas element concentrations do not vary much from mud to sand in the Rwenzori provinces. The same observation holds true for sands all along the western branch of the EARS (Garzanti et al., 2013b) and reflects different degrees of weathering (Nesbitt et al., 1997). Where physical processes are dominant, as in the Rwenzori provinces, the mud fraction contains minor secondary clay minerals, resulting in similar composition of sand and mud (Nesbitt and Young, 1996). In contrast, the different geochemical composition displayed by mud and sand fractions in the LAB and LGB results from greater quartz dilution and partly from incongruent dissolution of silicate

minerals, with loss of mobile cations during hydrolysis and formation of residual clay minerals (e.g., kaolinite; Bahlburg and Dobrzinski, 2011). Very low Na, Ca and Mg document strong selective dissolution of plagioclase and ferromagnesian silicates relative to more stable K-feldspar in the LAB/LGB provinces (Garzanti et al., 2013b).

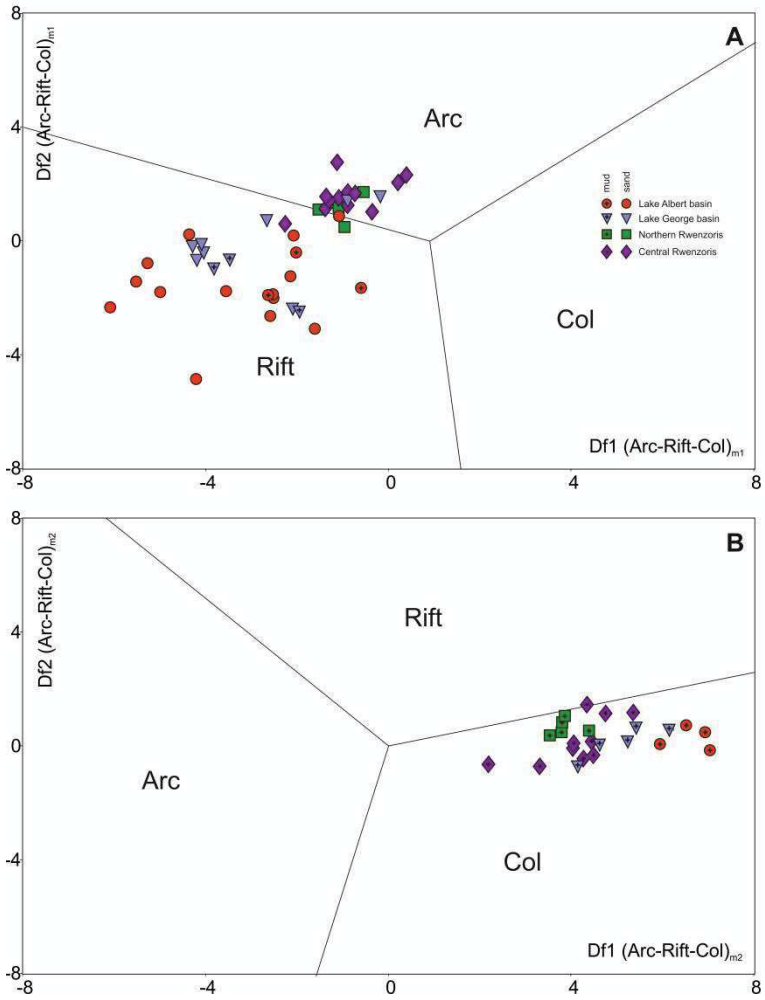

Figure 2-12. Discriminant function multidimensional diagram for (A) high-silica, and (B) low-silica clastic sediments (after Verma and Armstrong-Altrin, 2013).

2.6.5. Comparison of REE and Th/Sc ratio with potential source rocks

In this paragraph we compare the Th/Sc ratio (Fig. 2-10) and REE pattern (Fig. 2-11) of analyzed river samples with typical Ugandan basement rocks, including gneiss, schist, amphibolite, granite and quartzite. The dominant rock lithologies in the Albertine Rift are schist (4) and gneiss (5-7), and the geochemical fingerprint of most analyzed daughter sediments are consistent with such parent rocks. Some samples, chiefly from the LAB, have patterns resembling those of granitic rocks (1-3), characterized by prominent negative Eu anomaly, high Th/Sc ratio and varying LREE/HREE ratio. One sample from the CR compares with mafic source rocks as amphibolite (8) and meta-dolerite (9), identified by low Th/Sc ratio, no Eu anomaly, low ∑REE values and low LREE/HREE ratio. The REE pattern of samples from the NR province are characterized by no Eu anomaly, high LREE/HREE ratio

and Th/Sc ratio close to the UCC, matching the characteristics of a microcrystalline gneiss analyzed by Link (7; unpublished).

2.7 Conclusion

The petrographic, mineralogical and geochemical composition of modern sediments generated in different geomorphological settings along the Albertine Rift in Uganda (e.g., poorly-drained lowlands, high-altitude massifs) are of two fundamental types. The high-relief Rwenzori Mountains (NR and CR provinces) shed sands rich in feldspars and rock fragments with very rich heavy-mineral assemblages dominated by amphibole and epidote. Their ln(Q/F) and ln(Q/L) ratio, SiO_2/Al_2O_3 ratio and ZTR index indicate that these sediments have undergone only limited weathering, as confirmed by CIA, PIA and WIP indices, by αAl-values, and by similar geochemical composition of sand and mud samples. These results indicate that the exhumation of the young Rwenzori horst, leading to high topography and repeated cycles of glacial erosion, promotes rapid physical degradation rather than intense chemical alteration.

In contrast, the low-relief rift plateau (LAB and LGB provinces) generates sediments enriched in quartz by intense weathering prolonged over millions of years, during which chemical reactions led to extensive silicate dissolution and widespread development of thick lateritic soil covers. Presently, soil erosion is the prevailing process along much of the Albertine Rift, as indicated by the abundance of lateritic fragments in river sands. Chemical indices of weathering, although partly reflecting the lithology of source rocks, recycling and quartz dilution, suggest intense alteration for sediments of the Lake Albert Basin province, where indices reveal significantly stronger alteration for the mud fraction than for sand.

This study of modern sediments of the Albertine Rift shows that not only highly weathered and slightly weathered sands can be differentiated reliably, but also that the original provenance signatures of sediments generated from different source rocks and in different geomorphological settings can be identified even in areas characterized by extreme climatic conditions such as those of equatorial latitudes. We found that the imprint of source-rock lithology is best preserved by heavy minerals and geochemical parameters, especially non-mobile elements (e.g., Th/Sc ratio and REE). The majority of sediments in the Albertine Rift is derived from rocks intermediate between felsic and mafic suites and display similar composition to gneisses and schists of the Ugandan basement.

2.8 Acknowledgements

This study is integrated in the subproject B3 - Linking Source and Sink in the Rwenzori Mountains and adjacent rift basins, Uganda, which is part of the DFG-funded, interdisciplinary research program RiftLink – Rift Dynamics and Uplift and Climate Changes in Equatorial Africa (H1643–7/1). We would like to thank the Uganda National Council for Science and Technology (UNCST) and the Uganda Wildlife Authority (UWA) for research permissions, and also our Ugandan research partners from Makerere University for close cooperation. Many thanks go to A. Schumann for his on-site guidance and to our driver Kitam Ali. Alberto Resentini and Mara Limonta kindly analysed selected Rwenzori sands for petrography and heavy minerals; previous analyses by Marta Padoan, Giovanni Vezzoli and Alberto Resentini were also included in this study.

2.9 References

Aitchison, J., Egozcue, J. J., 2005. Compositional data analysis: where are we and where should we be heading? Mathematical Geology, 37, 829–850.

Albaric, J., Déverchère, J., Petit, C., Perrot, J., Le Gall, B., 2009. Crustal rheology and depth distribution of earthquakes: Insights from the central and southern East African Rift System. Tectonophysics, 468, 28–41.

Andò, S., Garzanti, E., Padoan, M., Limonta, M., 2012. Corrosion of heavy minerals during weathering and diagenesis: a catalogue for optical analysis. In: von Eynatten, H., Critelli, S., Ingersoll, R. V., Weltje, G. J., (Eds.), Actualistic models of sediment generation. Sedimentary Geology, 280, pp. 165–178.

Armstrong-Altrin, J. S., 2015. Evaluation of two multidimensional discrimination diagrams from beach and deep-sea sediments from the Gulf of Mexico and their application to Precambrian clastic sedimentary rocks. International Geology Review, 57, 1–16.

Armstrong-Altrin, J. S., Machain-Castillo, M. L., Rosales-Hoz, L., Carranza-Edwards, A., Sanchez-Cabeza, J.-A., Ruíz-Fernández, A. C., 2015. Provenance and depositional history of continental slope sediments in the Southwestern Gulf of Mexico unraveled by geochemical analysis. Continental Shelf Research, 95, 15–26.

Bahlburg, H., Dobrzinski, N., 2011. A review of the Chemical Index of Alteration (CIA) and its application to the study of Neoproterozoic glacial deposits and climate transitions. In: Arnaud, E., Halverson, G. P., Shields-Zhou, G. (Eds.), The Geological Record of Neoproterozoic Glaciations. Geological Society London, Memoirs, 36, pp. 81–92.

Barker, D. S., Nixon, P. H., 1989. High-Ca, low-alkali carbonatite volcanism at Fort Portal, Uganda. Contributions to Mineralogy and Petrology, 103, 166–177.

Basu, A., 1985. Influence of climate and relief on compositions of sands released at source areas. In: Zuffa, G. G. (Ed.), Provenance of arenites. Dordrecht, Reidel, NATO ASI Ser., 148, pp. 165–189.

Bauer F. U., Glasmacher U. A., Ring U., Schumann A., Nagudi B., 2010. Thermal and exhumation history of the central Rwenzori Mountains, Western Rift of the East African Rift System, Uganda. International Journal of Earth Sciences, 99, 1575–1597.

Belov, N. V., Belova, E. N., 1979. Reaction features of silica. In: Chernov, A. A. (Ed.), Growth of crystals. Springer US, pp. 1–5.

Bhatia, M. R., Crook, K. A., 1986. Trace element characteristics of graywackes and tectonic setting discrimination of sedimentary basins. Contributions to Mineralogy and Petrology, 92, 181–193.

Bishop, W. W., 1965. Quaternary geology and geomorphology in the Albertine Rift Valley, Uganda. In: Wright Jr., H. E., Frey, D. G. (Eds.), International studies on the Quaternary, pp. 293–321.

Burke, K., Gunnell, Y., 2008. The African erosion surface: A continental-scale synthesis of geomorphology, tectonics and environmetal change over the past 180 Million years. Geological Society of America Memoirs, 201, 1–66.

Chorowicz, J., 2005. The East African rift system. Journal of African Earth Sciences, 43, 379–410.

Cleary, W. J., Connolly, J. R., 1971. Distribution and genesis of quartz in a piedmont-coastal plain environment. Geological Society of America Bulletin, 82, 2755–2766.

Crook, K. A. W., 1968. Weathering and roundness of quartz sand grains. Sedimentology, 11, 171–182.

Cullers, R. L., 2000. The geochemistry of shales, siltstones and sandstones of Pennsylvanian–Permian age, Colorado, USA: implications for provenance and metamorphic studies. Lithos, 51, 181–203.

De Heinzelin, J., 1962. Les formations du Western Rift et de la cuvette congolaise. In Annales du Musée Royal de L'afrique Centrale, 40, 219–243.

Deer, W. A., Howie, R. A., Zussman, J., 1992. An Introduction to the Rock-Forming Minerals (2nd edition). Longman, Harlow.

Dixon, J. L., Heimsath, A. M., Kaste, J., Amundson, R., 2009a. Climate-driven processes of hillslope weathering. Geology, 37, 975–978.

Doornkamp, J. C., 1968. The role of inselbergs in the geomorphology of Southern Uganda. Transactions of the Institute of British Geographers, 44, 151–162.

Ebinger, C. J., 1989. Tectonic development on the western branch of the East African rift system. Geological Society of America Bulletin, 101, 885–903.

Ebinger, C. E., Scholz, C. A., 2012. Continental rift basins: the East African perspective. In: Busby, C., Azor, A. (Eds.), Tectonics of sedimentary basins: recent advances. Oxford, Wiley-Blackwell, pp. 185–208.

Eggermont, H., Damme, K. V., Russell, J. M., 2009. Rwenzori Mountains (Mountains of the Moon): Headwaters of the White Nile. In: Dumont, H. J. (Ed.), The Nile: Origin, Environments, Limnology and Human Use, Springer Science, pp. 243–261.

Fedo, C. M., Nesbitt, H. W., Young, G. M., 1995. Unraveling the effects of potassium metasomatism in sedimentary rocks and paleosols, with implications for paleoweathering conditions and provenance. Geology, 23, 921–924.

Fedo, C. M., Young, G. M., Nesbitt, H. W., Hanchar, J. M., 1997. Potassic and sodic metasomatism in the Southern Province of the Canadian Shield: Evidence from the Paleoproterozoic Serpent Formation, Huronian Supergroup. Canada. Precambrian Research, 84, 17–36.

Foley, S. F., Link, K., Tiberindwa, J. V., Barifaijo, E., 2012. Patterns and origin of igneous activity around the Tanzanian craton. Journal of African Earth Sciences, 62, 1–18.

Gabert, G., 1990. Lithostratigraphic and tectonic setting of gold mineralization in the Archean cratons of Tanzania and Uganda, East Africa. Precambrian Research, 46, 59–69.

Gaillardet, J., Dupré, B., Allègre, C. J., 1999. Geochemistry of large river suspended sediments: silicate weathering or recycling tracer?. Geochimica et Cosmochimica Acta, 63, 4037–4051.

Gao, S., Wedepohl, K. H., 1995. The negative Eu anomaly in Archean sedimentary rocks: Implications for decomposition, age and importance of their granitic sources. Earth and Planetary Science Letters, 133, 81–94.

Garzanti, E., Andò, S., 2007. Heavy mineral concentration in modern sands: implications for provenance interpretation. Developments in Sedimentology, 58, 517–545.

Garzanti, E., Resentini, A., 2015. Provenance control on chemical-weathering indices (Taiwan river sands). Sedimentary Geology, doi.org/10.1016/j.sedgeo.2015.06.013.

Garzanti, E., Andò, S., Vezzoli, G., 2008. Settling-equivalence of detrital minerals and grain-size dependence of sediment composition. Earth and Planetary Science Letters, 273, 138–151.

Garzanti, E., Andò, S., France-Lanord, C., Galy, V., Censi, P., Vignola, P., 2011. Mineralogical and chemical variability of fluvial sediments. 2. Suspended-load silt (Ganga-Brahmaputra, Bangladesh). Earth and Planetary Science Letters, 302, 107–120.

Garzanti, E., Andò, S., Vezzoli, G., Lustrino, M., Boni, M., Vermeesch, P., 2012. Petrology of the Namib sand sea: long-distance transport and compositional variability in the wind-displaced Orange Delta. Earth Science Reviews, 11, 173–189.

Garzanti, E., Padoan, M., Andò, S., Resentini, A., Vezzoli, G., Lustrino, M., 2013a. Weathering and relative durability of detrital minerals in equatorial climate: sand petrology and geochemistry in the East African Rift. The Journal of Geology, 121, 547–580.

Garzanti, E., Padoan, M., Peruta, L., Setti, M., Najman, Y.; Villa, I. M., 2013b. Weathering geochemistry and Sr-Nd fingerprints of equatorial upper Nile and Congo muds. Geochemistry, Geophysics, Geosystems, 14, 292–316.

Garzanti. E., Vermeesch, P., Padoan, M., Resentini, A., Vezzoli, G., Andò, S., 2014a. Provenance of passive-margin sand (southern Africa). The Journal of Geology, 122, 17–42.

Garzanti, E., Padoan, M., Setti, M., López-Galindo, A., Villa, I.M., 2014b. Provenance versus weathering control on the composition of tropical river mud (southern Africa). Chemical Geology, 366, 61–74.

Garzanti, E., Andò, S., Padoan, M., Vezzoli, G., El Kammar, A., 2015a. The modern Nile sediment system: Processes and products. Quaternary Science Reviews, 130, 9–56.

Garzanti, E., Resentini, A., Andò, S., Vezzoli, G., Pereira, A., Vermeesch, P., 2015b. Physical controls on sand composition and relative durability of detrital minerals during ultra-long distance littoral and aeolian transport (Namibia and southern Angola). Sedimentology, 62, 971–996.

Girty, G. H., Hanson, A. D., Knaack, C., Johnson, D., 1994. Provenance determined by REE, Th, and Sc analyses of metasedimentary rocks, Boyden Cave roof pendant, central Sierra Nevada, California. Journal of Sedimentary Research, 64, 68–73.

Grantham, J. H., Velbel, M. A., 1988. The influence of climate and topography on rock fragment abundance in modern fluvial sands of the southern Blue Ridge Mountains, North Carolina. Journal of Sedimentary Research, 58, 219–227.

Hammer, Ø., Harper, D. A. T., Ryan, P. D., 2001. PAST: Paleontological Statistics Software Package for Education and Data Analysis–Palaeontologia Electronica, 4, 9 pp.

Harnois, L., 1988. The CIW index: a new chemical index of weathering. Sedimentary Geology, 55, 319–322.

Hepworth, J. V., MacDonald, R., 1966. Orogenic belts of the northern Uganda basement. Nature, 210, 726–727.

Hubert, J. F., 1962. A zircon-tourmaline-rutile maturity index and the interdependence of the composition of heavy mineral assemblages with the gross composition and texture of sandstones. Journal of Sedimentary Research, 32, 440–450.

Ingersoll, R. V., Bullard, T. F., Ford, R. L., Grimm, J. P., Pickle, J. D., Sares, S. W., 1984. The effect of grain size on detrital modes: a test of the Gazzi-Dickinson point-counting method. Journal of Sedimentary Petrology, 54, 103–116.

Johnsson, M. J., 1993. The system controlling the composition of clastic sediments. In: Johnsson, M. J., Basu, A. (Eds.), Processes controlling the composition of clastic sediments. Geological Society of America Special Papers, 284, pp. 1–19.

Johnsson, M. J., Meade, R. H., 1990. Chemical weathering of fluvial sediments during alluvial storage: the Macuapanim Island point bar, Solimões River, Brasil. Journal of Sedimentary Petrology, 60, 827–842.

Johnsson, M. J., Stallard, R. F., Meade, R. H., 1988. First-cycle quartz arenites in the Orinoco River basin: Venezuela and Colombia. Journal of Geology, 96, 263–277.

Karl, M., 2008. Lithostratigraphische und strukturelle Kartierung im Zentralbereich des Rwenzori-Gebirges an der Grenze zwischen Uganda und dem Kongo, Diplomkartierung, Univ. Heidelberg, 182 p.

Koehn, D., Lindenfeld, M., Rümpker, G., Aanyu, K., Haines, S., Passchier, C. W., Sachau, T., 2010. Active transsection faults in rift transfer zones: evidence for complex stress fields and implications for crustal fragmentation processes in the western branch of the East African Rift. International Journal of Earth Sciences, 99, 1633–1642.

Kronberg, B. I., Nesbitt, H. W., Fyfe, W. S., 1987. Mobilities of alkalis, alkaline earths and halogens during weathering. Chemical geology, 60, 41–49.

Kuenen, Ph. H., 1959. Experimental abrasion, 3. Fluviatile action on sand. American Journal of Science, 257, 172–190.

Lee, Y. I., 2002. Provenance derived from the geochemistry of late Paleozoic–early Mesozoic mudrocks of the Pyeongan Supergroup, Korea. Sedimentary Geology, 149, 219–235.

Leggo, P. J., 1974. A geochronological study of the basement complex of Uganda. Journal of the Geological Society London, 130, 263–277.

Link, K., Koehn, D., Barth, M. G., Tiberindwa, J. V., Barifaijo, E., Aanyu, K., Foley, S. F., 2010. Continuous cratonic crust between the Congo and Tanzania blocks in western Uganda. International Journal of Earth Sciences, 99, 1559–1573.

Liu, Z., Colin, C., Huang, W., Le, K. P., Tong, S., Chen, Z., Trentesaux, A., 2007. Climatic and tectonic controls on weathering in south China and Indochina Peninsula: Clay mineralogical and geochemical investigations from the Pearl, Red, and Mekong drainage basins, Geochemistry, Geophysics, Geosystems, 8(5) Q05005. doi:10.1029/ 2006GC001490.

MacDonald, R., 1966. Geological map of Uganda. Department of Geological Survey and Mines, Uganda.

Mange, M. A., Maurer, H. F. W., 1992. Heavy minerals in colour. Chapman and Hall, London, 148 p.

McDonough, W. F., Sun, S. S., 1995. The composition of the Earth. Chemical Geology, 120, 223–253.

McFarlane, M. J., 1991. Some sedimentary aspects of lateritic weathering profile development in the major bioclimatic zones of tropical Africa. Journal of African Earth Sciences, 12, 267–282.

McLennan, S. M., Taylor, S. R., 1991. Sedimentary rocks and crustal evolution: tectonic setting and secular trends. The Journal of Geology, 99, 1–21.

McLennan, S. M., Hemming, S., McDaniel, D. K., Hanson, G. N., 1993. Geochemical approaches to sedimentation, provenance, and tectonics. Geological Society of America Special Papers, 284, 21–40.

Morton, A. C., 1985. Heavy minerals in provenance studies. In: Zuffa, G. G. (Ed.), Provenance of arenites. Dordrecht, Reidel, NATO ASI Ser. 148, pp. 249–277.

Morton, A. C., Hallsworth, C. R., 1994. Identifying provenance-specific features of detrital heavy mineral assemblages in sandstones. Sedimentary Geology, 90, 241–256.

Morton, A. C., Hallsworth, C. R., 1999. Processes controlling the composition of heavy mineral assemblages in sandstones. Sedimentary Geology, 124, 3–29.

Nagudi, B., Koeberl, C., Klötzli, U., 2001. Petrogenesis and geochronology of the Singo batholith using zircons. In: Schumann, A., (Ed.), Abstracts Regional Conference of the Geological Society of Uganda and the Geological Society of Africa, Kampala, pp. 36–37.

Nagudi, B., Koeberl, C., Kurat, G., 2003. Petrography and geochemistry of the Singo granite, Uganda, and implications for its origin. Journal of African Earth Science, 36, 73–87.

Nance, W. B., Taylor, S. R., 1976. Rare-earth element patterns and crustal evolution. 1. Australian post-Archean sedimentary rocks. Geochimica et Cosmochimica Acta, 40, 1539–1551.

Nesbitt, H. W., Young, G. M., 1982. Early Proterozoic climates and plate motions inferred from major element chemistry of lutites. Nature, 299, 715–717.

Nesbitt, H. W., Young, G. M., 1984. Prediction of some weathering trends of plutonic and volcanic rocks based on thermodynamic and kinetic considerations. Geochimica et Cosmochimica Acta, 48, 1523–1534.

Nesbitt, H. W., Young, G. M., 1996. Petrogenesis of sediments in the absence of chemical weathering: effects of abrasion and sorting on bulk composition and mineralogy. Sedimentology, 43, 341–358.

Nesbitt, H. W., Markowics, G., Price, R. C., 1980. Chemical processes affecting alkalis and alkaline earths during continental weathering. Geochimica et Cosmochimica Acta, 44, 1659–1666.

Nesbitt, H. W., Young, G. M., McLennan, S. M., Keays, R. R., 1996. Effects of chemical weathering and sorting on the petrogenesis of siliciclastic sediments, with implications for provenance studies. Journal of Geology, 104, 525–542.

Nesbitt, H. W., Fedo, C. M., Young, G. M., 1997. Quartz and feldspar stability, steady and non-steady-state weathering, and petrogenesis of siliciclastic sands and muds. Journal of Geology., 105, 173–191.

Ollier, C. D., 1990. Morphotectonics of the Lake Albert Rift Valley and its significance for continental margins. In: Logatchev, N. A., Zwart, H. J. (Eds.), Intracontinental Mountainous Terranes. Journal of Geodynamics, 11, pp. 343–355.

Osmaston, H. A., 1989. Glaciers, glaciations and equilibrium line altitude on the Rwenzori. In: Mahaney, W. C. (Ed.), Quaternary and Environmental Research on East African Mountains. Balkema, Rotterdam/Brookfield, pp. 31–104.

Parker, A., 1970. An index of weathering for silicate rocks. Geological Magazine, 107, 501–504.

Pickford, M., Senut, B., Poupeau, G., Brown, F., Haileab, B., 1991. Correlation of tephra layers from the Western Rift Valley (Uganda) to the Turkana Basin (Ethiopia/Kenya) and the Gulf of Aden. Stratigraphy, 313, 223–229.

Pickford, M., Senut, B., Hadoto, D., 1993. Geology and Palaeobiology of the Albertine Rift Valley Uganda-Zaire, Volume I: Geology, International Center for Training and Exchanges in the Geosciences, Orleans.

Roller, S., Hornung, J., Hinderer, M., Ssemmanda, I., 2010. Middle Miocene to Pleistocene sedimentary record of rift evolution in the southern Albertine Graben (Uganda). International Journal of Earth Sciences, 99, 1643–1661.

Rudnick, R. L., Gao, S., 2003. Composition of the continental crust. Treatise on Geochemistry, 3, 1–64.

Russell, R. D., Taylor, R. E., 1937. Roundness and shape of Mississippi River sands. The Journal of Geology, 45, 225–267.

Schlüter, T., 2008. Geological Atlas of Africa, 2nd edition, 307 p., Springer Verlag, Berlin.

Singh, P., 2009. Major, trace and REE geochemistry of the Ganga River sediments: influence of provenance and sedimentary processes. Chemical Geology, 266, 242–255.

Stallard, R. F., 1985. River chemistry, geology, geomorphology, and soils in the Amazon and Orinoco basins. In: Drever, J. I. (Ed.), The chemistry of weathering: Dodrecht, D. Reidel, pp. 293–316.

Suttner, L. J., Basu, A., Mack, G. H., 1981. Climate and the origin of quartz arenites. Journal of Sedimentary Petrology, 51, 1235–1246.

Taylor, R. G., Howard, K. W. F., 1998. Post-paleozoic evolution of weathered landsurfaces in Uganda by tectonically controlled deep weathering and stripping. Geomorphology, 25, 173–192.

Taylor, R. G., Howard, K. W. F., 1999a. Lithological evidence for the evolution of weathered mantles in Uganda by tectonically controlled cycles of deep weathering and stripping. Catena, 35, 65–94.

Taylor, R. G., Howard, K. W. F., 1999b. The influence of tectonic setting on the hydrological characteristics of deeply weathered terrains: evidence from Uganda. Journal of Hydrology, 218, 44–71.

Taylor, R. G., Mileham, L., Tindimugaya, C., Mwebembezi, L., 2009. Recent glacial recession and its impact on alpine riverflow in the Rwenzori Mountains of Uganda. Journal of African Earth Science, 55, 205–213.

Uganda Government, 1967. Uganda.Soils.

Van de Kamp, P. C., 2010. Arkose, subarkose, quartz Sand, and associated muds derived from felsic plutonic rocks in glacial to tropical humid climates. Journal of Sedimentary Petrology, 80, 895–918.

Van Loon, A. J., Mange, A. M. 2007. “In situ” dissolution of heavy minerals through extreme weathering, and the application of the surviving assemblages and their dissolution characteristics to correlation of Dutch and German silver sands. In: Mange, M. A., and Wright, D. T. (Eds.), Heavy minerals in use. Amsterdam, Elsevier, Developments in Sedimentology Series, 58, pp. 189–213.

Velbel, M. A., 1992. Geochemical mass balances and weathering rates in forested watersheds of the southern blue ridge. III. Cation budgets and the weathering rate of amphibole. American Journal of Earth Science, 292, 58–78.

Verma, S. P., Armstrong-Altrin, J. S., 2013. New multi-dimensional diagrams for tectonic discrimination of siliciclastic sediments and their application to Precambrian basins. Chemical Geology, 355, 117–133.

Weltje, G. J., von Eynatten, H., 2004. Quantitative provenance analysis of sediments: review and outlook. Sedimentary Geology, 171, 1–11.

White, A. F., Brantley, S. L., 2003. The effect of time on the weathering of silicate minerals: why do weathering rates differ in the laboratory and field?. Chemical Geology, 202, 479–506.

Yang, S., Li, C., Lee, C. B., Na, T. K., 2003. REE geochemistry of suspended sediments from the rivers around the Yellow Sea and provenance indicators. Chinese Science Bulletin, 48, 1135–1139.

Zuffa, G. G., 1985. Optical analysis of arenites: influence of methodology on compositional results. In: Zuffa, G. G. (Ed.), Provenance of arenites. Dordrecht, Reidel, NATO ASI Ser., 148, 165–189.

Chapter 3

3 Garnet and rutile mineral chemistry and zircon U-Pb ages of modern river sands along the western East African Rift (Albertine Rift, Uganda)

* unpublished manuscript

3.1 Abstract

Garnet, rutile and zircon are reliable indicator minerals for provenance reconstructions. This paper documents geochemical compositions of detrital garnet and rutile, and U-Pb ages of detrital zircon of modern stream sediments from the eastern rift shoulder of the Albertine Rift in western and southwestern Uganda, to test to what extend garnet, rutile and zircon reflect the framework geology of the study area. The analyzed river sediments represent two different geomorphological settings along the Albertine Rift, including the high-altitude > 5000 m high Rwenzori Mountains and poorly-drained lowlands of the rift plateau, in which two fundamental types of sediment is generated.

The results of this study show that all three mineral types very well reflect the geological situation in Uganda, and that different geological units are clearly distinguishable by the application of garnet, rutile and zircon. Streams that drain high-grade metamorphic rocks of the Neoarchean North Uganda Terrane (NUT) are characterized by high-almandine, low-spessartine garnet with two groups of varying grossular contents (< 10% and > 10%). Rutile is mainly of metapelitic origin according to Cr and Nb contents, and exhibits amphibolite-/eclogite-facies to granulite-facies Zr-in-rutile formation temperatures. The Neoarchean age of the NUT is confirmed by zircon U-Pb ages mainly ranging between ~2.7–2.4 Ga, with major cluster at 2.5–2.6 Ga. Rivers that mainly erode metasedimentary rocks of the Paleoproterozoic Rwenzori Fold Belt (RFB) are identified by almandine-spessartine garnet. Rutile formation temperatures are lower than for the NUT and mainly point to amphibolite-/eclogite-facies metamorphic conditions during rutile formation. Zircon geochronology exhibits two major populations at ~2.2–2.0 Ga and ~1.95–1.75 Ga, that correspond with the Eburnian Orogenic Cycle (2.20–1.85 Ga) in Uganda during which the fold belt evolved. Mixing of detritus from different sources within the Ugandan basement is indicated for Neoproterozoic platform sediments of the Bunyoro Group overlying the NUT in western and central Uganda. These rocks exhibit a wide range of zircon ages, including Mesoarchean, Neoarchean, Paleoproterozoic, Mesoproterozoic and Neoproterozoic ages, which do not reflect the actual depositional age of the Bunyoro Group of < 765–735 Ma. Rutile assemblages are similar to the Neoarchean units and might reflect primary erosion of the underlying basement or their recycled products within the Bunyoro Group.

3.2 Introduction

Heavy minerals are useful indicators for provenance determination, because their composition strongly depends on the composition of the parent rock (Morton, 1985). Provided that there are distinguishable differences within the source area, heavy minerals may be directly linked to the chemistry and tectonostratigraphic level of a specific rock suite. During the last decades, mineral chemical analyses and mineral dating became an integral part of many (sedimentary) provenance studies (Mange and Wright, 2007; von Eynatten and Dunkl, 2012, and references therein). Chemical analyses of a certain mineral type conducted by electron microprobe measurements provide a fast and precise way to receive essential information not only about the chemical/mineralogical composition of the source rock, but also about temperature and pressure conditions during rock formation. Furthermore, radiometric dating of detrital minerals by laser ablation-inductively coupled plasma-mass spectrometry

(LA-ICP-MS) is a key method for provenance reconstructions, because the age of a single grain can be directly associated with a certain crystallization event in the source area (Thomas, 2011; Gehrels, 2014). In this study, garnet and rutile were chosen for chemical analyses and zircon for mineral dating, because these minerals are by far the most frequently used mineral types in varietal studies, and they proofed to be reliable indicators in many provenance studies (e.g., Morton, 1985; Sabeen et al., 2002; Zack et al, 2004; Aubrecht et al., 2009; Morton and Chenery, 2009; Triebold et al., 2012; Andò et al., 2014; Schneider et al., 2016b, 2017). Garnet manifested as a sensitive index mineral, because of its wide range of compositional variations, mostly representing a solid solution of six principle end-members (almandine, pyrope, spessartine, grossular, andradite, and uvarovite), but also because of its importance in defining metamorphic conditions (Mange and Morton, 2007). Rutile shows host-rock specific geochemical variations, e.g., in the Cr and Nb contents, whereas the Zr content included in rutile gives information about temperature conditions during formation (summary in Meinhold, 2010). Geochronological studies have been applied on zircon, because it occurs in a variety of lithologies, it is ubiquitous in sediments, and resistant against metamorphism, which is an important aspect when studying the oldest cratons in the world. A further advantage of all of these mineral types is their high stability and resistance during transport and (chemical) weathering (Morton and Hallsworth, 1999). Although, the application of compositional data is highly promising, the results might be misleading, if not integrated with information from the whole sediment assemblage. This is especially the case when sediment derives from older recycled sedimentary rocks, which already experienced more than one sedimentary cycle. In this case, the heavy minerals might not reflect their actual rock suite, but the sources from which they originated in first place. Furthermore, external processes operating during transport and deposition might affect the heavy minerals (e.g., Morton and Hallsworth, 1999). Studies on garnet compositions emphasized the sensitivity of garnet against hydraulic sorting processes during transport (Krippner et al., 2015). The authors showed that the occurrence of certain garnet types depends on the analyzed grain size fraction, e.g., grossular-rich garnet is more frequent in smaller grain-size fractions, whereas pyrope-rich garnet shows higher abundances in the coarser grain-size fractions. This might lead to misinterpretation of heavy mineral suites and finally to incorrect provenance reconstructions.

In this study, we combined garnet and rutile mineral chemistry and U-Pb dating of detrital zircon on modern stream sediments along the Albertine Rift in western and southwestern Uganda to test to what extend the three mineral types reflect their underlying basement geology. Exposed rock suites within the study area include a variety of well distinguishable lithologies, including Archean high-grade crystalline terrains, Paleoproterozoic fold belts, and Neoproterozoic quartzose molasse-type platform sediments. This research aims at identifying the characteristics of the different lithologies in order to contribute to a broader understanding of the geological framework of Uganda, and to define potential sources for the Neogene rift sediment within the Albertine Graben, which is important for provenance and paleotectonic reconstructions of the northern western branch of the East African Rift System (EARS) (see chapters 4 – 7). Furthermore, the Albertine Rift offers a superb opportunity to test the reliability of garnet, rutile and zircon as fingerprinting minerals. In this tectonically active rift setting, thermal-induced rift-flank uplift results in contrasting topography between low-relief rift plateaus and adjacent high-altitude horsts such as the Rwenzori massif (Ebinger, 1989; Chorowicz, 2005). In vicinity to the equator, the climate is hot and humid, and chemical weathering may be so strong that provenance signatures may be largely lost and even detritus derived from crystalline basement rocks reduced to quartzose sand (Garzanti et al., 2013; Schneider et al., 2016b).

The stream sediments analyzed in this study have been previously studied for their petrographic and geochemical composition to quantify the effects of chemical weathering on the constitution of the sediment, and to ascertain whether the initial lithological signature is preserved in clastic sediments even under extreme climatic conditions (Schneider et al., 2016a). This study demonstrates that

sediment generated in different geomorphological settings along the Albertine Rift in Uganda (e.g., poorly-drained lowlands, high-altitude massifs) is of two fundamental types. The high-relief Rwenzori Mountains shed sand rich in feldspar and rock fragments with very rich heavy mineral assemblages dominated by amphibole and epidote. In this high-altitude setting, sediment generation is largely controlled by rapid physical degradation rather than intense chemical alteration. In contrast, sediment generation in low-relief plateau regions is largely the effect of intense chemical weathering leading to highly quartzose sand. Although, original provenance signatures might be blurred in areas characterized by extreme climatic conditions, it could be shown that the imprint of the source-rock lithology is partly preserved by heavy minerals and geochemical parameters, especially non-mobile elements (e.g., Th/Sc ratio and REE).

In this contribution, we present the first garnet and rutile compositional data, as well as U-Pb zircon ages for streams draining the Ugandan basement, which will enhance our understanding of the regional geology and erosional processes in this particular rift setting.

3.3 Geological and geochronological setting

The study area follows the eastern rift flank of the Albertine Rift in western and southwestern Uganda (0.1–1.5°N, 30.0–31.3°E). This includes the > 5000 m above sea level high Rwenzori Mountains, located between the sub-basins of Lake Albert and Lake George, where they form a promontory of the eastern rift shoulder of the Albertine Rift (Bauer et al., 2010, 2013; Ring, 2008, 2014). The geological record of Uganda covers more than three billion years. The uplifted basement along the eastern flank of the graben structure belongs to the proto-Congo Craton, and consists of Archean terranes, enclosed or penetrated by Paleo-, Meso- and Neoproterozoic fold belts (Westerhof et al., 2014). These mobile belts represent the Eburnian (2.20–1.85 Ga), Grenvillean (1.10–0.95 Ga) and Pan-African (0.75–0.50 Ga) Orogenic Cycles in Uganda (Condie, 1998, 2000, 2001). Each orogenic cycle was followed by deposition of post-orogenic molasse-type platform deposits (Fig. 3-1).

The Archean basement is divided into four tectono-thermal terranes, each of which experienced a different geodynamic evolution (Westerhof et al., 2014). The Tanzania Craton, which occupies major parts in southern-central Uganda, comprises the granite-greenstone suite of the Lake Victoria Terrane (LVT) and the granite-gneissic-migmatitic unit of the West Tanzania Terrane (WTT). For both terranes a Neoarchean age (~2.63–2.59 Ga and 2.65–2.64 Ga, respectively) has been determined (Mänttäri, 2014). The northern part of Uganda is composed of Archean high-grade gneissic-granulitic lithologies of the West Nile Block (WNB) and the North Uganda Terrane (NUT), both belonging to the NE Congo-Uganda Shield (Leggo, 1974). The WNB is composed of a Mesoarchean core (Uleppi Complex; > 3.08 Ga) overlain by mafic volcanic rocks of the War Group (~2.64 Ga) and accreted with Neoarchean (> 2.63–2.59 Ga) rocks of the Arua-Lobule Supergroup (Westerhof et al., 2014). The NUT is the largest tectono-thermal unit and occupies the northern part of the former ‘Ugandan Basement Complex’ (MacDonald, 1966) or ‘Archean Gneiss-Granulite Complex’ (Schlüter, 2008). The unit consists of a Mesoarchean nucleus (2.99 Ga), called the Karuma Complex, cropping out along the northern sector of the Albertine Graben (Westerhof et al., 2014). The complex is mainly composed of felsic and mafic granulitic metasedimentary rocks (van Straaten, 1971, 1976). Neoarchean supracrustal rocks of the NUT comprise granitoids, gneiss and migmatite of igneous or uncertain origin with most of the gneissose-migmatitic rocks showing U-Pb zircon ages between 2.6 and 2.5 Ga. The Rwenzori Fold Belt (RFB) occupies large parts of southern and southwestern Uganda, where it stretches from the western shore of Lake Victoria in the east towards the Rwenzori Mountains in the west. It separates the Archean granite-greenstone terranes of the Tanzanian Craton to the south from the Archean high-grade gneissic-granulitic terranes of the NUT. Lithologically, the mobile belt is composed of a gneissose-granitoid basement (2.21–2.15 Ga) related to the Eburnian I Orogenic Cycle

('Rukungiri Suite'), overlain by metasedimentary rocks (schist, phyllite, quartzite, and rare marble and calc-silicate), amphibolite and mafic volcanic rocks of the Buganda Group (~2.00–1.95 Ga). Within the RFB, syn-tectonic (1.99–1.96 Ga) and post-tectonic granitoids (1.85 Ga) were emplaced during the Eburnian II Orogenic Cycle. The Eburnian Orogenic event was shortly followed by deposition of post-tectonic molasse-type sediment of the Namuwasa (< 2.05 Ga and >1.85 Ga) and Bwezigoro groups (< 1.97 Ga) and the Kagera-Buhweju Supergroup (1.79 Ga). Mesoproterozoic rocks, largely correlated with the Grenvillean Orogenic Cycle (1.15–0.95 Ga), are represented by granitoids (1.40–1.33 Ga) and terrigenous metasediment of the North Kibaran Belt (~1.55−0.95 Ga) in southwestern Uganda, and by metamorphic volcanic rocks (0.98 Ga), metasediment (< 1.0 Ga) and rare ultramafic rocks of the Madi-Igisi Belt in northwestern Uganda; a narrow, intracratonic thrust and shear belt, separating the WNB from the NUT. In the early Neoproterozoic, extension of the proto-Congo Craton gave rise to deposition of platform rocks of the Malagarasi Supergroup during two depositional cycles between 880 and 820 Ma (Johnson et al. 2007), and at ~765 Ma (Key et al. 2001). In southern Uganda, these rocks are composed of molasse-type rocks (conglomerate, sandstone, siltstone) of the Mityana Group (890–790 Ma), cropping out in small patches west of Lake Victoria. In western-central Uganda, they belong to the Bunyoro Group cropping out in a sector that stretches from the eastern shore of Lake Albert towards Lake Kyoga in central Uganda (Bjørlykke, 1973, 1981). The rocks of this unit comprise shale, arkose, phyllite and quartzite that overlie basal tillite-like rocks. In places, the rocks of the Bunyoro Group show weak deformation and distinct tilting and folding (Westerhof et al., 2014). The glaciogenic deposits at the bottom of this group are assigned to represent ages of 765–735 Ma, whereas the overlying lithologies are consequently younger (Westerhof et al., 2014). The Pan-African Orogenic Cycle (~900−550 Ma), which led to the creation of the Gondwana Supercontinent, is represented by the East African Orogen (EAO). This poly-cycle mobile belt developed in northern Uganda between 830 Ma and 550 Ma and is composed of high-grade supracrustals, amphibolite, granitoid, granulite, and charnockite interlayered with older crust, and intruded by granitoids (950 Ma). A series of in situ Pan-African granitoid bodies (660 Ma) belonging to the E-W-trending Central African Fold Belt (CAFB) crop out in the northernmost part of Uganda (in the WNB and NUT). The Phanerozoic evolution of Uganda is associated with the breakup of the Gondwana continent leading to activation of older suture zones. It is manifested by the emplacement of a number of post-Pan-African (~550−440 Ma) alkaline complexes along a weakness zone that developed later into the eastern branch of the East African Rift System (EARS). Karoo sediments (290−180 Ma) are only present in small patches in southern Uganda. Most of these sediments were probably eroded in the course of the evolution and uplift of the EARS (Westerhof et al., 2014). Late Eocene-Neogene rifting and development of the EARS in Uganda is represented by the Elgon Complex in eastern Uganda, comprising basal sediment, covered predominantly by pyroclastic and volcanic rocks and associated carbonatite plugs and fenites of Neogene (20−18 Ma) age (Davies, 1952, 1956). The Albertine Supergroup that covers the Albertine Rift in western Uganda comprises strongly silica-undersaturated lavas including kamafugites and carbonatites (Barker and Nixon, 1989; Foley et al., 2012), and fluvio-lacustrine rift sediments (Pickford et al., 1993; Roller et al., 2010).

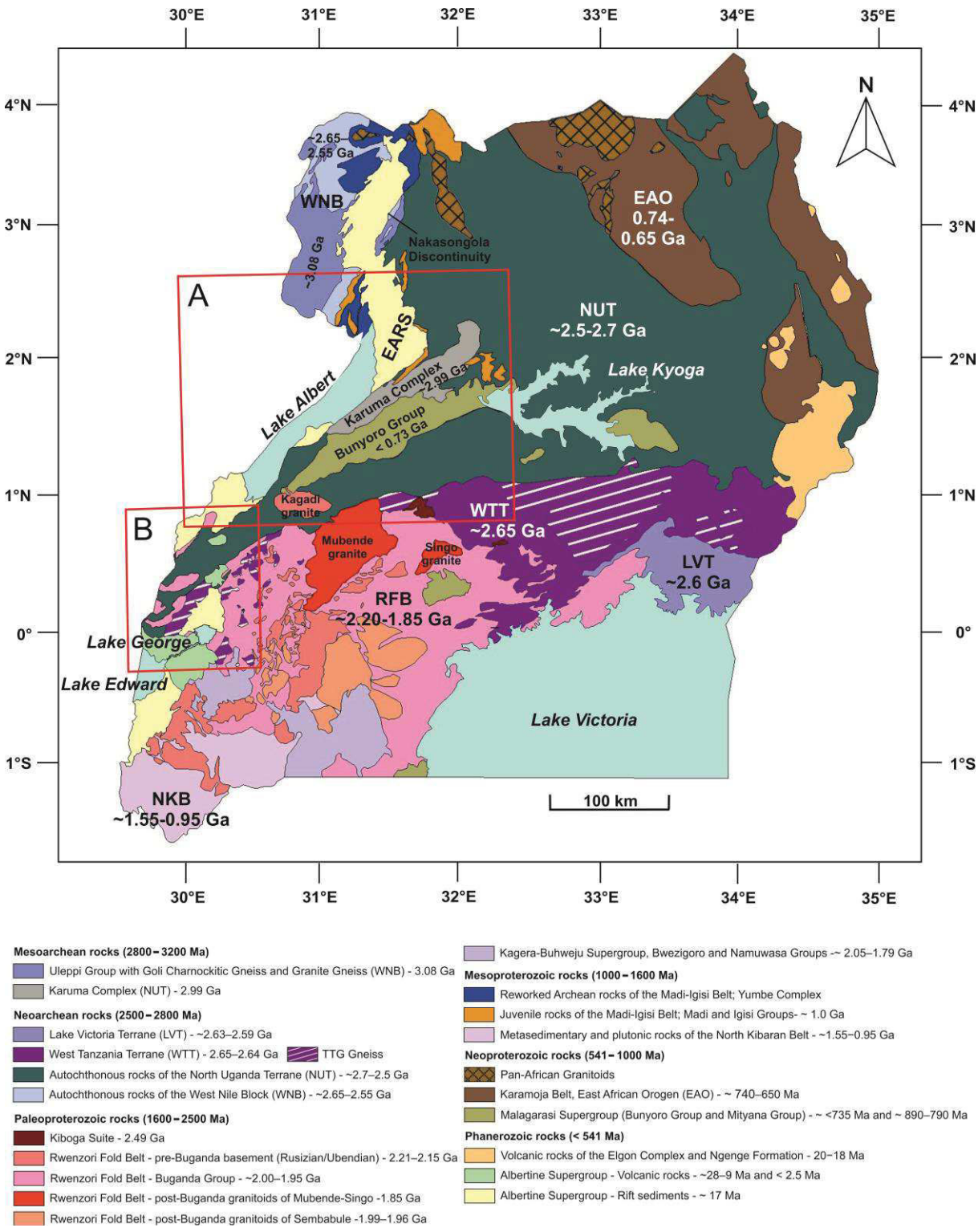

Figure 3-1. Geological and geochronological outline of Uganda after Westerhof et al. (2014) with age determinations adopted from Mänttäri (2014).

3.4 Methods

3.4.1 Sampling and sample description

Samples from fourteen rivers draining the Rwenzori Mountains and the eastern rift flank of the Albertine Rift were analyzed in this study (Figs. 3-2, 3-3). Rivers include major streams, but also lower-order tributaries. The samples represent different rock lithologies within the Ugandan basement. Rivers east of Lake Albert include the Wambabya and Muzizi Rivers, as well as two lower order tributaries to the Nkusi River, that either drain gneiss and granulite of the NUT, (meta-) sedimentary rocks of the Bunyoro Group, and/or the Kagadi granite complex belonging to the RFB. Rivers in southern Uganda that dewater into Lake George include the Dura River, the lower section of the Mpanga River, and three tributaries to both streams. Rivers draining the Rwenzori Mountains comprise the Dunga, Mubuku, Isebo, and Nyamwamba Rivers. Major rock lithologies for the samples in southern Uganda, including the Rwenzori Mountains, are the metamorphic basement of the RFB and/or the underlying Archean gneiss-granulite complex (NUT or TTG gneiss of the WTT).

Sample localities, river names / ID's and major basement lithologies are shown in Fig. 3-3. The analytical data referred to in this chapter are included in the Appendix.

Figure 3-2. Impressions of sampling sites for the modern river sediment.

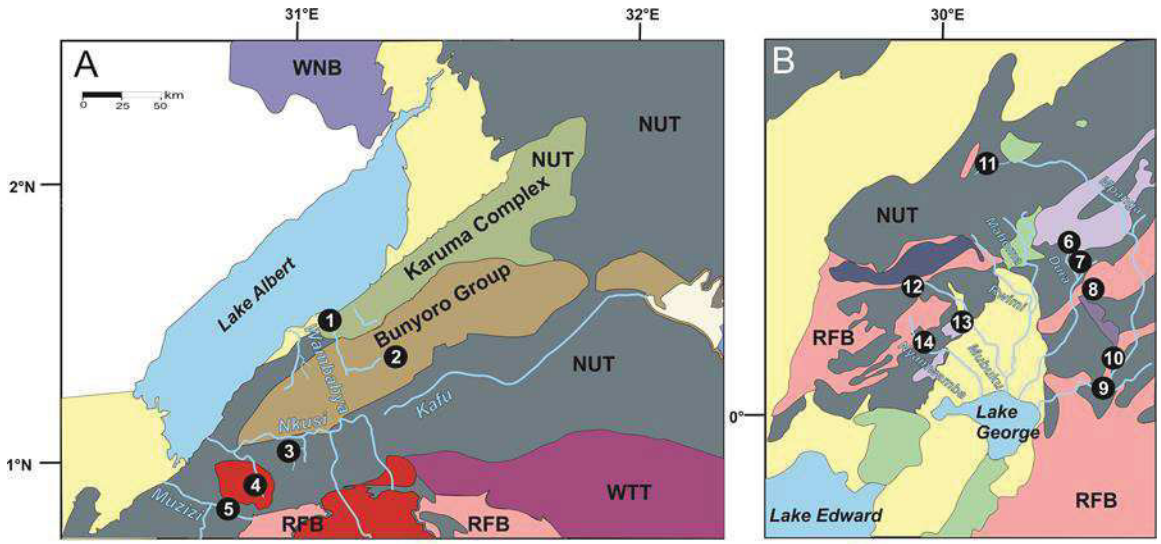

1 = Wambabya (GPS 58)
2 = trib. Wambabya (GPS 59)
3 = trib. Nkusi (GPS 64)
4 = trib. Nkusi 2 (GPS 65)
5 = Muzizi (GPS 66)
6 = Dura (GPS 70)
7 = trib. Dura (GPS 71)
8 = trib. Dura 2 (GPS 72)
9 = Mpanga (GPS 73)
10 = trib. Mpanga (GPS 75)
11 = Dunga (GPS 92)
12 = Mubuku (GPS 96)
13 = Isebo (GPS 97)
14 = Nyamwamba (GPS 98)

Heavy mineral distribution
Zircon
Tourmaline
Rutile
Epidote
Garnet
Amphibole
Sillimanite
Kyanite
Pyroxene
Other

Mesoarchean rocks (3200 - 2800 Ma)
Karuma Complex (metasedimentary granulite)
Neoarchean rocks (2800 - 2500 Ma)
West Tanzania Terrane (para- and orthogneiss, migmatite, granitoid)
North Uganda Terrane (granitoid, gneiss and migmatite of igneous or uncertain origin)
West Nile Block (granulite, charnockite, gneissose granitoid, metavolcanic and subvolcanic rocks, gneiss, schist)
Palaeoproterozoic rocks (2500 - 1600 Ma)
Rwenzori Fold Belt - Mubende-Singo Suite (porphyric granite; ~1.85 Ga)
Rwenzori Fold Belt - Buganda Group (slate, phyllite, mica schist)
Rwenzori Fold Belt - Buganda Group (quartzite)
Rwenzori Fold Belt - Buganda Group (amphibolite)
Rwenzori Fold Belt - Buganda Group (metasandstone)
Neoproterozoic rocks (1000 - 541 Ma)
Bunyoro Group (slate, shale, phyllite, sandstone, quartzite)
Phanerozoic rocks (< 541 Ma)
Albertine Group (volcanic rocks)
Albertine Group (rift sediment)

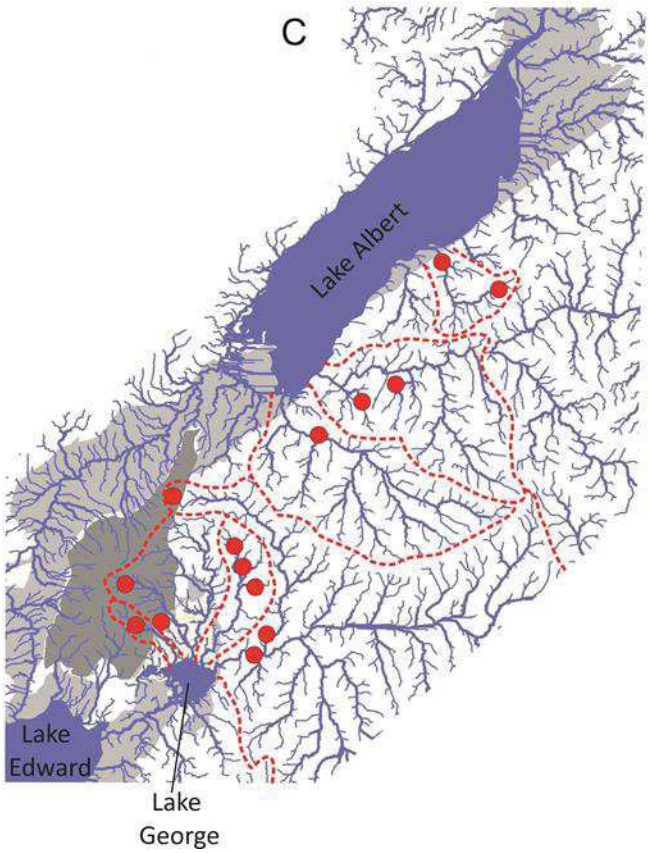

Figure 3-3 (previous page). Geological maps showing the sampling sites of analyzed modern river sands along the eastern rift flank of Lake Albert (A), and along the rift plateau north and east of Lake George and in the Rwenzori Mountains (B). Given are the river names, sample ID's and associated heavy mineral compositions for each sample as analyzed by Schneider et al. (2016a). (C) Modern hydrology of the study area with sampling sites (red points) and catchment boundaries (red dotted lines).

3.4.2 Garnet and rutile chemistry

Garnet and rutile chemistry was performed on 278 grains from five river sands, and 478 grains from eleven river sands, respectively. Heavy minerals from the grain size fraction 63–125 µm were separated by density settling in Na-polytungstate. Garnet and rutile grains were handpicked from the heavy mineral residues with a needle under the binocular microscope, placed on double-sided adhesive tape, mounted in epoxy resin, and polished. Bias has been avoided by randomly picking of every grain encountered during transverses across the residue. The samples were coated with carbon to ensure conductivity, and analyzed using a Jeol JXA-2800 electron microprobe equipped with a five wavelength dispersive spectrometer at the Johannes Gutenberg University of Mainz. An accelerating voltage of 15 kV and beam current of 20 nA was used for garnet element content of Si, Mg, Ca, Fe, Al, Ti, Cr and Mn with counting times of 15 s, except Ti, Cr and Mn with 30 s. Rutile grains were analyzed for Nb, Al, Cr, Zr and V with counting times of 200 s, Si and Fe with counting times of 100 s and Ti with counting times of 15 s. Measuring conditions include an accelerating voltage of 25 kV and a beam current of 80 nA.

The chemical composition of garnet was recalculated to the six end-members almandine, spessartine, pyrope, grossular, andradite, and uvarovite, with the structural formula based on 12 oxygen atoms and 8 cations (Deer et al., 1997). Fe^{2+} and Fe^{3+} contents were determined assuming stoichiometry. Rutile growth temperatures were calculated using the thermometer after Tomkins et al. (2007) in the α-quartz field after the following equation:

$$T(°C) = [(83.9 + 0.410 \times P)/(0.1428 - R \times \ln (Zr_{ppm})] - 273$$

with P is the pressure, 10 kbar, and R is the gas constant, 0.0083144 kJ K^{-1}.

3.4.3 Zircon geochronology

U-Pb zircon geochronology was carried out on nine river samples. Zircons of the grain size fraction 63–125 µm were separated from the bulk samples in heavy liquids (Na-polytungstate) and finally handpicked under a binocular microscope. Zircon grains were mounted in epoxy resin, sectioned and polished. Prior to analysis, cathodoluminescence (CL) images were conducted on all grains using a cathode luminescence detector connected to a Jeol JXA-2800 EMP device at the Johannes Gutenberg University Mainz to unveil internal structures and to target specific areas within them. U-Pb zircon geochronology was performed on 60 randomly picked grains by LA-ICP-MS using an Agilent 7500ce quadrupole inductively coupled mass spectrometer linked to an UP-213 Nd:YAG-laser system from New Wave with 213 nm wavelength at the Johannes Gutenberg University Mainz. Ablation was performed in a low-volume laminar flow cell, which is flushed by helium as carrier gas. Before reaching the torch, argon gas is added. All data were obtained from single spot measurements using a spot size of 30 µm and a total measuring time of 80 s, consisting of 30 s warm up, 30 s dwell and 20 s washout time. The repetition time was 10 Hz at an energy density of 3.6 J/cm^2. Calibration was assured by measuring the standard zircons 'GJ-1' (Jackson et al. 2004), 'Plesovice', '91500N', '91500A' and 'Temora' (Black et al., 2003; Nasdala et al., 2008) in defined intervals at the beginning,

during, and at the end of each measuring cycle. Following masses were analyzed: ^{202}Hg, ^{204}(Pb + Hg), ^{206}Pb, ^{207}Pb, ^{208}Pb, ^{232}Th, ^{235}U, and ^{238}U. Raw data were processed using Glitter Software (van Achterbergh et al., 2000). Probability density distribution and histogram plots were produced using Isoplot 3.75 (Ludwig, 2012). Zircon ages are defined as concordant, if Pb-Pb and U-Pb ages differ less than 10%. Zircons that yield discordant ages and those that give unreliable isotopic ages during measurement were not considered for data interpretation and for diagrams. Ages > 1 Ga were calculated using ^{207}Pb/^{206}Pb ratios, whereas ages < 1 Ga were obtained using ^{206}Pb/^{238}U. This is because ^{207}Pb/^{206}Pb ages become imprecise below < 1 Ga due to poorer counting statistics (Gerdes and Zeh, 2006; Sircombe, 2000). Furthermore, a total of 1898 zircon grains from the nine samples have been studied for their internal structures as revealed by CL images to conclude about the geologic history of the mineral grains, especially about magmatic and metamorphic (re-) crystallization events. Therefore, each of the counted grains was assigned to a certain morphotype group according to the template provided by Corfu et al. (2003).

3.5 Results

3.5.1 Garnet chemistry

The garnet compositions from five river sands are summarized in Table 3-1 and are shown as ternary diagrams using almandine plus spessartine (Al+Sp), pyrope (Pyr) and grossular (Gro) as poles (Fig. 3-4). The samples show variable garnet compositions. Overall, three garnet cluster could be identified.

Garnet of Cluster I is rich in almandine (~62–80%), low to medium in pyrope (~6–33%), low in spessartine (~1–8%) and grossular (~1–18%). This garnet dominates in a small tributary stream to the Nkusi River that drains gneissic rocks of the Archean NUT east of Lake Albert, but has not been recognized in any other locality.

Garnet of Cluster II is rich in almandine (~39–63%), medium in pyrope (~17–41%) with minor spessartine (~1–3%), but exhibits a higher grossular component (~10–21%) than garnet of Cluster I. It occurs in all samples from southwestern Uganda, and is dominant in the Dunga River that drains gneissic units of the northern flank of the Rwenzori Mountains.

Garnet of Cluster III represents an almandine-spessartine solid solution (~16–80% almandine; ~12–75% spessartine) with low pyrope (~8–14%) and grossular (<15%) contents. This garnet type is present in all rivers that receive input from medium- to high-grade metasedimentary rocks of the RFB and is dominant in the Nyamwamba River in the central Rwenzori Mountains that erodes schist of the Buganda Group. In a tributary stream of the Dura River (GPS 71), this garnet group shows a more distinct separation between the almandine and spessartine end-members and can be subdivided into garnet with a higher almandine content (~69–82%), and garnet with a higher spessartine component (~41–59%).

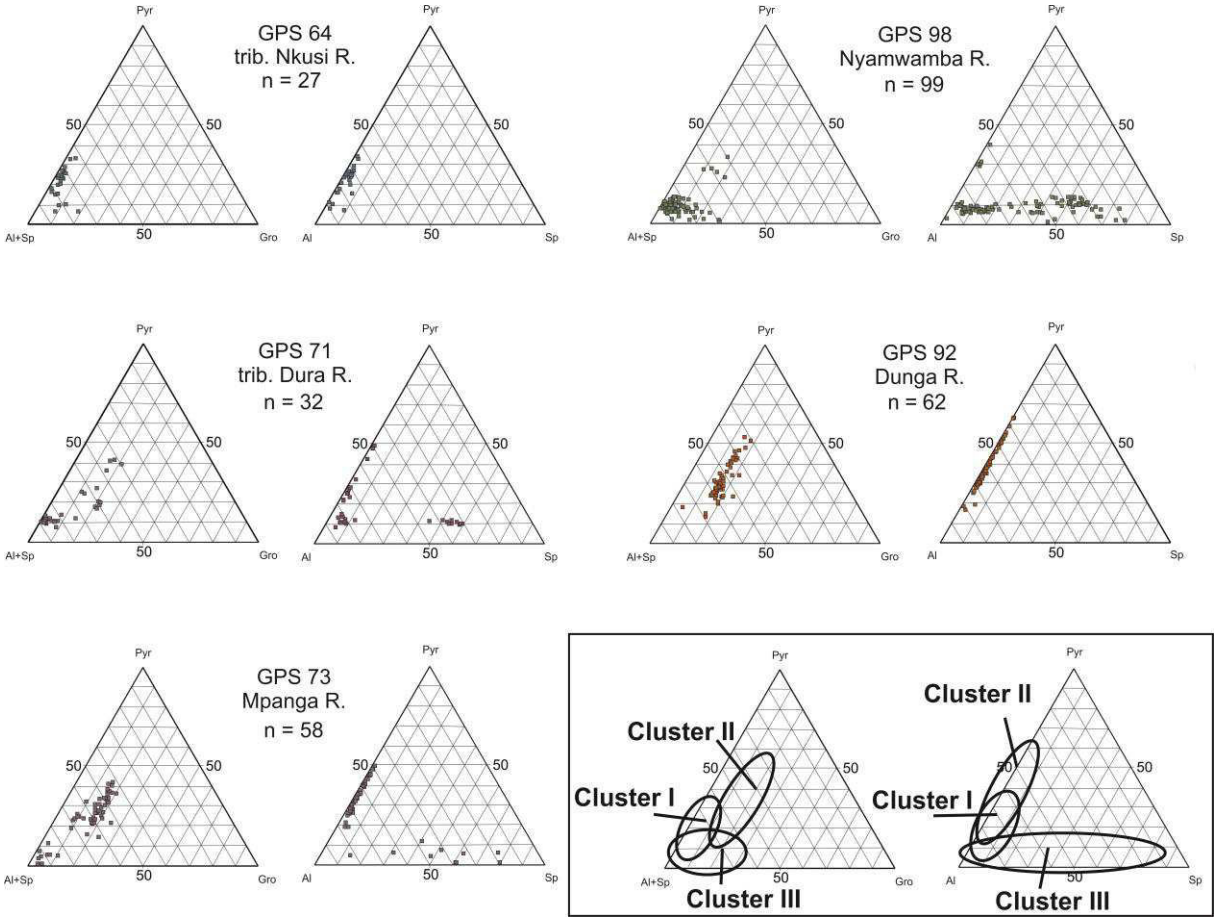

Figure 3-4. Results of garnet chemistry illustrated in Al+Sp-Gro-Pyr ternary diagrams with Al = almandine, Sp = spessartine, Gro = grossular, and Pyr = pyrope.

3.5.2 Rutile chemistry

The results of rutile measurements of eleven stream sediments are summarized in Table 3-1 and illustrated in Fig. 3-5. All analytical data are compiled in the Appendix.

For the majority of rutile grains representing streams along the eastern rift flank of Lake Albert, an origin from metapelitic rocks (78–92%) is indicated by Cr-Nb chemistry (Triebold et al., 2012). Zr-in-rutile thermometry indicates amphibolite-/eclogite-facies to granulite-facies conditions during rutile formation, mainly between ~555 and 890 °C, with most grains pointing to upper amphibolite-/eclogite-facies and lower granulite-facies conditions. Formation temperatures are slightly lower for the bulk of rutile grains from the Wambabya River eroding the (meta-) sedimentary Bunyoro Group. They exhibit upper amphibolite-/eclogite-facies conditions with few grains pointing to a granulitic source. One grain reveals a very high Zr-in-rutile temperature of 977 °C.

Rutile assemblages in rivers draining southern Uganda show distinct variations in Cr and Nb contents. The majority of rutile grains of the Mpanga River and of one of its tributary rivers represent an origin from metapelitic rocks (89% and 80%, respectively). Samples from the Dura River and its tributary are characterized by higher contents of metamafic rutile (45% and 56%). The tributary river is characterized by a bimodal array of rutile grains. The first rutile cluster shows high Cr contents between 3930 ppm and 8190 ppm, and low Nb contents mainly < 2000 ppm. The opposite is true for

the second cluster, identified by rutile grains exhibiting low Cr contents (92–1200 ppm) and high Nb concentrations, generally > 4000 ppm. With exception of the Mpanga River, rutile thermometry exhibits a narrow temperature range with most rutile formed under amphibolite-/eclogite-facies metamorphic conditions. The Mpanga River shows a bimodal frequency distribution of rutile temperatures with two peaks at ~590 °C and ~715 °C that correspond to medium amphibolite-/eclogite-facies conditions and upper amphibolite-/eclogite-facies conditions, respectively.

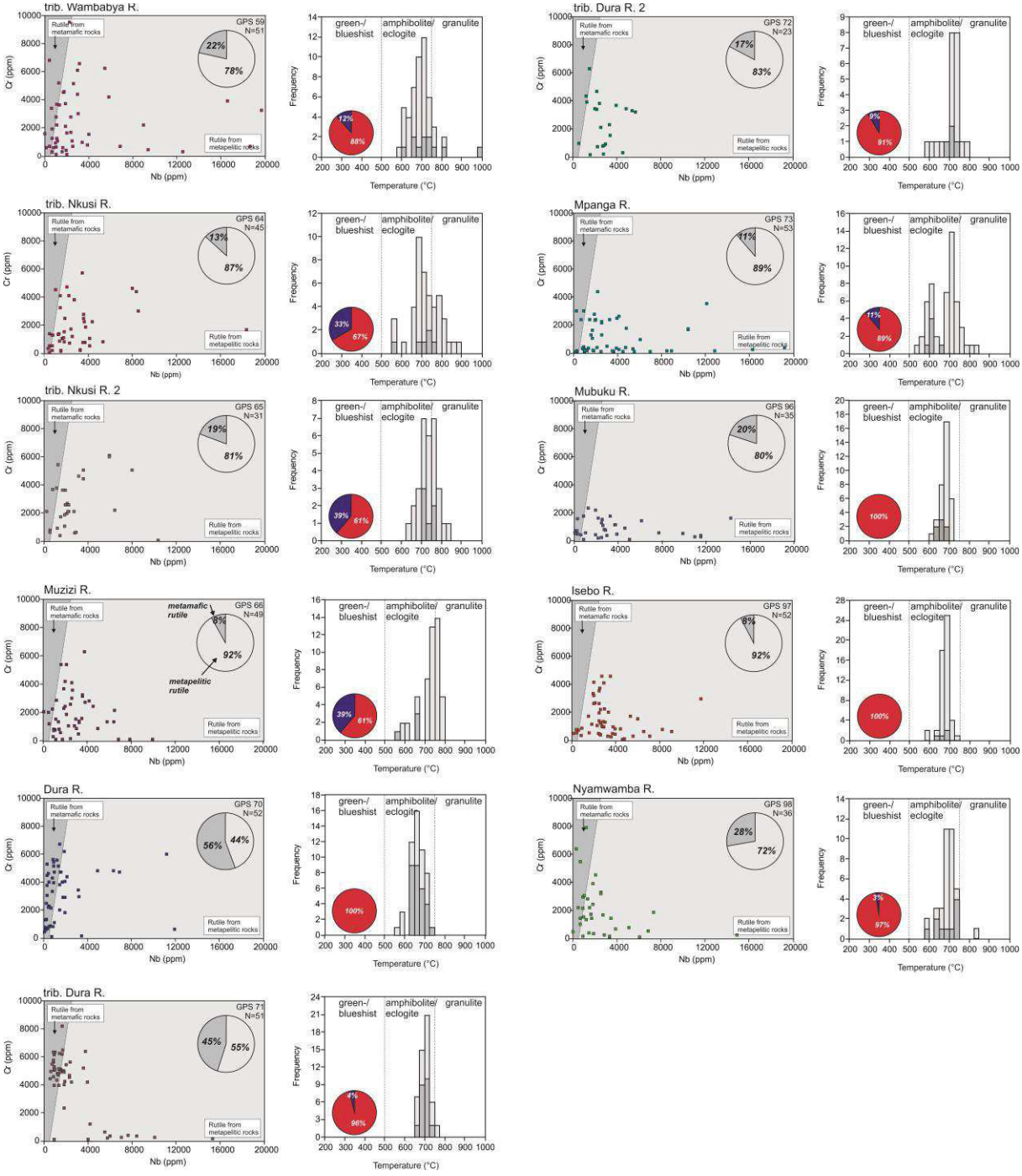

Figure 3-5. Rutile chemistry. (left) Cr vs. Nb plot with discrimination fields after Triebold et al. (2012), (right) Zr-in-rutile formation temperatures calculated after Tomkins et al. (2007).

Detrital rutile from rivers draining the Rwenzori Mountains exhibits different Cr and Nb contents. The samples are dominated by metapelitic rutile with 72% for the Nyamwamba River, 80% for the Mubuku River, and 92% for the Isebo River. Rutile in the Mubuku River shows less variability in Cr values (~90–2350 ppm), but a higher spread in the Nb content (~64–14260 ppm). In the Isebo River, most grains have Cr contents < 2000 ppm and variable Nb contents ranging between ~130 ppm and 11740 ppm. A subordinate group of rutile is characterized by variable Cr contents up to 5730 ppm, but a narrower range in Nb concentrations of ~2000–3000 ppm. In the Nyamwamba River, Cr and Nb contents are very variable with most of the grains having Cr concentrations < 3000 ppm and Nb contents < 4000 ppm. For all three rivers, rutile formation temperatures range between 595–730 °C, with most rutile having formed in a narrow temperature window between 660 °C and 700 °C (upper amphibolite-/eclogite-facies).

3.5.3 Zircon morphology and geochronology

Resultant concordant zircon U-Pb ages are illustrated in histograms and probability plots (Fig. 3-11) and on a geological map according to their sample locations (Fig. 3-12). The data are further summarized in Table 3-1. Cathodoluminescence (CL) images of selected zircon grains from each sample are shown in Fig. 3-10. All analytical results are given in the Appendix.

Zircon morphology

The morphology of analyzed zircon grains separated from nine Ugandan rivers is similar in all samples (Fig. 3-6). The grains appear as almost round to short prismatic crystals, although zircon with a length to width ratio of ~1.5–2.5 (long stubby to short stalky) is the most common one. Most grains have rounded to subrounded shapes; euhedral grains are rare. Few grains are broken.

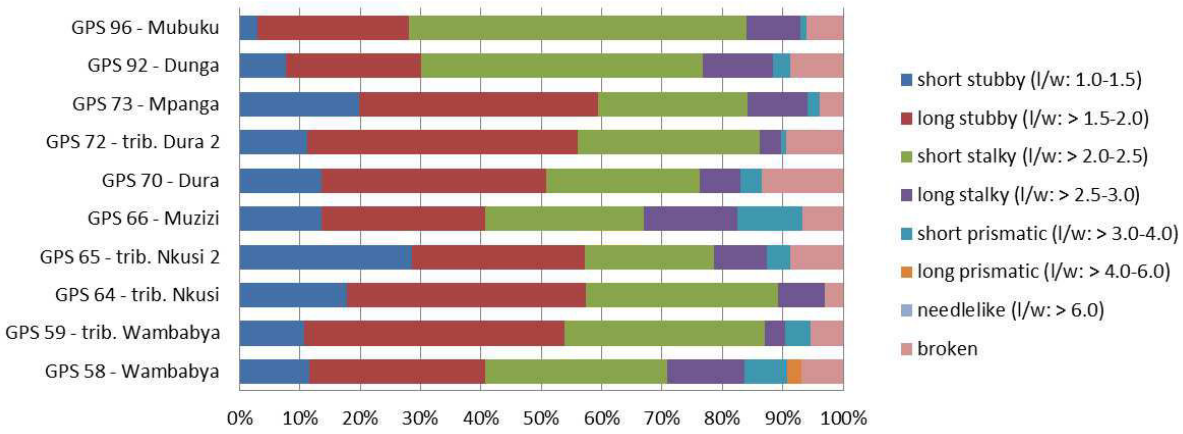

Figure 3-6. Classification of studied zircon grains according to their elongation (length/width ratio) after Gärtner et al. (2013).

The zircon crystals are typically colorless, yellowish, brownish, transparent, translucent to turbid (Fig. 3-7). Pinkish grains also occur and are especially common in rivers draining the Rwenzori Mountains (Mubuku, Dunga). The study of internal zircon structures yields similar results between all samples (Fig. 3-8). In CL images, the majority of zircon exhibits blurred, patchy or inhomogeneous structures, which do not allow recognition of pre-existing textures (‘auroral-light’ zoning) (Fig. 3-9A). Other

zircon grains appear nearly homogenous, but the zoning is still visible in places (Fig. 3-9D, E). Zircon showing irregular, convoluted, and thickened oscillatory zoning is common (Fig. 3-9F). Now and then, these grains are disturbed by recrystallized zones traversing original structures. A majority of zircon crystals exhibit large dark zoned or homogenous xenocrytic cores surrounded by lighter (almost) homogenous rims or bands (Fig. 3-9B). Magmatic zircon, characterized by a xenocrystic core enveloped by regular zoning is rare in the sands and reaches abundances up to 4% (Fig. 3-9I). This is also true for a tributary river to the Nkusi River, which drains the Kagadi granitic complex. Occasionally, zircon grains show irregular sector zoning, brecciated cores or veined textures (Fig. 3-9G, H).

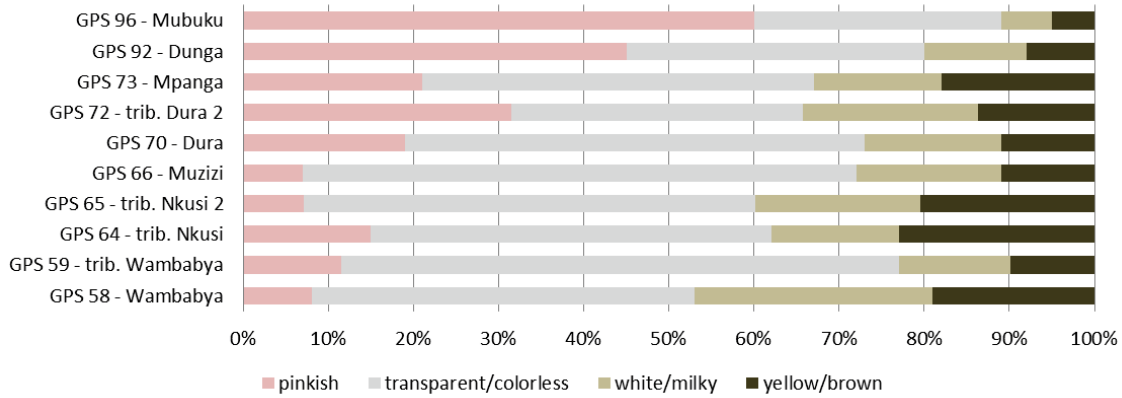

Figure 3-7. Distribution of zircon colors in the studied river sediments.

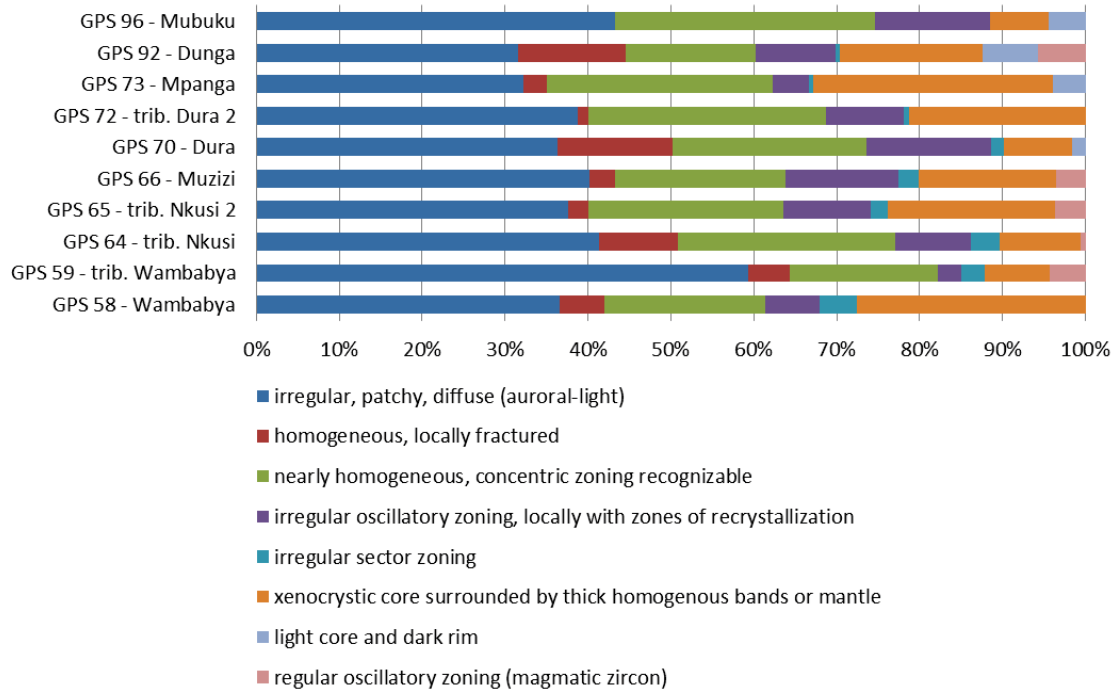

Figure 3-8. Distribution of internal zircon structures in the studied river sediments.

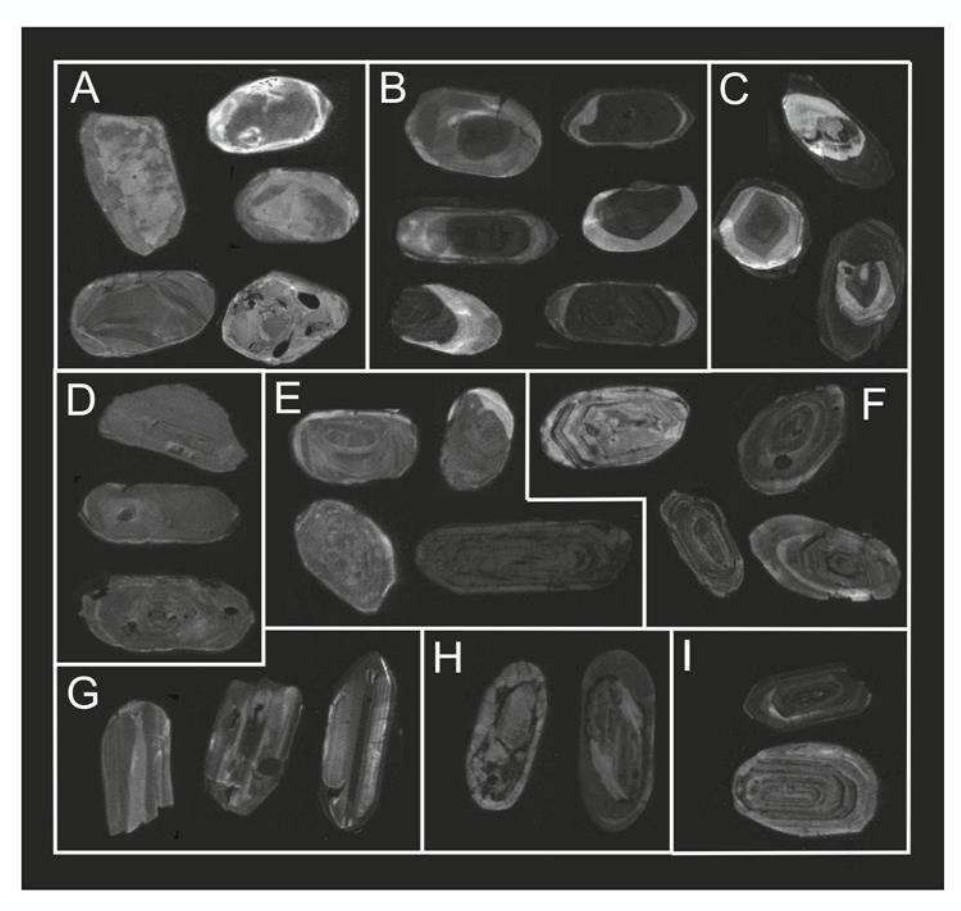

Figure 3-9. Variations of internal structures of studied zircon grains. All grains are between 63 and 125 µm in size. High-grade metamorphic zircon: (A) blurred, patchy, diffuse (auroral-light) or structureless textures (common in eclogite); (B) large dark inner core surrounded by thicker, nearly homogenous bands; cores can be homogenous or growth zoned; (C) broad (usually) irregular zoning; bands are more or less homogenous (typical for eclogite); (D) homogeneous unzoned zircon; (E) faintly zoned zircon locally with domains of recrystallization; (F) irregular oscillatory zoning; (G) irregular sector zoning; (H) left: fractured zircon with brecciated core, right: blurred core with recrystallization zones surrounded by homogenous mantle (typical for eclogite); Magmatic zircon:(I)regular oscillatory zoning.

Zircon U-Pb ages

Whilst the morphology of grains does not differ much between the samples, zircon ages are very varied in most rivers. Along the eastern rift shoulder of Lake Albert, two small streams that receive major input from the NUT, exhibit Paleoproterozoic to Neoarchean ages of 2380–2666 Ma and 2358–2753 Ma, respectively, with the majority of zircon grains yielding ages between 2500 and 2600 Ma. In the Wambabya River, two additional grains reveal late Paleoproterozoic ages of 1836 ± 104 Ma and 1871 ± 78 Ma. In the Muzizi River that erodes the NUT and metasedimentary rocks of the RFB, two major age populations occur. The first population (~48%) yields Paleoproterozoic ages between 1764 and 1891 Ma. The second group (~41%) consists of zircon ranging in age from 2319 and 2587 Ma, which corresponds to an early Paleoproterozoic to Neoarchean age. Furthermore, four zircon grains reveal mid-Paleoproterozoic ages of 2064 ± 63 Ma, 2109 ± 30 Ma, 2150 ± 87 Ma, 2195 ± 105 Ma. One grain shows an early Neoproterozoic age of 778 ± 14 Ma. The sample representing the Kagadi porphyric granite complex is dominated by zircon having early to late Paleoproterozoic ages between

1621 and 2496 Ma, with the dominant section between 2000 and 2200 Ma. Two zircon grains show a Neoarchean age of 2594 ± 46 Ma and 2641 ± 46 Ma. In a stream eroding sedimentary rocks of the Bunyoro Group, three major zircon populations are present. The first population consists of zircon yielding early Neoproterozoic to late Mesoproterozoic ages ranging between 848 Ma and 1182 Ma culminating between ~1000 Ma and 1100 Ma. A second population shows mid-Paleoproterozoic ages between 1815 and 2042 Ma. The third population displays Neoarchean ages between 2506 and 2785 Ma. Two grains yield a Mesoarchean age of 2853 ± 75 Ma and 2908 ± 50 Ma, whereas one grain exhibits an early Paleoproterozoic age of 2395 ± 88 Ma.

Figure 3-10. Selected representative CL images of U-Pb dated zircon grains from each sample with the location of the LA-ICP-MS analysis spot and related $^{207}Pb/^{206}Pb$ age (±1σ) for grains > 1.0 Ga and $^{206}Pb/^{238}U$ age (±1σ) for grains < 1.0 Ga. Ages are given in Ma.

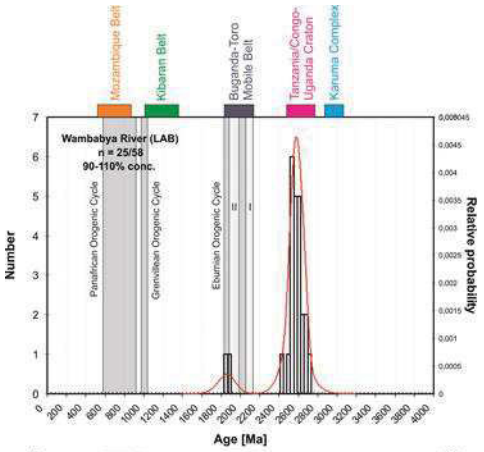
Mozambique Belt
Kibaran Belt
Buganda-Toro Mobile Belt
Tanzania/Congo-Uganda Craton
Karuma Complex
Wambabya River (LAB)
n = 25/58
90-110% conc.
Panafrican Orogenic Cycle
Grenvillean Orogenic Cycle
Eburnian Orogenic Cycle
II
I
Number
Relative probability
Age [Ma]

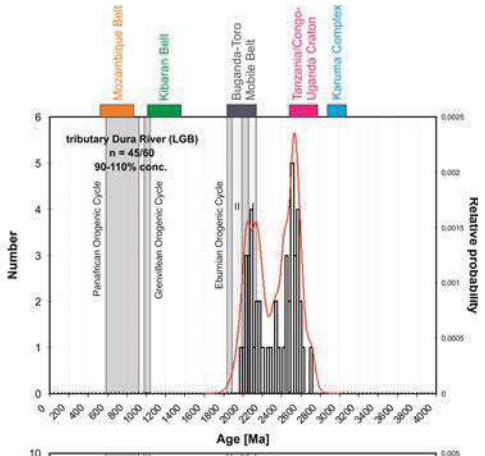
Mozambique Belt
Kibaran Belt
Buganda-Toro Mobile Belt
Tanzania/Congo-Uganda Craton
Karuma Complex
tributary Dura River (LGB)
n = 45/60
90-110% conc.
Panafrican Orogenic Cycle
Grenvillean Orogenic Cycle
Eburnian Orogenic Cycle
II
I
Number
Relative probability
Age [Ma]

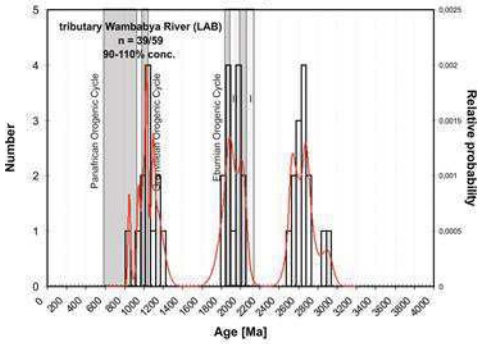
tributary Wambabya River (LAB)
n = 39/59
90-110% conc.
Panafrican Orogenic Cycle
Grenvillean Orogenic Cycle
Eburnian Orogenic Cycle
II
I
Number
Relative probability
Age [Ma]

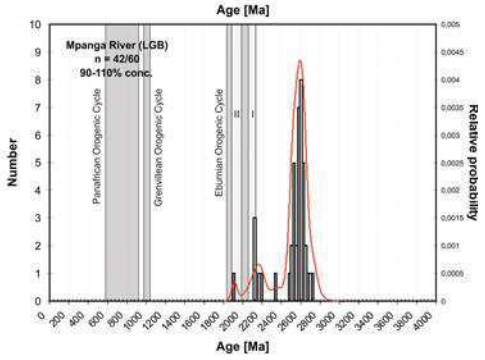
Mpanga River (LGB)
n = 42/60
90-110% conc.
Panafrican Orogenic Cycle
Grenvillean Orogenic Cycle
Eburnian Orogenic Cycle
II
I
Number
Relative probability
Age [Ma]

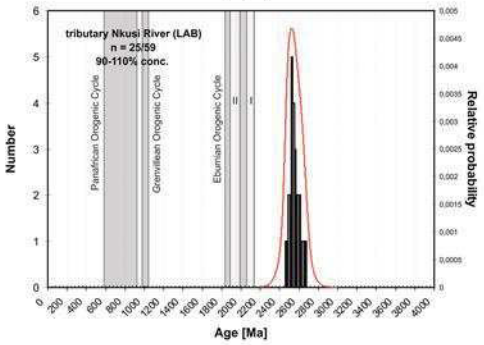
tributary Nkusi River (LAB)
n = 25/59
90-110% conc.
Panafrican Orogenic Cycle
Grenvillean Orogenic Cycle
Eburnian Orogenic Cycle
II
I
Number
Relative probability
Age [Ma]

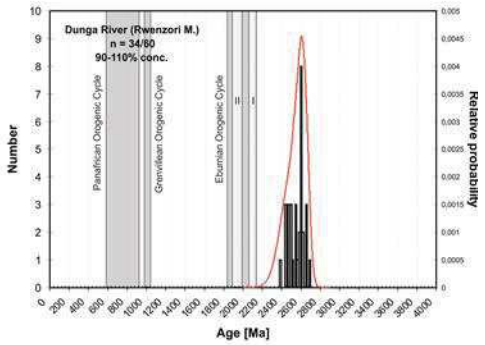
Dunga River (Rwenzori M.)
n = 34/60
90-110% conc.
Panafrican Orogenic Cycle
Grenvillean Orogenic Cycle
Eburnian Orogenic Cycle
II
I
Number
Relative probability
Age [Ma]

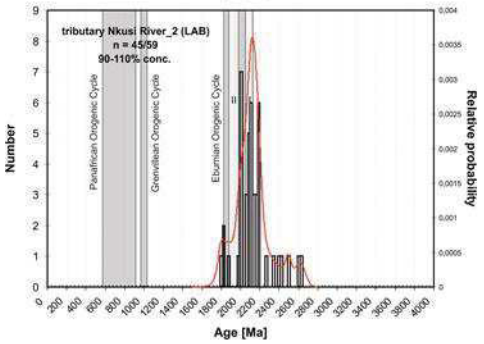
tributary Nkusi River_2 (LAB)
n = 45/59
90-110% conc.
Panafrican Orogenic Cycle
Grenvillean Orogenic Cycle
Eburnian Orogenic Cycle
II
Number
Relative probability
Age [Ma]

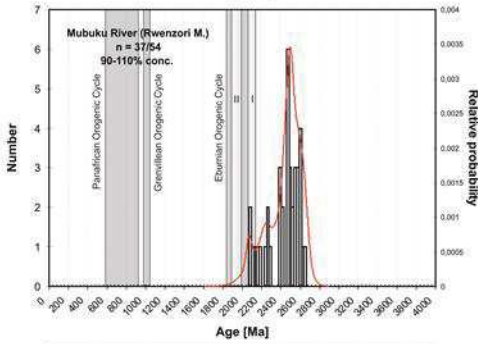
Mubuku River (Rwenzori M.)
n = 37/54
90-110% conc.
Panafrican Orogenic Cycle
Grenvillean Orogenic Cycle
Eburnian Orogenic Cycle
II
I
Number
Relative probability
Age [Ma]

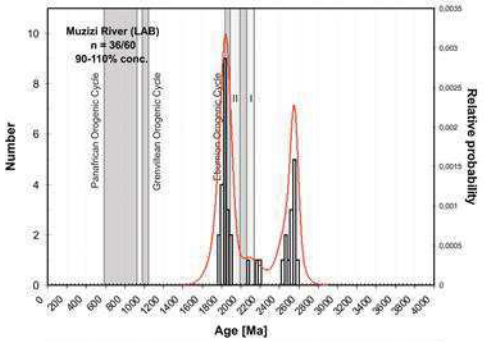
Muzizi River (LAB)
n = 36/60
90-110% conc.
Panafrican Orogenic Cycle
Grenvillean Orogenic Cycle
Eburnian Orogenic Cycle
II
I
Number
Relative probability
Age [Ma]


Paleozoic
Neo-protero-zoic
Meso-protero-zoic
Paleo-proterozoic
Neo-archean
Meso-archean
Paleo-archean
Eo-archean


Paleozoic
Neo-protero-zoic
Meso-protero-zoic
Paleo-proterozoic
Neo-archean
Meso-archean
Paleo-archean
Eo-archean

Figure 3-11 (previous page). Combined probability density distribution and histogram diagrams for concordant zircon U-Pb age data from the river samples with the ages of key tectonic sources.

Detrital zircon separated from the Mpanga River in southern Uganda exhibits Neoarchean ages of ~2490–2735 Ma. Most grains are in a range between ~2520 and 2620 Ma. A minor age population yields mid-Paleoproterozoic ages between ~2120 and 2190 Ma. Further Paleoproterozoic ages are at 1914 ± 28 Ma, 2276 ± 64 Ma and 2342 ± 50 Ma. In a small stream to the Dura River, zircon yields mid-Paleoproterozoic to Neoarchean ages between 1980 and 2716 Ma. The age histogram is characterized by a bimodal frequency distribution with age culminations at ~2000–2200 Ma (mid-Paleoproterozoic) and ~2450–2600 Ma (mainly Neoarchean).

In the Dunga River, which erodes the northern flank of the Rwenzori Mountains, one major age population exhibits early Paleoproterozoic (40%) to Neoarchean (60%) ages between 2373 and 2693 Ma. A single grain shows a slightly younger age of 2272 ± 77 Ma, which is also early Paleoproterozoic. In the Mubuku River, in the central Rwenzori Mountains, two zircon populations are distinguishable. Seventy eight percent of the analyzed zircon grains yield ages between 2360 and 2650 Ma that correspond with an early Paleoproterozoic to Neoarchean age. A smaller cluster includes early to mid-Paleoproterozoic ages between 2070 and 2295 Ma.

3.6 Discussion

3.6.1 Garnet chemistry

It has been noticed in several studies dealing with sediment generation in the equatorial part of Africa that garnet is commonly rare in modern streams (Ando et al., 2012; Garzanti et al., 2013; Schneider et al., 2016). This is despite the fact that amphibolite-facies metasedimentary rocks, which are the main proto-source for this mineral phase, underlie large parts of the African/Ugandan basement. The scarcity of the grains was interpreted by authors to be the result of intensive chemical weathering promoted by the hot-humid climate conditions in vicinity to the equator. Although, garnet from only five Ugandan stream sediments could be analyzed, the three garnet cluster identified during this study admit general statements about the underlying basement geology.

Almandine-rich garnet of Cluster I that represents gneiss and granitoid of the NUT is in close correspondence with garnet commonly formed in metasedimentary gneiss metamorphosed under pressure and temperature conditions transitional to amphibolite- to granulite-facies metamorphism (Aubrecht et al., 2009). Mn-rich garnet might also form in magmatic, felsic to intermediate source rocks (Krippner et al., 2014). However, an igneous origin for the garnet assemblage may be largely excluded, for two reasons: (1) garnet found in pegmatites commonly forms a solid solution between almandine and spessartine (Manning, 1983) and spessartine is low in all garnet grains, and (2) contribution from the nearby Kagadi porphyric granite is not indicated by zircon geochronology (see 3.5.3).

Cluster II garnet can be associated with either gneissic granitoid rocks of the NUT, or TTG gneiss of the WTT. In comparison with published data on garnet composition, they correspond best to garnet derived from metaigneous amphibolite, ecglogite and granulite (Krippner et al., 2014). Differences between garnet compositions from gneissic suites in southern and northern territories with one suite having a sedimentary origin and the other suite having an igneous origin resembles the inhomogeneity of the local basement.

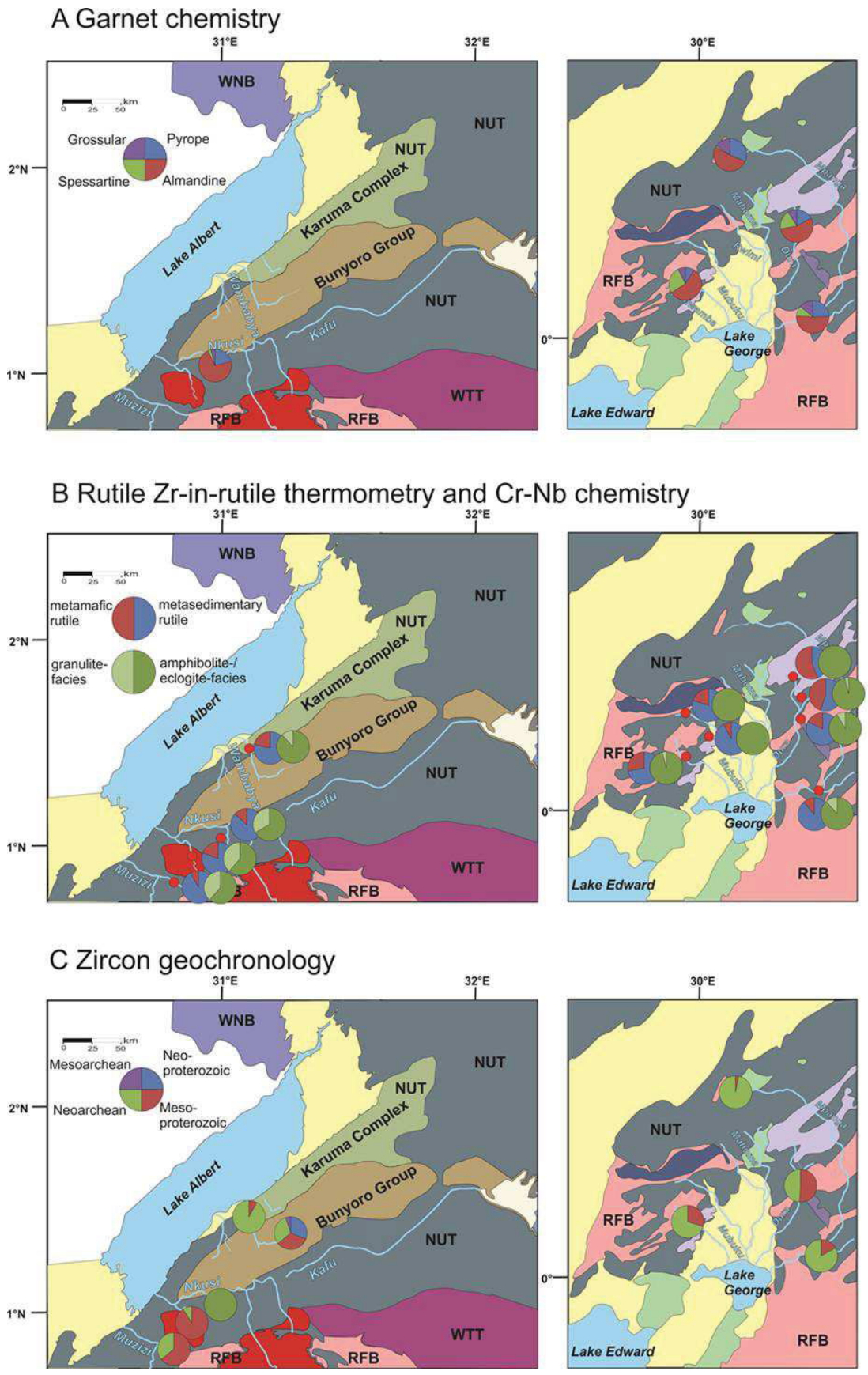

Figure 3-12. Pie charts illustrating the results of garnet, rutile and zircon analyses from each measured river sediment according to its sample location (in B: red dots).

River ID	River name	Tectono-thermal terrane	Cr-Nb chemistry		Zr-in-rutile thermometry				Zircon geochronology				Garnet chemistry			
			Metasedimentary rutile (%)	Metamafic rutile (%)	Temperature range (C°)	Temperature average (C°)	Amphibolite-/eclogite facies (%)	Granulie-facies (%)	Neoproterozoic (%)	Paleoproterozoic (%)	Neoarchean (%)	Mesoarchean (%)	Pyrope (%)	Almandine (%)	Spessartine (%)	Grossular (%)
GPS 58	Wambabya	NUT	-	-	-	-	-	-	0	8	92	0	-	-	-	-
GPS 59	tribut. Wambabya	BG	78	22	591-977	698	88	12	31	33	31	5	-	-	-	-
GPS 64	tribut.Nkusi	NUT	87	13	555-892	723	67	33	0	0	100	0	21	72	3	4
GPS 65	tribut. Nkusi	RFB	81	19	640-836	735	61	39	0	91	9	0	-	-	-	-
GPS 66	Muzizi	NUT	92	8	569-793	722	61	39	0	64	36	0	-	-	-	-
GPS 70	Dura	RFB	44	56	572-741	664	100	0	-	-	-	-	-	-	-	-
GPS 71	tribut. Dura	RFB	55	45	651-764	701	96	4	-	-	-	-	17	55	19	9
GPS 72	tribut. Dura	RFB	83	17	590-780	709	91	9	0	51	49	0	-	-	-	-
GPS 73	Mpanga	RFB	89	11	547-849	678	89	11	0	17	83	0	24	51	10	14
GPS 92	Dunga	NUT	-	-	-	-	-	-	0	3	97	0	32	51	2	16
GPS 96	Mubuku	RFB	80	20	618-712	680	100	0	-	-	-	-	-	-	-	-
GPS 97	Isebo	RFB	92	8	595-727	676	100	0	-	-	-	-	-	-	-	-
GPS 98	Nyamwamba	RFB	72	28	586-828	693	97	3	0	30	70	0	9	59	27	7

Table 3-1. Compiled results of garnet and rutile chemistry and zircon U-Pb geochronology of Ugandan rivers.

Cluster III garnet occurs in rivers that drain (major) parts of metasedimentary rocks of the RFB. This is in concert to the general description for this garnet type, commonly representing amphibolite-facies metasedimentary rocks (Mange and Morton, 2007; Aubrecht et al., 2009). A mixed source from both, high-grade gneiss of the NUT and the overlying metasedimentary units of the Buganda Group, is indicated for most sediments in southwestern Uganda by showing a combination of garnet from Cluster II and III. The more distinct separation between the almandine-rich and spessartine-rich garnet in a tributary stream of the Dura River, is likely due to the smaller number of analyzed grains in this sample.

3.6.2 Rutile chemistry

The overall similarity of rutile populations from four rivers along the eastern rift shoulder of Lake Albert is surprising at first sight, because the samples represent different source lithologies within the Ugandan basement. This includes Archean gneissic granitoid of the NUT, the Kagadi granite complex belonging to the RFB, as well as (meta-) sedimentary rocks of the Bunyoro Group. Differences between the sands are manifested in their petrographic and geochemical character, especially in the heavy mineral content and chemical ratios (Schneider et al., 2016), and also in zircon U-Pb ages (see section 3.5.3). A primary origin of rutile from (meta-) sedimentary rocks of the Bunyoro Group cannot be assumed, because this lithology is not assigned to underwent high-grade metamorphism (Westerhof et al., 2014). Therefore, it is likely that the rutile stems from the underlying gneissic-granitoid basement terrain, which is the most likely candidate for (very) high temperature rutile in this area. Furthermore, the possibility of a polyphase recycling of rutile needs to be considered.

Rutile that is present in streams crossing southern Uganda, including the Rwenzori Mountains, generally exhibits narrower temperature ranges than rutile along the rift shoulder, mainly in the amphibolite-/eclogite-facies metamorphic field. This is in concordance with major input from the Buganda Group of the RFB described to have experienced medium- to high-grade metamorphism

(Westerhof et al., 2014). Some minor contribution from granulite-facies rocks that sporadically crop out within the fold belt is indicated by some higher temperature rutile. In contrast to the rutile formation temperatures, that show little deviation between the samples, rutile shows distinct differences between Cr-Nb contents, implying a strong inhomogeneity between the different lithologies within this major tectonic unit. Possible source rocks for metapelitic rutile, which is dominant in most samples, are schistose rocks, including andalusite-cordierite schist, sillimanite-muscovite schists, or biotite schists. The source for metamafic rutile that is significant in the Dura River and its tributary might be ultramafic volcanic rocks of the Fort Portal volcanic field, which are present within the catchment area of both streams. In the Rwenzori Mountains, metamafic rutile may have derived from meta-tholeiitic lavas of the Stanley Volcanoes or from banded epidote-amphibolite resting in the central part of the Rwenzori Mountains.

3.6.3 Zircon gechronology

The analysis of zircon grains separated from nine Ugandan river sands shows that there is only minor derivation concerning the morphology of zircon between the samples, but distinct variation in obtained U-Pb ages. The stubby to stalky crystal morphology that is shown by the majority of grains indicates that the zircon crystallized in deep-seated, slowly cooled intrusions, rather than in rapidly crystallized, porphyric bodies (Corfu et al., 2003). (Well-) rounded outlines might result from abrasion during sediment transport. Internal structures, as revealed by CL imaging, are mostly characteristic for zircon that experienced high-grade metamorphism (Corfu et al., 2003), which is consistent with their source from old cratonic crust that experienced different high pressure and temperature events. Irregular oscillatory zoning, in which the initial igneous concentric zoning becomes progressively blurred, convoluted or thickened, might be associated with upper-amphibolite metamorphism (Hoskin and Black, 2000). This is also true for zircon exhibiting new-grown zones traversing older textures. However, recrystallized zones cutting through pre-existing structures might also hint to late- or post-magmatic processes and results from the expel of trace elements during crystallization (Pidgeon et al., 1998). On the other hand, chaotic, blurred to patchy pattern that characterize most of the zircon in each sample, as well as irregular sector zoning, homogenous grains or flowing textures, are all features described to be caused during granulite-facies metamorphic processes (Corfu et al., 2003). Zircon exhibiting dark zoned or unzoned xenocrystic cores enveloped by a (nearly) homogenous lighter rim or homogenous bands might derive from rocks that experienced eclogite metamorphism (Corfu et al., 2003). This kind of zircon has also been described by Link et al. (2010) to be present in Archean gneiss in southern Uganda. Veined and brecciated xenocrystic cores probably result from erosion during sedimentary processes. The absence or low quantity of magmatic zircon, respectively, reflects the dominance of metamorphic rocks in the Ugandan basement. Although, the occuring internal structures is conforming the regional basement, separation of distinct sources on the basis of zircon textures is not feasable, because the different morphological features can neither be associated to certain geological terrains (e.g., NUT or RFB), nor related to any age population.

In contrast to morphological features, U-Pb zircon ages show distinct variations. Overall, three prominent cluster at 2.7–2.4 Ga, ~2.2–2.0 and ~1.95–1.75 Ga, and minor populations at 2.9–2.85 Ga, 2.4–2.3 Ga and ~1200–900 Ma are distinguishable that correlate with major tectono-thermal events in the geodynamic history of the Ugandan basement. The omnipresence of zircon yielding Neoarchean ages reflects the widespread occurrence of Neoarchean rocks in Uganda, that crop out in the Lake Victoria Terrane (LVT), the West Tanzania Terrane (WTT), the West Nile Block (WNB), and the North Uganda Terrane (NUT). The NUT represents the major source for Neoarchean rocks in this study. Neoarchean zircons are dominant in the Dunga River of the northern Rwenzori Mountains, in a small tributary to the Nkusi River, and in the Wambabya River; all rivers mainly draining the NUT complex. Dominant Neoarchean ages range between 2.6 and 2.5 Ga what is consistent with age data

obtained from most gneissose-migmatitic rocks of the NUT (Link et al., 2010; Mänttäri, 2014). Some older grains with ages around 2.7 Ga probably represent older inherited zircons that have been assigned to be frequently present within this unit (Mänttäri, 2014). The youngest Neoarchean age known from the Ugandan basement has an age of 2.49 Ga and represents the formation of the suture between the WTT and the NUT (= Nakasongola Discontinuity) as result of a post-kinematic transtensional event (Ruotoistenmäki, 2014). Thus, the source for early Paleoproterozoic ages between 2.49 and 2.3 Ga, which are sporadically present in few rivers is enigmatic, because their age coincides with a period of tectonic quiescence that lasted until the onset of the Eburnian Orogenic Cycle some 200–100 Ma later. Westerhof et al. (2014) interpreted such zircons to have formed within smaller, local perturbances in the suture zone between the WTT and NUT. Zircons exhibiting Paleoproterozoic ages between ~2.2–2.0 Ga and ~1.9–1.75 Ga are also common in modern river sands. Major populations of this age are present in all streams that receive notable input from rocks of the RFB. This age group is dominant in a small stream draining the Kagadi porphyric granite complex, which has not been dated, before. As already indicated, mid-Paleoproterozoic ages are characteristic for the RFB in southern and southwestern Uganda, and can be correlated with the Eburnian Orogenic Cycle. Two major compressional phases at ~2.1–2.03 Ga (Eburnian I) and ~1.95 Ga (Eburnian II) resulted in the amalgamation of the Columbia (or Nuna) Supercontinent (Westerhof et al., 2014). Overall, the obtained zircon ages faithfully reflect major basement terrains in Uganda. An exception is one sample that represents the Neoproterozoic sedimentary Bunyoro Group (trib. Wambabya), which demonstrates a wide variety of zircon populations. Among Neoarchean and mid-Paleoproterozoic ages, they contain Mesoarchean ages between 2.9–2.85 Ga and late Mesoproterozoic to early Neoproterozoic ages of 1200–900 Ma. All of these zircons represent recycled grains that have their origin in different terrains of the Ugandan basement. Mesoarchean rocks represent the oldest exposures in the study area, and are restricted to small patches surrounded by Neoarchean basement. They occur in the Uleppi Complex (> 3.08 Ga) of the WNB in NW Uganda, in the Karuma Complex of the NUT (2.99 Ga), or in mafic enclaves in TTG gneiss of the WTT (3.1–2.8 Ga) (see also Schumann et al. 2004). According to the location of the river within the study area, it seems plausible that a high amount of the dated Mesoarchean zircons derive from the nearby located Karuma Group. Zircon ages around ~1.0 Ga can be correlated with the Grenvillean Orogenic Cycle (1100–950 Ma), formerly known as the ‘Mirian’ tectonic event (Hepworth and Macdonald, 1966), and are known from the Madi-Igisi Belt; an intracratonic, NNE-SSW directed thrust and strike-slip belt, which separates the WNB from the NUT. Because the Bunyoro Group itself is assigned to be younger than 765–735 Ma (Westerhof et al., 2014), it may be suspected that the zircons yielding ages of ~1200–900 Ma were recycled from ‘Mirian’ rocks during a former depositional cycle. The lack of Neoproterozoic zircons indicates the absence of Neoproterozoic magmatism within this rock suite.

Overall, the zircon crystals analyzed in this study very well reflect the geological situation in Uganda, and yielded faithfully the ages that were expected. We assume that every important zircon population is represented by the data set.

3.7 Conclusion

The present study provides evidence that detrital heavy mineral geochemistry and geochronology carried by modern streams are valuable indicators for provenance analysis, but that they reach limitations when derived from polycyclic sediments. We found that different tectonic settings or the weathering state of the sediment has obviously no influence on the composition of the mineral grains. Analysis on garnet and rutile chemistry with zircon U-Pb geochronology enabled us to characterize and discriminate different source rocks within the Ugandan basement, because the composition of heavy minerals varies with lithology and locality. Garnet geochemistry and Zr-in-rutile thermometry

are most suitable for distinguishing lithologies that experienced a different metamorphic overprint, which allowed us to separate between amphibolite-facies metamorphic rocks of the RFB and higher metamorphic amphibolite- to granulite-facies rocks of Archean gneissic-granulitic basement terrains. Cr and Nb contents in rutile provide decent information about mafic (e.g., amphibolite) or pelitic source lithologies (e.g., schist, phyllite) even within the same major thermal-tectono unit (RFB, NUT etc.). Zircon U-Pb ages reflect the long history of crustal evolution in Uganda by revealing ages spanning from the Mesoarchean to the Neoproterozoic. The majority of ages can be correlated with major crustal events in Uganda that include amalgamation of Archean lithospheric fragments and formation of fold belts related to the Eburnian, Grenvillean and Pan-African Orogenic Cycles. Multi-cycle sediments present in Neoproterozoic platform sediments of the Bunyoro Group demonstrate erosion and mixing of detritus from diverse source rocks in Uganda. High-grade metamorphic rutile together with Meso- and Neoarchean, and Paleo-, Meso-, and Neoproterozoic zircon populations are not assigned to be primary sourced from the platform sediments, but instead provide proof of former transportation and depositional cycles.

Overall, the application of garnet and rutile geochemistry together with U-Pb zircon geochronology proofed to very well reflect the geological situation in western and southwestern Uganda. First-cycle sediments give direct information about source lithologies, which underlines the usefulness of heavy minerals in sedimentary provenance analysis. However, the application of heavy minerals becomes problematic for polycyclic sediments that result from repeated geological cycles of sedimentation. Because of the durability of zircon, garnet and rutile, multicycle sedimentation is masked, which might lead to an incorrect interpretation of exclusively primary sources.

3.8 Acknowledgements

This study is part of the Forschergruppe ‘Riftlink’ funded by the DFG grant H1643–7/1. Special thanks go to the staff from the department of geoscience at the Johannes Gutenberg University of Mainz for their assistance during the analytical measurements. Dr. Stephan Buhre helped me with EMP analyses; Dr. Regina Mertz supported me during the LA-ICP-MS measurements; Klemens Link introduced me into zircon geochronology and helped with the evaluation of the final data set.

3.9 References

Abdelsalam, M. G., Katumwehe, A. B., Atekwana, E. A., Le Pera, A. K., Achang, M., 2016. The Paleoproterozoic Singo Granite in south-central Uganda revealed as a Nested Igneous Ring Complex using Geophysical Data. Journal of African Earth Sciences, 116, 198–212.

Andersen, T., 2005. Detrital zircons as tracers of sedimentary provenance: limiting conditions from statistics and numerical simulation. Chemical Geology, 216, 249–270.

Andò, S., Garzanti, E., Padoan, M., Limonta, M., 2012. Corrosion of heavy minerals during weathering and diagenesis: A catalogue for optical analysis. In: von Eynatten, H., Critelli, S., Ingersoll, R. V., Weltje, G. J. (Eds.), Actualistic models of sediment generation. Sedimentary Geology, 280, pp. 165–178.

Andò, S., Morton, A., Garzanti, E., 2014. Metamorphic grade of source rocks revealed by chemical fingerprints of detrital amphibole and garnet. In: Scott, R. A., Smyth, H. R., Morton, A. C., Richardson, N. (Eds.), Sediment provenance studies in hydrocarbon exploration and production. Geological Society of London, Special Publications, 386, pp. 351–371.

Aubrecht, R., Méres, Š., Sýkora, M., Mikus, T., 2009. Provenance of the detrital garnets and spinels from the Albian sediments of the Czorsztyn Unit (Pieniny Klippen Belt, Western Carpathians, Slovakia). Geologica Carpathica, 60, 463–483.

Barker, D. S., Nixon, P. H., 1989. High-Ca, low-alkali carbonatite volcanism at Fort Portal, Uganda. Contributions to Mineralogy and Petrology, 103, 166–177.

Bauer, F. U., Glasmacher U. A., Ring U., Schumann A., Nagudi B., 2010. Thermal and exhumation history of the central Rwenzori Mountains, Western Rift of the East African Rift System, Uganda. International Journal of Earth Sciences, 99, 1575–1597.

Bauer, F. U., Glasmacher, U. A., Ring, U., Karl, M., Schumann, A., Nagudi, B., 2013. Tracing the exhumation history of the Rwenzori Mountains, Albertine Rift, Uganda, using low-temperature thermochronology. Tectonophysics, 599, 8–28.

Bishop, W. W., 1965. Quaternary geology and geomorphology in the Albertine Rift Valley, Uganda. In: Wright Jr., H.E., Frey, D.G. (Eds.), International studies on the Quaternary, pp. 293–321.

Bjørlikke, K. O., 1973. Glacial conglomerates of late Precambrian age from the Bunyoro Series, W. Uganda. Geologische Rundschau, 62, 938–947.

Bjørlikke, K. O., 1981. Late Precambrian tillites of the Bunyoro Series, western Uganda. In: Hambrey, M. J., Harland, W. B. (Eds). Earth's Pre-Pleistocene Glacial Record. Cambridge University Press, Cambridge, pp. 151–152.

Black, L. P., Kamo, S. L., Allen, C. M., Aleinikoff, J. N., Davis, D. W., Korsch, R. J., Foudoulis, C., 2003. TEMORA 1: a new zircon standard for Phanerozoic U–Pb geochronology. Chemical Geology, 200, 155–170.

Bonini, M., Corti, G., Innocenti, F., Manetti, P., Mazzarini, F., Abebe, T., Pecskay, Z., 2005. Evolution of the Main Ethiopian Rift in the frame of Afar and Kenya rifts propagation. Tectonics, 24, 1–21.

Buchwaldt, R., Toulkeridis, T., Todt, W., Ucakuwun, E. K., 2008. Crustal age domains in the Kibaran belt of SW Uganda: Combined zircon geochronology and Sm–Nd isotopic investigation. Journal of African Earth Science, 51, 4–20.

Chorowicz, J., 2005. The East African rift system. Journal of African Earth Sciences, 43, 379–410.

Cohen, A. S., Soreghan, M. J., Scholz, C. A., 1993. Estimating the age of formation of lakes: an example from Lake Tanganyika, East African Rift system. Geology, 21, 511–514.

Cooke, H. B. S., 1958. Observations relating to the Quaternary environments in East and Southern Africa. Transactions of the Geological Society of South Africa, 60 Annex, 1–74.

Condie, K. C. 1998. Episodic continental growth and super continents: A mantle avalanche connection? Earth and Planetary Science Letters, 163, 97–108.

Condie, K. C. 2000. Episodic continental growths models: Afterthoughts and extensions. Tectonophysics, 322, 153–162.

Condie, K. C. 2001. Mantle Plumes and their record in earth history. Cambridge University Press, Cambridge, UK, 305 p.

Corfu, F., Hanchar, J. M., Hoskin, P. W., Kinny, P., 2003. Atlas of zircon textures. Reviews in mineralogy and geochemistry, 53, 469–500.

Davies, K. A. 1952. The building of Mount Elgon, East Africa. Memoir of the Geological Survey of Uganda, 7, 57 p.

Davies, K. A. 1956. The geology of south-east Uganda with special reference to the alkaline complexes. Memoir of the Geological Survey of Uganda, 8, 77 p.

Dechamps, R., Senut, B., Pickford, M., 1992. Fruits fossiles pliocènes et pléistocènes du Rift occidental ougandais. Signification paléoenvironnementale. Comptes rendus de l'Académie des sciences. Série 2, Mécanique, Physique, Chimie, Sciences de l'univers, Sciences de la Terre, 314, 325–331.

Deer, W., Howie, R., Zussman, J., 1997. The rock-forming minerals. Disilicates and ring silicates, Vol. 1B, 151–179.

Delvaux, D., Barth, A., 2010. African Stress Pattern from formal inversion of focal mechanism data. Implications for rifting dynamics. Tectonophysics, 482, 105–128.

DeMenocal, P., 1995. Plio-Pleistocene African Climate. Science, 270, 53–59.

DeMenocal, P., 2004. African climate change and faunal evolution during the Pliocene-Pleistocene. Earth and Planetary Science Letters, 220, 3–24.

De Waele, B., Johnson, S. P., Pisarevsky, S. A., 2008. Paleoproterozoic to Neoproterozoic growth and evolution of the eastern Congo Craton. Its role in the Rodenia puzzle. Precambrian Research, 160, 127–141.

Dickinson, W. R., 1970. Interpreting detrital modes of graywacke and arkose. Journal of Sedimentary Research, 40, 695–707.

Ebinger, C. J., 1989. Tectonic development on the western branch of the East African rift system. Geological Society of America Bulletin, 101, 885–903.

Ebinger, C. J., Deino, A. L., Tesha, A. L., Becker, T., Ring, U., 1993. Tectonic controls on rift basin morphology: evolution of the Northern Malawi (Nyasa) Rift. Journal of Geophysical Research: Solid Earth, 98, 17821–17836.

Flannery, J. W., Rosendahl, B. R., 1990. The seismic stratigraphy of Lake Malawi, Africa: implications for interpreting geological processes in lacustrine rifts. Journal of African Earth Sciences (and the Middle East), 10, 519–548.

Foley, S. F., Link, K., Tiberindwa, J. V., Barifaijo, E., 2012. Patterns and origin of igneous activity around the Tanzanian craton. Journal of African Earth Sciences, 62, 1–18.

Frihy, O. E., 2007. The Nile Delta: processes of heavy mineral sorting and depositional patterns. In: Mange, M. A., Wright, D. T. (Eds.), Heavy Minerals in Use. Developments in Sedimentology, 58. Elsevier, Amsterdam, pp. 345–391.

Gärtner, A., Linnemann, U., Sagawe, A., Hofmann, M., Ullrich, B., Kleber, A., 2013. Morphology of zircon crystal grains in sediment − characteristics, classifications, definitions. Geologica Saxonica, 59, 65–73.

Gani, N. D., Gani, M. R., Abdelsalam, M. G., 2007. Blue Nile incision on the Ethiopian Plateau: Pulsed plateau growth, Pliocene uplift, and hominin evolution. GSA Today, 17, 4–11.

Garzanti, E., Vezzoli, G., 2003. A classification of metamorphic grains in sands based on their composition and grade: Research Methods Papers. Journal of Sedimentary Research, 73, 830–837.

Garzanti, E., Padoan, M., Andò, S., Resentini, A., Vezzoli, G., Lustrino, M., 2013. Weathering and relative durability of detrital minerals in equatorial climate: sand petrology and geochemistry in the East African rift. The Journal of Geology, 121, 547–580.

Gautier, A., 1965. Geological Investigation in the Sinda Mohari (Ituri, NE-Congo). A Monograph on the Geological History of a Region in the Lake Albert Rift. Ganda-Congo Expedition. Ghent University, 158 p.

Gautier, A., 1970. Fossil freshwater mollusca of the Lake Edward–Lake Albert Rift. Annual Reports of the Royal Museum of Central Africa, Tervuren, 67, 1–144.

Gehrels, G., 2014. Detrital zircon U-Pb geochronology applied to tectonics. Annual Review of Earth and Planetary Sciences, 42, 127–149.

Gerdes, A., Zeh, A., 2006. Combined U–Pb and Hf isotope LA-(MC-) ICP-MS analyses of detrital zircons: comparison with SHRIMP and new constraints for the provenance and age of an Armorican metasediment in Central Germany. Earth and Planetary Science Letters, 249, 47–61.

Hepworth, J. V., MacDonald, R., 1966. Orogenic belts of the northern Uganda basement. Nature, 210, 726–727.

Hoskin, P. W. O., Black, L. P., 2000. Metamorphic zircon formation by solid-state recrystallization of protolith igneous zircon. Journal of metamorphic Geology, 18, 423–439.

Hubert, J. F., 1962. A zircon-tourmaline-rutile maturity index and the interdependence of the composition of heavy mineral assemblages with the gross composition and texture of sandstones. Journal of Sedimentary Research, 32, 440–450.

Jackson, S. E., Pearson, N. J., Griffin, W. L., Belousova, E. A., 2004. The application of laser ablation-inductively coupled plasma-mass spectrometry (la-icp-ms) to in situ U-Pb zircon geochronology. Chemical Geology, 211, 47–69.

Jacobs, B. F., Deino, A. L., 1996. Test of climate–leaf physiognomy regression models, their application to two Miocene floras from Kenya, and $^{40}Ar/^{39}Ar$ dating of the late Miocene Kapturo site. Palaeogeography, Palaeoclimatology, Palaeoecology, 123, 259–271.

Johnson, S. P., Waele, B. De, Tembo, F., Evans, D., Iizuka, T., Tani, K., 2007. Geochronology of the Zambezi supracrustal sequence, southern Zambia: a record of Neoproterozoic divergent processes along the southern margin of the Congo Craton. The Journal of Geology, 115, 355–374.

Karp, T., Scholz, C. A., McGlue, M. M., 2012. Structure and stratigraphy of the Lake Albert Rift, East Africa: Observations from seismic reflection and gravity data. In: Baganz, O. W., Bartov, Y., Bohacs, K., Nummedal, D. (Eds), Lacustrine sandstone reservoirs and hydrocarbon systems. AAPG Memoir, 95, pp. 299–318.

Key, R. M., Liyungu, A. K., Njamu, F. M., Somwe, V., Banda, J., Mosley, P. N., Armstrong, R. A. 2001. The western arm of the Lufilian Arc in NW Zambia and its potential for copper mineralisation. Journal of African Earth Science, 33, 503–528.

King, B. C., 1959a. Problems of the Precambrian of Central and Western Uganda, part I. Problems of correlation. Science Progress, London, 47, 528–542.

King, B. C., 1959b. Problems of the Precambrian of Central and Western Uganda, part II. Structures, metamorphism, and granites. Science Progress, London, 47, 723–744.

Krippner, A., Meinhold, G., Morton, A. C., von Eynatten, H., 2014. Evaluation of garnet discrimination diagrams using geochemical data of garnets derived from various host rocks. Sedimentary Geology, 306, 36–52.

Krippner, A., Meinhold, G., Morton, A. C., Russell, E., von Eynatten, H., 2015. Grain-size dependence of garnet composition revealed by provenance signatures of modern stream sediments from the western Hohe Tauern (Austria). Sedimentary Geology, 321, 25–38.

Leggo, P. J., 1974. A geochronological study of the basement complex of Uganda. Journal of the Geological Society of London, 130, 263–277.

Lenoir J.-L., Kuster D., Liegeois J. P., Utke A., Haider A., Matheis G., 1994. Origin and regional significance of late Precambrian and early Palaeozoic granitoids in the Pan-African belt of Somalia. Geologische Rundschau, 83, 624–641.

Link, K., Koehn, D., Barth, M. G., Tiberindwa, J. V., Barifaijo, E., Aanyu, K., Foley, S. F., 2010. Continuous cratonic crust between the Congo and Tanzania blocks in western Uganda. International Journal of Earth Sciences, 99, 1559–1573.

Lofty, M. F., 1997. Distributaion of heavy mineral grains by granulometric fractions in some modern Nile Delta coastal sands, Egypt. INQUA Commision on Quaternary Shorelines, Newsletter, 19, 33–41.

Ludwig, K. R., 2012. User's manual for Isoplot 3.75: A geochronological toolkit for Microsoft Excel: Berkeley Geochronology Center Special Publication, 5, 75 p.

MacDonald, R., 1966. Geological Map of Uganda. Department of Geological Survey and Mines, Uganda.

Macgregor, D. S., 2012. The development of the Nile drainage system: integration of onshore and offshore evidence. Petroleum Geoscience, 18, 417–431.

Macgregor, D. S., 2015. History of the development of the East African Rift System: A series of interpreted maps through time. Journal of African Earth Sciences, 101, 232–252.

Mänttäri, I., 2014. Mesoarchaean to Neoproterozoic U-Pb and Sm-Nd ages from Uganda. In: Lehto, T., Katto, E. (Eds.), GTK Consortium Geological Surveys in Uganda 2008−2012. Geological Survey of Finland, Special Paper 56, pp. 121–164.

Mange, M. A., Maurer, H. F. W., 1992. Heavy minerals in colour. Chapman and Hall, London, 148 p.

Mange, M. A., Morton, A. C., 2007. Geochemistry of heavy minerals. In: Mange, M. A., Wright, D. T. (Eds.), Heavy Minerals in Use. Developments in Sedimentology, 58. Elsevier, Amsterdam, pp. 345–391.

Mange, M. A., Wright, D. T. (Eds.), 2007. Heavy minerals in use: Developments in Sedimentology 58. Elsevier, Amsterdam, 1283 p.

Manning, D. A. C., 1983. Chemical variation in garnets from aplites and pegmatites, peninsular Thailand. Mineralogical Magazine, 47, 353–358.

Master, S., Bailie, R., 2000. Geochemistry of amphibolites from the Stanley Volcanics and Kilembe Schists, Buganda–Toro Supergroup, Ruwenzori Mountains, western Uganda. Journal of African Earth Science, 30, 59–60.

Master, S., Bekker, A., Karhu, J. A., 2013. Paleoproterozoic high δ 13 C carb marbles from the Ruwenzori Mountains, Uganda: Implications for the age of the Buganda Group. Chemical Geology, 362, 157–164.

Meinhold, G., 2010. Rutile and its applications in earth sciences. Earth-Science Reviews, 102, 1–28.

Morley, C. K., 1999. Geoscience of rift systems-evolution of East Africa. American Association of Petroleum Geologists Studies in Geology, 44, 242 p.

Morton, A. C., 1985. A new approach to provenance studies: electron microprobe analysis of detrital garnets from Middle Jurassic sandstones of the northern North Sea. Sedimentology, 32, 553–566.

Morton, A. C., Hallsworth, C. R., 1994. Identifying provenance-specific features of detrital heavy mineral assemblages in sandstones. Sedimentary Geology, 90, 241–256.

Morton, A. C., Hallsworth, C. R., 1999. Processes controlling the composition of heavy mineral assemblages in sandstones. Sedimentary Geology, 124, 3–29.

Morton, A., Chenery, S., 2009. Detrital rutile geochemistry and thermometry as guides to provenance of Jurassic–Paleocene sandstones of the Norwegian Sea. Journal of Sedimentary Research, 79, 540–553.

Nagudi, B., Koeberl, C., Kurat, G., 2003. Petrography and geochemistry of the Singo granite, Uganda, and implications for its origin. Journal of African Earth Science, 36, 73–87.

Nasdala, L., Hofmeister, W. G., Norberg, N., Mattinson, J. M., Corfu, F., Dorr, W., Kamo, S. L., Kennedy, A. K., Kronz, A., Reiners, P. W., Frei, D., Kosler, J., Wan, Y. S., Gotze, J., Hager, T., Kroner, A., Valley, J. W., 2008. Zircon M257—a homogeneous natural reference material for the ion microprobe U-Pb analysis of zircon. Geostandards and Geoanalytical Research, 32, 247–265.

Ollier, C. D., 1990. Morphotectonics of the Lake Albert Rift Valley and its significance for continental margins. Journal of Geodynamics, 11, 343–355.

Pickford, M., Senut, B., Poupeau, G., Brown, F., Haileab, B., 1991. Correlation of tephra layers from the Western Rift Valley (Uganda) to the Turkana Basin (Ethiopia/Kenya) and the Gulf of Aden. Stratigraphy, 313, 223–229.

Pickford, M., Senut, B., Hadoto, D., 1993. Geology and Palaeobiology of the Albertine Rift Valley, Uganda-Zaire. Vol. I: Geology. International Centre for Training and Exchanges in Geosciences, Occasional publications, 24, 1–190.

Pidgeon, R. T., Nemchin, A. A, Hitchen, G. J., 1998. Internal structures of zircons from Archean granites from the Darling Range batholith: Implications for zircon stability and the interpretation of zircon U-Pb ages. Contributions to Mineralogy and Petrology, 132, 288–299.

Rainaud, C., Master, S., Armstrong, R. A., Robb, L. J., 2005. Geochronology and nature of the Palaeoproterozoic basement in the Central African copperbelt (Zambia and the Democratic Republic of Congo), with regional implications. Journal of African Earth Science, 42, 1–31.

Ring, U., 2008. Extreme uplift of the Rwenzori Mountains in the East African Rift, Uganda: Structural framework and possible role of glaciations. Tectonics, 27. TC4018, doi: 10.1029/2007TC002176.

Ring, U., 2014. The East African Rift System. Australian Journal of Earth Sciences, 107, 132–146.

Ring, U., Betzler, C., 1995. Geology of the Malawi Rift: kinematic and tectono-sedimentary background to the Chiwondo Beds, northern Malawi. Journal of Human Evolution, 28, 7–21.

Ring, U., Betzler, C., Delvaux, D., 1992, Normal vs. strike-slip faulting during rift development in East Africa: The Malawi rift, Geology, 20, 1015–1018.

Roller, S., Hornung, J., Hinderer, M., Ssemmanda, I., 2010. Middle Miocene to Pleistocene sedimentary record of rift evolution in the southern Albertine Graben (Uganda). International Journal of Earth Sciences, 99, 1643–1661.

Rosendahl, B. R., Kilembe, E., Kaczmarick, K., 1992. Comparison of the Tanganyika, Malawi, Rukwa and Turkana Rift zones from analyses of seismic reflection data. Tectonophysics, 213, 235–256.

Ruotoistenmäki, T., 2014. Geophysical characteristics of Aswa shear, Nagasongola discontinuity and Ring dyke complex in Uganda. Journal of African Earth Sciences, 93, 23−41.

Sabeen, H. M., Ramanujam, N., Morton, A. C., 2002. The provenance of garnet: constraints provided by studies of coastal sediments from southern India. Sedimentary Geology, 152, 279–287.

Saemundsson, K., 2010. East African rift system. An overview. Paper presented at course V on exploration for geothermal resources, organized by UNU-GTP, GDC and KenGen, at Lake Bogoria and Lake Naivasha, Kenya, Oct. 29-Nov. 19, 2010.

Schlüter, T., 2008. Geological Atlas of Africa, 2nd edition, 307 p., Springer Verlag, Berlin.

Schneider, S., Hornung, J., Hinderer, M., Garzanti, E., 2016a. Petrography and geochemistry of modern river sediments in an equatorial environment (Rwenzori Mountains and Albertine rift, Uganda)—Implications for weathering and provenance. Sedimentary Geology, 336, 106–119.

Schneider, S., Hornung, J., Hinderer, M., 2016b. Evolution of the western East African Rift System reflected in provenance changes of Miocene to Pleistocene synrift sediments (Albertine Rift, Uganda). Sedimentary Geology, 343, 190–205.

Schneider, S., Hornung, J., Hinderer, M., 2017. Evolution of the northern Albertine Rift reflected in the provenance of synrift sediments (Nkondo-Kaiso area, Uganda). Journal of African Earth Sciences, 131, 183–197.

Sircombe, K. N., 2000. Quantitative comparison of large sets of geochronological data using multivariate analysis: a provenance study example from Australia. Geochimica et Cosmochimica Acta, 64, 1593–1616.

Stern, R. J., 1994. Arc assembly and continental collision in the Neoproterozoic East African Orogen: Implication for the consolidation of Gondwanaland. Annual Review of Earth and Planetary Sciences, 22, 319–351.

Tanner, P.W.G., 1971. The Stanley Volcanics Formation of Ruwenzori, Uganda.Annual Report. Research Institute for African Geology, 15. University of Leeds, pp. 8–11.

Taylor, R. G., Howard, K. W. F., 1999. The influence of tectonic setting on the hydrological characteristics of deeply weathered terrains: evidence from Uganda. Journal of Hydrology, 218, 44–71.

Thomas, W. A., 2011. Detrital-zircon geochronology and sedimentary provenance. Lithosphere, 3, 304–308.

Tomkins, H. S., Powell, R., Ellis, D. J., 2007. The pressure dependence of the zirconium-in-rutile thermometer. Journal of Metamorphic Geology, 25, 703–713.

Trauth, M. H., Maslin, M. A., Deino, A., Strecker, M. R., 2005. Late cenozoic moisture history of East Africa. Science, 309, 2051–2053.

Triebold, S., von Eynatten, H., Zack, T., 2012. A recipe for the use of rutile in sedimentary provenance analysis. Sedimentary Geology, 282, 268–275.

Van Achterbergh, E., Ryan, C. G., Jackson, S. E., Griffin, W. L., 2000. Data reduction software for LA-ICPMS: Appendix. In: Sylvester, P. J. (Ed.) Laser Ablation-ICP-mass spectrometry in the earth sciences: principles and applications, Vol. 29. Mineralogical Association of Canada Short Course Series, pp. 239–243.

Van Damme, D., Pickford, M., 1995. The late Cenozoic Ampullariidae (Mollusca, Gastropoda) of the Albertine Rift Valley (Uganda-Zaire). Hydrobiologia, 316, 1–32.

Van Damme, D., Pickford, M., 1998. The late Cenozoic Viviparidae (Mollusca, Gastropoda) of the Albertine Rift Valley (Uganda-Congo). Hydrobiologia, 390, 171–217.

Van Damme, D., Pickford, M., 2003. The late Cenozoic Thiaridae (Mollusca, Gastropoda, Cerithioidea) of the Albertine Rift Valley (Uganda-Congo) and their bearing on the origin and evolution of the Tanganyikanthalassoidmalacofauna. Hydrobiologia, 498, 1–83.

Van Straaten, H. P., 1971. Preliminary work on the Precambrian adjoining the Western Rift, north of Masindi, Bunyoro District (Sheet 39/I). Interim Res. Rept. I, Dept. Geol. Makerere Univ., Kampala.

Van Straaten, H.P., 1976. Präkambrium und junges Western Rift im Bunyoro Distrikt, NW-Uganda. Geologisches Jahrbuch, Reihe B, Heft 18, 95 p.

Von Eynatten, H., Gaupp, R., 1999. Provenance of Cretaceous synorogenic sandstones in the Eastern Alps: constraints from framework petrography, heavy mineral analysis and mineral chemistry. Sedimentary Geology, 124, 81–111.

Von Eynatten, H., Dunkl, I., 2012. Assessing the sediment factory: the role of single grain analysis. Earth-Science Reviews, 115, 97–120.

Westerhof, A. B. P., Härmä, P., Isabirye, E., Katto, E., Koistinen, T., Kuosmanen, E., Lehto, T., Lehtonen, M. I., Mäkitie, H., Manninen, T., Mänttäri, I., Pekkala, Y., Pokki, J., Saalmann, K., Virransalo, P., 2014. Geology and Geodynamic Development of Uganda with Explanation of the 1:1,000,000 -Scale Geological Map. Geological Survey of Finland, Special Paper, 55, 387 pages, 329 figures, 29 tables and 2 appendices.

Zack, T., Von Eynatten, H., Kronz, A. 2004. Rutile geochemistry and its potential use in quantitative provenance studies. Sedimentary Geology, 171, 37–58.

Chapter 4

4 Evolution of the western East African Rift System reflected in provenance changes of Miocene to Pleistocene synrift sediments (Albertine Rift, Uganda)

Sandra Schneider[1], Jens Hornung[1], Matthias Hinderer[1]

[1] Institute of Applied Geosciences, TU Darmstadt, Schnittspahnstrasse 9, D-64287 Darmstadt

4.1 Abstract

Miocene to Pleistocene synrift sediments in the Albertine Graben reflect the complex geodynamic evolution in the western branch of the East African Rift System. In this study we focus on the provenance of these siliciclastic deposits to identify sediment sources and supply paths with the ultimate goal to reconstruct the exhumation history of different tectonic blocks during prolonged rifting, with specific focus on the uplift of the Rwenzori Mountains in Uganda. We present framework and heavy mineral petrographic data combined with varietal studies of detrital garnet and rutile, based on logged sediment sections on the Ugandan side of Lake Albert (Kisegi-Nyabusosi area). The analyzed sedimentary units have a feldspatho-quartzose composition and distinct variations in heavy mineral assemblages and mineral chemical composition indicating two provenance changes. The Miocene part of the stratigraphy is dominated by garnet, zircon, tourmaline and rutile, whereas Pliocene to Pleistocene sediment yields high amounts of less stable amphibole and epidote. An abrupt switch in heavy mineral assemblages occurs during the early Pliocene (~5.5–5.0 Ma) and clearly postdates the formation of Palaeolake Obweruka at ~8 Ma. Provenance signatures point to major sediment supply from the northeast and subsequently from the southeast. We interpret this first shift as transition from the pre-rift to the syn-rift stage. In this scenario, formation of Palaeolake Obweruka is due to higher humidity in the upper Miocene, rather than forced rifting. A second change of sediment composition is documented by mineral geochemistry and coincides with fragmentation of Palaeolake Obweruka starting at ~2.5 Ma. Detrital garnet in sediment of Miocene to Pliocene age is rich in pyrope and almandine and calculated Zr-in-rutile temperatures range between ~550–950 °C. In contrast, garnet occurring in Pleistocene sediment (Nyabusosi Formation) has a higher spessartine component and rutile thermometry is consistent with a predominantly amphibolite-facies source. The most likely origin for the Pleistocene heavy mineral suites is the Rwenzori horst block, which delivered increasing amounts of sediment due to rapid uplift and high weathering during Pleistocene glacials.

4.2 Introduction

Sedimentary provenance analysis can be applied to reconstruct the spatial and temporal tectonic history of basins, because sediment composition reflects erosional unroofing, tectonic uplift, climatic, and environmental changes (Morton et al., 2002). In particular, heavy mineral analyses are a widely used technique to unravel the origin of modern and ancient siliciclastic material because, unlike quartz and feldspar, most heavy minerals are restricted to specific source rocks and parageneses (Mange and Wright, 2007). However, sediment composition does not simply reflect original source rock assemblages, but is modified by external processes, including weathering in the source area, abrasion and hydraulic sorting during transport, and diagenesis during burial (Morton and Hallsworth, 1994; Garzanti et al., 2010). Hydraulic sorting and burial diagenesis are believed to be the most crucial controlling factors (Morton and Hallsworth, 1999; Garzanti et al., 2010, 2011). For instance,

fractionation of sedimentary detritus by means of their size, shape, density, mechanic stability etc. during transport leads to enrichment of certain minerals in specific grain size fractions (Garzanti et al., 2011).

In sediment showing specific compositional modifications, changes in provenance signal can be obtained by (1) following the occurrence of diagnostic stable minerals (e.g., spinel; von Eynatten and Gaupp, 1999), (2) comparing the ratio of two stable minerals (e.g., apatite/tourmaline, garnet/zircon; Morton and Hallsworth, 1994), and (3) examining variations in the chemical composition of single grains of a certain mineral group, such as garnet and tourmaline (Morton, 1985; Zack et al., 2004).

Until now, only few provenance studies have been undertaken in rift deposits in the East African Rift System (EARS). Mathisen and Vondra (1983) studied heavy-mineral associations of Plio-Pleistocene fluvio-lacustrine sediments in the East Turkana Basin to unravel the timing of rifting, magmatism and drainage development. Roberts et al. (2012) used detrital zircon geochronology, tephro- and magnetostratigraphy to track past river courses in the Rukwa Basin.

In the Albertine Rift in the western branch of the EARS (Fig. 4-1), sediment accumulated during multiple rifting phases from the middle Miocene (~12.5 Ma; Pickford et al., 1993). Recently, detailed work started on the siliciclastic record by the hydrocarbon industry due to oil discoveries in the Albertine Graben and a collaborative research program (*Riftlink*, 2006–2015; Bauer et al., 2010a). A major focus of this research program was to understand the geodynamics, timing, and environmental impact of uplift of the Rwenzori Mountains (< 5100 m a.s.l.) (Ring, 2008). In this context, the sedimentary record around the Rwenzoris was used to reconstruct uplift over time. Roller et al. (2010) logged the entire sedimentary sequence on the northern side of the Rwenzoris within the southern Albertine Rift (Kisegi-Nyabusosi area) (Fig. 4-1D), i.e. and developed a depositional model. This paper complements this study by presenting the first petrographic, geochemical and provenance data of these Miocene to Pleistocene sediments.

The aim of this study is to unravel the Miocene to Pleistocene uplift pattern of the Rwenzoris and graben shoulders by identifying potential source areas, transportation paths and depocenters in and around the Albertine Graben. For fingerprinting and interpreting provenance data along the sedimentary sequence, pattern of modern river sands in the region were used (Garzanti et al., 2013; Schneider et al., 2016). The outcome of these studies demonstrates that specific provenance signatures, like heavy mineral composition, are still preserved in hot-humid environments, even in intensively weathered sediment produced in poorly-drained savannah lowlands of Uganda.

4.3 Geological setting

The East African Rift System (EARS) is an intracontinental rift zone that runs for over 4000 km through the African continent, from the Gulf of Aden southwards towards the Zambesi River in Mozambique, separating the Nubian plate from the Somalian plate (Chorowicz, 2005). In its central part, the EARS splits into the Eastern (Gregory) Rift and the Western Rift, both of which follow mobile Proterozoic belts that enclose the mechanically stronger Archean Tanzania Craton (McConnell, 1972) (Fig. 4-1A). The EARS has a complex tectonic architecture, due to the systematic linkage of single rift basins by intracontinental transform faults and their segmentation by transfer and accommodation zones (Bosworth et al., 1986; Ebinger, 1989; Morley, 1999; Acocella and Korme, 2002; Chorowicz, 2005; Koehn et al., 2010). Evidence for deformation of the continental crust in eastern Africa, including seismicity, active faulting and volcanics, reflects regional upwelling of the asthenosphere as well as local mantle flow (Calais et al., 2006). Sublithospheric flow regimes act on the Victoria microplate (Tanzania craton) between the western and eastern rift arms by forcing

counterclockwise rotation, causing movement in an east-south-east direction relative to the Nubian plate and the opening of the EARS at a rate of 6 mm/year (Calais et al., 2006; Stamps et al., 2008).

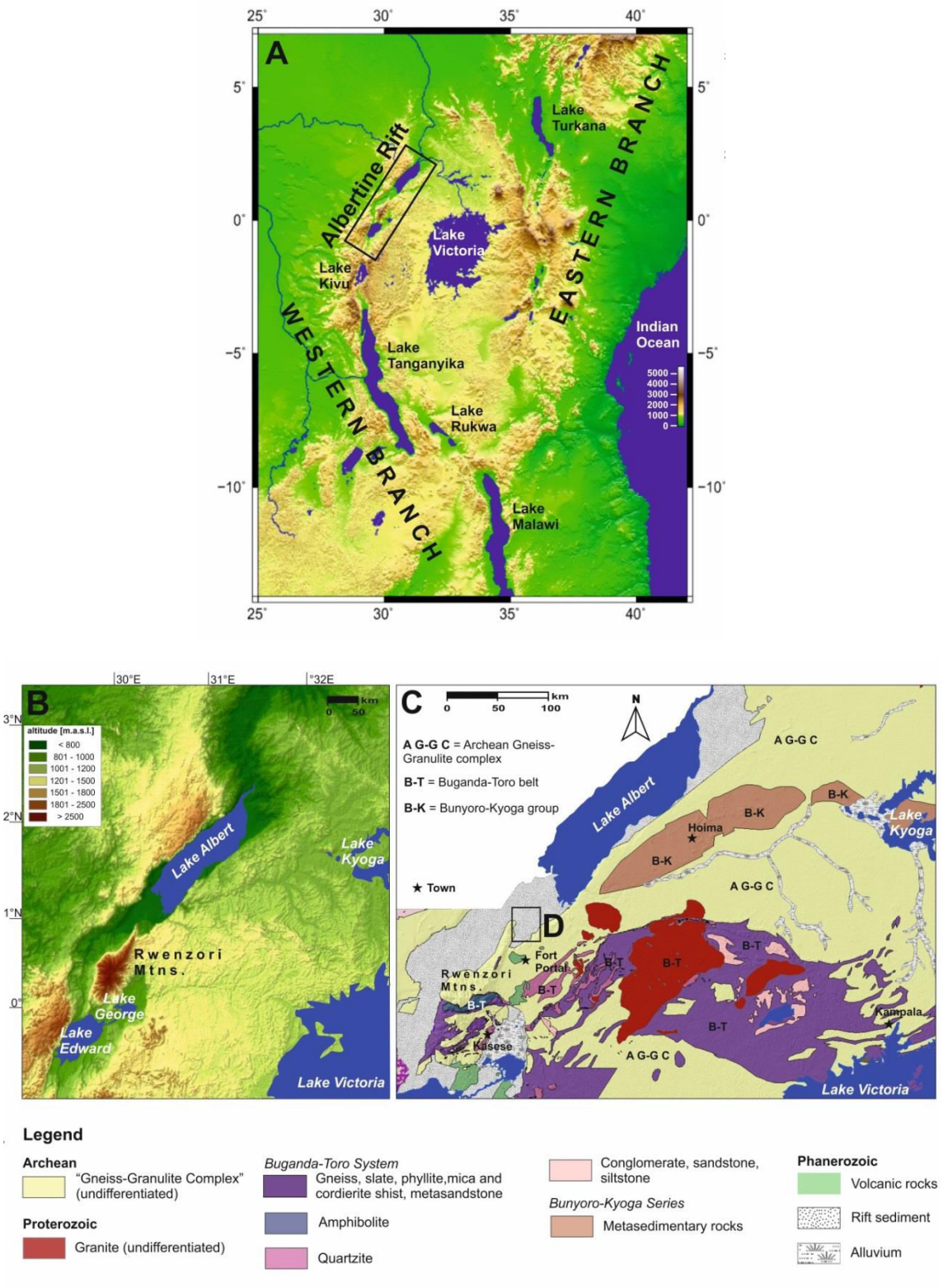

Figure 4-1. Study area. (A) Overview map of the central part of the East African Rift System, (B) Topographic overview map of the Albertine Rift, (C) Geology of western Uganda (modified after Schlüter, 2008), and (D) Location of the Kisegi-Nyabusosi area.

The overall direction of extension of the EARS has long been under debate (Acocella and Korme, 2002; Chorowicz, 2005) with suggested movement either roughly NW-SE (Chorowicz and Mukonki, 1979; Tiercelin et al., 1988; Versfelt and Rosendahl, 1989; Ring et al., 1992; Chorowicz et al., 1994), E-W (Morley, 1988; Ebinger, 1989; Bosworth et al., 1992; Stamps et al., 2008), or a combination of both directions (Boccaletti et al., 1998).

The ~500 km long, NE-SW trending Albertine Rift belongs to the northern sector of the Western Rift branch stretching from the Kivu volcanic province in the south (1°S) to the border between Uganda and South Sudan in the north (3°N), mainly between longitudes 29°E and 31°E (Fig. 4-1). Rifting processes induced the formation of a 50 km-wide en-echelon asymmetrical basin with a faulted escarpment on one side and a flexural warp or faulted monocline on the other (Ebinger, 1989). The Rwenzori horst block, ca. 50 wide and 120 km long, provides an extreme expression of rift-flank uplift between Lake Albert and Lake Edward and its highest summits reach more than 5000 m a.s.l. The Rwenzori Mountains represents the third highest mountain range in Africa and the highest without volcanic origin. This extreme topographic feature within an extensional tectonic setting is globally unique and has no counterpart in the eastern branch of the EARS (Ring, 2008; Bauer et al., 2010b).

The crystalline basement of the Albertine Rift is composed of Archean gneiss and granulite belonging to the Congo and Tanzania Cratons (Leggo, 1974), and low-grade to medium-grade Paleoproterozoic metasedimentary rocks of the Buganda-Toro belt (gneiss, amphibolite, quartzite, slate, phyllite and cordierite schist; King, 1959a, 1959b; King and de Swardt, 1970; Félix, 1972, 1975) (Fig. 4-1C). This mobile belt occupies major parts of southwestern Uganda, where it is thrusted northwards onto the Archean basement of the Tanzania Craton (Gabert, 1990; Link et al., 2010). In the central part of Uganda, metasedimentary rocks of the Buganda-Toro belt are penetrated by Paleoproterozoic granite (Nagudi et al., 2003, Abdelsalam et al., 2016). In a sector parallel to the eastern shore of Lake Albert and along the northern side of Lake Kyoga, low-grade Neoproterozoic slate and metasandstone overlie the cratonic basement with a basal metatillite (Bunyoro-Kyoga Group) (Bjørlikke, 1973; Schlüter, 2008).

Three major evolutionary stages have been assigned for the Albertine Rift from the middle Miocene time, based on morphotectonic, sedimentological and paleontological studies (Pickford et al., 1993). (1) During the Kisegi stage (~12.5–7 Ma) the Albertine Graben was more or less a shallow downwarp with an extension of 60 x 150–200 km that developed under arid to semi-arid climate conditions (Van Damme and Pickford, 1995). Sediment infill during that period was mainly caused by the proto-Nkusi River (Fig. 4-2A), which cuts through the western part of Uganda and, nowadays, terminates into Lake Albert (Bishop, 1965; Pickford et al., 1993). (2) The first major faulting episode took place at ~8 Ma. Graben formation and accelerated subsidence triggered the formation of Paleolake Obweruka, which extended ~550 km from near Kivu in the south to the Sudan/Uganda border in the north (Fig. 4-2B) (Ebinger, 1989; Pickford et al., 1993). The thicknesses of lacustrine deposits and biostratigraphic evidence indicate that the palaeolake was long-lived with assumed persistence from 7.5 to 2.5 Ma (Van Damme and Pickford, 2003). At that time, the climate shifted from semi-arid to humid sustaining a tropical semi-deciduous forest by ca. 6–7 Ma (Dechamps et al., 1992; Pickford, 1992, 1995; Jacobs and Deino, 1996). (3) The third stage was characterized by splitting of Palaeolake Obweruka into a southern and a northern basin as consequence of the beginning exhumation of the Rwenzori block (Fig. 4-2C). Uplift and warping of the local basement promoted disruption of the surface hydrology of Uganda, leading to river reversal of formerly westward flowing river basins (de Heinzelin, 1962; Bishop, 1965; Doornkamp, 1968; Taylor and Howard, 1999). Tectonically driven rift-flank uplift also had a strong impact on regional climate (e.g., deMenocal, 1995, 2004; Trauth et al., 2005), leading to drastic diminution of the tropical rainforest and to the expansion of wooded savanna environments around the Plio-Pleistocene boundary, similar to modern conditions (Dechamps et al., 1992).

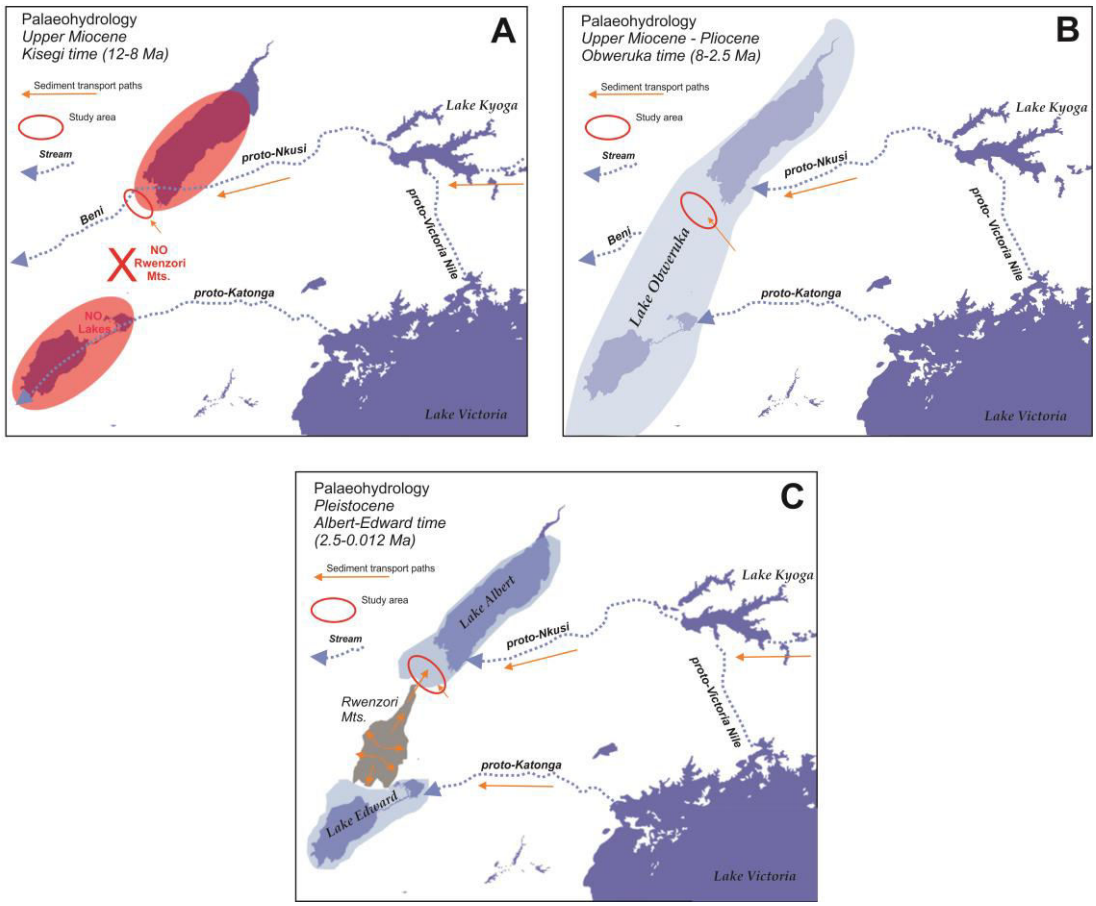

Figure 4-2. Palaeodrainage of Uganda during different stages of rift evolution (after Pickford et al., 1993).

4.4 Stratigraphy and Sedimentology

An up to 6 km thick sediment sequence was deposited in the Albertine Graben since the middle Miocene (Van Damme and Pickford, 2003; Abeinomugisha, 2010). Sedimentary successions are best exposed in four areas on the Ugandan side of the Lake Albert and Lake George sub-basins (Pickford et al., 1993; Roller et al., 2010). This study concentrates on the Kisegi-Nyabusosi area, which is located between Lake Albert and the northern tip of the Rwenzori Mountains (Fig. 4-1D). Here, rift sediments comprise unconsolidated siliciclastics from clay to coarse gravel with some ferruginous and calcareous intercalations that were deposited in a fluvio-lacustrine setting (Pickford et al., 1993; Roller et al., 2010). The sedimentary succession in the Kisegi-Nyabusosi area comprises ~660 stratigraphic meters and was divided by Pickford et al. (1993) into eight formations (Kisegi, Kakara, Oluka, Nyaburogo, Nyakabingo, Katorogo and Nyabusosi, capped by the Rwebishengo Beds) whose age was estimated by stages of freshwater mollusc associations in East Africa (Gautier, 1970, Pickford et al., 1993, Van Damme and Pickford, 2003) (Figs. 4-3, 4-4). Three molluscan associations that are present in other parts of the rift valley are missing in the Kisegi-Nyabusosi area at ~8.5 Ma, ~2.4 Ma and ~2.0 Ma (G2a, GX, GX'), suggesting breaks in the stratigraphic record (Gautier, 1970; Pickford et al., 1993; Senut and Pickford, 1994; Van Damme and Pickford, 1995, 1998, 2003, 2010) (Fig. 4-4). The duration of the hiatuses, however, is not exactly known. The following paragraph gives a short description of stratigraphic formations; detailed information is provided by Pickford et al. (1993) and Roller et al. (2010).

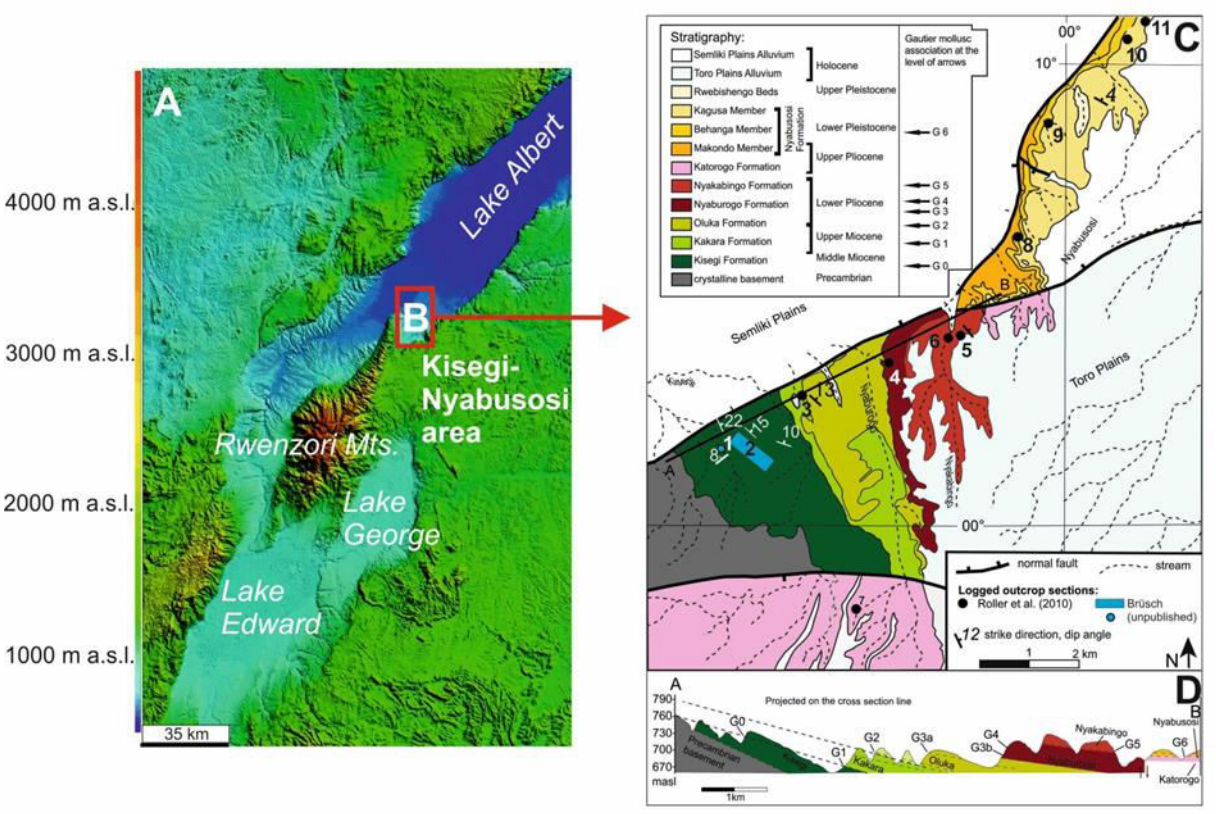

Figure 4-3. Geology of the study area. (A, B) Location of the Kisegi-Nyabusosi area in the Albertine Rift, (C) Geological map of the Kisegi-Nyabusosi area (after Pickford et al., 1993) showing the division of the sedimentary record into eight biostratigraphic formations based on datings of freshwater mollusc associations (Gautier, 1970; Van Damme and Pickford, 2003), (D) Superelevated cross section of the transect AB marked in the geological map.

Kisegi Formation (middle Miocene; 11 samples). The lower and middle part of the Kisegi Formation (~110 m thick) consist of predominantly medium-grained to coarse-grained sand bodies interpreted to be accumulated under semiarid climate conditions in a fluvial environment. The upper Kisegi Formation shows increasingly finer grain fractions (clay to fine sand) indicating an open lacustrine environment due to lake transgression and a more humid climate.

Kakara Formation (upper Miocene; 3 samples). The < 40 m thick Kakara Formation is a sand-prone unit, but silt and clay appear at the bottom and top of the formation. The lower part can be interpreted to be accumulated in a distal delta plain/palustrine environment, whereas the middle and upper parts show a lower delta plain setting (river mouth).

Oluka Formation (upper Miocene; 4 samples). The lower part of the 50–60 m thick formation is characterized by interlayering of clay and medium-grained sand interrupted by a ~8 m thick coarsening-up sand body. The middle section of this formation could not be logged systematically by Roller et al. (2010) due to poor exposure. Pickford et al. (1993) found a blackish iron-rich layer containing Gautier Mollusc associations (G2) and remains of late Miocene mammalian fauna. Overall, the grain size range decreases towards the top of the section and the occurrence of sandy beds becomes rare. Sediment of the Oluka Formation marks the transition from outer delta plain/palustrine conditions towards a (shallow) lacustrine depositional environment.

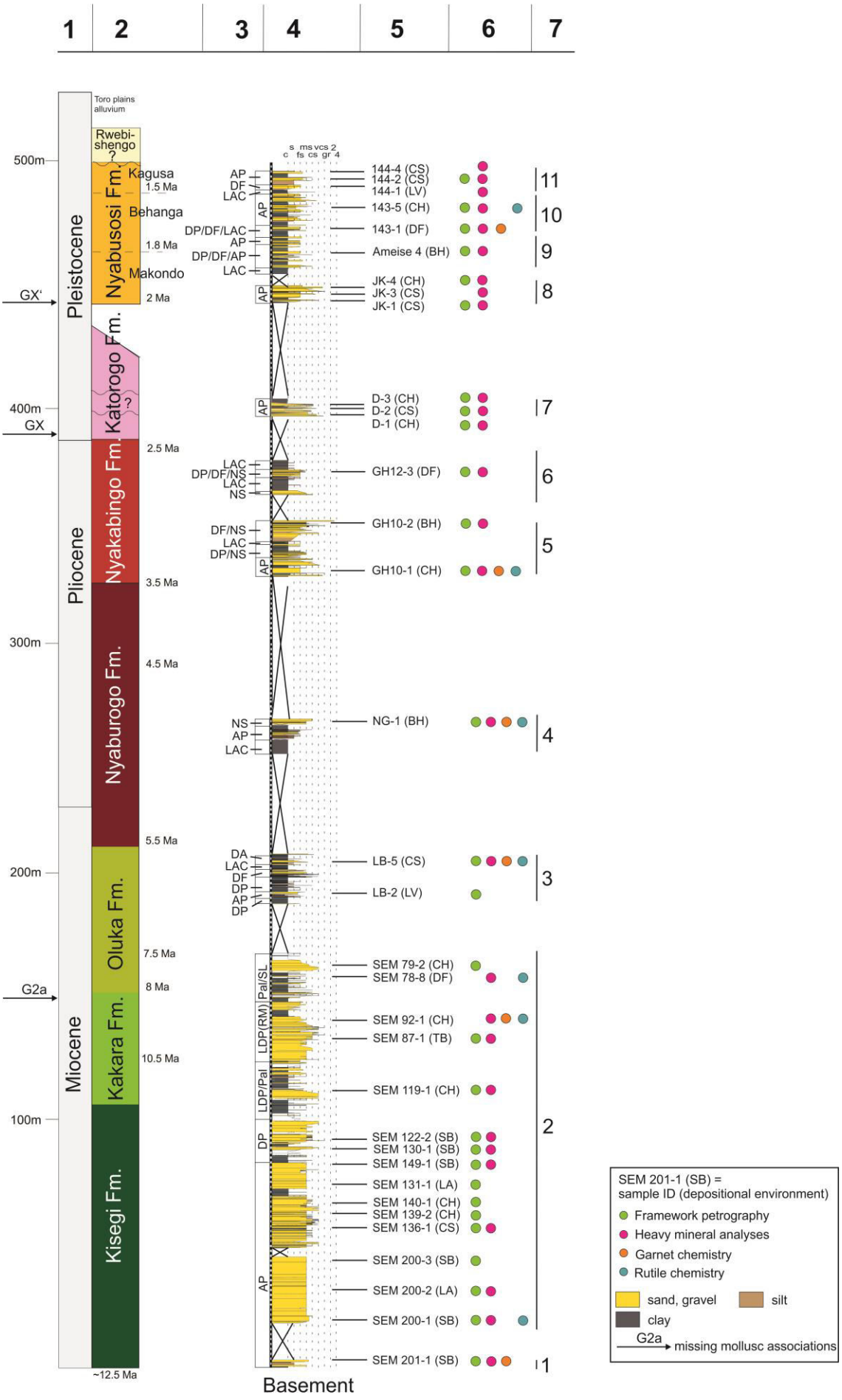
1
2
3
4
5
6
7
Toro plains alluvium
Rwebi-shengo ?
Kagusa
1.5 Ma
Behanga
1.8 Ma
Makondo
2 Ma
Nyabusosi Fm.
Katorogo Fm.
?
2.5 Ma
Nyakabingo Fm.
3.5 Ma
Nyaburogo Fm.
4.5 Ma
5.5 Ma
Oluka Fm.
7.5 Ma
8 Ma
Kakara Fm.
10.5 Ma
Kisegi Fm.
~12.5 Ma
Pleistocene
Pliocene
Miocene
500m
400m
300m
200m
100m
GX'
GX
G2a
s ms vcs 2
c fs cs gr 4
AP
DF
LAC
DP/DF/LAC
DP/DF/AP
DP/DF/NS
DF/NS
NS
DA
DP
LDP(RM) Pal/SL
LDP/Pal
144-4 (CS)
144-2 (CS)
144-1 (LV)
143-5 (CH)
143-1 (DF)
Ameise 4 (BH)
JK-4 (CH)
JK-3 (CS)
JK-1 (CS)
D-3 (CH)
D-2 (CS)
D-1 (CH)
GH12-3 (DF)
GH10-2 (BH)
GH10-1 (CH)
NG-1 (BH)
LB-5 (CS)
LB-2 (LV)
SEM 79-2 (CH)
SEM 78-8 (DF)
SEM 92-1 (CH)
SEM 87-1 (TB)
SEM 119-1 (CH)
SEM 122-2 (SB)
SEM 130-1 (SB)
SEM 149-1 (SB)
SEM 131-1 (LA)
SEM 140-1 (CH)
SEM 139-2 (CH)
SEM 136-1 (CS)
SEM 200-3 (SB)
SEM 200-2 (LA)
SEM 200-1 (SB)
SEM 201-1 (SB)
11
10
9
8
7
6
5
4
3
2
1
Basement
SEM 201-1 (SB) =
sample ID (depositional environment)
Framework petrography
Heavy mineral analyses
Garnet chemistry
Rutile chemistry
sand, gravel
silt
clay
G2a
missing mollusc associations

Figure 4-4 (previous page). Stratigraphy of the Kisegi-Nyabusosi: Sedimentological sections logged and interpreted with respect to architectual elements and depositional environment by Roller et al. (2010) and Brüsch (unpublished). (1) time epoch, (2) biostratigraphic formation (Pickford et al., 1993), (3) depositional environment of sediments. AP: alluvial plain, DP: delta plain, LDP: lower delta plain, Pal: palustrine, RM: river mouth, SL: shallow lacustrine, DF: delta front, LAC: lacustrine, DA: distal alluvial, NS: nearshore. (4) logged sedimentological sections; widths and colors of sections display grain sizes, (5) location, ID and architectural elements (in brackets) of analyzed samples. SB: sandy bedforms, LA: lateral accretion, CS: crevasse splay, CH: channel, TB: transverse bar, DF: delta foreset, LV: levee, BH: beach. (6) analytical methods used on the samples, (7) numbers refer to the ID of logged sections shown in Figure 4-2. Missing mollusc associations (G2a, GX and GX') mark breaks in the stratigraphy at ~8.5, ~2.4 and ~2.0 Ma.

Nyaburogo Formation (lower Pliocene - middle Pliocene; 1 sample). The Nyaburogo Formation is estimated to have a thickness of approximately 120 m (Pickford et al., 1993) of which 15 m was recorded by Roller et al. (2010). Overall, this unit is dominated by clay and silt with only few sandy intercalations at the top of the section. The depositional environment of the Nyaburogo Formation changes between lacustrine and alluvial/delta plain.

Nyakabingo Formation (upper Pliocene; 4 samples). The ~60 m thick unit is composed of clay, silt, sand and minor gravel. The gravel layers are generally impregnated by iron. Iron-impregnated horizons, however, also occur in sandy to silty sediment where they often show a high content of iron ooids. In addition, they are often rich in fossils, mostly shells of molluscs and bivalves. These layers rich in fossils and gravel are interpreted as beach deposits in a general lacustrine deltaic environment.

Katorogo Formation (lower Pleistocene; 3 samples). The Katorogo Formation consists of < 100 m thick poorly sorted sand with clayey intercalations that become dominant towards the top of the section. Sediment represents either clayey/silty floodplain fines or crevasse splay deposits interpreted to have been accumulated in an alluvial plain environment.

Nyabusosi Formation (lower Pleistocene; 9 samples). The ~50 m thick Nyabusosi Formation is divided into three members (Makondo, Behanga and Kagusa) and consists of alternating sandy and clayey beds. Several distinct ooidic iron crusts are distinguishable throughout the Behanga Member. The depositional environment fluctuates between fluvial-deltaic to shallow lacustrine, indicating considerable lake-level oscillations (Roller et al., 2010).

Rwebishengo Beds (middle Pleistocene). Rwebishengo Beds was not sampled.

4.5 Methods

4.5.1 Sampling

Sampling was carried out along 11 sections (Fig. 4-3) of rift sediment representing ~340 stratigraphic meters which have been logged in detail by Roller et al. (2010) and Brüsch (in prep.). During two field campaigns to the Ugandan part of the Albertine Rift in January-February 2012 and November-December 2012, a total of 34 sand samples was collected (Fig. 4-4). Where possible, samples were selected from fine-grained to medium-grained sand and taken randomly in order to cover each logged section from bottom to top. Samples encompass numerous depositional environments including fluvial (channel, lateral accretion), flood plain (crevasse splays), deltaic (transverse bar, delta forests) and lake deposits (beach, prodelta) (Fig. 4-4).

4.5.2 Framework petrography

Most (29) of the samples that represent the entire stratigraphic record were chosen for determination of the framework petrographic composition of rift sediments. The samples were sieved and the sand class 250–500 µm was used for petrographic investigations. Grains were embedded in epoxy resin and cut into standard polished thin sections. A total of 300 grains was counted in each thin section using an automatic point-counter, in order to identify the modal sand composition. All polymineralic grains were counted as lithic fragments (e.g., Decker and Helmold, 1985), hence, the Gazzi-Dickinson method (Dickinson, 1970) in which all subgrains (> 63 µm) within polymineralic fragments are classified in the category of the subgrain, was not applied. Metamorphic rock fragments were categorized into metapelite grains (e.g., micaeous or muscovite slate/phyllite/schist; Lmp), metapsammite/metafelsite grains (e.g., metasandstone/-siltstone, quartzite, gneiss; Lmf) and metabasite grains (e.g., amphibolite, prasinite; Lmb). Furthermore, a Principal Component Analysis (PCA) was performed using the free software package PAST – PAlaeontological Statistics (Hammer et al., 2001). All variables were normalized by dividing their standard deviations with the correlation matrix function (normalized var-covar) and transformed into centered log-ratio coordinates, in order to treat the data set systematically (Aitchison and Egozcue, 2005).

4.5.3 Heavy mineral analysis (HMA)

Heavy mineral analyses were performed on 28 samples, most of them identical to framework petrographic analysis. Some samples did not contain enough heavy minerals and had to be replaced by similar sand samples from the same formation. In one case, this could not be achieved. Heavy minerals (63–125 µm) were separated with sodium polytungstate (ρ = 2.855 g/cm^3) and grain mounts were impregnated with epoxy resin (n = 1.54). In each separate, 250 non-opaque and non-micaceous grains (Mange and Maurer, 1992) were counted using an automatic point counter.

To describe the degree of mineralogical maturity of studied sediment on the basis of heavy mineral assemblages, the ZTR index is used (Hubert, 1962). It is calculated by dividing the sum of zircon, tourmaline and rutile (= ZTR) by the amount of all transparent, non-micaceous heavy minerals. Moreover, we applied the garnet-zircon (GZi =100*garnet/garnet + zircon) and rutile-zircon (RuZi = 100*TiO_2 group minerals/TiO_2 group minerals + zircon) indices that were introduced to decipher changing provenance while overcoming the limits of conventional heavy mineral studies, e.g., hydraulic behavior, by comparing mechanically resistant minerals with similar properties (Morton and Hallsworth, 1994).

4.5.4 Mineral chemistry of detrital garnet and rutile

Rutile and garnet chemical compositions were analyzed from each formation (2 samples for rutile in the Oluka Formation). Preferentially, samples containing a high proportion of the analyzed mineral types were chosen. The Katorogo Formation had to be excluded, because it did not yield enough garnet and rutile. Overall, single grain analyses were performed on 540 detrital garnet grains from six samples and 312 rutile grains from seven samples. All occurring color varieties were included. Grains were handpicked under a binocular microscope, mounted in epoxy resin, cut into sections and polished. Prior to analysis, all samples were coated with carbon to ensure conductivity. Measurements were conducted by a Jeol JXA-2800 electron microprobe equipped with a five wavelength dispersive spectrometer at the Johannes Gutenberg University of Mainz. An accelerating voltage of 15 kV and beam current of 20 nA was used for garnet element content of Si, Mg, Ca, Fe, Al, Ti, Cr and Mn with

counting times of 15 s except Ti, Cr and Mn with 30 s. Rutile grains were analyzed for Nb, Al, Cr, Zr and V with counting times of 200 s, Si and Fe with counting times of 100 s and Ti with counting times of 15 s. Measuring conditions include an accelerating voltage of 25 kV and a beam current of 80 nA.

The chemical composition of garnet was recalculated to the six end-members almandine, spessartine, pyrope, grossular, andradite, and uvarovite, with the structural formula based on 12 oxygen atoms and 8 cations (Deer et al., 1992). Fe^{2+} and Fe^{3+} contents were determined, assuming stoichiometry.

Based on the Cr and Nb content, two major host lithologies for rutile, metamafic (e.g., mafic granulite, eclogite) and metapelitic rocks (e.g., felsic granulite, paragneiss, mica-shist), were distinguished (Zack et al., 2002, 2004; Triebold et al., 2007, 2012; Meinhold et al., 2008). Rutile growth temperatures were calculated using the thermometer after Tomkins et al. (2007) in the α-quartz field after the following equation:

$$T(°C) = [(83.9 + 0.410 \times P)/(0.1428 - R \times \ln(Zr_{ppm})] - 273$$

with P is the pressure, 10 kbar, and R is the gas constant, 0.0083144 kJ K−1.

4.6 Results

4.6.1 Framework petrographic composition

Thin section analyses show a weak degree of roundness of grains throughout the stratigraphy, with the majority of grains being subrounded to angular. Since sediment is largely unconsolidated, matrix or cement is absent. All sand samples show a feldspatho-quartzose composition (Garzanti et al., 2016). The quartz content of the three oldest formations Kisegi, Kakara and Oluka, here summarized as Group 1, ranges between ~64 and 87% (Fig. 4-5; Table A4-1, Appendix). K-feldspar shows abundances of 7–20% and is dominated by orthoclase and microcline. Plagioclase is less frequent with 2-9%. Feldspar grains are usually relatively fresh, but sometimes exhibit patchy sericitization. Rock fragments (1–14%) are of metamorphic origin and clearly dominated by metapsammites/-felsites, e.g., metasiltstone, quartz-sericite-grains, strongly foliated quartz-rich fragments with muscovite flakes, as well as coarse grained mosaic-like muscovite and biotite gneiss (Fig. 4-6). The highest amount of feldspar and rock fragments in Group 1 occurs in the lower Kisegi Formation.

The quartz content of Group 2 (Nyaburogo and Nyakabingo formations) is 60–75%. The amount of K-feldspar is 7–20%, i.e., similar to Group 1, whereas plagioclase (9–16%) is slightly enriched compared to Group 1. The spectrum of rock fragments (~4–5%) is again analogue to Group 1. The Nyakabingo Formation shows an increased amount of accessory minerals, i.e. heavy minerals and opaques (Fig. 4-5).

The quartz content of Group 3 (Katorogo and Nyabusosi formations) is 56–85% with highest values for the Katorogo Formation. Moreover, this is the only formation with a high content of polycrystalline quartz (Ø 41%). Feldspar (K-feldspar: 5–13%, plagioclase: 6–14%) is highest in the youngest Nyabusosi Formation, which is further characterized by notable amounts of mica (white > dark) up to 19% (Fig. 4-4C). Lithic fragments (1–13%) are dominated by felsic metamorphic grains, but also few metamafic fragments often rich in epidote and amphibole occur (up to 3%).

The differences in petrographic composition are displayed by biplots in Fig. 4-7. Samples of Group 1 mainly gather around the variables for monocrystalline quartz, K-feldspar, and chert. Sand of the Katorogo Formation (Group 2) is discriminated by its high amount of polycrystalline quartz, whereas Group 3 is separated by its contents of mica, rock fragments, heavy minerals and opaques.

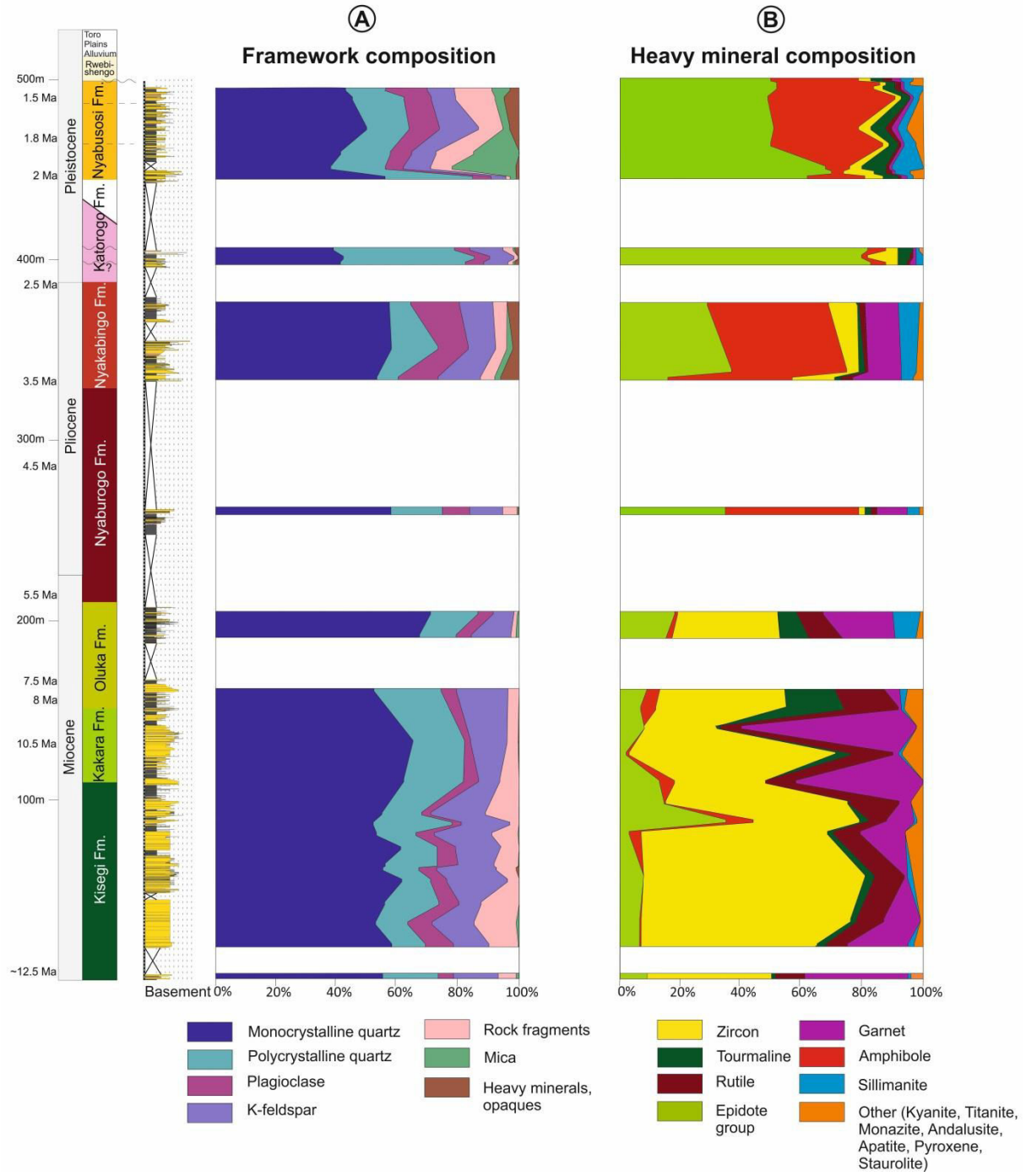

Figure 4-5. Distribution of (A) framework grains and (B) translucent heavy minerals in relation to the stratigraphic column.

4.6.2 Heavy mineral composition

Group 1 is predominated by zircon (24–73%), garnet (1–58%) becomes significant in the Kakara Formation, and epidote (2–33%) in the upper Kisegi Formation (Fig. 4-5). Further heavy minerals are tourmaline (< 19%), rutile (6–18%), amphibole (< 9%), sillimanite (< 9%) and kyanite (< 5%). Sporadically occurring and less important constituents are klinozoizite, monazite, staurolite, apatite and titanite (< 4%). The high amount of ultrastable minerals is reflected by high values of ZTR ratios varying between 32 and 87 (Table A4-2, Appendix).

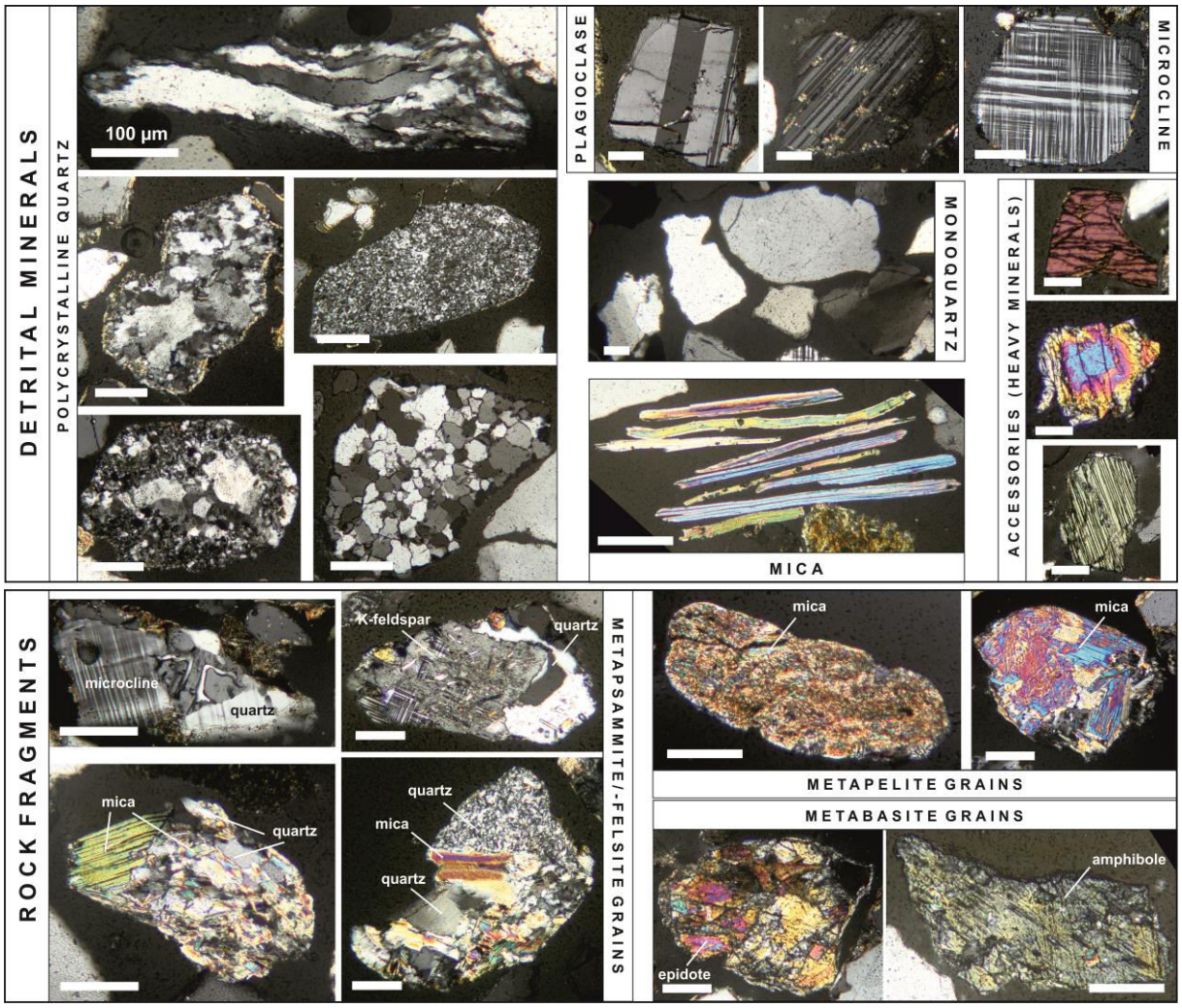

Figure 4-6. Microphotographs of framework grains. White scale bars are 100 µm. All photos with crossed-polars.

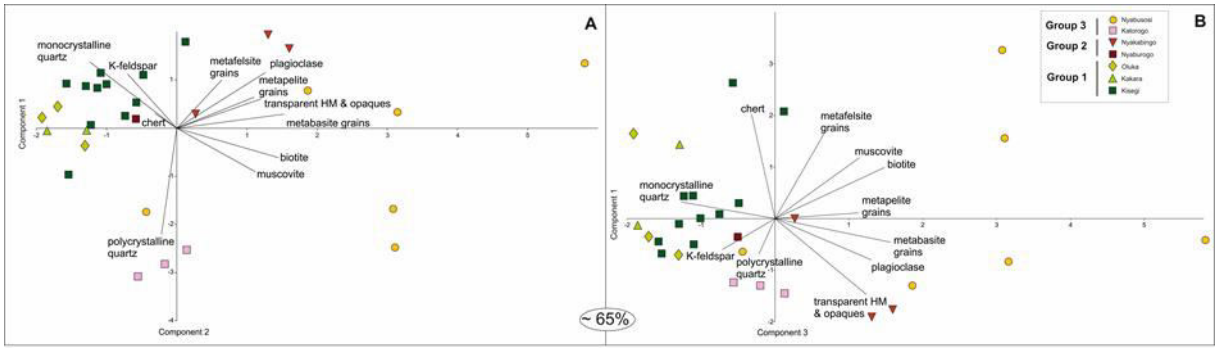

Figure 4-7. Biplots (first and second as well as first and third principal components) discriminating synrift sediments according to their framework petrographic composition. Together the first three components explain 65% of the total variability. In the first plot (A), four major groups with similar high relative variability (except chert) are distinguishable: 1) monocrystalline quartz, K-feldspar and chert (microcrystalline quartz), 2) polycrystalline quartz, 3) rock fragments, heavy minerals and opaques, and 4) mica. The second biplot (B) shows a spread of variables in all directions.

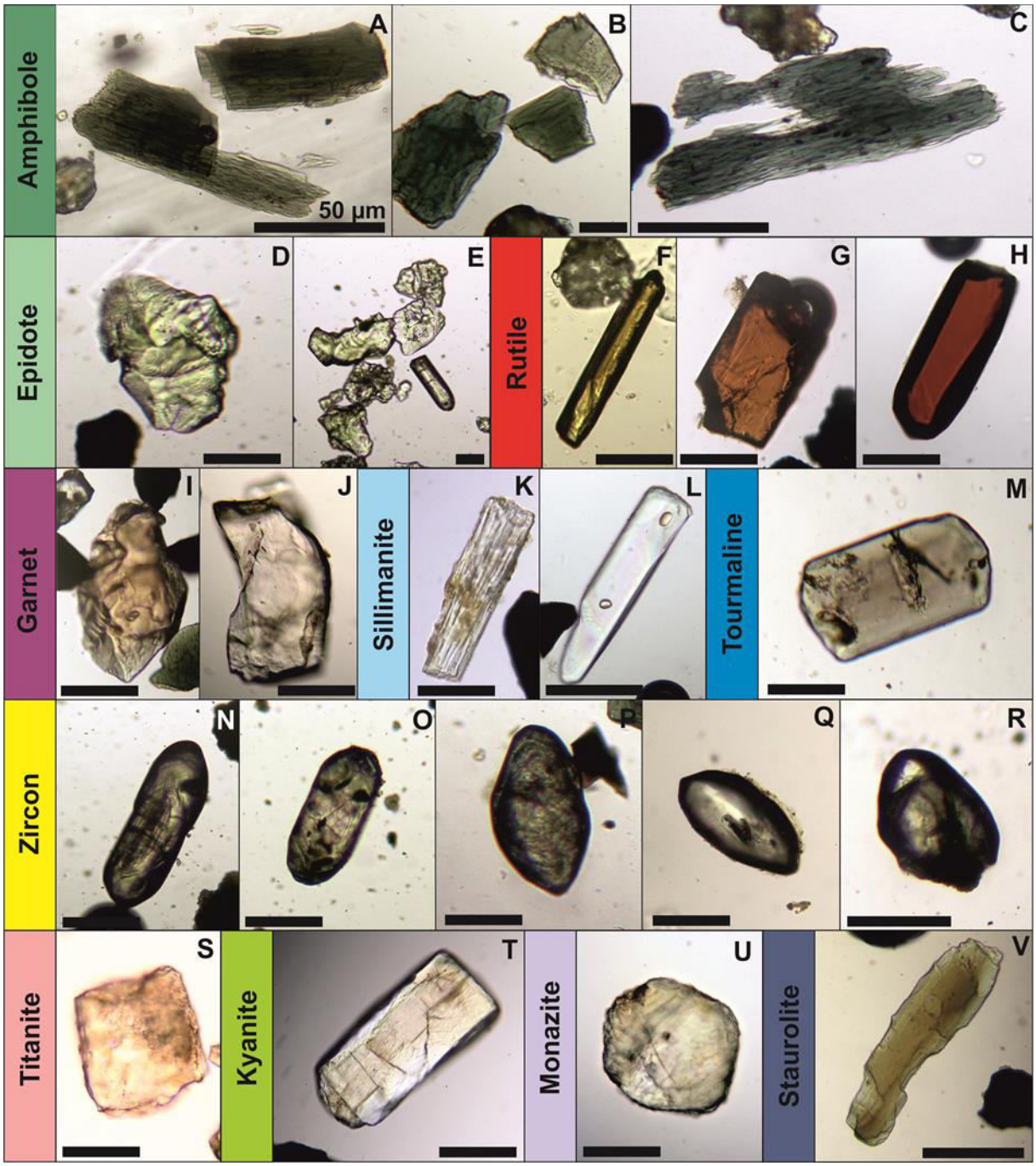

Figure 4-8. Photomicrographs of the most common heavy minerals. Black scale bars are 50 µm. (A, B, C) green-brown to blue-green irregular or rectangular hornblende fragments commonly displaying dissolution features, like corroded outlines and skeletal textures, (D, E) green to yellowish-green epidote grains with irregular habitus and patchy colour distribution, (F) yellowish-brown rutile with a slender, subrounded morphology, (G, H) red and reddish-brown angular to subrounded prismatic rutiles, (I, J) pinkish-orange and colorless irregular, feather-edged garnet fragments, (K) fibrous sillimanite (= fibrolite), (L) slender prismatic sillimanite, subrounded, (M) pinkish-green tourmaline with short prismatic morphology, (N, O, P) zircon grains with distinct zoning, and fluid and mineral inclusions, (Q, R) zircons grains without zoning, (S) colorless irregular titanite grain with yellowish to pale green tints, (T) colorless, tabular kyanite grain, (U) pale yellow, nearly colorless rounded spherical monazite grain, and (V) yellowish irregular staurolite fragment with corroded outline.

A major change in heavy mineral assemblages takes place with the onset of the Nyaburogo Formation, i.e., Group 2, and continues up to the top of Group 3 (Fig. 4-5). Heavy mineral compositions of these groups are dominated by epidote (16–82%) and amphibole (2–44%) with only minor zircon (2–14%) and garnet (1–16%). The highest amount of epidote occurs in sands of the Katorogo and Lower Nyabusosi formations (Group 3). Compared to Group 1, abundances of sillimanite (1–10%) and klinozoisite (< 8%) are slightly enriched, whereas rutile (< 4%) and kyanite (< 2%) slightly decrease. ZTR values are relatively low and range between 5 and 20. Other mineral indices proved to be less useful in this study. Both, the garnet-zircon and rutile-zircon indices show wide scattering (RuZi: 0–50; GZi: ~1–83) without a clear trend throughout the stratigraphy (Table A4-2, Appendix).

4.6.3 Mineral chemistry

Garnet

Results of chemical analysis of garnet grains from six samples are given in Table A4-3 (Appendix) and are shown in triangular plots after Mange and Morton (2007) and Aubrecht et al. (2009) (Fig. 4-9). Overall, three main cluster (I, II, III) of garnet compositions can be identified.

Cluster I consists of almandine- and pyrope-rich garnet that is low in grossular (< 10%) and spessartine. Within the discrimination diagram after Mange and Morton (2007) they plot in field A, which suggests garnets from high-grade metasedimentary rocks and charnockites. According to Aubrecht et al. (2009), their composition is closest to that from felsic and intermediate granulites.

Cluster II is characterized by higher almandine, lower pyrope, medium grossular (> 10%) and low spessartine. Within the diagram of Mange and Morton (2007) they occupy fields B (amphibolite-facies metasediment), and C (high-grade mafic rocks). According to Aubrecht et al. (2009), these garnets are equivalent to those formed within granulite-, eclogite- and amphibolite-facies rocks. Within the pyrope–almandine–spessartine diagram they plot in the fields 2, 5 and 7, mainly corresponding to high-grade ultramafic rocks, high-grade mafic rocks and amphibolite-facies rocks.

Cluster III includes almandine-spessartine garnets low in grossular and pyrope but relatively high in spessartine occupying field B after Mange and Morton (2007) and field 6/7 after Aubrecht et al. (2009). This garnet type is assigned to be derived from low-grade to medium-grade metasedimentary amphibolite-facies rocks (Krippner et al., 2014).

Group 1 (Kisegi, Kakara, Oluka) mainly shows garnet grains from Cluster I and Cluster II, and few from Cluster III in the Kisegi Formation. Garnet of the Kisegi and Kakara formations of Group 1 are predominantly from high-grade metasedimentary terrains (Cluster I). Group 2 (Nyaburogo, Nyakabingo) is characterized by garnet of Cluster II, whereby the high pyrope variety of this Cluster (similar to field 2, after Aubrecht et al. (2009)) is not present in the Nyaburogo Formation. In the Nyakabingo Formation also garnet of Cluster I occurs. For Group 3 (Katorogo, Nyabusosi), garnet chemistry is only available for the Nyabusosi Formation. This sample is dominated by garnet grains of Cluster III, but also contains some grains of Cluster II.

Rutile

Chemical analyses of rutile reveal large variations in trace element compositions with Al: ~20–2000 ppm, Si: ~70–5500 ppm, Nb: ~0–16900 ppm; Cr: ~30–5600 ppm; Fe: ~90–11300 ppm; V: ~0–9100 ppm, and Zr: ~80–4300 ppm (Table A4-4, Appendix). Variations of rutile chemistry in Group 1 and Group 2, however, are similar and show low Cr/Nb ratios (< 1) with Cr concentrations < 1000 ppm and Nb concentrations < 3000 ppm.

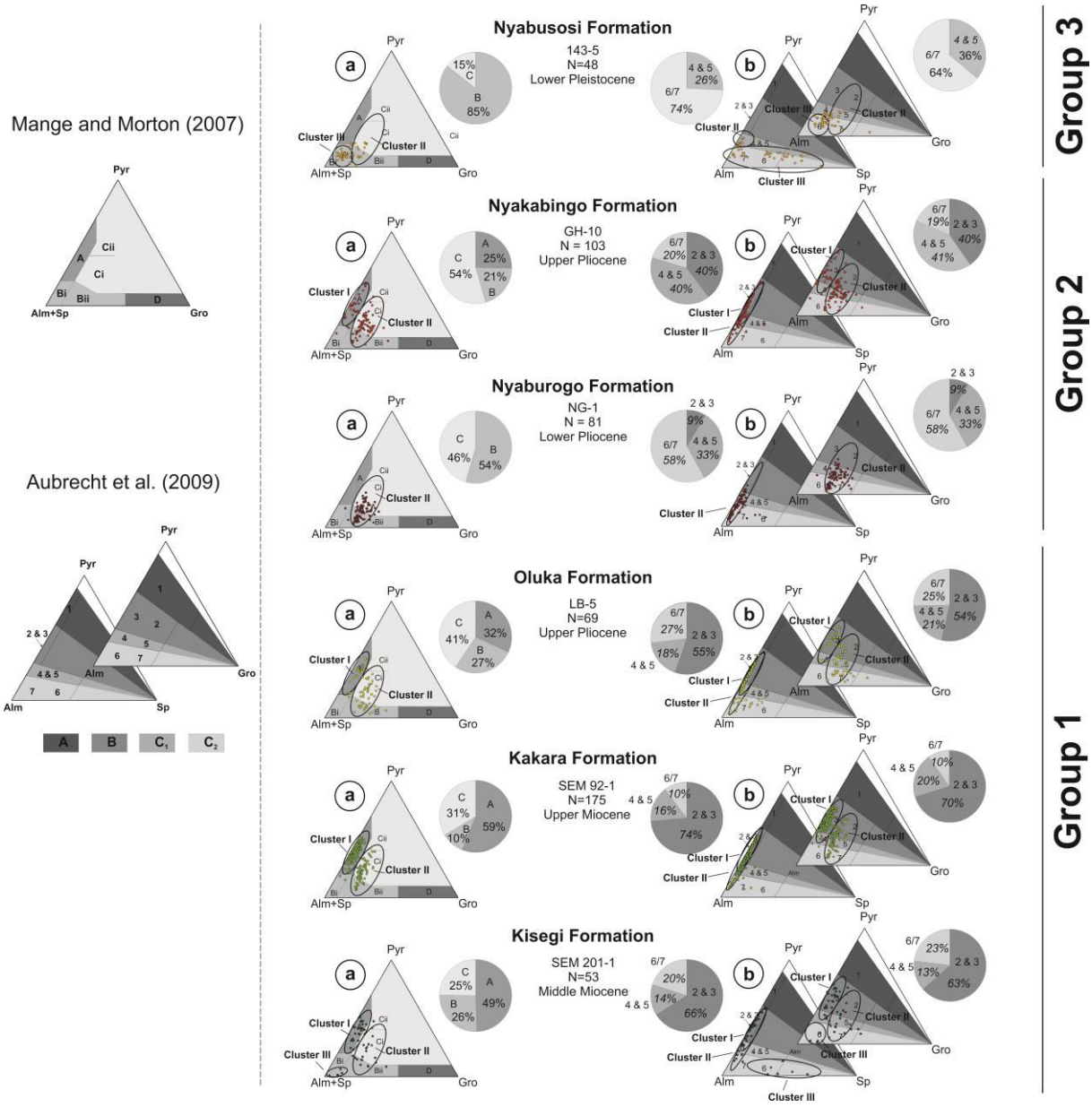

Figure 4-9. Garnet chemistry. (a) Discrimination diagram after Mange and Morton (2007) with the fields (A) mainly from high-grade granulite-facies metasedimentary rock or charnockite and intermediate felsic igneous rocks, (Bi) intermediate to felsic igneous rocks, (Bii) amphibolite-facies metasedimentary rocks, (Ci) mainly high-grade mafic rocks, (Cii) ultramafics with high Mg (pyroxenite and peridotite), (D) metasomatic rocks, very low-grade metamafic rocks and ultrahigh temperature metamorphosed calc-silicate granulite. (b) Alm-Sp-Pyr and Alm-Gro-Pyr plots after Aubrecht et al. (2009) with discrimination fields (A) high-pressure (HP) to ultrahigh-pressure (UHP) rocks, (B) eclogite- and granulite-facies rocks, (C1) higher amphibolite- to granulite-facies rocks and field (C2) amphibolite-facies rocks, but also other rocks such as blueschist, skarn, serpentinite and igneous rocks. Source rocks are further divided into 7 subgroups. (1) garnets UHP eclogite or garnet peridotite, (2) HP eclogite and HP mafic granulite, (3) felsic and intermediate granulite, (4) gneiss metamorphosed under pressure and temperature conditions transitional to granulite- and amphibolite-facies metamorphism, (5) amphibolite metamorphosed under pressure and temperature conditions transitional to granulite- and amphibolite-facies metamorphism, (6) gneiss metamorphosed under amphibolite-facies conditions, (7) amphibolite metamorphosed under amphibolite-facies conditions.

Alm = almandine, Sp = spessartine, Pyr = pyrope, Gro = grossular

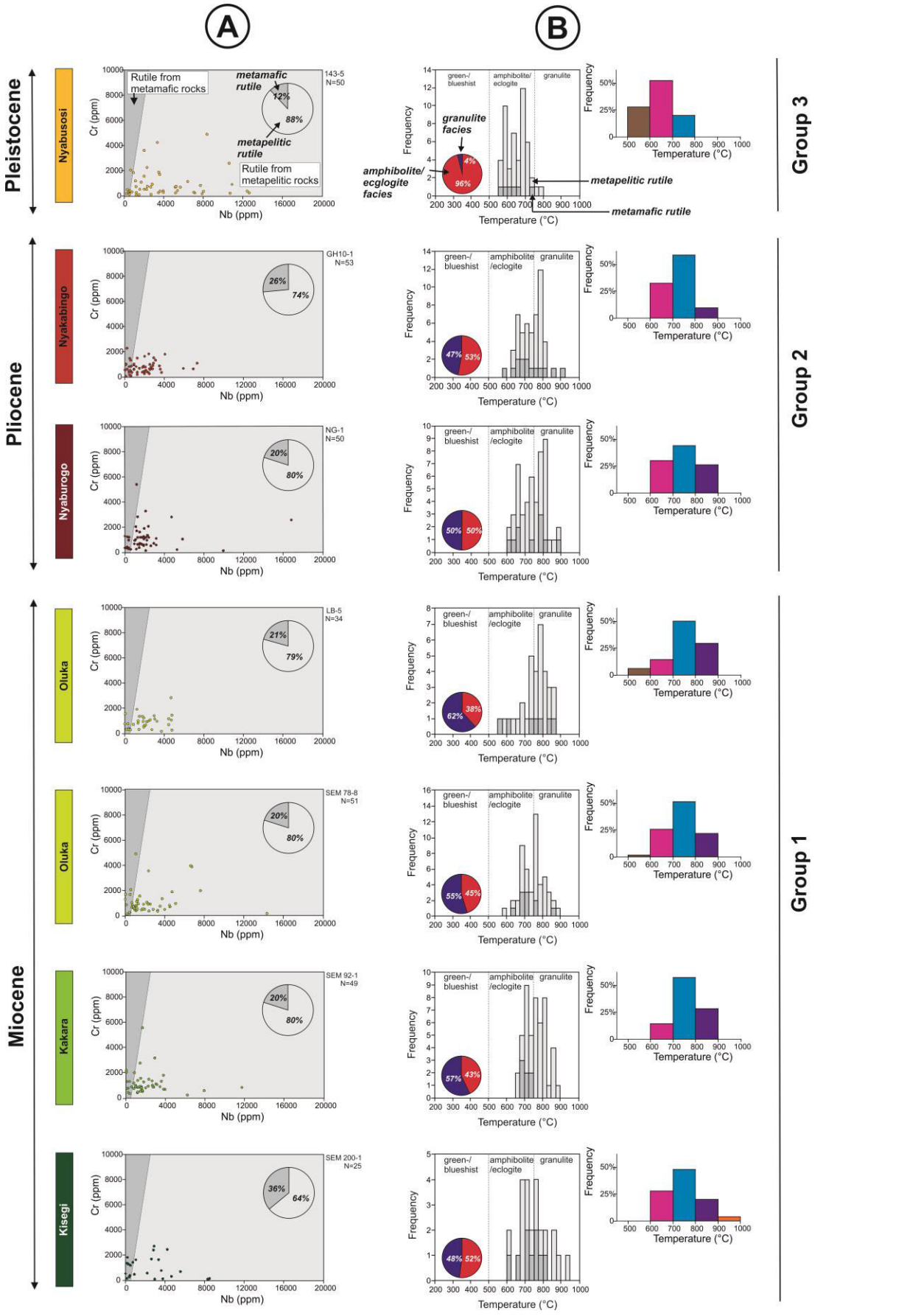

Figure 4-10. Rutile chemistry. (A) Cr-Nb plots discriminating rutile into metapelitic and metamafic rutile (Triebold et al., 2012), (B) calculated Zr-in-rutile formation temperatures (Tomkins et al., 2007).

According to the Cr-Nb diagram of Triebold et al. (2012), most of these rutiles are of metapelitic origin (64–80%) and only 20–36% are metamafic (Fig. 4-10A). The highest amount of metamafic rutiles occurs in the lower Kisegi Formation (Group 1). Rutile growth temperatures calculated after Tomkins et al. (2007) range between ~550 and 980 °C, which is equivalent to amphibolite-/eclogite- to granulite-facies conditions. There is no distinct trend between Groups 1 and 2, suggesting a mixed source for rutile (Fig. 4-10B).

In the single sample of Group 3 (Nyabusosi Formation), the majority of rutile grains are of metapelitic origin (88%). Some metapelitic grains exhibit high Nb values of > 3000 ppm. Rutile geothermometry reveals that granulite-facies grains are almost entirely absent and rutile from amphibolite-/eclogite-facies rocks becomes dominant, with formation temperatures between 550 and 750 °C. Overall, there is no contribution from green- or blueshist-facies rocks throughout the stratigraphy.

4.7 Discussion

The three groups defined according to their similar petrographic, heavy mineral and single grain composition can be used to set up a 3-stage evolutionary model of rifting and drainage systems in the Albertine Rift area. Hereby, the spatial distribution of different rock assemblages is considered, i.e., the Archean Tanzania Craton, the Paleoproterozoic Buganda-Toro belt, the Paleoproterozoic granites, and the Neoproterozoic Bunyoro-Kyoga Group. Specific attention is paid to the Rwenzori horst block to detect its uplift by provenance changes. Furthermore, petrographic signatures of modern river sands are used as reported from Schneider et al. (2016).

Stage 1. Middle to upper Miocene (Kisegi, Kakara, Oluka formations)

A distinct feature of Group 1 is the high content of zircon which correspond to modern sands draining the Archean Gneiss-Granulite complex (Tanzania Craton), granite, and metasedimentary rocks of the Bunyoro-Kyoga Group (Schneider et al., 2016). Garnet occurs either in rocks of the Buganda-Toro belt (garnet-mica schist, garnet-biotite schist, kyanite-garnet schist, mica-schist, amphibolite), or in bands separating gneissic units within the Archean Gneiss-Granulite complex (Appel et al., 2005; Karl, 2008; Link et al., 2010). Modern river sands show enhanced amounts of garnet only in rivers draining the Archean Gneiss-Granulite complex around the rift shoulders (Schneider et al., 2016). A major origin from this source is underlined by garnet and rutile chemistry, which mostly indicate a high-grade to very high-grade metamorphic source. This implies that sediment of Stage 1 was transported from basement rocks located east of Lake Albert with a main transport direction from the northeast (Fig. 4-11). In the lower Kisegi Formation some spessartine-rich garnet grains and metamafic rutiles indicate minor input from mafic medium-grade metasedimentary rocks from southern sources which became dominant during Stage 3.

The NE-SW directed supply system during the Miocene, as reconstructed from our provenance data, corresponds to the orientation of river valleys on the Ugandan Plateau until present (Pickford et al., 1993). We can therefore support previous assumptions concerning flow directions based on paleobiological evidence (Pickford et al., 1993) or paleocurrent indicators in Kisegi sediment (Bishop, 1965). Moreover, this is in line with geomorphological models of a westward directed river system draining the Ugandan Plateau and Albertine Rift area towards the Congo Basin and the Atlantic Ocean before this continent-wide system was dissected by formation of the western branch of the EARS (Cooke, 1958; Bishop, 1965; Taylor and Howard, 1999; summarized in Pickford et al., 1993). Gautier (1965) assumes that this flow system was installed during the middle Miocene when the Kenya Rift experienced a pulse of rifting and uplift (e.g., Smith, 1994). In general, modern rivers still follow this inherited drainage pattern, but are partly dissected and/or flow directions are inverted.

Stage 2. Early Pliocene – late Pliocene (Nyaburogo, Nyakabingo formations)

Between Group 1 and Group 2 a significant change in provenance is observed by a shift towards epidote-/amphibole-dominated heavy mineral assemblages and garnet and rutile chemistry, pointing to mostly moderately metamorphosed intermediate to mafic rocks (epidote-amphibolite facies). Similar signatures are observed in modern rivers (Schneider et al., 2016) draining the Archean Gneiss-Granulite complex in southwestern Uganda. Thus, we believe that sediment for Group 2 was most likely shed by Archean basement rocks located on the rift shoulder in a sector reaching from the northern part of the Rwenzori Mountains towards the rift shoulder east of the study area (Fig. 4-11). Although, the exact timing of this shift cannot be determined due to gaps in the sediment logs, it is likely to have occurred in the lower Pliocene between ~5.5 and 5.0 Ma.

Garnet types of Cluster I (high-grade metasedimentary rocks) and high-pyrope garnet of Cluster II (high-grade crustal rocks) lacking in the Nyaburogo Formation indicate an interruption of sediment input from high-grade metamorphic (granulite-facies) sources. We rule out that garnet varieties are affected by hydraulic sorting (see Krippner et al., 2015), because measured garnet grains are all in the same grain size range (63–125 µm). Reoccurrence of high-grade garnet accompanied by an increased amount of garnet and ZTR in the Nyakabingo Formation might be either caused by recycling of sediment from Group 1 and/or some regenerated sediment input from the same source shedding sediment of Group 1 (northeastern source), indicating that a tectonic pulse reinvigorated bedrock erosion. However, a more likely possibility displays unroofing of basement lithologies within the source area (northern Rwenzoris and rift shoulder east to the study area) leading to erosion of higher-grade metamorphic rocks. Nevertheless, the dominance of sediment in Stage 2 originating from moderately metamorphosed rocks gives evidence for a shift of major sediment supply from southern areas (SW Uganda) in the early Pliocene.

This first disturbance of the NE-SW-draining system (Stage 1) has been initiated most probably by uplift of the southern region forcing rivers to incise or redirect towards north. Furthermore, the shift in provenance at around 5.5–5.0 Ma is synchronous with a shift from an accommodation- to a supply-controlled system in synrift sedimentation (Roller et al., 2010). While in Stage 1, rift topography is not evident in the sedimentary record (pre-rift phase; Roller et al., 2010), the increased generation of accommodation space by subsidence of the rift floor concurrent with increased sediment input and uplift oft rift-flanks indicates a major tectonic pulse, i.e., the Albertine Rift graded into the syn-rift stage not before ca. 5 Ma.

This change in river network and sedimentation pattern in the early Pliocene is not reported in paleohydrological models so far, and lags behind the formation of the giant Palaeolake Obweruka at around 8 Ma spreading over ca. 500 km (Fig. 4-3). According to existing models, the formation of the lake marks the first major rifting pulse in the Albertine Rift (Pickford et al., 1993) that is reported to have occurred synchronous with formation and subsidence of the northern basin of Lake Tanganyika (Cohen et al., 1993) and the Malawi Basin (Ebinger, 1984, 1987, 1989; Flannery and Rosendahl, 1990). The Kenya Rift was also affected by major fault movements at that time (Pickford et al., 1993). Although some time lag between initiated tectonic activity and adaption of the river network and sedimentation pattern can be expected, the proximity of source-sink systems makes a response time of several million years improbable. The initiation of this large lake might instead be linked to increased humidity possibly in concert with increased downwarping of the region. This hypothesis is supported by climate indicators showing increased humidity in the Oluka Formation of the upper Miocene (Dechamps et al., 1992; Pickford, 1992).

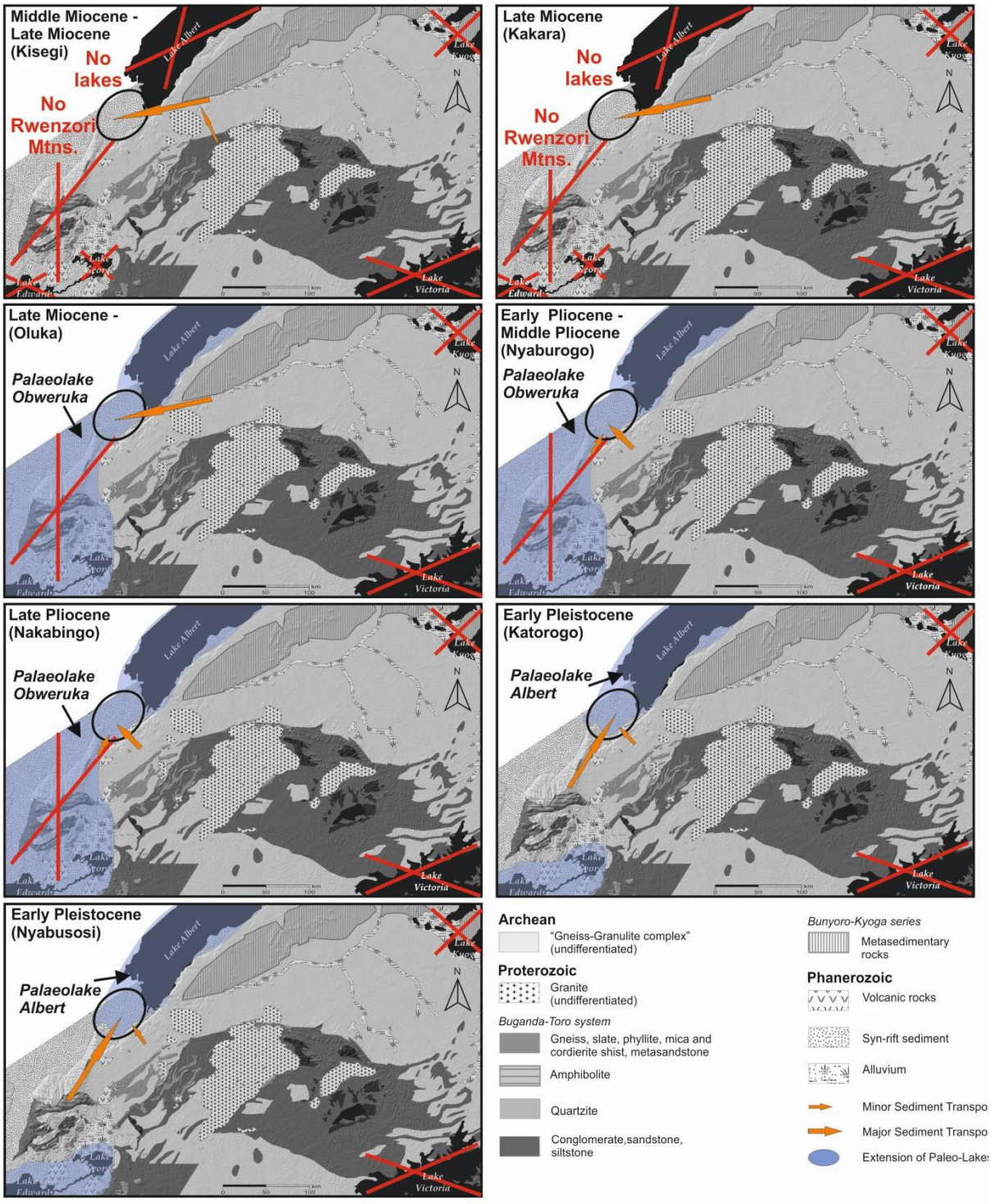

Figure 4-10. Sketch maps of the Albertine Rift showing interpreted sediment transport directions from the Middle Miocene to Pleistocene. Reconstruction of lake extension after Pickford et al. (1993).

Stage 3. Early Pleistocene (Katorogo, Nyabusosi)

Stage 3 differs significantly from the previous units by a provenance signature mainly from lower-grade metamorphic rocks. Sediment of the Katorogo Formation and the Nyabusosi Formation is rich in polycrystalline quartz, amphibole and epidote and shows a high amount of cluster III garnet (low-

medium grade metasediments) and low-temperature rutile (amphibolite-eclogite facies). These mineral suites can be assigned to the Buganda-Toro greenstone belt, also crossing the central and southern part of the Rwenzori Mountains. This is also confirmed by a similar composition between sediments of Group 3 and modern rivers draining the Rwenzori Mountains (Garzanti et al., 2013; Schneider et al., 2016) making this region as the most likely source in Stage 3 (Fig. 4-11). Increasing immaturity of sediments, indicated by higher amounts of rock fragments, including metabasite grains, mica and accessories, points to shorter distance transport. Accelerated uplift of the Rwenzori horst block is indicated by the increase of amphibole in the upper Nyabusosi Formation.

This second major change of the supply system between Stage 2 and 3 is well documented by provenance, onset of coarse-grained sediment facies, and biostratigraphic gaps. The gastropod associations (G2a, GX, GX') at ~2.4 Ma and ~2.0 Ma are missing. Due to the proximity of the signal, we suggest that this provenance change reflects the initiation of the extreme uplift of the Rwenzori fault block. The Buganda-Toro belt is also developed south of the Rwenzori horst block, but the coarse-grained sediment facies contradicts far-distance transport as well as the absence of volcanic grains from the Virunga Volcanic Province which had been active at this time and is well connected to the river system south of the Rwenzori Mountains around Lake Edward. Moreover, during the middle and upper Pleistocene repeated glaciations of the top regions of the Rwenzori Mountains down to ca. 2000 m accelerated erosion and sediment supply to surrounding areas (Kaufmann et al., 2015).

The timing and pattern of this second change of the supply system is in line with previous models. At the end of the Pliocene, Palaeolake Obweruka was fragmented into southern and northern basins occupied by the Paleolakes Lusso and Kaiso for another 0.5 million years (Van Damme and Pickford, 1995). Van Damme and Pickford (1995) link the fragmentation at ~2.5 Ma with the major uplift of the Rwenzori Mountains, which is supported by our provenance data. Linking provenance data with stratigraphy, the major uplift of the Rwenzori Mountains is likely to have started during the early Nyabusosi Formation (~1.8 Ma). The tectonic pulse around the Pliocene/Pleistocene boundary is also documented by initiation of inversion tectonics in the rift, e.g., the investigated Kisegi area due to strike-slip movements and rotation of the Rwenzori Block (Koehn et al., 2010). The beginning of extreme uplift of the Rwenzori horst block is coincident with other rifting events in East Africa, such as major faulting and subsidence in the Kenya Rift (Pickford, 1994) and rifting in the southern Lake Tanganyika Basin (Cohen et al., 1993) mainly caused by NW-SE striking extensional movement of the African and Somalian plates (Chorowicz, 2005) with an opening velocity of 2.1 mm/year for the Albertine Rift (Calais et al., 2006; Stamps et al., 2008).

4.8 Conclusion

The integration of provenance techniques, including framework petrography, heavy mineral content and chemical analysis of detrital garnet and rutile proved to be successful to discover significant changes in the detrital sources of synrift sediments in the Albertine Rift during the middle Miocene to Pleistocene. Overall, our provenance data allow to modify and refine existing evolutionary models for the western branch of the EARS.

We could identify three major stages of changing sediment supply to the southern Albertine Rift area which can be interpreted in terms of rifting activity:

- Stage 1 is characterized by a NE-SW trending supply system which is still inherited in current orientations of river valleys on the Ugandan Plateau. Detritus mainly derived from the Archean Gneiss-Granulite complex of the Tanzania craton in north-eastern Uganda.

- Stage 2: provenance signatures point to medium-grade to high-grade metamorphic terrains with some admixture of high-grade to granulite metamorphic rocks. This spectrum corresponds to significant input from Archean gneiss located in the south and south-east. This first transition of provenance signatures can be dated by biostratigraphy to the early Pliocene, i.e., between 5.5–5.0 Ma. This timing lags ca. 3 million years behind formation of the giant Palaeolake Obweruka at ca. 8 Ma which has been argued to reflect initiation of the synrift stage and graben formation (Pickford et al., 1993; Roller et al., 2010). Because a response time of the sediment supply system of over 3 million years is improbable, we suggest that the formation of Palaeolake Obweruka is primarily driven by increased humidity, but still represents the pre-rift stage of the Albertine Rift concurrent with regional downwarping. Here we suggest from provenance pattern that the synrift stage of the Albertine Rift has not started before ca. 5 Ma.

- Stage 3: after ca. 2.5 Ma provenance signals hint to predominantly low-grade metamorphic sources with a dominance of metasedimentary rocks. This makes the Buganda-Toro belt in the nearby Rwenzori horst block as the most probable source. The rifting process is now dominated by rapid uplift of rift shoulders, in particular the Rwenzori block which has reached more than 5000 m above sea level at present. Moreover, during the middle to upper Pleistocene the top area of the Rwenzori Mountains experienced repeated glaciation enhancing erosion and sediment supply. The tectonic pulse around the Pliocene/Pleistocene boundary is concurrent with the initiation of inversion tectonics in the Albertine Rift and increased rifting activities in other parts of the EARS indicating a regional change of the stress pattern.

4.9 Acknowledgements

The subproject B3 - Linking Source and Sink in the Rwenzori Mountains and adjacent rift basins, Uganda is funded by the DFG grant H1643–7/1 within the interdisciplinary research program RiftLink – Rift Dynamics and Uplift and Climate Changes in Equatorial Africa. We want to thank the Uganda National Council for Science and Technology (UNCST) and the Uganda Wildlife Authority (UWA) for research permissions. We thank our Ugandan research partners from Makerere University for close cooperation, A. Schumann for his on-site guidance and our driver Kitam Ali for his profound help and field endurance. Special thanks go to Dr. Stephan Buhre (Johannes Gutenberg University, Mainz) for his help with EMP analyses. We acknowledge detailed and stimulating reviews by Luca Carraciolo, Carita Augustsson and Jasper Knight.

4.10 References

Abdelsalam, M. G., Katumwehe, A. B., Atekwana, E. A., Le Pera, A. K., Achang, M., 2016. The Paleoproterozoic Singo Granite in south-central Uganda revealed as a Nested Igneous Ring Complex using Geophysical Data. Journal of African Earth Sciences, 116, 198–212.

Abeinomugisha, D., 2010. Development of a Petroleum System in a Young Rift Basin Prior to Continental Breakup: The Albertine Graben of the East African Rift System. In: AAPG International Convention and Exhibition, Sept. 12–15, 2010, Calgary, Alberta, Canada, unpublished.

Acocella, V., Korme, T., 2002. Holocene extension direction along the main Ethiopian Rift, East Africa. Terra Nova, 14, 191–197.

Aitchison, J., Egozcue, J. J., 2005. Compositional data analysis: where are we and where should we be heading? Mathematical Geology, 37, 829–850.

Appel, P., Schenk, V., Schumann, A., 2005. PT path and metamorphic ages of pelitic schists at Murchison Falls, NW Uganda Evidence for a Pan-African tectonometamorphic event in the Congo Craton. European Journal of Mineralogy, 17, 655–664.

Aubrecht, R., Méres, Š., Sýkora, M., Mikus, T., 2009. Provenance of the detrital garnets and spinels from the Albian sediments of the Czorsztyn Unit (Pieniny Klippen Belt, Western Carpathians, Slovakia). Geologica Carpathica, 60, 463–483.

Bauer, F. U., Koehn, D., Glasmacher, U. A., 2010a. Long-term rift evolution. International Journal of Earth Sciences, 99, 1483–1485.

Bauer, F. U., Glasmacher U. A., Ring U., Schumann A., Nagudi B., 2010b. Thermal and exhumation history of the central Rwenzori Mountains, Western Rift of the East African Rift System, Uganda. International Journal of Earth Sciences, 99, 1575–1597.

Bishop, W. W., 1965. Quaternary geology and geomorphology in the Albertine Rift Valley, Uganda. In: Wright Jr., H.E., Frey, D.G. (Eds.), International studies on the Quaternary, pp. 293–321.

Bjørlikke, K. O., 1973. Glacial conglomerates of late Precambrian age from the Bunyoro Series, W. Uganda. Geologische Rundschau, 62, 938–947.

Boccaletti, M., Bonini, M., Mazzuoli, R., Abebe, B., Piccardi, L., Tortorici, L., 1998. Quaternary oblique extensional tectonics in the Ethiopian Rift (Horn of Africa). Tectonophysics, 287, 97–116.

Bosworth, W., Lambiase, J., Keisler, R., 1986. A new look at Gregory's rift: the structural style of continental rifting. Eos, Transactions American Geophysical Union, 67, 577–583.

Bosworth, W., Strecker, M. R., Blisniuk, P. M., 1992. Integration of East African paleostress and present-day stress data: implications for continental stress field dynamics. Journal of Geophysical Research, 97, 11851–11865.

Brüsch, D., in prep. Miocene to Pleistocene environmental change in the western branch of the East African Rift from high-resolution records of synrift sediments (Albertine rift, Uganda). Dissertation, Technical University of Darmstadt.

Calais, E., Ebinger, C., Hartnady, C., Nocquet, J. M., 2006. Kinematics of the East African Rift from GPS and earthquake slip vector data. In: Yirgu, G., Ebinger, C.J., Maguire, P.K.H. (Eds.), Structure and evolution of the rifts systems within the Afar volcanic province, Northeast Africa. Geological Society, London, Special Publications, 259, pp. 9–22.

Chorowicz, J., 2005. The East African rift system. Journal of African Earth Sciences, 43, 379–410.

Chorowicz, J., Mukonki, M. B., 1979. Lintaments anciens, zones transformantes recentes et gtotectonique des fesses de I'Est Africain, d'aprts la teledetection et la microtectonique. Musee Royal d Afrique centrale, Tervuren (Belgique), Departement des Geologie et des Mines, Rapport annuel, 143–167.

Chorowicz, J., Collet, B., Bonavia, F. F., Korme, T., 1994. Northwest to north-northwest extension direction in the Ethiopian rift deduced from the orientation of extension structures and fault-slip analysis. Geological Society of America Bulletin, 106, 1560–1570.

Cohen, A. S., Soreghan, M. J., Scholz, C. A., 1993. Estimating the age of formation of lakes: an example from Lake Tanganyika, East African Rift system. Geology, 21, 511–514.

Cooke, H. B. S., 1958. Observations relating to the Quaternary environments in East and Southern Africa. Transactions of the Geological Society of South Africa, 60 Annex, 1–74.

Dechamps, R., Senut, B., Pickford, M., 1992. Fruits fossiles pliocènes et pléistocènes du Rift occidental ougandais. Signification paléoenvironnementale. Comptes rendus de l'Académie des sciences. Série 2, Mécanique, Physique, Chimie, Sciences de l'univers, Sciences de la Terre, 314, 325–331.

Decker, J., Helmold, K. P., 1985. The effect of grain size on detrital modes: a test of the Gazzi–Dickinson point-counting method — discussion. Journal of Sedimentary Petrology, 55, 618–620.

Deer, W. A., Howie, R. A., Zussman, J., 1992. An introduction to the rock-forming minerals, 2nd ed. Longman Scientific & Technical, Harlow.

De Heinzelin, J., 1962. Les formations du Western Rift et de la cuvette congolaise. Annales du Musée Royal de L'afrique Centrale, 40, 219–243.

DeMenocal, P., 1995. Plio-Pleistocene African Climate. Science, 270, 53–59.

DeMenocal, P., 2004. African climate change and faunal evolution during the Pliocene-Pleistocene. Earth and Planetary Science Letters, 220, 3–24.

Dickinson, W. R., 1970. Interpreting detrital modes of graywacke and arkose. Journal of Sedimentary Research, 40, 695–707.

Doornkamp, J. C., 1968. The role of inselbergs in the geomorphology of Southern Uganda. Transactions of the Institute of British Geographers, 44, 151–162.

Ebinger, C. J., Crow, M. J., Rosendahl, B. R., Livingstone, D. A., LeFournier, J., 1984. Structural evolution of Lake Malawi, Africa. Nature, 308, 627–629.

Ebinger, C. J., Rosendahl, B. R., Reynolds, D. J., 1987. Tectonic model of the Malaŵi rift, Africa. Tectonophysics, 141, 215–235.

Ebinger, C. J., 1989. Tectonic development on the western branch of the East African rift system. Geological Society of America Bulletin, 101, 885–903.

Félix, C., 1972. Evolution micro-structurale de micaschistes plurifaciels provenant de l'allochtone du massif du Ruwenzori (Zaïre). Annales de la Société géologique de Belgique, 95, 217–228.

Félix, C., 1975. Contribution à l'étude petrologique et géologique du Massif du Ruwenzori. Mémoires de l'Académie Royale des Sciences d'Outre-mer. Classe des sciences naturelles et médicales, 19, 1–67.

Flannery, J. W., Rosendahl, B. R., 1990. The seismic stratigraphy of Lake Malawi, Africa: implications for interpreting geological processes in lacustrine rifts. Journal of African Earth Sciences (and the Middle East), 10, 519–548.

Gabert, G., 1990. Lithostratigraphic and tectonic setting of gold mineralization in the Archean cratons of Tanzania and Uganda, East Africa. Precambrian Research, 46, 59–69.

Garzanti, E., 2016. From static to dynamic provenance analysis—Sedimentary petrology upgraded. Sedimentary Geology, 336, 3–13.

Garzanti, E., Andò, S., France-Lanord, C., Vezzoli, G., Censi, P., Galy, V., Najman, Y., 2010. Mineralogical and chemical variability of fluvial sediments: 1. Bedload sand (Ganga–Brahmaputra, Bangladesh). Earth and Planetary Science Letters, 299, 368–381.

Garzanti, E., Andó, S., France-Lanord, C., Censi, P., Vignola, P., Galy, V., Lupker, M., 2011. Mineralogical and chemical variability of fluvial sediments 2. Suspended-load silt (Ganga–Brahmaputra, Bangladesh). Earth and Planetary Science Letters, 302, 107–120.

Garzanti, E., Padoan, M., Andò, S., Resentini, A., Vezzoli, G., Lustrino, M., 2013. Weathering and relative durability of detrital minerals in equatorial climate: sand petrology and geochemistry in the East African Rift. The Journal of Geology, 121, 547–580.

Gautier, A., 1965. Geological investigation in the Sinda Mohari (Ituri, NE-Congo). A monograph on the geological history of a region in the Lake Albert Rift. Ganda-Congo Expedition, Ghent University, 158 pp.

Gautier, A., 1970. Fossil freshwater mollusca of the Lake Edward–Lake Albert Rift. Annual Reports of the Royal Museum of Central Africa, Tervuren, 67, 1–144.

Hammer Ø., Harper D. A. T., Ryan P. D., 2001. PAST: Paleontological Statistics Software Package for Education and Data Analysis. Palaeontol Electron 4. Available via http://palaeo-electronica.org/2001_1/past/issue1_01.htm

Hubert, J. F., 1962. A zircon-tourmaline-rutile maturity index and the interdependence of the composition of heavy mineral assemblages with the gross composition and texture of sandstones. Journal of Sedimentary Research, 32, 440–450.

Jacobs, B. F., Deino, A. L., 1996. Test of climate–leaf physiognomy regression models, their application to two Miocene floras from Kenya, and 40Ar/39Ar dating of the Late Miocene Kapturo site. Palaeogeography, Palaeoclimatology, Palaeoecology, 123, 259–271.

Karl, M., 2008. Lithostratigraphische und strukturelle Kartierung im Zentralbereich des Rwenzori-Gebirges an der Grenze zwischen Uganda und dem Kongo, Diplomkartierung, University of Heidelberg, 182 p.

Koehn, D., Lindenfeld, M., Rümpker, G., Aanyu, K., Haines, S., Passchier, C.W., Sachau, T., 2010. Active transsection faults in rift transfer zones: evidence for complex stress fields and implications for crustal fragmentation processes in the western branch of the East African Rift. International Journal of Earth Sciences, 99, 1633–1642.

Leggo, P. J., 1974. A geochronological study of the basement complex of Uganda. Journal of the Geological Society of London, 130, 263–277.

Link, K., Koehn, D., Barth, M. G., Tiberindwa, J. V., Barifaijo, E., Aanyu, K., Foley, S. F., 2010. Continuous cratonic crust between the Congo and Tanzania blocks in western Uganda. International Journal of Earth Sciences, 99, 1559–1573.

Kaufmann, G., Hinderer, M., Romanov, D., 2015. Shaping the Rwenzoris: balancing uplift, erosion, and glaciation. International Journal of Earth Sciences, 1–18.

King, B. C., 1959a. Problems of the Precambrian of Central and Western Uganda, part I. Problems of correlation. Science Progress, London, 47, 528–542.

King, B. C., 1959b. Problems of the Precambrian of Central and Western Uganda, part II. Structures, metamorphism, and granites. Science Progress, London, 47, 723–744.

King, B. C., de Swardt, A. M. J., 1970. Problems of structure and correlation in the Precambrian systems of Central and Western Uganda. Memoir of the Geological Survey of Uganda, 11, 133 p.

Krippner, A., Meinhold, G., Morton, A.C., von Eynatten, H., 2014. Evaluation of garnet discrimination diagrams using geochemical data of garnets derived from various host rocks. Sedimentary Geology 306, 36–52.

Krippner, A., Meinhold, G., Morton, A.C., Russell, E., von Eynatten, H., 2015. Grain-size dependence of garnet composition revealed by provenance signatures of modern stream sediments from the western Hohe Tauern (Austria). Sedimentary Geology 321, 25–38.

Mange, M. A., Maurer, H. F. W., 1992. Heavy minerals in colour. Chapman and Hall, London, 148 p.

Mange, M. A., Morton, A. C., 2007. Geochemistry of heavy minerals. In: Mange, M. A., Wright, D. T. (Eds.), Heavy Minerals in Use. Developments in Sedimentology, 58. Elsevier, Amsterdam, pp. 345–391.

Mange, M. A., Wright, D. T. (Eds.), 2007. Heavy minerals in use: Developments in Sedimentology 58. Elsevier, Amsterdam, 1283 p.

Mathisen, M. E., Vondra, C. F., 1983. Provenance of the Plio-Pleistocene sediments in the East Turkana basin, northern Kenya. Palaeogeography, Palaeoclimatology, Palaeoecology, 441, 141–168.

McConnell, R. B., 1972. Geological development of the rift system of eastern Africa. Geological Society of America Bulletin, 83, 2549–2572.

Meinhold, G., Anders, B., Kostopoulos, D., Reischmann, T., 2008. Rutile chemistry and thermometry as provenance indicator: an example from Chios Island, Greece. Sedimentary Geology, 203, 98–111.

Morley, C. K., 1988. Variable extension in Lake Tanganyika. Tectonics, 7, 785–801.

Morley, C. K., 1999. Geoscience of rift systems-evolution of East Africa. American Association of Petroleum Geologists Studies in Geology, 44, 242 pp.

Morton, A. C., 1985. Heavy minerals in provenance studies. In: Zuffa, G.G. (Ed.), Provenance of arenites. Dordrecht, Reidel, NATO ASI Series, 148, pp. 165–189.

Morton, A. C., Hallsworth, C. R., 1994. Identifying provenance-specific features of detrital heavy mineral assemblages in sandstones. Sedimentary Geology, 90, 241–256.

Morton, A. C., Hallsworth, C. R., 1999. Processes controlling the composition of heavy mineral assemblages in sandstones. Sedimentary Geology 124, 3–29.

Morton, A. C., Knox, R.W.B., Hallsworth, C. R., 2002. Correlation of reservoir sandstones using quantitative heavy mineral analysis. Petroleum Geoscience, 8, 251–262.

Nagudi, B., Koeberl, C., Kurat, G., 2003. Petrography and geochemistry of the Singo granite, Uganda, and implications for its origin. Journal of African Earth Science, 36, 73–87.

Pickford, M., 1992. Evidence for an arid climate in Western Uganda during the middle Miocene. Comptes rendus de l'Académie des sciences, 315, 1419–1424.

Pickford, M., 1994. Patterns of sedimentation and fossil distribution in the Kenya Rift valleys. Journal of African Earth Sciences, 18, 51–60.

Pickford, M., 1995. Fossil land snails of East Africa and their palaeoecological significance. Journal of African Earth Sciences, 20, 167–226.

Pickford, M., Senut, B., Hadoto, D., 1993. Geology and Palaeobiology of the Albertine Rift Valley, Uganda-Zaire. Vol. I: Geology. International Centre for Training and Exchanges in Geosciences, Occasional Publications, 24, 1–190.

Ring, U., 2008. Extreme uplift of the Rwenzori Mountains in the East African Rift, Uganda: Structural framework and possible role of glaciations. Tectonics, 27. TC4018, doi: 10.1029/2007TC002176.

Ring, U., Betzler, C., Delvaux, D., 1992. Normal vs. strike-slip faulting during rift development in East Africa: the Malawi rift. Geology, 20, 1015–1018.

Roberts, E. M., Stevens, N. J., O'connor, P. M., Dirks, P. H. G. M., Gottfried, M. D., Clyde, W. C., Clyde, R. A., Armstrong, A. I. S, Hemming, S., 2012. Initiation of the western branch of the East African Rift coeval with the eastern branch. Nature Geoscience, 5, 289–294.

Roller, S., Hornung, J., Hinderer, M., Ssemmanda, I., 2010. Middle Miocene to Pleistocene sedimentary record of rift evolution in the southern Albertine Graben (Uganda). International Journal of Earth Sciences, 99, 1643–1661.

Schlüter, T., 2008. Geological Atlas of Africa, 2nd edition, Springer Verlag, Berlin, 307 p.

Schneider, S., Hornung, J., Hinderer, M., Garzanti, E., 2016. Petrography and geochemistry of modern river sediments in an equatorial environment (Rwenzori Mountains and Albertine rift, Uganda)—Implications for weathering and provenance. Sedimentary Geology, 336, 106–119.

Senut, B., Pickford, M., 1994. Geology and Palaeobiology of the Albertine Rift Valley, Uganda-Zaire. International Centre for Training and Exchanges in Geosciences, Occasional Publications, 29, 1–423.

Smith, M., 1994. Stratigraphic and structural constraints on mechanisms of active rifting in the Gregory Rift, Kenya. Tectonophysics, 236, 3–22.

Stamps, D. S., Calais, E., Saria, E., Hartnady, C., Nocquet, J. M., Ebinger, C. J., Fernandes, R. M., 2008. A kinematic model for the East African Rift. Geophysical Research Letters, 35, L05304, doi:10.1029/2007GL032781.

Taylor, R. G., Howard, K. W. F., 1999. The influence of tectonic setting on the hydrological characteristics of deeply weathered terrains: evidence from Uganda. Journal of Hydrology, 218, 44–71.

Tiercelin, J. J., Chorowicz, J., Bellon, H., Richert, J. P., Mwanbene, J. T., Walgenwitz, F., 1988. East African Rift System: offset, age and tectonic significance of the Tanganyika-Rukwa-Malawi intracontinental transcurrent fault zone. Tectonophysics, 148, 241–252.

Tomkins, H. S., Powell, R., Ellis, D. J., 2007. The pressure dependence of the zirconium-inrutile thermometer. Journal of Metamorphic Geology, 25, 703–713.

Trauth, M. H., Maslin, M. A., Deino, A., Strecker, M. R., 2005. Late Cenozoic moisture history of East Africa. Science, 309, 2051–2053.

Triebold, S., von Eynatten, H., Luvizotto, G. L., Zack, T., 2007. Deducing source rock lithology from detrital rutile geochemistry: an example from the Erzgebirge, Germany. Chemical Geology, 244, 421–436.

Triebold, S., von Eynatten, H., Zack, T., 2012. A recipe for the use of rutile in sedimentary provenance analysis. Sedimentary Geology, 282, 268–275.

Van Damme, D., Pickford, M., 1995. The late Cenozoic Ampullariidae (Mollusca, Gastropoda) of the Albertine Rift Valley (Uganda-Zaire). Hydrobiologia, 316, 1–32.

Van Damme, D., Pickford, M., 1998. The late Cenozoic Viviparidae (Mollusca, Gastropoda) of the Albertine Rift Valley (Uganda—Congo). Hydrobiologia, 390, 171–217.

Van Damme, D., Pickford, M., 2003. The late Cenozoic Thiaridae (Mollusca, Gastropoda, Cerithioidea) of the Albertine Rift Valley (Uganda-Congo) and their bearing on the origin and evolution of the Tanganyikan thalassoid malacofauna. Hydrobiologia, 498, 1–83.

Van Damme, D., Pickford, M., 2010. The Late Cenozoic bivalves of the Albertine Basin (Uganda-Congo). Geo-Pal Uganda, 1–128.

Versfelt, J., Rosendahl, B. R., 1989. Relationships between pre-rift structure and rift architecture in Lakes Tanganyika and Malawi, East Africa. Nature, 337, 354–357.

Von Eynatten, H., Gaupp, R., 1999. Provenance of Cretaceous synorogenic sandstones in the Eastern Alps: constraints from framework petrography, heavy mineral analysis and mineral chemistry. Sedimentary Geology, 124, 81–111.

Zack, T., Kronz, A., Foley, S. F., Rivers, T., 2002. Trace element abundances in rutiles from eclogites and associated garnet mica schists. Chemical Geology, 184, 97–122.

Zack, T., Von Eynatten, H., Kronz, A. 2004a. Rutile geochemistry and its potential use in quantitative provenance studies. Sedimentary Geology, 171, 37–58.

Zack, T., Moraes, R., Kronz, A., 2004b. Temperature dependence of Zr in rutile: empirical calibration of a rutile thermometer. Contributions to Mineralogy and Petrology, 148, 471–488.

Chapter 5

5 Evolution of the northern Albertine Rift reflected in the provenance of synrift sediments (Nkondo-Kaiso area, Uganda)

Sandra Schneider[1], Jens Hornung[1], Matthias Hinderer[1]

[1] Institute of Applied Geosciences, TU Darmstadt, Schnittspahnstrasse 9, D-64287 Darmstadt

5.1 Abstract

Rift sediments are important archives for the evolution of the East African Rift System. We present a source-to-sink study of the Nkondo-Kaiso area in the northern Albertine Rift from a ~200 m thick late Miocene to early Pleistocene sediment succession. The multi-proxy provenance analysis includes framework petrography, heavy mineral studies and single grain studies of garnet and rutile. Mineral textures and provenance signatures indicate two major stages. Sediment of Stage 1 (late Miocene - late Pliocene; ~6.5–2.6 Ma) is less mature with quartz contents of 58–81%, K-feldspar of 9–15%, plagioclase of 4–15%, and rock fragments of 1–9%. Heavy mineral spectra are dominated by epidote and amphibole with minor abundances of zircon, sillimanite and garnet. Garnet is almandine-rich and can be grouped according to grossular contents (< 10% and > 10%). Rutile exhibits a wide range of Nb and Cr concentrations, most of them typical for a metapelitic origin. Zr-in-rutile formation temperatures range between ~570 and 940 °C. Garnet and rutile geochemistry mainly correspond to amphibolite- to granulite-facies igneous and metasedimentary rocks, which exist in the Mesoarchean Karuma Group and the Neoarchean granitoid gneiss of the North Uganda Terrane. Both are part of the adjacent eastern rift flank of the Albertine Rift. A slight change of heavy mineral composition at ~4.5 Ma can be correlated with onset of the synrift stage ~0.5–1.0 Ma later than in the southern Albertine Rift. Sediment of Stage 2 (early Pleistocene ~2.6–1.0 Ma) shows higher quartz contents of 82–93%, and lower contents of K-feldspar of 5–11%, plagioclase of 1–7%, and rock fragments of 1–2%. Stable heavy minerals (ZTR index: 19–63) and epidote dominate with minor amphibole and garnet. Rutile and garnet chemical compositions remain largely unchanged to Stage 1 pointing to the same primary source. Obviously, Pleistocene sediment was mainly recycled from sedimentary rocks of the Neoproterozoic Bunyoro Group, which originate from identical Archean rock assemblages. Ongoing river incision reactivated the primary Archean source in the upper part of Stage 2. In conclusion, Miocene to Pleistocene sediment of the Nkondo-Kaiso region is supplied from local sources of the rift flank and the adjacent Ugandan Plateau. Tectonic pulses at ~4.5 Ma, ~2.6 Ma, and ~1.5 Ma led to river incision and moderate expansion of drainage basins towards the east. These pulses are roughly coincident with other parts of the EARS but also show regional time lag and delayed response of the source-to-sink system.

5.2 Introduction

The East African Rift System (EARS) is the most prominent example of active continental rifting and its tectonic formation and evolution has been studied since decades (for summary see Chorowicz, 2005). However, the chronology and regional pattern of uplift and subsidence remains uncertain in many parts of the EARS. These uncertainties can be addressed by examining sediment infills of rift basins. In particular, provenance methods assist to reconstruct the parent rock assemblage and deduce rift evolution, tectonic segmentation, block uplift, and supply pattern since the Miocene when major

rifting started. Garzanti et al. (2013) and Schneider et al. (2016a) have demonstrated that even under extreme tropical weathering provenance signatures can be retrieved from modern river sands of the East African Rift region by integration of classical petrographic methods with modern geochemical approaches.

Schneider et al. (2016b) studied the provenance of middle Miocene to Pleistocene synrift sediment in the Kisegi-Nyabusosi area of the Albertine Rift, which is adjacent to the strongly uplifted Rwenzori basement block culminating to an altitude of 5109 m above sea level (Bauer et al., 2010, 2013; Ring, 2008, 2014) (Figs. 5-1, 5-2) and could distinguish three phases marked by correspondent provenance changes. The authors identified three stages of sediment supply changing from a northeastern source to southeastern and southern sources. Most probably, the southern source reflects the uplift of the Rwenzori Mountains, which has started at around 2.5 Ma (Schneider et al., 2016b). In this paper we extent the multi-proxy provenance study to the Miocene to Pleistocene onshore sediment in the Nkondo-Kaiso area of the central Albertine Rift. Similar to the Kisegi-Nyabusosi area in the south (Roller et al., 2010; Schneider et al., 2016b), the study is based on detailed sediment logging and biostratigraphic subdivision by Pickford et al. (1993). Around 100 km apart, these regions represent a proximal and distal setting with respect to the uplifted Rwenzori fault block. Major objectives are (i) to compare sediment sources at both sites, (ii) to identify regional variations in timing and intensity of rifting. In order to achieve these objectives, framework petrography, heavy mineral assemblages and the chemical composition of detrital garnet and rutile are integrated from both sites.

5.3 Albertine Rift

The NE-SW orientated Albertine Rift represents the northern segment of the more dissected western branch of the EARS (Fig. 5-1), generally characterized by deeper rift lakes, steeper escarpments, but lower volcanic activity than the eastern East African Rift (Ebinger, 1989). The Albertine Rift straddles over 500 km from Kivu in the south to the Uganda/Sudan border in the north, and is 45-50 km wide, defining the border between Uganda in the east and Congo to the west (Figs. 5-1, 5-2). The rift comprises several sub-basins, including the Lake Albert Basin, Lake Edward Basin and Lake Kivu Basin (from north to south; Chorowicz, 2005). According to seismic-reflection surveys and gravity data sets from ongoing exploration, the Lake Albert sub-basin represents a symmetrical full-graben (Karp et al., 2012). In contrast, uplift of rift shoulders is rather asymmetric. While in the central and northern Albertine Graben the western Congolese rift flank is uplifted higher up to 2.2 km, in the south the eastern rift flank is anomalous upthrusted to ca. 5 km (Rwenzori fault block) and separates the Lake Albert sub-basin from the Lake Edward/George sub-basins (Ollier, 1990; Chorowicz, 2005) (Figs. 5-1, 5-3).

The Ugandan basement through which the rift propagates spans more than three billion years, and is composed of welded Archean lithospheric fragments, intersected or surrounded by Proterozoic fold belts (Westerhof et al., 2014) (Figs. 5-2, 5-3). Westerhof et al. (2014) divide the basement complex into five tectono-thermal terranes, each marked by a particular geodynamic evolution (Fig. 5-3). The southern-central part of Uganda is built up by an Archean granite-greenstone belt of the Lake Victoria Terrane (LVT) and the West Tanzania Terrane (WTT), both belonging to the Tanzania Craton (Fig. 5-2). Archean high-grade gneissic-granulitic rocks of northern-central Uganda, formerly known as the ‘Gneiss-Granulite Complex’ (Schlüter, 2008), belong to the West Nile Block (WNB) and the North Uganda Terrane (NUT), both considered to be part of the NE Congo-Uganda Block (Congo Craton) (Leggo, 1974) (Fig. 5-2). The NUT consists of a Mesoarchean nucleus – the Karuma Complex – cropping out along the northern part of the Albertine Graben (Fig. 5-3). Granulitic rocks dominate in the northern part of this unit, whereas the southern part includes

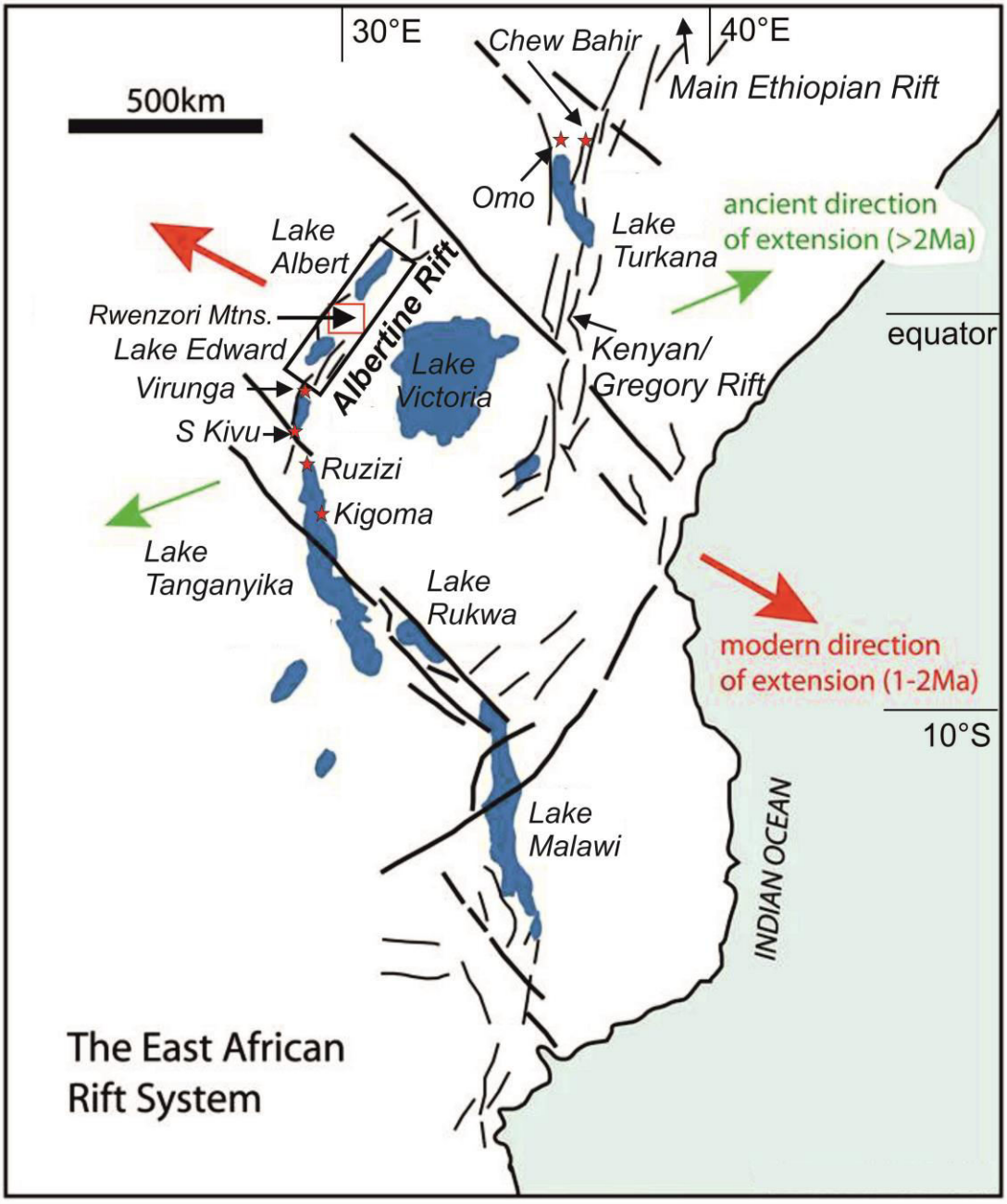

Figure 5-1. Overview of the East African Rift System (EARS) and its simplified tectonic structure. Modified after Rosendahl et al. (1992). The Albertine Rift forms the northernmost part of the western branch of the EARS.

granulitic migmatite and granitoid with a granitic to granodioritic composition (van Straaten, 1971, 1976). In vicinity to the study area, the rock is composed of Fe-Mg silicates, K-feldspar, plagioclase and quartz with notable amounts of retrograde amphibole and other high-grade minerals, like garnet (Westerhof et al., 2014). The bulk of the NUT is composed of granitoid, gneiss and migmatite of igneous or uncertain origin (Westerhof et al., 2014). Along the Albertine Rift, they occur as foliated to massive migmatised granitic and granodiorite gneiss with K-feldspar, plagioclase and quartz as major minerals, whereas hornblende and epidote are common minerals in mafic inclusions (Westerhof et al., 2014). The Paleoproterozoic Rwenzori Fold Belt (RFB; also known as the Buganda-Toro mobile belt, Schlüter, 2008) crops out in southern Uganda, where it overlies the western segment of the Tanzania Craton (Figs. 5-2, 5-3). The fold belt represents a duplex system that consists of northward thrusted thick-skinned nappes composed of Archean crust and Paleoproterozoic cover units (Link et al., 2010).

The basement of the Rwenzori Fold Belt is composed of gneiss and granitoid rocks and overlain by the Buganda Group with cordierite-, garnet-, staurolite-, andalusite-, and sillimanite-bearing mica schist, phyllite, quartzite, and rare marble and calc-silicate rocks (King, 1959a, 1959b; Schlüter, 2008; Master et al., 2013). In some parts, especially in the Rwenzori Mountains, the Buganda Group is covered by thick amphibolite and other mafic metavolcanic rocks (Tanner, 1971; Master and Bailie, 2000). Paleoproterozoic granitic batholiths have been emplaced within this belt during syn-tectonic and post-tectonic magmatism (Nagudi et al., 2003; Abdelsalam et al., 2016). Mesoproterozoic rocks are represented by granitoid and terrigenous metasedimentary rocks of the North Kibaran Belt in southwestern Uganda (Buchwaldt et al., 2008), as well as by metamorphic volcanic rocks, metasedimentary rocks and rare ultramafics of the Madi-Igisi Belt in northwestern Uganda (Mänttäri, 2014). The Neoproterozoic Bunyoro Group contains slate, phyllite, tillite, sandstone, and mudstone. It is exposed along the eastern rift shoulder of Lake Albert towards the eastern part of Lake Kyoga, where it partly overlies rocks of the North Uganda Terrane (Fig. 5-3) (Bjørlikke, 1973; Schlüter, 2008, Westerhof et al., 2014). The northernmost part of Uganda belongs to the Neoproterozoic East African Orogen (EAO) (Stern, 1994) represented by high-grade supracrustal rocks, amphibolite, granitoid, granulite, charnockite, and intruded granitoids (Westerhof, 2014).

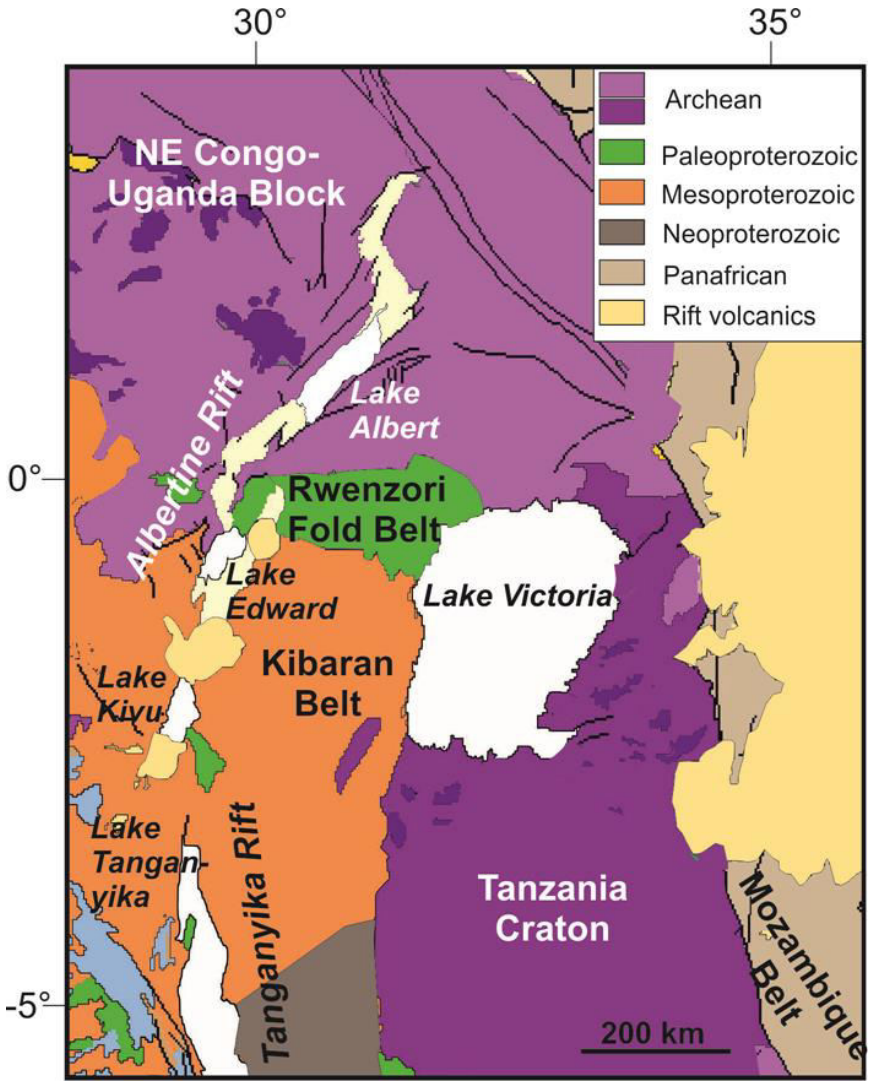

Figure 5-2. Geological outline of eastern Africa (modified after Lenoir et al., 1994; Morley, 1999; Rainaud et al., 2005; De Waele et al., 2008; Westerhof et al., 2014).

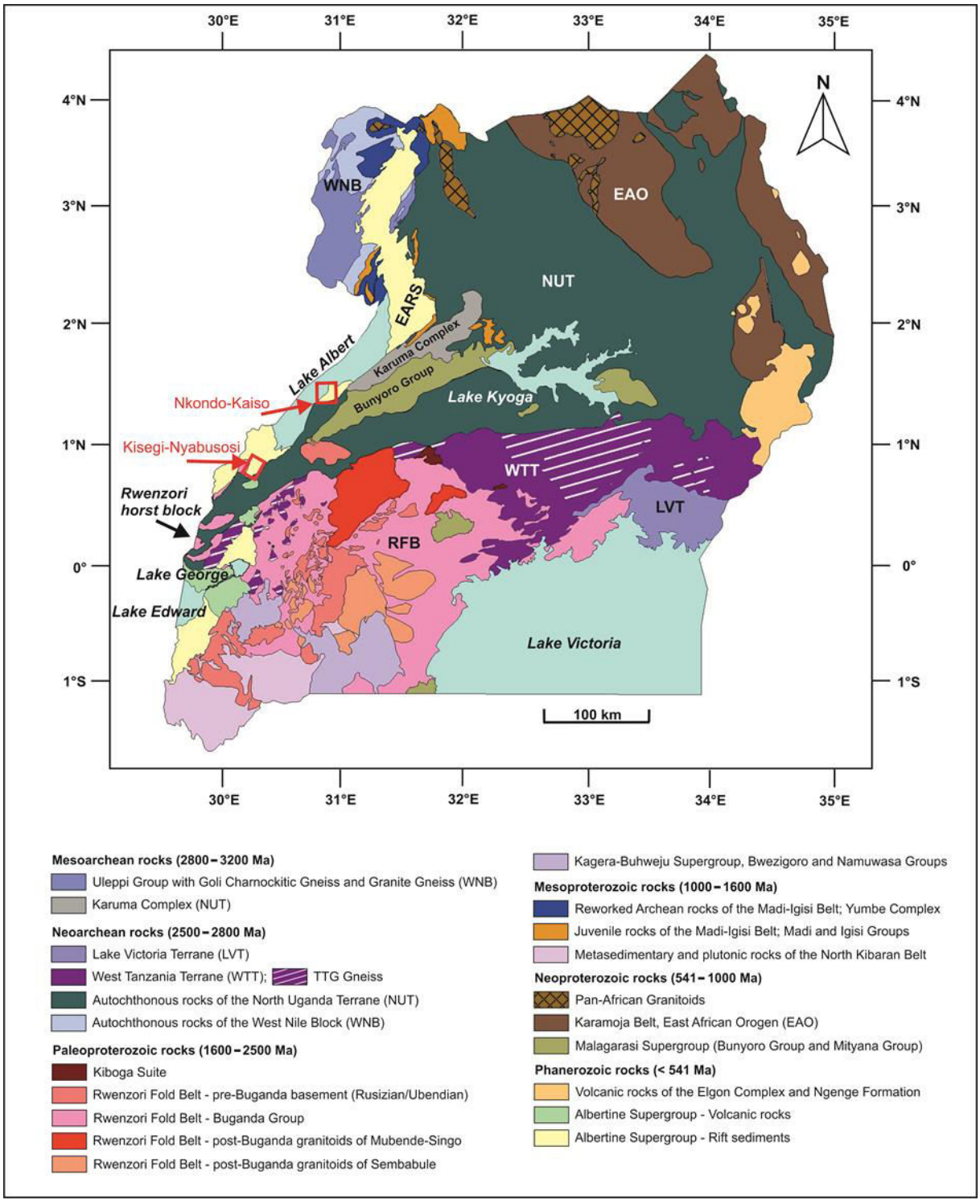

Figure 5-3. Geological map of Uganda (after Westerhof et al., 2014). The basement is divided into the five tectono-thermal units West Nile Block (WNB), North Uganda Terrane (NUT), Rwenzori Fold Belt (RFB), West Tanzania Terrane (WTT), Lake Victoria Terrane (LVT). EAO = East African Orogen, EARS = East African Rift System. The location of studied areas is given in red squares.

The Albertine Rift cuts diagonally through the Archean and Proterozoic units. Subsidence was initiated at ~18–20 Ma (Delvaux and Barth, 2010) and the first sediment is recorded at ~12.5 Ma (Pickford et al., 1993). According to geomorphological models (Bishop, 1965; Pickford et al., 1993),

as well as our provenance analysis in the southern Lake Albert sub-basin (Kisegi-Nyabusosi area; Schneider et al., 2016b), the detritus was supplied by a westward-directed river system draining the Ugandan plateau and Albertine Rift area towards the Congo Basin and the Atlantic Ocean (Cooke, 1958; Gautier, 1965; Bishop, 1965; Taylor and Howard, 1999; summarized in Pickford et al., 1993). Onset of volcanism is reported from the Virunga Province at ~12 Ma (Ebinger, 1989). Major faulting at ~8 Ma and accelerated subsidence (Ring et al., 1992; Ebinger et al., 1993; Ring and Betzler, 1995) triggered the formation of Paleolake Obweruka (Fig. 5-10), which extended ~550 km from near Kivu in the south to the Sudan/Uganda border in the north and lasted from 7.5 to 2.5 Ma (Ebinger, 1989; Pickford et al., 1993). The transition from the pre-rift to the syn-rift stage is assigned to have occurred ~5.5–5.0 Ma when the rift sediment shows a major compositional change that implies a shift from northwestern to southwestern supply areas (Schneider et al., 2016b). Facies analysis supports this assumption by indicating a change from an accommodation- to a supply-controlled system in synrift sedimentation (Roller et al., 2010). Erosional unconformities, coarser grained sediment input and a shift in provenance give evidence to increased tectonic activity at ~2.5 Ma and accelerated uplift of rift flanks including exhumation of the Rwenzori fault block and separation of Paleolake Obweruka (Pickford et al., 1993; Schneider et al., 2016b). Regional uplift and transition to a highly fluctuating global icehouse climate led to increasingly arid conditions in the Pleistocene (e.g., deMenocal, 1995, 2004; Trauth et al., 2005). A Pliocene humid tropical semi-deciduous forest was replaced by a wooded savanna environment around the Plio-Pleistocene boundary (Dechamps et al., 1992).

5.4 Stratigraphy

The sedimentary fill of the Lake Albert Basin reaches a maximum thickness of ~5 km (Karp et al., 2012). Sedimentary successions are only accessible at few localities onshore around Lake Albert. The Kisegi-Nyabusosi area in the southern Lake Albert sub-basin (Fig. 5-3) provides the longest record down to the basal pre-rift infill at ~12.5 Ma (Pickford et al., 1993; Roller et al., 2010). In the central Albertine Graben, the Nkondo-Kaiso area offers onshore exposures of synrift sediment over an area of about 9 km^2 and a thickness of ca. 200 m (Fig. 5-4, 5-5). It is bordered by Lake Albert to the west (618 m above sea level) and the eastern rift flank to the east that reaches elevations of ~1300 m above sea level. According to biostratigraphic dating, the lowermost sediment is ca. ~6.5 Ma old and reaches up to the middle Pleistocene. Sediment is mostly terrigenous and fine- to medium-grained with few conglomerate beds (Fig. 5-5). Sedimentary structures and facies associations show fluvio-deltaic to lacustrine depositional environments. Few tephra layers are intercalated (Fig. 5-4, 5-5) and were used by Pickford et al. (1991) for additional age constraints. Pickford et al. (1993) subdivided the sediment succession of Nkondo-Kaiso into five formations (Nkondo, Warwire, Kyeoro, Kaiso Village and Museta beds formations) (Fig. 5-5). Stratigraphic ages are based on correlations of fossil mammal and gastropod associations mostly with the eastern rift branch of the EARS, (Gautier, 1970; Pickford et al., 1993; van Damme and Pickford, 1995, 1998, 2003), as well as on relative thephrostratigraphy (Pickford et al., 1991). The tephra layers in the Nkondo-Kaiso area are highly altered which makes them unsuitable for radiometric dating. Instead, Pickford et al. (1991) used geochemical fingerprinting to correlate some of them with radiometrically dated volcanic ash layers in the eastern rift branch of the EARS. Exact stratigraphic dating of the sediment succession in the onshore Nkondo-Kaiso area are tainted with some uncertainties, because: (1) parts of the sedimentary sequences are inaccessible and covered by thick soils or dense vegetation and could not be logged, (2) the duration of hiatuses is unclear, (3) only some of the fossil species found in the Albertine Rift have been encountered at other localities, (4) tephra layers are only sporadically present in the Warwire Formation and Kaiso Village Formation and, (5) the fingerprinting method only represents probable correlations. The following brief description of the formations is based on Pickford et al. (1993) and own observations.

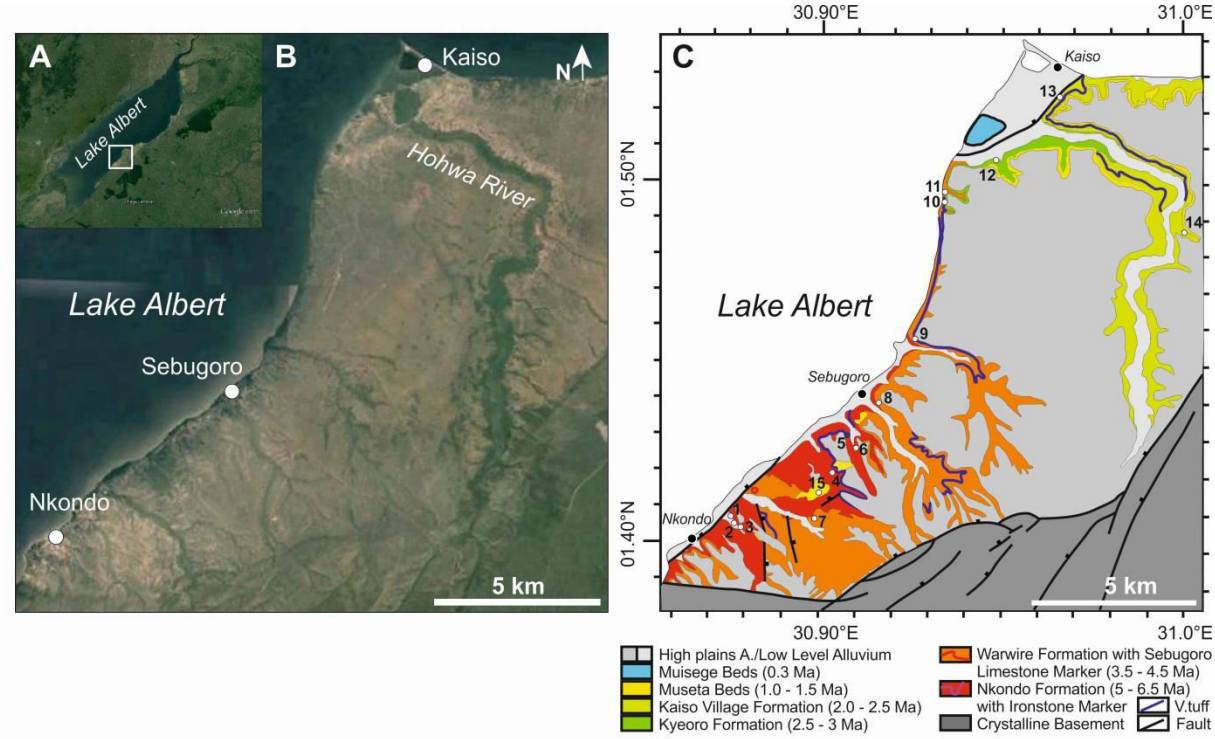

Figure 5-4. Satellite overview map of the (A) northern Albertine Rift, and (B) Nkondo-Kaiso area (Google Earth, July 2016). (C) Geological map of the Nkondo-Kaiso (after Pickford et al., 1993) with location of logged sedimentary outcrops.

The lowermost formation in the Nkondo-Kaiso area, the Nkondo Formation, is ~70 m thick ranging from the late Miocene to the early Pliocene. It comprises two members. The lower Nkondo Member is up to 40 m thick and shows intercalations between sand, silt and clay with ooidic and sandy ironstone layers. The ~30 m Nyawaiga Member consists almost exclusively of grey and brown clay. Silty and sandy intercalations are very rare. The depositional environment of the Nkondo Formation grades from fluvial-deltaic to deep lacustrine conditions. Both, biostratigraphy as well as facies interpretations correlate the Nkondo Formation with the Upper Oluka Formation of the Kisegi-Nyabusosi area.

The Warwire Formation rests unconformably on the Nkondo Formation with a 10 cm thick basal microconglomerate followed by approximately 80 m of clay, silt and sand alternations. Several iron crusts and iron-hydroxide impregnated horizons are present. The unit is rich in fossils and yields abundant mollusc associations (Pickford et al., 1993). Two volcanic ash layers have been recorded within this formation, described and correlated by Pickford et al. (1991). The grayish-brown, some cm thick Warwire Tuff crops out in the lower part of the formation (Fig. 5-5) and is correlated with the Lomogol Tuff from the Turkana Basin and an unnamed tuff from the Ethiopian Rift dated to 3.6 Ma. The younger, ~45 cm thick Kyampanga Tuff matches the composition of the Lokochot Tuff, also from the Turkana Basin, and is dated to 3.45 Ma. Based on the dating of these tephra layers and correlations of mollusc associations, the basis of the Warwire Formation might be as old as 4 Ma (Pickford et al., 1993) and an early to late Pliocene age can be assigned. The depositional environment of the Warwire Formation is marked by an interplay of lacustrine, fluvial and alluvial fan deposits.

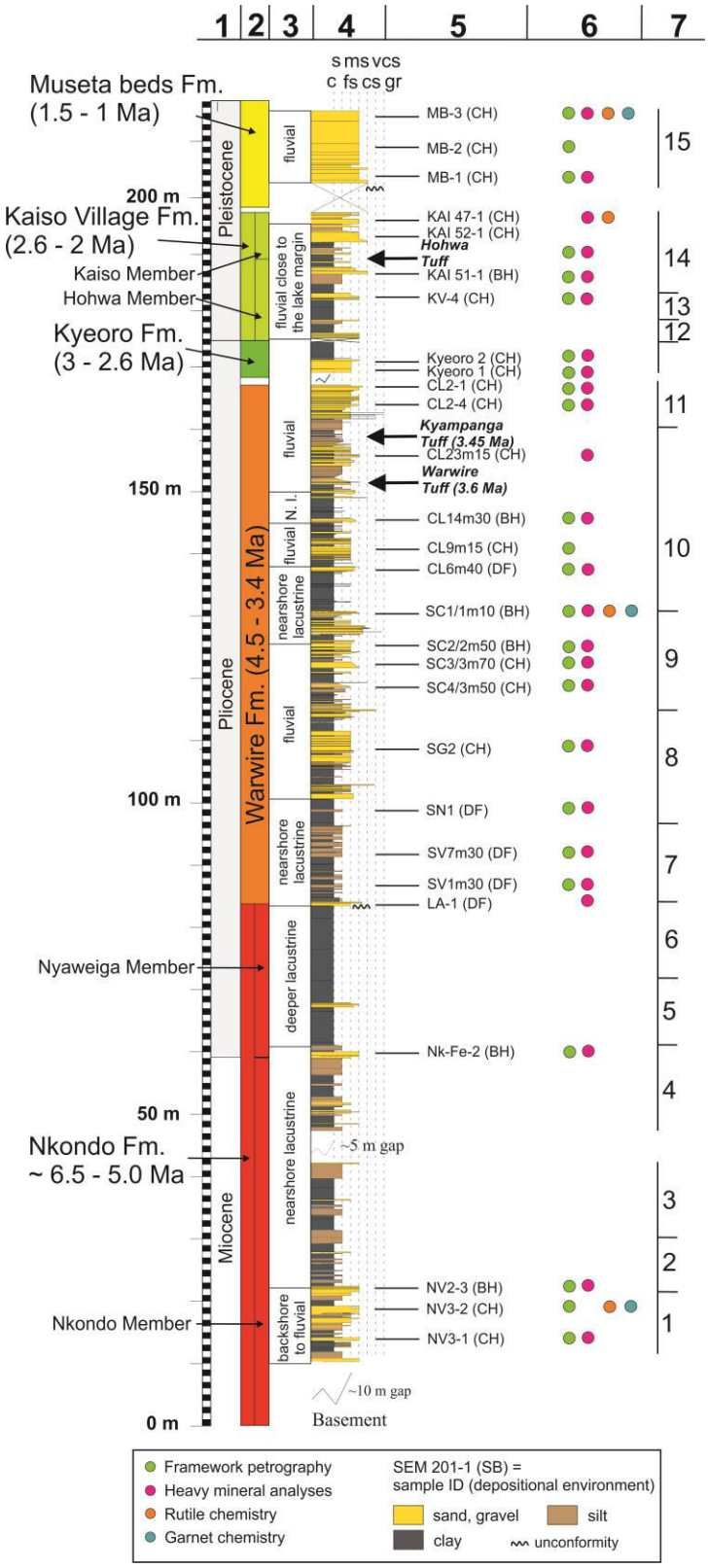

Figure 5-5. Stratigraphy of the Nkondo-Kaiso area: (1) time epoch, (2) biostratigraphic formation (Pickford et al., 1993), (3) depositional environment of sediments, (4) logged sedimentological sections; widths and colors of sections display grain sizes, (5) location, ID and architectural elements (in brackets) of analyzed samples. CH: channel, DF: delta foreset, BH: beach. (6) analytical methods applied on the samples, (7) numbers refer to the ID of logged sections shown in figure 5-4. c = clay, s = silt, fs = fine sand, ms = medium sand, cs = coarse sand, vcs = very coarse sand, gr = gravel.

The late Pliocene Kyeoro Formation has a thickness of at least 8 m, but the base is not accessible due to modern alluvium coverage. The sedimentary exposures consist of 2 m predominantly fine sand followed by ~3 m clay. The sediment was probably accumulated in a fluvial environment near a lake margin.

The following ~23 m thick, early Pleistocene Kaiso Village Formation consists of two members. The ~16 m thick Hohwa Member is predominantly composed of clayey sediment with few sandy interbeds. Mammal associations correspond to an early age of ~2.6 Ma (Pickford et al., 1993). The 2–8 cm thin Hohwa Tuff of unknown age (Pickford et al., 1991) forms the lower boundary of the overlying Kaiso Village Member (Fig. 5-5), which is composed of ~7 m thick clay, silt and sand with an overall coarsening-up trend. The Kaiso Village Formation represents a fluvial floodplain environment near the lakeshore. Pickford et al. (1993) estimated an age of ~2.3 Ma for the basis of this member.

The Museta beds Formation lies unconformably on the Kaiso Village Formation. Mammal associations make an age of ~1.5–1.0 Ma probable (Pickford et al., 1993). The unit is dominated by ~12 m thick medium sand representing channel deposits in a fluvial environment.

5.5 Methods

5.5.1 Sampling

A total of 28 sand samples from 16 logged sections with a total thickness of ~200 m were collected (Fig. 5-5). Sediment samples were selected at a mean interval of ca. 5 to 10 m and preferentially taken from medium-grained sand layers. All formations are represented with a minimum of 2 samples from the 5 m thick Kyeoro Formation and 14 samples from the 80 m thick Warwire Formation. All sediment samples are non-cemented and matrix-free.

5.5.2 Framework petrography

Twenty-five samples were sieved and the medium sand fraction (250–500 µm) was investigated by point-counting of 300 grains using the 'traditional' method. Hence, sand sized crystals (> 0.063 mm) within rock fragments were counted in the category of the rock fragment in which they appear (e.g., von Eynatten and Gaupp, 1999) and not as monomineralic grains (Gazzi-Dickinson method; Dickinson, 1970). Metamorphic rock fragments were categorized into felsic (metapelite, Lmp; metapsammite, metafelsite; Lmf) and mafic (metabasite; Lmb) detritus (Garzanti and Vezzoli, 2003). Quartz grains were subdivided into monocrystalline quartz (Qm), polycrystalline quartz (Qp; 2 or more subgrains) and microcrystalline quartz (chert).

5.5.3 Heavy mineral analysis

Twenty-five of the 28 samples were analyzed for their heavy mineral content. Three samples that were point-counted did not yield enough heavy minerals and were replaced by others, taken within the same stratigraphic unit and locality (Fig. 5-5). Heavy minerals of the grain size fraction 63–125 µm were separated with Na-polytungstate (ρ = 2.855 g/cm^3), mounted on glass slides and impregnated with epoxy resin. In each slide, 250 non-opaque and non-micaceous grains (Mange and Maurer, 1992) were counted with an automatic point counter. From individual frequencies, the garnet-zircon (GZi = 100*garnet/(garnet + zircon)) and rutile-zircon (RuZi = 100*TiO_2 group minerals/(TiO_2 group minerals + zircon)) indices were calculated (Morton and Hallsworth, 1994). These indices can be

supportive in unravelling changing provenance, because they may sort out effects of e.g., weathering and hydraulic sorting by comparing minerals with similar properties. The degree of the mineralogical maturity of studied sediment is described by the ZTR index (Hubert, 1962), calculated as the sum of zircon, tourmaline and rutile (= ZTR) divided by the sum of transparent and non-micaceous heavy minerals.

5.5.4 Mineral chemistry of detrital garnet and rutile

Single grain analysis of mineral chemistry was conducted on 252 detrital garnet grains from the Nkondo Formation (n = 85), Warwire Formation (n = 121) and Museta beds Formation (n = 46), and on 175 rutile grains representing the Nkondo Formation (n = 47), Warwire Formation (n = 65), Kaiso Village Formation (n = 18) and Museta beds Formation (n = 45). We have chosen samples that contain a high proportion of the analyzed mineral types. The Kaiso Village Formation had to be excluded for garnet chemistry, because it did not yield enough garnet grains. Garnet and rutile grains were hand-picked from the heavy mineral residuum under a binocular microscope and placed on synthetic mounts. Chemical analysis of both was performed with a Jeol JXA-2800 electron microprobe equipped with a five wavelength dispersive spectrometer at the Johannes Gutenberg University of Mainz.

Operation conditions for garnet included accelerating voltage of 15 kV and beam current of 20 nA. Garnet was analyzed in respect of Si, Mg, Ca, Fe and Al with counting times of 15 s, and Ti, Cr and Mn with counting times of 30 s. Rutile grains were analyzed for Nb, Al, Cr, Zr and V with counting times of 200 s, Si and Fe with counting times of 100 s and Ti with counting times of 15 s. Measuring conditions include an accelerating voltage of 25 kV and a beam current of 80 nA.

Garnet analyses were recalculated to the six end-members almandine, spessartine, pyrope, grossular, andradite, and uvarovite with the structural formula based on 12 oxygen atoms and 8 cations (Deer et al., 1997). The Fe^{2+} and Fe^{3+} contents were determined by stoichiometry. Rutile growth temperatures were calculated using the thermometer after Tomkins et al. (2007) in the α-quartz field (see Triebold et al., 2012) using the following equation:

$$T(°C) = [(83.9 + 0.410 \times P)/(0.1428 - R \times \ln(Zr_{ppm})] - 273$$

where P is the pressure, 10 kbar, and R is the gas constant, 0.0083144 kJ K−1.

5.6 Results

5.6.1 Framework petrography

Point-counting results are presented in Table A5-1 (Appendix). Throughout the stratigraphy, the majority of grains are subrounded to angular. Quartz, feldspar and rock fragments appear mostly fresh and largely uncorroded. Weathering features, like etch-pits and re-entrants, are rare. The sediment composition is feldspatho-quartzose, but with marked differences between the lower part – the Nkondo, Warwire, Kyeoro formations – and upper part – the Kaiso Village and Museta beds formations – of the sedimentary record (Fig. 5-6). The Nkondo, Warwire, and Kyeoro formations, in the following called Group 1, have quartz concentrations of 58–81% (Qm: 45–71%, Qp: 3–20%). The

amount of K-feldspar of 9–15% remains similar throughout Group 1. Plagioclase ranges between 4% and 15% and is less frequent than K-feldspar in the Nkondo Formation and the lowest part of the Warwire Formation, but increases to similar abundances as K-feldspar upsection. Rock fragments of 1–9% are dominated by metapsammite/-felsite grains, which are mainly parageneses of quartz-feldspar-(mica) of medium- to high metamorphic rank (e.g., gneiss). Metapelite (e.g., clayey or micaceous fragments) or metabasite grains (e.g., epidote- and amphibole-rich fragments) occur only sporadically. Accessory minerals include mica flakes, heavy minerals and opaque phases (< 7%).

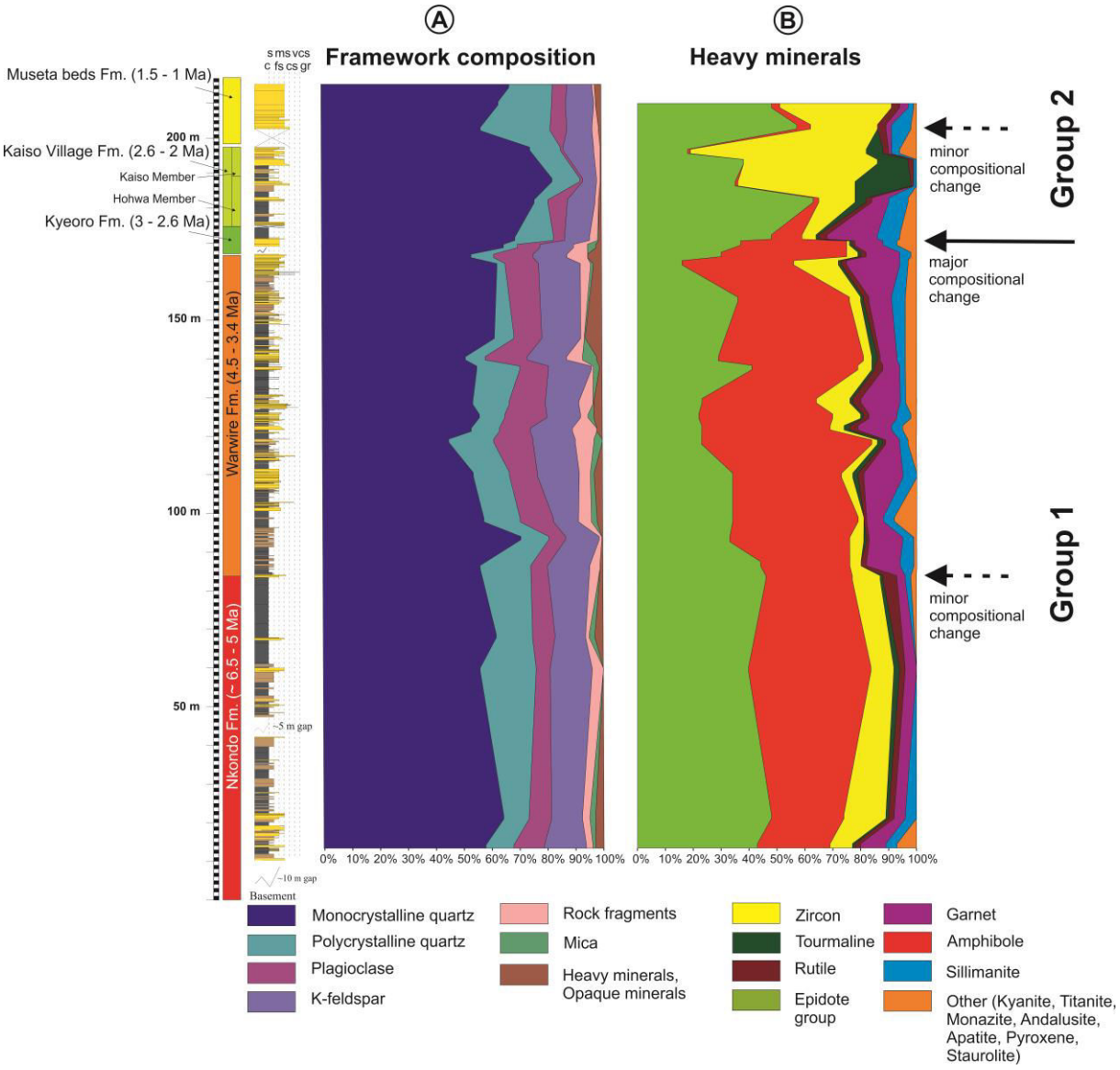

Figure 5-6. Distribution of (A) framework grains and (B) translucent heavy minerals in relation to the stratigraphic column. c = clay, s = silt, fs = fine sand, ms = medium sand, cs = coarse sand, vcs = very coarse sand, gr = gravel.

The upper part of the stratigraphy, in the following called Group 2, is characterized by a higher quartz content of 82–93% (Qm: 57–83%, Qp: 5–25%) at the expense of feldspar and rock fragments. K-feldspar shows amounts of 5–11% and prevails over plagioclase (1–7%). Rock fragments are rare (1–2%) and dominated by metapsammite/-felsite grains. Among high-grade metamorphic fragments that are similar to Group 1, few low-grade metamorphic metasiltstone lithics occur. Metabasite grains are sporadically present in the Museta beds Formation. Mica is virtually absent in Group 2. Other accessory phases, like heavy minerals and opaques, occur with abundances of < 3%.

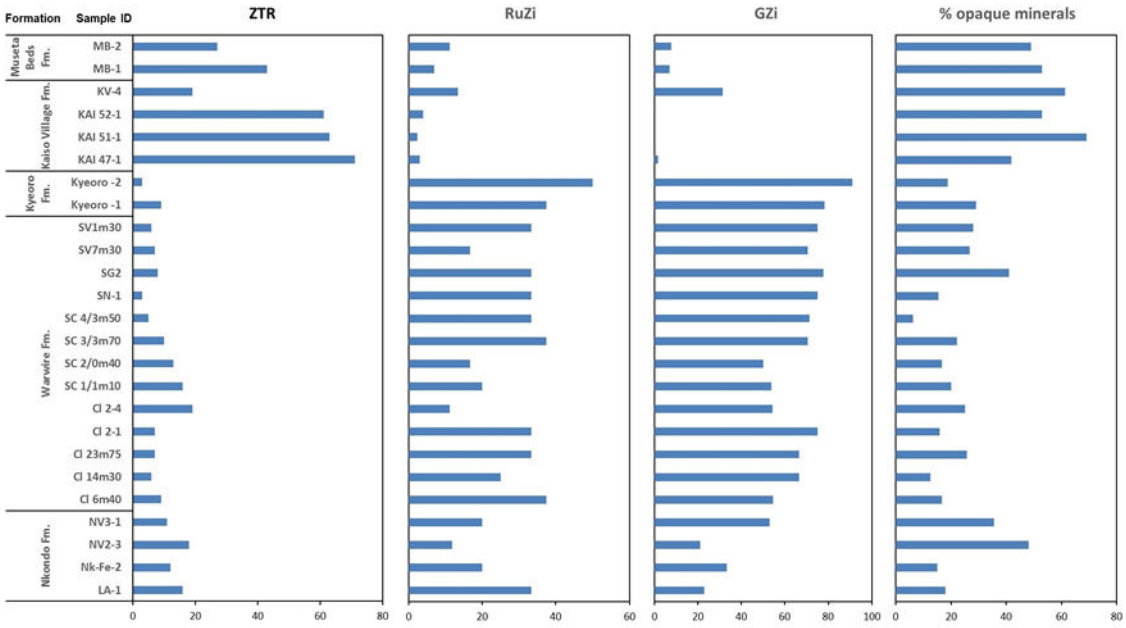

Figure 5-7. Different heavy mineral indices and percentage of opaque minerals of the analyzed samples, plotted in their inferred stratigraphical order. Formation thickness is not to scale. ZTR = zircon-tourmaline-rutile index; RuZi = rutile-zircon index; GZi = garnet-zircon index.

5.6.2 Heavy mineral composition

The heavy mineral data are given in Table A5-2 (Appendix). Heavy mineral assemblages of Group 1 show 6–48% opaque phases (Fig. 5-7). The transparent heavy mineral fraction mainly consists of epidote (14–48%) and amphibole (mainly green to bluish-green hornblende; 11–61%) with smaller proportions of zircon (1–16%), garnet (3–19%) and sillimanite (< 8%), and rare rutile (1–5%), clinozoisite (< 5%), titanite (< 3%), tourmaline, and kyanite (both < 2%) (Fig. 5-6). The ZTR index shows values between 3 and 19 (Fig. 5-7). Provenance-sensitive garnet:zircon (GZi) and rutile:zircon (RuZi) heavy mineral indices show moderate mean values for the Nkondo Formation (GZi ~33 and RuZi ~21), and higher mean values for the Warwire Formation (GZi ~66 and RuZi ~28) and the Kyeoro Formation (GZi ~78 and RuZi ~38) (Fig. 5-7). Heavy mineral assemblages of Group 2 show higher amounts of opaque minerals (42–78%). The transparent heavy mineral fraction is characterized by a significant decrease of amphibole (< 5%) and garnet (< 6%), paralleled by an increase of zircon (13–63%). Tourmaline (4–20%) shows enhanced abundances in the Kaiso Village Formation, but was not determined in the Museta beds Formation. The higher amount of ultrastable minerals in Group 2 is reflected by a ZTR index of 19 to 71. Mineral indices are moderate for the Hohwa Member of the

Kaiso Village Formation (GZi = 32 and RuZi = 13), and low for the Kaiso Village Member (GZi = 0 and RuZi ~3) and the Museta beds Formation (GZi ~5 and RuZi ~8) (Fig. 5-7).

The texture of heavy mineral grains is generally similar in both groups. Most amphibole, epidote and garnet grains show a slight to advanced stage of corrosion (Fig. 5-8). Corrosion pits and re-entrants up to hacksaw terminations are frequent for amphibole. Most garnet and epidote grains show corroded outlines, but are only sporadically deeply etched. Zircon and rutile grains are commonly subrounded to rounded, whereas tourmaline reveals an angular to subrounded appearance. In most cases, the ZTR minerals remain largely unweathered. This is also true for most prismatic sillimanite and kyanite grains, that appear to be remarkable fresh and mostly uncorroded. Some broken grains indicate mechanical rupture (Andò et al., 2012).

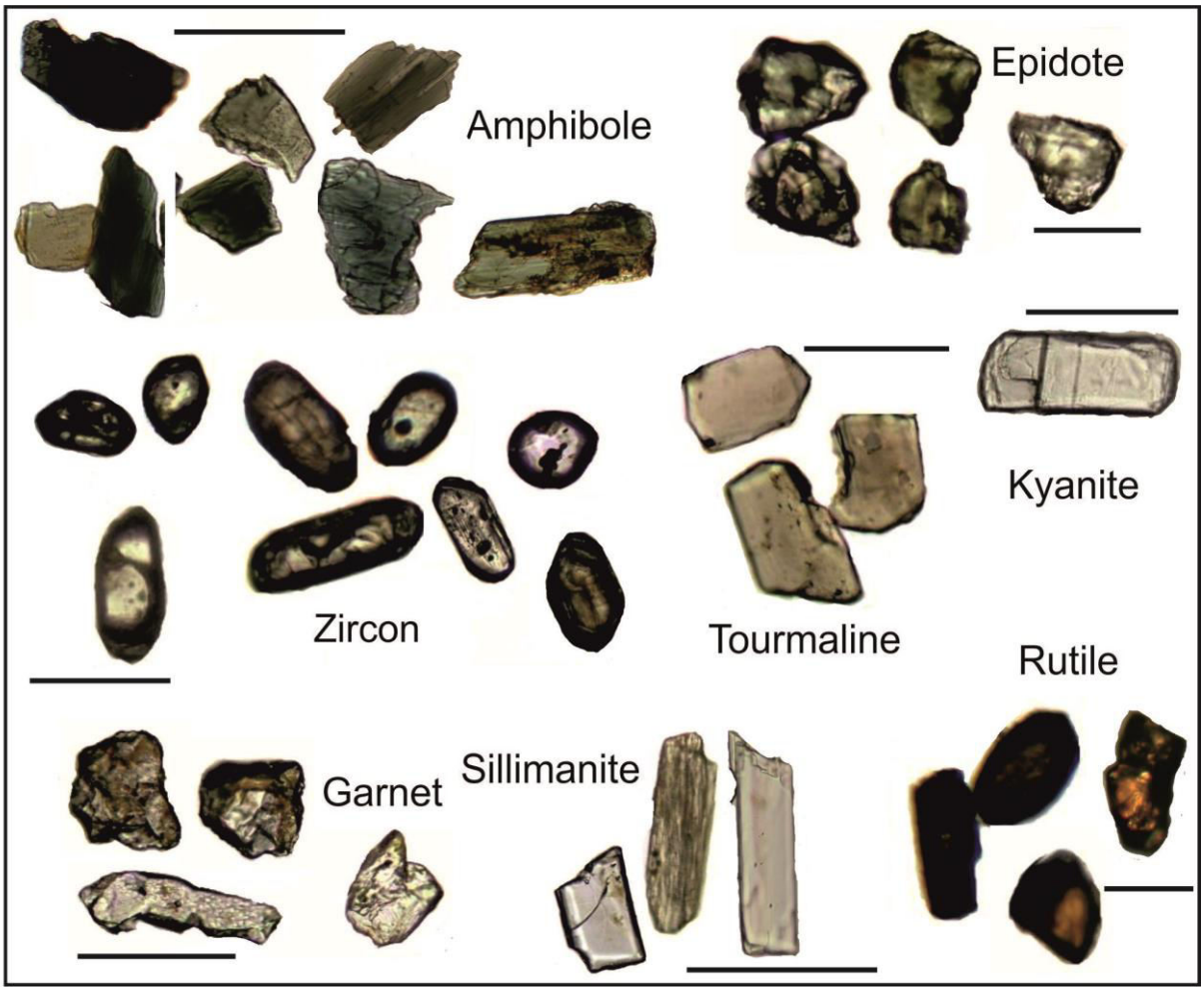

Figure 5-8. Photo table of the most frequent heavy minerals. Black scale bars are 100 µm.

5.6.3 Garnet chemistry

The garnet compositions are shown as ternary diagrams using almandine plus spessartine (Alm+Sp), pyrope (Pyr) and grossular (Gro) as poles (Fig. 5-9). Overall, there is little variation of garnet compositions among Group 1 (Nkondo and Warwire formations) and Group 2 (Museta beds

Formation). The garnet is dominated by high-almandine, low-spessartine, and low- to medium-pyrope (4–44%) (Table A5-3, Appendix). Both sediment groups contain a bimodal array of garnet compositions with populations of < 10% (Cluster I) and > 10% grossular (Cluster II) (Fig. 5-9). The composition of Cluster I is representative for garnet derived from granulite-facies metasedimentary rocks or charnockite, whereas Cluster II corresponds to garnet formed in metaigneous granulite, eclogite and amphibolite rocks (Mange and Morton, 2007; Aubrecht et al., 2009; Krippner et al., 2014). The low-pyrope variety of Cluster II has also been described to be common in amphibolite-facies metasedimentary rocks (Mange and Morton, 2007).

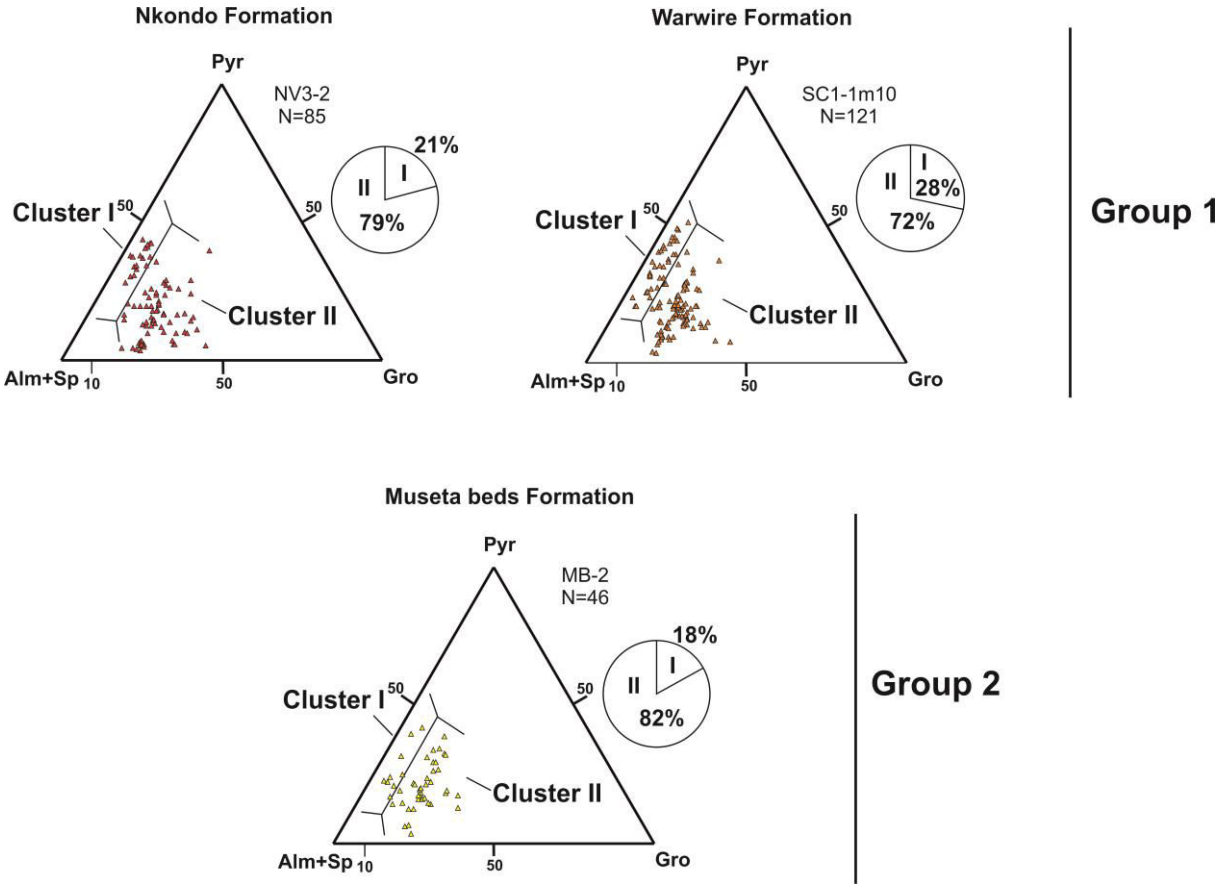

Figure 5-9. Garnet chemistry illustrated in Alm+Sp-Gro-Pyr ternary diagrams with Alm = almandine, Sp = spessartine, Gro = grossular, and Pyr = pyrope.

5.6.4 Rutile chemistry

Detrital rutile from the four analyzed samples has large compositional variations with Al < 1634 ppm, Si ~83–391 ppm, Nb ~5–14470 ppm, Cr ~68–3823 ppm, Fe ~44–20055 ppm, V < 7926 ppm, and Zr ~106–4722 ppm (Table A5-4, Appendix). The Zr concentrations indicate rutile growth temperatures for Group 1 (Nkondo Formation and Warwire Formation) between ~570 and 940 °C, corresponding to amphibolite-/eclogite- and granulite-facies formation temperatures (Tomkins et al., 2007) (Fig. 5-10B). The majority of rutile represents a temperature range of 700–800 °C, hence upper amphibolite-/eclogite- and lower granulite-facies conditions. In both sediment groups, ca. two third of the rutile shows Cr/Nb ratios < 2, assigned to metapelitic rocks. One third is in accordance with an origin from

metamafic lithologies (31% and 32%; Fig. 5-10A). In contrast to Group 1, all rutile grains from the Kaiso Village Formation (Group 2) indicate a metapelitic origin and 80% of rutile yields temperatures between 700 and 800 °C (granulite-facies). In the Museta beds Formation (Group 2) the chemical composition of rutile is similar to Group 1, but with less spread of formation temperatures.

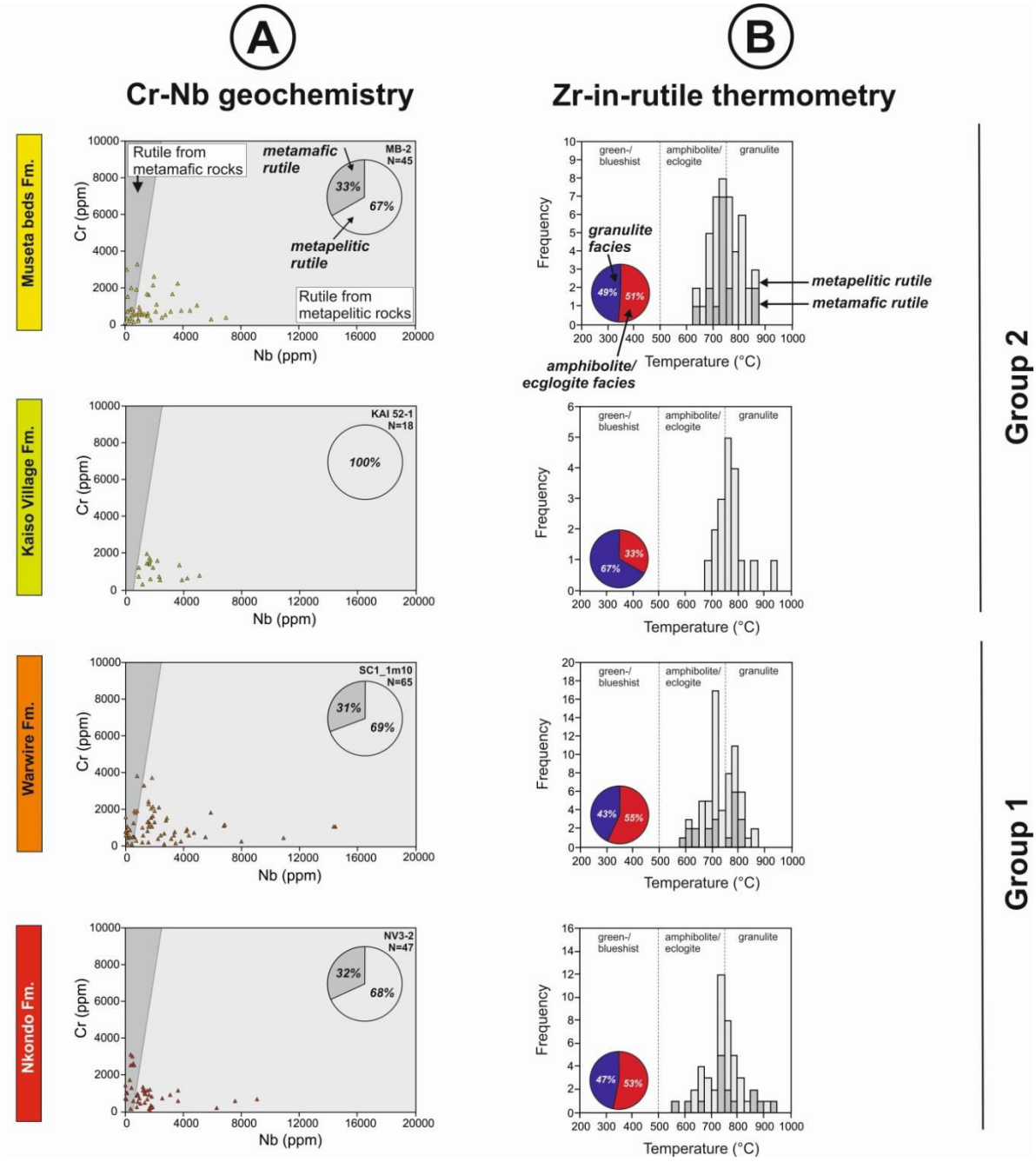

Figure 5-10. Rutile chemistry. (A) Cr vs. Nb with discrimination fields after Triebold et al. (2012), (B) Zr-in-rutile formation temperatures (Tomkins et al., 2007).

5.7 Discussion

Stage 1. Late Miocene - late Pliocene (Nkondo, Warwire, Kyeoro formations)

Provenance signatures of Group 1 sediment fits to source rocks of the surrounding eastern flank of the Albertine Rift (Fig. 5-11). The dominance of metamorphic heavy minerals, the almandine-rich garnet, the mainly metapelitic origin of rutile and its high formation temperatures together with mainly felsic high-grade metamorphic rock fragments indicate an origin from amphibolite- to granulite-facies metaigneous and metasedimentary source rocks. Two possible rock suites can be identified, both belonging to the North Uganda Terrane. One of them comprises Neoarchean gneissic granitoid, which occupies large parts of the Ugandan basement and is also exposed along the rift shoulder east of the study area (Schlüter, 2008; Westerhof et al., 2014). The other potential source area is the Mesoarchean Karuma Complex that crops out in a SW-NE-trending belt along the northern sector of the Albertine Rift (Figs. 5-3, 5-11). Major rock assemblages in the southern part of the Karuma Complex include granulitic migmatite and granitoid with a granitic to granodioritic composition (van Straaten 1971, 1976). Though rocks of the Karuma Complex are generally considered to have experienced a higher metamorphic overprint (granulite metamorphic conditions and amphibolite-grade retromorphism) than the Neoarchean rocks of the NUT (Westerhof et al., 2014), an overlap in composition and metamorphic rank is likely. Thus, a distinct separation between these units is unfeasible, and both areas need to be taken into account as potential source for sediment of Group 1.

After a hiatus of about 0.5 Ma, sediment composition in the Warwire Formation tends towards amphibole-dominated heavy mineral assemblages together with raised contents of garnet, sillimanite, and plagioclase. Rutile and garnet chemistry remain consistent between the Nkondo Formation and the Warwire Formation. A possible reason for this minor change in sediment composition is a shift in the mixture of the Neoarchean and Mesoarchean source rocks of the North Ugandan Terrance towards slightly enhanced erosion of the granulitic gneiss of the Karuma Complex. Differential weathering between the Nkondo Formation and the Warwire Formation, which might have been triggered by the climate shift from humid to more arid conditions during the Pliocene (Dechamps et al., 1992; Jacobs and Deino, 1996), is not indicated by the texture of grains remaining similar in both formations. Hydraulic sorting can be largely excluded, because it does not explain the increase of garnet together with amphibole, because both minerals are described to show a different hydraulic behavior during transport (Lofty, 1997). Significant unroofing and erosion of deeper, higher metamorphic rocks, which would explain increase of high-grade metamorphic minerals is not displayed by garnet and rutile chemistry, which are consistent between the Nkondo and Warwire Formation.

The hiatus between the Nkondo and Wawire formations between 5.0 and 4.5 Ma may be interpreted as transition into the synrift stage. Although this has affected sedimentation, provenance pattern did not change significantly, pointing to persistence of relatively local sources and slow dissection and headward cutting of the rift-flank even under increased tectonic activity and increased river gradients. In contrast, the southern Albertine Rift (Kisegi-Nyabusosi area) shows a significant provenance shift ca. 0.5 to 1 Ma earlier at around 5.5 to 5.0 Ma (Schneider et al., 2016b). This might be due to a higher sensitivity to axial drainage and/or a northward progradation of tectonic faulting activity. The early Pliocene tectonic pulse and shift in sediment composition is contemporaneous to overall tectonic activity in the EARS and coincides with (1) major topography development in Ethiopia and southward propagation of rift the segment (Gani et al., 2007; Macgregor, 2012), (2) major subsidence in Turkana, Omo and Chew Bahir rifts, (3) rifting in Kigoma basins (Macgregor, 2015), in the northern Lake Malawi Basin (Flannery and Rosendahl, 1990) and the Ruzizi Basin (Chorowicz, 2005) (Fig. 5-1).

Stage 2. Early Pleistocene (Kaiso Village, Museta beds formations)

Provenance data point to an extension of the source area for Group 2 to the Neoproterozoic Bunyoro Group on the Ugandan plateau east of the Albertine Rift (Figs. 5-3, 5-11). The petrographic composition of Group 2 strongly resembles the composition of modern river sands draining this group (Schneider et al., 2016a). The Bunyoro Group crops out at a length of ~250 km and width of ~20–50 km and is composed of Neoproterozoic arkose, mudstone, shale, phyllite and quartzite that overlie basal tillitic rocks (Bjørlykke, 1973; Schlüter, 2008). East of the study area, this unit forms a flat-lying sediment platform, resting unconformable on the Archean basement, and partly covering the source region of Group 1 (Fig. 5-3, 5-11). A major argument is the higher compositional maturity compared to Group 1, which can be explained by recycling of older sediment. This is supported by the higher amounts of opaque phases, zircon and tourmaline at the expense of amphibole and garnet indicating a reworked source. The presence of some low-grade metasedimentary rock fragments in the sediment of the Kaiso Village Formation supports this theory. Moreover, garnet and rutile chemistry remain similar to Group 1 and may reflect either continuous sediment input from underlying amphibolite-facies to granulite-facies Archean rocks or their recycled products in the Bunyoro Group. Some gneissic rock fragments composed of quartz and feldspar, point to the primary Archean source. A stronger reinvigoration of sediment input from the Archean basement is indicated for the early Pleistocene Museta beds Formation (~1.5–1.0 Ma) by a slight increase of plagioclase, K-feldspar, garnet, amphibole and sillimanite together with decrease in quartz, zircon and tourmaline. The nearly complete absence of tourmaline in this formation remains uncertain at this point.

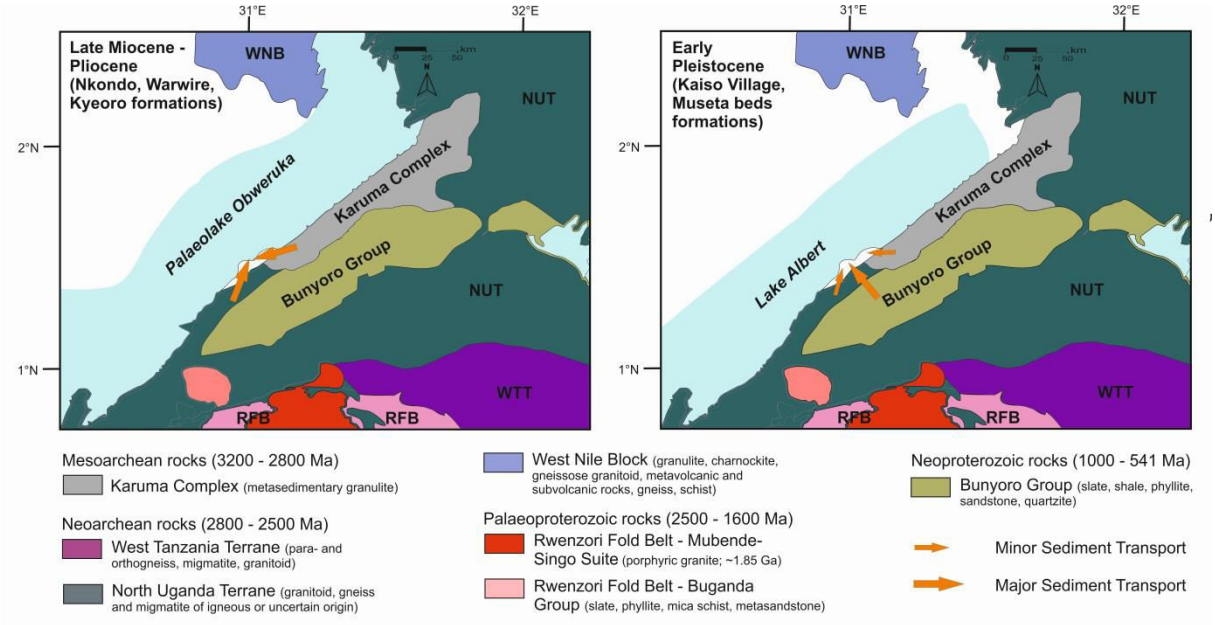

Figure 5-11. Sketch maps of the Albertine Rift showing interpreted sediment transport directions from the late Miocene to early Pleistocene. Geology after Westerhof et al. (2014), and reconstruction of lake extension after Pickford et al. (1993). WNB = West Nile Block, NUT = North Uganda Terrane, RFB = Rwenzori Fold Belt, WTT = West Tanzania Terrane.

Several findings argue against another major control of the increased compositional maturity of Group 2, although some impact cannot be ruled out. Enhanced removal of unstable mineral phases due to chemical weathering in the source area or after deposition is not indicated by the texture of minerals exhibiting for both sediment groups a similar corrosion and weathering degree. Furthermore, it does not explain the decrease of rutile and garnet, both assigned to be considerable stable towards dissolution (Hubert, 1962). As pointed out before, a more arid climate in the Pleistocene (Dechamps et al., 1992) also does not call for a significant increase in weathering intensity. Strong control of hydraulic sorting during transport seems also improbable, because ultradense zircon and opaque minerals would be expected to accumulate concomitantly with rutile and garnet due to their hydraulic equivalence, rather than with less dense tourmaline and epidote (Morton and Hallsworth, 1994, 1999; Lofty, 1997; Frihy, 2007).

The shift in sediment provenance at ~2.6 Ma is contemporaneous to the southern Albertine Graben where the extreme uplift of the Rwenzori Mountains was initiated at this time (Pickford et al., 1993; Schneider et al., 2016b). A further tectonic pulse can be assumed at 2.0–1.5 Ma when provenance signatures shifted again and an unconformity was formed at the base of the Museta beds Formation. Enhanced sediment supply from the Archean basement during the Pleistocene may be due to incision of river valleys deeper into the basement. Similarly, a tectonic pulse is observed in the Kisegi-Nyabusosi area at ~1.8 Ma interpreted to mark the beginning of major uplift of the Rwenzori Mountains (Schneider et al., 2016b). Again, also other parts of the EARS show tectonic pulses at this time, e.g., southern Lake Tanganyika (Cohen et al., 1993), southern Main Ethiopian Rift (Bonini et al., 2005), southern Gregory Rift (Saemundsson, 2010) and Lake Malawi Rift (Macgregor, 2015) (Fig. 5-1).

5.8 Conclusion

The provenance of late Miocene to early Pleistocene rift sediment in the northern Albertine Rift (Nkondo-Kaiso area) was restored based on sediment modal compositions and chemical compositions of detrital garnet and rutile. A major change of sediment composition occurred at around 2.6 Ma when sediment became more mature. Potential source rocks, however, show only minor shifts. Rutile and garnet chemistry remains largely unchanged over the entire sedimentary succession from the latest Miocene to the early Pleistocene (~5.5–1.0 Ma). Most probably, the higher maturity in the Pleistocene results from additional supply from Neoproterozoic metasedimentary rocks, which are recycled from the same Archean basement rocks as the older Cenozoic sediment. In summary, the following scenario can be proposed:

- From ~6.5–4.5 Ma (pre-rift) sediment was supplied from the adjacent plateau from nearby sources, i.e., Neoarchean granitoids and the Mesoarchean Karuma Complex both belonging to the North Ugandan Terrane.

- From ~4.5–2.6 Ma (syn-rift) tectonic activity increased. Sediment supply continued to be mainly from nearby Archean basement sources; however, incision and headward cutting moved the mixture towards increased input from granulitic rocks of the Mesoarchean Karuma Complex. The basal shift at ~4.5 Ma lags ~0.5–1.0 Ma behind the southern Albertine Rift, which can be explained by delayed adaption of drainage systems and/or a northward progradation of rifting.

- From ~2.6–1.0 Ma (late syn-rift, inverted rift) a major tectonic pulse contemporaneous to the beginning of the extreme uplift of the Rwenzori fault block

led to increased erosion and expansion of downcutting rivers into the Ugandan Plateau to the east. This led to supply from a new source area, i.e., the Neoproterozoic Bunyoro Group that was also supplied from Archean basement rocks. Hence, Pleistocene sediment underwent twofold recycling.

The proposed provenance changes in the Nkondo-Kaiso area largely coincide in timing with major faulting episodes in other parts of the EARS, suggesting that tectonic movements in eastern Africa act at a global scale. The periods of compositional change are also coincident to provenance shifts in the southern Albertine Rift (Kisegi-Nyabusosi area), although some time lag indicates that tectonics in this particular basin are also subject to regional variations. The higher intensity of rifting activity in the southern Albertine sub-basin, culminating in the strongly exhumed Rwenzori Mountains, is also manifested in provenance pattern. In contrast to the Kisegi-Nyabusosi region, where three significant stages of sediment supply changing from a northeastern source to southeastern and southern sources were identified, provenance shifts in the further to the north located Nkondo-Kaiso area are less pronounced and sediment supply is mainly from local sources of the adjacent rift flank.

5.9 Acknowledgements

This study is part of the Forschergruppe 'Riftlink' funded by the DFG grant H1643–7/1. We thank the Ugandan National Council for Science and Technology for permitting the research work in Uganda and the Uganda Wildlife Authority for their support and permission to work in the national parks. Many thanks to our Ugandan research partners from Makerere University for cooperation, in particular Andreas Schumann for his on-site guidance and our driver Kitam Ali for his profound help and field endurance. Special thanks go to Dr. Stephan Buhre (Johannes Gutenberg University, Mainz) for his help with EMP analyses. Dennis Brüsch and Christina Bonanati contributed to this paper by sediment logging and facies analysis in the field as well as drawing of sedimentary logs. The article benefited greatly from careful reviews by Luca Carraciolo and Carita Augustsson.

5.10 References

Abdelsalam, M. G., Katumwehe, A. B., Atekwana, E. A., Le Pera, A. K., Achang, M., 2016. The Paleoproterozoic Singo Granite in south-central Uganda revealed as a Nested Igneous Ring Complex using Geophysical Data. Journal of African Earth Sciences, 116, 198–212.

Andò, S., Garzanti, E., Padoan, M., Limonta, M., 2012. Corrosion of heavy minerals during weathering and diagenesis: A catalogue for optical analysis. In: von Eynatten, H., Critelli, S., Ingersoll, R.V., Weltje, G.J. (Eds.), Actualistic models of sediment generation. Sedimentary Geology 280, pp. 165–178.

Aubrecht, R., Méres, Š., Sýkora, M., Mikus, T., 2009. Provenance of the detrital garnets and spinels from the Albian sediments of the Czorsztyn Unit (Pieniny Klippen Belt, Western Carpathians, Slovakia). Geologica Carpathica, 60, 463–483.

Bauer, F. U., Glasmacher U. A., Ring U., Schumann A., Nagudi B., 2010. Thermal and exhumation history of the central Rwenzori Mountains, Western Rift of the East African Rift System, Uganda. International Journal of Earth Sciences, 99, 1575–1597.

Bauer, F. U., Glasmacher, U. A., Ring, U., Karl, M., Schumann, A., Nagudi, B., 2013. Tracing the exhumation history of the Rwenzori Mountains, Albertine Rift, Uganda, using low-temperature thermochronology. Tectonophysics, 599, 8–28.

Bishop, W. W., 1965. In: Wright Jr., H. E., Frey, D. G. (Eds.), Quaternary Geology and Geomorphology in the Albertine Rift Valley, Uganda. International Studies on the Quaternary, pp. 293–321.

Bjørlikke, K. O., 1973. Glacial conglomerates of late Precambrian age from the Bunyoro Series, W. Uganda. Geologische Rundschau, 62, 938–947.

Bonini, M., Corti, G., Innocenti, F., Manetti, P., Mazzarini, F., Abebe, T., Pecskay, Z., 2005. Evolution of the Main Ethiopian Rift in the frame of Afar and Kenya rifts propagation. Tectonics, 24, 1–21.

Buchwaldt, R., Toulkeridis, T., Todt, W., Ucakuwun, E. K., 2008. Crustal age domains in the Kibaran belt of SW Uganda: Combined zircon geochronology and Sm–Nd isotopic investigation. Journal of African Earth Science, 51, 4–20.

Chorowicz, J., 2005. The East African rift system. Journal of African Earth Sciences, 43, 379–410.

Cohen, A. S., Soreghan, M. J., Scholz, C. A., 1993. Estimating the age of formation of lakes: an example from Lake Tanganyika, East African Rift system. Geology, 21, 511–514.

Cooke, H. B. S., 1958. Observations relating to the quaternary environments in east and southern Africa. Transactions of the Geological Society of South Africa, 60 (Annex), 1–74.

Dechamps, R., Senut, B., Pickford, M., 1992. Fruits fossiles pliocènes et pléistocènes du Rift occidental ougandais. Signification paléoenvironnementale. Comptes rendus de l'Académie des sciences. Série 2, Mécanique, Physique, Chimie, Sciences de l'univers, Sciences de la Terre, 314, 325–331.

Deer, W., Howie, R., Zussman, J., 1997. The rock-forming minerals. Disilicates and ring silicates. Vol. 1B, 151–179.

Delvaux, D., Barth, A., 2010. African Stress Pattern from formal inversion of focal mechanism data. Implications for rifting dynamics. Tectonophysics, 482, 105–128.

DeMenocal, P., 1995. Plio-Pleistocene African Climate. Science, 270, 53–59.

DeMenocal, P., 2004. African climate change and faunal evolution during the Pliocene-Pleistocene. Earth and Planetary Science Letters, 220, 3–24.

De Waele, B., Johnson, S. P., Pisarevsky, S. A., 2008. Paleoproterozoic to Neoproterozoic growth and evolution of the eastern Congo Craton. Its role in the Rodenia puzzle. Precambrian Research, 160, 127–141.

Dickinson, W. R., 1970. Interpreting detrital modes of graywacke and arkose. Journal of Sedimentary Research, 40, 695–707.

Ebinger, C. J., 1989. Tectonic development on the western branch of the East African rift system. Geological Society of America Bulletin 101, 885–903.

Ebinger, C. J., Deino, A. L., Tesha, A. L., Becker, T., Ring, U., 1993. Tectonic controls on rift basin morphology: evolution of the Northern Malawi (Nyasa) Rift. Journal of Geophysical Research: Solid Earth, 98, 17821–17836.

Flannery, J. W., Rosendahl, B. R., 1990. The seismic stratigraphy of Lake Malawi, Africa: implications for interpreting geological processes in lacustrine rifts. Journal of African Earth Sciences (and the Middle East), 10, 519–548.

Frihy, O. E., 2007. The Nile Delta: processes of heavy mineral sorting and depositional patterns. In: Mange, M.A., Wright, D.T. (Eds.), Heavy Minerals in Use. Developments in Sedimentology, 58. Elsevier, Amsterdam, pp. 345–391.

Gani, N. D., Gani, M. R., Abdelsalam, M. G., 2007. Blue Nile incision on the Ethiopian Plateau: Pulsed plateau growth, Pliocene uplift, and hominin evolution. GSA Today, 17, 4.

Garzanti, E., Vezzoli, G., 2003. A classification of metamorphic grains in sands based on their composition and grade: Research Methods Papers. Journal of Sedimentary Research, 73, 830–837.

Garzanti, E., Padoan, M., Andò, S., Resentini, A., Vezzoli, G., Lustrino, M., 2013. Weathering and relative durability of detrital minerals in equatorial climate: sand petrology and geochemistry in the East African rift. The Journal of Geology, 121, 547–580.

Gautier, A., 1965. Geological Investigation in the Sinda Mohari (Ituri, NE-Congo). A Monograph on the Geological History of a Region in the Lake Albert Rift. Ganda-Congo Expedition. Ghent University, 158 pp.

Gautier, A., 1970. Fossil freshwater mollusca of the Lake Edward–Lake Albert Rift. Annual Reports of the Royal Museum of Central Africa, Tervuren 67, 1–144.

Hubert, J. F., 1962. A zircon-tourmaline-rutile maturity index and the interdependence of the composition of heavy mineral assemblages with the gross composition and texture of sandstones. Journal of Sedimentary Research, 32, 440–450.

Jacobs, B. F., Deino, A.L., 1996. Test of climate–leaf physiognomy regression models, their application to two Miocene floras from Kenya, and 40Ar/39Ar dating of the late Miocene Kapturo site. Palaeogeography, Palaeoclimatology, Palaeoecology, 123, 259–271.

Karp, T., Scholz, C. A., McGlue, M. M., 2012. Structure and stratigraphy of the Lake Albert Rift, East Africa: Observations from seismic reflection and gravity data. In: Baganz, O. W., Bartov, Y., Bohacs, K., Nummedal, D. (Eds), Lacustrine sandstone reservoirs and hydrocarbon systems. AAPG Memoir, 95, pp. 299–318.

King, B. C., 1959a. Problems of the Precambrian of Central and Western Uganda, part I. Problems of correlation. Science Progress, London, 47, 528–542.

King, B. C., 1959b. Problems of the Precambrian of Central and Western Uganda, part II. Structures, metamorphism, and granites. Science Progress, London, 47, 723–744.

Krippner, A., Meinhold, G., Morton, A. C., von Eynatten, H., 2014. Evaluation of garnet discrimination diagrams using geochemical data of garnets derived from various host rocks. Sedimentary Geology, 306, 36–52.

Leggo, P. J., 1974. A geochronological study of the basement complex of Uganda. Journal of the Geological Society of London, 130, 263–277.

Lenoir J-L, Kuster D., Liegeois J. P., Utke A., Haider A., Matheis G., 1994. Origin and regional significance of late Precambrian and early Palaeozoic granitoids in the Pan-African belt of Somalia. Geologische Rundschau, 83, 624–641.

Link, K., Koehn, D., Barth, M. G., Tiberindwa, J. V., Barifaijo, E., Aanyu, K., Foley, S. F., 2010. Continuous cratonic crust between the Congo and Tanzania blocks in western Uganda. International Journal of Earth Sciences, 99, 1559–1573.

Lofty, M. F., 1997. Distributaion of heavy mineral grains by granulometric fractions in some modern Nile Delta coastal sands, Egypt. INQUA Commision on Quaternary Shorelines, Newsletter 19, 33–41.

Macgregor, D. S., 2012. The development of the Nile drainage system: integration of onshore and offshore evidence. Petroleum Geoscience, 18, 417–431.

Macgregor, D. S., 2015. History of the development of the East African Rift System: A series of interpreted maps through time. Journal of African Earth Sciences, 101, 232–252.

Mänttäri, I., 2014. Mesoarchaean to Neoproterozoic U-Pb and Sm-Nd ages from Uganda. In: Lehto, T., Katto, E. (Eds.), GTK Consortium Geological Surveys in Uganda 2008−2012. Geological Survey of Finland, Special Paper, 56.

Mange, M. A., Maurer, H. F. W., 1992. Heavy minerals in colour. Chapman and Hall, London, 148 pp.

Mange, M. A., Morton, A. C., 2007. Geochemistry of heavy minerals. In: Mange, M. A., Wright, D. T. (Eds.), Heavy Minerals in Use. Developments in Sedimentology, 58. Elsevier, Amsterdam, pp. 345–391.

Master, S., Bailie, R., 2000. Geochemistry of amphibolites from the Stanley Volcanics and Kilembe Schists, Buganda–Toro Supergroup, Ruwenzori Mountains, western Uganda. Journal of African Earth Science, 30, 59–60.

Master, S., Bekker, A., Karhu, J. A., 2013. Paleoproterozoic high δ 13 C carb marbles from the Ruwenzori Mountains, Uganda: Implications for the age of the Buganda Group. Chemical Geology, 362, 157–164.

Morley, C. K., 1999. Geoscience of rift systems-evolution of East Africa. American Association of Petroleum Geologists Studies in Geology, 44, 242 pp.

Morton, A. C., Hallsworth, C. R., 1994. Identifying provenance-specific features of detrital heavy mineral assemblages in sandstones. Sedimentary Geology, 90, 241–256.

Morton, A. C., Hallsworth, C. R., 1999. Processes controlling the composition of heavy mineral assemblages in sandstones. Sedimentary Geology, 124, 3–29.

Nagudi, B., Koeberl, C., Kurat, G., 2003. Petrography and geochemistry of the Singo granite, Uganda, and implications for its origin. Journal of African Earth Science, 36, 73–87.

Ollier, C. D., 1990. Morphotectonics of the Lake Albert Rift Valley and its significance for continental margins. Journal of Geodynamics, 11, 343–355.

Pickford, M., Senut, B., Poupeau, G., Brown, F., Haileab, B., 1991. Correlation of tephra layers from the Western Rift Valley (Uganda) to the Turkana Basin (Ethiopia/Kenya) and the Gulf of Aden. Stratigraphy, 313, 223–229.

Pickford, M., Senut, B., Hadoto, D., 1993. Geology and Palaeobiology of the Albertine Rift Valley, Uganda-Zaire. Vol. I: Geology. International Centre for Training and Exchanges in Geosciences, Occasional publications, 24, 1–190.

Rainaud, C., Master, S., Armstrong, R. A., Robb, L. J., 2005. Geochronology and nature of the Palaeoproterozoic basement in the Central African copperbelt (Zambia and the Democratic Republic of Congo), with regional implications. Journal of African Earth Science, 42, 1–31.

Ring, U., 2008. Extreme uplift of the Rwenzori Mountains in the East African Rift, Uganda: Structural framework and possible role of glaciations. Tectonics, 27.

Ring, U., 2014. The East African Rift System. Australian Journal of Earth Sciences, 107, 132–146.

Ring, U., Betzler, C., 1995. Geology of the Malawi Rift: kinematic and tectono-sedimentary background to the Chiwondo Beds, northern Malawi. Journal of Human Evolution, 28, 7–21.

Ring, U., Betzler, C., Delvaux, D., 1992, Normal vs. strike-slip faulting during rift development in East Africa: The Malawi rift, Geology, 20, 1015–1018.

Roller, S., Hornung, J., Hinderer, M., Ssemmanda, I., 2010. Middle Miocene to Pleistocene sedimentary record of rift evolution in the southern Albertine Graben (Uganda). International Journal of Earth Sciences, 99, 1643–1661.

Rosendahl, B. R., Kilembe, E., Kaczmarick, K., 1992. Comparison of the Tanganyika, Malawi, Rukwa and Turkana Rift zones from analyses of seismic reflection data. Tectonophysics, 213, 235–256.

Saemundsson, K., 2010. East African rift system. An overview. Paper presented at course V on exploration for geothermal resources, organized by UNU-GTP, GDC and KenGen, at Lake Bogoria and Lake Naivasha, Kenya, Oct. 29-Nov. 19, 2010.

Schlüter, T., 2008. Geological Atlas of Africa, 2nd edition, 307 p., Springer Verlag, Berlin.

Schneider, S., Hornung, J., Hinderer, M., Garzanti, E., 2016a. Petrography and geochemistry of modern river sediments in an equatorial environment (Rwenzori Mountains and Albertine rift, Uganda)—Implications for weathering and provenance. Sedimentary Geology, 336, 106–119.

Schneider, S., Hornung, J., Hinderer, M., 2016b. Evolution of the western East African Rift System reflected in provenance changes of Miocene to Pleistocene synrift sediments (Albertine Rift, Uganda). Sedimentary Geology, 343, 190–205.

Stern, R. J., 1994. Arc assembly and continental collision in the Neoproterozoic East African Orogen: Implication for the consolidation of Gondwanaland. Ann. Rev. Earth. Plan. Sci. 22, 319–351.

Tanner, P. W. G., 1971. The Stanley Volcanics Formation of Ruwenzori, Uganda. Annual Report. Research Institute for African Geology, 15. University of Leeds, pp. 8–11.

Taylor, R. G., Howard, K. W.F., 1999. The influence of tectonic setting on the hydrological characteristics of deeply weathered terrains: evidence from Uganda. Journal of Hydrology, 218, 44–71.

Tomkins, H. S., Powell, R., Ellis, D. J., 2007. The pressure dependence of the zirconium-in-rutile thermometer. Journal of Metamorphic Geology, 25, 703–713.

Trauth, M. H., Maslin, M. A., Deino, A., Strecker, M. R., 2005. Late cenozoic moisture history of East Africa. Science, 309, 2051–2053.

Triebold, S., von Eynatten, H., Zack, T., 2012. A recipe for the use of rutile in sedimentary provenance analysis. Sedimentary Geology, 282, 268–275.

Van Damme, D., Pickford, M., 1995. The late Cenozoic Ampullariidae (Mollusca, Gastropoda) of the Albertine Rift Valley (Uganda-Zaire). Hydrobiologia, 316, 1–32.

Van Damme, D., Pickford, M., 1998. The late Cenozoic Viviparidae (Mollusca, Gastropoda) of the Albertine Rift Valley (Uganda-Congo). Hydrobiologia, 390, 171–217.

Van Damme, D., Pickford, M., 2003. The late Cenozoic Thiaridae (Mollusca, Gastropoda, Cerithioidea) of the Albertine Rift Valley (Uganda-Congo) and their bearing on the origin and evolution of the Tanganyikanthalassoidmalacofauna. Hydrobiologia, 498, 1–83.

Van Straaten, H. P., 1971. Preliminary work on the Precambrian adjoining the Western Rift, north of Masindi, Bunyoro District (Sheet 39/I). Interim Res. Rept. I, Dept. Geol. Makerere Univ., Kampala.

Van Straaten, H. P., 1976. Prakambrium und junges Western Rift im Bunyoro Distrikt, NW-Uganda. Geologisches Jahrbuch, Reihe B, Heft 18, 95 pp.

Von Eynatten, H., Gaupp, R., 1999. Provenance of Cretaceous synorogenic sandstones in the Eastern Alps: constraints from framework petrography, heavy mineral analysis and mineral chemistry. Sedimentary Geology, 124, 81–111.

Westerhof, A. B. P., Härmä, P., Isabirye, E., Katto, E., Koistinen, T., Kuosmanen, E., Lehto, T., Lehtonen, M. I., Mäkitie, H., Manninen, T., Mänttäri, I., Pekkala, Y., Pokki, J., Saalmann, K., Virransalo, P., 2014. Geology and Geodynamic Development of Uganda with Explanation of the 1:1,000,000 -Scale Geological Map. Geological Survey of Finland, Special Paper, 55, 387 pages, 329 figures, 29 tables and 2 appendices.

Chapter 6

6 New insights into the evolution of the western East African Rift System (Albertine Rift, Uganda) through bulk rock geochemistry and zircon U-Pb geochronology

* unpublished manuscript

6.1 Abstract

In this study, bulk rock geochemistry and zircon geochronological data provide constraints on the provenance and depositional history of Miocene-Pleistocene rift sediments from two areas (Kisegi-Nyabusosi, Nkondo-Kaiso) in the central and southern Albertine Rift in western Uganda. The new provenance data suggest that the rift fill was supplied by high- to low-grade metamorphic and granitoidic rocks from Archean cratons (e.g., North Uganda Terrane, Karuma Complex), as well as Paleoproterozoic (Rwenzori Fold Belt) and Neoproterozoic lithologies (Bunyoro Group, East African Orogen). The data also indicate that the southern and eastern margins of the Lake Albert Basin were supplied by different independently operating drainage systems, which were prone to modifications during ongoing rifting and tectonic uplift.

The Miocene sediment (~17.0–5.0 Ma) in the southern Albertine Rift (Kisegi-Nyabusosi area) was supplied via a widely-branched, westward-directed 'proto-Nkusi-Victoria Nile' river system that flowed from the Kenyan margin through Uganda and the Albertine Rift, and further to the Congo Basin. The dominance of Neoarchean zircon U-Pb ages (~2500–2700 Ma) suggests major input from Neoarchean terranes, which are widespread in the Ugandan basement. This together with significant amounts of Pan-African zircon ages indicates that source areas may have extended towards the at least 400 km away East African Orogen in northeastern Uganda, maybe also Kenya. Since ~5.0 Ma, this large-scale hydrological network was mainly disrupted as indicated by lack of Neoproterozoic zircon and distinctively lower ratios for 'provenance-sensitive' geochemical parameters, such as La/Sc, La/Co, Th/Cr, Th/Co, Zr/Sc, and Th/Sc. This provenance change is interpreted to represent a phase of first major rifting affecting the Albertine Graben concurrent with the transition from the pre-rift into the syn-rift stage with enhanced subsidence and uplift of rift flanks and the Ugandan plateau. Delivering streams were largely deflected to the margin of the Albertine Basin. Although zircon and geochemical data remain similar to the Pliocene section, a further shift of provenance pattern at the Pliocene-Pleistocene interface (~2.5 Ma) manifests by the occurrence of pinkish zircon grains and is concurrent with the beginning uplift of the Rwenzori Mountains and initiation of inversion tectonics in the rift sector. In the Nkondo-Kaiso area further to the north, Pliocene (~5.1–4.0 Ma) sediment is mainly shed from the adjacent rift flank. Zircon U-Pb ages indicate major derivation from Neoarchean lithologies (2600–2700 Ma; North Uganda Terrane) and minor input from Neoproterozoic (Bunyoro Group) and Mesoarchean rocks (Karuma Group) cropping out in vicinity to the rift margin. Since the early Pleistocene (~2.6 Ma), the rift sediment exhibits a more quartzose composition reflected by high SiO_2 contents (~80%), increased mean K_2O/Na_2O ratios (~2.7), marked depletion in mobile elements, and relative increase of elemental ratios critical of the source rock composition (La/Sc, La/Co, Th/Co, and Th/Cr). The higher maturity is interpreted to result from enhanced input from recycled sedimentary rocks of the Neoproterozoic Bunyoro Group, which implies some eastward propagation of the drainage network. Following river incision led to reinvigoration of input from Archean basement rocks of the graben shoulder. Overall, the new provenance-based evolution model helps to refine existing tectonic and paleodrainage models for the Albertine Rift and contributes towards a broader understanding of the history of the northern Western Rift branch.

6.2 Introduction

The East African Rift System (EARS) is the most prominent tectonic and geomorphological feature in Africa and the classical example for an active continental rift. The rift valley is traditionally divided into an eastern and western branch; both consisting of several individual, narrow, roughly N-S aligned tectonic basins, which are flanked by broad uplifted shoulders that may be elevated several thousand meters above surrounding areas (Chorowicz, 2005; Ring, 2014). In the extreme case of the Rwenzori Mountains within the Albertine Graben in the Western Rift, basement uplift accounts for more than 4 km (Ring, 2008; Bauer et al., 2010, 2013). Although, the EARS has been intensively studied since decades (see Chorowicz, 2005), many uncertainties concerning the timing of onset and long-term evolution of rifting remain. One possible way to address these uncertainties is to study the interior of the individual rift segments, because the sedimentary infill exhibits the only complete record of the internal and external processes controlling rift evolution. In particular, sedimentary provenance analysis can be effective in reconstructing block uplift, unroofing patterns, landscape fragmentation and drainage evolution.

In this contribution, we study the Miocene-Pleistocene sediment cropping out in two localities within the Albertine graben valley (Kisegi-Nyabusosi and Nkondo-Kaiso) in the western branch of the EARS to reconstruct the evolutionary history of this particular basin. Recently, the sedimentary successions were analyzed for their provenance by integrating framework petrography, heavy mineral analyses and single grain chemistry of detrital garnet and rutile (Schneider et al., 2016b, 2017) (Fig. 6-7). Compositional variations within the stratigraphy of both areas were interpreted to represent changes in the source rocks as result of a shift in sediment supply pattern. In the Kisegi-Nyabusosi area, which is located adjacent to the northern tip of the Rwenzori Mountains, three varying provenances were determined. The first change in sediment composition is mainly shown by a switch from zircon-garnet-dominated to epidote-amphibole-dominated heavy mineral assemblages and by the absence of high almandine-pyrope garnet (grossular <10%), and was interpreted to reflect the transition from the pre-rift to the syn-rift stage in the early Pliocene (~5.5–5.0 Ma). The second provenance change that manifests by the occurrence of spessartine-rich garnet and ‘colder’ Zr-in-rutile temperatures marks the beginning uplift of the nearby Rwenzori horst block, starting at ~2.5 Ma. In the Nkondo-Kaiso area further to the north, two main provenance stages were determined. Pliocene sediment points to a proximal source close to the fault scarp with major transport from high-grade rocks of the North Uganda Terrane (NUT). The increase of more stable minerals (e.g., quartz, zircon) at the Pliocene-Pleistocene transition was interpreted to reflect admixing of recycled sedimentary rocks of the Bunyoro Group that partly overlies basement rocks in the east, because external processes, like weathering and hydraulic sorting could be largely excluded. Schneider et al. (2016b, 2017) insinuate that the timing of compositional changes corresponds roughly between the Kisegi-Nyabusosi area and Nkondo-Kaiso area and is closely related to tectonic activity affecting this particular rift sector and overall tectonic events in the East African Rift.

The aim of this study is to extend the multi-proxy approach of Schneider et al. (2016b, 2017) to validate the proposed provenance model and to tackle remaining uncertainties concerning source areas and drainage pathways. In particular, this includes verification of the proposed large-scale river system that is supposed to have existed during the Miocene and was later disrupted by the uplift of rift flanks bounding the Albertine Rift. Although, a distal sediment transport from northern sources with major contribution from the Neoarchean NUT is indicated for the Miocene sediment of the Kisegi-Nyabusosi area by the data set of Schneider et al. (2016b), the dimension of sediment sources and the operating drainage network could not be specified by the applied methodical approach. Further verifications are also necessary for the later segmentation of this continental-wide river network in the early Pliocene. Although this shift is indicated by heavy mineral assemblages and garnet chemistry, it is not shown by rutile chemistry, which remains similar to the underlying succession. In the Nkondo-Kaiso region,

uncertainties remain concerning the higher maturity of the Pleistocene sediment as revealed by high abundances of quartz and the occurrence of more resistant heavy minerals, interpreted to be caused by additional input from the (meta-)sedimentary Bunyoro Group. This is still afflicted with uncertainties, because garnet and rutile chemistry remain analogue to the Pliocene sediment sections.

Furthermore, spatial correlations and interpretations between the two studied areas (Kisegi-Nyabusosi vs. Nkondo-Kaiso) need to be adjusted, especially with regard to the lately revised biostratigraphic age model for the Albertine Rift (Simon et al., 2017). Finally, the provenance-based evolutionary model is discussed with existing tectonic, sedimentological and drainage models for the Albertine Rift.

The methodological approach of this study includes combined analysis of zircon U-Pb ages and bulk rock geochemistry. U-Pb zircon geochronology is applied in order to determine the time of formation of the zircon grains, which, ideally, can be directly linked to a specific magmatic or metamorphic event in the study area (Thomas, 2011; Gehrels, 2014). Bulk rock geochemical analysis is used to discriminate and classify the sediment according to its elemental interior. Some trace elements are sensitive indicators of either felsic (e.g. Th, U, Zr, Hf, Nb, Ta, Y) or mafic rocks (e.g. Ni, Co, Cr, V, Cu; Bhatia and Crook, 1986; Cullers, 2000; Lee, 2002) and can therefore be used to decipher the provenance of siliciclastic rocks. Element concentrations and ratios also provide information about fractionation processes during transport and about the weathering degree of sediments, because changes in the mineralogical composition are also reflected in the geochemistry of sediments (Cullers, 1988, 2000).

6.3 Geological setting

The EARS, the most prominent example of an intra-plate ridge system, developed successively during the Cenozoic, and was most probably initiated by the impingement of a mantle plume underneath eastern Africa (Ebinger, 1989; Chorowicz, 2005; Ring, 2014). Traditionally, the EARS is divided into two main branches; an older, volcanically-active eastern branch and a younger, less volcanically-active western branch (Ring, 2014). The eastern branch runs over circa 2200 km from the Afar triangle in the north, through the Ethiopian and Kenyan rifts towards the North Tanzanian Divergence in the south (Fig. 6-1). The western branch extends over circa 2100 km from the Albertine Rift in the north, through the Kivu and Tanganyika rifts towards the Malawi Rift in the south. At the Mbeya triple junction (Macheyeki et al. 2008), the western branch unites with the re-emerging eastern branch. Each rift branch consists of diachronous, narrow, elongated, more or less N-S trending individual sectors, linked and segmented by intracontinental transform, transfer and accommodation zones (Chorowicz, 2005). The rift valleys are flanked to both sides by thermally uplifted shoulders, comprising parallel mountain lines, plateaus, or volcanic massifs (Chorowicz, 2005). Both, the eastern and western rift arm show distinct differences concerning age, volcanic activity, and overall morphology, most probably determined by the location and movement direction of the mantle plume underneath of Africa and the composition of the lithosphere through which the rift propagates (Ring, 2014).

The Albertine Rift constitutes the northern of three sectors collectively forming the western arm of the EARS, with the national border between Uganda and the Democratic Republic of Congo (DRC) passing through the center of the rift valley. Structurally, the rift segment consists of several dissected asymmetric graben depocenters, each separated by NW-SE or W-E trending basement heights or ‘Accommodation Zones’ (AZs), some of them associated with volcanics (Rubondo, 2005). The basin is bounded by a large border fault on one side and a set of smaller step faults on the other side (Lukaye et al., 2016). Active rifting in the Albertine Rift is evident from seismic investigations (Morley et al., 1990; McGlue et al., 2006) and geomorphological studies (Pickford et al., 1993), and manifests by subsidence of the rift floor and associated uplift of rift flanks. The lowest point is located within Lake

Albert (618 m a.s.l.), while the border faults flanking the rift have been elevated to >1 km to the east and ~3 km to the west. The highest uplift are the Rwenzori Mountains (>5000 m a.s.l.) that represent a tilted block composed of dissected Precambrian basement rocks located between Lake Albert and Lake Edward (Ollier, 1990).

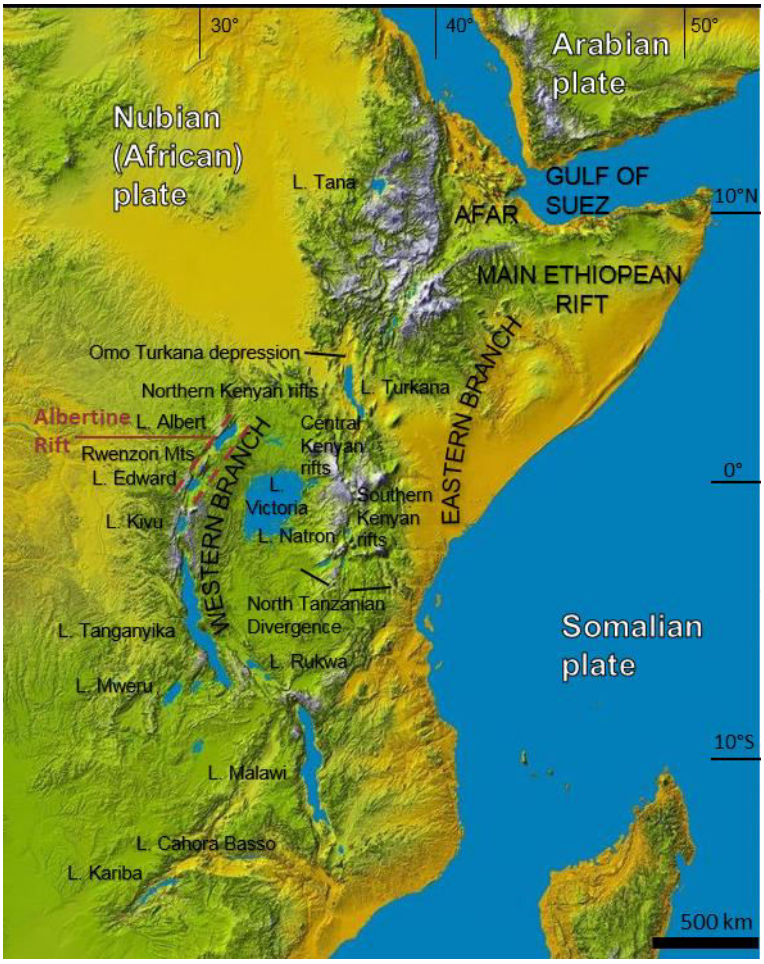

Figure 6-1. Morphological overview of the East Africa Rift System with location of the Albertine Rift. The basemap (Digital Elevation Model) is a SSRT image provided by the NASA.

The Albertine Rift formed as a result of multiple rifting phases. The onset of rifting and timing of various tectonic events is still not clear. There is largely agreement between most researchers that rifting and sedimentation in this rift sector date from Neogene to Recent and that there were at least three major stages of tectonic activity during which faulting and rift flank uplift took place (Pickford et al., 1993). The onset of sedimentation is controversially discussed with proposed ages for the earliest subsurface sediment in the southern Lake Albert Basin ranging from early Miocene (Lukaye, 2009; Simon, 2015) to early Pliocene (RPS Energy, 2008), whereas earliest surface exposures are assigned to be middle Miocene in age (Pickford et al., 1993; Van Damme and Pickford, 2003), or older (Lukaye et al., 2016). Most recent studies plead for an age of ~17.0 Ma (Simon et al., 2017). First major faulting took place at ~8.0 Ma. Associated rift-flank uplift (Ring et al., 1992; Ebinger et al., 1993; Ring and Betzler, 1995) and accelerated subsidence triggered the formation of a paleolake (Lake Obweruka), which extended ~550 km from near Kivu in the south to the Sudan/Uganda border in the north and lasted from 7.5 to 2.5 Ma (Ebinger, 1989; Pickford et al., 1993). The transition from the pre-rift to the syn-rift stage is assigned to have started at 6.2 Ma based on studies on sedimentology and

deformation pattern (Simon et al., 2017) (Fig. 6-2). Schneider et al. (2016b) propose some later ages between ~5.5–5.0 Ma for the transition into the syn-rift stage, based on a provenance shift observed within the rift sediment. Rift flanks are assigned to become climatically significant since 4.0 Ma (Pickford et al., 1993). A further period of tectonic activity at ~2.5 Ma was accompanied by uplift of the rift walls (Pickford et al., 1993; Schneider et al., 2016b). The exhumation of the Rwenzori Mountains is believed to have started at this time, forcing the separation of Paleolake Obweruka into present Lake Albert and Lake Edward (Pickford et al., 1993; MacPhee, 2006; Bauer et al., 2010, 2012, 2016).

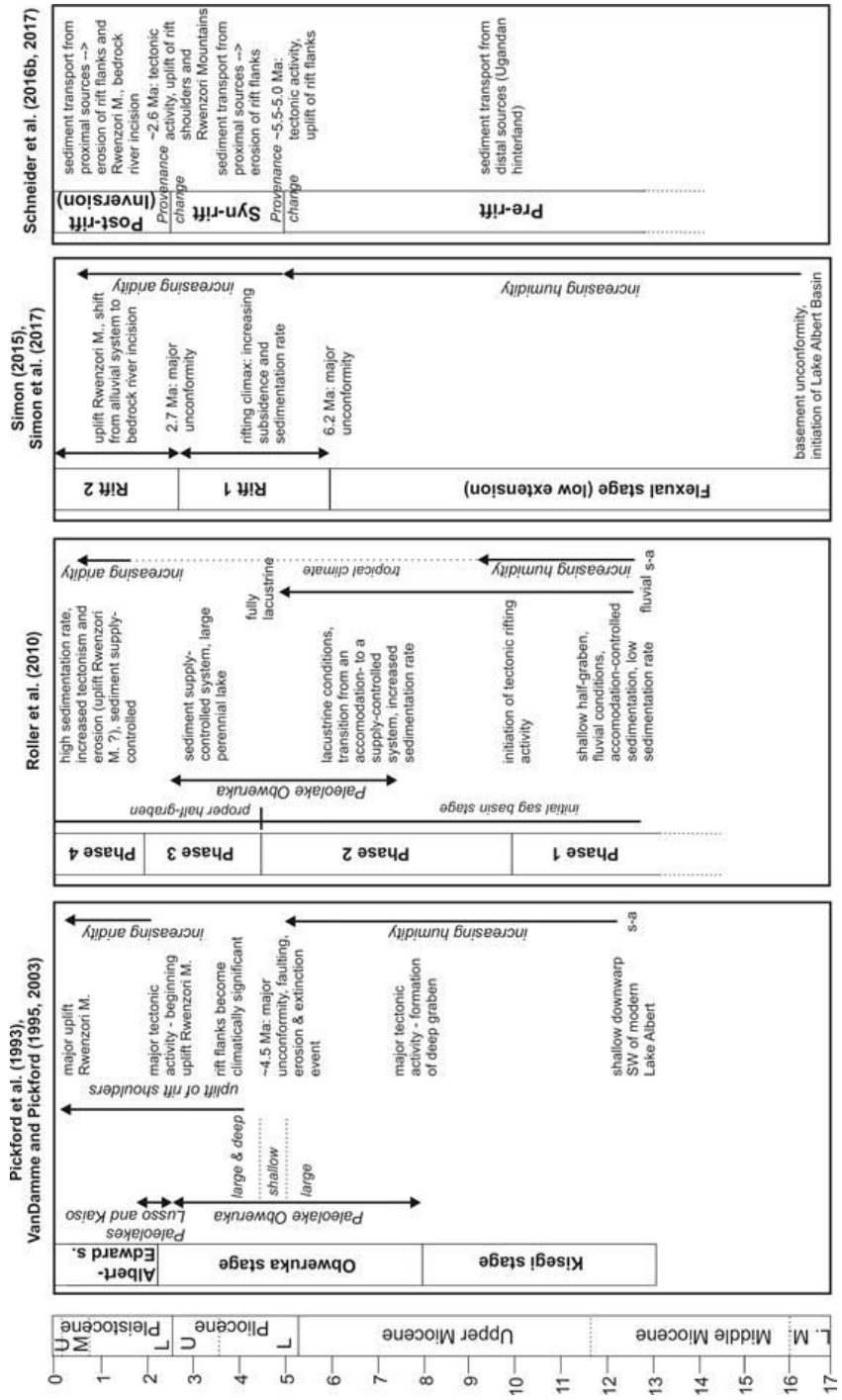

Figure 6-2. Recent models for the sedimento-tectonic evolution of the Albertine Rift.

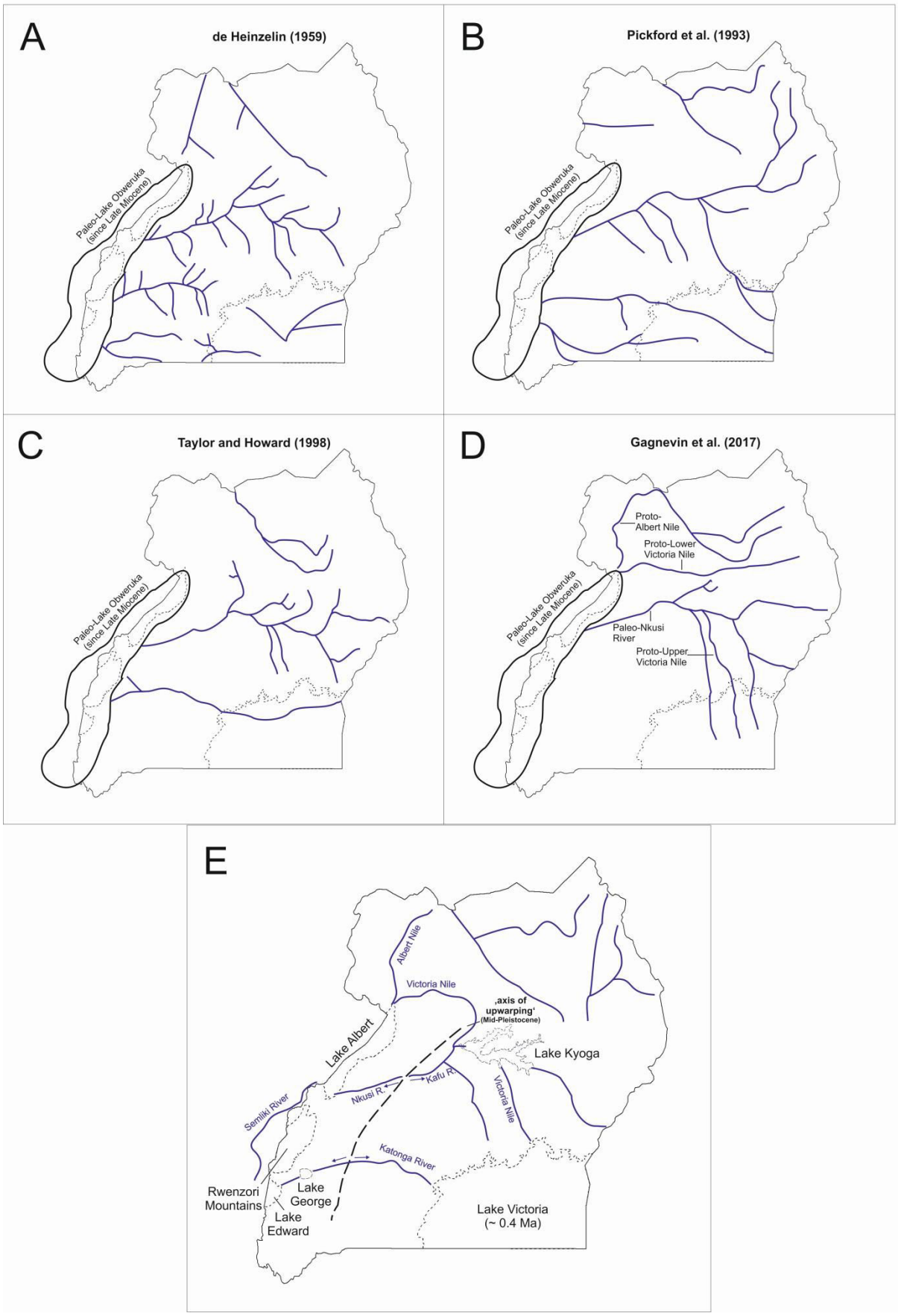

Figure 6-3. A-D: Different models for the Miocene to Pleistocene drainage of Uganda. E: Modern drainage of Uganda.

However, the proposed time frame for sedimentation and tectonics in the Albertine Rift is tainted with some uncertainties, because direct dating is missing. Stratigraphic ages are based on correlations of fossil mammals and gastropod associations (Gautier, 1970; Pickford et al., 1993; van Damme and Pickford, 1995, 1998, 2003; Simon, 2015), as well as tephra layers (Pickford et al., 1991), mostly with the eastern rift branch of the EARS. There are also controversies concerning the drainage evolution in Uganda. Although it is generally agreed that drainage during the Miocene to middle Pleistocene was westward directed towards the rift and further eastward into the Congo Basin, there are several interpretations concerning the configuration (e.g., dimension, river direction) of the hydrographic network (Fig. 6-3). While most authors assume drainage via a widely-branched 'proto-Nkusi River system', which was extensively fed by rivers draining the region now covered by Lake Victoria, Pickford et al. (1993) also propose a connection to rivers traversing the northeastern part of Uganda. The continental-wide drainage system was modified since ~0.4 Ma by river reversal as consequence of rift flank uplift and northward tilting ('axis of upwarping'; Doornkamp, 1968). Reversed flow directions and downwarping of the country east of the axis led to the creation of Lake Kyoga and Lake Victoria by either flooding of former headwaters or pooling of waters (Doornkamp, 1968; Ollier, 1990; Taylor and Howard, 1999) and to the capture of the upper Nile by the Victoria Nile (Talbot and Williams, 2009). Outflow from the rift is now northwards into South Sudan via the Albert Nile. Regional tectonic uplift also had a severe influence on climate evolution (e.g., deMenocal, 1995, 2004; Trauth et al., 2005), manifested in diminution of the tropical rainforest and expansion of savanna environments by during the Plio-Pleistocene boundary (Dechamps et al., 1992). Surface and subsurface investigations indicate that the Albertine Rift is filled with several thousand meters thick sedimentary successions. Drilling in the Semliki Basin revealed a ~3000 m thick sedimentary succession without reaching the basement, while geophysical surveys indicate a ~6 km sequence below southern Lake Albert (Lukaye et al., 2016). Maximum estimated thicknesses for the Neogene sediment that is exposed in valleys surrounding Lake Albert vary from ~600 m (Wayland, 1925; Pickford et al., 1993) up to 'at least' 1300 m (Bishop, 1965). The sediment is mainly composed of fluvial and deltaic deposits in the top and bottom of the sedimentary record and lacustrine deposits in the middle and reveals a variety of lithologies, including conglomerate, sand, silt, clay, chert, shale, oil shale, and coal-bearing horizons.

6.4 Geology and geochronology of Uganda

If not cited otherwise, the following overview about the Ugandan geology follows the description given by Westerhof et al. (2014, and references therein), whereas the rock ages are reported according to Mänttäri (2014, and references therein).

The Ugandan basement spans more than 3 billion years. Structurally, it constitutes the northern part of the proto-Congo Craton, and is composed of welded Archean nuclei and Paleo-, Meso-, and Neoproterozoic mobile belts, associated with the Eburnian (~2.1–1.85 Ga), Grenvillean (~1.1–0.95 Ga) and Pan-African (~0.9–0.55 Ga) Orogenic Cycles (Fig. 6-4) . The two major Archean 'building blocks' are the Tanzania Craton and the NE Congo-Uganda Shield, further divided into smaller tectono-thermal terranes, each of which experienced a different geodynamic evolution. The Tanzania Craton, which occupies major parts in southern-central Uganda, comprises the granite-greenstone suite of the Lake Victoria Terrane (LVT) and the granito-gneissic-migmatitic suite of the West Tanzania Terrane (WTT). For both terrains a Neoarchean age (~2.63–2.59 Ga and 2.65–2.64 Ga, respectively) has been determined. The northern part of Uganda is composed of Archean high-grade gneissic-granulitic terranes of the West Nile Block (WNB) and the NUT, both belonging to the NE Congo-Uganda Shield. The WNB consists of a Mesoarchean nucleus (Uleppi Complex; >3.08 Ga) covered by mafic volcanic rocks of the War Group (~2.64 Ga) and mingled with Neoarchean (>2.63–2.59 Ga)

rocks of the Arua-Lobule Supergroup. The NUT is the largest tectono-thermal unit and occupies the northern part of the formerly called 'Ugandan Basement Complex' or 'Archean Gneiss-Granulite Complex' (MacDonald, 1966). It is separated from the WTT by the Nakasongola Discontinuity (pre-2.6 Ga), and from the WNB by the Madi-Igisi Belt (~1.0 Ga), and surrounded by Neoproterozoic Pan-African fold belts to the north and east. The NUT includes Mesoarchean granulitic metasedimentary rocks (Karuma Complex; 2.99 Ga), and Neoarchean (2.8–2.5 Ga) granitoid, gneiss and migmatite of igneous or uncertain origin. Metasedimentary rocks (e.g., micaeous schist, amphibolite, quartzite, calcsilicate) of Paleoproterozoic age represent the Eburnian Orogenic Cycle in Uganda (~2.2–1.8 Ga), and are present within the Rwenzori Fold Belt (RFB, or Buganda-Toro System according to Schlüter, 2008) that occupies large parts in central and southwestern Uganda (King, 1959a, 1959b; Schlüter, 2008; Master et al., 2013). Rocks of this belt are folded and thrusted northward onto Archean basement rocks (Link et al., 2010) with folding and intensity of metamorphic overprint decreasing southwards (Schlüter, 2008) and roughly from west to east (Taylor and Howard, 1998). Older gneissose/granitoidic rocks (2.21–2.15 Ga; Eburnian I) are overlain by metasediment and mafic volcanic rocks of the Buganda Group (~2.0–1.95 Ga). Within the RFB, several syn- and post-tectonic granitic bodies were emplaced (e.g., Singo or Mubende granite; Nagudi et al., 2003; Abdelsalam, 2016), for which an age of 1.99–1.96 Ga, and 1.85 Ga, respectively, has been assumed (Eburnian II). The Eburnian Orogenic Cycle was shortly followed by deposition of post-tectonic molasses-type sediment (1.79 Ga). Mesoproterozoic rocks largely correlate with the Grenvillean Orogenic Cycle (1.15–0.95 Ga). They include granitoid (1.40–1.33 Ga) and terrigenous metasediment of the North Kibaran Belt (~1.55–0.95 Ga) in southwestern Uganda, as well as metamorphic volcanics (0.98 Ga), metasediment (<1.0 Ga), and rare ultramafics of the Madi-Igisi Belt in northwestern Uganda; a narrow, intracratonic, thrust and shear belt, separating the WNB from the NUT. In the early Neoproterozoic, extension of the proto-Congo Craton gave rise to the deposition of platform rocks of the Malagarasi Supergroup during two depositional cycles between 880 and 820 Ma (Johnson et al., 2007), and since ~765 Ma (Key et al., 2001). In southern Uganda, these rocks are composed of molasses-type sediment (conglomerate, sandstone, siltstone) of the Mityana Group (890–790 Ma), cropping out in small patches west of Lake Victoria. In western-central Uganda, they belong to the Bunyoro Group (765–735 Ma), a 250 km long and 20–50 km wide belt stretching along the eastern shore of Lake Albert towards Lake Kyoga in central Uganda. In this region, mudstone, sandstone, and low-grade metamorphic schist, slate, orthoquartzite, and phyllite overlie a basal tillite (Bjørlikke, 1973; Schlüter, 2008; Westerhof et al., 2014). Correlation with similar deposits in central Africa suggests that these tilloids have an age between 765 Ma and 735 Ma (Key et al. 2001), largely coeval with the global Sturtian glaciation. The Pan-African Orogenic Cycle (~900–550 Ma), which led to the creation of the Gondwana Supercontinent, is represented by the East African Orogen (EAO) in the northeast (Stern, 1994). This orogen represents a poly-cycle mobile belt that developed between 830 Ma and 550 Ma, and is composed of high-grade supracrustals, amphibolite, granitoid, granulite, charnockite interlayered with older crust, and intruded by granitoids (950 Ma). A series of in situ Pan-African granitoid bodies (660 Ma) belonging to the E-W-trending Central African Fold Belt (CAFB) crop out in the northernmost part of Uganda (in the WNB and NUT). The Phanerozoic evolution of Uganda is associated with the breakup of the Gondwana continent leading to activation of older suture zones. In Uganda, this phase is characterized by emplacement of a number of post-Pan-African (~550 to ~440 Ma) alkaline complexes along a weakness zone that developed later into the Western Branch of the EARS. Karoo sediments (290–180 Ma) are only present in small patches in southern Uganda. Most of this sediment was probably eroded with the evolution and uplift of the EARS (Westerhof et al., 2014). Late Eocene-Neogene rifting and development of the EARS in Uganda is represented by the Elgon Complex in eastern Uganda, comprising basal sediment, covered predominantly by pyroclastic and volcanic rocks and associated carbonatite plugs and fenites of Neogene (20–18 Ma) age. The Albertine Group laid down in the Albertine Rift in the western branch of the EARS is

composed of strongly silica-undersaturated lavas, including kamafugite and carbonatite (Barker and Nixon, 1989; Foley et al., 2012), as well as Miocene to Pleistocene fluvio-lacustrine rift sediment (Pickford et al., 1993; Roller et al., 2010).

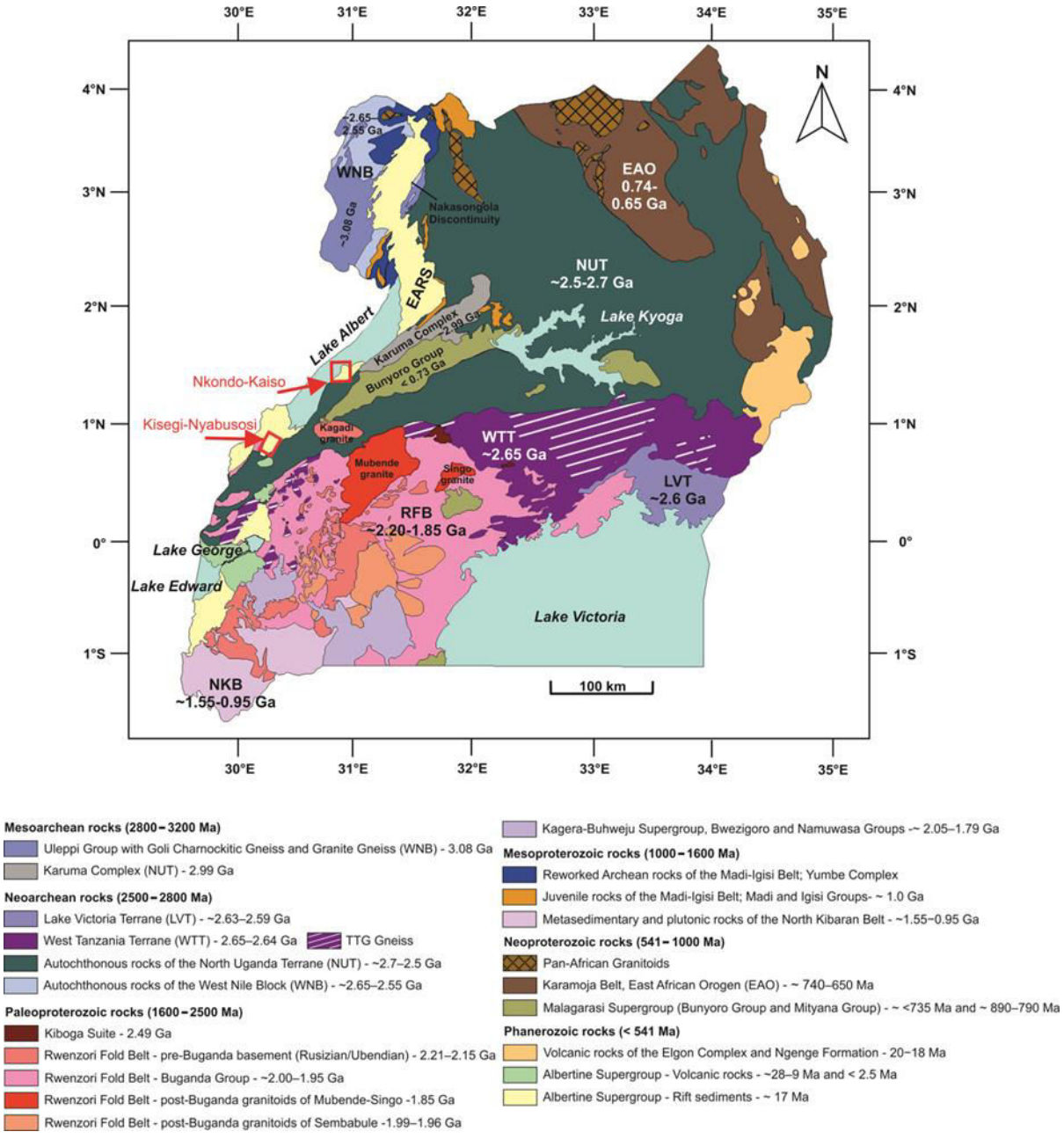

Figure 6-4. Geological and geochronological outline of Uganda after Westerhof et al. (2014) with age determinations adopted from Mänttäri (2014) and location of studied areas (in red boxes).

6.5 Stratigraphy and sedimentology

The rift sediment analyzed in this study crops out in two localities in the northern Albertine Rift. The Kisegi-Nyabusosi area adjoins Lake Albert to the south. To the southwest it is bounded by the

northern tip of the Rwenzori horst block and by the rift shoulder to the east. The Kaiso-Nkondo area is located at the eastern shoreline of Lake Albert. To its eastern side it is bordered by the rift shoulder of the Albertine Rift, which has been uplifted in this area ~1.3 km. The stratigraphy of both areas is subdivided into several formations, members and beds based on mammalian biostratigraphy (Pickford et al., 1993; Van Damme and Pickford, 1995, 2003; Simon, 2015; Simon et al., 2017) and tephrostratigraphy (Pickford et al., 1991). Recently, the age model of the sedimentary infilling has been revised by combination of biostratigraphic data (mammals), sequential correlations of outcrops and subsurface wells and validation of paleoprecipitation variation curves available for the East African Rift System (Simon, 2015; Simon et al., 2017). According to this study, the initiation of the Albertine Rift started much earlier (~17.0 Ma) than previously thought. A brief description of the sedimentary record deposited in both study areas is given in the following section. Stratigraphic subdivisions and ages of the successions rely on published biostratigraphic data presented by Pickford et al. (1993) and later revisions made by Simon (2015). The description of sedimentological features follows Roller et al. (2010), Lukaye et al. (2016) and own observations. For more detailed descriptions see Schneider et al. (2016b, 2017).

Exposed deposits in the Kisegi-Nyabusosi area (Fig. 6-6) show the most complete sedimentary record in the Albertine Rift, spanning from middle Miocene to Recent. The oldest sediment, overlying metamorphic basement, is assigned to the ~110 m thick Kisegi Formation (early Miocene; ~17.0 Ma). Following a basal conglomerate, this formation consists of predominantly amalgamated, cross-bedded, medium-grained to coarse-grained sand bodies interpreted to be accumulated in a fluvial environment. The presence of abundant gypsum precipitates indicates warm to hot, semiarid climate conditions. The upper Kisegi Formation (now Kasande Formation; Lukaye et al., 2016; 12.5 Ma) shows increasingly finer grain-size fractions (bleached fine sand to clay) indicating an open lacustrine environment due to lake transgression and a more humid climate. The following <40 m thick Kakara Formation (11.5–9.0 Ma) is dominated by sand, with some intercalated silty and clayey layers at the bottom and top of the formation. The sediment accumulated in a distal delta plain/palustrine environment merging into a lower delta plain setting (river mouth). The lower part of the 50–60 m thick Oluka Formation (6.5–5.0 Ma) is composed of alternations between clay and medium-grained sand with a general fining-upward trend, disrupted by a ~8 m thick coarsening-up sand body in the lower section. Sediment of the Oluka Formation marks the transition from outer delta plain/palustrine conditions towards a (shallow) lacustrine depositional environment. The Nyaburogo Formation (5.0–4.2 Ma) is estimated to have a thickness of approximately 120 m (Pickford et al., 1993) of which 15 m was recorded by Roller et al. (2010). Overall, this unit is dominated by clay and silt with only few sandy intercalations at the top of the section. The depositional environment of the Nyaburogo Formation changes from lacustrine towards alluvial/delta plain. Palynomorph associations suggest transition from humid to a drier climate during the early stage of this formation (Lukaye, 2009). The ~60 thick Nyakabingo Formation (4.0–2.5 Ma) is composed of light gray to greenish clay, iron-stained silt, sand and minor gravel accumulated in a lacustrine deltaic environment. The <100 m thick Katorogo Formation (≈2.5 Ma(?)) consists of poorly sorted sand with clayey intercalations that become dominant in the upper part of the section. Sediment represents either clayey/silty floodplain fines or crevasse splay deposits interpreted to have been accumulated in an alluvial plain environment. The ~50 m thick Nyabusosi Formation (≈1.5 Ma) is divided into three members – Makondo, Behanga and Kagusa – and consists of alternating sandy and clayey beds. Several distinct ooidic iron crusts are distinguishable throughout the Behanga Member. The depositional environment fluctuates between fluvial-deltaic to shallow lacustrine, indicating considerable lake-level oscillations (Roller et al., 2010). In the Kaiso-Nkondo region (Fig. 6-5), the base of the stratigraphy is not exposed. The oldest sediment is allocated to the Nkondo Formation deposited in a fluvial-deltaic to deep lacustrine depositional environment (~70 m thick). The sediment is composed of intercalations between sand, silt and clay (Nkondo Member) fining-upwards into clayey deposits (Nyawaiga Member). New age data imply that the Nkondo

formation is younger than previously presumed. Instead of a late Miocene to early Pliocene age (Pickford et al, 1993), Simon (2015) assigns this formation to be fully Pliocene in age (5.1–4.6 Ma), and to correlate with the Nyaburogo Fm. in the southern Lake Albert sub-basin. The overlying Warwire Formation (≈4 Ma) is composed of a 10 cm thick basal microconglomerate, followed by approximately 80 m of clay, silt and sand alternations, that represent an interplay between lacustrine, fluvial and alluvial fan settings. Several iron crusts and iron-hydroxide impregnated horizons are distinguishable, as well as two volcanic ash layers (Warwire Tuff, 3.6 Ma, and Kyampagna Tuff, 3.45 Ma) (Pickford et al., 1991). The at least 8 m thick Kyeoro Formation (~4–2.5 Ma) comprises sand and clay accumulated in a fluvial environment near a lake margin. The following ~23 m thick Kaiso Village Formation (2.6–2.0 Ma) is predominantly composed of clayey sediments intercalated with sandy interbeds (Hohwa Member) and is coarsening-upwards into a silty-sandy unit (Kaiso Village Member). The Hohwa Tuff of unknown age is intercalated between the two members (Pickford et al., 1991). The Kaiso Village Formation represents a fluvial floodplain environment near the lakeshore. The Museta beds Formation (1.5–1.0 Ma) lies unconformably on the Kaiso Village Formation and is dominated by ~12 m thick medium sand representing channel deposits in a fluvial environment.

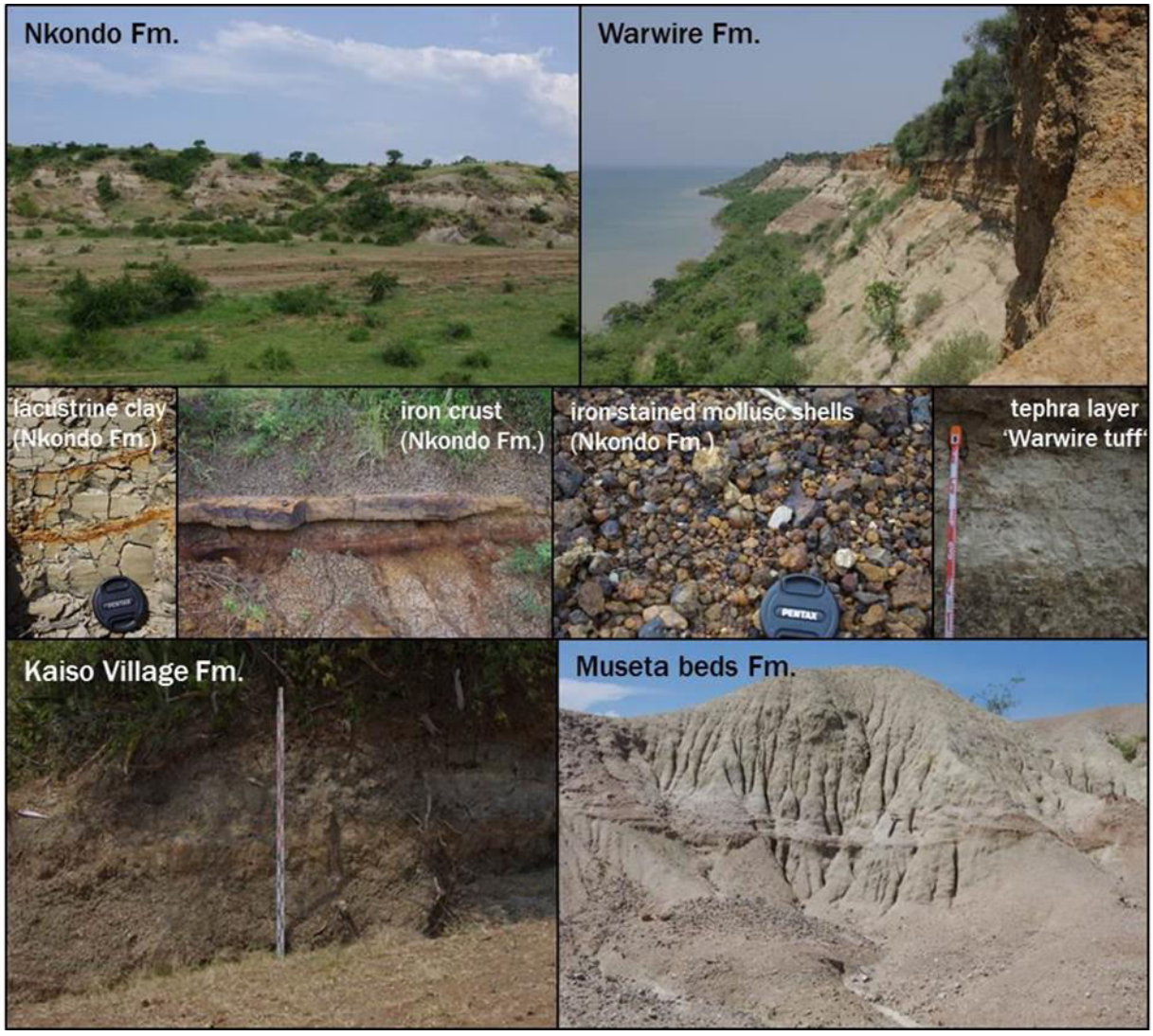

Figure 6-5. Sedimentary outcrops logged in the Nkondo-Kaiso area.

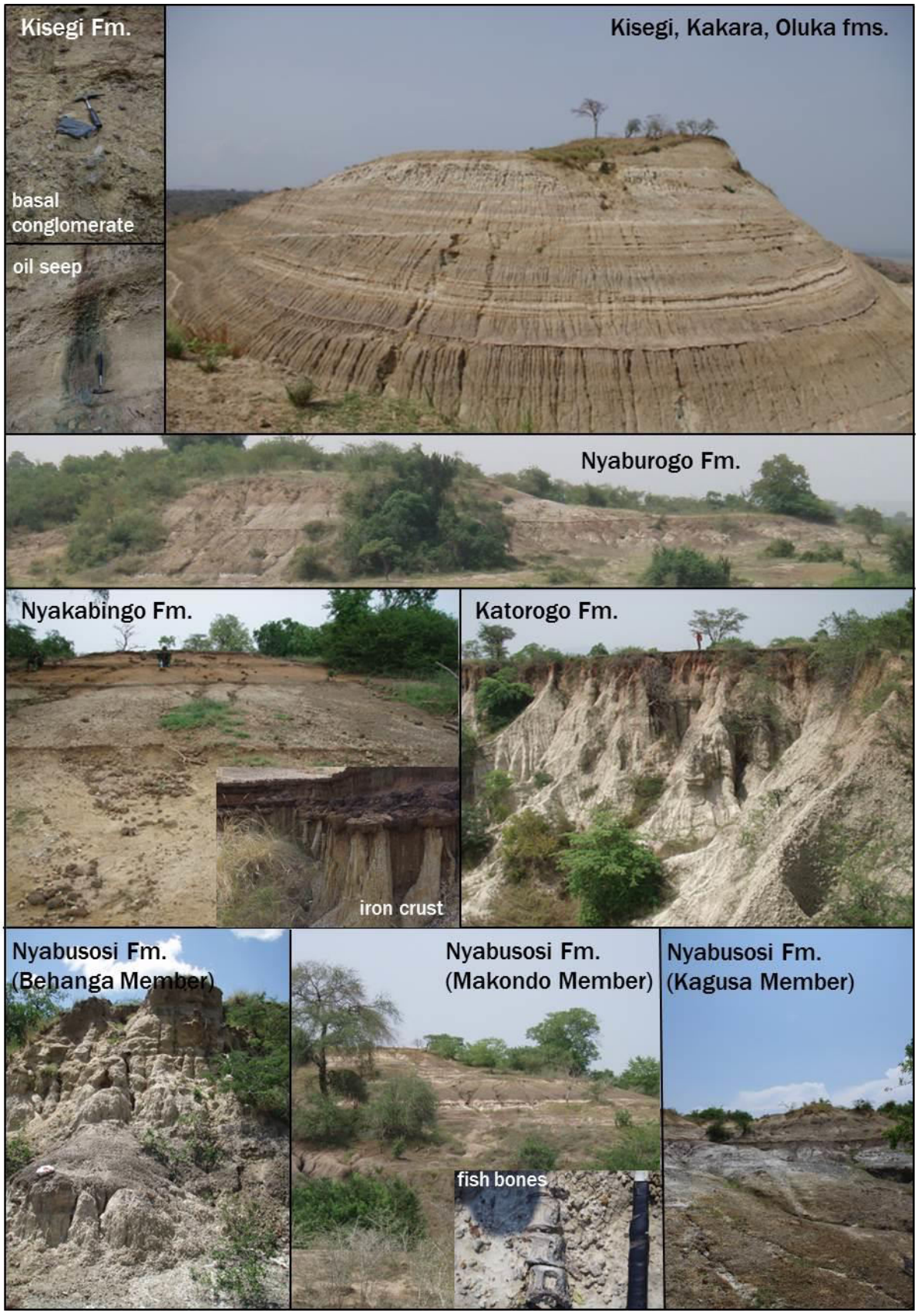

Figure 6-6. Impressions of logged sediment exposures in the Kisegi-Nyabusosi area.

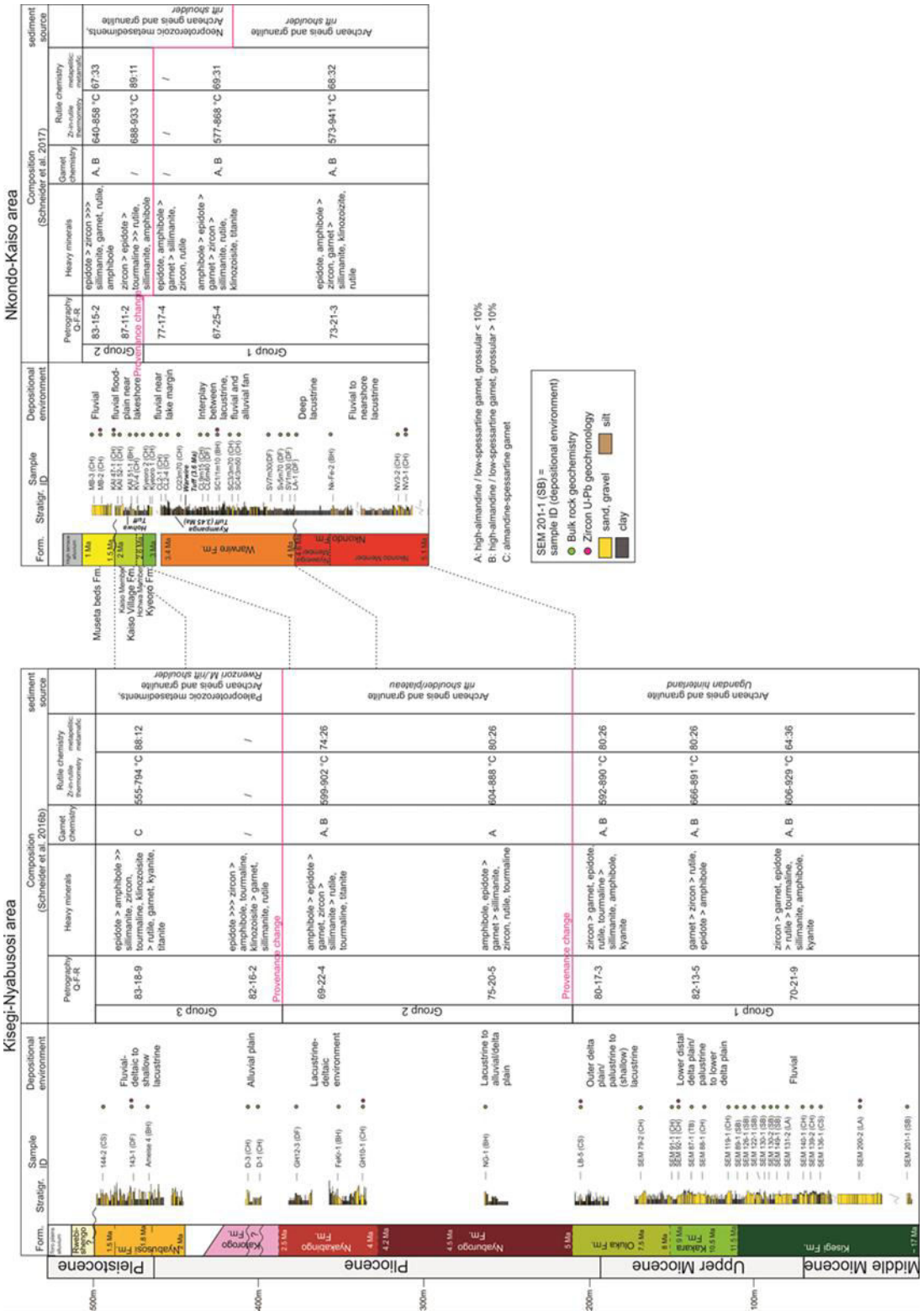

Figure 6-7. Stratigraphy of the Kisegi-Nyabusosi and Nkondo-Kaiso areas showing logged sedimentological sections (widths and colors display grain sizes) interpreted with respect to depositional environment by Roller et al. (2010) and Brüsch (unpublished); location, ID and architectural elements (in brackets) of analyzed samples with SB: sandy bedforms, LA: lateral accretion, CS: crevasse splay, CH: channel, TB: transverse bar, DF: delta foreset, LV: levee, BH: beach; analytical methods used on the samples; results from petrographic observations and chemical analysis of garnet and rutile and interpreted provenance from Schneider et al. (2016b, 2017). Biostratigraphic formations after Pickford et al. (1993).

6.6 Methods

6.6.1 Sampling

The samples analyzed in this study were previously studied for their petrographic and single grain geochemical composition by Schneider et al. (2016b, 2017). Sampling procedures and location of logged outcrop sections are described in named publications. The location of samples within the stratigraphic record of both areas is shown in Fig. 6-7. Whole-rock chemical data and zircon analytical data referred to in this chapter are given in the Appendix.

6.6.2 Bulk-rock geochemistry

Geochemical analyses were performed on 29 samples from the Kisegi-Nyabusosi area, and 24 samples from the Nkondo-Kaiso area, respectively. Prior to analysis, the samples were wet sieved, and the sand fraction (0.063–2 mm) was powdered using a disc mill. The sand-sized material was then analyzed for their major and trace element concentrations, including REE, at the laboratory ALS minerals (Spain). Major elements and a few minor elements were quantified using ICP-OES/AES and the majority of trace elements was determined by ICP-MS, following a lithium metaborate/tetraborate fusion for the resistate elements (Si, Al, Fe, Ti, Ca, Na, K, Mn, P, Mg, Ba, Ce, Cr, Cs, Ga, Ge, Nb, Rb, REE, Sn, Sr, Ta, Th, U, V, W, Y, Zr), an acid solution treatment for the base metals (Ag, Ca, Co, Cu, Li, Mo, Ni, Pb, Sc, Zn), and aqua regia treatment for As, Bi, Hg, In, Re, Sb, Se, Te and Tl. For further information concerning analyzing procedures, geostandards and elemental precisions visit www.alsglobal.com. For the evaluation and interpretation of the geochemical dataset, element concentrations were normalized to the Upper Continental Crust (UCC; Rudnick and Gao, 2003). REE are discussed with reference to CI Carbonaceous Chondrites (McDonough and Sun, 1995). To obtain information on the degree of (paleo-)weathering of the sediment, the Chemical Index of Alteration (CIA; Nesbitt and Young, 1982) and the Weathering Index of Parker (WIP; Parker, 1970) were calculated after following formulas:

$$CIA = [Al_2O_3) / (Al_2O_3 + CaO^* + Na_2O + K_2O] \bullet 100 \quad [1]$$

$$WIP = [(Ca) / 0.7) + (2\,Na / 0.35) + (2\,K / 0.25) + (Mg / 0.9)] \bullet 100 \quad [2]$$

* CaO in silicate-bearing minerals only

No correction for CaO incorporated in carbonates and phosphates was performed, because such phases were never observed in the analyzed samples. With increasing weathering intensity, the value of the CIA increases, whereas the WIP decreases. Al-rich phyllosilicates have high CIA values (kaolinite and chlorite ~100, illite and smectite ~80 and muscovite ~75), unweathered feldspars values of ~50, and biotite, hornblende and pyroxene of 50–55, 10–30, and 0–10, respectively (Nesbitt and Young, 1982). Since the WIP measures the absolute concentration of mobile Na, K, Mg and Ca in the sediment, this index is strongly influenced by quartz dilution (Garzanti and Resentini, 2016).

6.6.3 Zircon U-Pb geochronology

U-Pb zircon geochronology was carried out on nine rift sediments (Kisegi-Nyabusosi: 5; Kaiso-Nkondo: 4), one from each formation except for the Nyaburogo and Katorogo formations in the

Kisegi-Nyabusosi area and the Kyeoro Formation in the Kaiso-Nkondo area. Zircons from the grain size fraction 63–125 µm were separated from the bulk sediment by standard techniques. After zircon enrichment via density separation (Na-polytungstate), the hand-picked zircons were mounted on a double-sided adhesive tape, bedded in epoxy resin and polished to reveal a section of the inner core. Prior to analysis, cathodoluminescence (CL) images were taken from all samples using a cathode luminescence detector connected to a Jeol JXA-2800 EMP device at the Johannes Gutenberg University Mainz. The purpose of CL images is to study internal structures of zircons, e.g., the texture of core and rims, which may give important information about (re-) crystallization events during magmatic and metamorphic processes (Corfu et al., 2003b). U-Pb isotope analysis was carried out by LA-ICP-MS using an Agilent 7500ce quadrupole inductively coupled mass spectrometer linked to an UP-213 Nd:YAG-laser system from New Wave with 213 nm wavelength at the Johannes Gutenberg University Mainz. Ablation was performed in a low-volume laminar flow cell, which is flushed by Helium as carrier gas. Before reaching the torch Argon gas is added. In each sample, 55 to 60 randomly selected zircons were analyzed. All data were obtained from single spot core measurements using a spot size of 30 µm and a total measuring time of 80 s, consisting of 30 s warm up, 30 s dwell and 20 s washout time. The repetition time was 10 Hz at an energy density of 3.6 J/cm^2. Calibration was assured by measuring the standard zircons 'GJ-1' (Jackson et al., 2004), 'Plesovice', '91500N', '91500A', and 'Temora' (Black et al., 2003; Nasdala et al., 2008) in defined intervals at the beginning, during and at the end of each measuring cycle. Following masses were analyzed: ^{202}Hg, ^{204}(Pb + Hg), ^{206}Pb, ^{207}Pb, ^{208}Pb, ^{232}Th, ^{235}U, and ^{238}U. Raw data were processed using Glitter Software (van Achterbergh et al., 2000). Combined probability density distribution and histogram diagrams were produced using Isoplot 3.75 (Ludwig, 2012).

Zircon ages are defined as concordant, if Pb-Pb and U-Pb ages differ less than 10%. Zircons that yield discordant ages and those that give unreliable isotopic ages during measurement were not considered for diagrams and data interpretation. Ages >1 Ga were calculated using ^{207}Pb/^{206}Pb ratios, whereas ages <1 Ga were obtained using ^{206}Pb/^{238}U. This is because ^{207}Pb/^{206}Pb ages become imprecise below <1 Ga due to poorer counting statistics (Gerdes and Zeh, 2006; Sircombe, 2000).

6.7 Geochemical Results

For a clear and consistent description and interpretation of the data set, the results are presented according to the lithostratigraphic grouping proposed by Schneider et al., (2016b, 2017).

6.7.1 Kisegi-Nyabusosi area

Group 1: Middle to upper Miocene (~17.0–5.0 Ma; Kisegi, Kakara, Oluka formations)

According to the sandclass-scheme after Herron (1988), which discriminates sediments and sedimentary rocks based on logarithmic ratios of SiO_2/Al_2O_3 versus Fe_2O_3/K_2O, the sediment of Group 1 is classified as subarkose, sublitharenite or litharenite (Fig. 6-8). One sample from the Kisegi Formation plots in the field for arkose. SiO_2/Al_2O_3 ratios of the sediment range between 6.6 and 46.7 (mean 17.7), and are generally >10, which is consistent with a high compositional maturity for the majority of samples (Cox et al., 1995). SiO_2 concentrations range from 72.7 wt.% to 94.8 wt.% with mean values of 83.2 wt.% for the Kisegi Formation, 86.0 wt% for the Kakara Formation and 84.9 wt.% for the Oluka Formation. Al_2O_3 values are between 2.0 and 11.1 wt.% (mean 5.6 wt.%), while K_2O ranges between 1.2–2.9 wt%. Concentrations of Fe_2O_3 are 0.6–6.2 wt.%, with highest values for the lower part of this Group 1. The values of MgO, CaO, TiO_2, MnO, and P_2O_5 are generally very low, mainly <1 wt.%. The ratio of K_2O/Na_2O, which largely displays the proportion between K-feldspar

and plagioclase (Pettijohn et al., 1972), reveals values between 1.3 and 5.8, suggesting enrichment of K-feldspar over plagioclase in the samples.

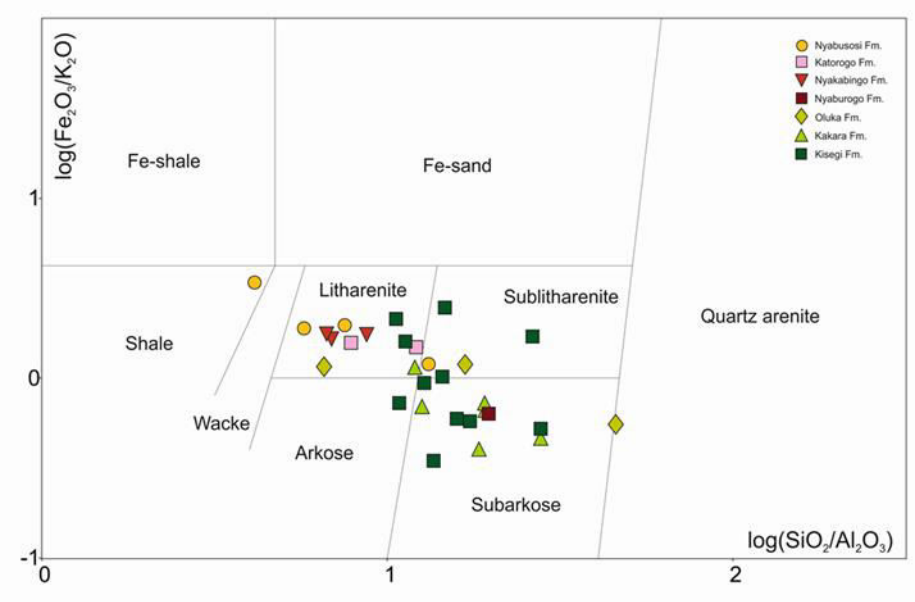

Figure 6-8. Chemical classification scheme for the sediment of the Kisegi-Nyabusosi area after Herron (1988).

Multi-element diagrams normalized to Upper Continental Crust composition indicate depletion for the mobile trace elements Cs, Rb, and Sr, and for the Transition Trace Elements (TEE) Sc, V, Co, Cu, Ni, and Zn (Fig. 6-9). Concentrations of the High Field Strength Elements (HFSE) Zr, Hf, Th, Nb, Ta, and U are similar or enriched compared with the UCC. Total rare earth element (∑REE) values vary strongly throughout the stratigraphy of Group 1 and are in a range between ~42 and 336. The highest values reveal some samples from the Kisegi Formation. Values for anomalous Eu (Eu/Eu*) range between 0.81 and 1.12, indicating that the sediment of Kisegi (mean 0.95), Kakara (mean 0.88), and Oluka (mean 0.87) are characterized by a missing or only slight Eu anomaly (Fig. 6-10). Furthermore, most sediments of the lower part of the stratigraphy show fractionation within the REE, indicated by La_N/Yb_N ratios of 8.9–68.1, La_N/Sm_N ratios of 3.3–11.4, and Gd_N/Yb_N ratios of 1.2–4.4 (Fig. 6-11). Fractionation is most distinctive for the Kisegi Formation. Values for anomalous Ce (Ce/Ce*) are similar in all sands and range between 0.93 and 1.26, e.g., no anomalous Ce was measured. The sediment of Group 1 has Th/Sc ratios between 1.4 and 4.5 accompanied by varying Zr/Sc ratios between 33.3 and 292 (Fig. 6-13), that indicate according to McLennan et al. (1993) pronounced sediment reworking for most sediments that is consistent with observed zircon enrichment (Schneider et al., 2016b). With exception of Th/Cr (0.01–0.1), the provenance sensitive element ratios La/Sc (6.8–22.3), La/Co (1.1–33.5) and Th/Co (0.2–6.5) (Cullers, 1988, 2000) are relatively high and indicate a felsic provenance for the sediments (Fig. 6-12). The weathering degree of the samples reflected by the Chemical Index of Alteration (CIA; Nesbitt and Young, 1982) ranges between 56 and 69 suggesting only mild to moderate weathering for all analyzed samples (Fig. 6-14). WIP values are between 13 and 39 and hint to some quartz enrichment for few samples.

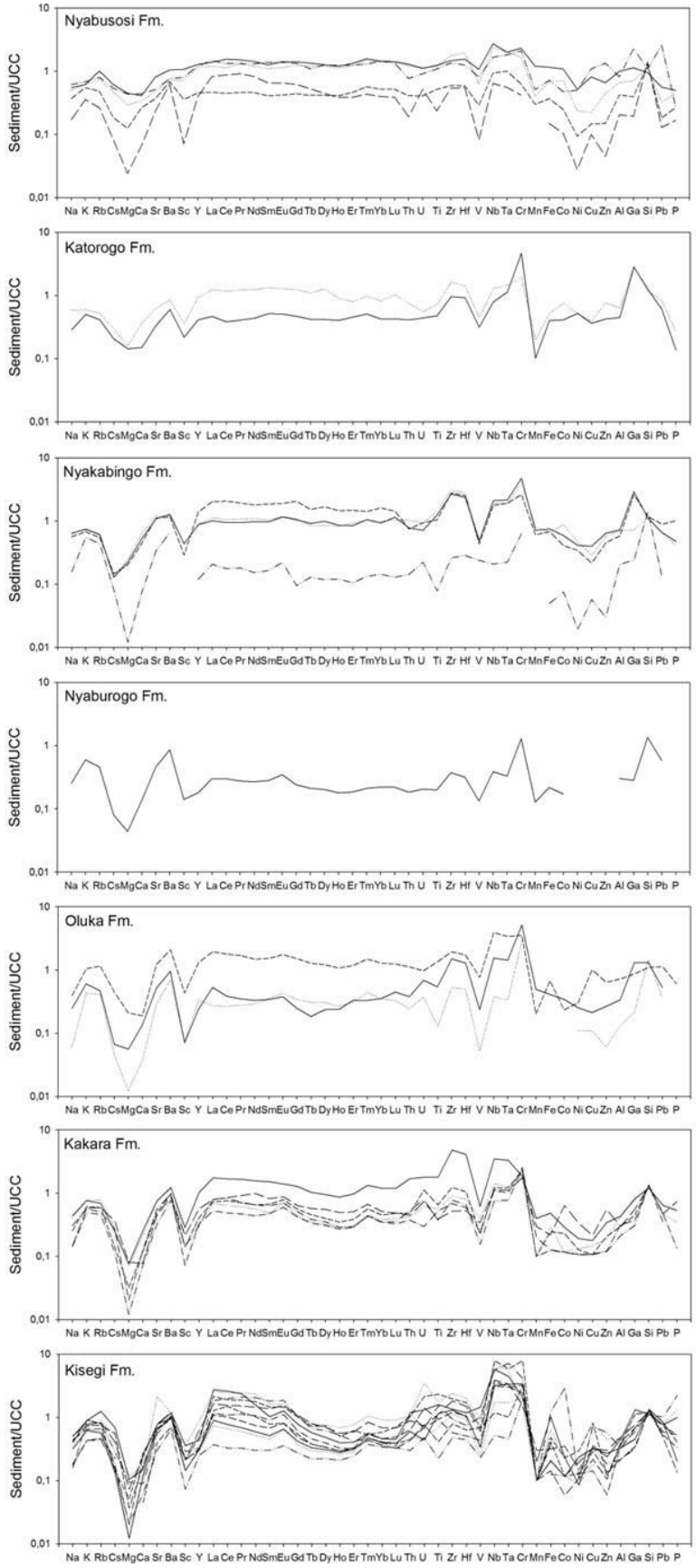

Figure 6-9. Geochemistry of rift sediments in the Kisegi-Nyabusosi area. UCC-normalized elements (Rudnick and Gao, 2003) are arranged following the periodic table group by group (after Garzanti et al., 2013).

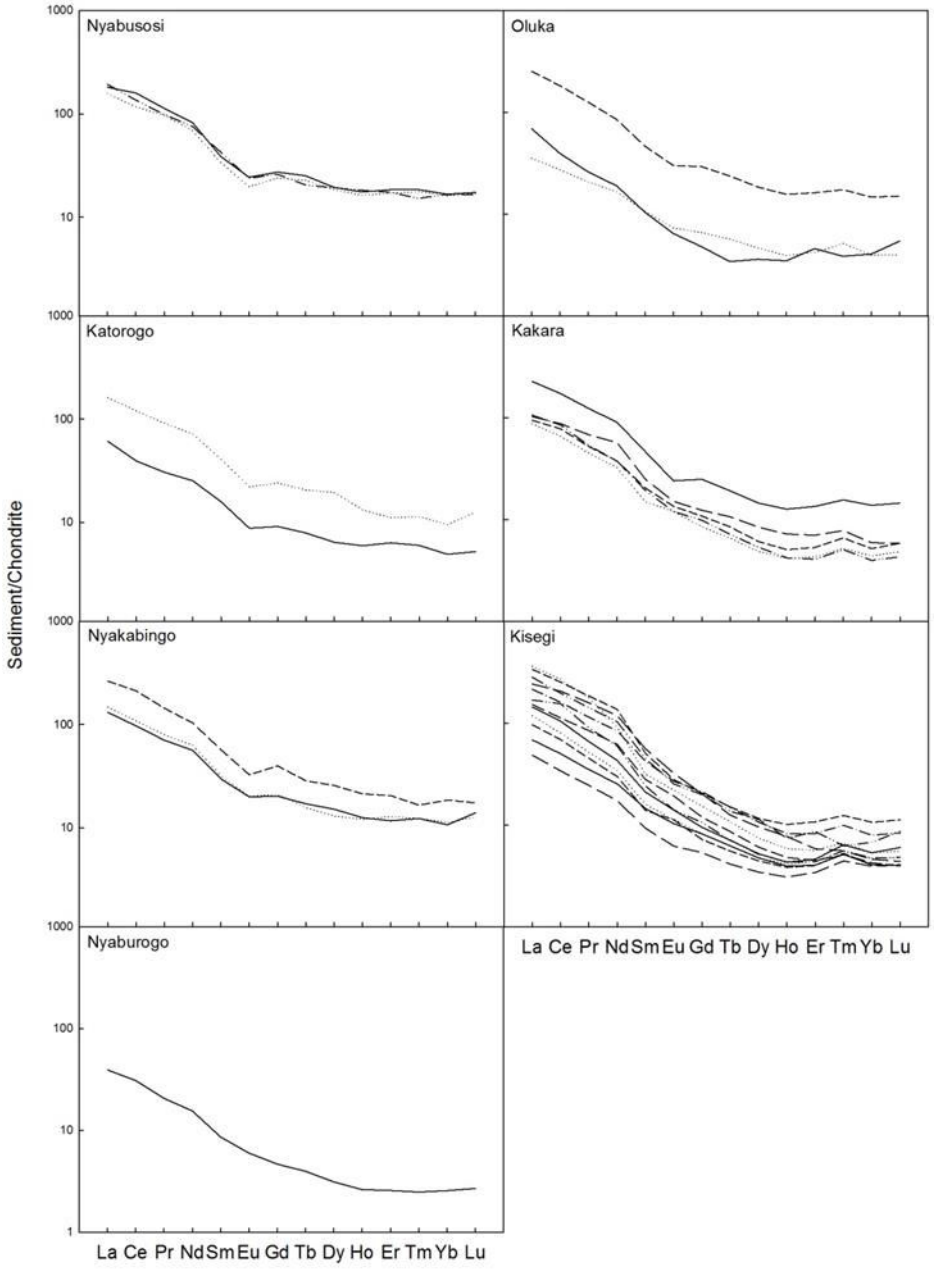

Figure 6-10. REE pattern for the rift sediment in the Kisegi-Nyabusosi area normalized to CI carbonaceous chondrites (McDonough and Sun, 1995).

Group 2. Lower Pliocene to upper Pliocene (~5.0–2.5 Ma; Nyaburogo, Nyakabingo formations)

Geochemically, the one sample representing the Nyaburogo Formation is classified as subarkose. The sand shows a high compositional maturity with a SiO_2 value of 94.8 wt.%, SiO_2/Al_2O_3 ratio of ~ 19, and K_2O/Na_2O ratio of 2. In contrast, the concentrations of Al_2O_3, K_2O, Fe_2O_3, Na_2O, CaO, MgO, MnO and TiO_2 are generally low and comparable with those of Group 1. This is also true for trace elements, which are largely depleted in terms of the UCC. Sediment of the following Nyakabingo Formation is classified as litharenite. In comparison to the Nyaburogo Formation, the samples show lower mean SiO_2 values of ~75 wt.% together with higher mean concentrations for all other major constituents, lower SiO_2/Al_2O_3 ratios (~7.5) and K_2O/Na_2O ratios (~1).

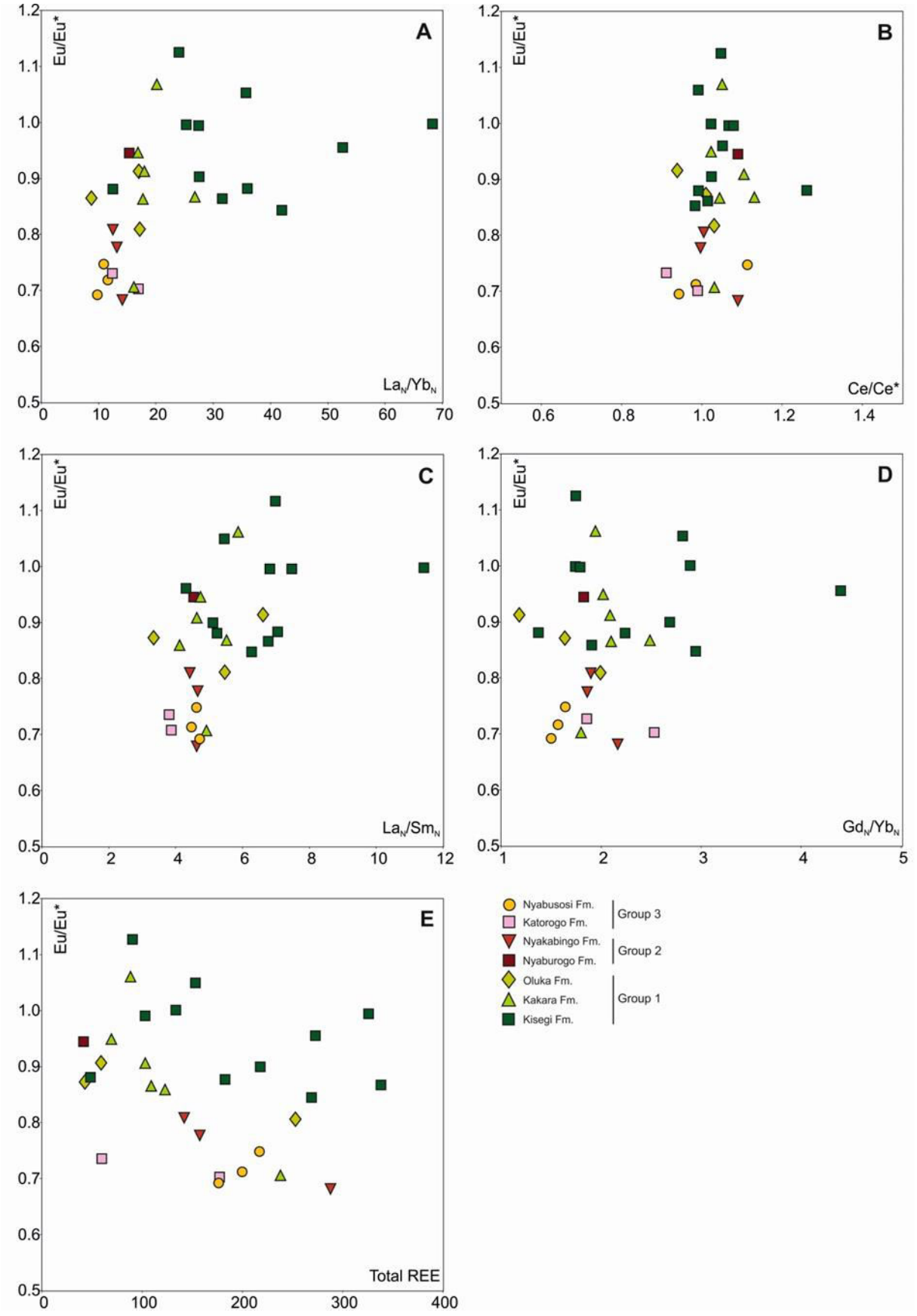

Figure 6-11. Diagrams illustrating the Eu anomaly (Eu/Eu*) in relation to (A) the fractionation of LREE and HREE (La_N/Yb_N), (B) anomalous Ce (Ce/Ce*), (C) the fractionation within the LREE (La_N/Sm_N), (D) the fractionation within the HREE (Gd_N/Yb_N), and(E)the total REE content for the sand of the Kisegi-Nyabusosi area.

Most trace elements show similar concentrations to the UCC (Fig. 6-9). Exceptions are Zr, Hf, and Ga that exhibit concentrations up to three times higher than the UCC. Rb, Cs, Cu, Sc and Zn are depleted compared to the UCC standard. As is shown in Fig. 6-11, the sand of the Nyaburogo Formation is characterized by a very low total REE content (∑REE = ~42) and lack of Eu anomaly (Eu/Eu* = 0.95). In contrast, sand of the Nyakabingo Formation exhibits higher ∑REE concentrations (∑REE ~143–289), and values for anomalous Eu/Eu* that are in a range of ~0.6 and ~0.8, i.e., the samples are characterized by a negative Eu anomaly. Fractionation within the REE with respect to the Eu-anomaly is similar between both formations. The ratio between the light REE and heavy REE (La_N/Yb_N) ranges between ~12 and 15. The sand is characterized by flat heavy rare earth element (HREE) profiles (Gd_N/Yb_N = ~2). Zr/Sc (~36–133) and Th/Sc (~1–2) ratios are slightly higher for sand of the Nyakabingo Formation than for sand of the Nyaburogo Formation, indicating a more felsic provenance and a higher recycling component for the Nyakabingo Formation (Fig. 6-13). La/Sc (4.7–16.6), La/Co (2.3–8.9), Th/Cr (0.02–0.03), and Th/Co (0.7–1.1) ratios are similar between the two formations, and, besides Th/Cr ratios, match the composition of the UCC (Fig. 6-12). An exception is one sediment from the Nyakabingo Formation, in which La/Co and La/Sc ratios are considerable higher and comparable to Group 1. CIA values of 61–65 are similar between both formations and indicate slight to moderate weathering for sediment of Group 2 (Fig. 6-14). The calculated WIP values are lower in the Nyaburogo Formation (WIP = 23) than in the Nykabingo Formation (WIP = 34–38), reflecting higher quartz dilution for the lower part of this group, which is consistent with the high SiO_2 value.

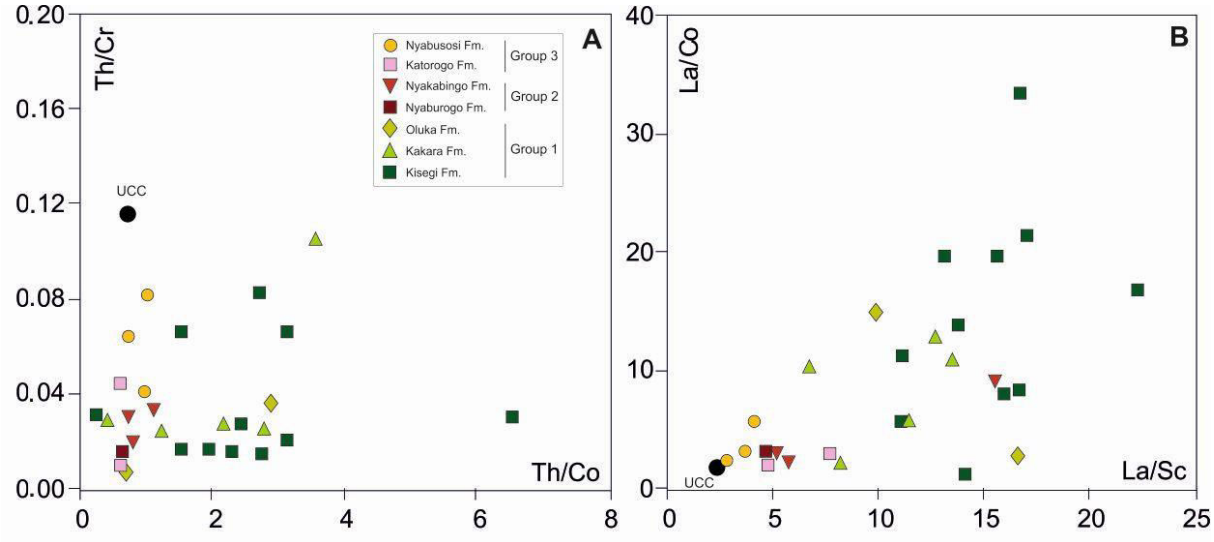

Figure 6-12. Diagrams illustrating the ratio of 'provenance-sensitive' elements (Cullers, 1988, 2000) with respect to the Upper Continental Crust (UCC; Rudnick and Gao, 2003) in the sand of the Kisegi-Nyabusosi area.

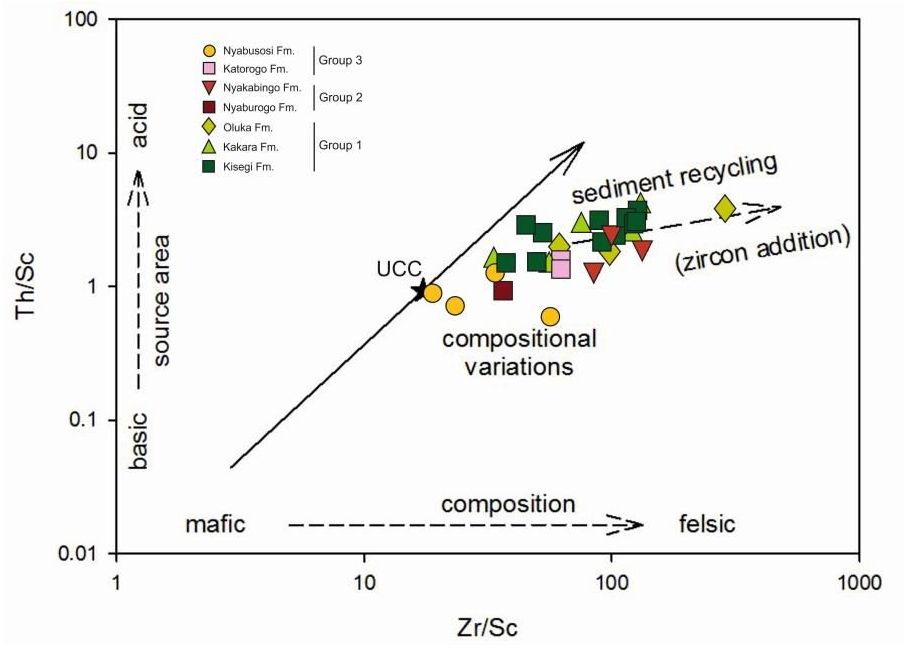

Figure 6-13. Discrimination diagram after McLennan et al. (1993) for the rift sediment in the Kisegi-Nyabusosi area demonstrating compositional variations (Th/Sc) and sediment recycling (Zr/Sc).

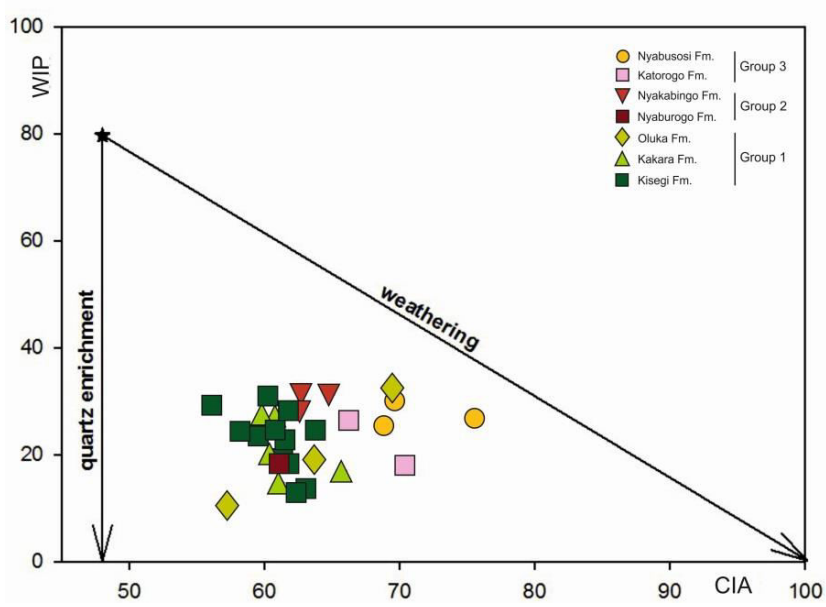

Figure 6-14. Weathering degree and trend of the studied samples in the Kisegi-Nyabusosi area exemplified in the CIA/WIP diagram (after Garzanti et al., 2013).

Figure 6-15 (next page). Different geochemical parameters for the analyzed samples from both, the Kisegi-Nyabusosi area and Kaiso-Nkondo area, plotted in their inferred stratigraphical order. Formation thickness is not to scale.

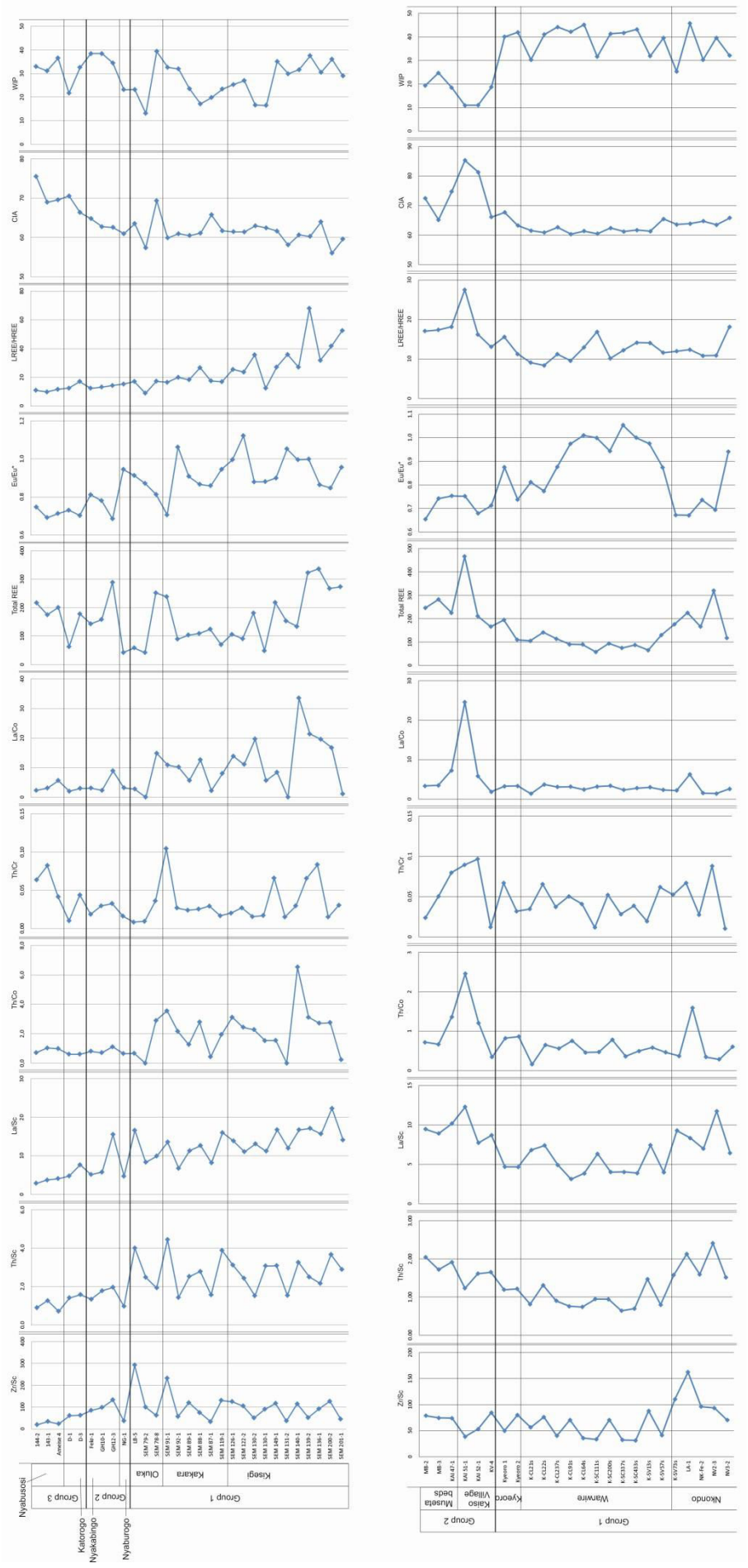
WIP
CIA
LREE/HREE
Eu/Eu*
Total REE
La/Co
Th/Cr
Th/Co
La/Sc
Th/Sc
Zr/Sc
Group 3
Group 2
Group 1
Nyabusosi
Katorogo
Nyakabingo
Nyaburogo
Kisegi
Kakara
Oluka
Mussata beds
Kaiso Village
Kyerora
Warrire
Nkondo

Group 3. Lower Pleistocene (~2.5–1.0 Ma; Katorogo, Nyabusosi formations)

Sediment of Group 3 is classified as litharenite (Fig. 6-8). One sample from the Nyabusosi Formation plots in the field for shale. In general, the Katorogo Formation shows higher SiO_2 contents of ~80 wt.% and higher SiO_2/Al_2O_3 ratios of ~10 than the Nyabusosi Formation, which exhibits SiO_2 values of ~71 wt% and SiO_2/Al_2O_3 ratios of ~6. As consequence of higher SiO_2 contents in the Katorogo Formation, other major element concentrations are lower in this formation. The K_2O/Na_2O ratio is similar throughout Group 3, largely between 0.9 and 1.5, suggesting nearly equal proportions of K-feldspar and plagioclase. As shown in Fig. 6-9, the majority of trace elements in sand of the Katorogo Formation is depleted in comparison to the UCC standard. Exceptions are Ba, Hf, Zr, Ga, Ni and Co, which are similar or slightly enriched to the UCC. In the Nyabusosi Formation, depletion is indicated for the mobile elements, as well as for Ni, Cu, and Zn. All other elements largely match the composition of the UCC. Chondrite-normalized REE pattern (Fig. 6-10) show light rare earth element enrichment (La_N/Yb_N ~12) and flat heavy rare earth element profiles (Gd_N/Yb_N ~1.8) with a negative Eu anomaly (Eu/Eu* ~0.7). The provenance sensitive ratios La/Sc (~2.7–7.7), La/Co (~2.3–5.6), Th/Cr (~0.04–0.8), and Th/Co (~0.7–1.0) are similar to Group 2. The sediment of Group 3 has varying Zr/Sc ratios between ~19 and ~63, and Th/Sc ratios between ~0.7 and 1.6. These ratios are lowest in the Nyabusosi Formation, not only in comparison to the Katorogo Formation, but compared to all samples in the Kisegi-Nyabusosi area, indicating that this sediment has been least affected by sedimentary recycling (Fig. 6-13). Weathering indices exhibit values of 64–75 for the CIA and values of 22–36 for the WIP point to a moderate weathering degree, marginally higher than for sand of Group 1 and Group 2 (Fig. 6-14).

6.7.2 Nkondo-Kaiso area

Group 1. Lower Pliocene to upper Pliocene (~5.1–2.6 Ma; Nkondo, Warwire, Kyeoro formations)

According to the *sandclass*-scheme after Herron (1988), the majority of sediments from the Nkondo, Warwire and Kyeoro formations are classified as litharenite or arkose. One sample from the Warwire Formation is classified as subarkose, and one sample from the Nkondo Formation is discriminated as

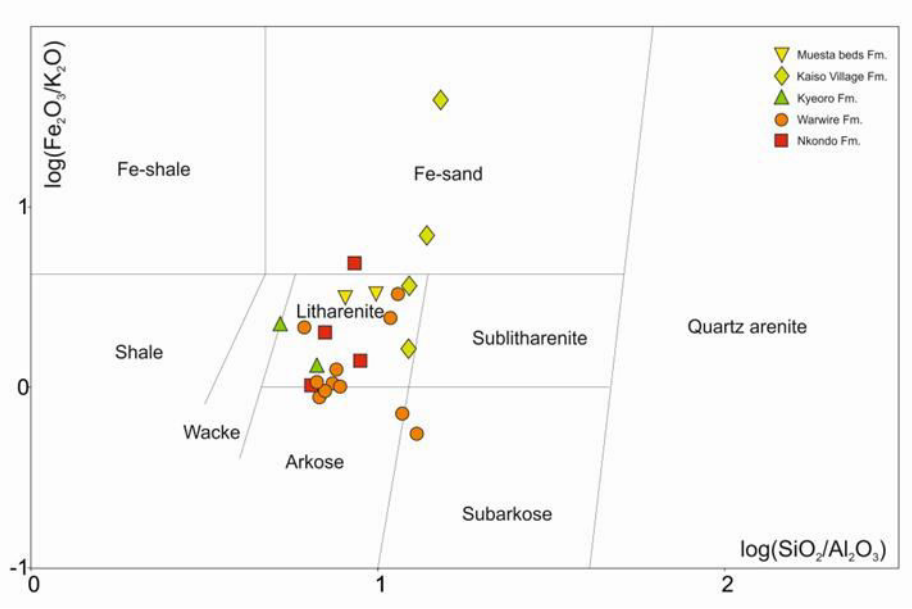

Figure 6-16. Chemical classification scheme for the sediment of the Nkondo-Kaiso area after Herron (1988).

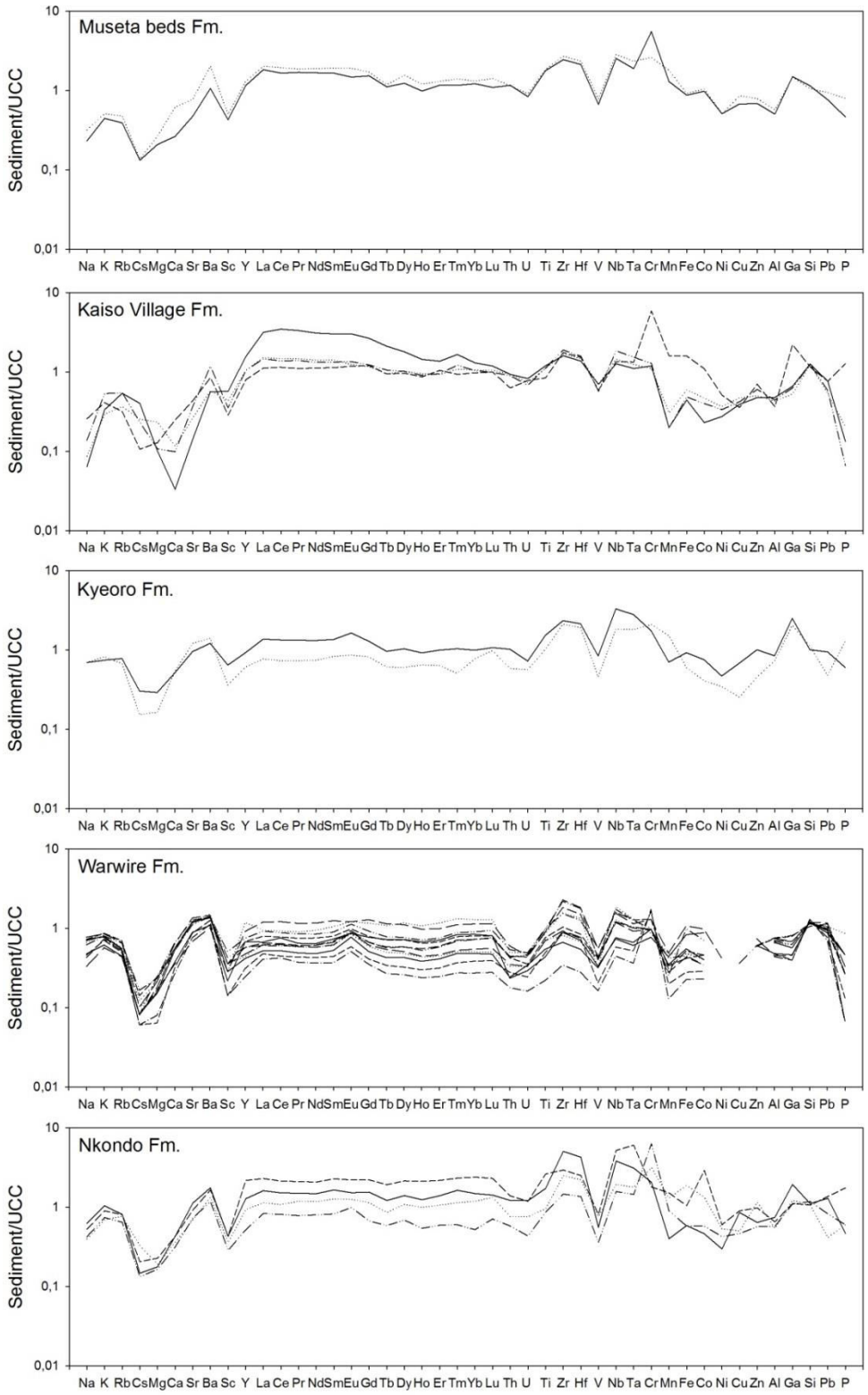

Figure 6-17. Geochemistry of rift sediments in the Nkondo-Kaiso area. UCC-normalized elements (Rudnick and Gao, 2003) are arranged following the periodic table group by group (after Garzanti et al. (2013).

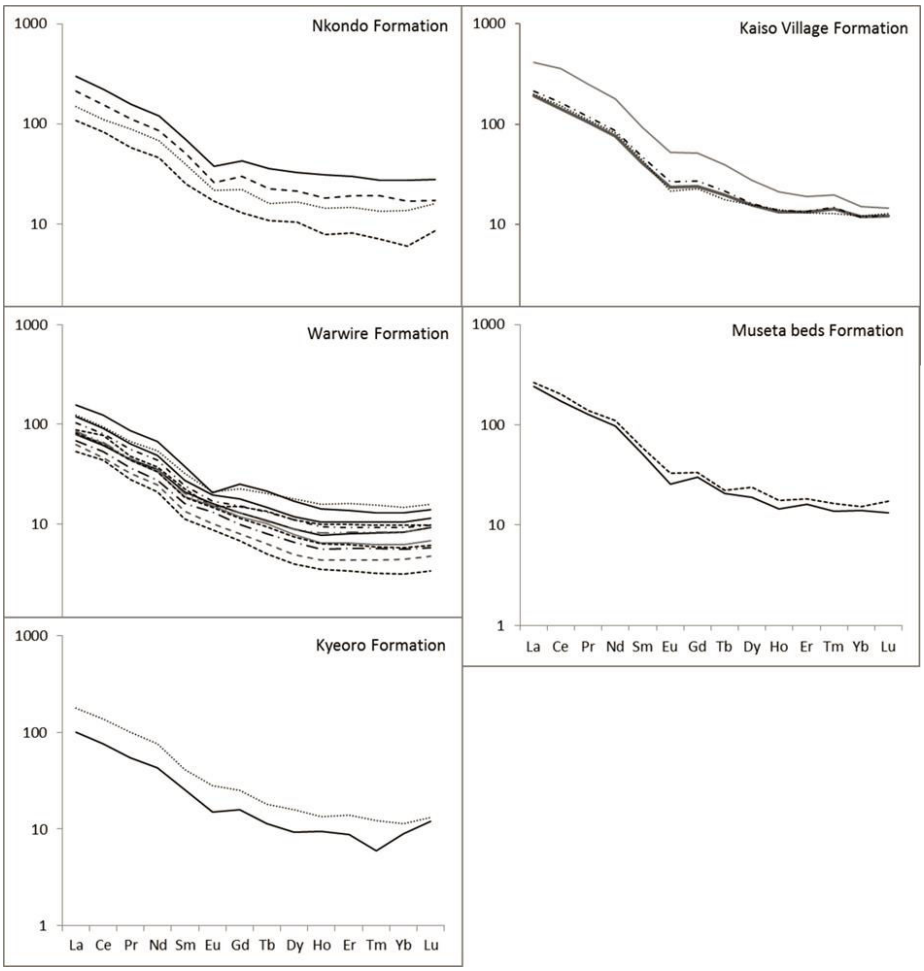

Figure 6-18. REE pattern for the rift sediment in the Nkondo-Kaiso area normalized to CI carbonaceous chondrites (McDonough and Sun, 1995).

Fe-bearing sandstone (Fig. 6-16). The sediment displays medium to high SiO_2 values that range between 67–87 wt.%, with highest concentrations in the Warwire Formation (~79 wt.%). SiO_2/Al_2O_3 ratios range between ~5 and ~13, and are marginally higher in the Warwire Formation. Analysed concentrations for mobile elements are ~1–2.5 wt.% for Na_2O and CaO, 1.6–2.9 for K_2O, and <0.7 for MgO. K_2O/Na_2O ratios of ~1–2 are lowest in the Warwire and Kyeoro formations. Al_2O_3 reaches values of 8–13 wt.%. As demonstrated in multielement spider diagrams (Fig. 6-17), Mg is strongly depleted compared to the UCC, whereas Na, Ca, Al and K show only slight depletion. Fe_2O3 (~1–10 wt.%), TiO_2 (<1.7 wt.%), and MnO (<0.2 wt.%) are lower in the Warwire Formation than in the Nkondo and Kyeoro formations. Trace element concentrations, illustrated with respect to the UCC, show strong depletion for Cs. Sr, Ba and Pb match the composition of the UCC. Provenance indicative elements, such as Th, Zr, Sc, Co and Nb are generally similar or raised compared to the UCC standard. In general, the lowest median trace element abundances are indicated for sand of the Warwire Formation, which is depleted in most trace elements relative to the other formations as well as to the UCC, including Cs, Sc, Y, Th, U, Zr, Hf, V, Nb, Ta, Cr, Co, Ga. The concentrations of Ni, Co and Zn are under detection limit. The highest overall values for the minor elements, including Rb, Y, Th, U, Zr, Hf, V, Nb, Ta, Co, Ni, Cu, Zn and Pb, were measured for the Nkondo Formation.

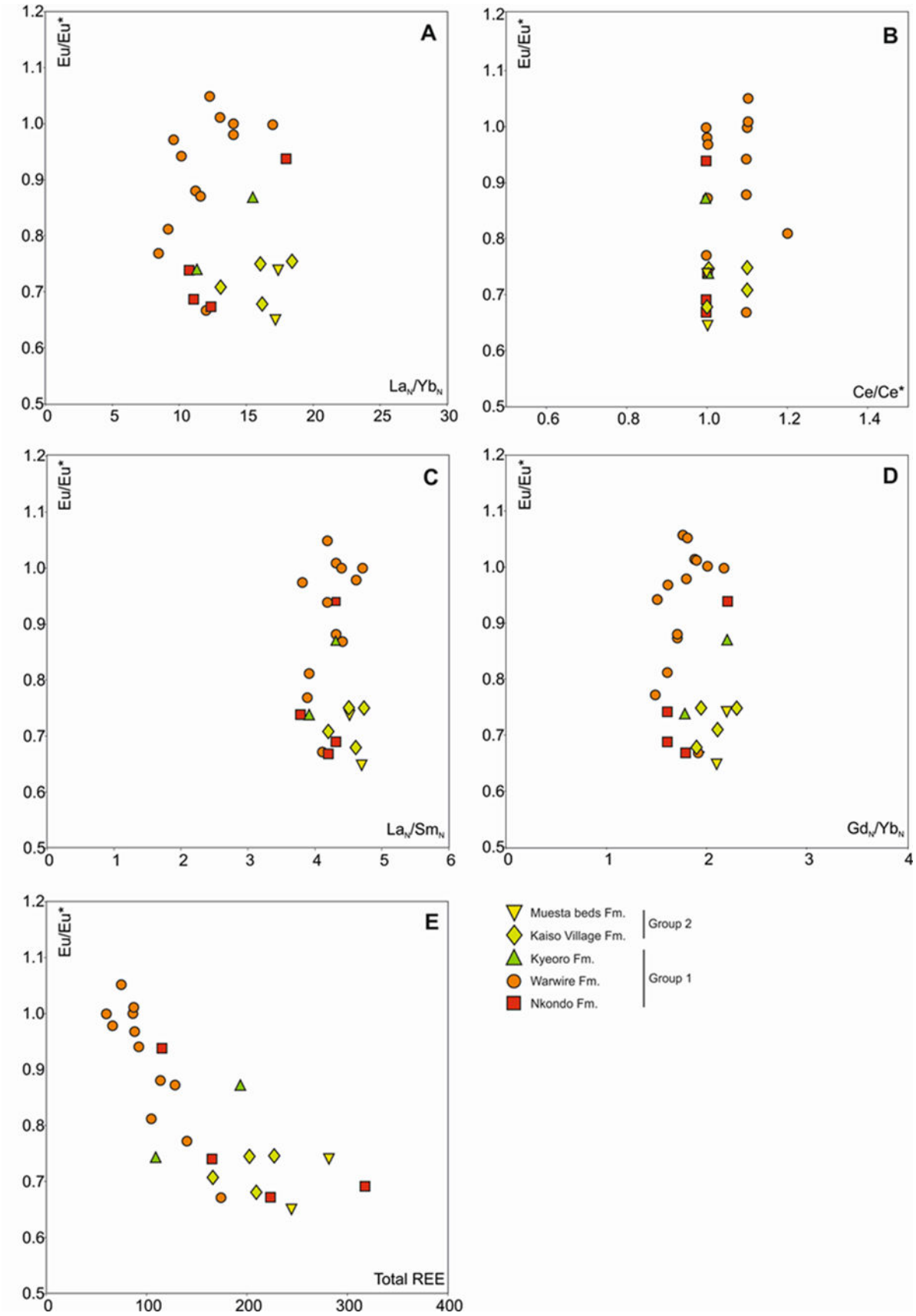

Figure 6-19. Diagrams illustrating the Eu anomaly (Eu/Eu*) in relation to (A) the fractionation of LREE and HREE (La_N/Yb_N), (B) anomalous Ce (Ce/Ce*), (C) the fractionation within the LREE (La_N/Sm_N), (D) the fractionation within the HREE (Gd_N/Yb_N), and(E)the total REE content for the sand of the Nkondo-Kaiso area.

Fig. 6-17 shows REE values compared to the UCC, and in Fig. 6-18 REE values are discussed with reference to chondrite. ∑REE values range between ~58 and 320 with highest values for the Nkondo Formation (~207) and lowest ∑REE values for the Warwire Formation (~102). Chondrite-normalized pattern are similar throughout Group 1 and characterized by LREE enrichment (La_N/Yb_N ~8–18) and flat HREE (Gd_N/Yb_N ~1.5–2.2). A negative Eu anomaly is indicated for the majority of samples of the Nkondo Formation and the Kyeoro Formation (both Eu/Eu* ~0.8) (Fig. 6-19). In contrast, most samples from the Warwire Formation are characterized by a missing Eu anomaly (Eu/Eu* >0.9). The Ce/Ce* values cluster around 1 in all samples, i.e. no anomalous cerium is detected. Th/Sc (0.6–2.4), Zr/Sc (31.6–162.3), La/Sc (3.2–11.8), Th/Co (0.16–1.6), La/Co (1.4–6.3) ratios are higher in the Nkondo Formation than in the Warwire and Kyeoro formations, indicating a more felsic composition for this sediment (Figs. 6-20, 6-21). With values between 60–68 for the CIA and 25–46 for the WIP, weathering indices point to a low to moderate weathering degree (Fig. 6-22).

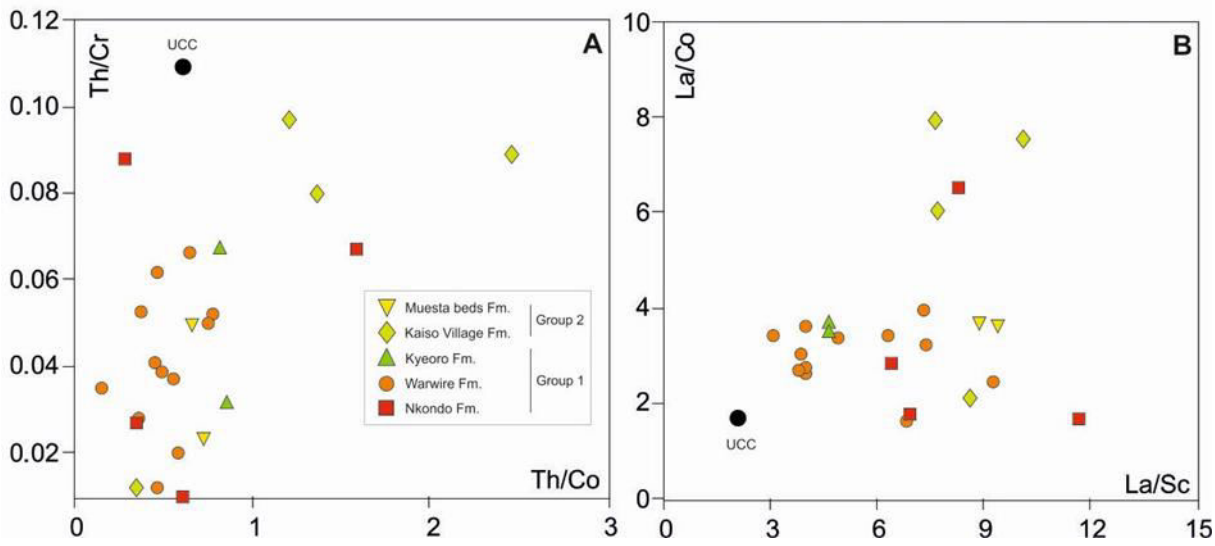

Figure 6-20. Diagrams illustrating the ratio of 'provenance-sensitive' elements (Cullers, 1988, 2000) with respect to the Upper Continental Crust (UCC; Rudnick and Gao, 2003) in the sand of the Nkondo-Kaiso area.

Group 2. Lower Pleistocene (~2.6–1.0 Ma; Kaiso Village, Museta beds formations)

The sediment from Group 2 is chemically classified as litharenite; two samples from the Kaiso Village Formation plot in the field for iron-bearing sand (Fig. 6-16). Overall, SiO_2 values are higher in the Kaiso Village Formation (~82.5 wt.%) than in the Museta beds Formation (~73.6 wt.%). In turn, the Kaiso Village Formation shows lower values for other major elements; not only in comparison with the Museta beds Formation, but also compared to Group 1. This is also indicated by multivariate diagrams normalized to the UCC (Fig. 6-17), which show stronger depletion in major elements, which is most striking for Na, Ca, Mn and P in the Kaiso Village Formation. Trace element pattern are similar to Group 1. Mobile elements and the TTE are generally depleted with respect to the UCC, whereas concentrations of the HFSE are close or raised compared to the UCC. All samples show high Cr concentrations, which are more than six times higher than the UCC in sediment of the Museta beds Formation. ∑REE values are in a range between ~166 and 282 (Fig. 6-19). The highest values occur in the Museta beds Formation. Chondrite-normalized pattern are similar to Group 1 and show LREE enrichment and flat HREE pattern with negative Eu anomalies of ~0.7 (Fig. 6-18). The ratio between the light REE and heavy REE ranges between ~13 and 28 for the Kaiso Village Formation, and are ~17 for the Museta beds Formation. As for Group 1, the Ce/Ce* values cluster around 1. The ratios of

La/Sc (~6.4–12.3), Th/Co (~0.3–2.5), La/Co (~1.8–7.3), Th/Cr (~0.02–0.1) are generally higher in the middle to upper part of the Kaiso Village Formation (Fig. 6-20). The opposite is true for Th/Sc (~1.2–2.0) and Zr/Sc (~74–84.8) ratios, which have higher ratios in the lower Kaiso Village Formation and Museta beds Formation (Fig. 6-21). The CIA and WIP values are in a range of 65–85, and 11–25, respectively, revealing a moderate to high weathering degree for sediment of Group 2 (Fig. 6-22). CIA values correlate weakly negative with Al_2O_3 (r = - 0.35) and strongly negative with CaO (r = - 0.72), Na_2O (r = - 0.75) and K_2O (r = - 0.73) throughout the Nkondo-Kaiso area, reflecting that in this area weathering indices might mirror a decrease in feldspar minerals.

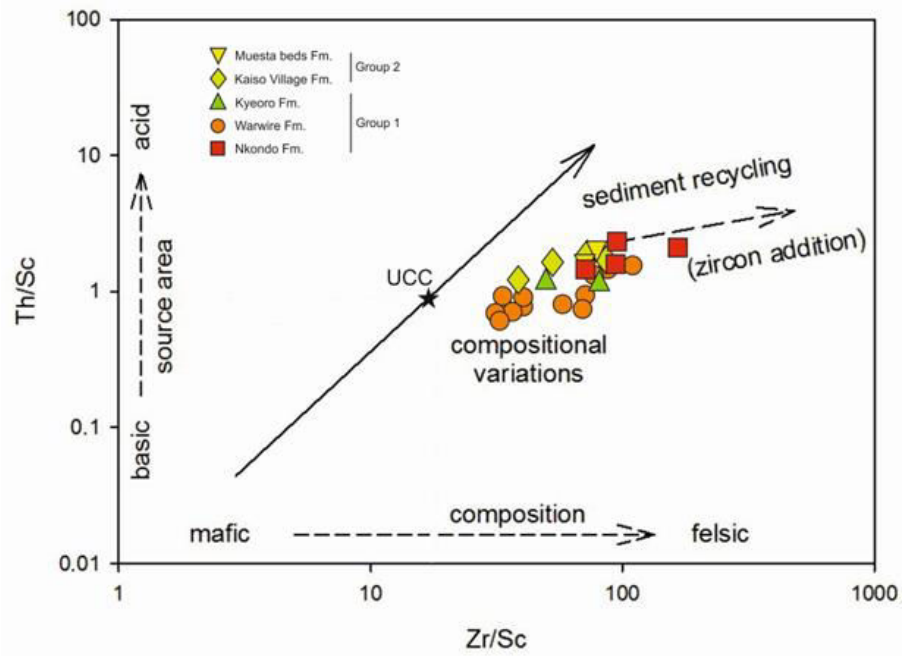

Figure 6-21. Discrimination diagram after McLennan et al. (1993) for the rift sediment in the Nkondo-Kaiso area demonstrating compositional variations (Th/Sc) and sediment recycling (Zr/Sc).

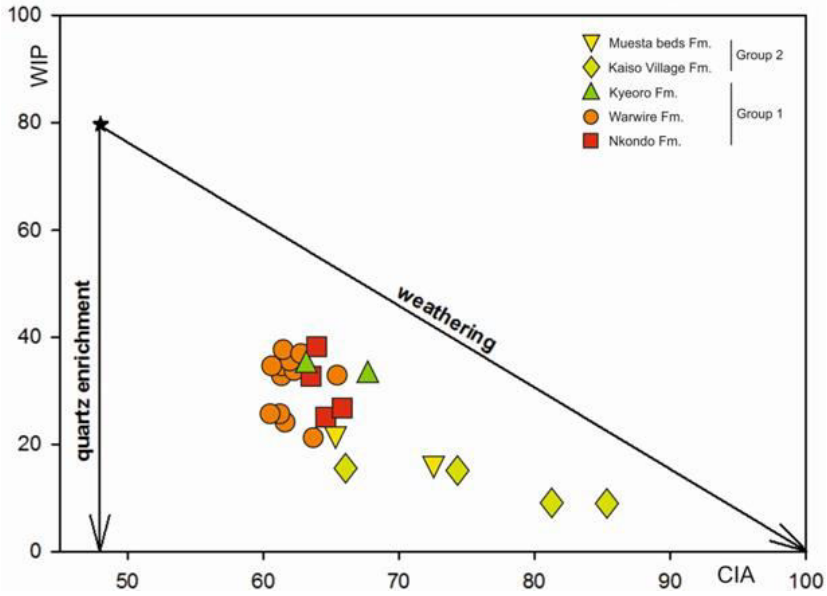

Figure 6-22. Weathering degree and trend of the studied samples in the Nkondo-Kaiso area exemplified in the CIA/WIP diagram (after Garzanti et al., 2013).

6.8 Zircon morphology and geochronology

6.8.1 Kisegi-Nyabusosi area

Group 1: Middle to upper Miocene (~17.0–5.0 Ma; Kisegi, Kakara, Oluka formations)

Detrital zircon in the Kisegi, Kakara and Oluka formations is transparent, translucent to turbid, but almost exclusively colorless (Fig. 6-23). Some completely turbid grains exhibit a milky shine. The majority of analyzed zircon grains is rounded and appears as long stubby or short stalky grains with a length/width ratio between 1.5 and 2.5 (Fig. 6-24), assigned to be characteristic for zircon that crystallized in deep-seated, slowly cooled intrusions (Corfu et al., 2003b). Some long prismatic, idiomorphic grains occur. The Kisegi Fm. and Kakara Fm. also exhibit a higher content of broken grains. The internal structure of zircon is variable as indicated by CL images and typical for grains that experienced (high-grade) metamorphism (Figs. 6-25, 6-27). The majority of zircon exhibits blurred, patchy or inhomogeneous structures, which do not allow recognition of pre-existing textures. Such so called ‘auroral-light” zoning is described to be typical for zircon that experienced high-pressure events, e.g., eclogite metamorphism (Corfu et al., 2003a, b). Other zircon grains are either fully homogenous or pre-existing oscillatory zoning might be suspected. A common feature is irregular oscillatory zoning, in which former igneous concentric zones are preserved, but became thickened and convoluted during metamorphic recrystallization (Corfu et al., 2003b). These zircons might also show recrystallized zones traversing older structures. Zircon with xenocrystic cores is common. Some zircon shows distinct zonation between core and rim. Core and surrounding mantle are usually homogenous, but in some cases, core and/or rim might be also zoned. The ratio between core and mantle is variable. Grains might either have a large inner sector surrounded by a thin rim or the core is surrounded by a thick mantle or, less common, thick bands. The long prismatic grains might also display longitudinal zonation. A correlation between internal zircon structures and zircon ages was generally not shown during this study.

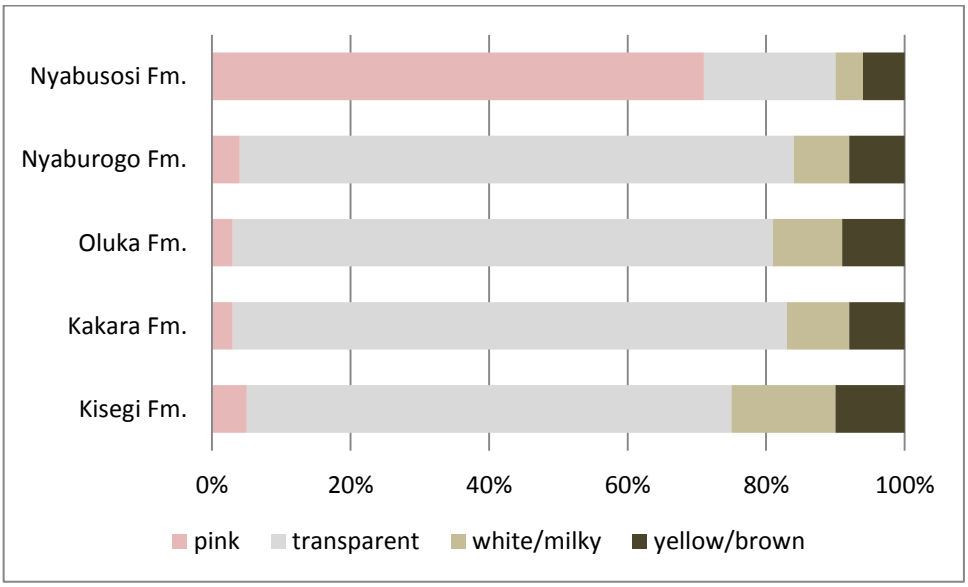

Figure 6-23. Distribution of zircon colors in the studied rift sediment of the Kisegi-Nyabusosi area.

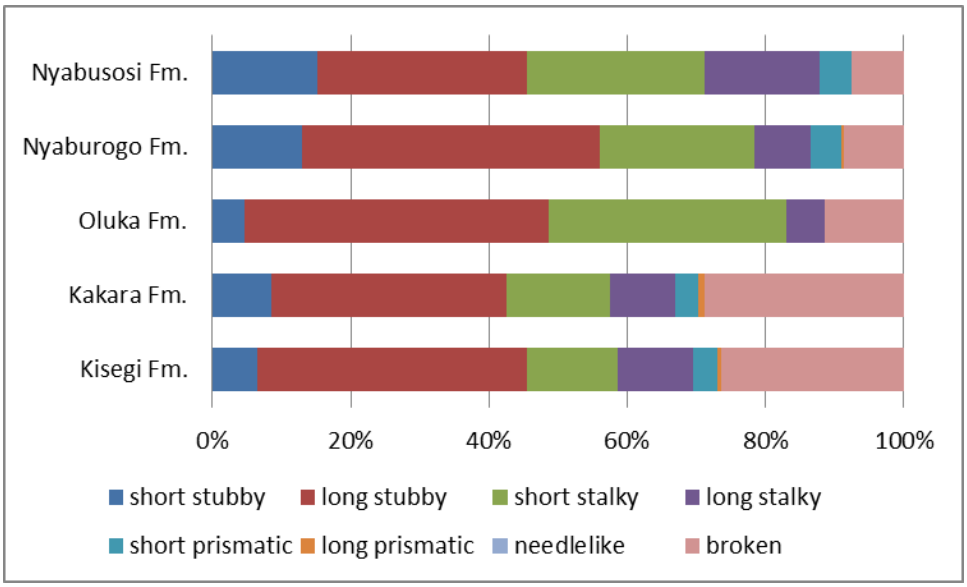

Figure 6-24. Classification of studied zircon grains from the Kisegi-Nyabusosi area according to their elongation (length/width ratio) after Gärtner et al. (2013).

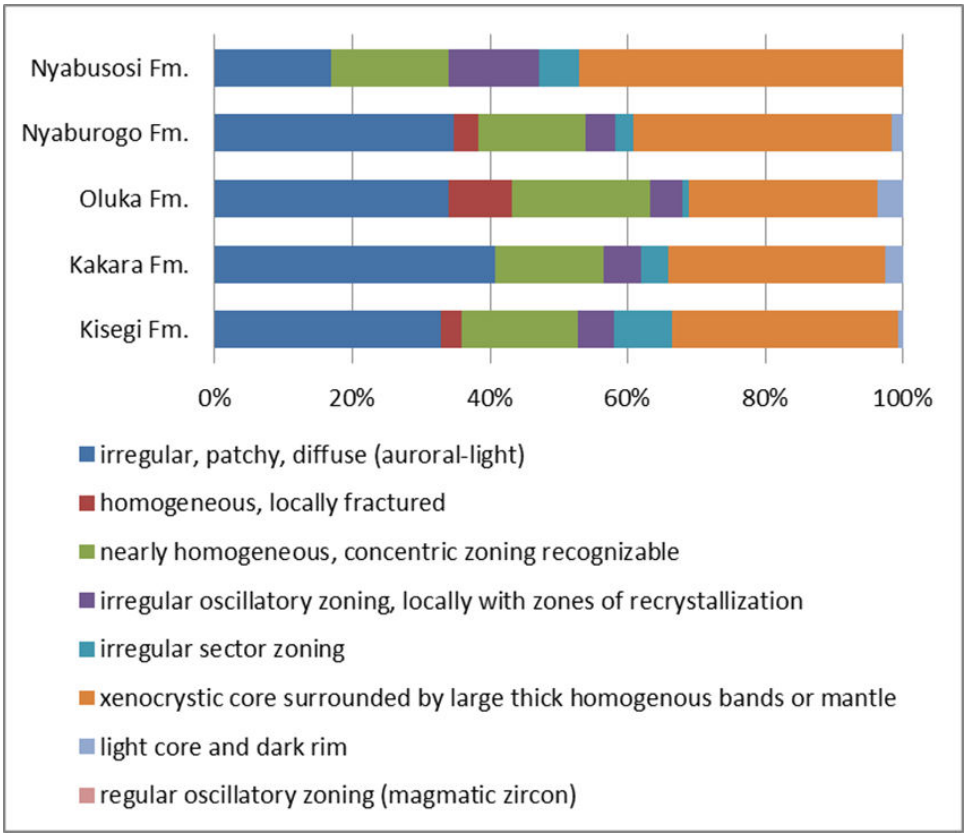

Figure 6-25. Distribution of internal zircon structures in the studied samples of the Kisegi-Nyabusosi area.

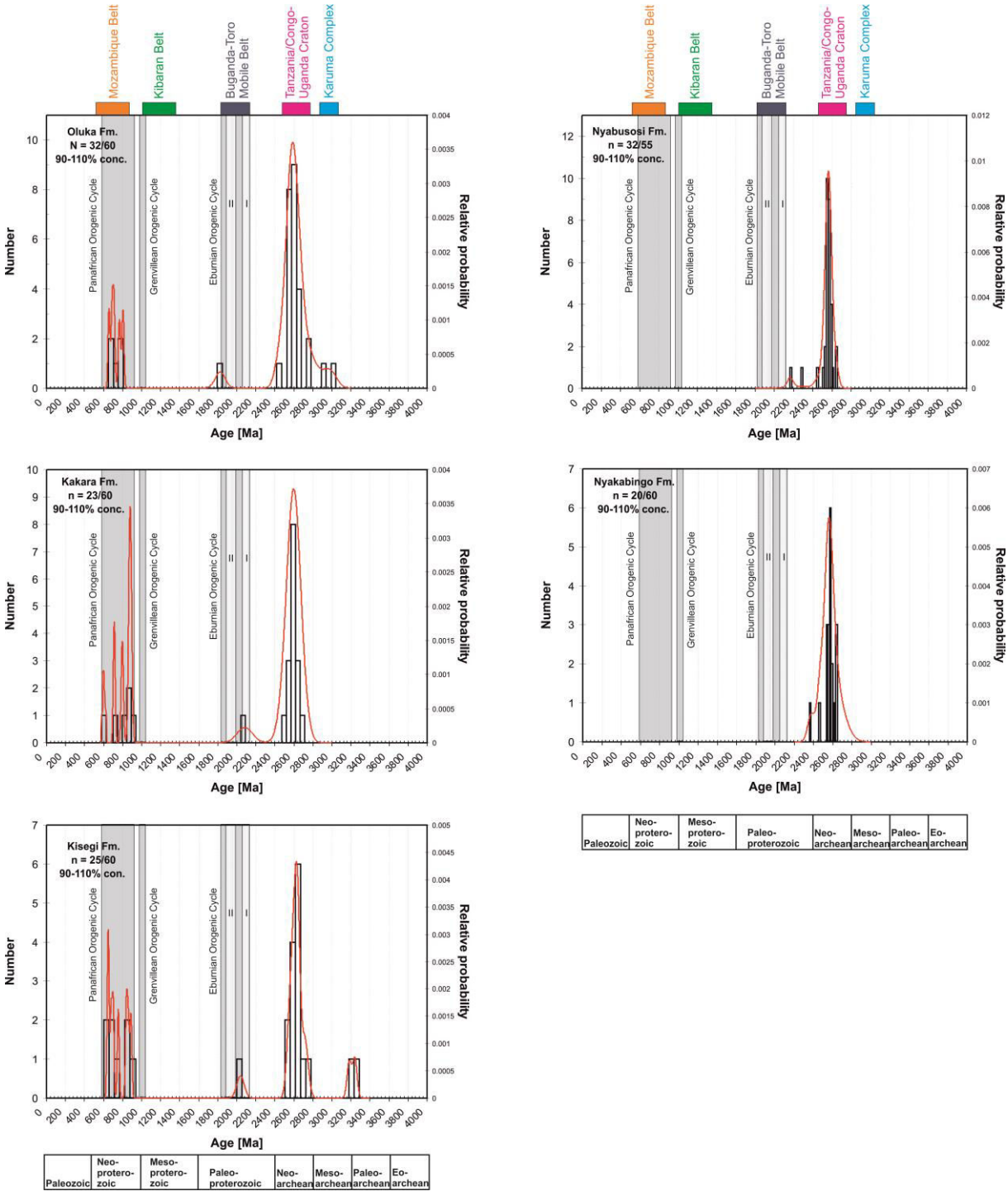

Figure 6-26. Combined probability density distribution and histogram diagrams for concordant zircon U-Pb age data from the rift sediment of the Kisegi-Nyabusosi area with the ages of key tectonic sources.

Detrital zircon in sediment of Group 1 exhibits a wide age spectrum, with similar age populations among the three formations (Fig. 6-26). The major zircon population yields Neoarchean ages of ~2550–2740 Ma for the Kisegi Formation, 2510–2700 Ma for the Kakara Formation, and ~2550–2750 Ma for the Oluka Formation. In the Kisegi Formation, a further population produces Neoproterozoic ages at ~640–890 Ma. Few individual grains disclose ages of 2040 ± 39 Ma (Paleoproterozoic), 3184 ± 24 Ma and 3243 ± 22 Ma (Mesoarchean). The sample from the Kakara Formation contains a minor Neoproterozoic zircon cluster at ~590–890 Ma. One grain shows an individual age of 2084 ± 81 Ma (Paleoproterozoic). In the Oluka Formation, a smaller group yields Neoproterozoic ages between ca. 660 and 805 Ma. Further obtained ages are at 1827 ± 52 Ma, 2443 ± 49 Ma (both Paleoproterozoic), 2891 ± 82 Ma and 2993 ± 65 Ma (both Mesoarchean).

Group 2. Lower Pliocene to upper Pliocene (~5.0–2.5 Ma; Nyaburogo, Nyakabingo formations)

Zircon from the Nyakabingo Formation is typically colorless, transparent, translucent to turbid, long stubby to short stalky (l:w ~1.5–2.5) (Figs. 6-23, 6-24). Pinkish and yellowish grains also occur. Internal structures are similar to the grains present in Group 1 (Fig. 6-25). In CL images, most grains either exhibit an undulous, inhomogeneous or chaotic internal structure or are characterized by a distinct core enveloped by irregular oscillatory zoning (Fig. 6-27). Few grains exhibit a thicker rather homogeneous rim, while some grains disclose large, dark, and homogeneous cores surrounded by a thin rim. The concordance-filtered ages of 60 zircon grains give a major zircon population at ~2540–2640 Ma (mainly Neoarchean). Two further grains reveal early-Paleoproterozoic ages of 2374 ± 66 Ma and 2471 ± 30 Ma. Mesoarchean and Neoproterozoic ages are missing in this Group.

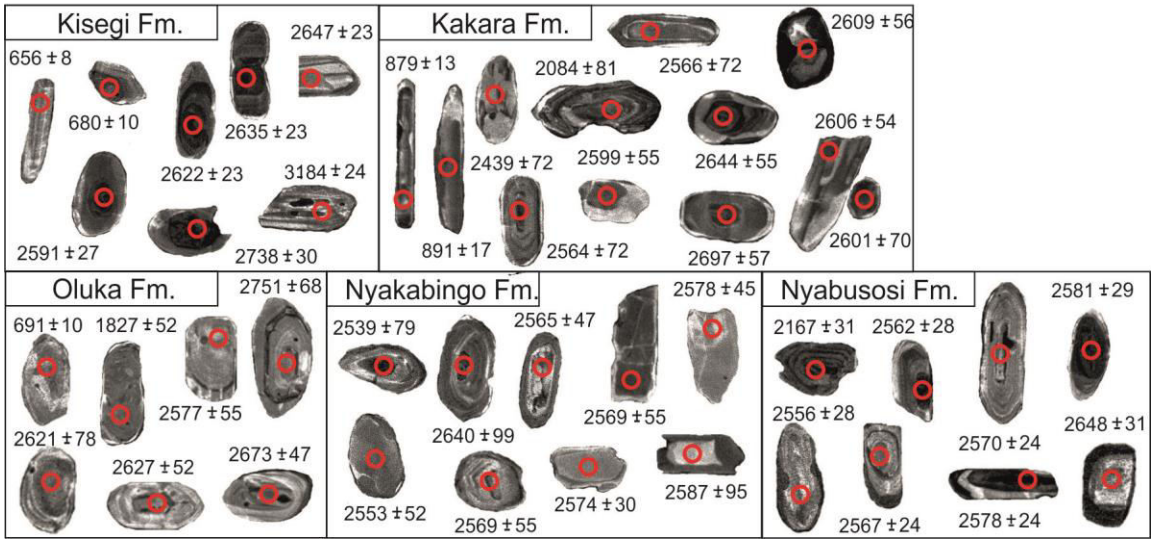

Figure 6-27. Selected representative CL images of U-Pb dated zircon grains from each sample with the location of the LA-ICP-MS analysis spot and related $^{207}Pb/^{206}Pb$ age (±1σ) for grains >1.0 Ga and $^{206}Pb/^{238}U$ age (±1σ) for grains <1.0 Ga. Ages are given in Ma.

Group 3. Lower Pleistocene (~2.5–1.0 Ma; Katorogo, Nyabusosi formations)

In contrast to zircon from the previous two groups, the Nyabusosi Formation yields a high amount of pinkish zircon grains that appear either translucent or turbid (Fig. 6-23). Transparent, colorless and

yellowish zircon grains are subordinated. The morphology varies from almost round to long prismatic although zircon with a length/width ratio of ~1.5–2.5 is the most common one (Fig. 6-24). In CL images, most zircon exhibits a large dark xenocrytic core surrounded by a thinner light mantle (Fig. 6-27). Other zircons are either homogenous or characterized by irregular oscillatory zoning or rather blurred internal structure. A total of fifty-five zircon domains were dated. Of these, twenty-two analyses were ignored for data interpretation due to high discordancy. The $^{207}Pb/^{206}Pb$ ages are similar to the ages observed in Group 2 by giving a narrow range of Neoarchean ages between ~2510–2650 Ma, culminating at ~2570 Ma (Fig. 6-26). Three grains yield Paleoproterozoic ages of 2167 ± 31 Ma, 2299 ± 143 Ma, and 2453 ± 35 Ma.

6.8.2 Nkondo-Kaiso area

Group 1. Lower Pliocene to upper Pliocene (~5.1–2.6 Ma; Nkondo, Warwire, Kyeoro formations)

Detrital zircon grains from Group 1 are dominantly colorless, transparent to turbid (Fig. 6-28). Sporadically, yellowish, brownish or light pinkish grains occur. Most zircon grains show a long stubby elongation with a length/width ratio between >1.5–2.0, followed by short stalky grains with a length/width ratio between >2.0 and 2.5 (Fig. 6-29). Elongated prismatic grains occur only sporadically. According to CL images, most zircon crystals show blurred, chaotic structures or are nearly homogenous to weakly zoned (Figs. 6-30, 6-32). Irregular concentric oscillatory zoning also occurs. Zircon diplaying xenocrytic cores enveloped by thick homogenous mantle are especially common in the Warwire Formation. Few grains disclose planar or sector zoning.

In Group 1, twenty out of sixty analyzed zircon crystals yielded concordant ages. The age spectra indicate that the majority of zircon in both formations has Neoarchean ages, largely between ~2560–2790 Ma (Nkondo Fm.) and ~2580–2680 Ma (Warwire Fm.) (Fig. 6-31). In the Nkondo Formation, three further ages were determined at 732 ± 10 Ma (Neoproterozoic), 2201 ± 44 Ma (Palaeoproterozoic) and 3342 ± 36 (Paleoarchean). In the Warwire Formation, two grains exhibit Neoproterozoic ages at 921 ± 14 Ma and 952 ± 17 Ma. Three grains reveal Mesoarchean ages between 2890 and 3100 Ma.

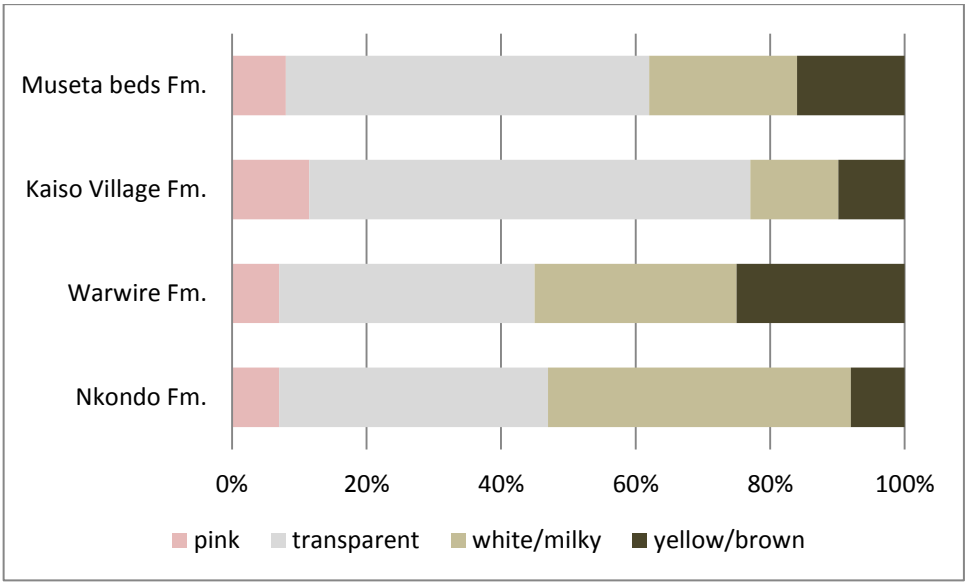

Figure 6-28. Distribution of zircon colors in the studied rift sediment of the Nkondo-Kaiso area.

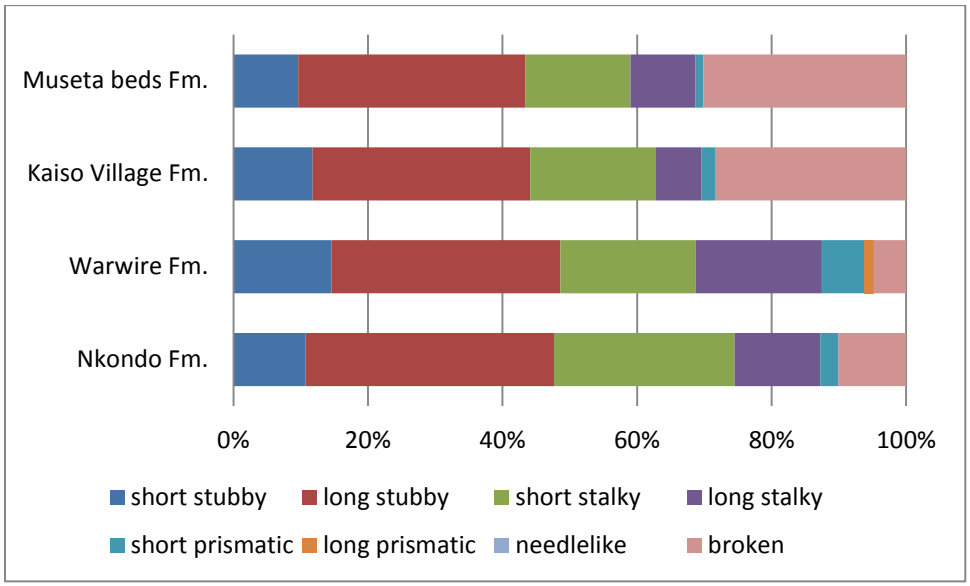

Figure 6-29. Classification of studied zircon grains from the Nkondo-Kaiso area according to their elongation (length/width ratio) after Gärtner et al. (2013).

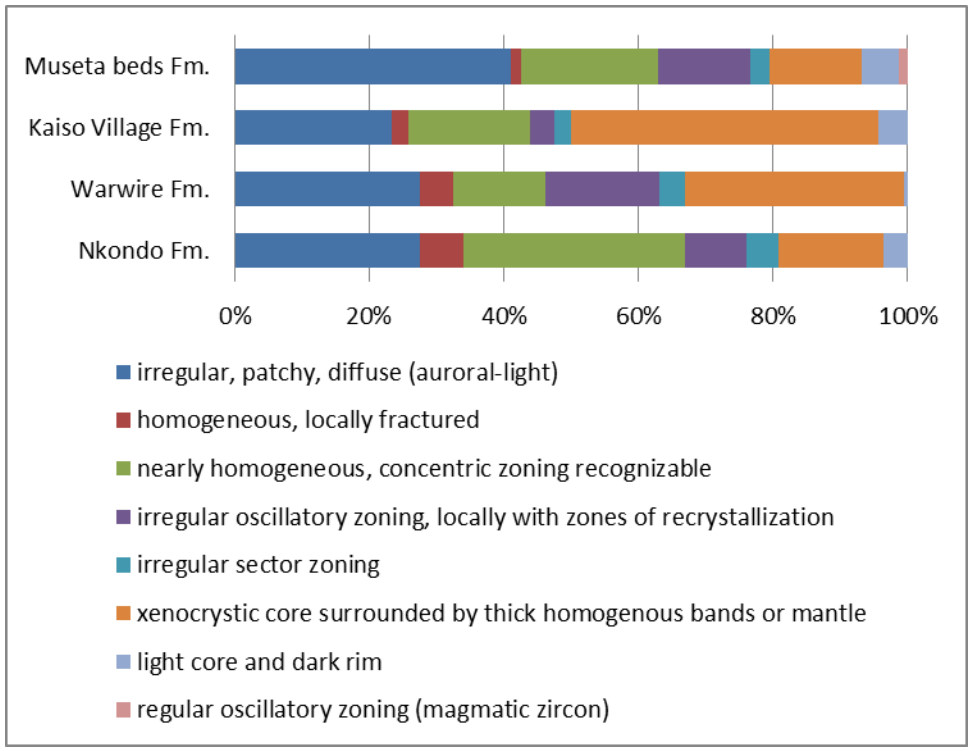

Figure 6-30. Distribution of internal zircon structures in the studied samples of the Nkondo-Kaiso area.

Group 2. Lower Pleistocene (~2.6–1.0 Ma; Kaiso Village, Museta beds formations)

Zircon in the Kaiso Village Formation and Museta beds Formation is mainly colorless, transparent to translucent. Few grains show a pinkish, yellowish to brownish tinge (Fig. 6-28). Most grains display a long stubby or short stalky morphology (l:w ~1.5–2.5) (Fig. 6-29). Broken crystals are common. CL images reveal that most crystals from the Kaiso Village Formation have a xenocrystic core surrounded by an unzoned mantle, whereas the Museta beds Formation is dominated by zircon showing heterogeneous patchy and convoluted pattern or irregular concentric zones (Fig. 6-30).

In Group 2, forty-five (Kaiso Village Formation) and forty (Museta beds Formation) out of sixty measured zircon grains yielded concordant ages (Fig. 6-31). In the Kaiso Village Formation, the most prominent zircon population shows Neoarchean ages between ~2510–2750 Ma. Few grains yield either Neoproterozoic (~650 and 950 Ma) or Paleoproterozoic (~2020 and 2340 Ma) ages. In the Museta beds Formations, the majority of zircon grains cluster between ~2410–2590 Ma, which is consistent with early Paleoproterozoic to late Neoarchean ages. Four further ages at 692 ± 10 (Neoproterozoic), ~2300 ± 44 Ma (Palaeoproterozoic) 2730 ± 22 Ma and 2734 ± 38 Ma (both Neoarchean) were determined.

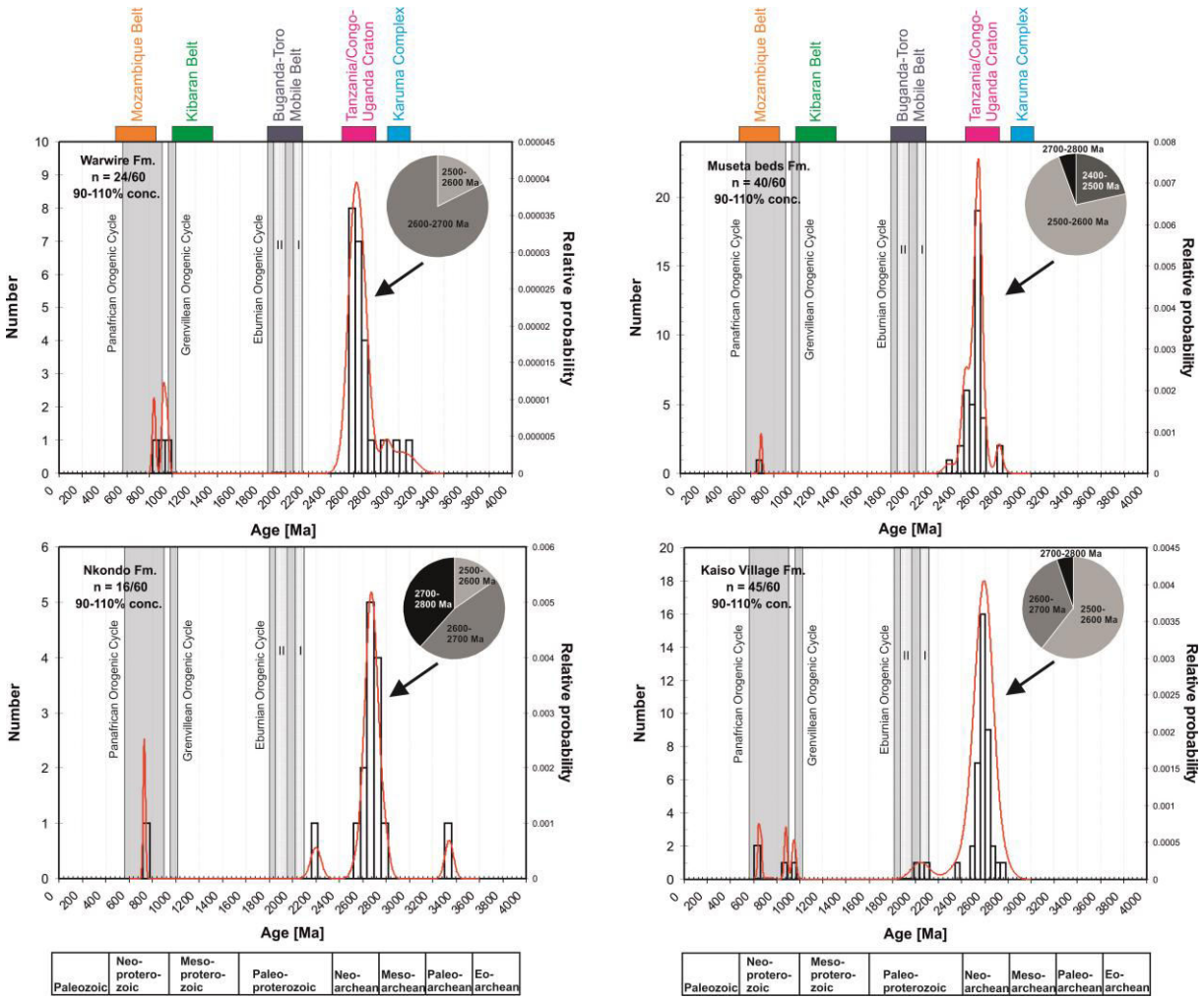

Figure 6-31. Combined probability density distribution and histogram diagrams for concordant zircon U-Pb age data from the rift sediment of the Kisegi-Nyabusosi area with the ages of key tectonic sources.

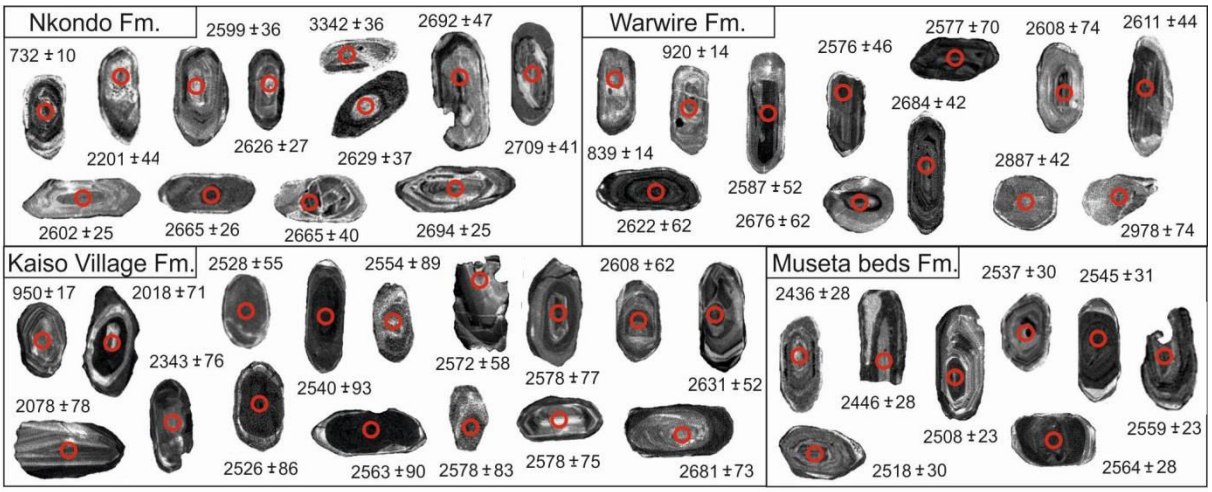

Figure 6-32. Selected representative CL images of U-Pb dated zircon grains from each sample with the location of the LA-ICP-MS analysis spot and related $^{207}Pb/^{206}Pb$ age (±1σ) for grains >1.0 Ga and $^{206}Pb/^{238}U$ age (±1σ) for grains <1.0 Ga. Ages are given in Ma.

6.9 Discussion

6.9.1 Sediment sources

6.9.1.1 Kisegi-Nyabusosi area

Group 1. Middle to upper Miocene (~17.0–5.0 Ma; Kisegi, Kakara, Oluka formations)

According to Schneider et al. (2016b), the sediment of Group 1 is predominantly composed of quartz, K-feldspar, minor plagioclase, and a high amount of the most durable heavy minerals (ZTR, garnet), which combined with amphibolite- to granulite-facies garnet and rutile suggest input from acidic high-grade to very high-grade metamorphic source rocks of Archean gneissic-granulitic cratons. The data set of this study mainly attests to the interpretations drawn from petrographic and single-grain geochemical analysis, but is also further able to specify distinct source areas. The geochemical data set confirms an origin from acidic rocks (e.g., granitoids). In particular, the high values of the provenance sensitive element ratios La/Sc, La/Co, Th/Cr, Th/Co, Th/Sc, and Zr/Sc (Cullers, 1988, 2000) concurs with high amounts of zircon in the samples, while sporadically occurring higher Gd_N/Yb_N ratios >2 might reflect the high garnet content in this sand (Brown and Rushmer, 2006; Hall and Hughes, 2012). The dearth of Eu-anomalies suggests that the sediment received input from source rocks that have not undergone intracrustal differentiation to the degree that separates significant amounts of plagioclase (Gao and Wedepohl, 1995). This together with significant LREE enrichment, and flat to depleted HREE is a typical feature for Archean rocks (McLennan and Taylor, 1991), and closely resembles REE pattern observed in river sediment that drains Neoarchean rock suites (NUT) of the Ugandan basement (Schneider et al., 2016a). The prominent zircon cluster at ~2500–2700 Ma confirms significant input from Neoarchean rocks. Possible sources are the granite-greenstone suites of the LVT and the WTT, as well as the granito-gneissic-migmatitic suites of the WNB and the NUT. Because the NUT constitutes major parts of central and northern Uganda, and crops out along the rift shoulder east to the study area, it seems plausible that this suite contributed significant amounts of detritus to the sediment of Group 1. A further zircon cluster at ~600–900 Ma points to input from Neoproterozoic rocks. Such rock suites are well documented in the Karamoja Belt in eastern Uganda, which belongs to the EAO (Stern, 1994). Rare Paleoproterozoic zircons at ~1.8 Ma and ~2.1–2.0 Ma can be correlated

with the Eburnian I and Eburnian II Orogenic Cycles that are represented by the RFB in southern Uganda. The few Mesoarchean zircons may have either derived from the Karuma Complex of the NUT (2.99 Ga), or from mafic enclaves in TTG gneiss of the WTT (3.1–2.8 Ga) (Schumann et al. 2004). Since the other zircon age spectra indicate an origin from eastern and southern basement domains, denudation from the TTG gneiss seems to be most coherent. Furthermore, an origin from recycled sedimentary rocks of the Bunyoro Group, that overlies Archean lithologies in western and central Uganda, needs to be considered, because zircons with ages of ~800–1300 Ma, 1.8–2.0 Ga, 2.5–2.7 Ga and 2.8 Ga have also been reported from streams draining this rock suite (Schneider et al., in prep.). Internal structures of zircon as revealed by CL imaging underline the geological situation in the study area and are mostly characteristic for zircon that experienced high-grade metamorphism (Corfu et al., 2003b). The stubby to stalky crystal morphology that is shown by the majority of grains attests to this by indicating that the zircon crystallized in deep-seated, slowly cooled intrusions, rather than in rapidly crystallized, porphyric bodies (Corfu et al., 2003b). (Well-) rounded outlines as well as broken grains might result from abrasion during sediment transport. Taking collectively, geochemistry, zircon geochronology, as well as mineral chemical and petrographic data gathered by Schneider et al. (2016b), the sediment of Group 1 derived from a variety of source rocks located in central, southern and eastern Uganda, maybe across the border in western Kenya. This is consistent with a westward directed drainage system. A climate shift concomitant with an increase in humidity from the Kisegi Formation towards the Oluka Formation, which was proposed based on facies analysis of the sedimentary successions (Roller et al., 2010), the appearance of abundant fossil fruits in upper Miocene strata (Pickford et al., 1993), and analysis on palynomorphs (Simon et al., 2017), is not manifested in the petrographic and geochemical composition of the sand. In general, all sediment samples show a similar only slight weathering degree, indicated by low to moderate weathering indices (CIA, WIP).

Group 2. Lower Pliocene to upper Pliocene (~5.0–2.5 Ma; Nyaburogo, Nyakabingo formations)

Sediment of Group 2 is predominantly composed of quartz, K-feldspar and plagioclase, but with a slightly higher content of feldspar, mica, and accessory minerals for sediment of the Nyakabingo Formation (Schneider et al., 2016b). The geochemical dataset approves to the higher compositional maturity of the Nyaburogo Formation, i.e., by showing higher SiO_2/Al_2O_3 ratios. Quartz dilution together with lower amounts of zircon in this sand might also explain the very low ∑REE content in the Nyaburogo Formation. The presence of negative Eu-anomalies for sand of the Nyakabingo Formation, that are also observed in sediment of the following Group 3, seems also to be partly depend on the total REE content, because a linear relationship between the ∑REE and Eu/Eu* is partly indicated for the samples. A distinct feature of Group 2 is the ratios of La/Sc, La/Co, Th/Cr, Th/Co, Zr/Sc, and Th/Sc, which are distinctively lower in comparison to Group 1, largely comparable to the composition of the UCC. The signified compositional change is concurrent with a change of heavy mineral assemblages, which are mainly dominated by amphibole and epidote since the onset of Group 2 (Fig.). The higher Zr/Sc ratio for sediment of the Nyakabingo Formation is probably due to the marginally higher zircon content in this sand. The provenance change that is indicated by bulk rock geochemistry is also accompanied by zircon geochronology, mainly due to the absence of Neo- and Paleoproterozoic, as well as Mesoarchean zircon in the sediment of Group 2. The narrow zircon population at ~2470–2640 Ma in sand of the Nyakabingo Formation indicates major input from Neoarchean rocks, most probably from gneissic units of the NUT that crops out along the nearby rift flank. Two individual zircon ages at ~2374 ± 35 Ma and 2471 ± 29 Ma coincide with a period of tectonic calm in Uganda, and are interpreted by Westerhof et al. (2014) to represent local perturbances preceding the Eburnian Orogenic Cycle. Overall, bulk rock geochemistry and zircon geochronology follows petrographic observations and indicate first transition of provenance signatures with the onset

of the Nyaburogo Formation. Even though zircon geochronology is not available for the Nyaburogo Formation itself, the shift at the Miocene/Pliocene boundary is well marked by heavy minerals and bulk rock geochemical data. The data set implies that sediment transport from the Ugandan hinterland (East African Orogen) was largely disrupted. The composition of the sediment, in particular the epidote-amphibole-dominated heavy mineral suites, amphibolite- to granulite-facies garnet and rutile as well as dominant Neoarchean zircon ages strongly resembles the signature of modern rivers draining the NUT implying that sediment of Group 2 was probably mainly shed from proximal sources along the rift shoulder, which confirms previous interpretations concerning source rocks and transport pathways (Schneider, 2016b). The timing of this change of sediment supply pattern coincides with a period when Paleolake Obweruka became large and deep (Pickford et al., 1993), and correlates well with a 'Major Flooding Surface' (S4m) identified by Simon (2015) at 4.9 Ma, held to represent the most distal environment. It is therefore likely that, at this time, the Albertine Rift experienced a period of uplift and basin subsidence, during which rift shoulders formed local topographic highs that were eroded. The shift in provenance data lags more than 1 Ma behind a basin-wide unconformity at 6.2 Ma, interpreted to represent the transition from the initial rift stage into the syn-rift stage (Simon, 2015). The time delay might be explained by a longer response time of the drainage system to adapt to the modified environmental conditions. An aridification trend during the Pliocene, which was identified by several authors (e.g., Simon et al., 2017) is not intended by sediment composition that shows similar weathering indices as the Miocene section.

Group 3. Lower Pleistocene (~2.5 Ma to present; Katorogo, Nyabusosi formations)

According to Schneider et al. (2016b), the sediment of Group 3 is composed of quartz, K-feldspar, and plagioclase. The Nyabusosi Formation reveals higher amounts of rock fragments, also metabasite grains, and mica, which is reflected by the geochemical data, i.e. by low SiO_2/Al_2O_3 ratios <10. Geochemically, the composition of Group 3 is similar to Group 2, particularly to the Nyakabingo Formation. La/Sc, La/Co, Th/Cr, Th/Co, Zr/Sc, and Th/Sc together with REE pattern suggest a source of intermediate to acidic composition, comparable with Upper Continental Crust material. Zircon ages of Group 3 are similar to the zircon ages obtained for the Nyakabingo Formation of Group 2. The prominent cluster at 2510–2650 Ma can be associated with chief derivation from Neoarchean rocks, most probably also from the NUT. A distinct change from mainly colorless zircon crystals (Group 2) towards a strong dominance of pinkish grains suggests that the sediment derived from a different domain of the basement block than sediment of Group 2. Notable amounts of pinkish zircon has only been observed in rivers draining the Rwenzori horst block (Schneider et al., in prep.), which makes derivation from this location probable. Two individual Paleoproterozoic ages of 2166 ± 31 Ma and 2299 ± 143 Ma might attest to this, because they largely coincide with the earliest phase of the Eburian I Orogenic Cycle in Uganda and deposition of the gneissose/granitoid basement of the RFB assigned to the Rukungiri Suite (2.21–2.15 Ga), which mainly crops out in southern Uganda, but also forms the northern tip of the Rwenzori Mountains. Overall, the age information, in conjunction with the geochemical data set indicate that sand of Group 3 was transported from proximal sources along the rift shoulder, most probably with major contribution from the Rwenzori Mountains. This attests to the previous interpretation drawn from petrography and mineral chemistry (Schneider et al., 2016b), e.g., by higher content of mica, the occurrence of metabasite grains, and lower-grade metamorphic (amphibolite-facies) garnet and rutile. Interpretations correlate well with a major basin-wide unconformity at 2.7 Ma (Simon, 2015) and also approve thermochronological data (MacPhee, 2006; Bauer et al., 2010, 2012, 2016) indicating exhumation of the Rwenzori Mountains at the Pliocene-Pleistocene boundary.

6.9.1.2 Kaiso area

Group 1. Lower Pliocene to upper Pliocene (~5.1–2.6 Ma; Nkondo, Warwire, Kyeoro formations)

Sediment of the Nkondo, Warwire and Kyeoro formations is dominated by quartz, K-feldspar, plagioclase, and minor quartz-feldspar-rich metamorphic rock fragments (Schneider et al., 2017). This together with the whole rock geochemical data indicates that sediment of Group 1 was mainly delivered from felsic to intermediate source rocks. A slightly higher mafic composition for sand of the Warwire and Kyeoro formations is demonstrated by lower Th/Sc ratios, less depletion in Eu, lower total REE values, as well as lower K_2O/Na_2O ratios, and matches the relative higher plagioclase and amphibole content in this sand. Weathering indices (CIA and WIP) suggest that the sand of Group 1 was only slightly affected by weathering processes. The prominent zircon population at ~2600–2700 Ma indicates that sediment of Group 1 received major input from Neoarchean rocks, which are widely exposed in the Ugandan basement. Considering the geographic position of the Nkondo-Kaiso area within the rift valley, the most probable source area represents the NUT, because this complex occupies major domains in central and northern Uganda. The small amount of early Neoarchean zircon ages between 2700 and 2800 Ma that are present in the Nkondo Formation also affirm contribution from this complex. In general, these ages are rare in Uganda, but are known from the Kaseeta potassium granite gneiss that belongs to the NUT and crops out along the eastern rift shoulder in direct vicinity to the study area (Westerhof et al., 2014). The few Mesoarchean ages between ~2.89 and 3.1 Ga, observed in the Warwire Formation, most probably indicate input from granulitic gneiss of the proximal Karuma Group that represents the Mesoarchean nucleus of the NUT. Some influence of this complex might also attest to the slight compositional shift that occurs between the Nkondo Formation and Warwire Formation (e.g., higher amphibole and plagioclase). Few individual Neo- and Paleoproterozoic zircon grains that can be correlated with either the RFB in southern Uganda (2201 ± 40 Ma), the Pan-African Karamoja Belt in eastern Uganda (653 ± 12 Ma, 839 ± 14 Ma), and the Madi-Igisi Belt in northern Uganda (~1000 Ma), respectively, probably represent recycled grains that were presumably shed from the nearby sedimentary Bunyoro Group that partly overlies the Archean basement in western and central Uganda. The occurrence of similar Neo- and Paleoproterozoic ages within this lithology is affirmed by analysis of zircon grains from a stream eroding this rock suite (Chapter 3). The origin for one concordant Paleoarchean age of 3342 ± 36 Ma (Nkondo Fm.) is difficult to interpret, because Paleoarchean ages are not known from the Ugandan basement. Cahen (1954) reported a poorly constraint age of 3.42 Ga from the Bomu-Kibalian Shield in the northeast Congo. It is very likely that this individual zircon grain also represents a recycled component. Overall, the new data set attests to previous interpretations derived from petrographic and mineral chemical studies (Schneider et al., 2017). It suggests that detritus of Group 1 mainly derived from medium- to high-grade gneissic granitoid of the NUT, which is conforming to heavy mineral assemblages dominated by epidote, amphibole and garnet, as well as to garnet and rutile chemistry implying major derivation from amphibolite- to granulite-facies metamorphic rocks (Schneider et al., 2017). Some sediment transport from the Bunyoro Group, which was not implied by petrographic studies, is probable due to the presence of recycled zircon. Minor transport from the Karuma Group is indicated since the onset of the Warwire Formation (~4.5 Ma), likely caused by northward progradation of the axial drainage system due to tectonic faulting activity. This together with river incision might explain the slight compositional shift between the Nkondo Fm. and Warwire Fm. The transition between both formations, marked by a hiatus of 0.5 Ma, has recently been interpreted to represent the initiation of the synrift stage in the northern Lake Albert sub-basin, because it correlated with the first severe provenance change in the Kisegi-Nyabusosi area (Schneider et al., 2017). However, this interpretation needs to be revised according to the new age model recently proposed for the Albertine Rift (Simon, 2015). Based on the new biostratigraphic ages, the onset of the Nkondo Formation at ~5.1 Ma already matches the transition into the synrift stage in the southern rift basin, whereas the Nkondo/Warwire

boundary (~4.5− 4.0 Ma) matches the transit between the Nyaburogo Fm. and Nyakabingo Fm. Sediment of the pre-rift stage is not exposed in the Nkondo-Kaiso area.

Group 2. Lower Pleistocene (~2.6–1.0 Ma; Kaiso Village, Museta beds formations)

Petrographically, the sediment of Group 2 is similar to Group 1, but with relative increase in quartz at the expense of plagioclase in the Kaiso Village Formation. The heavy mineral suites differ markedly from those of the Nkondo, Warwire and Kyeoro formations by showing dominant zircon and epidote, with subordinate tourmaline in the Kaiso Village Formation, and garnet, amphibole and sillimanite in the Museta beds formation (Schneider et al., 2017). Generally, the quartz-rich character of the sand, trace-element concentrations comparable to the UCC, enrichment in LREE, negative Eu anomalies and the flat HREE patterns suggest an origin from acidic to intermediate igneous rocks. The higher content of quartz and other stable minerals, especially in the Kaiso Village Formation, is reflected by high SiO_2 contents (~80 %), increased mean K_2O/Na_2O ratios of ~2.7, marked depletion in mobile elements, and relative increase of elemental ratios critical of the source rock composition, such as La/Sc, La/Co, Th/Co, and Th/Cr. The relative high total REE content and the negative Eu-anomaly also reflects the decrease of plagioclase and the enrichment of ultradense minerals, e.g., zircon, in the samples (Garzanti et al., 2011). Detrital zircon age spectra are similar to Group 1 and indicate major derivation from Neoarchean rocks. Few individual Neo- and Mesoproterozoic grains probably represent recycled grains, shed from the nearby Bunyoro Group. Interestingly, a rejuvenating trend within the Neoarchean age range is observed from sediment of Group 1 throughout Group 2, which might imply erosion of different sources within the same major tectonic terrane. While most Neoarchean zircon ages from sediment of Group 1 range between 2600 and 2700 Ma, this age range becomes less prominent in the Kaiso Village Formation and is completely absent in sand of the Museta beds Formation. Instead, sediment of Group 2 is characterized by continuous increase of zircon ages between 2500 and 2600. The Museta beds Formation also shows ages of ~2400–2500 Ma. These early Paleoproterozoic ages are rare in the Ugandan basement. Ages ~2490 Ma are known from granite and feldspar porphyry of the Kiboga suite near the boundary between the NUT and the WTT (Westerhof et al., 2014) and occur in few rivers draining the NUT (Chapter 3). A possible scenario for the slight shift in zircon ages might be incision and expansion of river courses from the rift shoulder further to the Ugandan plateau region in the east. In this course, stronger erosion of the Neoproterozoic Bunyoro Group that covers large parts of the Ugandan plateau east of the Albertine Rift would be expected. Input of recycled sedimentary material from the Bunyoro Group would also explain raised weathering indices (e.g., CIA) that cannot be explained sufficiently by chemical weathering, for two reasons. Firstly, weathering alone can hardly explain the strong relative increase in epidote, which cannot be considered as more stable than amphibole, garnet, and sillimanite during weathering (Velbel, 1999), and secondly, chemical weathering should have affected the entire region, but is not documented in the sediment of the Kisegi-Nyabusosi area. We therefore believe that, in this case, the high weathering indices are rather a provenance signal and reflect recycling of older sedimentary material.

Although, the new data set supports previous interpretations based on petrographic and heavy mineral assemblages (Schneider et al., 2017), they provide no significant new findings to back up former assumptions, especially concerning an origin from the Bunyoro Group. Contrary to expectations, the sediment shows no increase in Neo- or Mesoproterozoic grains, which were however detected in significant abundances in one river sediment draining the Bunyoro Group (Schneider et al., in prep.). Possible explanations for the similarity of zircon ages throughout the entire stratigraphy of the Nkondo-Kaiso region might be heterogeneities within the Bunyoro Group leading to an uneven distribution of zircon populations. Over time, unroofing leads to exposure and erosion of different

parts / rocks (e.g., tilloids, quartzite) of the lithology, which might be dominated by grains recycled from Neoarchean basement. Furthermore, only one river sample was analyzed concerning zircon ages, i.e., the composition of other parts within this lithology is unknown.

6.9.2 Paleotectonic implications

Based on the compilation of this new geochemical and geochronological data set with published data on petrography and mineral chemistry collected for the sediment of the Kisegi-Nyabusosi and Kaiso-Nkondo area (Schneider et al., 2016b, 2017), following paleotectonic implications for the evolution of the Albertine Rift can be drawn that allow re-evaluation of existing evolutionary models for the northern Western Branch of the EARS (Fig. 6-33).

Early rift stage (~17.0–5.0 Ma)

The onset of sedimentation in the Albertine Rift at ~17.0 Ma (Simon, 2015) is characterized by first faulting and deposition of the fluvial Kisegi Formation in a shallow downwarp southwest of modern Lake Albert (Pickford et al., 1993). As is known from sedimentological studies and facies analysis (Roller et al, 2010, and own work), the depositional environment was characterized by limited accommodation space where strongly amalgamated sandy bedforms were produced in an alluvial plain setting. The new provenance data clearly demonstrate that early sediment was transported into the Kisegi-Nyabusosi area from distal source areas in the Ugandan hinterland, probably also in western Kenya. Mixing of detritus from a variety of different source rocks in eastern, southern and central Uganda is mainly manifested in U-Pb ages of zircon, implying that the drainage system during the Miocene was characterized by a widely-branched river network. While only the NUT could be identified as possible source on the basis of petrographic and heavy mineral data (Schneider et al., 2016b), zircon U-Pb ages help to identify several other potential sources that extend towards the at least 400 km away located East African Orogen, including parts of southern Uganda that are nowadays occupied by Lake Victoria. This is an important finding, because it provides the definite evidence for a continental-wide, westward-directed drainage system, assumed to be initiated by uplift of the Kenyan Rift margin to the east (Gautier, 1965). Our data strongly agree with other paleohydrological models (e.g., Pickford et al., 1993; Taylor and Howard, 1998, 1999; Gagnevin et al., 2017), that propose drainage via the paleo-Nkusi River with its large regional catchment, including input from the Victoria Nile. Our drainage model further validates the hydrological model proposed by Pickford et al. (1993), who described a connection also to river catchments in northeastern Uganda (East African Orogen), which was not insinuated by most other authors (Fig. 6-3).

Ongoing subsidence in the Albertine Rift manifests in sedimentation, e.g., by transition from an accommodation-controlled system to a supply-controlled system during which the Kakara and Oluka formations were deposited (Roller et al., 2010). The change from mainly fluvial conditions towards palustrine/shallow lacustrine conditions marks the onset of Paleolake Obweruka that drowned the study area around 8.0 Ma. Facies changes are accompanied by minor changes in sediment composition, e.g., by slight decrease of zircon in heavy mineral suites, also deflected by REE data and provenance sensitive geochemical ratios. Although the change of the depositional environment / transport velocity had some influence on compositional ratios, provenance data do not imply a change of sediment sources, but remain more or less the same for another ~3.0 Ma. As the regional drainage still freely enters the basin, the influence of rift shoulder topography, assigned to have already begun to evolve along the basin margins, had not yet been prominent enough to severely influence local drainage pattern. It is therefore likely that the formation of Palaeolake Obweruka was not solely

initiated by a period of faulting in the Albertine Rift, but has also been triggered by increase of humidity in the Late Miocene (Simon, 2015; Lukaye et al., 2016). As insinuated by Pickford et al. (1993), drainage continued to be from west to east into Lake Obweruka and further to the Congo. Although, climate changes since the early Miocene to a maximum of humidity in the late Miocene are manifested by abundant fossil fruits in upper Miocene strata (Pickford et al., 1993) and palynofacies associations (Simon, 2015; Lukaye et al., 2016; Simon et al., 2017), they are not disclosed by the composition of the rift sediment.

Syn-rift stage (~5.0–2.6 Ma)

The database of this study indicates that the Albertine Rift glided into the actual syn-rift stage not before ~5.0 Ma. Taking into account a longer response time of the drainage system to adapt, the provenance model correlates broadly with a basin-wide unconformity at 6.2 Ma, interpreted to represent the onset of the major rifting phase ('rifting climax') characterized by high subsidence rates (>500m/Ma up to 600–800 m/Ma) and sedimentation rates (2.4x103 km^3/Ma) (Simon, 2015). A change in the provenance signal between the Oluka Formation and Nyaburogo Formation in the Kisegi-Nyabusosi area indicates that, only at this time, rift shoulders became topographic barriers that influenced sediment transport into the rift. Although, the westward-directed drainage from the Ugandan hinterland into Lake Obweruka is described to have persisted during the Pliocene, the sediment volume reaching the rift had obviously been reduced (Simon et al., 2017). We believe that streams delivering sediment to the Nyaburogo and Nyakabingo formations were largely deflected to the margin of the Albertine Basin and sediment transport was now mainly restricted to proximal sources, with the rising rift shoulders being the most dominant sediment source. This change of provenance pattern coincides with a period when Lake Obweruka became large and deep (Pickford et al., 1993; Van Damme and Pickford, 2003), indicating that rift shoulders and accommodation space became prominent and formed a steep-walled basin. This assumption goes along with former interpretations, stating that rift shoulders became climatically significant in the early Pliocene (~4 Ma) and that Palaeolake Obweruka was already partly divided into a southern and a northern basin by the rising Rwenzori Mountains (Van Damme and Pickford, 2003). The missing of Pan-African zircon ages in the Pliocene sediment further indicates disconnection of the northeastern drainage system from the 'paleo-Nkusi-Victoria Nile system'. The data suggest that drainage was mainly from central-southern areas, similar to interpretations made by de Heinzelin (1959), Taylor and Howard (1998) and Gagnevin et al. (2017). The provenance-based drainage model is thus in opposite to the hydrological model of Pickford et al. (1993), assuming continuing transport from northern sources and disruption of the drainage network not before the late Pleistocene, when tilting and river reversal led to the creation of Lake Kyoga and Lake Victoria and connection to the river Nile system (Talbot and Williams, 2009). According to provenance data, the drainage system on the Ugandan Plateau must have been disrupted earlier at least since the early Pliocene. Regional rivers from the northeast did not enter the southern Albertine Graben anymore.

In the Nkondo-Kaiso area, early Pliocene (~5.1 Ma) sediment accumulated in a lacustrine-influenced depositional environment, largely simultaneously to the transition between the pre-rift and syn-rift phase in the Kisegi-Nyabusosi area. In contrast to the southern Lake Albert sub-basin, rivers flowing into the northern Albertine Rift presumably belonged to an independent, much smaller hydrographic network, which was not connected to the large continental-wide drainage system delivering sediment to the southern Albertine Rift. Provenance data imply dominant erosion from the NUT and minor transport from the Bunyoro Group, both exposed along the eastern shoulder of the rift valley. The minor shift in sediment composition between the Nkondo Formation and Warwire Formation at 4.6–4.0 Ma is also manifested in sedimentation by the transition from deeper lacustrine towards nearshore

lacustrine strata, as well as by a widespread unconformity between both formations probably caused by a faulting episode (Pickford et al., 1993). Provenance pattern indicate incision of rivers into deeper strata of basement lithologies together with some additional input from northern sources (Karuma Complex), which suggest northward progradation of tectonic faulting activity. However, provenance pattern did not change significantly, pointing to persistence of relatively local sources.

Rift inversion stage (~2.6 Ma to present)

A further provenance change at the Pliocene-Pleistocene interface, largely concurrent in both the Kisegi-Nyabusosi area and Nkondo-Kaiso area, marks the transition into the final rifting phase characterized by fast uplift of rift shoulders and initiation of inversion tectonics in the Albertine Rift. The shift in sediment composition coincides with a basin-wide unconformity, assigned to represent the onset of a second rifting phase with less accommodation and sedimentation rates (subsidence rate: 450 to 250 m/Ma; sedimentation rate: 1.5x103 km^3/Ma) and controlled by normal faults (Simon, 2015). Although U-Pb zircon ages and geochemical parameter in Pleistocene sand of the Kisegi-Nyabusosi area did not change much compared to the Pliocene, a major provenance change at this time is well defined by garnet and rutile chemistry, indicating input from lower-grade (amphibolite-facies) metasedimentary rocks of the RFB, also cropping out in the Rwenzori Mountains (Schneider et al., 2016b). Major transport from the Rwenzori Mountains is also supported by increase of rock fragments, mica and pinkish zircon grains. Provenance data very well match other observations, e.g., (i) mapping and paleontological studies of sedimentary succession of the Kisegi-Nyabusosi area revealing tilting and truncation during the Pliocene-Pleistocene boundary (Pickford et al., 1993), (ii) thermochronological studies (MacPhee, 2006; Bauer et al., 2010a, 2012, 2016) indicating a major period of exhumation of the Rwenzori Mountains at this time, (iii) the occurrence of Podocarpus pollen characteristic for elevations >1000 m; thus, approving to the growth of a close relief, and (iv) sedimentation occurred along two major depocenters located adjacent to the Rwenzori horst block (Simon, 2015).

Sediment supply to the Nkondo-Kaiso area persisted from proximal sources along the rift margin. The higher volume of more mature, quartzose material (Kaiso Village Formation), which is related to increased input from the (meta-)sedimentary Bunyoro Group, suggests that the catchment area might have expanded further to the east as rifting proceeds, probably as consequence of uplift and incision of former footwall-derived rivers. River incision especially plays a role for the Museta beds Formation, during which deeper stratigraphic levels are exposed and reinvigorate delivery from the Archean basement into the rift. Our observations are concurrent with interpretations made by Simon (2015), who suggested a shift from an alluvial system to a network of bedrock river incision during the Pleistocene.

Overall, provenance data imply only small-scale changes concerning sediment transport directions for both study areas compared to the previous rifting phase with major supply from the uplifted rift margin. As reported by other authors, the regional drainage of Uganda persisted until the mid-Pleistocene, when tilting of rift shoulders in consequence of footwall uplift led to the initiation of the ‘axis of upwarping’ located 13–32 km east of the western rift (Doornkamp, 1968). River reversal and downwarping of the country east of the axis led to the creation of Lake Kyoga and Lake Victoria by either flooding of former headwaters or pooling of waters (Doornkamp, 1968; Ollier, 1990; Taylor and Howard, 1999b) and to modifications of the hydrological network. However, the drainage interpreted from Pleistocene sediments in the Albertine Rift did not change much over time and is still similar until the present-day.

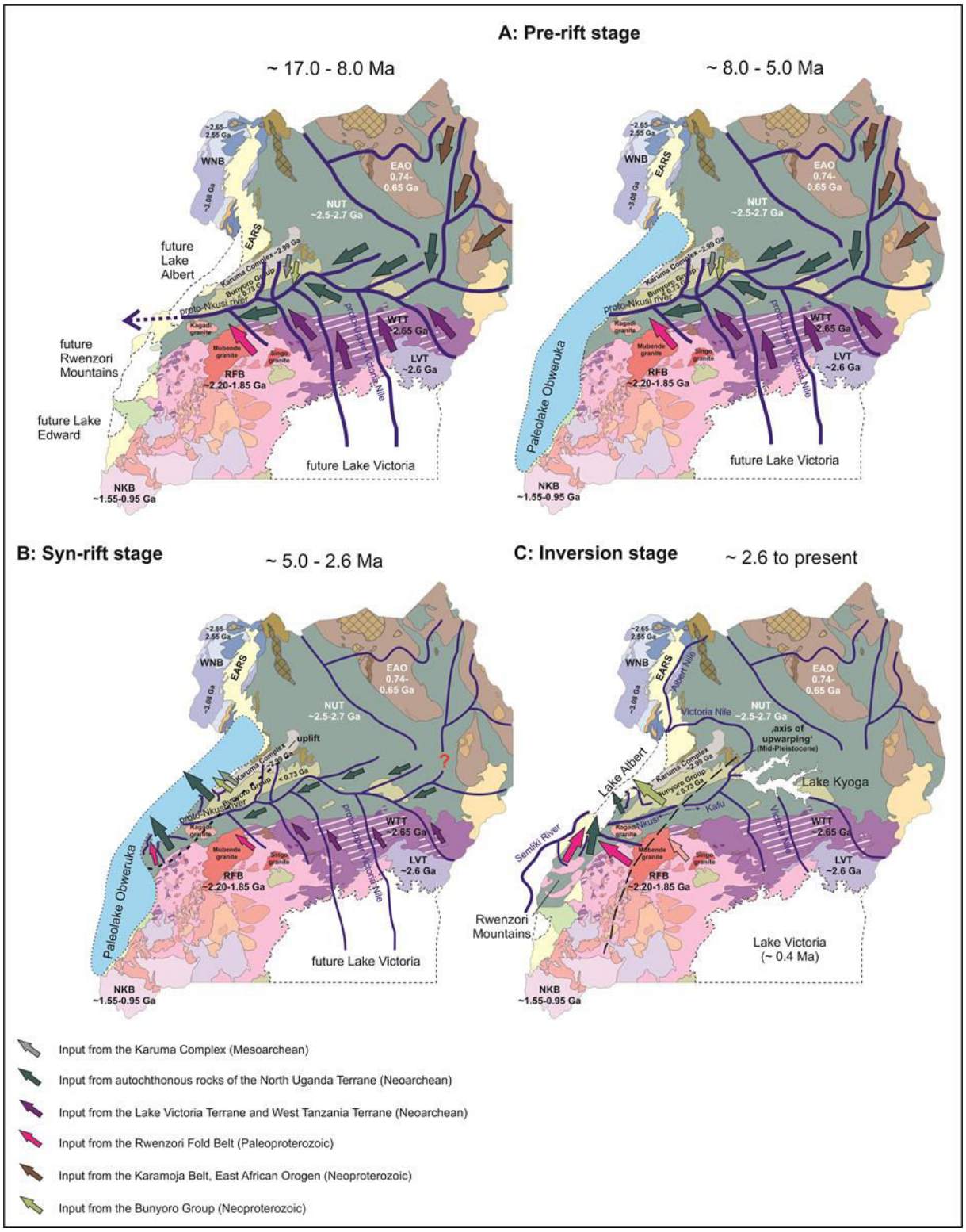

Figure 6-33. Provenance-based drainage model for Uganda during different stages of rift evolution with inferred sediment input directions. Reconstruction of lake extension after Pickford et al. (1993).

6.10 Conclusions

Integration of data from bulk rock geochemistry and U-Pb zircon geochronology from Miocene-Pleistocene rift sediment in two study areas (Kisegi-Nyabusosi and Nkondo-Kaiso) in the Albertine Rift provides constraints about the provenance of the rift infill. This study shows that from the late Miocene onwards there were important episodes of tectonic activity affecting the northern section of the Western Rift valley. The long-term result to these tectonic events was the development of broadly uplifted mountainous regions straddling parallel to the rift valley, with uplift rates ranging from ~1–3 km a.s.l in different parts of the system. Uplift culminates in the 5109 m a.s.l. Rwenzori Mountains, representing the highest rift-flank uplift on Earth.

In particular, this study reveals compositional differences of the sedimentary inventory of the Albertine Rift, indicating that the spatial and temporal sediment supply resulted from different independently operating transport systems. The change of compositional pattern largely at the Miocene-Pliocene (~5.0 Ma) and Pliocene-Pleistocene interface (~2.6 Ma) mark the initiation of different rifting phases through which the Albertine Rift passed during its evolution. The new data set partly refines existing tectonic models and paleodrainage directions for the Lake Albert sediment system, especially concerning the dimension and configuration of the regional hydrographic network.

Overall, three different evolutionary stages can be identified based on provenance pattern:

Pre-rift stage (~17.0–5.0 Ma) – Miocene sediment is only exposed in the southern Albertine Basin (Kisegi-Nyabusosi area). Provenance pattern indicate that sediment supply was mainly from a widely-branched, continental-wide river network that delivered sediment from northern, central, and southern sources in Uganda with major input from Archean cratonic terrains and the more distal Neoproterozoic Pan-African belt near the Kenya margin. This supply supports existing paleodrainage models (e.g., Pickford et al., 1993) proposing derivation via a 'proto-Nkusi-Victoria Nile' river system, which, in contrast to the present day, was connected to a large-scale catchment area, before this river network was disrupted due to local uplift.

Syn-rift stage (~5.0–2.6 Ma) – A provenance change during the Miocene-Pliocene boundary marks the onset of the major rifting phase in the Albertine Rift characterized by subsidence and uplift of rift walls. Less variability of zircon U-Pb ages indicates disruption of sediment transport from the Ugandan hinterland. Supply into the southern (Kisegi-Nyabusosi area) and central (Nkondo-Kaiso area) rift sector was now mainly from proximal sources with the Archean cratonic basement (NUT) of the rising rift shoulders representing the most dominant sediment source.

Rift inversion stage (~2.6 to present) – A further change of compositional pattern concurrent in both study areas during the Pliocene-Pleistocene transition signifies the initiation of the last rifting phase, which is well correlated with a regional unconformity at 2.7 Ma (Simon et al., 2017) and the beginning of the major uplift of the Rwenzori Mountains (MacPhee, 2006; Bauer et al., 2010, 2012, 2015). Strongest evidence is the appearance of pinkish zircon grains in sand of the southern sub-basin (Kisegi-Nyabusosi area) which can be assigned to dominant sediment input from the rising Rwenzori horst block. In the Nkondo-Kaiso region, uplift and river incision induced additional input from the Neoproterozoic (meta-)sedimentary Bunyoro Group located further to the east and leading to a higher maturity of the Pleistocene sediment.

This study further highlights the importance of compositional provenance analysis to fully understand sediment supply into depositional systems. Zircon U-Pb geochronology proofed to be a powerful application to decipher certain source areas, because each obtained age population could be linked to a certain tectono-thermal terrane in the regional basement. In particular, this method provided final evidence for a large scale transport system supplying the Miocene sediment of the Kisegi-Nyabusosi

area, as well as its later disruption by either the presence or missing of certain age groups. The bulk geochemical data set also allowed drawing conclusions about external factors controlling sediment deposition, such as weathering and recycling, and particularly helped to reveal sediment input from polycycle lithologies (Bunyoro Group), where zircon ages failed.

6.11 Acknowledgements

This study is part of the Forschergruppe 'Riftlink' funded by the DFG grant H1643–7/1. We thank the Ugandan National Council for Science and Technology for permitting the research work in Uganda and the Uganda Wildlife Authority for their support and permission to work in the national parks. Many thanks to our Ugandan research partners from Makerere University for cooperation, in particular Andreas Schumann for his on-site guidance and our driver Kitam Ali for his profound help and field endurance. Special thanks go to Dr. Stephan Buhre (Johannes Gutenberg University, Mainz) for his help with CL imaging and Dr. Regina Mertz-Kraus for her assistance during LA-ICP-MS measurements. Klemens Link kindly introduced me into zircon geochronology and helped with the evaluation of the final data set.

6.12 References

Abdelsalam, M. G., Katumwehe, A. B., Atekwana, E. A., Le Pera, A. K., Achang, M., 2016. The Paleoproterozoic Singo Granite in south-central Uganda revealed as a Nested Igneous Ring Complex using Geophysical Data. Journal of African Earth Sciences, 116, 198–212.

Barker, D. S., Nixon, P. H., 1989. High-Ca, low-alkali carbonatite volcanism at Fort Portal, Uganda. Contributions to Mineralogy and Petrology, 103, 166–177.

Bauer, F. U., Glasmacher U. A., Ring U., Schumann A., Nagudi B., 2010. Thermal and exhumation history of the central Rwenzori Mountains, Western Rift of the East African Rift System, Uganda. International Journal of Earth Sciences, 99, 1575–1597.

Bauer, F. U., Glasmacher, U. A., Ring, U., Karl, M., Schumann, A., Nagudi, B., 2013. Tracing the exhumation history of the Rwenzori Mountains, Albertine Rift, Uganda, using low-temperature thermochronology. Tectonophysics, 599, 8–28.

Bauer, F. U., Glasmacher, U. A., Ring, U., Grobe, R. W., Mambo, V. S., Starz, M., 2016. Long-term cooling history of the Albertine Rift: new evidence from the western rift shoulder, DR Congo. International Journal of Earth Sciences, 105, 1707–1728.

Bhatia, M. R., Crook, K. A., 1986. Trace element characteristics of graywackes and tectonic setting discrimination of sedimentary basins. Contributions to Mineralogy and Petrology, 92, 181–193.

Bishop, W. W., 1965. Quaternary geology and geomorphology in the Albertine Rift Valley, Uganda. In: Wright Jr., H. E., Frey, D. G. (Eds.), International studies on the Quaternary, pp. 293–321.

Bjørlikke, K. O., 1973. Glacial conglomerates of late Precambrian age from the Bunyoro Series, W. Uganda. Geologische Rundschau, 62, 938–947.

Black, L. P., Kamo, S. L., Allen, C. M., Aleinikoff, J. N., Davis, D. W., Korsch, R. J., Foudoulis, C., 2003. TEMORA 1: a new zircon standard for Phanerozoic U–Pb geochronology. Chemical Geology, 200, 155–170.

Brown, M., Rushmer, T. (Eds.), 2006. Evolution and differentiation of the continental crust. Cambridge University Press, 553 pp.

Cahen, L., 1954. Geologie du Congo Belge. Vaillant Carmanne, Liege, 577 pp.

Chorowicz, J., 2005. The East African rift system. Journal of African Earth Sciences, 43, 379–410.

Cullers, R., 1988. Mineralogical and chemical changes of soil and stream sediment formed by intense weathering of the Danburg granite, Georgia, USA. Lithos, 21, 301–314.

Cullers, R. L., 2000. The geochemistry of shales, siltstones and sandstones of Pennsylvanian–Permian age, Colorado, USA: implications for provenance and metamorphic studies. Lithos, 51, 181–203.

Corfu, F., Ravna, E. J. K., Kullerud, K., 2003a. A late Ordovician U-Pb age for the Tromsø nappe complex, uppermost allochthon of the Scandinavian. Caledonides, Contributions to Mineralogy and Petrology, 145, 502–513.

Corfu, F., Hanchar, J. M., Hoskin, P. W., Kinny, P., 2003b. Atlas of zircon textures. Reviews in mineralogy and geochemistry, 53, 469–500.

Cox, R., Lowe, D. R., Cullers, R. L., 1995. The influence of sediment recycling and basement composition on evolution of mudrock chemistry in the southwestern United States. Geochimica et Cosmochimica Acta, 59, 2919–2940.

Dechamps, R., Senut, B., Pickford, M., 1992. Fruits fossiles pliocènes et pléistocènes du Rift occidental ougandais. Signification paléoenvironnementale. Comptes rendus de l'Académie des sciences. Série 2, Mécanique, Physique, Chimie, Sciences de l'univers, Sciences de la Terre, 314, 325–331.

De Heinzelin, J., 1959. Les formations du Western Rift et de la cuvette Congolaise. Actes IVe Congres Panafricain Prehistoire, section I. Annales du Musée Royal de L'afrique Centrale, Sciences Humaines, 40, 219–243.

DeMenocal, P., 1995. Plio-Pleistocene African Climate. Science, 270, 53–59.

DeMenocal, P., 2004. African climate change and faunal evolution during the Pliocene-Pleistocene. Earth and Planetary Science Letters, 220, 3–24.

Doornkamp, J. C., 1968. The role of inselbergs in the geomorphology of Southern Uganda. Transactions of the Institute of British Geographers, 44, 151–162.

Ebinger, C. J., 1989. Tectonic development on the western branch of the East African rift system. Geological Society of America Bulletin, 101, 885–903.

Ebinger, C. J., Deino, A. L., Tesha, A. L., Becker, T., Ring, U., 1993. Tectonic controls on rift basin morphology: evolution of the Northern Malawi (Nyasa) Rift. Journal of Geophysical Research: Solid Earth, 98, 17821–17836.

Foley, S. F., Link, K., Tiberindwa, J. V., Barifaijo, E., 2012. Patterns and origin of igneous activity around the Tanzanian craton. Journal of African Earth Sciences, 62, 1–18.

Gärtner, A., Linnemann, U., Sagawe, A., Hofmann, M., Ullrich, B., Kleber, A., 2013. Morphology of zircon crystal grains in sediment − characteristics, classifications, definitions. Geologica Saxonica, 59, 65–73.

Gagnevin, D., Tyrrell, S., Morton, A. C., Leather, J., Lee, N., Floch, B. L., Frei, D., Lukaye, J., 2017. Sand supply to the Lake Albert Basin (Uganda) during the Miocene-Pliocene: A multiproxy provenance approach. Geochemistry, Geophysics, Geosystems, 18, 2133–2148.

Gao, S., Wedepohl, K. H., 1995. The negative Eu anomaly in Archean sedimentary rocks: Implications for decomposition, age and importance of their granitic sources. Earth and Planetary Science Letters, 133, 81–94.

Garzanti, E., Andó, S., France-Lanord, C., Censi, P., Vignola, P., Galy, V., Lupker, M., 2011. Mineralogical and chemical variability of fluvial sediments 2. Suspended-load silt (Ganga–Brahmaputra, Bangladesh). Earth and Planetary Science Letters, 302, 107–120.

Garzanti, E., Padoan, M., Andò, S., Resentini, A., Vezzoli, G., Lustrino, M., 2013. Weathering and relative durability of detrital minerals in equatorial climate: sand petrology and geochemistry in the East African Rift. The Journal of Geology, 121, 547–580.

Garzanti, E., Resentini, A., 2016. Provenance control on chemical indices of weathering (Taiwan river sands). Sedimentary Geology, 336, 81–95.

Gautier, A., 1965. Geological Investigation in the Sinda Mohari (Ituri, NE-Congo). A Monograph on the Geological History of a Region in the Lake Albert Rift. Ganda-Congo Expedition. Ghent University, 158 pp.

Gautier, A., 1970. Fossil freshwater mollusca of the Lake Edward–Lake Albert Rift. Annual Reports of the Royal Museum of Central Africa, Tervuren, 67, 1–144.

Gehrels, G., 2014. Detrital zircon U-Pb geochronology applied to tectonics. Annual Review of Earth and Planetary Sciences, 42, 127–149.

Gerdes, A., Zeh, A., 2006. Combined U–Pb and Hf isotope LA-(MC-) ICP-MS analyses of detrital zircons: comparison with SHRIMP and new constraints for the provenance and age of an Armorican metasediment in Central Germany. Earth and Planetary Science Letters, 249, 47–61.

Hall, R. P., Hughes, D. J., 2012. Early Precambrian basic magmatism. Springer Science & Business Media, 496 pp.

Herron, M. M., 1988. Geochemical classification of terrigenous sands and shales from core or log data. Journal of Sedimentary Petrology, 58, 820–829.

Jackson, S. E., Pearson, N. J., Griffin, W. L., Belousova, E. A., 2004. The application of laser ablation-inductively coupled plasma-mass spectrometry (la-icp-ms) to in situ U-Pb zircon geochronology. Chemical Geology, 211, 47–69.

Johnson, S. P., Waele, B. De, Tembo, F., Evans, D., Iizuka, T., Tani, K., 2007. Geochronology of the Zambezi supracrustal sequence, southern Zambia: a record of Neoproterozoic divergent processes along the southern margin of the Congo Craton. The Journal of Geology, 115, 355–374.

Key, R. M., Liyungu, A. K., Njamu, F. M., Somwe, V., Banda, J., Mosley, P. N., Armstrong, R. A. 2001. The western arm of the Lufilian Arc in NW Zambia and its potential for copper mineralisation. Journal of African Earth Science. 33, 503–528.

King, B. C., 1959a. Problems of the Precambrian of Central and Western Uganda, part I. Problems of correlation. Science Progress, London, 47, 528–542.

King, B. C., 1959b. Problems of the Precambrian of Central and Western Uganda, part II. Structures, metamorphism, and granites. Science Progress, London, 47, 723–744.

Lee, Y. I., 2002. Provenance derived from the geochemistry of late Paleozoic–early Mesozoic mudrocks of the pyeongan supergroup, Korea. Sedimentary Geology, 149, 219–235.

Link, K., Koehn, D., Barth, M. G., Tiberindwa, J. V., Barifaijo, E., Aanyu, K., Foley, S. F., 2010. Continuous cratonic crust between the Congo and Tanzania blocks in western Uganda. International Journal of Earth Sciences, 99, 1559–1573.

Ludwig, K. R., 2012. User's manual for Isoplot 3.75: A geochronological toolkit for Microsoft Excel: Berkeley Geochronology Center Special Publication No. 5, 75 pp.

Lukaye, J. M., 2009. Biostratigraphy and Palynofacies of Four Exploration Wells from the Albertine Graben, Uganda. American Association of Petroleum Geologists, Search & Discovery Article, 50169. http://www.searchanddiscovery.net/documents/2009/50169lukaye/ndx_lukaye.pdf.

Lukaye, J., Worsley, D., Kiconco, L., Nabbanja, P., Abeinomugisha, D., Amusugut, C., Njabire, N., Nuwagaba, R., Mugisha, F., Ddungu, T., Sserubiri, T., Sserubiri, T., 2016. Developing a Coherent Stratigraphic Scheme of the Albertine Graben-East, Africa. Journal of Earth Science and Engineering, 6, 264–294.

Macheyeki, A. S., Delvaux, D., De Batist, M., Mruma, A., 2008. Fault kinematics and tectonic stress in the seismically active Manyara–Dodoma Rift segment in Central Tanzania–Implications for the East African Rift. Journal of African Earth Sciences, 51, 163–188.

Mänttäri, I., 2014. Mesoarchaean to Neoproterozoic U-Pb and Sm-Nd ages from Uganda. In: Lehto, T., Katto, E. (Eds.), GTK Consortium Geological Surveys in Uganda 2008−2012. Geological Survey of Finland, Special Paper 56.

Master, S., Bekker, A., Karhu, J. A., 2013. Paleoproterozoic high δ 13 C carb marbles from the Ruwenzori Mountains, Uganda: Implications for the age of the Buganda Group. Chemical Geology, 362, 157–164.

MacDonald, R., 1966. Geological Map of Uganda. Department of Geological Survey and Mines, Uganda.

MacPhee, D., 2006. Exhumation, Rift-flank uplift, and Thermal Evolution of the Rwenzori Mountains Determined by Combined (U–Th)/He and U–Pb thermochronometry. Master thesis, Massachusetts Institute of Technology.

McDonough, W. F., Sun, S. S., 1995. The composition of the earth. Chemical Geology, 120, 223–253.

McGlue, M. M., Scholz, C. A., Karp, T., Ongodia, B., Lezzar, K. E., 2006. Facies architecture of flexural margin lowstand delta deposits in Lake Edward, East African rift: constraints from seismic reflection imaging. Journal of Sedimentary Research, 76, 942–958.

McLennan, S. M., Taylor, S. R., 1991. Sedimentary rocks and crustal evolution: tectonic setting and secular trends. The Journal of Geology, 1–21.

McLennan, S. M., Hemming, S., McDaniel, D. K., Hanson, G. N., 1993. Geochemical approaches to sedimentation, provenance, and tectonics. Geological Society of America Special Papers, 284, 21–40.

Morley, C. K., Nelson, R. A., Patton, T. L., Munn, S. G., 1990. Transfer zones in the East African rift system and their relevance to hydrocarbon exploration in rifts. American Association of Petroleum Geologists Bulletin, 74, 1234–1253.

Nagudi, B., Koeberl, C., Kurat, G., 2003. Petrography and geochemistry of the Singo granite, Uganda, and implications for its origin. Journal of African Earth Science, 36, 73–87.

Nasdala, L., Hofmeister, W. G., Norberg, N. ,Mattinson, J. M., Corfu, F., Dorr, W., Kamo, S. L., Kennedy, A. K., Kronz, A., Reiners, P. W., Frei, D., Kosler, J., Wan, Y. S., Gotze, J., Hager, T., Kroner, A., Valley, J. W., 2008. Zircon M257—a homogeneous natural reference material for the ion microprobe U-Pb analysis of zircon. Geostandards and Geoanalytical Research, 32, 247–265.

Nesbitt, H. W., Young, G. M., 1982. Early Proterozoic climates and plate motions inferred from major element chemistry of lutites. Nature, 299, 715–717.

Ollier, C. D., 1990. Morphotectonics of the Lake Albert Rift Valley and its significance for continental margins. Journal of Geodynamics, 11, 343–355.

Parker, A., 1970. An index of weathering for silicate rocks. Geological Magazine, 107, 501–504.

Pettijohn, F. J., Potter, P. E., Siever, R., 1972. Sand and Sandstone. Springer, Berlin Heidelberg New York.

Pickford, M., Senut, B., Poupeau, G., Brown, F., Haileab, B., 1991. Correlation of tephra layers from the Western Rift Valley (Uganda) to the Turkana Basin (Ethiopia/Kenya) and the Gulf of Aden. Stratigraphy, 313, 223–229.

Pickford, M., Senut, B., Hadoto, D., 1993. Geology and Palaeobiology of the Albertine Rift Valley, Uganda-Zaire. Vol. I: Geology. International Centre for Training and Exchanges in Geosciences, Occasional publications, 24, 1–190.

Ring, U., 2008. Extreme uplift of the Rwenzori Mountains in the East African Rift, Uganda: Structural framework and possible role of glaciations. Tectonics, 27, 1–19.

Ring, U., 2014. The East African Rift System. Australian Journal of Earth Sciences, 107, 132–146.

Ring, U., Betzler, C., Delvaux, D., 1992. Normal vs. strike-slip faulting during rift development in East Africa: the Malawi rift. Geology, 20, 1015–1018.

Ring, U., Betzler, C., 1995. Geology of the Malawi Rift: kinematic and tectono-sedimentary background to the Chiwondo Beds, northern Malawi. Journal of Human Evolution 28, 7–21.

Roller, S., Hornung, J., Hinderer, M., Ssemmanda, I., 2010. Middle Miocene to Pleistocene sedimentary record of rift evolution in the southern Albertine Graben (Uganda). International Journal of Earth Sciences, 99, 1643–1661.

RPS Energy, 2008. Palynological Analysis of the Turaco-3 and Turaco-2 Wells, Block 3A, Albert Basin, Uganda. 32 pp. + 4 encl. Confidential Report.

Rubondo, E., 2005. The hydrocarbon potential of the Albertine Graben, Uganda. Petroleum Exploration and Production Department, Ministry of Energy and Mineral Development, 22 pp.

Rudnick, R. L., Gao, S., 2003. Composition of the continental crust. Treatise on Geochemistry, 3, 1–64.

Schlüter, T., 2008. Geological Atlas of Africa, 2nd edition, Springer Verlag, Berlin, 307 pp.

Schneider, S., Hornung, J., Hinderer, M., Garzanti, E., 2016a. Petrography and geochemistry of modern river sediments in an equatorial environment (Rwenzori Mountains and Albertine rift, Uganda)—Implications for weathering and provenance. Sedimentary Geology, 336, 106–119.

Schneider, S., Hornung, J., Hinderer, M., 2016b. Evolution of the western East African Rift System reflected in provenance changes of Miocene to Pleistocene synrift sediments (Albertine Rift, Uganda). Sedimentary Geology, 343, 190–205.

Schneider, S., Hornung, J., Hinderer, M., 2017. Evolution of the northern Albertine Rift reflected in the provenance of synrift sediments (Nkondo-Kaiso area, Uganda). Journal of African Earth Sciences, 131, 183–197.

Schneider, S., Hornung, J., Hinderer, M., in prep. Garnet and rutile mineral chemistry and zircon U-Pb ages of modern river sands along the western East African Rift (Albertine Rift, Uganda).

Schumann, A., Schenk, V., Kulyanyingi, P. K., Morelli, C., Barton, E., Garbe-Schonberg, D., 2004. Evidence for the widespread occurrence of neo-Archean GGM-type granitoids in eastern Uganda: Orleans, Abstracts, 20th Colloquium of African Geology, 366.

Simon, B. 2015. Rift du Lac Albert, Ouganda, Rift Est Africain : Déformation, érosion, sédimentation et bilan de matière depuis 17 Ma, Université de Rennes 1, Rennes, 403 pp.

Simon, B., Guillocheau, F., Robin, C., Dauteuil, O., Nalpas, T., Pickford, M., Senut, B., Lays, P., Bourges, P., Bez, M., 2017. Deformation and sedimentary evolution of the Lake Albert Rift (Uganda, East African Rift System). Marine and Petroleum Geology, 86, 17–37.

Sircombe, K. N., 2000. Quantitative comparison of large sets of geochronological data using multivariate analysis: a provenance study example from Australia. Geochimica et Cosmochimica Acta, 64, 1593–1616.

Stern, R. J., 1994. Arc assembly and continental collision in the Neoproterozoic East African Orogen: Implication for the consolidation of Gondwanaland. Ann. Rev. Earth. Plan. Sci. 22, 319–351.

Talbot, M. R., Williams, M. A., 2009. Cenozoic evolution of the Nile Basin. In: Dumont, H. J. (Ed.), The Nile: Origin, Environments, Limnology and Human Use, Springer Netherlands, pp. 37-60.

Taylor, R. G., Howard, K. W. F., 1998. Post-Palaeozoic evolution of weathered landsurfaces in Uganda by tectonically controlled deep weathering and stripping. Geomorphology, 25, 173–192.

Taylor, R. G., Howard, K. W. F., 1999. The influence of tectonic setting on the hydrological characteristics of deeply weathered terrains: evidence from Uganda. Journal of Hydrology, 218, 44–71.

Thomas, W. A., 2011. Detrital-zircon geochronology and sedimentary provenance. Lithosphere, 3, 304–308.

Trauth, M. H., Maslin, M. A., Deino, A., Strecker, M. R., 2005. Late cenozoic moisture history of East Africa. Science, 309, 2051–2053.

Van Achterbergh, E., Ryan, C. G., Jackson, S. E., Griffin, W. L., 2000. Data reduction software for LA-ICPMS: Appendix. In: Sylvester, P. J. (Ed.), Laser Ablation-ICP-mass spectrometry in the earth sciences: principles and applications, Vol. 29. Mineralogical Association of Canada Short Course Series, pp. 239–243.

Van Damme, D., Pickford, M., 1995. The late Cenozoic Ampullariidae (Mollusca, Gastropoda) of the Albertine Rift Valley (Uganda-Zaire). Hydrobiologia, 316, 1–32.

Van Damme, D., Pickford, M., 1998. The late Cenozoic Viviparidae (Mollusca, Gastropoda) of the Albertine Rift Valley (Uganda-Congo). Hydrobiologia, 390, 171–217.

Van Damme, D., Pickford, M., 2003. The late Cenozoic Thiaridae (Mollusca, Gastropoda, Cerithioidea) of the Albertine Rift Valley (Uganda-Congo) and their bearing on the origin and evolution of the Tanganyikan thalassoid malacofauna. Hydrobiologia, 498, 1–83.

Velbel, M. A., 1999. Bond strength and the relative weathering rates of simple orthosilicates. American Journal of Science, 299, 679–696.

Wayland, E. J., 1925. Petroleum in Uganda. Nature, 115, 980–980.

Westerhof, A.B.P., Härmä, P., Isabirye, E., Katto, E., Koistinen, T., Kuosmanen, E., Lehto, T., Lehtonen, M.I., Mäkitie, H., Manninen, T., Mänttäri, I., Pekkala, Y., Pokki, J., Saalmann, K., Virransalo, P., 2014. Geology and Geodynamic Development of Uganda with Explanation of the 1:1,000,000 -Scale Geological Map. Geological Survey of Finland, Special Paper 55, 387 pages, 329 figures, 29 tables and 2 appendices.

Chapter 7

7 Synthesis

7.1 Provenance of the rift sediment – A statistical approach

In this thesis, a combination of different methodological approaches was applied on the rift sediment in the Albertine Rift in order to reconstruct their parent-rock assemblage(s). Overall, four different provenance suites were interpreted by combined information provided by the multi-proxy approach: (1) the gneissic-granulitic Archean North Uganda Terrane (NUT), (2) the Paleoproterozoic metasedimentary Rwenzori Fold Belt (RFB), (3) Neoproterozoic recycled (meta-)sedimentary rocks of the Bunyoro Group (BG), and (4) a mixed 'distal' provenance that includes rocks from the East African Orogen (EAO), Lake Victoria Terrane (LVT), West Tanzania Terrane (WTT), NUT etc. So far, the data collected from each method were more or less interpreted independently from each other, partly in different chapters/articles of this thesis.

This chapter aims at integrating the results obtained from the different applied methods by using a statistical approach. Multivariate statistical analyses of compositional data (e.g., principal component analysis [PCA], cluster analysis [CA], multidimensional scaling [MDS]) are powerful and informative tools in provenance studies, because they (i) allow for evaluating large data sets, (ii) present a reasonable way to identify patterns in data, (iii) underline their differences and similarities, and (iv) help to 'unmix' processes or sources (Smith, 2002; Dietze et al., 2012). One of the most common used dimension-reducing statistical techniques is PCA that allows transformation of a large set of correlated variables to a smaller set of uncorrelated variables, called principle components, that still contains most of the information of the original data set. Thus, this statistical/mathematical procedure aims at visualizing the relationship (similarities and dissimilarities) among entries by projecting high dimensional data down to two or three dimensions while preserving the relative distance between the observations (Aitchison, 1986). Strictly, PCA is a special case of classical MDS in which the dissimilarities are Euclidean distances (Vermeesch, 2013). Although it could be shown that both approaches lead to the same results (Lacher and O'Donnell, 1988; Vermeesch, 2013), PCA has the advantage that results can be visualized in biplots, which depict both the configuration and the endmember compositions (Vermeesch et al., 2016). Biplots thus facilitate the interpretation of statistical results regarding the underlying processes (Aitchison and Greenacre, 2002), which is seen here as a benefit for giving this method priority.

To interpret the data collected during this study in a meaningful way, the data set needs to be reduced to a small number of variables that reveal the highest variability. Thus, the goal of this approach is to find the best possible discrimination for the rift sediment and to associate it with different rock suites of the Ugandan basement. The characteristics of different basement rocks are known from studies on modern river sediments, which were analyzed by the same analytical approach (Schneider et al., 2016a, in prep.(a)). The river sediment covers three of the four implicated provenance suites. Each rock suite shows specific characteristics that may act as a fingerprint.

a) Provenance pattern in modern river sands

A total of 51 modern river sediments along the eastern flank of the Albertine Rift were analyzed for their bulk petrographic and geochemical composition as well as heavy mineral assemblages (Schneider et al., 2016a). Garnet chemistry is available from five samples, rutile chemistry from eleven samples and zircon U-Pb ages from nine samples (Schneider et al., in prep.(a)).

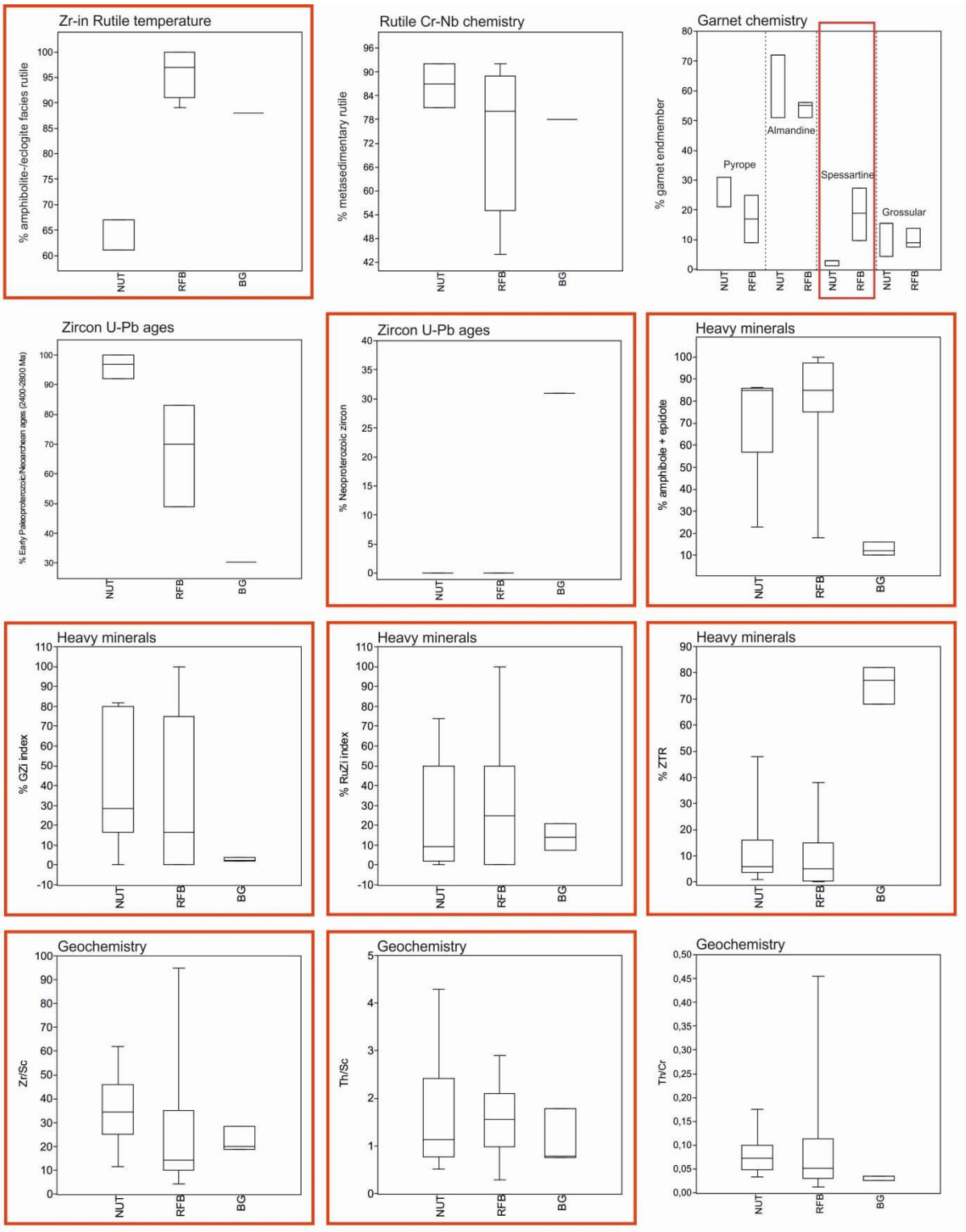

Continued on the next page.

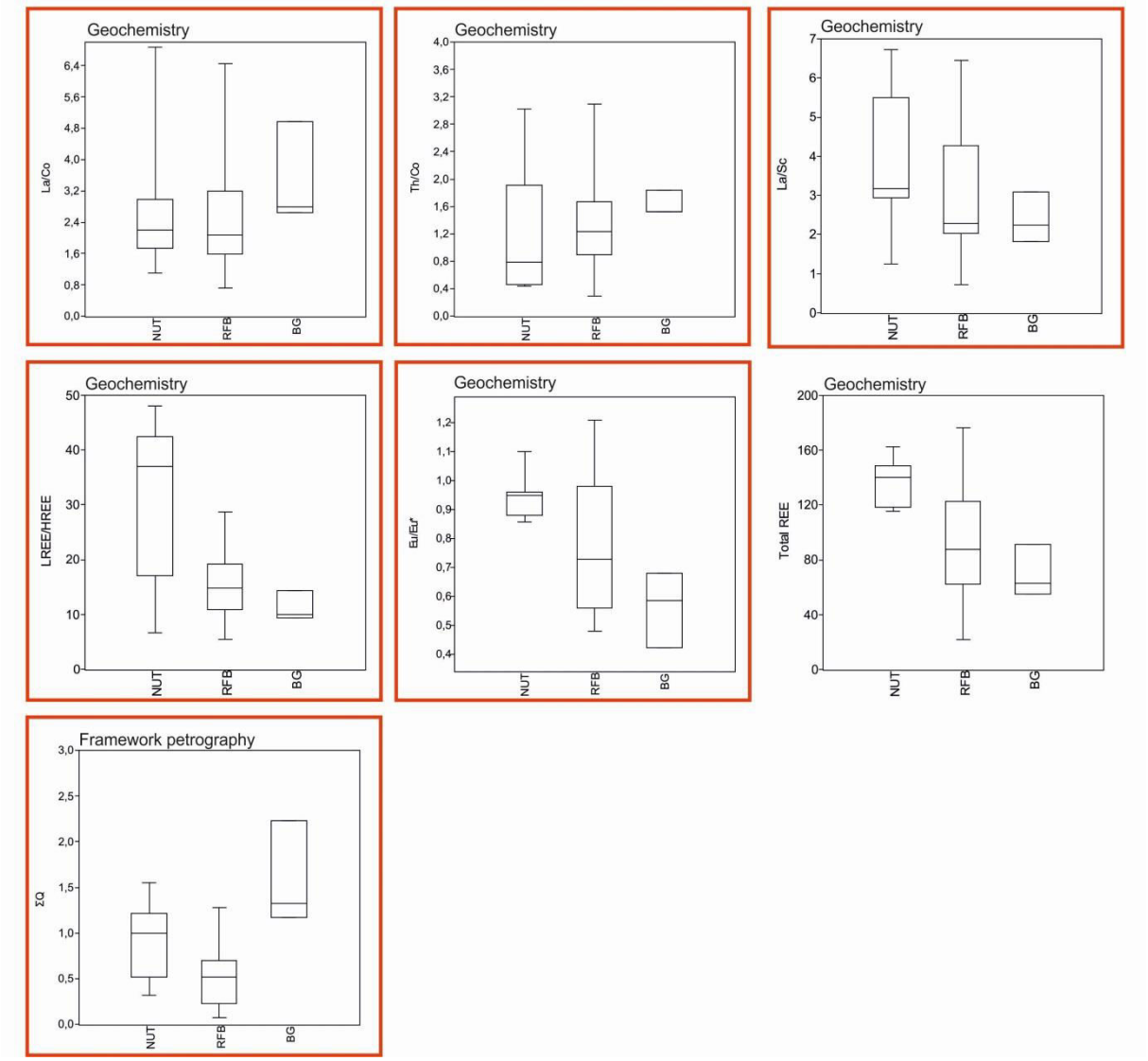

Figure 7-1. Box plots showing the variability of provenance-reliable parameters in modern river sediments that drain different rock suites of the regional basement. Parameters framed in red boxes depict the strongest variability and were chosen for statistical treatment (PCA) of the data set.
NUT = North Uganda Terrane, RFB = Rwenzori Fold Belt, BG = Buganda Group.

In a first step, the modern river samples were divided into three groups according to their underlying basement lithology.

a. *North Uganda Terrane (NUT)* – representative for the entire Ugandan Archean basement
b. *Rwenzori Fold Belt (RFB)* – Paleoproterozoic metasedimentary and granitoid rocks, partly intermingled with Archean gneiss
c. *Bunyoro Group (BG)* – Neoproterozoic recycled (meta-)sedimentary rocks

Only samples that allocate to one of these lithologies unequivocally were selected, i.e., sediment that represents a mixture of different basement suites is not considered for data evaluation.

To single out the characteristics of the three source areas, the most reliable provenance parameters from every available method were selected:

- Bulk rock petrography: ∑Q (= total quartz)
- Bulk rock geochemistry: La/Co, Th/Co, Th/Cr, La/Sc, Th/Sc, Zr/Sc, La_N/Yb_N, Eu/Eu*, ∑REE
- Heavy minerals: % of amphibole + epidote, ZTR, RuZi, GZi
- Garnet chemistry: % of pyrope, % of almandine, % of spessartine, % of grossular
- Rutile chemistry: % of amphibole-facies rutile, % of metasedimentary rutile
- Zircon U-Pb ages: % of early Paleoproterozoic/Neoarchean ages (2400–2800 Ma), % of Neoproterozoic zircon

Both, the total quartz content (∑Q) and the ZTR index reflect the occurrence of ultrastable minerals in the sediment and might therefore be influenced by external controlling factors such as recycling and weathering (e.g., Johnsson, 1993; Morton and Hallsworth, 1999). However, in case of this study, these parameters are seen as valuable provenance indices for recycled sediment of the Bunyoro Group. Moreover, the Eu-anomaly (Eu/Eu*) might also be partly sensitive to weathering processes as indicated by studies on modern river sand (Schneider et al., 2016a). Therefore, only 'unweathered' samples from the Rwenzori Mountains were selected for characterization of the NUT and RFB suites in order not to falsify the data.

Garnet and rutile chemistry as well as zircon geochronology were applied on only few river sediments, and the results may be partly statistically insignificant. This is especially the case for the Bunyoro Group for which only one sample has been analyzed for rutile chemistry and zircon geochronology. Garnet chemistry is not available at all for the Bunyoro Group.

Fig. 7-1 illustrates the variability of provenance-reliable variables obtained from the different applied methods for the modern river sand. Samples from the Bunyoro Group usually show the strongest contrast between all three groups. Compared to the samples from the NUT and RFB, they show distinct higher values for ∑Q, ZTR, Neoproterozoic zircon, La/Co and Th/Co, and lower values for amphibole + epidote, the GZi index, La_N/Yb_N, Eu/Eu*, ∑REE, Th/Cr, and Neoarchean zircon. The NUT and RFB exhibit strong overlap concerning many variables. This is especially true for heavy mineral spectra and bulk geochemical data. An exception are REE values (La_N/Yb_N, Eu/Eu*, ∑REE), which are generally higher in NUT samples. The strongest variation between the NUT and RFB is reflected by results obtained from varietal studies. Sediment from the RFB is characterized by higher values for amphibolite-facies rutile and spessartine-rich garnet, whereas the NUT naturally has higher amounts of Neoarchean zircon.

Based on the discrimination pattern of the three major rock lithologies of the Ugandan basement, following variables are considered for statistical treatment of the rift sediment:

- the geochemical ratios La/Sc, La/Co, Th/Co, La_N/Yb_N, Eu/Eu*,
- the total quartz content (∑Q = monoquartz + polyquartz + chert),
- the heavy mineral indices RuZi, GZi, and ZTR,
- the sum of amphibole and epidote,
- the spessartine concentration of garnet,
- the proportion of amphibole-/eclogite-facies rutile, and
- the amount of Neoproterozoic zircon.

The chosen variables best mirror changes in the provenance of the studied sediment.

b) Principal Component Analysis (PCA) / Biplot analysis

Calculation of the PCA was performed using the free software package PAST – PAlaeontological Statistics (Hammer et al., 2001). All data obtained during this study belong to the group of compositional data, e.g., they are non-negative and sum up to 100%, and are thus dependent on each other. In order to treat the data set systematically, all variables were normalized by division of their standard deviations by using the correlation matrix function (normalized var-covar) and transformed into centered log-ratio coordinates (Aitchison and Egozcue, 2005). Data points are illustrated in a scatter plot (biplot) showing the first two principle components. Biplots are an ideal way for graphic representation of the variability of covariance data sets, because they represent both the samples and the variables of compositional data (Gabriel, 1971; Aitchison, 1990). The principle components (or eigenvectors) represent linear combinations of the original variables. Their direction in a particular orthogonal dimension explains their contribution to the variance of the data set. The first principal component has the strongest influence on the variability in the data, whereas each succeeding component determines the remaining variabilities.

For biplot interpretation, following information should be kept in mind (von Eynatten et al., 2003):

(1) The squared distance between the variable and the origin of the biplot (corresponds to the center of the whole data set) matches the variance of the variable, i.e., a small angle between the line of a variable and the axis implies a strong influence of the variable on the corresponding principal component.
(2) The squared distance between two variables is a measure for the variance between these variables, i.e., the ratio between variables that plot close together within the biplot is nearly constant.
(3) The distance between two data (sample) points represents the (dis-)similarity of the two samples, i.e., clustering of samples within the biplot implicates similarities in compositional pattern.

The result of the PCA is shown in Fig. 7-2. The first two principle components explain ~63% of the total variance of the data set. Overall, four major groups are distinguishable; each of them correlated with a major basement terrane in the study area. Each provenance suite occupies one field of the biplot. Field 1 is determined by the GZi and RuZi indices and represents input from Archean basement rocks (NUT). Field 2 includes the spessartine concentration of garnet and the proportion of amphibole-/eclogite-facies rutile. This group is highly associated with the RFB. The variable for the total content of amphibole and epidote clusters largely between the two fields, because these heavy minerals are related to both the NUT and RFB. Field 3 is controlled by the total quartz content ($\sum$Q), as well as La/Co and Th/Co ratios and linked to the Bunyoro Group. Neoproterozoic zircon in conjunction with a second cluster containing La_N/Yb_N, La/Sc and Th/Sc rule Field 4. This field represents a fourth provenance with input from mainly acidic Neoarchean and Pan-African rocks (e.g., EAO). The variable for ZTR is afflicted to both Field 3 and Field 4, which reflects the high amount of ultrastable heavy minerals (e.g., zircon, tourmaline, and rutile) in these lithologies.

Clustering of the rift sediment within the plot shows distinct separation between the samples of each group that supports major interpretations proposed during this thesis. There is strong similarity between the sand of Group 1 from the Nkondo-Kaiso area (Nkondo Fm., Warwire Fm., Kyeoro Fm.) and Group 2 from the Kisegi-Nyabusosi area (Nyaburogo Fm., Nyakabingo Fm.). Generally, the samples are mostly located within Field 1, which is due to their abundant amount of feldspar, amphibole-/epidote-dominated heavy mineral assemblages, low ZTR indices and relatively lower values for provenance sensitive La_N/Yb_N, La/Sc, Th/Co, and La/Co ratios. All of these samples are interpreted to receive major input from the local Archean basement of the NUT. As expected, the

samples of Group 3 from the Kisegi-Nyabusosi area (Katorogo Fm., Nyabusosi Fm.) plot in Field 2. Their composition is largely similar to the sand shed by the RFB. This group is assumed to (partly) represent erosion of the uplifting Rwenzori Mountains. The samples from Group 1 (Kisegi Fm., Kakara Fm., Oluka Fm.) of the Kisegi-Nyabusosi area are associated with Field 4. Their composition is characterized by quartz, K-feldspar and minor plagioclase, a considerable amount of Pan-African zircon grains, high ZTR values, missing Eu-anomaly and high values of the provenance sensitive element ratios La/Sc, Th/Sc, and Zr/Sc. This sediment is mainly associated with acidic Neoarchean and Pan-African rocks carried into the Albertine Rift by a large-scale river network. Sediment from Group 2 of the Nkondo-Kaiso area is rich in quartz and shows also high ZTR values. In contrast to most sediment from Group 1 of the Kisegi-Nyabusosi area, they show marked depletion in mobile elements and a lower amount of feldspar. The PCA indicates a high compositional maturity that is most likely related to input from recycled (meta-)sedimentary rocks of the Bunyoro Group.

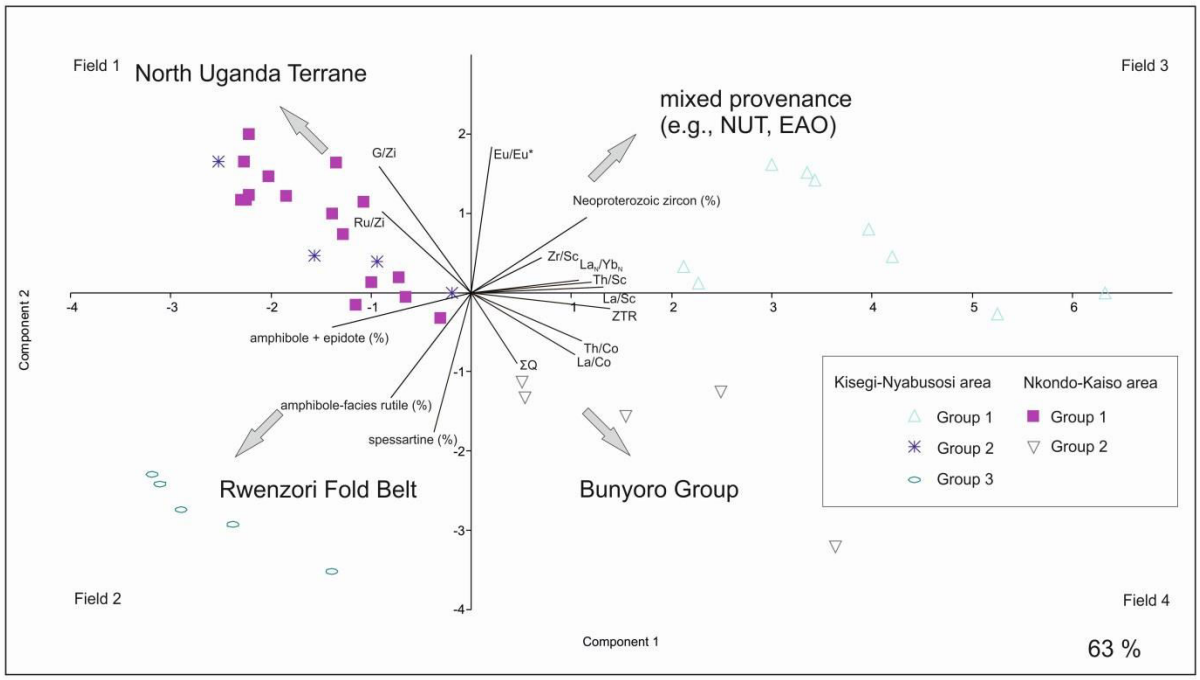

Figure 7-2. Biplot for the rift fill in the Kisegi-Nyabusosi area and Nkondo-Kaiso area discriminating the sand according to their major provenance. Axes are the first and second principal components. The percentage indicates proportions of total variability explained by an individual biplot.

7.2 Sedimento-tectonic model for the evolution of the Albertine Rift

Sedimentary provenance analysis of the rift sediment in the Albertine Rift indicates two major compositional changes largely at the Miocene-Pliocene transition (~5.0 Ma) and Pliocene-Pleistocene transition (~2.6 Ma), that are likely the result of changes in source rocks caused by shifts in the sediment supply system (Schneider et al., 2016b, 2017, in prep.(b)). Changes in drainage pattern are likely to be linked to different tectonic and structural phases affecting the Albertine Rift during its evolution. Based on these new insights into erosion, sediment transfer, and uplift pattern, a paleotectonic model that presents a more detailed picture of the spatial-temporal evolution of the northern western branch of the East African Rift can be established (Fig. 7-3, 7-4).

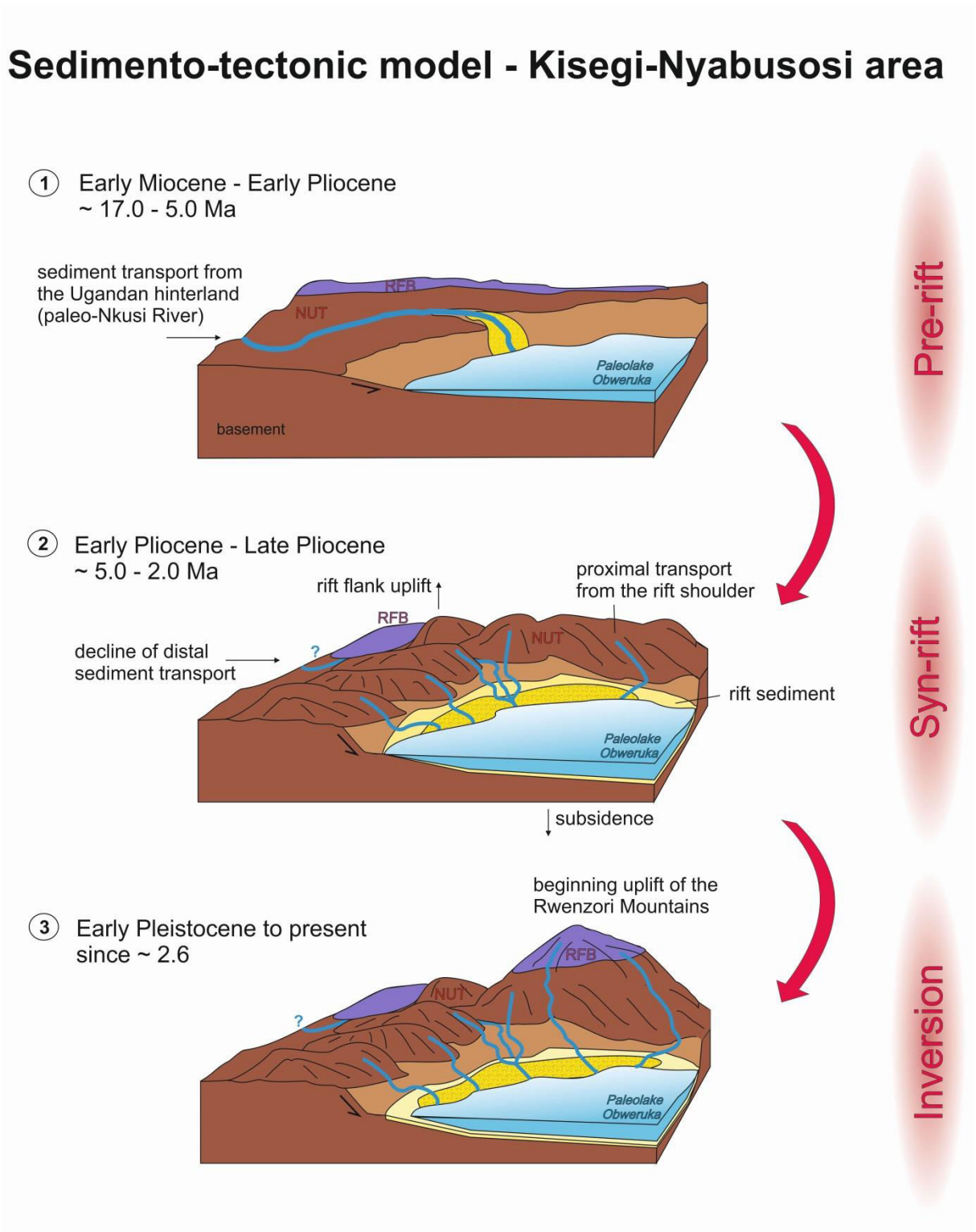

Figure 7-3. Provenance-based sedimento-tectonic model for the Kisegi-Nyabusosi area.

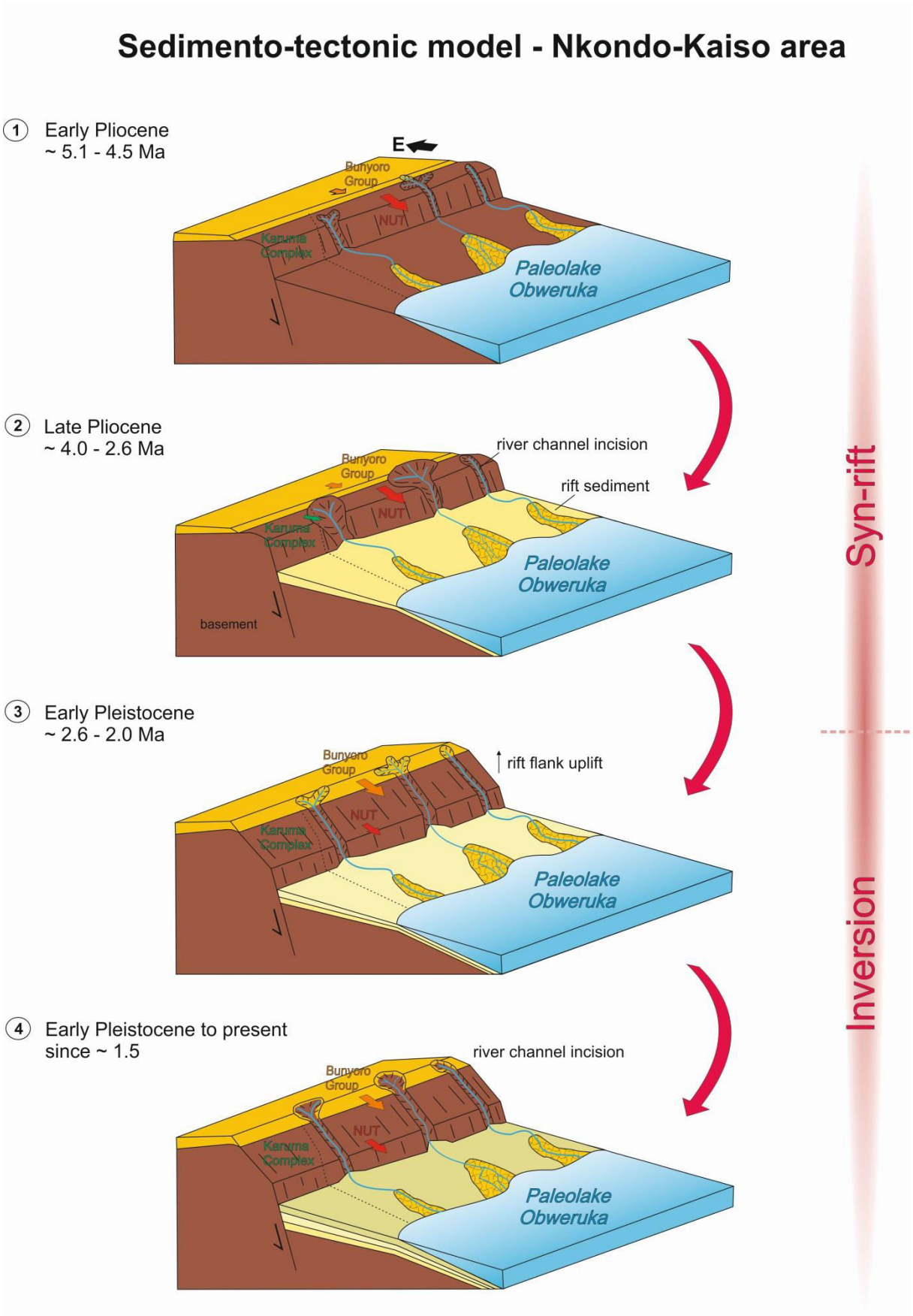

Figure 7-4. Provenance-based sedimento-tectonic model for the Nkondo-Kaiso area.

Pre-rift phase (~17.0–5.0 Ma)

The onset of sedimentation in the Albertine Rift is characterized by first faulting and deposition of the fluvial Kisegi Formation in a more or less shallow downwarp located southwest of modern Lake Albert (Pickford et al., 1993). The Kisegi valley in the southern rift basin is the only known place in the graben, where this earliest sediment is exposed. The age of initial sedimentation is still controversially discussed, but recent studies plead for an initial age of 17.0 ± 0.8 Ma (Simon, 2015).

As is known from facies analysis and biostratigraphic work (Roller et al., 2010; Lukaye et al., 2016), the depositional environment was characterized by limited accommodation space where strongly amalgamated sand bodies were accumulated in an alluvial plain setting. At this time, sedimentation in the rift was mainly accommodation-controlled (Roller et al., 2010).

Transport of sedimentary detritus within a fairly stable fluvial environment is reflected by the relative monotonous composition of these earliest rift sediments, dominated by quartz, abundant feldspar, minor plagioclase and quartz-/feldspar-rich rock fragments. Garnet and rutile chemistry indicate a mixed provenance from high-grade to very high-grade (amphibolite- to granulite-facies) metacrustal and metasedimentary rocks. This together with zircon-controlled heavy mineral suites, high values of the provenance sensitive element ratios La/Sc, Th/Sc, and Zr/Sc, high ZTR and ∑REE, as well as dominant occurrence of Neoarchean zircon ages suggests derivation from acidic Neoarchean rocks, such as the gneissic-granulitic Neoarchean North Uganda Terrane (NUT) in central and northern Uganda as well as the granite-greenstone suites of the Lake Victoria Terrane (LVT) and the West Tanzania Terrane (WTT) in southern Uganda. Separation of the different Neoarchean terranes (NUT, LVT, WTT) by, e.g. zircon U-Pb ages, is not feasible, because these rock suites show strong similarity in formation ages (~2.5–2.6 Ga). In addition, a high amount of Pan-African zircon ages suggests erosion of the at least 400 km away located Karamoja Belt belonging to the East African Orogen (EAO). Pan-African ages cannot be related to any other basement lithology on the Ugandan plateau. These ages are missing in modern river sands along the rift shoulder (Schneider et al., in prep. (a)), because these rivers are nowadays disconnected from the EAO. This in conjunction with some minor input from Paleoproterozoic (RFB) and Mesoarchean (Karuma Group) lithologies implies a widely-branched river network on the East African Plateau during the Miocene. In particular, the new zircon geochronological data validate existing drainage models that propose a large-scale westward directed river system that flowed from the Kenya Rift through the Ugandan Plateau and Albertine Rift towards the Congo Basin and further to the Atlantic Ocean before this continent-wide system was dissected by formation of the western branch of the EARS (Cooke, 1958; Bishop, 1965; Taylor and Howard, 1999; summarized in Pickford et al., 1993). The dominance of the most durable minerals (ZTR, garnet) might also attest to a long-distance transport.

Ongoing rifting in the Albertine Rift manifests in sedimentation by transition from an accommodation-controlled system to a supply-controlled system during which the upper Kisegi, Kakara and Oluka formations deposit. An increase of finer and thinner beds towards the end of the Miocene reflects the change from mainly fluvial conditions towards a palustrine/shallow lacustrine depositional setting. The distinct change in sedimentology and facies since the upper Kisegi Formation was interpreted by some authors to mark first rifting in the Albertine Rift (Roller et al., 2010; Lukaye et al., 2016), whereas the boundary between the Kakara Formation and Oluka Formation is assigned to represent the onset of Paleolake Obweruka that drowned the study area from ca. 8 Ma (Ebinger, 1989; Pickford et al., 1993). The change in the depositional environment and sedimentation pattern had only minor impact on the composition of the sediment, which remains more or less the same for another ~3.0 Ma. The increase of finer grain size fractions might be seen in sediment composition by a slight, but constant decrease in rock fragments towards the Oluka Formation, because rock fragments tend to be less abundant in finer grain size classes due to their decomposition into their individual components.

Some lower proportions of ultradense zircon together with minor increase of rutile, tourmaline, garnet and epidote might be due to the establishment of a lower-energetic regime. High fluctuations within heavy mineral assemblages probably also result from grain sorting effects caused by a relative high frequency of paleo-environmental facies shifts and related transport processes. However, a correlation between grain size, depositional environment and the abundance of certain mineral species is not indicated. The occurrence of similar types of detrital components, together with analogue zircon U-Pb ages, and chemical data of garnet and rutile throughout the lower part of the Kisegi-Nyabusosi area indicates constant input from the same source for the Miocene sediment. Although, local sorting effects might cause some fluctuations in the ratio of certain mineral species, the overall composition is in first place controlled by the source rock(s).

As the regional drainage still freely enters the basin, the influence of rift shoulder topography, assigned to have already begun to evolve along the basin margins (Pickford et al., 1993), had not yet been prominent enough to severely influence local drainage pattern. It is therefore likely that the formation of Palaeolake Obweruka was not solely initiated by a period of faulting in the Albertine Rift, but has also been triggered by an increase of humidity in the late Miocene.

There is commonality between most researchers concerning the climate evolution during the Miocene. Abundant evaporitic gypsum precipitations together with the occurrence of fossil ferns and pollen typical for dry open grassland environments (internal data from my colleague D. Brüsch) support the assumption of a semi-arid local climate at the beginning of rifting (Kisegi Fm.). Based on facies analysis of the sedimentary successions (Roller et al., 2010) and the appearance of abundant fossil fruits in upper Miocene strata (Pickford et al., 1993), a climate shift from hot and dry (semi-arid) climate in the beginning of sedimentation to a more humid climate towards the Oluka Formation was suggested. Lukaye (2009) already proposed a climate change during the upper Kisegi Formation, where he noted a change in palynofacies associations.

The proposed climate shift is not inferred by the composition of the sediment. A change from semi-arid to more humid conditions would probably result in higher weathering intensities and leaching of ‘instable’ constituents, such as ferromagnesian minerals or feldspar. However, the occurrence of abundant feldspar minerals throughout the stratigraphy, constant K-feldspar/plagioclase ratios and K/Na ratios, as well as low loss of mobile elements reflected by low to moderate weathering indices (CIA, WIP) speaks against intensification of weathering towards the late Miocene.

In the Nkondo-Kaiso area, Miocene sediment is not exposed. Sedimentation in this region started not before the early Pliocene (~5.1 Ma).

Syn-rift phase (~5.0–2.6 Ma)

The database of this study shows a distinct change in the composition of the sediment in the Kisegi-Nyabusosi area between the Oluka Formation and Nyaburogo Formation at ~5.0 Ma, interpreted to represent the transition from the pre-rift into the syn-rift stage characterized by enhanced subsidence of the rift floor and uplift of rift shoulders. The first provenance shift in the Kisegi-Nyabusosi area is indicated by several parameters, including heavy mineral assemblages, trace element ratios and zircon age data together with slight shifts in the modal composition. The dominance of Neoarchean zircon together with epidote-amphibolite-rich heavy mineral suites, high values for RuZi and GZi indices, and high-grade metamorphic garnet and rutile strongly resemble the signature of rivers draining the NUT, which makes this terrane the most probable source for the Pliocene sediment. Some Paleoproterozoic zircon grains indicate minor contribution from Paleoproterozoic rocks of the RFB. The absence of Neoproterozoic zircon populations suggests disruption of sediment transport from

northeastern sources. Streams delivering sediment to the Kisegi-Nyabusosi area (Nyaburogo and Nyakabingo formations) were probably deflected to the margin of the Albertine Basin and sediment transport was now mainly restricted to proximal sources with the rising rift shoulders representing the most dominant sediment source. This assumption is supported by lack of low-grossular garnet in the Nyaburogo Formation, which reflects reduction of the catchment area. The high-grossular garnet in this formation matches the chemical composition of garnet carried by modern rivers draining the NUT of the northern Rwenzori Mountains (Schneider et al., in prep.(a)), hinting to input from southern sources. Reoccurrence of high-grade low-grossular garnet accompanied by an increased amount of garnet and ZTR in the following Nyakabingo Formation might be either signify expansion of the drainage system towards the rift plateau of the Albertine Rift, where modern river sands carry these garnet grains (Schneider et al., in prep.(a)), or might be seen as an indicator for river incision and unroofing of the regional basement leading to erosion of higher metamorphic stratigraphic levels.

Overall, the change of provenance pattern in the Kisegi-Nyabusosi area coincides with a period when Lake Obweruka became large and deep (Pickford et al., 1993; Van Damme and Pickford, 2003), and correlates well with a Maximum Flooding Surface (S4m) at 4.9 Ma (Simon, 2015). It seems conceivable that, only at this time, rift shoulders and accommodation zones became prominent topographic barriers that formed a basin that was closed on all sides and influenced sediment transport into the rift. The provenance-based tectonic model lags ~1 Ma behind a basin-wide unconformity at 6.2 Ma, interpreted by Simon (2015) to represent the transition into the syn-rift stage. It might therefore be likely that the source-to-sink system needs a longer response time to adjust to the new regional conditions.

Initiation of sedimentation in the ~100 km further to the north located Nkondo-Kaiso area started only at ~5.1 Ma (Simon, 2015) with deposition of the lacustrine Nkondo Formation and mainly coincides with the onset of the syn-rift stadium in the Kisegi-Nyabusosi area. Epidote-/amphibole-dominated heavy mineral assemblages together with high-grade (amphibolite-/granulite-facies) garnet and rutile as well as dominance of Neoarchean zircon spectra suggest major derivation from the NUT, which crops out close to the fault scarp. Some Neoproterozoic zircon grains indicate minor input from the (meta-)sedimentary Bunyoro Group, which overlies parts of the NUT east of the study area. A minor compositional change is observed between the Nkondo Formation and the following Warwire Formation at ~4.0 Ma that matches the transit between the Nyaburogo Formation and Nyakabingo Formation in the southern rift basin. A slight increase of amphibole, garnet, sillimanite, and plagioclase together with few Mesoarchean grains that were not investigated in the underlying Nkondo Formation hints to some additional input from the granulitic Karuma Complex located northeast of the study area, and suggests either northward progradation of rivers or increased bedrock incision leading to erosion of fresher rock material. The minor shift in sediment composition is also manifested in sedimentation by the transition from deeper lacustrine towards nearshore lacustrine strata, as well as a widespread unconformity between both formations assigned to represent a faulting episode (Pickford et al., 1993). Garnet and rutile chemistry as well as zircon ages remain similar between both formations, suggesting relative stable input from analogue source rocks.

Pliocene climate conditions are controversially discussed. Some researchers assume that the climate was humid during the early Pliocene (Dechamps et al., 1992) and became again more arid towards the late Pliocene (Dechamps et al., 1992; Jacobs and Deino, 1996). Roller et al. (2010) proposes a tropical climate throughout the entire Pliocene, whereas Lukaye (2009) suggests a drier climate during the early Pliocene. However, as for the previous pre-rift phase, climate changes are not inferred by the composition of the sediment.

Rift inversion phase (~2.6–1.0 Ma)

Well-correlated compositional changes in both the Kisegi-Nyabusosi area and Nkondo-Kaiso area at ~2.6 Ma mark a further period of tectonic movement in the Albertine Rift that is related to the uplift of the Rwenzori Mountains. Provenance pattern, e.g., the occurrence of spessartine-rich garnet and 'colder' Zr-in-rutile temperatures in Pleistocene sand of the Kisegi-Nyabusosi area (Katorogo Fm. and Nyabusosi Fm.) hint to input from lower-grade (amphibolite-facies) metasedimentary sources, which suggests major derivation from the RFB that stretches along southwestern Uganda towards the Rwenzori Mountains. The appearance of pinkish zircon grains in the rift sediment underlines major transport from the Rwenzori Mountains, because such zircon crystals are only observed in significant amounts in rivers draining this mountain range (Schneider et al., in prep.(a)). The major uplift of the Rwenzori Mountains is likely to have started during the early Nyabusosi Formation (~1.8 Ma) as reflected by increase of rock fragments and mica. At this time, the rifting process in the Albertine Rift is dominated by rapid uplift and erosion of rift shoulders.

In contrast, sediment supply in the Nkondo-Kaiso area is still mainly from proximal sources along the rift margin. However, the data set shows higher contents of ultrastable minerals (quartz, ZTR) especially in the Kaiso Village Formation that implies increased input from recycled sediments of the Bunyoro Group. A rejuvenation trend in Neoarchean zircon ages suggests that the catchment area might have expanded further to the east as rifting proceeds, probably as consequence of incision of former footwall-derived rivers. Overall, provenance pattern imply that drainage pathways did not change significantly and sediment transport persisted from relatively local sources.

The second provenance change correlates well with a major basin-wide unconformity at 2.7 Ma (Simon, 2015) as well as thermochronological data (MacPhee, 2006; Bauer et al., 2010, 2012, 2015) indicating exhumation of the Rwenzori Mountains at the Pliocene-Pleistocene boundary. A major phase of aridity well identified at ~2.5 Ma (Bonnefille, 2010) contrasts some higher values of weathering indices (CIA) in the sands, which in this case might be rather controlled by provenance than by weathering.

7.3 The Albertine Rift on an EARS-wide scale

A primary goal of this study was to correlate the different sediment exposures deposited in the southern (Kisegi-Nyabusosi) and central (Nkondo-Kaiso) part of the Albertine Rift and to put them into proper context with regional events in other domains of the EARS.

Miocene-Pliocene transition (~5.0 Ma) – the first provenance change in the Kisegi-Nyabusosi area at ~5.0 Ma can be correlated with several tectonic events in the EARS (Fig. 7-5). Major tectonic activity at this time is chiefly associated with main rifting in the eastern rift branch, largely expressed by major subsidence and development of topography (Macgregor, 2015).

In Ethiopia, this period corresponds with southward propagation of the rift sector, as well as growth of the topography, as revealed by studies on river incision (Gani et al., 2007) and surge in Nile sedimentation (Macgregor, 2012). Major fault movements are known from the Kenya Rift (Pickford et al., 1993), expressed by main subsidence and sedimentation in the Turkana, Omo and Chew Bahir Rifts (Macgregor, 2012), and also by thermochronological data, which indicate denudation and uplift of the rift shoulders largely between 7 and 4 Ma on the eastern side and between 5 and 2 Ma on the western side of the Central Kenyan Rift (Spiegel et al., 2007). The western rift branch is characterized by formation and subsidence of the northern Tanganyika Basin (Cohen et al., 1993) and northern Malawi Basin (Ebinger, 1989; Ebinger et al., 1984, 1987; Flannery and Rosendahl, 1990), rifting in

the Kigoma Basins (Macgregor, 2015) and the Ruzizi Basin (Chorowicz, 2005), as well reactivation of the Rukwa Basin (Wescott et al., 1991).

Pliocene-Miocene transition (~2.6 Ma) – the second provenance change at ~2.6 Ma, coeval with the initiation of the uplift of the Rwenzori Mountains, can also be correlated to other parts of the EARS that show tectonic pulses at the same time (Fig. 7-6). It could be related to major faulting and subsidence in the Kenya Rift (Pickford, 1994), rift propagation of the Malawi Rift and Tanyanyika Rift (Macgregor, 2015), rifting in the southern Main Ethiopian Rift (Bonini et al., 2005), and formation of a full graben in the southern Gregory Rift (Saemundsson, 2010). This pulse also matches extensional phases observed for the Natron, Manyara and Eyasi Basins near the North Tanzanian Divergence (Foster et al., 1997; Le Gall et al., 2008).

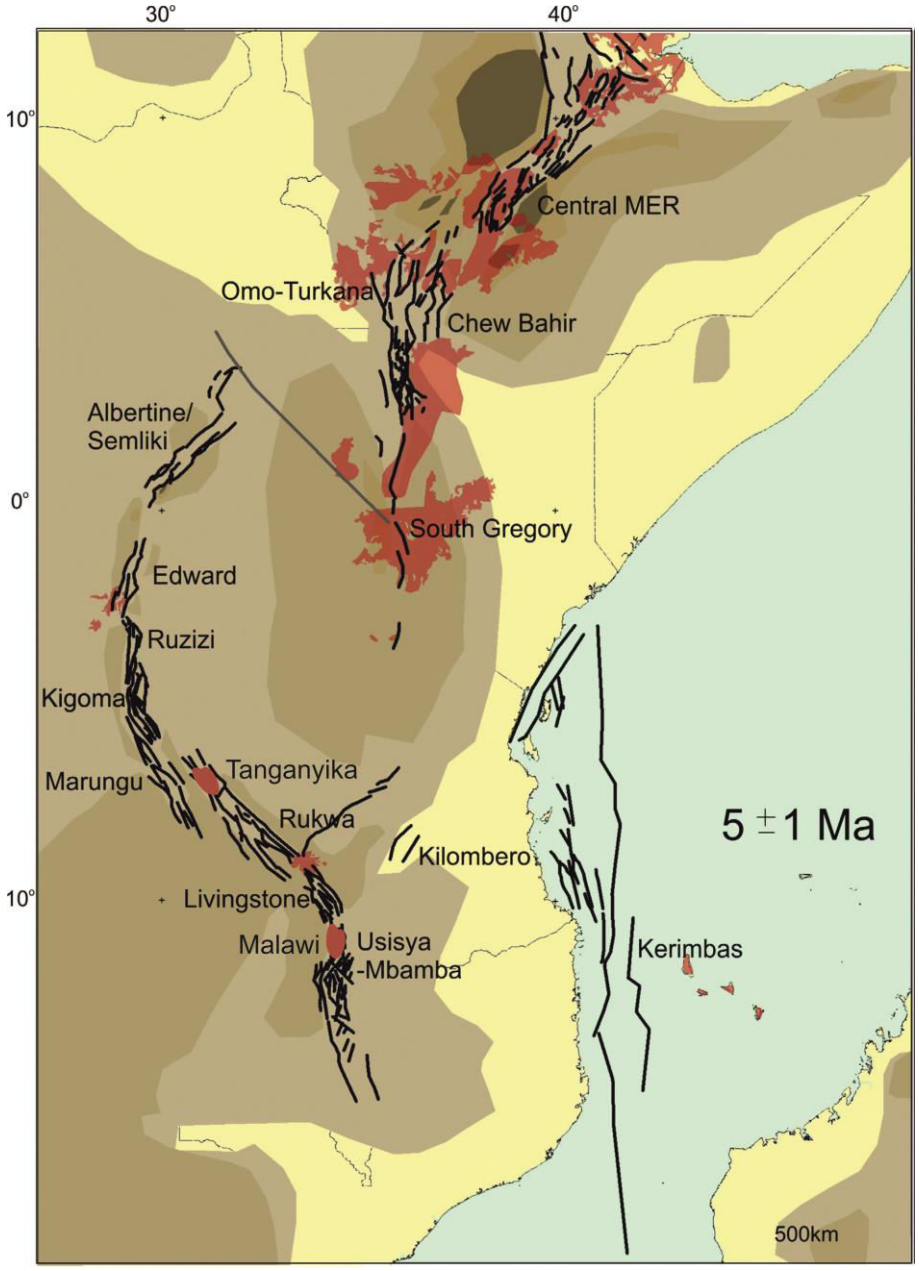

Figure 7-5. Time reconstruction map showing key areas of major tectonic events in the EARS at 5 ± 1 Ma (modified after Macgregor, 2012).

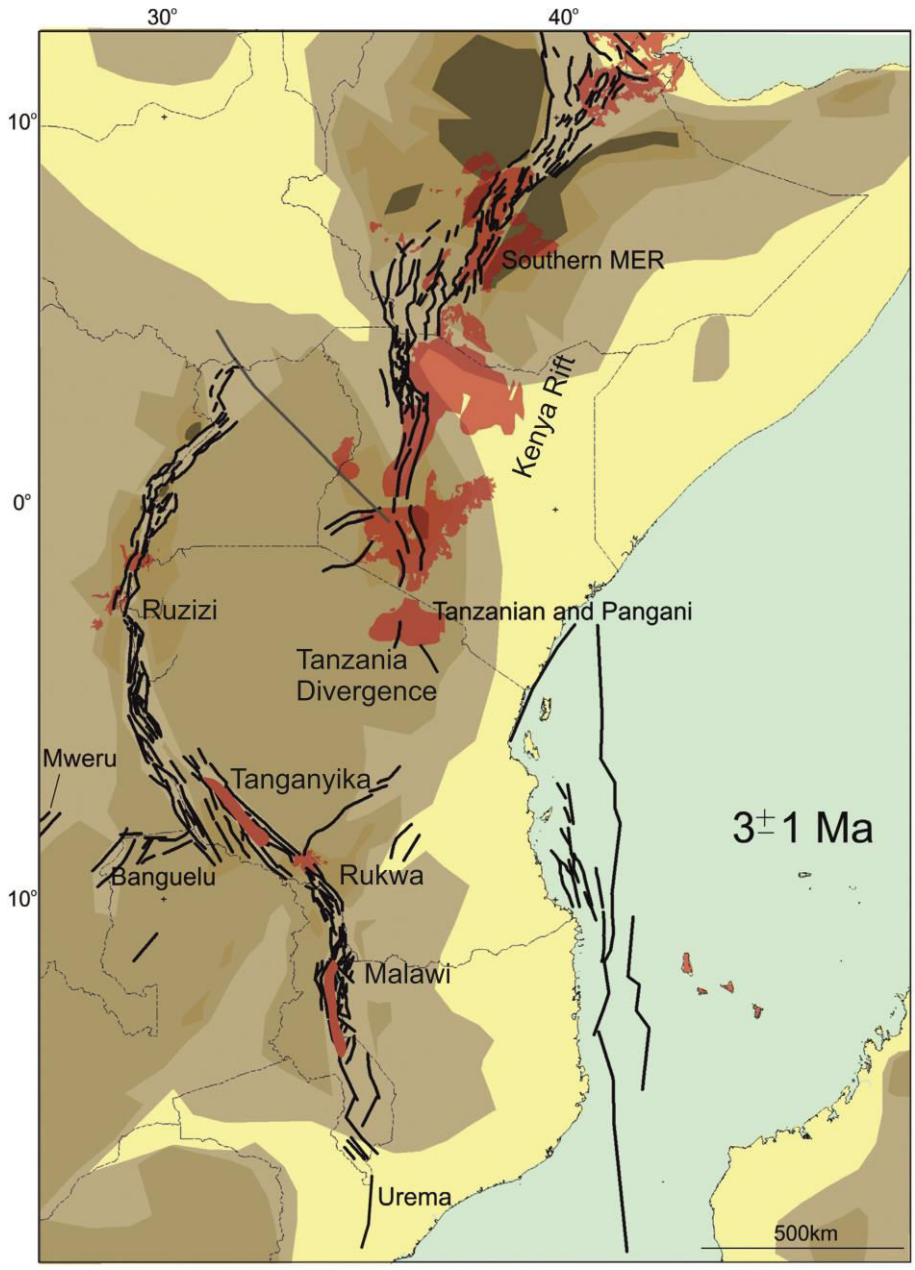

Figure 7-6. Time reconstruction map showing key areas of major tectonic events in the EARS at 3 ± 1 Ma (modified after Macgregor, 2012).

7.4 The application of multi-proxy sedimentary provenance analysis in tropical rift settings

The potential of sedimentary provenance analysis (SPA) for reconstructing paleo-earth systems has been demonstrated in multitude studies (e.g., Weltje and von Eynatten, 2004; Caracciolo et al., 2016). Provenance data can play a key role in unravelling (1) paleogeographic/-geologic settings, (2) the nature of uplift, (3) igneous and crustal evolution, (4) sediment recycling, (5) drainage pattern, (6) depositional systems, and (7) climatic conditions by 'simply' reading the composition and texture of sediments or sedimentary rocks. Despite the fact that the application of SPA may also be highly promising in rift settings, where the displacement geometry along the border fault system mainly

controls sediment-supply rates, accommodation space, regional drainage and climate pattern, this kind of study is still underrepresented in the EARS.

In this study, SPA has been applied on the Neogene rift infill and modern river sediment in and around the Albertine Rift in the western branch of the EARS with the major aim to reconstruct the evolutionary history of this particular rift basin since its initiation in the Miocene. For several reasons, the Albertine Rift provided a superb opportunity to test the potential of SPA. Besides for a tectonically active rift setting, where thermal-induced rift-flank uplift results in contrasting climate, vegetation, and topography between low-relief rift plateaus and adjacent high-altitude horsts such as the Rwenzori massif, the Albertine Rift is also located in vicinity to the Equator where precipitation and average temperatures are among the highest on Earth. Such a climatic setting may provide a challenge in provenance studies, because chemical weathering may be so strong that provenance signatures may be largely lost. Furthermore, the regional geology along the Albertine Rift and Ugandan plateau shows strong commonality and exposed rocks mainly include crystalline metamorphic lithologies that entirely belong to the Precambrian basement of cratonic Africa, i.e., identification and separation of potential sediment sources provides a challenging task.

To tackle these difficulties and to reconstruct sediment provenance in a successful manner, a multi-proxy approach has been applied on both the modern sediment and rift sediment that involves a combination of different interdisciplinary methods that have been proven to be successful in many provenance studies. They include 'traditional' petrographic-mineralogical analysis (framework and heavy mineral studies), as well as 'innovative' geochemical (bulk rock geochemistry, single-grain garnet and rutile chemistry) and geochronological methods (Zircon U-Pb ages). The purpose of integrating different methods was to select parameters that are most suitable for identifying the proto-source of the sediment and that also allows identification of parameters most feasible for singling out external processes such as (chemical) weathering, hydraulic sorting, or mixing of detritus from varying host lithologies that might modify sediment during erosion, dispersal and deposition.

The study on modern river sediment taken along the rift shoulder of the Albertine Rift, including the Rwenzori Mountains, provided the base for this study and was mainly conducted to define the signature of different rock suites of the regional basement that can later be identified in the Neogene rift sediment. Compilation of a basal data set for some major basement lithologies seemed to be mandatory for this study, because several parameters, like garnet and rutile chemical data, are not available at all for Ugandan basement rocks.

The analysis of modern river sediment met expectations and led to two substantial findings. Firstly, climate and topography are important factors in controlling sand composition along the Albertine Rift. This study showed that modern sediment generation produces two types of sediment characterized by different weathering degree. Along the rift shoulder/plateau, where prolonged pedogenic processes lead to highly weathered regolith, even detritus derived from crystalline basement rocks reduced to quartzose sand with quartz content up to 98%. In contrast, the effect of chemical weathering is hampered in areas characterized by higher relief, here the Rwenzori Mountains, because of increased surface energy gradients/erosion rates resulting in only mildly weathered feldspar-/lithoclast-rich sand. The different degree of weathering intensity is well exemplified when comparing sediment that originates from Archean crystalline basement rocks exposed along the rift shoulder with quartz content of ~67%, K/Na ratio of ~2.3, ZTR of ~24 and CIA of ~90 with less weathered sediment derived from the same lithology exposed in the Rwenzori Mountains showing lower quartz content of ~45%, K/Na ratio ~1.2, ZTR of ~5 and CIA of ~65. Quantification of the weathering degree was best accomplished by petrographic and bulk rock geochemical data, including the ratio and texture of framework components (QFR), weathering indices (e.g., CIA, PIA), concentrations of mobile elements (K, Na, Ba, Sr, Rb), α-values as well as K_2O/Na_2O ratios, because all of these parameters are

able to give information about the loss of instable minerals (e.g., feldspar) and increase of stable minerals (e.g., quartz), respectively.

Most importantly for this study was the finding that original provenance signatures imprinted in the sediment can still be identified even in highly weathered sands. While the modal composition and major elements turned out to be commonly unsuitable to uncover initial provenance signatures, heavy minerals (assemblage and single-grain) and trace elements (including REE) proofed to be still selective. The data set shows that particularly heavy mineral assemblages and indices together with geochemical parameters are suitable for identifying sand derived from (meta-)sedimentary lithologies (Bunyoro Group), which compared to the surrounding crystalline basement rocks show higher values for ZTR (~77), La/Co (~3.7) and Th/Co (~1.6), and lower values for GZi (~3), La_N/Yb_N (~11), ∑REE (~74), and Eu/Eu* (~0.6). Separation of crystalline basement terranes, here the NUT and RFB, proofed not to be feasible by these parameters, because both suites show strong overlap in their framework grains, bulk geochemical composition, and especially heavy mineral assemblages, characterized by high amounts of epidote and amphibole (up to 100%). A clear separation between both terranes could be achieved by single-grain studies on zircon, garnet and rutile that certainly turned out to be powerful applications during this study. Both, garnet compositions and the Zr content in rutile are able to provide information about metamorphic conditions during rock formation and could therefore be used to separate sand derived from medium- to high-grade metamorphic rocks of the RFB showing predominantly amphibolite-facies rutile and spessartine-rich garnet, from sand derived from high- to very high-grade metamorphic rocks of the NUT, dominated by amphibolite- to granulite-facies rutile and almandine-rich garnet. Furthermore, Cr and Nb contents in rutile provide decent information about metapelitic (e.g., schist) and (meta-)mafic (e.g., Si-undersaturated volcanics) source lithologies even within the same major tectono-thermal unit (e.g., RFB). Zircon U-Pb geochronology refines the separation of both lithologies by showing Paleoproterozoic ages for the RFB and Neoarchean ages for the NUT. Because garnet, rutile and zircon could be usually clearly allocated to a certain lithology they were also able to uncover mixing of different rock types during sediment dispersal. However, as seen by studying river sediment from the (meta-)sedimentary Bunyoro Group, garnet, rutile and zircon might also be misleading. Because of their mechanical durability, they can survive more than one sedimentary cycle, which might lead to an incorrect interpretation of exclusively primary sources.

The results obtained from the modern sediment provided a fundamental base for source rock/area interpretation and could be largely transferred to the ancient rift sediment within the Albertine Graben on the basis of which provenance shifts at the Miocene-Pliocene transition (~5.0 Ma) and Pliocene-Pleistocene transition could be identified (~2.6 Ma).

In particular, the signature of the Archean NUT and Paleoproterozoic RFB could be clearly retrieved within the ancient sedimentary record. The dominance of Neoarchean zircon together with epidote-amphibolite-rich heavy mineral suites, high values for RuZi and GZi indices, and high-grade metamorphic garnet and rutile in the Pliocene successions of both, the Kisegi-Nyabusosi and Nkondo-Kaiso area, strongly resemble the signature of rivers draining the NUT along the rift shoulder, which made this terrane the most probable source for this part of the sedimentary record. On the other hand, the occurrence of almandine-spessartine garnet and lower amphibolite-facies Zr-in-rutile temperatures in the Pleistocene sediment of the Kisegi-Nyabusosi area could be correlated to the signature of rivers draining the RFB. However, specification of distinct supply areas within these terranes was not possible on the basis of these methodological applications. Final evidence for dominant sediment supply from the Rwenzori Mountains for the Pleistocene succession in the Kisegi-Nyabusosi area was only given by the occurrence of pinkish zircon grains in the rift sand, which are a common feature in

river sands draining the Rwenzori horst, and a higher immaturity of the modal composition pointing to enhanced erosion from uplifting basement rocks.

The analysis of modern river sand became even more important for sand shed by metasedimentary rock suites, here the Pleistocene sediment in the Nkondo-Kaiso area, characterized by high compositional maturity with high quartz contents, high element ratios, and ZTR-dominated heavy mineral suites, high weathering indices (e.g. CIA), low concentrations of mobile elements (K, Na, Ba, Sr, Rb), as well as high K_2O/Na_2O ratios. While in case of modern river sediment, all of these parameters could be used to separate higher weathered sediment from only mildly weathered sediment, they proofed to be misleading for the Pleistocene succession. Here, ratios and indices did not reflect increase in the weathering degree, but were caused by input from already altered material from (meta-)sedimentary rocks of the Bunyoro Group. The final proof for input from the Bunyoro Group could be derived by comparing the signature of the Pleistocene sediment with this of the river sediment draining this rock suite. Especially the high amount of tourmaline together with higher ratios for La/Co and Th/Co could be used to connect both suites. As was already shown by analysis of the modern river sediment, garnet, rutile and zircon, which remain analogue to the underlying Pliocene succession, are misleading for interpreting supply from (meta-)sedimentary rocks, because they represent recycled grains and are thus indicative for sources they derived from in first place.

		Modern river sediments					Rift sediments				
		Source rock/area		Weathering/climate	Sorting/recycling	Mixing	Source rock/area		Weathering/climate	Sorting/recycling	Mixing
		crystalline source	metasedimentary source				crystalline source	metasedimentary source			
Framework composition	QFL ratio	x(x)	xx(x)	xx	xx	o	x(x)	xxx	x	xx	o
	Rock fragments	xx	x	o	x	xx	x	x	o	x	x
Heavy mineral analysis	Bulk composition	xx	xx	x	xx	x(x)	xx	xx	x	xx	x(x)
	Indices (ZTR, GZi, RuZi)	xx	xxx	x	xx	x(x)	xx	xxx	x	xx	x(x)
Bulk rock geochemistry	Major elements	x(x)	xx	xx	xx	o	x(x)	xxx	x	xx	o
	Trace element ratios	xx	xx	o	xx	x	xx	xx	o	xx	x
	REE	xx	xx	o	xx	x	xx	xx	o	xx	x
	Weathering indices (CIA, WIP)	x	x(x)	xxx	x(x)	o	x	xx	x	x	o
	α-values	x	x(x)	xxx	x	o	-	-	-	-	-
Garnet chemistry		xxx	o	o	o	xx	xxx	o	o	o	xx
Rutile chemistry	Zr-in-rutile thermometry	xxx	o	o	o	xx	xxx	o	o	o	xx
	Cr-Nb chemistry	x	o	o	o	x(x)	o	o	o	o	x
Zircon studies	Zircon U-Pb geochronology	xxx	o	o	o	xxx	xxx	o	o	o	xxx
	Zircon morphology	x	o	o	o	x	x	o	o	o	x

xxx excellent indicator
xx good indicator
x minor indcator
o no indicator

Table 7-1. Applicability of applied methods for identifying different 'provenance parameters'(source rock/area and external factors controlling sediment composition) for modern river sediments and Neogene rift sediments in the Albertine Rift.

The signature obtained from modern river sand can also indirectly assist to recover source areas, as seen while studying the Miocene sedimentary record in the Kisegi-Nyabusosi area. While garnet and rutile chemistry indicated a mixed provenance from high-grade to very high-grade (amphibolite- to granulite-facies) metacrustal and metasedimentary rocks, on the basis of which gneissic-granulitic Archean terranes could be identified as possible source, heavy mineral assemblages characterized by high amounts of garnet and ZTR together with high element ratios of La/Sc, Th/Sc, Zr/Sc, and ∑REE showed conflicting results to epidote-amphibole-rich heavy mineral suites in modern rivers draining Archean terranes along the rift shoulder. Because of this, these parameters could be used as an indicator for a more acid source area located further away from the rift valley in the Ugandan hinterland. The dominance of the most durable minerals might also be seen as an indicator for hydraulic sorting during dispersal, which may also be a proof of a long-distance transport. In case of the Miocene succession, zircon geochronology surely provided the most indicative method for source determination, because varying occurring zircon populations, including Mesoarchean, Neoarchean, Paleoproterozoic and Neoproterozoic grains, could be directly linked to the age of different basement lithologies in the local basement. Zircon geochronology turned out to be an exclusive method that provided evidence for a widely-branched 'continental-wide' transport system extending to the at least 400 km away located East African Orogen (EAO) in northeastern Uganda and helped to specify source areas or the dimension of the drainage network, which was not able by other methods.

Interpretations concerning source areas could be well verified by statistical treatment of the data set by Principal Component Analysis (PCA). PCA assisted to find the best possible discrimination function for the rift sediment according to their similarities and differences, and helped to connect them to the signature of modern rivers draining different rock suites in the Ugandan basement. The best discriminant input variables can be identified when comparing multiple parameters from different rock lithologies of the regional basement or river sediment draining these lithologies, respectively. Overall, this study highly emphasizes the utilization of statistical approaches to integrate large provenance data sets.

While most of the methods applied during this study showed to be helpful in recovering provenances to some degree, some techniques including zircon morphology, Cr-Nb chemistry of rutile and determination of rock fragments in thin sections proofed to be less informative and can therefore not be recommended when studying sediment in similar areas (Table 7-1). Studying internal structures of zircon crystals demonstrated to be a very time-consuming method that compared to the chronological information only partly helped to distinguish between magmatic and metamorphic zircon. This method is not useful for distinguishing sediment sources in areas where the basement is characterized by regional commonality, because all samples contain a similar array of morphotype classes. Even though, Cr and Nb contents in rutile worked well for river sediments and were able to distinguish metapelitic from mafic lithologies, it did not proof to be relevant for discriminating rift sediment. Cr and Nb ratios remained similar throughout the stratigraphic column in both study areas, indicating dominant input from metapelitic sources. The observation of rock fragments also remains insufficient, because they could only be distinguished according to their protolith composition (metapelite, metapsammite/metafelsite, and metabasite grain). A detailed study of mineral parageneses was not practicable, which is mainly due to the small grain size of the clasts in the analyzed grain size fraction. Furthermore, the majority of rock fragments in the sand constitutes of quartz-feldspar intergrowths, and can therefore not give much information on the source rock.

A pitfall during this study proofed to be interpretations concerning long-term climate shifts from humid to arid climate conditions that are well documented for Eastern Africa since the Miocene, and have also been investigated during sedimentological and paleontological studies in the Albertine Rift (Pickford et al., 1993, Lukaye et al., 2016). They could not be inferred on the basis of provenance

data. This might probably be because the duration of time, during which the rift sediment has been exposed to the climate conditions, was too short to severely modify compositional pattern. Furthermore, as in the modern case of the Rwenzori Mountains, rapid erosion of detritus from the uplifted rift shoulder leads to physical destruction of sedimentary material in first place. Thus, the rift sediment is largely controlled by the composition of the certain source rock. It must also be kept in mind that SPA is not an exclusive method that allows to fully understand the complexity of all the products and processes within rift settings. For a comprehensive reconstruction of the entire basin evolution, SPA needs to be applied in conjunction with other approaches, such as sedimentological, paleontological and geophysical studies, which give additional information on, e.g., depositional environments, climate evolution, or the architecture of basins.

Take-home message:

Despite the fact that few questions, especially the climatic ones, remained unsolved during this thesis, this study very well demonstrates that multi-proxy SPA presents a satisfactorily tool in investigating compositional shifts in the sedimentary interior of rift basins in tropical regions that may also work well for reconstructing major tectonic stages in other rift sectors in the East African Rift. In case of the Albertine Rift, SPA assisted to recover three major rifting stages that are likely to be linked to tectonic activity affecting this particular basin during its evolution, and helped to refine existing drainage models for Uganda. This study highly recommends the application of multi-proxy approaches when studying sediment in areas where there is commonality in the regional basement and/or where sediment is modified by external processes. It could be shown that no single signal is capable of clearly distinguishing between different source rocks/areas, but that the complementary information provided by each method summarizes to an overall picture. Single-grain methods (garnet and rutile chemistry, zircon U-Pb ages) are most suitable for distinguishing between rock lithologies characterized by different metamorphic overprint and age. Framework grains and major elements are indicators for both weathering or recycled sedimentary sources. To single out the dominant process, other parameters like heavy mineral assemblages or trace element ratios might be helpful that may be linked to the signature of potential source rocks/areas. This study further highlights the usefulness of modern river sands for characterizing potential source rocks. The compilation of a basal data set for major basement terranes is especially meaningful for settings where the basement geology is poorly constraint and/or certain analytical data are missing. This study clearly shows that only the linkage between the signature of river sand (or basement terranes, respectively) and rift sand, which is best achieved by statistical treatment (PCA) of the data set, helps to clearly interpret proto-sources. Otherwise, interpretations concerning sediment sources might have been more difficult or equivocal.

7.5 References

Aitchison, J., 1986. The Statistical Analysis of Compositional Data. London, Chapman & Hall, 416 p.

Aitchison, J., 1990. Relative variation diagrams for describing patterns of compositional variability. Mathematical Geology, 22, 487–511.

Aitchison, J., Greenacre, M., 2002. Biplots of compositional data. Journal of the Royal Statistical Society: Series C (Applied Statistics), 51, 375–392.

Aitchison, J., Egozcue, J. J., 2005. Compositional data analysis: where are we and where should we be heading? Mathematical Geology, 37, 829–850.

Bauer, F. U., Glasmacher U. A., Ring U., Schumann A., Nagudi B., 2010. Thermal and exhumation history of the central Rwenzori Mountains, Western Rift of the East African Rift System, Uganda. International Journal of Earth Sciences, 99, 1575–1597.

Bauer, F. U., Karl, M., Glasmacher, U. A., Nagudi, B., Schumann, A., Mroszewski, L., 2012. The Rwenzori Mountains of western Uganda–Aspects on the evolution of their remarkable morphology within the Albertine Rift. Journal of African Earth Sciences, 73, 44–56.

Bauer, F. U., Glasmacher, U. A., Ring, U., Karl, M., Schumann, A., Nagudi, B., 2013. Tracing the exhumation history of the Rwenzori Mountains, Albertine Rift, Uganda, using low-temperature thermochronology. Tectonophysics, 599, 8–28.

Bishop, W. W., 1965. Quaternary geology and geomorphology in the Albertine Rift Valley, Uganda. In: Wright Jr., H. E., Frey, D. G. (Eds.), International studies on the Quaternary, pp. 293–321.

Bonini, M., Corti, G., Innocenti, F., Manetti, P., Mazzarini, F., Abebe, T., Pecskay, Z., 2005. Evolution of the Main Ethiopian Rift in the frame of Afar and Kenya rifts propagation. Tectonics, 24, 1–21.

Bonnefille, R., 2010. Cenozoic vegetation, climate changes and hominid evolution in tropical Africa. Global and Planetary Change, 72, 390–411.

Caracciolo, L., Garzanti, E., Von Eynatten, H., Weltje, G. J., 2016. Sediment generation and provenance: processes and pathways. Sedimentary Geology, 336, 1–2.

Chorowicz, J., 2005. The East African rift system. Journal of African Earth Sciences, 43, 379–410.

Cohen, A.S., Soreghan, M.J., Scholz, C.A., 1993. Estimating the age of formation of lakes: an example from Lake Tanganyika, East African rift system. Geology, 21, 511–514.

Cooke, H. B. S., 1958. Observations relating to the Quaternary environments in East and Southern Africa. Transactions of the Geological Society of South Africa, 60, 1–74.

Dechamps, R., Senut, B., Pickford, M., 1992. Fruits fossiles pliocènes et pléistocènes du Rift occidental ougandais. Signification paléoenvironnementale. Comptes rendus de l'Académie des sciences. Série 2, Mécanique, Physique, Chimie, Sciences de l'univers, Sciences de la Terre, 314, 325–331.

Dietze, E., Hartmann, K., Diekmann, B., Ijmker, J., Lehmkuhl, F., Opitz, S., Stauch, G., Wünnemann, B., Borchers, A., 2012. An end-member algorithm for deciphering modern detrital processes from lake sediments of Lake Donggi Cona, NE Tibetan Plateau, China. Sedimentary Geology, 243, 169–180.

Ebinger, C. J., 1989. Tectonic development on the western branch of the East African rift system. Geological Society of America Bulletin, 101, 885–903.

Ebinger, C. J., Crow, M. J., Rosendahl, B. R., Livingstone, D. A., LeFournier, J., 1984. Structural evolution of Lake Malaŵi, Africa. Nature, 308, 627-629.

Ebinger, C. J., Rosendahl, B. R., Reynolds, D. J., 1987. Tectonic model of the Malawi rift, Africa. Tectonophysics, 141, 215–235.

Flannery, J. W., Rosendahl, B. R., 1990. The seismic stratigraphy of Lake Malawi, Africa: implications for interpreting geological processes in lacustrine rifts. Journal of African Earth Sciences, 10, 519–548.

Foster, A., Ebinger, C., Mbede, E., Rex, D., 1997. Tectonic development of the northern Tanzanian sector of the East African Rift System. Journal of the Geological Society, 154, 689–700.

Gabriel, K. R., 1971. The biplot-graphic display of matrices with applications to principal component analysis. Biometrika, 58, 453–467.

Gani, N. D. S., Gani, M. R., Abdelsalem, M. G., 2007. Blue Nile incision on the Ethiopian Plateau; pulsed plateau growth, Pliocene uplift and hominid evolution. GSA Today, 17, 4–11.

Hammer, Ø., Harper, D. A. T., Ryan, P. D., 2001. PAST: Paleontological Statistics Software Package for Education and Data Analysis–Palaeontologia Electronica, 4, 9 pp.

Jacobs, B. F., Deino, A. L., 1996. Test of climate–leaf physiognomy regression models, their application to two Miocene floras from Kenya, and $^{40}Ar/^{39}Ar$ dating of the late Miocene Kapturo site. Palaeogeography, Palaeoclimatology, Palaeoecology, 123, 259–271.

Johnsson, M. J., 1993. The system controlling the composition of clastic sediments. In: Johnsson, M. J., Basu, A. (Eds.), Processes controlling the composition of clastic sediments. Geological Society of America Special Papers, 284, pp. 1–19.

Lacher, D. A., O'Donnell, E. D., 1988. Comparison of multidimensional scaling and principal component analysis of interspecific variation in bacteria. Annals of Clinical & Laboratory Science, 18, 455–462.

Le Gall, B., Nonnotte, P., Rolet, J., Benoit, M., Guillou, H., Mousseau-Nonnotte, M., Albaric, J., Déverchère, J., 2008. Rift propagation at craton margin.: Distribution of faulting and volcanism in the North Tanzanian Divergence (East Africa) during Neogene times. Tectonophysics, 448, 1–19.

Lukaye, J. M., 2009. Biostratigraphy and Palynofacies of Four Exploration Wells from the Albertine Graben, Uganda. American Association of Petroleum Geologists, Search & Discovery Article, 50169. http://www.searchanddiscovery.net/documents/2009/50169lukaye/ndx_lukaye.pdf.

Lukaye, J., Worsley, D., Kiconco, L., Nabbanja, P., Abeinomugisha, D., Amusugut, C., Njabire, N., Nuwagaba, R., Mugisha, F., Ddungu, T., Sserubiri, T., Sserubiri, T., 2016. Developing a Coherent Stratigraphic Scheme of the Albertine Graben-East, Africa. Journal of Earth Science and Engineering, 6, 264–294.

Macgregor, D. S., 2012. The development of the Nile drainage system: integration of onshore and offshore evidence. Petroleum Geoscience, 18, 417–431.

Macgregor, D., 2015. History of the development of the East African Rift System: a series of interpreted maps through time. Journal of African Earth Sciences, 101, 232–252.

MacPhee, D., 2006. Exhumation, Rift-flank uplift, and Thermal Evolution of the Rwenzori Mountains Determined by Combined (U–Th)/He and U–Pb thermochronometry. Master thesis, Massachusetts Institute of Technology.

Morton, A. C., Hallsworth, C. R., 1999. Processes controlling the composition of heavy mineral assemblages in sandstones. Sedimentary Geology, 124, 3–29.

Pickford, M., 1994. Patterns of sedimentation and fossil distribution in the Kenya Rift valleys. Journal of African Earth Sciences, 18, 51–60.

Pickford, M., Senut, B., Hadoto, D., 1993. Geology and Palaeobiology of the Albertine Rift Valley, Uganda-Zaire. Vol. I: Geology. International Centre for Training and Exchanges in Geosciences, Occasional Publications, 24, 1–190.

Roller, S., Hornung, J., Hinderer, M., Ssemmanda, I., 2010. Middle Miocene to Pleistocene sedimentary record of rift evolution in the southern Albertine Graben (Uganda). International Journal of Earth Sciences, 99, 1643–1661.

Saemundsson, K., 2010. East African rift system. An overview. In: Paper Presented at Course V on Exploration for Geothermal Resources, Organized by UNU-GTP, GDC and KenGen, at Lake Bogoria and Lake Naivasha, Kenya, Oct. 29-Nov. 19, 2010.

Schneider, S., Hornung, J., Hinderer, M., Garzanti, E., 2016a. Petrography and geochemistry of modern river sediments in an equatorial environment (Rwenzori Mountains and Albertine rift, Uganda)—Implications for weathering and provenance. Sedimentary Geology, 336, 106–119.

Schneider, S., Hornung, J., Hinderer, M., 2016b. Evolution of the western East African Rift System reflected in provenance changes of Miocene to Pleistocene synrift sediments (Albertine Rift, Uganda). Sedimentary Geology, 343, 190–205.

Schneider, S., Hornung, J., Hinderer, M., 2017. Evolution of the northern Albertine Rift reflected in the provenance of synrift sediments (Nkondo-Kaiso area, Uganda). Journal of African Earth Sciences, 131, 183–197.

Schneider, S., Hornung, J., Hinderer, M., in prep.(a). Garnet and rutile mineral chemistry and zircon U-Pb ages of modern river sands along the western East African Rift (Albertine Rift, Uganda).

Schneider, S., Hornung, J., Hinderer, M., in prep.(b). New insights into the evolution of the western East African Rift System (Albertine Rift, Uganda) through bulk rock geochemistry and zircon U-Pb geochronology.

Simon, B. 2015. Rift du Lac Albert, Ouganda, Rift Est Africain : Déformation, érosion, sédimentation et bilan de matière depuis 17 Ma, Université de Rennes 1, Rennes, 403 pp.

Smith, L. I., 2002. A tutorial on principal components analysis. Cornell University, USA, 51, 26 pp.

Spiegel, C., Kohn, B. P., Belton, D. X., Gleadow, A. J., 2007. Morphotectonic evolution of the central Kenya rift flanks: Implications for late Cenozoic environmental change in East Africa. Geology, 35, 427–430.

Taylor, R. G., Howard, K. W. F., 1999. The influence of tectonic setting on the hydrological characteristics of deeply weathered terrains: evidence from Uganda. Journal of Hydrology, 218, 44–71.

Vermeesch, P., 2013. Multi-sample comparison of detrital age distributions. Chemical Geology, 341, 140–146.

Vermeesch, P., Resentini, A., Garzanti, E., 2016. An R package for statistical provenance analysis. Sedimentary Geology, 336, 14–25.

von Eynatten, H., Barceló-Vidal, C., Pawlowsky-Glahn, V., 2003. Composition and discrimination of sandstones: a statistical evaluation of different analytical methods. Journal of Sedimentary Research, 73, 47–57.

Weltje, G. J., von Eynatten, H., 2004. Quantitative provenance analysis of sediments: review and outlook. Sedimentary Geology, 171, 1–11.

Wescott, W. A., Krebs, W. K., Engelhardt, D. W., Cunningham, S. M., 1991. New biostratigraphic age dates from the Lake Rukwa rift basin in Western Tanzania. American Association of Petroleum Geologists Bulletin, 75, 1255–1263.

Appendix – Chapter 2

A2-1 – Sample list

Tectonic province	sample ID	river/lake name	site	longitude	latitude	altitude [m.a.s.l]	kind of water body	underlying basement
Lake Albert basin	1	Nile*	Pakwach	2,46014	31,50703	680	river	Recycled sediments Albertine Graben
	2	Para*	Para Safari Lodge	2,29000	31,56611	633	river	Recycled sediments Albertine Graben
	3	Bulisa*	Bulisa	2,12194	3,14464	645	river	Recycled sediments Albertine Graben
	4	Jolya*	Rabongo Forest	2,14806	31,70583	740	river	Archean Gneiss-Granulite Complex + Recycled sediments Albertine Graben
	5	Waiga 1*	Rabongo Forest	2,05917	31,71667	695	river	Archean Gneiss-Granulite Complex
	6	Waiga 2*	Kigoya	1,99278	31,47556	635	river	Archean Gneiss-Granulite Complex + Recycled sediments Albertine Graben
	7	Waisoke*	Bugoigo	1,93028	31,42833	625	river	rchean Gneiss-Granulite Complex + Metasediments Bunyoro-Kyoga Series + Recycled sediments Albertine Graben
	8	Lake Albert*	Butiaba	1,81806	31,32083	620	lake	rchean Gneiss-Granulite Complex + Metasediments Bunyoro-Kyoga Series + Recycled sediments Albertine Graben
	9	Waki*	Biso	1,70944	31,37639	990	river	Archean Gneiss-Granulite Complex + Metasediments Bunyoro-Kyoga Series
	10	Kafu*	Kibangya	1,54339	32,04137	1100	river	Archean Gneiss-Granulite Complex
	11	Wambabya	Kaiso-Tonya	1,55854	31,10358	624	river	Archean Gneiss-Granulite Complex + Metasediments Bunyoro-Kyoga Series
	12	tribut. Wambabya	Hoima	1,41485	31,33691	1039	river	Metasediments Bunyoro-Kyoga Series
	13	tribut. Wambabya	Kiziranfumbi	1,33454	31,21181	1068	river	Metasediments Bunyoro-Kyoga Series
	14	tribut. Wambabya	Muntenne	1,29849	31,14634	1055	river	Metasediments Bunyoro-Kyoga Series
	15	tribut. Nkusi	SW Kabwoya	1,18802	31,03452	1086	river	Metasediments Bunyoro-Kyoga Series
	16	Nkusi 1	Kitoma	1,12961	30,99481	1052	river	Archean Gneiss-Granulite Complex + Metasediments Bunyoro-Kyoga Series
	17	Nkusi 2*	Pachwa	1,13000	30,89528	1020	river	Archean Gneiss-Granulite Complex + Metasediments Bunyoro-Kyoga Series
	18	tribut. Nkusi	SW Kitoma	1,07989	30,94480	1101	river	Archean Gneiss-Granulite Complex
	19	tribut. Nkusi	SW Kyangamwoyo	0,96402	30,83797	1182	river	Granites
	20	Muzizi	W Nyakalengija	0,87096	30,72939	1142	river	Archean Gneiss-Granulite Complex
Lake George basin	21	Kazinga*	Katunguru	-0,12500	30,04806	917	river	Recycled sediments Lake Edward Graben
	22	Crater Lake	Durama	0,49667	30,33113	1382	lake	Quartzites Buganda-Toro System + Volcanics
	23	Dura	north Kibale	0,45849	30,38005	1253	river	Quartzites Buganda-Toro System + Archean Gneiss-Granulite Complex
	24	tribut. Dura	Kibale	0,43675	30,39327	1224	river	Quartzites Buganda-Toro System + Archean Gneiss-Granulite Complex
	25	tribut. Dura	Kahunge	0,33994	30,42848	1233	river	Quartzites/Metasediments Buganda-Toro System
	26	tribut. Mpanga	Kamwenge	0,17076	30,48593	1376	river	Metasediments Buganda-Toro System
	27	Mpanga south 1	NE of Mpanga	0,10872	30,41391	1173	river	Metasediments Buganda-Toro System + Archean Gneiss-Granulite Complex
	28	Mpanga south 2	Rwenjaza	0,10075	30,46152	1170	river	Metasediments Buganda-Toro System + Archean Gneiss-Granulite Complex
Northern Rwenzoris	29	Dunga	N Bubandi	0,65596	30,17274	1659	river	Archean Gneiss-Granulite Complex
	30	Kazi	Bubandi	0,61985	30,15832	1701	river	Archean Gneiss-Granulite Complex
	31	Igasa	Kateebwa	0,57218	30,19127	1533	river	Archean Gneiss-Granulite Complex
	32	Mahoma*	Kisomoro	0,54333	30,16861	1545	river	Archean Gneiss-Granulite Complex
	33	Mpanga north 1*	Fort Portal	0,65944	30,29306	1495	river	Archean Gneiss-Granulite Complex + Volcanics
	34	Mpanga north 2	E Fort Portal	0,64312	30,39307	1423	river	Archean Gneiss-Granulite Complex
Central Rwenzoris	35	Rwimi 1*	Rwimi	0,37306	30,21083	1060	river	Metasediments Buganda-Toro System
	36	Rwimi 2	SE Rwimi	0,34174	30,23936	1044	river	Metasediments Buganda-Toro System + Archean Gneiss-Granulite Complex
	37	Butawu	N Mutwanga	0,34543	29,78432	1837	river	Metasediments Buganda-Toro System
	38	tribut. Butawu	N Kalonge	0,34492	29,80871	2050	river	Metasediments Buganda-Toro System
	39	tribut. Butawu	N Kalonge	0,36114	29,84782	3775	river	Metasediments Buganda-Toro System
	40	tribut. Butawu	N Kalonge	0,34084	29,81627	2048	river	Metasediments Buganda-Toro System
	41	Mugusu	SE Mount Speke	0,39095	29,92072	3454	river	Metasediments Buganda-Toro System
	42	Mubuku 4	SW Nyabitaba Hut, C. Rwenzoris	0,34718	29,95928	2910	river	Metasediments Buganda-Toro System
	43	Bujuku	W Nyabitaba Hut, C. Rwenzoris	0,35808	29,97175	2590	river	Metasediments Buganda-Toro System + Archean Gneiss-Granulite Complex
	44	Mubuku 1	W Nyabitaba Hut, C. Rwenzoris	0,35800	29,97197	2581	river	Metasediments Buganda-Toro System + Archean Gneiss-Granulite Complex
	45	Isebo 1	E Nyabitaba Hut, C. Rwenzoris	0,36235	29,99877	2108	river	Archean Gneiss-Granulite Complex
	46	Mubuku 2	Bugoye	0,30675	30,10111	1253	river	Archean Gneiss-Granulite Complex
	47	Isebo 2	N Mubuku	0,26706	30,11022	1144	river	Metasediments Buganda-Toro System + Archean Gneiss-Granulite Complex
	48	Mubuku*	Mubuku	0,26111	30,12167	1105	river	Metasediments Buganda-Toro System + Archean Gneiss-Granulite Complex
	49	Nyamwamba	Kilembe	0,21374	30,00580	1399	river	Metasediments Buganda-Toro System + Archean Gneiss-Granulite Complex
	50	Nyamagasani	Kyarumba	0,12307	29,94980	1253	river	Metasediments Buganda-Toro System
	51	Nyamagasani 2*	Kagando	0,00917	29,89889	1051	river	Archean Gneiss-Granulite Complex + Volcanics

*samples adopted from Garzanti et al. (2013a)

A2-2 – Analytical procedure (bulk rock geochemistry)

Laboratory		Actlabs (Canada)		ALS Minerals (Spain)	
Analyzed grain size fraction		mud (<63 µm)		sand (0.063-2 mm)	
Analyte Symbol	**Unit Symbol**	**Detection Limit**	**Analysis Method**	**Detection Limit**	**Analysis Method**
SiO2	%	0.01	ICP-OES	0.01	ICP-AES
Al2O3	%	0.01	ICP-OES	0.01	ICP-AES
Fe2O3(T)	%	0.01	ICP-OES	0.01	ICP-AES
MnO	%	0.001	ICP-OES	0.01	ICP-AES
MgO	%	0.01	ICP-OES	0.01	ICP-AES
CaO	%	0.01	ICP-OES	0.01	ICP-AES
Na2O	%	0.01	ICP-OES	0.01	ICP-AES
K2O	%	0.01	ICP-OES	0.01	ICP-AES
TiO2	%	0.001	ICP-OES	0.01	ICP-AES
P2O5	%	0.01	ICP-OES	0.01	ICP-AES
BaO	%	-	-	0.01	ICP-AES
SrO	%	-	-	0.01	ICP-AES
Cr2O3	%	-	-	0.01	ICP-AES
LOI	%	0.01	ICP-OES	0.01	ICP-AES
Sc	ppm	1	ICP-OES	1	ICP-AES
Be	ppm	1	ICP-OES	-	ICP-MS
V	ppm	5	ICP-OES	5	ICP-MS
Cr	ppm	20	ICP-MS	10	ICP-MS
Co	ppm	1	ICP-MS	1	ICP-AES
Ni	ppm	20	ICP-MS	1	ICP-AES
Cu	ppm	10	ICP-MS	1	ICP-AES
Zn	ppm	30	ICP-MS	2	ICP-AES
Cd	ppm	-	-	0.5	ICP-AES
Ga	ppm	1	ICP-MS	0.01	ICP-MS
Ge	ppm	1	ICP-MS	5	ICP-MS
As	ppm	5	ICP-MS	0.1	ICP-MS
Rb	ppm	2	ICP-MS	0.2	ICP-MS
Sr	ppm	2	ICP-OES	0.1	ICP-MS
Y	ppm	2	ICP-OES	0.5	ICP-MS
Zr	ppm	4	ICP-OES	2	ICP-MS
Nb	ppm	1	ICP-MS	0.2	ICP-MS
Mo	ppm	2	ICP-MS	1	ICP-AES
Ag	ppm	0.5	ICP-MS	0.5	ICP-AES
In	ppm	0.2	ICP-MS	-	ICP-MS
Sn	ppm	1	ICP-MS	1	ICP-MS
Sb	ppm	0.5	ICP-MS	0.05	ICP-MS
Cs	ppm	0.5	ICP-MS	0.01	ICP-MS
Ba	ppm	3	ICP-OES	0.5	ICP-MS
Bi	ppm	0.4	ICP-MS	0.01	ICP-MS
La	ppm	0.1	ICP-MS	0.5	ICP-MS
Ce	ppm	0.1	ICP-MS	0.5	ICP-MS
Pr	ppm	0.05	ICP-MS	0.03	ICP-MS
Nd	ppm	0.1	ICP-MS	0.1	ICP-MS
Sm	ppm	0.1	ICP-MS	0.03	ICP-MS
Eu	ppm	0.05	ICP-MS	0.03	ICP-MS
Gd	ppm	0.1	ICP-MS	0.05	ICP-MS
Tb	ppm	0.1	ICP-MS	0.01	ICP-MS
Dy	ppm	0.1	ICP-MS	0.05	ICP-MS
Ho	ppm	0.1	ICP-MS	0.01	ICP-MS
Er	ppm	0.1	ICP-MS	0.03	ICP-MS
Tm	ppm	0.05	ICP-MS	0.01	ICP-MS
Yb	ppm	0.1	ICP-MS	0.03	ICP-MS
Lu	ppm	0.04	ICP-MS	0.01	ICP-MS
Hf	ppm	0.2	ICP-MS	0.2	ICP-MS
Ta	ppm	0.1	ICP-MS	0.1	ICP-MS
W	ppm	1	ICP-MS	1	ICP-MS
Tl	ppm	0.1	ICP-MS	0.02	ICP-MS
Pb	ppm	5	ICP-MS	2	ICP-AES
Th	ppm	0.1	ICP-MS	0.05	ICP-MS
U	ppm	0.1	ICP-MS	0.05	ICP-MS

A2-3 – Framework petrography (point-counting results)

T+A1:AC33ectonic province	Sample ID	River/Lake	Site	Operator	GSZ (range)	monocrystalline quartz	polycrystalline quartz	plagioclase	albitized feldspars	K-feldspar	volcanic grains	felsic plutonic grains	intermediate plutonic grains	arenaceous grains	chert grains	metapelite grains	metapsammite grains	metafelsite grains	metabasite grains	micas	transparent heavy minerals	opaque minerals	non-carbonate intrabasinal grains	altered undetermined grains	TOTAL	Q	F	R
Lake Albert basin	1	Nile*	Pakwach	A.Resentini	250-1000	82	12	2	0	2	0	0	0	0	0	0	0	0	0	0	1	0	0	0	100	94	4	2
	2	Paraa*	Paraa Safari Lodge	A.Resentini	250-1000	83	12	0	0	1	0	0	0	0	0	0	0	0	0	0	0	1	2	0	100	96	1	3
	3	Bulisa*	Bulisa	A.Resentini	250-1000	90	8	0	0	0	0	0	0	0	0	0	0	0	0	0	0	0	0	0	100	98	1	1
	4	Jolya*	Rabongo Forest	A.Resentini	250-1000	49	26	4	0	7	0	2	0	0	0	0	0	1	0	1	0	0	10	0	100	75	11	14
	5	Waiga*	Rabongo Forest	G.Vezzoli	250-1000	17	42	4	0	3	0	6	0	1	0	0	1	3	7	0	12	0	4	0	100	59	7	34
	6	Waiga*	Kigoya	A.Resentini	250-1000	63	30	0	0	1	0	2	0	0	0	0	0	1	0	0	1	0	2	0	100	93	1	6
	7	Waisoke*	Bugoigo	A.Resentini	250-1000	44	34	3	0	5	0	0	0	0	0	0	0	0	1	0	4	0	8	0	100	78	8	14
	8	Lake Albert*	Butiaba	A.Resentini	250-1000	66	29	1	0	1	0	0	0	0	0	0	0	0	0	0	1	2	1	0	100	95	1	3
	9	Waki*	Biso	A.Resentini	250-1000	37	55	1	0	1	0	0	0	0	0	0	2	0	0	0	0	0	4	0	100	92	1	7
	10	Kafu*	Kibangya	A.Resentini	250-1000	83	5	5	0	5	0	1	0	0	0	0	1	0	0	0	0	0	1	0	100	88	10	3
	11	Wambabya	Kaiso-Tonya	S. Schneider	250-500	58	9	1	0	7	0	1	0	0	0	0	1	11	1	2	6	0	3	0	100	67	8	25
	12	tribut. Wambabya	Hoima	S. Schneider	250-500	52	5	1	0	5	0	0	0	0	1	0	1	2	0	0	0	0	33	0	100	57	6	37
	13	tribut. Wambabya	Kiziranfumbi	S. Schneider	250-500	55	3	1	0	4	0	0	0	0	0	0	1	1	0	0	0	0	35	0	100	58	5	37
	14	tribut. Wambabya	Munteme	S. Schneider	250-500	59	10	1	0	4	0	0	0	0	0	0	0	3	0	0	0	0	23	0	100	69	5	26
	15	tribut. Nkusi	SW Kabwoya	S. Schneider	250-500	47	7	1	0	5	0	0	0	0	1	1	1	1	0	<1	<1	0	36	0	100	54	6	40
	16	Nkusi 1	Kitoma	S. Schneider	250-500	61	5	1	0	14	0	1	0	0	0	0	2	2	0	0	0	0	14	0	100	66	15	19
	17	Nkusi 2*	Pachwa	G.Vezzoli	250-1000	59	6	1	0	10	1	1	0	0	0	0	0	0	0	0	0	0	22	0	100	65	11	24
	18	tribut. Nkusi	SW Kitoma	S. Schneider	250-500	74	1	1	0	9	0	0	0	0	0	0	1	5	0	0	0	0	9	0	100	75	10	15
	19	tribut. Nkusi	SW Kyangamwoyo	S. Schneider	250-500	84	1	1	0	7	0	0	0	0	1	1	2	0	0	0	0	0	3	0	100	85	8	7
	20	Muzizi	W Nyakalengija	S. Schneider	250-500	59	10	6	0	13	0	0	0	0	0	0	2	3	1	2	1	0	3	0	100	69	19	12
Lake George basin	21	Kaziinga*	Katunguru	A.Resentini	250-1000	55	9	10	0	6	0	2	0	0	0	1	1	2	5	1	3	0	2	1	100	64	17	19
	22	Crater Lake	Durama	S. Schneider	250-500	13	43	1	0	1	4	0	0	0	0	1	1	3	4	1	2	0	26	0	100	56	2	42
	23	Dura	north Kibale	S. Schneider	250-500	45	11	4	0	9	0	0	0	0	0	0	7	3	1	1	1	0	19	0	101	56	13	31
	24	tribut. Dura	Kibale	S. Schneider	250-500	44	12	10	0	19	0	0	0	0	0	0	3	8	0	<1	<1	0	4	0	100	56	29	15
	25	tribut. Dura	Kahunge	S. Schneider	250-500	74	4	1	0	5	0	0	0	0	0	0	0	13	0	1	0	0	2	0	100	78	6	16
	26	tribut. Mpanga	Kamwenge	S. Schneider	250-500	65	9	6	0	10	0	0	0	0	0	0	2	5	0	<1	2	0	1	0	100	74	16	10
	27	Mpanga south 1	NE of Mpanga	S. Schneider	250-500	73	4	2	0	6	0	0	0	0	0	0	8	2	0	1	2	0	2	0	100	77	8	15
Northern Rwenzoris	29	Dunga	N Bubandi	S. Schneider	250-500	40	10	13	0	9	0	0	0	0	0	0	4	8	4	<1	4	2	6	0	100	50	22	28
	30	Kazi	Bubandi	S. Schneider	250-500	18	6	14	0	9	0	0	0	0	0	0	9	20	11	1	5	2	5	0	100	24	23	53
	31	Igasa	Kateebwa	S. Schneider	250-500	24	10	12	0	11	2	0	0	0	0	0	9	16	6	2	4	1	3	0	100	34	23	43
	32	Mahoma*	Rubona	A.Resentini	250-1000	29	26	8	0	5	0	2	0	0	0	1	5	1	3	0	8	2	9	1	100	55	12	33
	33	Mpanga north 1*	Fort Portal	A.Resentini	250-1000	46	15	9	0	3	0	0	0	0	0	0	0	1	1	1	12	3	10	0	100	61	11	28
Central Rwenzoris	35	Rwimi 1*	Rwimi	A.Resentini	250-1000	22	16	22	3	10	0	3	0	0	0	3	5	4	7	0	4	0	1	0	100	37	36	27
	37	Butawu	N Mutwanga	A.Resentini	300-500	49	7	2	0	1	0	0	0	0	0	10	20	1	0	8	1	0	0	1	100	56	3	41
	38	tribut. Butawu	N Kalonge	A.Resentini	300-500	5	4	7	0	0	0	0	0	0	0	1	0	6	34	0	38	0	0	5	100	9	7	84
	39	tribut. Butawu	N Kalonge	A.Resentini	300-500	3	4	9	0	0	0	0	0	0	0	1	1	4	23	0	51	0	0	3	100	7	9	84
	40	tribut. Butawu	N Kalonge	A.Resentini	<500	10	8	22	0	1	0	1	0	0	0	1	2	3	12	7	28	0	4	1	100	18	23	59
	46	Mubuku 2	Bugoye	S. Schneider	250-500	20	5	3	0	11	0	0	0	0	0	8	7	17	20	6	3	0	0	0	100	25	14	61
	47	Isebo	N Mubuku	S. Schneider	250-500	26	15	11	0	15	0	0	0	0	0	0	6	10	9	5	2	0	1	0	100	41	26	33
	48	Mubuku*	Mubuku	G.Vezzoli	250-1000	19	9	20	0	11	0	9	0	0	0	1	2	6	12	6	4	0	0	0	100	29	31	41
	49	Nyamwamba	Kilembe	S. Schneider	250-500	20	14	8	0	6	0	0	0	0	0	0	10	19	13	6	2	1	1	0	100	34	14	52
	51	Nyamagasani 2*	Kagando	A.Resentini	250-1000	27	14	12	1	10	0	2	0	0	0	1	7	4	2	3	7	2	4	0	100	41	24	35

*samples adopted from Garzanti et al. (2013a)

A2-4 – Heavy mineral analysis (point-counting results)

Tectonic province	sample ID	river/lake name	site	Operator	GSZ (range)	zircon	tourmaline	rutile	Ti Oxides	titanite	apatite	monazite	epidote	garnet	staurolite	andalusite	kyanite	sillimanite	amphibole	pyroxene	total	ZTR	Gzi	Ruzi
Lake Albert basin	2	Paraa*	Paraa Safari Lodge	M.Padoan	63-250	61	1	27	0	1	0	1	5	1	0	0	4	1	0	0	100	89	1	30
	3	Bulisa*	Bulisa	M.Padoan	63-250	34	1	36	1	0	0	2	11	0	0	0	16	0	0	0	100	71	0	52
	4	Jolya*	Rabongo Forest	M.Padoan	63-250	16	1	7	3	4	0	1	29	0	0	0	12	0	26	0	100	24	0	30
	5	Waiga*	Rabongo Forest	M.Padoan	63-250	5	2	1	1	0	0	0	27	3	0	0	0	0	59	0	100	8	35	15
	6	Waiga*	Kigoya	M.Padoan	63-250	7	1	9	5	2	0	0	40	0	1	0	15	4	14	2	100	17	7	58
	7	Waisoke*	Bugoigo	M.Padoan	63-250	5	1	5	1	3	0	1	44	10	0	0	1	0	29	0	100	11	65	48
	8	Lake Albert*	Butiaba	M.Padoan	63-250	14	0	0	0	5	5	10	24	10	0	0	0	0	19	14	100	14	40	0
	9	Waki*	Biso	M.Padoan	63-250	26	6	2	1	1	0	0	17	2	1	0	5	20	21	0	100	34	5	5
	11	Wambabya	Kaiso-Tonya	S. Schneider	63-125	10	5	1	0	1	3	1	21	0	0	0	1	3	52	2	100	16	0	9
	12	tribut. Wambabya	Hoima	S. Schneider	63-125	25	41	2	0	0	2	7	5	1	0	0	0	5	11	1	100	68	4	7
	13	tribut. Wambabya	Kiziranfumbi	S. Schneider	63-125	49	19	13	0	0	4	1	8	1	0	0	0	1	4	0	100	81	2	21
	14	tribut. Wambabya	Munteme	S. Schneider	63-125	40	35	7	0	0	2	1	4	1	0	0	0	2	8	0	100	82	2	15
	15	tribut. Nkusi	SW Kabwoya	S. Schneider	63-125	25	48	4	0	0	7	2	1	1	0	0	0	3	9	0	100	77	4	14
	16	Nkusi 1	Kitoma	S. Schneider	63-125	37	8	3	0	0	3	3	19	2	0	0	1	4	19	1	100	48	5	8
	17	Nkusi 2*	Pachwa	S. Schneider	63-125	17	17	0	3	3	0	0	28	0	0	0	6	6	19	3	100	33	0	0
	18	tribut. Nkusi	SW Kitoma	S. Schneider	63-125	46	1	1	0	0	8	6	9	12	0	1	0	2	14	0	100	48	21	2
	19	tribut. Nkusi	SW Kyangamwoyo	S. Schneider	63-125	61	5	1	0	1	0	6	13	1	0	0	0	0	12	0	100	67	2	2
	20	Muzizi	W Nyakalengija	S. Schneider	63-125	11	6	1	0	2	3	3	6	0	0	0	0	4	64	0	100	18	0	8
Lake George basin	21	Kazinga*	Katunguru	M.Padoan	63-250	0	2	2	1	0	0	0	29	0	0	0	0	2	64	0	100	4	0	80
	22	Crater Lake	Durama	S. Schneider	63-125	1	1	3	0	2	1	0	31	1	0	0	2	2	46	10	100	5	50	75
	23	Dura	north Kibale	S. Schneider	63-125	1	3	1	0	1	2	0	33	1	0	0	1	2	52	3	100	5	50	50
	24	tribut. Dura	Kibale	S. Schneider	63-125	6	2	2	0	2	2	1	34	1	0	0	2	3	44	1	100	10	14	25
	25	tribut. Dura	Kahunge	S. Schneider	63-125	29	6	3	0	1	8	2	5	1	0	1	1	28	13	2	100	38	3	9
	26	tribut. Mpanga	Kamwenge	S. Schneider	63-125	5	2	1	0	1	0	1	20	1	0	1	0	2	65	1	100	8	17	17
	27	Mpanga south 1	NE of Mpanga	S. Schneider	63-125	7	7	3	0	1	2	1	33	1	0	0	1	16	25	3	100	17	13	30
Northern Rwenzoris	29	Dunga	N Bubandi	S. Schneider	63-125	1	0	0	0	0	3	0	18	4	0	0	2	0	68	4	100	1	80	0
	30	Kazi	Bubandi	S. Schneider	63-125	3	1	1	0	0	2	0	37	2	0	1	2	1	48	3	100	4	40	14
	31	Igasa	Kateebwa	S. Schneider	63-125	5	1	1	0	0	4	0	42	2	0	1	0	0	43	2	100	6	29	9
	32	Mahoma*	Rubona	M.Padoan	63-250	2	1	6	0	0	1	0	63	0	0	2	0	0	23	0	100	9	17	74
	33	Mpanga north 1*	Fort Portal	M.Padoan	63-250	1	2	1	0	1	1	0	13	4	0	0	1	0	43	30	100	4	82	50
Central Rwenzoris	35	Rwimi 1*	Rwimi	M.Padoan	63-250	0	0	0	0	0	0	0	3	0	0	0	0	0	96	0	100	0	/	/
	37	Butawu	N Mutwanga	M.Limonta	> 15	0	0	0	0	0	0	0	5	0	0	0	0	0	95	0	100	0	/	/
	38	tribut. Butawu	N Kalonge	M.Limonta	> 15	0	1	0	0	0	0	0	41	0	0	1	1	1	51	0	100	2	50	50
	39	tribut. Butawu	N Kalonge	M.Limonta	> 15	0	1	0	0	0	0	0	19	0	0	0	1	0	78	0	100	1	/	/
	40	tribut. Butawu	N Kalonge	M.Limonta	> 15	0	0	0	5	0	0	0	13	0	0	2	0	0	76	2	100	0	100	/
	46	Mubuku 2	Bugoye	S. Schneider	63-125	0	0	1	0	1	2	1	14	1	0	0	0	1	77	3	100	1	100	100
	47	Isebo	N Mubuku	S. Schneider	63-125	3	10	2	0	1	2	0	37	1	0	0	0	4	38	2	100	15	25	40
	48	Mubuku*	Mubuku	M.Padoan	63-250	0	1	0	0	0	0	0	13	0	0	0	0	0	85	1	100	1	/	/
	49	Nyamwamba	Kilembe	S. Schneider	63-125	1	7	1	0	2	1	1	32	3	0	0	1	2	48	1	100	9	75	50
	51	Nyamagasani 2*	Kagando	M.Padoan	63-250	1	17	11	1	1	0	0	54	4	0	0	0	0	9	0	100	30	82	92

*samples adopted from Garzanti et al. (2013a)

A2-5a Bulk rock geochemistry (sand fraction)

Sand Fraction

Tectonic province	sample ID	river/lake name	site	Laboratory	Class	SiO2	Al2O3	Fe2O3	MnO	MgO	CaO	Na2O	K2O	TiO2	P2O5	LOI	Total	Sc	V	Cr	Co	Ni	Cu	Zn	Ga	As	Rb	Sr	Y	Zr	Nb
					(µm)	wt%	wt%	wt%	wt%	wt%	wt%	wt%	wt%	wt%	wt%	wt%		ppm	ppm	ppm	ppm	ppm	ppm	ppm	ppm	ppm	ppm	ppm	ppm	ppm	ppm	ppm
Lake Albert basin	3	Bulisa*	Bulisa	ACME	63-2000	96.98	0.71	0.86	0.01	0.01	0.02	0.01	0.05	0.37	0.02	1.00	100.04	<1	20.00	27.37	1.40	1.30	2.50	5.00	1.30	0.90	2.10	4.80	2.90	238.10	5.90
	5	Waiga*	Rabongo Forest	ACME	63-2000	80.49	5.81	5.14	0.10	1.19	2.10	1.01	0.84	1.49	0.14	1.50	99.81	10.00	88.00	75.26	13.70	9.70	7.10	44.00	8.40	<0.5	18.20	144.50	15.50	459.00	24.30
	6	Waiga*	Kigoya	ACME	63-2000	94.50	1.86	1.93	0.03	0.05	0.20	0.24	0.41	0.40	0.05	0.30	99.97	<1	20.00	27.37	3.50	3.30	3.80	70.00	2.40	<0.5	7.50	38.70	6.50	220.90	6.90
	9	Waki*	Biso	ACME	63-2000	93.80	1.16	2.78	0.05	0.06	0.07	0.04	0.16	0.86	0.05	0.90	99.93	2.00	40.00	61.58	6.60	6.20	9.90	40.00	2.10	<0.5	4.10	9.70	5.20	347.90	12.10
	11	Wambabya	Kaiso-Tonya	ALS	63-2000	88.70	3.50	2.28	0.03	0.30	0.59	0.48	1.10	0.34	0.06	1.23	98.66	5.00	35.00	130.00	4.00	4.00	8.00	20.00	6.90	0.30	32.70	33.30	37.30	310.00	11.50
	12	tribut. Wambabya	Hoima	ALS	63-2000	72.40	4.40	18.80	0.05	0.16	0.03	<0.01	0.52	0.26	0.37	4.68	101.72	7.00	95.00	210.00	3.00	8.00	24.00	54.00	8.50	14.80	26.20	12.20	12.60	140.00	6.50
	13	tribut. Wambabya	Kiziranfumbi	ALS	63-2000	71.90	4.95	17.95	0.04	0.16	0.03	<0.01	0.42	0.33	0.32	5.04	101.18	8.00	111.00	230.00	4.00	10.00	24.00	28.00	9.20	14.00	23.60	15.20	13.20	150.00	9.00
	14	tribut. Wambabya	Munteme	ALS	63-2000	80.00	3.21	11.10	0.04	0.10	0.06	<0.01	0.40	0.33	0.13	3.36	98.77	5.00	90.00	270.00	4.00	16.00	23.00	35.00	6.40	14.40	19.00	8.90	11.00	140.00	5.70
	15	tribut. Nkusi	SW Kabwoya	ALS	63-2000	69.00	6.19	17.70	0.06	0.17	0.11	<0.01	0.68	0.42	0.18	5.26	99.83	6.00	227.00	310.00	7.00	10.00	28.00	33.00	10.60	25.50	37.40	12.80	16.50	170.00	10.60
	16	Nkusi 1	Kitoma	ALS	63-2000	75.80	6.61	11.75	0.06	0.34	0.40	0.63	1.82	0.33	0.11	3.76	101.70	5.00	130.00	290.00	5.00	10.00	19.00	21.00	9.80	13.60	58.50	32.20	7.60	140.00	7.30
	17	Nkusi 2*	Pachwa	ACME	63-2000	76.57	6.78	9.00	0.04	0.09	0.09	0.26	2.76	0.48	0.13	3.60	99.80	4.00	110.00	130.00	4.00	6.00	15.40	574.00	8.60	8.30	78.70	52.00	11.40	180.40	13.50
	18	tribut. Nkusi	SW Kitoma	ALS	63-2000	87.10	2.38	5.54	0.06	<0.01	<0.01	0.08	0.30	0.97	0.11	1.71	98.31	4.00	70.00	350.00	9.00	10.00	15.00	20.00	4.80	2.00	10.50	12.90	6.80	180.00	15.90
	19	tribut. Nkusi	SW Kyangamwoyo	ALS	63-2000	91.50	1.28	2.83	0.05	0.02	0.03	<0.01	0.26	1.37	0.03	0.95	98.35	3.00	48.00	260.00	3.00	7.00	6.00	18.00	3.20	0.50	8.30	8.40	11.80	440.00	29.70
	20	Muzizi	W Nyakalengija	ALS	63-2000	92.00	3.19	2.45	0.04	0.20	0.25	0.32	1.32	0.71	<0.01	0.91	101.44	3.00	36.00	160.00	4.00	11.00	6.00	19.00	4.60	0.20	42.30	28.20	11.40	250.00	7.40
Lake George basin	21	Kazinga	Katunguru	ALS	63-2000	88.52	4.02	3.85	0.05	0.09	0.10	0.17	0.91	0.27	0.05	1.46	99.48	4.00	55.00	190.00	5.00	20.00	10.00	30.00	6.00	5.00	42.00	22.00	9.80	130.00	4.90
	21	Kazinga	Katunguru	ALS	63-2000	81.70	6.63	2.54	0.04	0.80	1.50	1.41	1.70	0.39	0.08	1.32	98.19	5.00	52.00	160.00	6.00	15.00	8.00	28.00	8.20	0.20	48.60	120.50	11.20	90.00	7.20
	22	Crater Lake	Durama	ALS	63-2000	68.90	5.46	17.30	0.05	1.25	1.02	0.10	0.24	0.50	0.15	4.62	99.64	30.00	413.00	240.00	13.00	43.00	114.00	50.00	10.90	1.60	10.10	60.70	8.40	90.00	14.30
	23	Dura	north Kibale	ALS	63-2000	84.70	4.00	6.17	0.10	0.34	0.79	0.36	0.66	0.39	0.19	3.25	101.02	7.00	102.00	200.00	16.00	14.00	17.00	37.00	6.40	1.10	22.70	57.10	8.90	100.00	17.00
	24	tribut. Dura	Kibale	ALS	63-2000	93.60	3.11	1.49	0.02	0.08	0.21	0.38	1.34	0.13	0.05	1.29	101.76	2.00	13.00	180.00	4.00	5.00	4.00	16.00	4.20	0.20	38.20	33.90	7.00	70.00	5.80
	25	tribut. Dura	Kahunge	ALS	63-2000	93.10	2.17	2.10	0.01	0.06	0.03	0.02	0.61	0.21	0.01	0.88	99.25	2.00	27.00	250.00	1.00	6.00	3.00	7.00	4.00	0.30	25.20	6.50	5.80	80.00	4.40
	26	tribut. Mpanga	Kamwenge	ALS	63-2000	91.60	2.77	1.58	0.01	0.10	0.26	0.37	1.16	0.19	0.04	0.67	98.81	2.00	16.00	160.00	2.00	4.00	6.00	11.00	4.40	0.40	25.50	21.70	9.80	190.00	6.70
	27	Mpanga south 1	NE of Mpanga	ALS	63-2000	88.70	3.65	3.14	0.04	0.09	0.12	0.24	0.87	0.28	0.05	1.36	98.59	3.00	40.00	200.00	4.00	6.00	4.00	22.00	5.70	0.70	39.60	25.00	9.90	140.00	6.10
Northern Rwenzoris	29	Dunga	N Bubandi	ALS	63-2000	75.50	7.93	8.03	0.11	1.42	1.69	1.62	1.54	1.18	0.15	1.32	100.62	10.00	170.00	160.00	18.00	31.00	14.00	68.00	13.10	0.50	34.30	195.00	7.80	350.00	29.60
	30	Kazi	Bubandi	ALS	63-2000	72.70	10.25	6.57	0.08	1.46	1.80	1.60	3.04	0.87	0.12	2.35	101.01	9.00	145.00	130.00	14.00	18.00	12.00	65.00	14.60	0.20	72.80	266.00	8.30	260.00	17.90
	31	Igasa	Kateebwa	ALS	63-2000	75.70	9.18	5.11	0.09	1.22	1.75	1.88	2.32	0.72	0.13	1.88	100.12	9.00	103.00	140.00	13.00	22.00	11.00	44.00	12.70	0.30	52.10	219.00	7.80	310.00	17.90
	32	Mahoma	Rubona	ALS	63-2000	71.88	10.66	5.98	0.10	1.42	1.77	2.13	2.11	0.90	0.20	2.67	99.82	9.00	116.00	200.00	17.00	30.00	10.00	70.00	14.00	5.00	49.00	273.00	8.90	262.00	28.80
	33	Mpanga north 1*	Fort Portal	ACME	63-2000	69.79	6.60	13.55	0.10	1.86	2.69	0.96	0.69	1.19	0.22	2.10	99.75	18.00	275.00	109.47	20.60	20.10	34.80	91.00	12.40	0.90	16.10	201.30	9.70	208.30	23.70
	34	Mpanga north 2	E Fort Portal	ALS	63-2000	77.52	7.29	5.28	0.18	1.25	2.10	1.33	1.72	0.50	0.27	2.46	99.88	9.00	81.00	210.00	12.00	20.00	10.00	40.00	9.00	5.00	32.00	278.00	7.60	227.00	18.40
Central Rwenzoris	35	Rwimi 1*	Rwimi	ACME	63-2000	69.87	12.36	4.90	0.07	1.68	2.19	2.72	3.44	0.56	0.12	1.90	99.81	12.00	101.00	41.05	14.30	8.30	11.90	138.00	13.10	0.60	75.50	138.90	12.60	94.30	21.00
	36	Rwimi 2	SE Rwimi	ALS	63-2000	70.15	10.92	6.48	0.09	1.70	2.40	2.72	2.54	0.90	0.18	1.42	99.51	14.00	146.00	200.00	16.00	30.00	20.00	60.00	15.00	5.00	62.00	144.00	17.00	238.00	36.70
	37	Butawu	N Mutwanga	ALS	63-2000	75.77	10.00	3.32	0.04	1.10	0.85	1.40	3.84	0.40	0.06	1.66	98.44	6.00	53.00	290.00	8.00	< 20	10.00	50.00	13.00	< 5	111.00	109.00	10.50	106.00	8.10
	41	Mugusu	SE Mount Speke	ALS	63-2000	67.30	15.11	3.33	0.08	1.13	1.96	4.54	3.05	0.40	0.07	1.46	98.43	6.00	63.00	150.00	9.00	< 20	< 10	50.00	18.00	< 5	63.00	348.00	14.90	84.00	9.00
	45	Isebo 1	E Nyabitaba Hut, C. Rwenzoris	ALS	63-2000	74.04	11.03	3.11	0.05	1.00	1.41	2.50	3.41	0.39	0.06	1.27	98.26	6.00	53.00	340.00	7.00	< 20	< 10	40.00	13.00	< 5	76.00	155.00	10.30	85.00	6.60
	46	Mubuku 2	Bugoye	ALS	63-2000	63.00	12.75	8.39	0.13	3.15	4.48	2.68	2.11	0.95	0.11	2.14	99.98	21.00	182.00	160.00	20.00	37.00	24.00	75.00	17.20	0.10	67.30	157.00	21.50	140.00	10.30
	47	Isebo 2	N Mubuku	ALS	63-2000	75.30	10.50	3.59	0.05	0.54	0.66	1.68	3.44	0.52	0.07	2.53	98.98	6.00	61.00	140.00	8.00	16.00	7.00	27.00	13.50	0.40	108.50	98.20	9.20	160.00	13.70
	48	Mubuku*	Mubuku	ACME	63-2000	68.04	12.45	5.87	0.08	2.56	3.43	2.47	2.64	0.53	0.07	1.70	99.84	17.00	118.00	54.74	17.30	12.90	18.30	64.00	13.80	<0.5	73.30	162.90	12.70	70.50	6.50
	49	Nyamwamba	Kilembe	ALS	63-2000	72.00	12.10	6.09	0.08	1.14	1.32	2.03	3.00	0.68	0.08	1.89	100.51	11.00	97.00	180.00	12.00	26.00	32.00	50.00	16.60	0.70	125.50	92.50	15.70	110.00	10.30
	50	Nyamagasani	Kyarumba	ALS	63-2000	71.30	11.54	5.90	0.08	1.41	1.74	1.98	2.80	0.72	0.08	1.53	99.07	12.00	98.00	230.00	13.00	30.00	20.00	60.00	16.00	5.00	110.00	105.00	18.00	126.00	10.50
	51	Nyamagasani 2*	Kagando	ACME	63-2000	70.50	11.40	5.57	0.08	1.67	2.30	2.75	2.58	0.76	0.18	2.18	100.06	13.00	127.00	120.00	12.00	21.00	16.00	56.00	15.40	1.00	72.10	131.50	15.30	180.00	29.70

Sand Fraction

Tectonic province	sample ID	river/lake name	site	Laboratory	Class	Mo	Sn	Sb	Cs	Ba	Bi	La	Ce	Pr	Nd	Sm	Eu	Gd	Tb	Dy	Ho	Er	Tm	Yb	Lu	Hf	Ta	W	Tl	Th	Pb	U
					(µm)	ppm	ppm	ppm	ppm	ppm	ppm	ppm	ppm	ppm	ppm	ppm	ppm	ppm	ppm	ppm	ppm	ppm	ppm	ppm	ppm	ppm	ppm	ppm	ppm	ppm	ppm	ppm
Lake Albert basin	3	Bulisa*	Bulisa	ACME	63-2000	0.10	<1	<0.1	<0.1	35.00	<0.1	4.00	17.30	0.90	3.10	0.59	0.11	0.50	0.08	0.50	0.11	0.36	0.06	0.47	0.08	5.80	0.40	<0.5	<0.1	2.30	4.30	0.40
	5	Waiga*	Rabongo Forest	ACME	63-2000	0.30	1.00	<0.1	<0.1	283.00	<0.1	31.80	60.70	7.37	26.50	4.80	0.84	4.33	0.61	3.11	0.57	1.81	0.26	1.86	0.26	11.70	1.60	0.60	<0.1	13.20	9.70	1.70
	6	Waiga*	Kigoya	ACME	63-2000	0.20	8.00	<0.1	<0.1	138.00	<0.1	13.90	26.00	3.22	10.20	2.05	0.30	1.80	0.26	1.51	0.27	0.76	0.13	0.84	0.12	5.40	0.60	<0.5	<0.1	5.30	18.00	1.00
	9	Waki*	Biso	ACME	63-2000	0.40	1.00	<0.1	<0.1	66.00	<0.1	28.40	55.80	6.04	18.60	3.09	0.16	2.32	0.28	1.26	0.19	0.57	0.08	0.66	0.11	9.20	0.70	29.00	<0.1	21.90	7.10	1.40
	11	Wambabya	Kaiso-Tonya	ALS	63-2000	1.00	2.00	<0.05	0.28	293.00	0.04	27.50	56.40	6.49	24.10	4.55	0.63	4.56	0.80	5.49	1.25	4.03	0.66	4.13	0.63	7.40	1.20	1.00	<0.5	12.10	12.00	1.85
	12	tribut. Wambabya	Hoima	ALS	63-2000	3.00	1.00	0.79	0.76	148.50	0.12	12.80	25.30	2.94	11.00	2.14	0.48	2.17	0.33	2.07	0.43	1.32	0.28	1.37	0.22	3.30	0.40	1.00	<0.5	5.52	16.00	2.26
	13	tribut. Wambabya	Kiziranfumbi	ALS	63-2000	4.00	5.00	0.82	0.71	99.00	0.13	19.90	35.60	4.27	15.70	2.93	0.59	2.64	0.39	2.40	0.52	1.43	0.27	1.39	0.21	3.50	0.50	1.00	<0.5	6.08	20.00	1.79
	14	tribut. Wambabya	Munteme	ALS	63-2000	5.00	<1	1.26	0.50	87.70	0.09	11.20	24.10	2.40	8.50	1.62	0.32	1.71	0.29	1.90	0.40	1.11	0.24	1.13	0.17	3.40	0.30	1.00	<0.5	6.81	13.00	2.90
	15	tribut. Nkusi	SW Kabwoya	ALS	63-2000	7.00	1.00	2.18	1.86	137.50	0.21	18.50	39.00	4.32	15.40	2.88	0.55	2.73	0.46	2.88	0.59	1.68	0.32	1.52	0.22	3.90	0.70	1.00	<0.5	10.70	26.00	1.97
	16	Nkusi 1	Kitoma	ALS	63-2000	5.00	4.00	1.22	1.12	288.00	0.11	16.00	40.20	3.42	11.90	2.06	0.40	1.74	0.26	1.51	0.29	0.82	0.17	0.85	0.13	3.40	0.50	1.00	<0.5	12.35	24.00	1.71
	17	Nkusi 2*	Pachwa	ACME	63-2000	2.70	1.00	1.00	0.80	433.00	0.10	40.20	98.80	8.95	30.10	4.91	0.56	3.99	0.50	2.56	0.42	1.10	0.16	1.00	0.14	4.20	0.70	<0.5	<0.1	26.90	28.80	4.70
	18	tribut. Nkusi	SW Kitoma	ALS	63-2000	3.00	<1	0.16	0.24	77.10	0.04	26.90	66.90	5.96	20.00	3.22	0.22	2.25	0.29	1.42	0.27	0.68	0.16	0.67	0.11	4.40	1.00	1.00	<0.5	17.15	14.00	1.38
	19	tribut. Nkusi	SW Kyangamwoyo	ALS	63-2000	3.00	7.00	0.20	0.11	50.00	0.02	55.70	116.50	12.55	42.80	6.64	0.18	4.47	0.53	2.49	0.43	1.14	0.18	1.09	0.18	11.00	5.00	1.00	<0.5	42.20	20.00	1.88
	20	Muzizi	W Nyakalengija	ALS	63-2000	2.00	1.00	<0.05	0.26	281.00	0.02	18.60	42.40	4.25	14.90	2.65	0.43	2.22	0.33	1.94	0.42	1.24	0.21	1.35	0.22	6.40	0.90	1.00	<0.5	10.30	8.00	1.42
Lake George basin	21	Kazinga	Katunguru	ALS	63-2000	3.00	1.00	0.20	1.00	189.00	0.30	9.18	21.50	2.02	7.37	1.37	0.26	1.25	0.23	1.58	0.33	1.00	0.16	1.17	0.22	3.90	0.55	0.90	0.19	5.64	14.00	1.92
	21	Kazinga	Katunguru	ALS	63-2000	2.00	1.00	0.05	0.68	355.00	0.03	18.50	37.60	4.23	14.80	2.54	0.48	2.08	0.32	1.80	0.36	1.13	0.21	1.14	0.19	2.30	0.60	1.00	<0.5	9.20	10.00	1.04
	22	Crater Lake	Durama	ALS	63-2000	2.00	1.00	0.10	0.17	105.50	0.06	15.40	44.80	3.60	13.50	2.54	0.64	1.99	0.30	1.80	0.36	1.01	0.22	1.12	0.17	2.10	0.70	1.00	<0.5	6.81	10.00	1.40
	23	Dura	north Kibale	ALS	63-2000	2.00	1.00	0.05	0.29	233.00	0.03	25.30	52.10	4.95	16.90	2.74	0.62	2.19	0.30	1.67	0.33	0.92	0.15	0.88	0.14	2.40	0.90	1.00	<0.5	6.77	10.00	1.59
	24	tribut. Dura	Kibale	ALS	63-2000	3.00	1.00	<0.05	0.24	213.00	0.01	10.70	21.20	2.32	8.20	1.49	0.28	1.26	0.19	1.12	0.23	0.68	0.12	0.72	0.11	1.90	0.40	1.00	<0.5	4.20	9.00	1.46
	25	tribut. Dura	Kahunge	ALS	63-2000	3.00	2.00	<0.05	0.24	103.50	0.02	4.20	8.90	0.94	3.30	0.62	0.11	0.66	0.13	0.89	0.21	0.67	0.13	0.77	0.12	2.20	0.40	1.00	<0.5	3.09	3.00	0.66
	26	tribut. Mpanga	Kamwenge	ALS	63-2000	2.00	1.00	<0.05	0.14	275.00	0.03	12.90	26.40	3.03	11.00	2.06	0.30	1.74	0.26	1.61	0.34	1.03	0.17	1.06	0.17	4.70	0.60	<1	<0.5	5.80	7.00	0.97
	27	Mpanga south 1	NE of Mpanga	ALS	63-2000	2.00	1.00	0.06	0.76	199.00	0.06	12.80	30.00	2.84	10.10	1.88	0.34	1.67	0.25	1.58	0.35	1.02	0.18	1.19	0.18	3.50	0.50	1.00	<0.5	5.99	7.00	1.26
Northern Rwenzoris	29	Dunga	N Bubandi	ALS	63-2000	1.00	2.00	0.05	0.42	682.00	0.02	31.40	75.10	6.79	23.90	3.72	0.95	2.53	0.31	1.62	0.30	0.77	0.13	0.74	0.12	8.10	2.20	1.00	<0.5	8.30	9.00	1.52
	30	Kazi	Bubandi	ALS	63-2000	1.00	1.00	<0.05	0.50	945.00	0.01	30.70	65.20	7.09	25.30	4.02	0.96	2.78	0.33	1.70	0.31	0.83	0.14	0.83	0.14	7.00	1.30	1.00	<0.5	13.05	11.00	1.63
	31	Igasa	Kateebwa	ALS	63-2000	<1	1.00	<0.05	0.32	809.00	0.01	26.70	53.50	6.05	21.30	3.46	0.88	2.54	0.30	1.62	0.31	0.82	0.14	0.81	0.14	7.70	1.00	1.00	<0.5	10.20	8.00	1.38
	32	Mahoma	Rubona	ALS	63-2000	3.00	2.00	0.20	0.70	990.00	0.10	37.00	78.90	7.38	26.80	4.32	1.10	2.71	0.36	1.78	0.31	0.84	0.12	0.77	0.13	6.20	1.77	0.60	0.26	9.77	14.00	1.53
	33	Mpanga north 1*	Fort Portal	ACME	63-2000	1.50	2.00	0.10	0.20	297.00	<0.1	22.50	62.80	5.41	20.10	3.40	0.79	2.63	0.39	1.98	0.35	1.00	0.18	1.09	0.16	5.30	1.90	0.70	<0.1	9.10	11.40	2.90
	34	Mpanga north 2	E Fort Portal	ALS	63-2000	3.00	1.00	0.20	0.40	1036.00	0.10	26.50	53.80	5.47	19.60	3.21	0.86	2.19	0.30	1.47	0.26	0.73	0.10	0.64	0.10	3.30	0.88	1.10	0.16	6.93	10.00	1.10
Central Rwenzoris	35	Rwimi 1*	Rwimi	ACME	63-2000	0.20	2.00	<0.1	0.60	491.00	<0.1	24.50	48.20	5.80	19.50	3.53	0.75	2.89	0.44	2.53	0.45	1.31	0.22	1.57	0.19	3.00	1.60	0.80	<0.1	18.70	7.90	4.20
	36	Rwimi 2	SE Rwimi	ALS	63-2000	3.00	4.00	0.20	0.60	448.00	0.20	31.40	65.30	7.01	25.40	4.60	0.98	3.48	0.54	2.99	0.60	1.65	0.25	1.72	0.29	6.50	3.48	1.20	0.27	23.80	16.00	5.30
	37	Butawu	N Mutwanga	ALS	63-2000	4.00	2.00	< 0.2	1.40	687.00	0.20	16.60	30.70	3.68	13.80	2.58	0.52	1.88	0.31	1.71	0.33	0.98	0.15	1.04	0.18	3.00	0.70	1.80	0.47	13.30	21.00	4.63
	41	Mugusu	SE Mount Speke	ALS	63-2000	3.00	2.00	< 0.2	0.90	1096.00	0.40	38.40	79.70	8.83	32.50	5.67	1.21	3.57	0.49	2.63	0.48	1.42	0.21	1.40	0.22	2.50	0.88	0.90	0.32	17.00	27.00	6.76
	45	Isebo 1	E Nyabitaba Hut, C. Rwenzoris	ALS	63-2000	6.00	1.00	< 0.2	0.90	656.00	< 0.1	15.60	34.90	3.64	13.20	2.60	0.59	2.06	0.32	1.83	0.35	1.01	0.15	1.00	0.17	2.50	0.69	0.60	0.36	7.58	19.00	1.69
	46	Mubuku 2	Bugoye	ALS	63-2000	<1	2.00	<0.05	1.18	411.00	0.04	24.20	49.50	6.06	22.80	4.54	1.11	4.13	0.65	3.66	0.74	2.21	0.39	2.23	0.35	3.80	0.90	1.00	<0.5	10.95	11.00	2.31
	47	Isebo 2	N Mubuku	ALS	63-2000	1.00	3.00	<0.05	2.19	613.00	0.07	19.20	39.20	4.31	15.10	2.58	0.56	2.08	0.31	1.65	0.31	0.96	0.18	1.00	0.16	4.10	1.20	2.00	<0.5	9.84	12.00	2.62
	48	Mubuku*	Mubuku	ACME	63-2000	0.20	1.00	<0.1	1.20	487.00	<0.1	12.30	23.60	3.09	11.60	2.26	0.61	2.25	0.37	2.21	0.43	1.28	0.20	1.33	0.20	2.00	0.50	0.70	0.10	5.00	5.90	1.30
	49	Nyamwamba	Kilembe	ALS	63-2000	1.00	3.00	0.06	3.13	485.00	0.15	22.90	46.20	5.45	19.20	3.70	0.75	3.17	0.48	2.68	0.54	1.63	0.30	1.74	0.27	3.20	1.00	2.00	<0.5	12.30	16.00	3.27
	50	Nyamagasani	Kyarumba	ALS	63-2000	3.00	5.00	0.30	2.90	464.00	0.60	20.40	43.40	4.77	17.90	3.72	0.73	3.12	0.51	2.97	0.61	1.73	0.27	1.85	0.32	3.70	1.00	1.40	0.53	11.70	23.00	3.76
	51	Nyamagasani 2*	Kagando	ACME	63-2000	1.00	3.00	<0.05	0.73	419.00	0.04	29.80	59.10	6.71	23.50	4.08	0.90	3.13	0.47	2.56	0.49	1.54	0.27	1.53	0.24	4.70	2.70	1.00	<0.5	18.35	11.00	4.68

A2-5b Bulk rock geochemistry (mud fraction)

MUD Fraction

Tectonic province	sample ID	river/lake name	site	Laboratory	Class	Mo	Sn	Sb	Cs	Ba	Bi	La	Ce	Pr	Nd	Sm	Eu	Gd	Tb	Dy	Ho	Er	Tm	Yb	Lu	Hf	Ta	W	Tl	Th	Pb	U
					(µm)	ppm	ppm	ppm	ppm	ppm	ppm	ppm	ppm	ppm	ppm	ppm	ppm	ppm	ppm	ppm	ppm	ppm	ppm	ppm	ppm	ppm	ppm	ppm	ppm	ppm	ppm	ppm
Lake Albert basin	11	Wambabya	Kaiso-Tonya	Actlabs	<63	3.00	10.00	< 0.5	1.30	406.00	< 0.4	112.00	237.00	24.70	92.90	17.00	2.34	13.50	2.20	13.20	2.60	8.10	1.29	9.00	1.56	59.40	3.80	< 1	0.10	43.30	36.00	10.40
	12	tribut. Wambabya	Hoima	Actlabs	<63	5.00	7.00	1.50	1.60	293.00	< 0.4	46.70	95.50	9.88	36.70	6.90	1.41	6.00	1.10	6.80	1.50	4.70	0.75	5.10	0.86	26.30	1.50	2.00	< 0.1	16.20	26.00	6.60
	13	tribut. Wambabya	Kiziranfumbi	Actlabs	<63	5.00	40.00	1.20	1.80	176.00	< 0.4	70.70	141.00	14.60	53.70	10.30	1.79	7.80	1.30	8.60	1.80	5.70	0.94	6.90	1.16	40.60	2.80	3.00	0.30	20.40	26.00	7.70
	14	tribut. Wambabya	Munteme	Actlabs	<63	6.00	30.00	1.40	1.20	329.00	< 0.4	83.60	171.00	16.40	59.30	10.70	1.80	8.40	1.50	9.30	1.90	5.90	0.96	6.70	1.19	40.20	2.00	3.00	0.30	32.70	28.00	11.00
	15	tribut. Nkusi	SW Kabwoya	Actlabs	<63	4.00	12.00	0.80	3.30	245.00	< 0.4	73.10	159.00	16.90	63.00	11.20	1.82	9.00	1.50	8.90	1.80	5.50	0.83	5.50	0.95	29.70	2.00	2.00	< 0.1	24.80	18.00	6.00
	16	Nkusi 1	Kitoma	Actlabs	<63	5.00	26.00	0.80	3.50	455.00	< 0.4	78.10	186.00	17.10	60.40	11.00	1.29	8.30	1.40	7.70	1.60	4.60	0.69	4.90	0.78	24.60	2.70	3.00	0.60	45.30	45.00	7.50
	18	tribut. Nkusi	SW Kitoma	Actlabs	<63	4.00	38.00	< 0.5	0.80	387.00	< 0.4	171.00	367.00	36.50	129.00	21.70	1.60	15.70	2.20	11.60	2.20	6.40	1.01	7.30	1.28	69.00	4.20	2.00	< 0.1	95.30	50.00	13.40
	19	tribut. Nkusi	SW Kyangamwoyo	Actlabs	<63	3.00	18.00	< 0.5	0.80	249.00	< 0.4	237.00	505.00	49.80	175.00	28.90	1.36	20.80	2.90	14.80	2.90	8.60	1.40	9.90	1.75	81.20	3.40	1.00	< 0.1	163.00	51.00	15.00
	20	Muzizi	W Nyakalengija	Actlabs	<63	3.00	17.00	< 0.5	1.30	489.00	< 0.4	113.00	221.00	24.60	89.90	17.00	2.79	13.10	2.10	12.40	2.50	7.70	1.21	8.50	1.47	46.10	3.20	2.00	0.80	54.80	41.00	11.40
Lake George basin	21	Kazinga	Katunguru	Actlabs	<63	< 2	8.00	< 0.5	1.60	506.00	< 0.4	158.00	333.00	37.70	134.00	18.90	4.22	11.80	1.60	8.60	1.60	5.10	0.77	5.10	0.88	16.10	10.10	< 1	< 0.1	34.40	36.00	5.70
	22	Crater Lake	Durama	Actlabs	<63	3.00	10.00	< 0.5	0.80	554.00	< 0.4	204.00	462.00	46.50	167.00	22.40	5.44	12.90	1.50	6.90	1.10	3.10	0.41	2.60	0.41	9.80	12.20	1.00	< 0.1	41.70	20.00	7.60
	23	Dura	north Kibale	Actlabs	<63	2.00	13.00	< 0.5	0.90	812.00	< 0.4	134.00	284.00	29.50	105.00	15.50	3.44	10.30	1.40	7.10	1.30	3.80	0.56	3.80	0.63	13.70	7.60	1.00	< 0.1	34.00	17.00	9.60
	24	tribut. Dura	Kibale	Actlabs	<63	< 2	13.00	< 0.5	1.30	636.00	< 0.4	119.00	236.00	25.40	93.70	16.60	2.40	12.70	2.00	11.20	2.10	6.20	1.00	7.00	1.16	26.80	4.70	1.00	0.10	49.20	39.00	19.30
	25	tribut. Dura	Kahunge	Actlabs	<63	2.00	18.00	< 0.5	1.30	446.00	< 0.4	55.30	123.00	12.10	45.00	8.60	1.41	7.40	1.30	8.30	1.80	5.80	1.01	7.00	1.24	28.50	2.60	< 1	< 0.1	32.90	20.00	7.40
	26	tribut. Mpanga	Kamwenge	Actlabs	<63	4.00	32.00	< 0.5	0.80	581.00	< 0.4	133.00	269.00	30.50	116.00	22.20	2.85	18.30	3.00	17.70	3.70	11.20	1.84	12.90	2.30	90.90	4.50	1.00	< 0.1	58.10	42.00	14.50
	27	Mpanga south 1	NE of Mpanga	Actlabs	<63	2.00	32.00	< 0.5	1.40	760.00	< 0.4	143.00	300.00	31.10	116.00	21.20	3.59	17.50	3.10	19.00	4.00	12.50	2.05	14.30	2.42	67.00	4.00	2.00	< 0.1	61.80	34.00	13.60
	28	Mpanga south 2	Rwenjaza	Actlabs	<63	< 2	4.00	< 0.2	1.10	1024.00	93.20	189.00	20.60	74.00	12.80	2.41	9.31	1.43	8.21	1.65	4.97	0.78	5.41	0.96	51.40	4.31	1.20	0.33	24.00	37.60	< 0.1	7.87
Northern Rwenzoris	29	Dunga	N Bubandi	Actlabs	<63	< 2	9.00	< 0.5	1.00	1023.00	< 0.4	140.00	318.00	31.60	114.00	16.40	4.27	9.70	1.20	6.00	1.00	2.90	0.42	2.90	0.55	33.60	9.30	2.00	< 0.1	35.10	25.00	7.60
	30	Kazi	Bubandi	Actlabs	<63	< 2	12.00	< 0.5	1.00	941.00	< 0.4	128.00	275.00	28.70	103.00	15.30	3.61	9.30	1.10	5.60	1.00	2.70	0.38	2.60	0.46	23.60	8.00	1.00	0.40	31.30	17.00	6.80
	31	Igasa	Kateebwa	Actlabs	<63	< 2	18.00	< 0.5	0.70	978.00	< 0.4	117.00	245.00	26.30	95.40	13.90	3.42	9.10	1.10	5.50	1.00	2.90	0.42	2.80	0.54	30.80	8.30	1.00	< 0.1	32.90	18.00	9.90
	32	Mahoma	Rubona	Actlabs	<63	< 2	4.00	< 0.2	1.10	973.00	149.00	321.00	34.20	123.00	17.90	4.44	10.40	1.27	6.32	1.07	3.01	0.43	3.09	0.57	36.20	10.20	0.80	0.28	17.00	38.90	< 0.1	9.23
	34	Mpanga north 1	E Fort Portal	Actlabs	<63	< 2	2.00	< 0.2	1.30	1608.00	155.00	320.00	34.70	123.00	17.80	4.37	10.70	1.25	5.94	0.97	2.67	0.36	2.29	0.37	7.40	7.46	0.90	0.27	17.00	34.60	< 0.1	6.62
Central Rwenzoris	35	Rwimi 1	Rwimi	Actlabs	<63	< 2	3.00	< 0.5	1.20	480.00	< 0.4	70.80	140.00	15.20	55.60	9.30	2.07	6.80	1.00	5.30	1.00	2.90	0.44	2.80	0.48	12.00	4.30	< 1	< 0.1	25.40	19.00	9.30
	36	Rwimi 2	SE Rwimi	Actlabs	<63	< 2	7.00	0.30	1.50	627.00	120.00	231.00	25.10	89.80	14.70	3.40	10.10	1.46	8.13	1.57	4.59	0.73	5.18	0.96	35.10	10.50	2.00	0.36	44.00	46.40	0.20	16.40
	46	Mubuku 2	Bugoye	Actlabs	<63	< 2	4.00	< 0.5	1.40	336.00	< 0.4	39.00	78.00	8.85	33.70	6.60	1.59	5.50	0.90	5.40	1.10	3.10	0.50	3.30	0.55	10.50	1.40	< 1	< 0.1	14.40	19.00	5.10
	47	Isebo	N Mubuku	Actlabs	<63	< 2	27.00	< 0.5	3.60	594.00	< 0.4	94.90	195.00	20.80	76.10	13.00	2.65	10.10	1.60	9.70	2.00	6.00	0.97	6.90	1.19	33.10	6.20	2.00	< 0.1	38.20	27.00	11.90
	49	Nyamwamba	Kilembe	Actlabs	<63	< 2	9.00	< 0.5	4.70	556.00	< 0.4	68.40	141.00	15.10	55.90	10.40	2.05	7.90	1.20	6.90	1.30	3.90	0.61	4.20	0.71	10.80	2.30	3.00	0.60	24.60	29.00	16.40
	50	Nyamagasani	Kyarumba	Actlabs	<63	< 2	7.00	< 0.2	2.00	453.00	38.80	81.70	8.71	32.50	6.32	1.54	5.27	0.83	4.91	0.98	2.85	0.43	2.95	0.51	9.90	2.12	< 0.5	0.36	31.00	17.70	< 0.1	5.94

MUD Fraction

Tectonic province	sample ID	river/lake name	site	Laboratory	Class	SiO2	Al2O3	Fe2O3	MnO	MgO	CaO	Na2O	K2O	TiO2	P2O5	LOI	Total	Sc	V	Cr	Co	Ni	Cu	Zn	Ga	As	Rb	Sr	Y	Zr	Nb
					(µm)	wt%	wt%	wt%	wt%	wt%	wt%	wt%	wt%	wt%	wt%	wt%		ppm	ppm	ppm	ppm	ppm	ppm	ppm	ppm	ppm	ppm	ppm	ppm	ppm	ppm
Lake Albert basin	11	Wambabya	Kaiso-Tonya	Actlabs	<63	67.71	10.66	8.39	0.15	0.51	0.91	0.47	1.52	1.13	0.19	7.60	99.25	18.00	102.00	60.00	13.00	< 20	30.00	60.00	19.00	< 5	62.00	75.00	70.00	2445.00	44.00
	12	tribut. Wambabya	Hoima	Actlabs	<63	53.46	9.47	26.64	0.09	0.31	0.16	0.04	1.02	0.89	0.46	8.20	100.70	15.00	172.00	180.00	9.00	30.00	40.00	90.00	15.00	27.00	47.00	30.00	39.00	1128.00	22.00
	13	tribut. Wambabya	Kiziranfumbi	Actlabs	<63	56.79	10.97	20.55	0.06	0.28	0.19	0.04	0.70	1.26	0.39	7.87	99.10	16.00	168.00	210.00	8.00	30.00	40.00	50.00	16.00	22.00	44.00	36.00	49.00	1686.00	34.00
	14	tribut. Wambabya	Munteme	Actlabs	<63	66.92	8.88	12.30	0.15	0.29	0.41	0.14	1.17	1.57	0.18	7.23	99.25	13.00	128.00	200.00	16.00	30.00	40.00	80.00	14.00	19.00	48.00	32.00	54.00	1685.00	26.00
	15	tribut. Nkusi	SW Kabwoya	Actlabs	<63	72.56	8.10	8.58	0.23	0.31	0.33	0.07	0.91	1.17	0.14	6.87	99.28	10.00	137.00	110.00	16.00	20.00	20.00	50.00	13.00	9.00	57.00	32.00	48.00	1268.00	24.00
	16	Nkusi 1	Kitoma	Actlabs	<63	55.40	15.09	14.91	0.24	0.38	0.38	0.22	1.68	1.34	0.24	10.71	100.60	13.00	196.00	130.00	21.00	30.00	30.00	50.00	22.00	11.00	98.00	58.00	42.00	982.00	42.00
	18	tribut. Nkusi	SW Kitoma	Actlabs	<63	60.50	12.23	13.80	0.23	0.30	0.39	0.29	1.35	4.53	0.17	6.74	100.50	20.00	262.00	330.00	19.00	50.00	50.00	110.00	21.00	7.00	49.00	71.00	59.00	2893.00	62.00
	19	tribut. Nkusi	SW Kyangamwoyo	Actlabs	<63	62.95	13.86	8.63	0.14	0.17	0.20	0.14	1.41	3.47	0.16	7.30	98.43	15.00	171.00	130.00	11.00	50.00	30.00	80.00	24.00	< 5	44.00	43.00	73.00	3177.00	54.00
	20	Muzizi	W Nyakalengija	Actlabs	<63	57.35	16.92	10.93	0.10	0.75	0.94	0.41	1.78	1.69	0.20	9.37	100.40	20.00	178.00	120.00	22.00	40.00	30.00	110.00	24.00	< 5	84.00	69.00	70.00	1761.00	37.00
Lake George basin	21	Kazinga	Katunguru	Actlabs	<63	62.30	10.29	8.34	0.14	2.19	4.80	1.51	1.69	2.65	0.42	4.58	98.90	18.00	160.00	240.00	20.00	50.00	30.00	100.00	18.00	< 5	67.00	349.00	45.00	613.00	108.00
	22	Crater Lake	Durama	Actlabs	<63	49.65	10.37	20.97	0.19	2.74	2.76	0.40	0.69	2.70	0.42	7.96	98.84	38.00	443.00	360.00	33.00	80.00	110.00	110.00	23.00	< 5	32.00	260.00	24.00	405.00	205.00
	23	Dura	north Kibale	Actlabs	<63	52.27	12.28	12.85	0.55	1.02	3.13	0.68	1.05	3.12	0.55	12.18	99.69	23.00	220.00	150.00	48.00	60.00	40.00	130.00	20.00	< 5	41.00	209.00	33.00	565.00	136.00
	24	tribut. Dura	Kibale	Actlabs	<63	62.12	12.77	6.61	0.17	0.55	1.47	0.98	2.73	1.95	0.25	9.71	99.33	15.00	127.00	100.00	23.00	30.00	30.00	130.00	19.00	< 5	87.00	122.00	58.00	1021.00	57.00
	25	tribut. Dura	Kahunge	Actlabs	<63	69.95	13.55	7.33	0.05	0.31	0.26	0.15	2.82	1.11	0.11	5.32	101.00	12.00	121.00	170.00	6.00	20.00	10.00	50.00	20.00	< 5	113.00	39.00	50.00	1100.00	33.00
	26	tribut. Mpanga	Kamwenge	Actlabs	<63	71.55	9.81	8.51	0.08	0.49	1.32	1.11	2.39	1.21	0.18	3.80	100.40	21.00	109.00	160.00	9.00	< 20	30.00	70.00	19.00	< 5	69.00	89.00	93.00	3731.00	49.00
	27	Mpanga south 1	NE of Mpanga	Actlabs	<63	68.96	10.85	7.35	0.31	0.39	1.15	1.18	2.12	2.01	0.21	5.73	100.30	13.00	119.00	150.00	23.00	30.00	20.00	100.00	17.00	< 5	77.00	189.00	113.00	2728.00	46.00
	28	Mpanga south 2	Rwenjaza	Actlabs	<63	62.61	11.45	8.05	0.38	0.70	1.87	1.59	1.79	1.79	0.27	8.79	99.27	12.00	92.00	60.00	25.00	30.00	20.00	80.00	16.00	< 5	55.00	303.00	49.50	2100.00	71.10
Northern Rwenzoris	29	Dunga	N Bubandi	Actlabs	<63	53.48	15.54	11.87	0.21	2.04	3.48	2.60	2.06	2.13	0.57	5.16	99.15	18.00	229.00	90.00	30.00	50.00	30.00	130.00	27.00	< 5	55.00	515.00	26.00	1434.00	122.00
	30	Kazi	Bubandi	Actlabs	<63	50.69	17.00	10.10	0.21	2.07	3.37	1.93	2.30	1.55	0.44	11.30	100.90	19.00	186.00	70.00	28.00	30.00	30.00	120.00	25.00	< 5	80.00	474.00	25.00	989.00	128.00
	31	Igasa	Kateebwa	Actlabs	<63	53.54	15.16	10.82	0.27	1.96	3.54	2.30	1.80	1.76	0.52	7.34	99.01	20.00	200.00	110.00	29.00	50.00	30.00	110.00	25.00	< 5	57.00	468.00	25.00	1345.00	119.00
	32	Mahoma	Rubona	Actlabs	<63	52.00	15.16	11.69	0.22	2.17	3.63	2.38	1.89	2.15	0.61	6.68	98.56	17.00	204.00	80.00	30.00	50.00	30.00	110.00	26.00	< 5	57.00	507.00	30.70	1520.00	131.00
	34	Mpanga north 1	E Fort Portal	Actlabs	<63	45.41	13.56	12.05	0.45	1.62	3.29	1.53	1.37	1.57	1.06	15.95	97.85	16.00	167.00	60.00	24.00	30.00	30.00	110.00	20.00	< 5	48.00	470.00	27.40	453.00	114.00
Central Rwenzoris	35	Rwimi 1	Rwimi	Actlabs	<63	59.95	12.94	7.60	0.13	2.21	3.51	2.61	1.81	1.00	0.40	8.39	100.50	20.00	157.00	90.00	20.00	30.00	40.00	100.00	21.00	< 5	79.00	218.00	26.00	437.00	71.00
	36	Rwimi 2	SE Rwimi	Actlabs	<63	56.64	12.52	11.06	0.19	2.47	4.87	2.29	1.56	1.58	0.95	4.44	98.57	29.00	225.00	70.00	24.00	40.00	30.00	130.00	21.00	< 5	65.00	318.00	46.70	1440.00	148.00
	46	Mubuku 2	Bugoye	Actlabs	<63	52.64	13.42	10.32	0.18	4.11	5.92	2.47	1.44	1.22	0.22	6.58	98.52	29.00	233.00	160.00	33.00	60.00	60.00	120.00	20.00	< 5	55.00	193.00	29.00	396.00	20.00
	47	Isebo	N Mubuku	Actlabs	<63	59.32	14.34	8.97	0.14	1.16	2.23	1.81	2.42	1.35	0.26	6.30	98.31	17.00	151.00	140.00	16.00	30.00	20.00	80.00	22.00	< 5	105.00	191.00	56.00	1298.00	72.00
	49	Nyamwamba	Kilembe	Actlabs	<63	56.77	13.89	8.38	0.20	1.70	2.25	1.50	2.14	1.00	0.27	12.09	100.20	16.00	128.00	140.00	34.00	50.00	120.00	150.00	19.00	< 5	115.00	129.00	36.00	389.00	30.00
	50	Nyamagasani	Kyarumba	Actlabs	<63	53.81	14.57	10.08	0.20	4.03	5.33	2.58	1.60	1.15	0.24	5.45	99.05	27.00	214.00	80.00	35.00	50.00	60.00	130.00	20.00	< 5	67.00	193.00	29.20	379.00	37.40

Tectonic province	sample ID	river/lake name	site	weathering indices						alpha values															
				SAND FRACTION			MUD FRACTION			SAND FRACTION								MUD FRACTION							
				CIA	PIA	WIP	CIA	PIA	WIP	α^{Al}_{Na}	α^{Al}_{Ca}	α^{Al}_{Sr}	α^{Al}_{Mg}	α^{Al}_{K}	α^{Al}_{Ba}	α^{Al}_{Rb}	α^{Al}_{Cs}	α^{Al}_{Na}	α^{Al}_{Ca}	α^{Al}_{Sr}	α^{Al}_{Mg}	α^{Al}_{K}	α^{Al}_{Ba}	α^{Al}_{Rb}	α^{Al}_{Cs}
Lake Albert basin	3	Bulisa*	Bulisa	92	99	1	-	-	-	17	9	3	11	3	1	2	-	-	-	-	-	-	-	-	-
	5	Waiga 1*	Rabongo Forest	63	69	6	-	-	-	1	1	1	1	1	1	2	-	-	-	-	-	-	-	-	-
	6	Waiga 2*	Kigoya	49	49	25	-	-	-	2	2	1	6	1	1	2	-	-	-	-	-	-	-	-	-
	9	Waki*	Biso	82	93	2	-	-	-	7	4	3	3	1	1	2	-	-	-	-	-	-	-	-	-
	11	Wambabya	Kaiso-Tonya	62	69	11	79	87	16	3	2	5	2	1	1	1	6	8	4	7	3	2	2	3	4
	12	tribut. Wambabya	Hoima	89	100	4	89	98	8	158	55	16	5	3	2	2	3	85	22	15	5	3	2	3	3
	13	tribut. Wambabya	Kiziranfumbi	92	100	3	92	98	6	178	62	14	5	4	3	3	3	99	22	15	6	5	5	4	3
	14	tribut. Wambabya	Munteme	87	97	3	84	93	10	115	20	16	5	3	3	2	3	23	8	13	5	3	2	3	4
	15	tribut. Nkusi	SW Kabwoya	89	98	5	86	95	8	223	21	21	6	3	3	2	2	42	9	12	4	3	2	2	1
	16	Nkusi 1	Kitoma	70	83	16	87	96	15	4	6	9	3	1	2	2	3	25	15	13	7	3	3	2	2
	17	Nkusi 2*	Pachwa	67	93	26	-	-	-	6	19	3	12	0	1	1	3	-	-	-	-	-	-	-	-
	18	tribut. Nkusi	SW Kitoma	86	96	2	86	94	12	11	89	8	39	3	2	3	5	15	12	8	7	3	2	4	8
	19	tribut. Nkusi	SW Kyangamwoyo	81	100	2	89	97	12	46	16	7	11	2	2	2	5	36	26	15	13	3	4	5	9
	20	Muzizi	W Nyakalengija	63	79	11	84	92	18	4	5	5	3	1	1	1	6	15	7	12	4	3	3	3	7
Lake George basin	21	Kazinga*	Katunguru	59	63	22	56	58	32	2	2	2	1	1	1	2	4	7	2	0	5	6	0	0	7
	22	Crater Lake	Durama	80	82	6	73	75	17	20	2	4	1	8	4	8	15	9	1	2	1	5	1	5	7
	23	Dura	north Kibale	69	74	8	72	75	20	4	2	3	2	2	1	2	6	6	1	3	2	4	1	5	7
	24	tribut. Dura	Kibale	62	75	11	71	80	29	3	6	4	6	1	1	1	6	5	3	5	4	2	2	2	5
	25	tribut. Dura	Kahunge	77	100	4	81	96	21	39	27	15	6	1	1	1	4	32	19	16	7	2	2	2	5
	26	tribut. Mpanga	Kamwenge	61	70	10	67	75	25	3	4	6	5	1	1	2	9	3	3	5	3	1	1	2	6
	27	Mpanga south 1	NE of Mpanga	75	91	7	71	79	23	5	11	6	7	1	1	1	2	3	4	3	5	2	1	2	4
	28	Mpanga south 2	Rwenjaza	77	91	7	69	74	26	9	15	8	7	2	1	1	2	3	2	2	3	2	1	3	5
Northern Rwenzoris	29	Dunga	N Bubandi	62	66	23	66	69	37	2	2	2	1	2	1	3	9	2	2	1	1	3	1	4	8
	30	Kazi	Bubandi	61	68	33	69	74	37	2	2	2	1	1	1	2	9	3	2	2	1	3	1	3	9
	31	Igasa	Kateebwa	61	65	29	67	70	34	2	2	2	1	1	1	2	13	2	2	2	1	3	1	4	11
	32	Mahoma*	Rubona	64	69	29	66	69	36	2	2	2	1	2	1	3	7	2	2	1	1	3	1	4	7
	33	Mpanga north 1*	Fort Portal	50	50	26	-	-	-	2	1	1	1	2	1	3	10	-	-	-	-	-	-	-	-
	34	Mpanga north 2	E Fort Portal	59	61	24	69	72	30	2	1	1	1	1	0	3	8	3	2	2	1	3	1	5	6
Central Rwenzoris	35	Rwimi 1*	Rwimi	51	51	64	-	-	-	1	1	2	1	1	1	1	6	-	-	-	-	-	-	-	-
	36	Rwimi 2	SE Rwimi	59	62	36	59	61	35	1	2	3	1	1	2	2	8	2	1	2	1	3	1	3	4
	41	Mugusu	SE Mount Speke	61	65	46	62	65	42	1	3	2	2	2	1	3	8	2	2	2	1	2	1	2	3
	42	Mubuku 4	SW Nyabitaba Hut, C. Rwenzoris	-	-	-	57	58	42	-	-	-	-	-	-	-	-	2	1	4	1	4	4	5	4
	43	Bujuku	W Nyabitaba Hut, C. Rwenzoris	-	-	-	59	60	39	-	-	-	-	-	-	-	-	5	2	0	3	20	0	1	19
	44	Mubuku 1	W Nyabitaba Hut, C. Rwenzoris	62	73	36	59	61	43	3	4	4	2	1	1	1	3	2	1	4	1	3	3	3	3
	45	Isebo 1	E Nyabitaba Hut, C. Rwenzoris	60	66	39	64	67	44	2	3	3	2	1	1	2	6	2	2	3	1	2	2	3	4
	46	Mubuku 2	Bugoye	58	60	40	58	59	41	2	1	4	1	2	2	3	5	2	1	3	1	3	3	4	5
	47	Isebo 2	N Mubuku	64	75	33	69	75	32	2	6	5	3	1	1	1	2	3	2	4	2	2	2	2	2
	48	Mubuku*	Mubuku	49	49	61	-	-	-	1	1	2	1	1	1	1	3	-	-	-	-	-	-	-	-
	49	Nyamwamba	Kilembe	66	73	33	70	76	31	2	3	6	2	1	2	1	2	3	2	5	1	2	2	2	2
	50	Nyamagasani	Kyarumba	64	70	33	61	62	40	2	2	5	1	1	2	1	2	2	1	4	1	3	2	3	4
	51	Nyamagasani 2*	Kagando	60	64	37	62	65	36	1	2	4	1	2	2	2	7	2	1	3	1	2	2	2	5

*samples adopted from Garzanti et al. (2013a)

Appendix – Chapter 3

A3-1 – Rutile chemistry

	Sample ID	River name	Al ppm	Si ppm	Nb ppm	Cr ppm	Fe ppm	Ti ppm	V ppm	Zr ppm	Total %
Detection limit			0.001	0.003	0.004	0.0017	0.002	0.02	0.002	0.027	
1	GPS 59	trib. Wambabya	302	178	2932	1120	1237	585182	1324	432	98.78
2	GPS 59	trib. Wambabya	373	119	1711	4529	749	583443	1709	455	98.85
3	GPS 59	trib. Wambabya	249	572	5639	153	5156	580446	706	321	98.87
4	GPS 59	trib. Wambabya	349	111	1776	4555	759	587340	1734	512	99.52
5	GPS 59	trib. Wambabya	29	99	1343	3642	309	588479	4280	877	99.84
6	GPS 59	trib. Wambabya	39	82	2006	122	2219	592616	2161	307	99.93
7	GPS 59	trib. Wambabya	208	108	716	1914	490	591297	3255	1604	99.93
8	GPS 59	trib. Wambabya	46	109	5864	4185	678	586261	2209	289	99.94
9	GPS 59	trib. Wambabya	300	349	6881	647	3384	586680	1334	249	99.97
10	GPS 59	trib. Wambabya	22	84	1123	3678	65	589318	5381	814	100.08
11	GPS 59	trib. Wambabya	37	117	1047	2767	527	594714	1660	384	100.21
12	GPS 59	trib. Wambabya	291	147	3402	2046	689	591477	3070	529	100.27
13	GPS 59	trib. Wambabya	234	156	1608	140	2128	596812	1833	244	100.53
14	GPS 59	trib. Wambabya	37	88	2972	6076	455	591417	1685	529	100.54
15	GPS 59	trib. Wambabya	246	216	4366	1438	4906	591297	600	282	100.56
16	GPS 59	trib. Wambabya	104	110	3923	781	3448	593575	919	684	100.59
17	GPS 59	trib. Wambabya	93	120	3388	976	1177	594474	3452	948	100.77
18	GPS 59	trib. Wambabya	57	98	679	250	910	599930	2650	475	100.84
19	GPS 59	trib. Wambabya	66	86	1012	927	1633	600409	1444	204	100.96
20	GPS 59	trib. Wambabya	215	93	629	3361	1384	599090	715	351	100.97
21	GPS 59	trib. Wambabya	51	99	1988	380	852	597951	4507	691	101.09
22	GPS 59	trib. Wambabya	80	118	144	566	595	602807	2077	420	101.13
23	GPS 59	trib. Wambabya	37	95	2990	4380	680	597711	921	190	101.17
24	GPS 59	trib. Wambabya	231	118	2504	1070	3254	597052	2603	1838	101.45
25	GPS 59	trib. Wambabya	103	106	445	646	957	603707	2173	799	101.49
26	GPS 59	trib. Wambabya	21	151	1081	94	697	603047	3629	235	101.49
27	GPS 59	trib. Wambabya	29	92	3994	1504	664	598311	3755	768	101.52
28	GPS 59	trib. Wambabya	344	168	4431	514	2899	599750	829	260	101.53
29	GPS 59	trib. Wambabya	140	165	1195	1048	1779	603107	1392	430	101.54
30	GPS 59	trib. Wambabya	35	81	1109	1261	1115	603107	2315	321	101.56
31	GPS 59	trib. Wambabya	253	104	3171	6570	637	597172	1475	460	101.64
32	GPS 59	trib. Wambabya	66	86	2651	5123	954	599570	1121	356	101.65
33	GPS 59	trib. Wambabya	37	83	28	1584	435	605565	2002	591	101.72
34	GPS 59	trib. Wambabya	64	116	687	270	2831	605865	746	364	101.82
35	GPS 59	trib. Wambabya	62	145	2039	1611	730	605745	1736	194	102.04
36	GPS 59	trib. Wambabya	102	151	16637	3923	4780	584642	1481	708	102.07
37	GPS 59	trib. Wambabya	70	98	2542	668	2007	605865	1254	791	102.22
38	GPS 59	trib. Wambabya	104	91	1611	276	1480	608203	786	1045	102.27
39	GPS 59	trib. Wambabya	7	63	2271	9545	332	593875	1844	6054	102.33
40	GPS 59	trib. Wambabya	64	88	8973	2170	1510	598251	2595	406	102.34
41	GPS 59	trib. Wambabya	36	107	3053	3002	737	605145	2911	417	102.57
42	GPS 59	trib. Wambabya	60	79	9383	411	4951	598731	1317	649	102.60
43	GPS 59	trib. Wambabya	73	96	2361	2755	784	605265	3723	574	102.61
44	GPS 59	trib. Wambabya	91	164	12583	277	5079	597292	1277	137	102.82
45	GPS 59	trib. Wambabya	88	104	1077	608	11582	602807	657	562	102.91
46	GPS 59	trib. Wambabya	159	118	1084	2205	727	611740	1238	776	103.01
47	GPS 59	trib. Wambabya	186	126	2363	1672	836	610421	2482	193	103.05
48	GPS 59	trib. Wambabya	131	123	1912	3728	430	611200	1785	561	103.31
49	GPS 59	trib. Wambabya	40	93	1293	5186	209	611081	2012	651	103.43
50	GPS 59	trib. Wambabya	82	100	719	1217	874	614618	1935	1079	103.44
51	GPS 59	trib. Wambabya	30	72	808	588	727	617076	1856	489	103.61
52	GPS 64	trib.Nkusi	33	126	18385	1667	5171	570734	4557	881	100.26
53	GPS 64	trib.Nkusi	134	184	5337	798	1824	608443	1020	951	103.12
54	GPS 64	trib.Nkusi	92	91	2541	1208	305	595553	4041	3257	101.18
55	GPS 64	trib.Nkusi	31	86	2246	4085	626	608623	940	1363	103.00
56	GPS 64	trib.Nkusi	80	110	2311	705	876	613958	2942	617	103.60
57	GPS 64	trib.Nkusi	102	108	470	538	634	602627	5347	965	101.80
58	GPS 64	trib.Nkusi	106	110	1813	798	1045	593755	2229	2410	100.38
59	GPS 64	trib.Nkusi	18	110	2721	3821	127	604186	5823	1207	103.00
60	GPS 64	trib.Nkusi	59	107	3683	788	1930	596153	1274	778	100.80
61	GPS 64	trib.Nkusi	38	81	475	1401	22309	583503	1922	102	101.64
62	GPS 64	trib.Nkusi	102	290	737	198	1869	613778	630	342	102.99
63	GPS 64	trib.Nkusi	19	106	1329	1406	190	602208	3499	1445	101.70
64	GPS 64	trib.Nkusi	255	111	3744	1846	983	612999	2536	486	103.83
65	GPS 64	trib.Nkusi	93	159	4089	1039	1262	607424	1767	109	102.66

Rutile chemistry cont.

	Sample ID	River name	Al ppm	Si ppm	Nb ppm	Cr ppm	Fe ppm	Ti ppm	V ppm	Zr ppm	Total %
Detection limit			0.001	0.003	0.004	0.0017	0.002	0.02	0.002	0.027	
66	GPS 64	trib.Nkusi	71	97	375	316	218	615397	3045	871	103.40
67	GPS 64	trib.Nkusi	27	115	2545	1201	550	610661	3859	690	103.27
68	GPS 64	trib.Nkusi	39	100	2037	4729	259	590517	2305	1603	100.26
69	GPS 64	trib.Nkusi	35	113	1868	2493	260	615637	802	1172	103.73
70	GPS 64	trib.Nkusi	40	115	3511	751	3207	599270	1493	606	101.50
71	GPS 64	trib.Nkusi	67	122	1428	3253	1194	601488	1949	523	101.67
72	GPS 64	trib.Nkusi	132	86	4338	2234	645	595733	3223	586	101.16
73	GPS 64	trib.Nkusi	30	106	750	526	268	604666	4288	796	101.90
74	GPS 64	trib.Nkusi	102	111	1372	840	480	591477	4248	487	99.85
75	GPS 64	trib.Nkusi	49	113	712	1279	213	605085	2083	594	101.69
76	GPS 64	trib.Nkusi	52	114	794	1272	218	604726	2204	526	101.65
77	GPS 64	trib.Nkusi	40	144	1502	137	522	616176	1990	193	103.45
78	GPS 64	trib.Nkusi	38	95	1460	4120	634	616896	2142	1210	104.43
79	GPS 64	trib.Nkusi	37	97	3598	2770	130	605685	4915	439	102.95
80	GPS 64	trib.Nkusi	44	89	8374	4398	1348	593155	1604	1067	101.68
81	GPS 64	trib.Nkusi	10	87	1288	1318	668	612699	2788	81	103.16
82	GPS 64	trib.Nkusi	51	98	1005	4544	264	611081	2192	876	103.35
83	GPS 64	trib.Nkusi	37	100	1506	217	2568	609882	1171	381	102.64
84	GPS 64	trib.Nkusi	42	99	2442	1722	2581	604546	2009	472	102.32
85	GPS 64	trib.Nkusi	40	94	8553	3019	6030	600169	823	552	103.21
86	GPS 64	trib.Nkusi	83	95	3578	2462	1299	604186	3679	416	102.63
87	GPS 64	trib.Nkusi	323	201	3481	5700	1313	608982	591	326	103.49
88	GPS 64	trib.Nkusi	35	86	8003	4618	473	598131	2975	2148	102.74
89	GPS 64	trib.Nkusi	148	112	1843	1517	955	600649	3721	1623	101.76
90	GPS 64	trib.Nkusi	139	151	4119	549	892	599210	2370	452	101.31
91	GPS 64	trib.Nkusi	77	105	487	63	731	618275	2144	512	103.73
92	GPS 64	trib.Nkusi	144	122	3246	263	1387	620373	1228	352	104.52
93	GPS 64	trib.Nkusi	31	96	3611	2226	1686	593395	3013	1236	100.88
94	GPS 64	trib.Nkusi	42	102	3274	203	1739	601848	2180	444	101.64
95	GPS 64	trib.Nkusi	48	94	1653	1028	914	615937	1873	701	103.71
96	GPS 64	trib.Nkusi	87	150	1755	1080	913	618455	2470	1725	104.44
97	GPS 65	trib.Nkusi 2	292	194	1876	1037	1130	613838	2013	267	103.44
98	GPS 65	trib.Nkusi 2	212	187	2070	1966	450	606045	2645	925	102.42
99	GPS 65	trib.Nkusi 2	246	201	774	3686	229	590577	1945	653	99.72
100	GPS 65	trib.Nkusi 2	287	166	10346	68	5986	603767	1301	728	103.77
101	GPS 65	trib.Nkusi 2	393	146	538	769	346	600469	1730	1033	100.90
102	GPS 65	trib.Nkusi 2	242	141	3565	5069	751	609282	1866	2074	103.83
103	GPS 65	trib.Nkusi 2	328	249	1525	1730	2439	597771	1316	849	101.03
104	GPS 65	trib.Nkusi 2	312	223	1433	376	2310	613539	1463	398	103.34
105	GPS 65	trib.Nkusi 2	307	190	2780	569	2383	606165	1033	515	102.32
106	GPS 65	trib.Nkusi 2	230	166	2132	2668	799	611800	2720	650	103.53
107	GPS 65	trib.Nkusi 2	247	200	2238	2081	560	611440	4001	1085	103.64
108	GPS 65	trib.Nkusi 2	248	184	5933	6104	785	601488	1351	1111	102.87
109	GPS 65	trib.Nkusi 2	317	203	1915	3598	801	591956	2930	596	100.39
110	GPS 65	trib.Nkusi 2	247	215	5931	6002	766	602148	1321	1110	102.96
111	GPS 65	trib.Nkusi 2	303	198	2119	2594	847	606584	2766	674	102.68
112	GPS 65	trib.Nkusi 2	277	208	2204	2120	546	610121	4030	1133	103.44
113	GPS 65	trib.Nkusi 2	310	171	1850	1875	1999	596153	2374	577	100.88
114	GPS 65	trib.Nkusi 2	266	156	1944	2568	692	609042	2220	385	102.88
115	GPS 65	trib.Nkusi 2	391	190	3598	4419	843	593635	1967	1232	101.05
116	GPS 65	trib.Nkusi 2	285	212	1683	3613	916	609102	1335	836	103.00
117	GPS 65	trib.Nkusi 2	255	174	1173	3744	310	612999	1222	780	103.44
118	GPS 65	trib.Nkusi 2	244	187	2243	2577	576	600949	2412	1405	101.77
119	GPS 65	trib.Nkusi 2	306	174	2925	603	4575	606524	1092	867	102.84
120	GPS 65	trib.Nkusi 2	254	176	7996	5048	1375	598071	940	1376	102.54
121	GPS 65	trib.Nkusi 2	270	179	1245	5435	315	598791	1461	1143	101.47
122	GPS 65	trib.Nkusi 2	268	166	557	630	180	599210	5124	599	101.12
123	GPS 65	trib.Nkusi 2	242	171	2698	2115	2001	608922	1669	1538	103.23
124	GPS 65	trib.Nkusi 2	345	188	6413	2179	1822	594594	1870	460	101.31
125	GPS 65	trib.Nkusi 2	245	190	3162	4642	725	580625	4582	720	99.15
126	GPS 65	trib.Nkusi 2	278	156	245	2090	2131	593575	1667	579	100.12
127	GPS 65	trib.Nkusi 2	248	164	1221	889	556	596692	2351	423	100.42
128	GPS 66	Muzizi	245	171	3213	482	4243	587999	2342	794	99.91
129	GPS 66	Muzizi	292	163	3278	1311	548	594414	2041	310	100.39
130	GPS 66	Muzizi	270	181	6433	1342	1682	590577	2107	316	100.48

Rutile chemistry cont.

	Sample ID	River name	Al ppm	Si ppm	Nb ppm	Cr ppm	Fe ppm	Ti ppm	V ppm	Zr ppm	Total %
Detection limit			0.001	0.003	0.004	0.0017	0.002	0.02	0.002	0.027	
131	GPS 66	Muzizi	248	163	2131	5392	211	575050	4266	1263	98.12
132	GPS 66	Muzizi	347	179	994	800	849	592316	4208	845	100.09
133	GPS 66	Muzizi	287	151	7846	120	4581	587400	1578	959	100.49
134	GPS 66	Muzizi	247	182	1203	2848	454	594534	2096	1167	100.46
135	GPS 66	Muzizi	280	160	4181	2793	351	585901	3468	888	99.67
136	GPS 66	Muzizi	264	178	5798	1349	4229	581824	1765	974	99.40
137	GPS 66	Muzizi	266	171	2455	129	1642	600349	2058	965	101.34
138	GPS 66	Muzizi	301	151	1437	825	965	588479	2767	557	99.25
139	GPS 66	Muzizi	348	163	1111	778	2819	594594	779	144	100.12
140	GPS 66	Muzizi	254	157	2142	1877	271	591896	2516	719	99.97
141	GPS 66	Muzizi	280	159	3780	6298	386	585541	1248	802	99.75
142	GPS 66	Muzizi	303	165	456	1994	256	601728	1317	389	101.10
143	GPS 66	Muzizi	254	165	949	739	1952	597532	2359	1399	100.89
144	GPS 66	Muzizi	288	214	1734	104	2612	601428	1234	167	101.30
145	GPS 66	Muzizi	288	171	4969	853	2644	579906	2265	1160	98.71
146	GPS 66	Muzizi	265	191	4557	2437	1240	577328	1485	1058	98.09
147	GPS 66	Muzizi	315	183	2489	2578	474	581285	1304	1023	98.28
148	GPS 66	Muzizi	270	157	1399	1324	1344	595613	1441	552	100.35
149	GPS 66	Muzizi	251	134	1989	2444	826	601129	1909	808	101.58
150	GPS 66	Muzizi	250	158	1871	3672	157	592975	3185	1076	100.56
151	GPS 66	Muzizi	289	149	919	311	4065	588299	1490	829	99.39
152	GPS 66	Muzizi	258	167	85	2055	1450	598910	877	101	100.65
153	GPS 66	Muzizi	263	160	3497	1587	600	584103	3226	1061	99.08
154	GPS 66	Muzizi	256	165	3052	870	3279	576549	1826	626	97.77
155	GPS 66	Muzizi	254	172	1429	821	2262	594054	1716	1145	100.31
156	GPS 66	Muzizi	257	206	2986	1533	2647	595014	956	752	100.72
157	GPS 66	Muzizi	236	170	2315	1065	4185	595194	528	202	100.65
158	GPS 66	Muzizi	254	163	1605	5387	1080	594174	1163	566	100.73
159	GPS 66	Muzizi	292	156	2604	3012	515	596213	1095	974	100.81
160	GPS 66	Muzizi	267	198	563	1178	666	584282	1580	352	98.18
161	GPS 66	Muzizi	281	178	3822	2720	630	582124	2648	1236	98.94
162	GPS 66	Muzizi	278	160	6502	2148	1376	580745	2725	1307	99.21
163	GPS 66	Muzizi	263	212	1142	1526	1453	592736	1527	561	99.90
164	GPS 66	Muzizi	256	175	845	2242	358	590278	1727	372	99.38
165	GPS 66	Muzizi	263	155	3565	3134	297	591237	2151	797	100.27
166	GPS 66	Muzizi	302	237	9907	85	6271	583503	1880	143	100.39
167	GPS 66	Muzizi	249	165	2827	1033	3973	587280	1773	765	99.68
168	GPS 66	Muzizi	280	185	3573	3262	649	581105	1510	1050	98.60
169	GPS 66	Muzizi	262	191	1130	92	3944	587280	2052	800	99.29
170	GPS 66	Muzizi	293	137	3251	1400	1493	591357	3309	768	100.33
171	GPS 66	Muzizi	252	172	6848	81	5346	589198	1285	588	100.63
172	GPS 66	Muzizi	264	196	2670	3571	217	589019	2629	815	99.90
173	GPS 66	Muzizi	248	161	1974	4215	113	598551	2828	1228	101.55
174	GPS 66	Muzizi	278	174	1543	583	2700	599870	956	619	101.12
175	GPS 66	Muzizi	245	166	1882	2306	428	589438	2760	951	99.70
176	GPS 66	Muzizi	268	171	2629	4111	726	592256	1575	1093	100.47
177	GPS 70	Dura	237	209	41	448	887	602268	2529	235	101.14
178	GPS 70	Dura	246	166	6331	4835	2636	585961	1320	706	100.37
179	GPS 70	Dura	231	175	1476	3793	1058	583083	784	227	98.47
180	GPS 70	Dura	242	197	507	2295	127	589258	4662	342	99.61
181	GPS 70	Dura	254	178	1961	4039	1489	598311	1503	375	101.35
182	GPS 70	Dura	556	124	990	1082	2805	596093	2924	335	100.82
183	GPS 70	Dura	265	197	2099	4379	1516	600589	879	666	101.76
184	GPS 70	Dura	231	171	980	4711	1293	602328	1643	394	101.96
185	GPS 70	Dura	254	156	331	648	871	599870	2760	292	100.86
186	GPS 70	Dura	255	170	1523	4703	717	605385	1309	294	102.39
187	GPS 70	Dura	238	233	3225	2937	1634	607663	1006	145	102.85
188	GPS 70	Dura	233	141	1858	6183	301	595074	1604	481	100.98
189	GPS 70	Dura	248	143	827	5634	837	599270	1349	651	101.49
190	GPS 70	Dura	248	187	308	3769	251	597052	2586	272	100.78
191	GPS 70	Dura	203	141	3464	138	2958	603886	1492	104	102.06
192	GPS 70	Dura	266	173	1964	1835	3108	601548	976	344	101.70
193	GPS 70	Dura	226	145	883	5168	622	601249	871	296	101.58
194	GPS 70	Dura	225	156	1454	6728	270	590278	3351	376	100.47
195	GPS 70	Dura	237	168	288	3058	367	593575	4601	310	100.43

Rutile chemistry cont.

	Sample ID	River name	Al ppm	Si ppm	Nb ppm	Cr ppm	Fe ppm	Ti ppm	V ppm	Zr ppm	Total %
Detection limit			0.001	0.003	0.004	0.0017	0.002	0.02	0.002	0.027	
196	GPS 70	Dura	236	180	263	1338	602	595014	5671	562	100.64
197	GPS 70	Dura	703	151	11954	642	5590	589138	2255	526	101.83
198	GPS 70	Dura	245	161	596	879	927	610181	2757	845	102.77
199	GPS 70	Dura	220	195	476	3987	988	605385	1482	355	102.18
200	GPS 70	Dura	263	180	11185	6011	3658	591417	1167	381	102.38
201	GPS 70	Dura	259	211	507	803	668	603167	6551	554	102.12
202	GPS 70	Dura	245	165	858	823	1182	593875	1785	555	99.91
203	GPS 70	Dura	242	183	785	3357	574	594774	2947	309	100.53
204	GPS 70	Dura	247	204	686	2159	1983	595074	2149	654	100.53
205	GPS 70	Dura	247	154	199	588	476	599690	3487	293	100.86
206	GPS 70	Dura	263	115	1747	2926	1677	601309	651	320	101.50
207	GPS 70	Dura	242	172	1965	2902	1096	612340	555	368	103.27
208	GPS 70	Dura	228	171	1696	4003	878	587580	817	276	99.27
209	GPS 70	Dura	253	152	4895	4822	2268	590038	1387	551	100.73
210	GPS 70	Dura	263	160	279	4468	1645	608922	1031	409	102.86
211	GPS 70	Dura	274	159	1673	3984	874	594234	824	309	100.39
212	GPS 70	Dura	233	178	887	3955	1094	597652	2275	513	101.13
213	GPS 70	Dura	285	163	244	2480	215	611081	4534	252	103.21
214	GPS 70	Dura	251	156	3151	3442	948	595913	757	412	100.84
215	GPS 70	Dura	261	179	6879	4731	2005	591357	1433	415	101.21
216	GPS 70	Dura	326	267	704	97	1949	604666	3314	121	101.91
217	GPS 70	Dura	261	181	1302	5151	944	593995	1277	438	100.59
218	GPS 70	Dura	243	158	403	4616	2180	602148	1126	440	101.89
219	GPS 70	Dura	225	170	205	705	483	602088	4166	262	101.38
220	GPS 70	Dura	258	160	1556	4723	1204	594174	1277	443	100.63
221	GPS 70	Dura	260	158	912	5454	1951	600110	965	473	101.71
222	GPS 70	Dura	261	153	117	762	620	594534	2741	219	99.90
223	GPS 70	Dura	269	177	179	1289	421	595613	4355	381	100.45
224	GPS 70	Dura	239	187	430	2170	253	597112	6295	429	101.19
225	GPS 70	Dura	273	182	1421	1990	2326	600229	984	130	101.26
226	GPS 70	Dura	251	252	756	4287	792	591057	974	255	99.77
227	GPS 70	Dura	273	226	309	5271	960	578647	6361	304	98.73
228	GPS 70	Dura	268	196	1219	5593	944	603946	684	349	102.20
229	GPS 71	trib. Dura	36	102	3750	6404	3161	593215	1171	628	101.41
230	GPS 71	trib. Dura	45	110	832	5625	676	604426	1146	622	102.25
231	GPS 71	trib. Dura	70	143	1796	3996	645	607903	910	414	102.65
232	GPS 71	trib. Dura	31	112	15309	157	9387	589798	928	379	102.68
233	GPS 71	trib. Dura	31	110	921	3935	930	610601	2313	455	103.22
234	GPS 71	trib. Dura	22	84	1219	4820	1485	595673	923	559	100.80
235	GPS 71	trib. Dura	66	87	4154	1201	1471	601129	2667	655	101.91
236	GPS 71	trib. Dura	11	102	2462	4177	179	596153	1453	952	100.91
237	GPS 71	trib. Dura	27	107	855	4588	818	607184	1799	734	102.69
238	GPS 71	trib. Dura	20	80	991	6360	1010	589918	2130	528	100.17
239	GPS 71	trib. Dura	28	112	1635	8189	1929	604246	1030	561	102.95
240	GPS 71	trib. Dura	29	129	548	4436	863	608383	2056	512	102.83
241	GPS 71	trib. Dura	27	94	7645	392	3466	602627	2291	711	102.88
242	GPS 71	trib. Dura	47	108	3996	92	3794	599270	1094	325	101.45
243	GPS 71	trib. Dura	47	105	1531	5118	1293	609282	1071	483	103.16
244	GPS 71	trib. Dura	7	88	909	5066	1568	606045	1384	551	102.60
245	GPS 71	trib. Dura	37	107	1666	6489	1445	601488	1800	478	102.25
246	GPS 71	trib. Dura	6	100	873	5755	1520	586860	2032	360	99.58
247	GPS 71	trib. Dura	44	113	10066	239	4478	584822	2284	500	100.42
248	GPS 71	trib. Dura	22	92	1536	5089	982	598791	1200	529	101.37
249	GPS 71	trib. Dura	14	77	1791	2353	2364	605625	920	323	102.24
250	GPS 71	trib. Dura	17	107	1376	5084	987	596452	1265	495	100.96
251	GPS 71	trib. Dura	24	104	1313	5145	554	612879	1875	572	103.74
252	GPS 71	trib. Dura	22	100	1331	3937	1308	590098	1553	566	99.82
253	GPS 71	trib. Dura	104	104	2010	5433	1697	597472	1254	305	101.40
254	GPS 71	trib. Dura	19	115	1296	4694	991	593395	3111	563	100.70
255	GPS 71	trib. Dura	53	106	920	108	1656	617495	1185	523	103.67
256	GPS 71	trib. Dura	97	102	8398	323	3397	596452	2259	581	101.93
257	GPS 71	trib. Dura	49	105	5497	615	3176	588839	3470	726	100.41
258	GPS 71	trib. Dura	29	125	1618	6213	1196	598431	2078	521	101.70
259	GPS 71	trib. Dura	27	115	1415	6234	1210	586561	1276	565	99.57
260	GPS 71	trib. Dura	31	100	3914	4189	1572	591537	1544	429	100.55

Rutile chemistry cont.

	Sample ID	River name	Al ppm	Si ppm	Nb ppm	Cr ppm	Fe ppm	Ti ppm	V ppm	Zr ppm	Total %
Detection limit			**0.001**	**0.003**	**0.004**	**0.0017**	**0.002**	**0.02**	**0.002**	**0.027**	
261	**GPS 71**	**trib. Dura**	24	87	872	6345	1347	591596	1839	682	100.47
262	**GPS 71**	**trib. Dura**	42	115	1169	4320	1410	599810	1121	441	101.40
263	**GPS 71**	**trib. Dura**	20	119	965	5103	947	602028	1094	479	101.79
264	**GPS 71**	**trib. Dura**	25	90	1758	4991	1388	591297	1616	363	100.25
265	**GPS 71**	**trib. Dura**	25	90	3580	5209	2451	598251	988	792	101.90
266	**GPS 71**	**trib. Dura**	16	101	1494	4887	3024	593275	982	637	100.74
267	**GPS 71**	**trib. Dura**	30	94	2288	4519	1056	607543	1011	613	102.86
268	**GPS 71**	**trib. Dura**	12	100	1251	4772	777	599870	1512	559	101.48
269	**GPS 71**	**trib. Dura**	14	82	918	5304	1471	592795	1387	496	100.41
270	**GPS 71**	**trib. Dura**	4	82	697	5502	1244	604606	2126	649	102.48
271	**GPS 71**	**trib. Dura**	26	101	598	4949	1259	609342	1276	304	102.98
272	**GPS 71**	**trib. Dura**	120	100	7037	237	3742	603107	820	1065	102.70
273	**GPS 71**	**trib. Dura**	54	110	2273	4666	1506	606404	1067	619	102.78
274	**GPS 71**	**trib. Dura**	21	118	2338	5645	442	603886	5408	619	103.08
275	**GPS 71**	**trib. Dura**	19	86	1803	4931	1577	599390	1323	589	101.62
276	**GPS 71**	**trib. Dura**	61	92	5743	195	4330	604186	1350	586	102.76
277	**GPS 71**	**trib. Dura**	70	115	5966	316	3685	601189	1037	873	102.21
278	**GPS 71**	**trib. Dura**	28	104	887	6149	752	609582	1638	724	103.31
279	**GPS 71**	**trib. Dura**	8	112	1903	4219	951	593695	2970	718	100.76
280	**GPS 72**	**trib. Dura 2**	268	155	1549	141	1530	601488	644	136	100.99
281	**GPS 72**	**trib. Dura 2**	276	175	2233	711	1600	600409	1500	199	101.18
282	**GPS 72**	**trib. Dura 2**	253	155	2796	187	1792	590278	1330	258	99.51
283	**GPS 72**	**trib. Dura 2**	236	138	4870	3413	549	595014	1466	400	101.01
284	**GPS 72**	**trib. Dura 2**	264	178	1227	4323	756	591656	1205	446	100.01
285	**GPS 72**	**trib. Dura 2**	236	173	2555	2107	4561	591297	807	543	100.38
286	**GPS 72**	**trib. Dura 2**	338	171	2986	915	5314	592076	1318	549	100.61
287	**GPS 72**	**trib. Dura 2**	267	173	1298	3915	1221	594534	1495	574	100.58
288	**GPS 72**	**trib. Dura 2**	289	173	5364	3298	1009	603647	973	603	102.56
289	**GPS 72**	**trib. Dura 2**	273	150	1482	6295	430	592436	2136	609	100.63
290	**GPS 72**	**trib. Dura 2**	269	177	3370	1515	693	590637	2427	612	99.95
291	**GPS 72**	**trib. Dura 2**	255	197	1522	6278	1349	590577	1112	642	100.32
292	**GPS 72**	**trib. Dura 2**	263	173	5710	3201	319	594774	2886	652	101.33
293	**GPS 72**	**trib. Dura 2**	333	208	2394	3823	597	598910	1542	740	101.42
294	**GPS 72**	**trib. Dura 2**	252	144	3337	2280	2314	606584	1468	750	102.85
295	**GPS 72**	**trib. Dura 2**	244	169	2834	807	2299	604006	1417	751	102.09
296	**GPS 72**	**trib. Dura 2**	242	136	2150	3364	456	612100	931	773	103.36
297	**GPS 72**	**trib. Dura 2**	272	180	2729	768	2340	605625	1468	778	102.36
298	**GPS 72**	**trib. Dura 2**	295	167	4545	272	3576	597172	1350	841	101.37
299	**GPS 72**	**trib. Dura 2**	286	199	556	973	939	593275	5961	883	100.51
300	**GPS 72**	**trib. Dura 2**	238	151	3942	3686	2721	589079	2589	887	100.55
301	**GPS 72**	**trib. Dura 2**	213	188	2207	4668	149	601069	3764	1153	102.24
302	**GPS 72**	**trib. Dura 2**	282	144	2018	3448	3407	597352	162	1238	101.34
303	**GPS 73**	**Mpanga**	43	123	6948	100	7461	594234	1404	515	101.80
304	**GPS 73**	**Mpanga**	103	402	3018	460	2550	597592	1811	160	101.02
305	**GPS 73**	**Mpanga**	34	100	1349	346	4822	614138	166	118	103.51
306	**GPS 73**	**Mpanga**	47	75	2517	2142	458	616476	2073	707	104.08
307	**GPS 73**	**Mpanga**	33	97	3938	2467	506	603347	2838	879	102.35
308	**GPS 73**	**Mpanga**	83	95	8500	122	14303	594954	702	577	103.22
309	**GPS 73**	**Mpanga**	54	132	2460	98	3791	612399	839	140	103.32
310	**GPS 73**	**Mpanga**	93	194	851	292	2891	613299	1604	662	103.31
311	**GPS 73**	**Mpanga**	42	137	908	432	2762	613658	1313	160	103.24
312	**GPS 73**	**Mpanga**	39	102	1989	2376	1752	600169	2204	660	101.55
313	**GPS 73**	**Mpanga**	20	97	1665	1053	3650	606165	1395	651	102.45
314	**GPS 73**	**Mpanga**	35	90	2165	4380	848	599030	1672	799	101.50
315	**GPS 73**	**Mpanga**	34	98	1906	2328	1735	601488	2208	694	101.75
316	**GPS 73**	**Mpanga**	82	97	271	131	2139	610421	933	381	102.41
317	**GPS 73**	**Mpanga**	76	108	24257	87	14147	590457	937	533	105.10
318	**GPS 73**	**Mpanga**	88	175	2565	2226	2197	599990	1900	194	101.56
319	**GPS 73**	**Mpanga**	25	103	4096	243	2673	604186	4220	1000	102.76
320	**GPS 73**	**Mpanga**	40	106	16288	250	11426	591836	631	475	103.51
321	**GPS 73**	**Mpanga**	133	103	5511	90	6440	618694	267	212	105.24
322	**GPS 73**	**Mpanga**	86	98	19224	388	9967	586800	785	1305	103.11
323	**GPS 73**	**Mpanga**	60	99	6040	964	2973	620793	924	561	105.40
324	**GPS 73**	**Mpanga**	68	132	1667	1632	475	593575	1625	633	99.97
325	**GPS 73**	**Mpanga**	109	329	3619	116	5322	580565	776	622	98.58

Rutile chemistry cont.

	Sample ID	River name	Al ppm	Si ppm	Nb ppm	Cr ppm	Fe ppm	Ti ppm	V ppm	Zr ppm	Total %
Detection limit			0.001	0.003	0.004	0.0017	0.002	0.02	0.002	0.027	
326	GPS 73	Mpanga	32	112	965	113	1983	597172	1999	117	100.42
327	GPS 73	Mpanga	43	108	758	354	309	602508	3463	2296	101.64
328	GPS 73	Mpanga	36	121	3497	151	4630	598551	750	71	101.30
329	GPS 73	Mpanga	69	93	4133	2644	994	589618	1468	1002	100.00
330	GPS 73	Mpanga	183	103	8878	125	4913	599750	1040	952	102.66
331	GPS 73	Mpanga	38	99	1831	158	3375	587939	1326	825	99.27
332	GPS 73	Mpanga	82	138	3283	2366	129578	487102	298	238	103.85
333	GPS 73	Mpanga	28	100	1464	2373	992	595553	2803	129	100.57
334	GPS 73	Mpanga	26	111	4781	1786	3495	584222	2395	587	99.57
335	GPS 73	Mpanga	49	72	5363	294	3701	593155	903	273	100.63
336	GPS 73	Mpanga	58	179	209	109	2634	602867	790	113	101.16
337	GPS 73	Mpanga	51	86	250	2982	2903	614078	321	166	103.47
338	GPS 73	Mpanga	25	102	1012	250	2108	609822	1107	107	102.42
339	GPS 73	Mpanga	84	93	4735	384	5541	596752	461	919	101.49
340	GPS 73	Mpanga	22	72	879	2995	1277	604966	508	168	101.81
341	GPS 73	Mpanga	53	106	1600	1306	614	604066	1765	414	101.65
342	GPS 73	Mpanga	49	109	12862	155	9510	587760	1296	629	102.06
343	GPS 73	Mpanga	47	121	672	2365	2086	597711	794	179	100.66
344	GPS 73	Mpanga	42	109	963	162	2949	592676	1389	93	99.73
345	GPS 73	Mpanga	73	118	122	66	3794	590457	578	157	99.23
346	GPS 73	Mpanga	46	74	1221	140	2148	608143	448	759	102.16
347	GPS 73	Mpanga	71	111	2147	367	1832	605205	795	1559	102.01
348	GPS 73	Mpanga	62	97	4489	95	3587	593215	1119	418	100.51
349	GPS 73	Mpanga	44	105	1885	2779	2309	603227	1687	652	102.11
350	GPS 73	Mpanga	122	106	12093	3523	4142	589019	256	742	101.67
351	GPS 73	Mpanga	78	98	3900	316	3612	595733	702	651	100.85
352	GPS 73	Mpanga	47	73	2554	1272	6081	584103	1239	628	99.33
353	GPS 73	Mpanga	48	222	1776	186	9577	586920	1552	134	100.07
354	GPS 73	Mpanga	39	112	10416	1648	7112	582244	1306	467	100.56
355	GPS 73	Mpanga	44	120	10416	1717	7070	581884	1230	509	100.50
356	GPS 96	Mubuku	260	159	1295	2349	2049	600469	1200	500	101.38
357	GPS 96	Mubuku	298	184	64	568	874	598551	2269	371	100.53
358	GPS 96	Mubuku	379	176	11534	298	9856	574870	1755	384	99.88
359	GPS 96	Mubuku	305	305	3897	483	5344	590397	604	412	100.29
360	GPS 96	Mubuku	251	177	2472	233	2981	600529	1315	396	101.39
361	GPS 96	Mubuku	354	238	10975	306	9011	580026	1636	392	100.49
362	GPS 96	Mubuku	361	202	2185	196	4335	590337	1415	502	99.92
363	GPS 96	Mubuku	245	168	9849	542	7481	580386	1114	446	100.04
364	GPS 96	Mubuku	216	180	591	411	2735	586321	1799	311	98.76
365	GPS 96	Mubuku	256	187	2555	1509	5416	580506	661	390	98.58
366	GPS 96	Mubuku	267	164	2740	814	4988	589318	466	596	99.89
367	GPS 96	Mubuku	253	177	274	1573	360	591656	6316	441	100.18
368	GPS 96	Mubuku	263	182	1011	555	3570	596572	1207	538	100.65
369	GPS 96	Mubuku	255	193	1948	419	3819	600649	1327	261	101.48
370	GPS 96	Mubuku	349	175	11534	377	6012	597891	709	532	102.93
371	GPS 96	Mubuku	309	171	325	467	677	606045	2867	226	101.85
372	GPS 96	Mubuku	228	182	126	698	543	592256	3641	249	99.65
373	GPS 96	Mubuku	232	151	2970	395	7152	583203	859	482	99.24
374	GPS 96	Mubuku	287	144	2871	775	4207	589678	1837	623	100.07
375	GPS 96	Mubuku	251	191	2483	1287	3708	590158	2183	460	100.12
376	GPS 96	Mubuku	242	186	244	705	1601	597592	2008	335	100.49
377	GPS 96	Mubuku	242	194	118	519	787	588539	2417	403	98.87
378	GPS 96	Mubuku	329	179	4631	919	5062	584822	1343	567	99.64
379	GPS 96	Mubuku	278	158	2191	1638	4289	577748	849	536	97.95
380	GPS 96	Mubuku	314	192	817	1766	3672	591357	1047	475	99.94
381	GPS 96	Mubuku	284	155	5051	114	8217	581225	931	570	99.42
382	GPS 96	Mubuku	229	137	1945	2170	4347	590457	963	540	100.13
383	GPS 96	Mubuku	360	190	14260	1627	12204	573671	819	560	100.62
384	GPS 96	Mubuku	278	163	7684	564	4942	588059	1645	528	100.64
385	GPS 96	Mubuku	292	168	2619	1088	4319	587999	1699	409	99.77
386	GPS 96	Mubuku	237	146	3283	1784	5133	580985	934	577	98.85
387	GPS 96	Mubuku	339	159	6115	1444	6968	573731	1031	529	98.39
388	GPS 96	Mubuku	264	161	3675	1132	4106	595913	2035	419	101.28
389	GPS 96	Mubuku	270	145	825	88	3203	584642	1200	201	98.43
390	GPS 96	Mubuku	216	277	3732	1131	4093	588119	2141	409	100.02

Rutile chemistry cont.

	Sample ID	River name	Al ppm	Si ppm	Nb ppm	Cr ppm	Fe ppm	Ti ppm	V ppm	Zr ppm	Total %
Detection limit			0.001	0.003	0.004	0.0017	0.002	0.02	0.002	0.027	
391	GPS 97	Isebo	69	123	6556	617	6033	602088	765	147	102.73
392	GPS 97	Isebo	74	89	1509	1732	3837	599690	640	153	101.29
393	GPS 97	Isebo	43	103	3318	2007	3522	613539	1145	250	103.99
394	GPS 97	Isebo	37	105	407	526	3200	616296	1296	285	103.69
395	GPS 97	Isebo	42	100	3966	790	2805	606824	937	309	102.63
396	GPS 97	Isebo	68	88	2528	3710	3748	600229	479	321	101.86
397	GPS 97	Isebo	41	94	5334	1707	3596	599750	3317	350	102.36
398	GPS 97	Isebo	40	88	3263	278	5709	617855	1596	351	104.86
399	GPS 97	Isebo	41	100	2586	1247	3943	606344	2514	366	102.86
400	GPS 97	Isebo	39	95	2454	3514	2518	603227	2596	369	102.47
401	GPS 97	Isebo	27	79	4391	814	2660	605145	2588	369	102.68
402	GPS 97	Isebo	39	130	2746	1027	4705	599390	1934	369	101.72
403	GPS 97	Isebo	35	110	2744	4573	3014	607963	635	378	103.24
404	GPS 97	Isebo	20	113	127	456	2853	612939	1897	381	103.13
405	GPS 97	Isebo	42	107	3025	1286	4002	592736	2480	382	100.68
406	GPS 97	Isebo	34	140	3525	4557	3473	602987	947	386	102.67
407	GPS 97	Isebo	11	82	2801	971	4567	602508	1289	394	102.10
408	GPS 97	Isebo	91	178	1999	3171	3279	603826	173	400	102.19
409	GPS 97	Isebo	61	100	2593	382	4368	604366	1035	403	102.22
410	GPS 97	Isebo	40	81	2105	2653	4236	606284	1113	404	102.82
411	GPS 97	Isebo	13	98	1937	3327	3041	613958	789	405	103.93
412	GPS 97	Isebo	47	105	2582	2216	4247	589858	4781	406	100.71
413	GPS 97	Isebo	30	97	410	785	1661	607603	4446	410	102.57
414	GPS 97	Isebo	49	110	5582	298	5562	615877	1343	411	104.87
415	GPS 97	Isebo	15	108	2865	1321	3248	623910	1230	412	105.52
416	GPS 97	Isebo	38	87	2488	2603	4489	616596	781	414	104.58
417	GPS 97	Isebo	34	107	3555	262	5874	601009	2044	415	102.22
418	GPS 97	Isebo	40	100	8218	783	6543	601608	1491	420	103.20
419	GPS 97	Isebo	25	112	884	864	3674	614857	650	422	103.58
420	GPS 97	Isebo	33	115	1978	2616	3405	607843	1418	423	102.97
421	GPS 97	Isebo	29	115	3935	408	4413	610181	1065	429	103.43
422	GPS 97	Isebo	75	89	11744	2953	10183	577688	1285	438	100.74
423	GPS 97	Isebo	29	98	2455	1956	4048	598431	784	440	101.37
424	GPS 97	Isebo	29	107	831	360	6759	601548	1946	443	102.00
425	GPS 97	Isebo	31	114	2913	959	10416	605025	1120	445	103.50
426	GPS 97	Isebo	33	110	1830	1133	4616	603467	1814	446	102.24
427	GPS 97	Isebo	61	82	2554	435	4710	611500	1332	452	103.52
428	GPS 97	Isebo	59	110	1975	4169	3469	614917	468	454	104.27
429	GPS 97	Isebo	76	159	578	707	39099	578167	1478	456	103.45
430	GPS 97	Isebo	77	92	2296	1037	3914	596393	1329	466	100.93
431	GPS 97	Isebo	61	94	2897	4109	3149	595194	1132	473	101.18
432	GPS 97	Isebo	31	105	2410	469	10338	597652	990	484	102.08
433	GPS 97	Isebo	49	115	1590	545	4372	604546	1189	493	102.15
434	GPS 97	Isebo	183	113	3676	462	5339	599810	706	509	101.80
435	GPS 97	Isebo	156	80	2984	2241	5355	601368	1023	517	102.29
436	GPS 97	Isebo	97	99	3731	941	6686	599570	846	521	102.08
437	GPS 97	Isebo	148	105	4798	80	4254	600589	1777	537	102.05
438	GPS 97	Isebo	110	96	9078	631	7026	609162	890	580	104.60
439	GPS 97	Isebo	68	93	2498	1397	4365	603047	1489	635	102.27
440	GPS 97	Isebo	31	96	6010	1521	5199	606824	990	645	103.55
441	GPS 97	Isebo	211	459	4609	57	3908	592016	226	656	100.36
442	GPS 97	Isebo	58	170	7058	287	3649	597112	1212	731	101.71
443	GPS 98	Nyamwamba	247	172	1239	7907	2018	598191	1014	723	101.92
444	GPS 98	Nyamwamba	229	205	1527	2180	3029	600529	1623	361	101.61
445	GPS 98	Nyamwamba	286	174	979	1533	1187	611620	1408	500	102.95
446	GPS 98	Nyamwamba	285	176	3313	81	5423	598431	396	463	101.43
447	GPS 98	Nyamwamba	269	208	1314	2815	2372	587760	3610	569	99.82
448	GPS 98	Nyamwamba	255	148	2704	1664	2710	594294	2019	712	100.75
449	GPS 98	Nyamwamba	289	160	1696	1455	4713	588239	2612	575	99.96
450	GPS 98	Nyamwamba	227	142	677	1450	12515	602328	2681	796	103.47
451	GPS 98	Nyamwamba	297	143	905	125	1283	606944	2347	662	102.12
452	GPS 98	Nyamwamba	344	184	5059	751	4231	597172	1054	289	101.51
453	GPS 98	Nyamwamba	268	181	2513	3295	1881	607603	437	482	102.78
454	GPS 98	Nyamwamba	1314	186	16	497	2583	612819	2710	131	103.38
455	GPS 98	Nyamwamba	254	178	2569	3211	1812	613239	573	526	103.73

Rutile chemistry cont.

	Sample ID	River name	Al ppm	Si ppm	Nb ppm	Cr ppm	Fe ppm	Ti ppm	V ppm	Zr ppm	Total %
Detection limit			0.001	0.003	0.004	0.0017	0.002	0.02	0.002	0.027	
456	GPS 98	Nyamwamba	356	228	6855	530	6690	590997	623	441	101.12
457	GPS 98	Nyamwamba	303	198	6033	102	6520	600110	1291	574	102.52
458	GPS 98	Nyamwamba	273	158	269	6383	479	597472	1073	222	101.05
459	GPS 98	Nyamwamba	266	169	499	2174	2896	608203	485	455	102.52
460	GPS 98	Nyamwamba	293	246	930	2132	993	611740	829	703	102.98
461	GPS 98	Nyamwamba	263	172	1829	3925	5475	602807	942	543	102.66
462	GPS 98	Nyamwamba	260	177	3313	126	4322	592136	1808	440	100.43
463	GPS 98	Nyamwamba	253	172	894	2964	403	599690	2944	398	101.29
464	GPS 98	Nyamwamba	264	161	1829	2444	3841	596512	806	475	101.06
465	GPS 98	Nyamwamba	274	186	1892	342	915	608683	3036	564	102.65
466	GPS 98	Nyamwamba	243	179	1477	402	3965	600110	1455	454	101.38
467	GPS 98	Nyamwamba	259	144	665	5457	205	581045	9706	692	99.70
468	GPS 98	Nyamwamba	250	668	7353	1883	6211	587340	692	1930	101.05
469	GPS 98	Nyamwamba	250	189	667	1418	1851	596812	2773	715	100.78
470	GPS 98	Nyamwamba	272	166	14890	264	10027	575230	1292	618	100.46
471	GPS 98	Nyamwamba	335	191	3457	1418	4406	604186	194	376	102.43
472	GPS 98	Nyamwamba	241	187	1633	1714	4030	589798	653	129	99.73
473	GPS 98	Nyamwamba	280	243	676	1010	3356	609522	2107	292	102.91
474	GPS 98	Nyamwamba	304	147	2845	236	4021	600110	963	532	101.53
475	GPS 98	Nyamwamba	313	187	1216	1354	5400	596692	2786	716	101.44
476	GPS 98	Nyamwamba	309	181	3904	679	4546	612100	887	548	103.86
477	GPS 98	Nyamwamba	259	202	2062	4516	5561	584342	1659	580	99.86
478	GPS 98	Nyamwamba	267	171	1051	3034	1003	602448	2544	722	101.87

A3-2 – Garnet chemistry

	Sample ID	River	SiO2	TiO2	Al2O3	Cr2O3	FeO mass-%	MnO	MgO	CaO	Na2O	Total
detection limit			0.016	0.011	0.014	0.013	0.022	0.012	0.009	0.014	0.012	
1	GPS 64	trib. Nkusi	36.99	0.03	21.23	0.02	33.78	3.65	1.57	3.25	0.00	100.52
2	GPS 64	trib. Nkusi	37.79	0.02	22.09	0.07	32.08	0.82	5.98	1.26	0.07	100.18
3	GPS 64	trib. Nkusi	38.01	0.01	22.26	0.05	32.62	0.54	5.98	1.19	0.09	100.74
4	GPS 64	trib. Nkusi	37.67	0.00	22.43	0.10	30.21	1.04	7.11	1.33	0.00	99.89
5	GPS 64	trib. Nkusi	37.67	0.00	21.78	0.04	35.12	0.25	2.49	3.91	0.00	101.26
6	GPS 64	trib. Nkusi	37.54	0.01	21.97	0.02	35.09	0.67	4.34	1.22	0.10	100.95
7	GPS 64	trib. Nkusi	38.56	0.00	22.42	0.11	29.12	0.94	8.34	1.07	0.00	100.55
8	GPS 64	trib. Nkusi	37.17	0.00	21.63	0.03	35.47	1.08	2.44	2.16	0.00	99.98
9	GPS 64	trib. Nkusi	38.97	0.04	22.52	0.06	28.59	0.53	8.73	1.18	0.00	100.62
10	GPS 64	trib. Nkusi	37.11	0.06	21.90	0.00	35.50	0.55	3.94	0.87	0.05	99.99
11	GPS 64	trib. Nkusi	36.98	0.01	21.71	0.05	31.90	3.47	3.63	1.95	0.03	99.72
12	GPS 64	trib. Nkusi	37.39	0.00	21.40	0.07	32.44	0.88	1.64	6.23	0.01	100.06
13	GPS 64	trib. Nkusi	37.71	0.01	21.92	0.06	32.56	0.41	5.71	1.54	0.02	99.93
14	GPS 64	trib. Nkusi	38.07	0.00	22.15	0.05	31.15	1.12	6.70	0.96	0.00	100.20
15	GPS 64	trib. Nkusi	38.06	0.00	22.31	0.15	32.26	1.14	6.15	1.17	0.00	101.24
16	GPS 64	trib. Nkusi	37.70	0.00	22.09	0.10	32.37	2.22	4.96	1.14	0.01	100.59
17	GPS 64	trib. Nkusi	37.05	0.00	21.83	0.07	31.91	1.28	5.65	1.23	0.00	99.01
18	GPS 64	trib. Nkusi	37.71	0.00	22.47	0.06	30.53	1.49	6.60	0.91	0.09	99.86
19	GPS 64	trib. Nkusi	38.36	0.00	22.26	0.02	31.92	1.52	6.35	0.90	0.00	101.33
20	GPS 64	trib. Nkusi	37.76	0.02	21.92	0.00	31.28	1.53	6.10	0.96	0.06	99.63
21	GPS 64	trib. Nkusi	38.01	0.00	21.91	0.01	31.50	1.61	5.99	0.95	0.04	100.02
22	GPS 64	trib. Nkusi	38.05	0.00	22.21	0.08	31.50	0.50	6.47	1.70	0.00	100.51
23	GPS 64	trib. Nkusi	37.77	0.00	22.03	0.04	31.34	1.52	6.10	1.07	0.04	99.91
24	GPS 64	trib. Nkusi	37.92	0.00	22.27	0.00	32.35	1.70	5.51	0.80	0.02	100.57
25	GPS 64	trib. Nkusi	37.87	0.00	21.88	0.06	35.07	0.76	3.95	1.56	0.01	101.16
26	GPS 64	trib. Nkusi	37.87	0.00	22.18	0.09	31.89	1.35	6.11	1.04	0.07	100.60
27	GPS 64	trib. Nkusi	38.28	0.00	21.93	0.12	34.06	0.47	5.14	1.47	0.00	101.46

Garnet chemistry cont.

	Sample ID	River	SiO2	TiO2	Al2O3	Cr2O3	FeO	MnO	MgO	CaO	Na2O	Total
							mass-%					
detection limit			0.016	0.011	0.014	0.013	0.022	0.012	0.009	0.014	0.012	
28	GPS 92	Dunga	39.03	0.04	22.11	0.15	25.13	0.46	7.67	6.05	0.03	100.68
29	GPS 92	Dunga	38.68	0.01	21.70	0.04	27.21	0.63	5.14	7.48	0.00	100.89
30	GPS 92	Dunga	38.95	0.04	22.02	0.05	25.36	0.38	7.79	5.91	0.00	100.49
31	GPS 92	Dunga	39.17	0.02	21.98	0.05	25.25	0.42	7.12	6.82	0.00	100.82
32	GPS 92	Dunga	39.83	0.04	22.54	0.05	21.34	0.37	10.28	5.78	0.00	100.22
33	GPS 92	Dunga	38.98	0.08	21.90	0.15	26.05	0.66	6.88	6.03	0.00	100.72
34	GPS 92	Dunga	39.51	0.06	21.99	0.07	24.41	0.90	7.76	6.03	0.02	100.74
35	GPS 92	Dunga	38.72	0.02	22.10	0.00	26.13	0.43	6.86	6.14	0.00	100.40
36	GPS 92	Dunga	41.11	0.04	21.33	0.04	24.60	0.52	7.10	7.07	0.00	101.81
37	GPS 92	Dunga	39.10	0.01	22.04	0.10	25.36	0.58	7.13	6.28	0.00	100.60
38	GPS 92	Dunga	38.89	0.06	22.02	0.11	24.60	0.58	7.93	6.07	0.00	100.25
39	GPS 92	Dunga	37.95	0.00	21.64	0.04	25.36	0.57	5.94	7.34	0.00	98.84
40	GPS 92	Dunga	38.12	0.08	21.73	0.11	27.40	0.57	5.97	6.30	0.00	100.28
41	GPS 92	Dunga	38.94	0.00	22.42	0.25	23.41	0.75	8.61	5.93	0.00	100.31
42	GPS 92	Dunga	38.92	0.00	22.04	0.06	24.21	0.69	7.50	6.59	0.00	100.01
43	GPS 92	Dunga	39.16	0.08	21.68	0.17	23.88	0.43	8.75	5.89	0.00	100.04
44	GPS 92	Dunga	38.94	0.05	22.30	0.09	25.18	0.59	7.35	5.95	0.00	100.45
45	GPS 92	Dunga	39.95	0.00	22.81	0.05	19.83	0.36	11.45	5.91	0.00	100.37
46	GPS 92	Dunga	39.62	0.00	22.15	0.10	20.44	0.32	8.88	8.18	0.12	99.80
47	GPS 92	Dunga	38.13	0.01	21.66	0.05	30.38	0.84	3.40	6.74	0.05	101.26
48	GPS 92	Dunga	40.35	0.01	23.11	0.08	17.90	0.29	12.59	6.10	0.00	100.44
49	GPS 92	Dunga	39.08	0.04	22.17	0.27	23.81	0.47	8.51	5.99	0.01	100.34
50	GPS 92	Dunga	39.90	0.03	22.59	0.06	18.89	0.43	11.76	5.90	0.02	99.58
51	GPS 92	Dunga	38.88	0.02	21.72	0.22	26.54	0.61	6.51	6.20	0.02	100.72
52	GPS 92	Dunga	39.03	0.04	22.02	0.11	23.84	0.49	8.23	6.00	0.01	99.77
53	GPS 92	Dunga	39.50	0.04	22.82	0.04	21.71	0.32	9.06	6.89	0.05	100.43
54	GPS 92	Dunga	39.31	0.06	22.16	0.12	24.80	0.47	8.06	6.12	0.03	101.13
55	GPS 92	Dunga	38.50	0.07	21.54	0.00	27.04	0.60	5.27	7.53	0.00	100.55
56	GPS 92	Dunga	38.68	0.00	21.72	0.20	26.70	0.84	6.47	5.97	0.00	100.58
57	GPS 92	Dunga	38.67	0.00	22.11	0.07	25.66	0.45	5.99	7.44	0.03	100.42
58	GPS 92	Dunga	39.19	0.03	22.06	0.16	24.91	0.67	7.62	5.86	0.08	100.58
59	GPS 92	Dunga	38.78	0.06	22.16	0.10	26.08	0.55	7.08	5.89	0.04	100.74
60	GPS 92	Dunga	39.07	0.08	22.19	0.11	23.59	0.45	8.57	5.90	0.00	99.96
61	GPS 92	Dunga	39.96	0.05	22.67	0.22	18.83	0.31	11.32	6.52	0.04	99.92
62	GPS 92	Dunga	39.71	0.05	22.86	0.16	20.60	0.44	10.92	5.82	0.00	100.55
63	GPS 92	Dunga	38.79	0.07	22.33	0.11	24.61	0.47	7.75	6.22	0.04	100.38
64	GPS 92	Dunga	39.08	0.01	22.30	0.06	23.90	0.51	8.17	6.07	0.02	100.12
65	GPS 92	Dunga	39.34	0.05	22.34	0.10	22.30	0.48	9.22	6.43	0.07	100.32
66	GPS 92	Dunga	38.36	0.03	21.80	0.07	25.02	0.63	6.18	7.32	0.00	99.41
67	GPS 92	Dunga	38.14	0.01	21.85	0.09	27.43	0.63	5.84	6.49	0.03	100.51
68	GPS 92	Dunga	38.62	0.07	21.96	0.08	25.97	0.74	6.89	6.18	0.00	100.51
69	GPS 92	Dunga	39.03	0.09	21.99	0.05	23.95	0.40	8.77	5.81	0.00	100.09
70	GPS 92	Dunga	39.71	0.00	22.68	0.11	20.57	0.53	10.69	5.92	0.01	100.23
71	GPS 92	Dunga	38.58	0.01	21.95	0.05	25.24	0.48	7.29	6.09	0.02	99.70
72	GPS 92	Dunga	39.27	0.01	22.55	0.09	21.51	0.50	10.04	6.12	0.04	100.13
73	GPS 92	Dunga	38.48	0.01	21.97	0.06	26.69	0.57	6.17	6.16	0.00	100.11
74	GPS 92	Dunga	38.48	0.04	21.76	0.04	25.82	0.60	7.13	5.83	0.00	99.69
75	GPS 92	Dunga	39.52	0.00	21.94	0.03	27.56	0.60	6.35	5.04	0.00	101.04
76	GPS 92	Dunga	38.71	0.00	22.09	0.09	25.35	0.56	7.69	6.11	0.00	100.59
77	GPS 92	Dunga	38.51	0.05	21.92	0.11	27.24	0.60	6.18	6.16	0.04	100.80
78	GPS 92	Dunga	38.60	0.03	21.93	0.00	26.84	0.59	6.54	5.99	0.04	100.56
79	GPS 92	Dunga	38.09	0.04	21.58	0.01	30.70	0.26	3.94	5.81	0.02	100.44
80	GPS 92	Dunga	39.74	0.03	23.01	0.11	15.99	0.26	12.76	6.63	0.02	98.55
81	GPS 92	Dunga	40.08	0.05	22.97	0.06	18.87	0.39	12.23	5.82	0.00	100.47
82	GPS 92	Dunga	40.08	0.05	22.97	0.06	18.87	0.39	12.23	5.82	0.00	100.47
83	GPS 92	Dunga	40.20	0.04	23.27	0.02	14.54	0.18	13.78	7.12	0.00	99.16
84	GPS 92	Dunga	39.61	0.02	22.65	0.05	19.38	0.47	10.92	6.46	0.04	99.59
85	GPS 92	Dunga	39.63	0.01	22.34	0.29	19.48	0.51	11.17	5.97	0.03	99.43
86	GPS 92	Dunga	40.51	0.00	23.14	0.06	15.25	0.21	14.65	5.15	0.00	98.97
87	GPS 92	Dunga	38.27	0.02	22.06	0.04	23.78	0.44	8.57	6.29	0.01	99.47
88	GPS 92	Dunga	37.61	0.01	21.92	0.11	31.84	2.26	4.56	2.11	0.05	100.47
89	GPS 92	Dunga	37.90	0.07	21.79	0.06	25.17	0.51	7.56	6.09	0.05	99.20
90	GPS 98	Nyamwamba	37.50	0.02	21.36	0.00	36.74	2.54	2.08	1.05	0.00	101.29
91	GPS 98	Nyamwamba	37.05	0.00	21.78	0.00	31.20	7.77	1.86	1.48	0.02	101.16
92	GPS 98	Nyamwamba	37.45	0.15	21.16	0.00	14.62	16.43	0.53	8.05	0.02	98.41
93	GPS 98	Nyamwamba	37.34	0.06	21.66	0.04	20.70	15.94	2.39	1.91	0.03	100.06
94	GPS 98	Nyamwamba	36.98	0.00	21.76	0.00	24.97	13.66	2.60	0.44	0.00	100.41
95	GPS 98	Nyamwamba	37.07	0.00	21.69	0.03	27.22	11.39	2.16	0.59	0.00	100.15
96	GPS 98	Nyamwamba	37.20	0.10	21.67	0.00	15.62	22.13	1.47	2.62	0.00	100.81
97	GPS 98	Nyamwamba	37.66	0.00	21.45	0.01	12.25	22.60	3.23	1.94	0.01	99.16

Garnet chemistry cont.

	Sample ID	River	SiO2	TiO2	Al2O3	Cr2O3	FeO	MnO	MgO	CaO	Na2O	Total
							mass-%					
detection limit			0.016	0.011	0.014	0.013	0.022	0.012	0.009	0.014	0.012	
98	GPS 98	Nyamwamba	36.78	0.00	21.33	0.02	26.58	13.12	1.53	0.41	0.00	99.78
99	GPS 98	Nyamwamba	36.69	0.10	20.98	0.04	15.25	22.64	2.14	0.54	0.01	98.38
100	GPS 98	Nyamwamba	37.23	0.00	21.54	0.04	36.61	2.65	1.81	1.21	0.08	101.16
101	GPS 98	Nyamwamba	37.45	0.00	21.51	0.04	18.72	17.80	3.44	0.79	0.04	99.80
102	GPS 98	Nyamwamba	36.85	0.00	21.44	0.02	14.69	22.14	3.14	0.46	0.03	98.77
103	GPS 98	Nyamwamba	37.06	0.02	21.45	0.01	34.22	5.36	1.91	0.85	0.09	100.98
104	GPS 98	Nyamwamba	37.28	0.00	21.48	0.00	11.97	25.25	2.68	0.17	0.04	98.87
105	GPS 98	Nyamwamba	37.24	0.00	21.17	0.00	10.80	28.51	1.90	0.23	0.04	99.90
106	GPS 98	Nyamwamba	37.21	0.00	21.55	0.08	13.93	25.16	2.38	0.64	0.01	100.97
107	GPS 98	Nyamwamba	37.08	0.00	21.50	0.05	32.98	6.77	2.04	0.82	0.00	101.24
108	GPS 98	Nyamwamba	36.87	0.03	21.36	0.00	33.66	5.56	1.50	1.59	0.00	100.57
109	GPS 98	Nyamwamba	37.26	0.03	21.54	0.00	18.56	19.48	2.60	0.84	0.00	100.31
110	GPS 98	Nyamwamba	37.00	0.05	21.22	0.05	15.93	21.95	2.50	0.39	0.04	99.12
111	GPS 98	Nyamwamba	37.21	0.00	21.59	0.07	30.80	7.99	2.45	0.62	0.14	100.87
112	GPS 98	Nyamwamba	37.07	0.00	21.56	0.06	26.01	10.08	2.33	2.29	0.04	99.45
113	GPS 98	Nyamwamba	37.89	0.00	21.66	0.05	24.39	0.80	6.00	7.03	0.01	97.83
114	GPS 98	Nyamwamba	37.00	0.03	21.09	0.03	25.94	6.77	1.69	1.66	0.03	94.25
115	GPS 98	Nyamwamba	36.74	0.00	21.19	0.03	32.15	6.85	1.60	1.14	0.00	99.69
116	GPS 98	Nyamwamba	37.01	0.00	21.22	0.05	32.52	6.31	1.52	1.36	0.05	100.04
117	GPS 98	Nyamwamba	38.44	0.01	21.97	0.09	28.49	0.49	7.15	2.93	0.00	99.56
118	GPS 98	Nyamwamba	36.82	0.00	21.57	0.06	36.43	1.48	2.43	1.25	0.02	100.06
119	GPS 98	Nyamwamba	36.98	0.01	21.52	0.01	30.22	7.33	2.10	1.57	0.05	99.80
120	GPS 98	Nyamwamba	37.52	0.00	21.36	0.02	32.76	1.54	2.51	3.27	0.00	98.98
121	GPS 98	Nyamwamba	36.73	0.00	21.22	0.03	32.47	3.87	1.58	1.47	0.04	97.42
122	GPS 98	Nyamwamba	37.04	0.21	20.77	0.08	15.94	14.77	0.27	9.23	0.00	98.31
123	GPS 98	Nyamwamba	36.64	0.00	21.34	0.02	28.49	6.92	1.63	1.88	0.00	96.92
124	GPS 98	Nyamwamba	36.56	0.00	21.17	0.02	23.61	15.13	1.56	0.62	0.02	98.70
125	GPS 98	Nyamwamba	36.86	0.07	21.32	0.05	13.83	24.25	2.55	0.33	0.07	99.32
126	GPS 98	Nyamwamba	37.09	0.03	20.76	0.05	14.27	23.75	2.63	0.67	0.03	99.28
127	GPS 98	Nyamwamba	37.00	0.04	21.19	0.04	31.60	4.39	1.97	1.45	0.00	97.68
128	GPS 98	Nyamwamba	37.14	0.01	21.33	0.03	21.91	15.19	2.77	0.76	0.06	99.20
129	GPS 98	Nyamwamba	36.83	0.18	20.82	0.00	9.98	25.04	0.87	4.47	0.00	98.19
130	GPS 98	Nyamwamba	35.68	0.00	21.01	0.02	32.13	1.78	4.75	0.94	0.00	96.32
131	GPS 98	Nyamwamba	37.01	0.00	21.30	0.07	33.36	4.19	1.82	1.17	0.07	98.99
132	GPS 98	Nyamwamba	36.78	0.00	20.98	0.04	29.32	6.85	1.86	1.73	0.03	97.59
133	GPS 98	Nyamwamba	36.93	0.00	21.13	0.06	11.16	26.44	2.15	0.95	0.05	98.87
134	GPS 98	Nyamwamba	36.94	0.00	21.39	0.05	34.64	4.32	1.83	1.13	0.04	100.34
135	GPS 98	Nyamwamba	36.54	0.01	20.51	0.02	21.94	16.64	1.54	0.77	0.05	98.01
136	GPS 98	Nyamwamba	36.42	0.00	21.05	0.03	21.35	17.38	1.42	0.48	0.07	98.20
137	GPS 98	Nyamwamba	36.95	0.00	21.19	0.01	27.69	6.48	1.75	1.52	0.00	95.59
138	GPS 98	Nyamwamba	36.70	0.02	21.12	0.00	32.90	1.44	2.19	1.18	0.00	95.55
139	GPS 98	Nyamwamba	36.72	0.06	21.06	0.00	29.72	6.00	1.60	1.06	0.00	96.23
140	GPS 98	Nyamwamba	36.62	0.00	21.25	0.05	21.18	16.10	2.19	0.58	0.08	98.04
141	GPS 98	Nyamwamba	38.35	0.00	21.68	0.17	25.60	0.77	7.10	3.82	0.00	97.49
142	GPS 98	Nyamwamba	36.87	0.00	21.30	0.05	22.59	15.82	2.30	0.52	0.08	99.53
143	GPS 98	Nyamwamba	38.11	0.01	21.75	0.11	26.05	0.69	7.21	3.85	0.07	97.86
144	GPS 98	Nyamwamba	37.13	0.05	21.05	0.05	14.55	23.26	2.36	0.68	0.00	99.13
145	GPS 98	Nyamwamba	37.07	0.02	21.20	0.00	14.59	21.97	3.40	0.29	0.07	98.61
146	GPS 98	Nyamwamba	37.19	0.00	21.13	0.07	14.92	21.64	2.80	1.11	0.00	98.86
147	GPS 98	Nyamwamba	36.93	0.04	21.20	0.02	31.57	7.28	1.55	1.20	0.07	99.85
148	GPS 98	Nyamwamba	37.15	0.02	21.43	0.00	32.23	5.88	1.77	1.40	0.04	99.91
149	GPS 98	Nyamwamba	37.03	0.01	21.25	0.07	37.32	0.81	2.53	1.04	0.00	100.06
150	GPS 98	Nyamwamba	36.43	0.00	20.89	0.06	23.53	15.47	1.44	0.55	0.07	98.44
151	GPS 98	Nyamwamba	36.97	0.04	21.11	0.07	15.21	23.72	2.60	0.28	0.00	100.00
152	GPS 98	Nyamwamba	36.85	0.06	20.83	0.02	8.90	30.51	0.55	2.20	0.00	99.91
153	GPS 98	Nyamwamba	37.03	0.02	21.44	0.03	31.90	6.39	1.62	1.62	0.05	100.10
154	GPS 98	Nyamwamba	36.98	0.00	21.26	0.06	31.49	6.23	1.72	1.60	0.00	99.34
155	GPS 98	Nyamwamba	39.08	0.05	22.30	0.01	22.64	0.59	8.75	6.06	0.03	99.51
156	GPS 98	Nyamwamba	37.29	0.12	20.91	0.01	15.27	21.36	3.42	0.81	0.06	99.25
157	GPS 98	Nyamwamba	36.82	0.00	21.08	0.00	12.78	24.72	2.65	0.67	0.05	98.78
158	GPS 98	Nyamwamba	36.47	0.00	20.67	0.02	13.38	25.97	1.79	0.54	0.08	98.93
159	GPS 98	Nyamwamba	36.81	0.33	20.29	0.03	6.75	29.31	0.50	5.14	0.00	99.16
160	GPS 98	Nyamwamba	36.71	0.00	21.25	0.01	34.47	4.15	1.41	1.55	0.10	99.64
161	GPS 98	Nyamwamba	37.11	0.03	21.44	0.03	36.05	3.60	1.70	1.21	0.01	101.17
162	GPS 98	Nyamwamba	36.89	0.14	21.07	0.08	11.51	25.85	0.92	4.30	0.00	100.76
163	GPS 98	Nyamwamba	35.68	0.00	20.36	0.00	30.93	6.02	1.71	4.36	0.02	99.09
164	GPS 98	Nyamwamba	36.63	0.01	21.21	0.05	36.67	2.41	1.74	1.21	0.03	99.95
165	GPS 98	Nyamwamba	36.73	0.00	21.38	0.00	36.41	2.98	1.43	1.65	0.06	100.64
166	GPS 98	Nyamwamba	36.73	0.00	21.43	0.00	33.35	5.92	1.48	1.42	0.08	100.41
167	GPS 98	Nyamwamba	37.07	0.04	21.25	0.00	22.19	16.55	1.49	0.84	0.00	99.44

Garnet chemistry cont.

	Sample ID	River	SiO2	TiO2	Al2O3	Cr2O3	FeO	MnO	MgO	CaO	Na2O	Total
							mass-%					
detection limit			0.016	0.011	0.014	0.013	0.022	0.012	0.009	0.014	0.012	
168	GPS 98	Nyamwamba	37.24	0.00	21.51	0.01	38.01	1.12	2.04	1.24	0.00	101.17
169	GPS 98	Nyamwamba	36.14	0.78	20.81	0.01	18.08	20.27	2.28	0.53	0.09	99.00
170	GPS 98	Nyamwamba	36.70	0.01	21.51	0.04	35.67	3.46	1.62	1.23	0.00	100.24
171	GPS 98	Nyamwamba	36.55	0.00	21.12	0.07	33.81	5.00	1.67	1.21	0.00	99.43
172	GPS 98	Nyamwamba	37.13	0.00	21.27	0.03	30.89	4.21	2.06	4.08	0.05	99.72
173	GPS 98	Nyamwamba	37.39	0.02	21.15	0.07	17.49	17.85	3.15	2.35	0.00	99.46
174	GPS 98	Nyamwamba	37.03	0.00	21.19	0.02	36.77	2.50	1.53	1.21	0.00	100.25
175	GPS 98	Nyamwamba	36.99	0.04	20.98	0.05	13.62	23.67	3.05	0.34	0.07	98.81
176	GPS 98	Nyamwamba	37.01	0.01	20.76	0.01	17.66	19.87	2.96	0.82	0.02	99.12
177	GPS 98	Nyamwamba	36.99	0.00	21.23	0.02	6.91	31.90	1.99	0.21	0.00	99.24
178	GPS 98	Nyamwamba	36.95	0.04	21.06	0.00	13.54	23.67	2.43	0.57	0.07	98.33
179	GPS 98	Nyamwamba	36.80	0.02	21.00	0.09	36.71	2.85	1.27	1.63	0.00	100.37
180	GPS 98	Nyamwamba	36.65	0.00	21.31	0.00	30.92	9.12	1.86	0.61	0.00	100.47
181	GPS 98	Nyamwamba	36.60	0.01	21.62	0.03	35.25	3.71	1.61	1.65	0.00	100.49
182	GPS 98	Nyamwamba	36.99	0.00	21.49	0.03	36.83	1.49	2.29	1.11	0.02	100.25
183	GPS 98	Nyamwamba	37.07	0.03	21.25	0.00	36.43	2.62	1.88	1.42	0.01	100.71
184	GPS 98	Nyamwamba	37.08	0.02	21.47	0.05	32.55	3.18	2.01	3.99	0.09	100.45
185	GPS 98	Nyamwamba	37.32	0.00	21.34	0.09	15.06	21.19	3.43	0.36	0.00	98.79
186	GPS 98	Nyamwamba	37.33	0.00	21.41	0.00	17.37	21.28	2.75	0.88	0.08	101.10
187	GPS 98	Nyamwamba	36.91	0.00	21.35	0.02	35.00	3.12	1.91	2.03	0.01	100.34
188	GPS 98	Nyamwamba	36.69	0.00	21.32	0.00	36.93	2.60	1.36	1.14	0.00	100.04
189	GPS 98	Nyamwamba	36.92	0.00	20.80	0.02	32.97	0.36	0.59	8.10	0.02	99.77
190	GPS 71	trib. Dura	36.77	0.00	21.40	0.05	32.63	4.92	2.93	0.76	0.04	99.50
191	GPS 71	trib. Dura	37.01	0.00	21.35	0.01	16.49	21.19	2.94	0.84	0.00	100.83
192	GPS 71	trib. Dura	39.45	0.02	22.83	0.09	19.61	0.37	10.66	6.82	0.02	99.89
193	GPS 71	trib. Dura	36.75	0.00	21.48	0.05	34.13	3.08	3.00	0.71	0.00	99.20
194	GPS 71	trib. Dura	39.07	0.00	22.24	0.11	21.86	0.61	9.33	6.14	0.00	99.35
195	GPS 71	trib. Dura	36.73	0.07	21.43	0.10	15.72	22.29	2.72	0.42	0.04	100.52
196	GPS 71	trib. Dura	37.10	0.02	21.49	0.09	18.42	17.58	2.61	3.19	0.00	100.50
197	GPS 71	trib. Dura	37.10	0.03	21.36	0.05	35.52	2.06	1.99	1.64	0.00	99.75
198	GPS 71	trib. Dura	36.96	0.04	21.34	0.00	30.97	2.19	3.36	1.05	0.00	95.91
199	GPS 71	trib. Dura	36.98	0.02	21.60	0.03	36.20	1.50	3.26	1.03	0.01	100.63
200	GPS 71	trib. Dura	37.19	0.00	21.45	0.06	13.73	25.48	2.52	0.68	0.00	101.11
201	GPS 71	trib. Dura	36.84	0.12	21.20	0.06	13.71	24.54	2.35	0.98	0.02	100.81
202	GPS 71	trib. Dura	36.87	0.00	21.45	0.08	34.81	3.66	2.48	0.56	0.00	99.91
203	GPS 71	trib. Dura	36.94	0.05	21.04	0.07	13.93	24.57	2.48	0.92	0.08	101.08
204	GPS 71	trib. Dura	36.97	0.08	21.10	0.04	14.96	23.24	2.54	0.60	0.03	100.57
205	GPS 71	trib. Dura	39.62	0.01	22.74	0.09	17.83	0.50	10.89	6.52	0.00	98.20
206	GPS 71	trib. Dura	37.37	0.00	21.33	0.00	34.05	3.12	2.72	1.54	0.03	100.16
207	GPS 71	trib. Dura	37.88	0.03	21.71	0.02	25.98	1.22	4.72	7.87	0.00	99.42
208	GPS 71	trib. Dura	37.03	0.03	21.32	0.08	35.08	2.33	2.63	1.81	0.00	100.32
209	GPS 71	trib. Dura	39.39	0.04	22.42	0.17	20.28	0.53	10.51	6.23	0.05	99.62
210	GPS 71	trib. Dura	37.01	0.05	21.68	0.05	15.15	22.88	2.88	0.81	0.02	101.53
211	GPS 71	trib. Dura	37.90	0.09	21.57	0.00	26.51	0.56	5.05	8.21	0.01	99.90
212	GPS 71	trib. Dura	38.49	0.07	21.92	0.16	25.44	0.64	6.96	6.20	0.00	99.88
213	GPS 71	trib. Dura	38.21	0.00	21.43	0.02	26.47	0.56	4.98	8.36	0.00	100.03
214	GPS 71	trib. Dura	36.92	0.08	21.49	0.08	35.96	2.53	2.60	1.04	0.02	100.73
215	GPS 71	trib. Dura	37.93	0.00	21.39	0.01	27.74	0.56	4.33	8.21	0.00	100.17
216	GPS 71	trib. Dura	38.27	0.02	21.51	0.02	27.51	0.62	4.24	8.23	0.10	100.51
217	GPS 71	trib. Dura	37.09	0.11	21.49	0.04	15.82	22.97	2.49	0.60	0.03	101.64
218	GPS 71	trib. Dura	38.30	0.00	22.11	0.15	28.33	0.50	6.21	4.41	0.05	100.06
219	GPS 71	trib. Dura	37.16	0.01	21.55	0.08	33.26	1.88	3.63	1.07	0.00	98.65
220	GPS 71	trib. Dura	38.20	0.00	21.92	0.13	28.38	0.55	6.34	4.47	0.09	100.08
221	GPS 71	trib. Dura	36.96	0.02	21.48	0.01	12.85	24.21	2.73	0.43	0.00	98.68
222	GPS 73	Mpanga	37.63	0.02	21.79	0.04	26.55	1.22	3.66	8.36	0.04	99.32
223	GPS 73	Mpanga	38.09	0.00	21.49	0.08	26.98	0.80	5.33	6.80	0.01	99.58
224	GPS 73	Mpanga	38.46	0.02	21.62	0.08	25.66	0.36	6.89	6.16	0.01	99.25
225	GPS 73	Mpanga	39.32	0.00	22.08	0.16	21.39	0.41	9.90	6.01	0.02	99.29
226	GPS 73	Mpanga	39.48	0.02	22.16	0.22	21.78	0.53	9.46	6.33	0.00	99.98
227	GPS 73	Mpanga	36.97	0.07	20.90	0.06	17.73	21.97	1.90	0.37	0.07	100.04
228	GPS 73	Mpanga	38.20	0.04	21.57	0.07	24.79	0.60	6.99	6.61	0.00	98.87
229	GPS 73	Mpanga	37.06	0.23	20.55	0.04	11.68	25.87	1.44	1.43	0.05	98.35
230	GPS 73	Mpanga	38.37	0.02	21.41	0.10	25.58	0.44	6.77	6.25	0.05	98.99
231	GPS 73	Mpanga	38.31	0.01	21.94	0.08	26.78	0.79	5.63	6.43	0.03	100.00
232	GPS 73	Mpanga	36.72	0.07	21.19	0.00	6.69	34.37	0.37	0.08	0.02	99.51
233	GPS 73	Mpanga	39.42	0.04	22.29	0.13	20.46	0.46	9.88	6.37	0.02	99.07
234	GPS 73	Mpanga	39.50	0.03	22.26	0.09	22.02	0.37	9.17	6.26	0.02	99.72
235	GPS 73	Mpanga	38.82	0.09	21.72	0.10	24.40	0.53	7.00	7.11	0.03	99.80
236	GPS 73	Mpanga	36.70	0.00	21.21	0.04	34.67	5.34	1.19	0.76	0.08	99.99
237	GPS 73	Mpanga	39.14	0.03	21.99	0.12	22.63	0.39	8.64	6.85	0.05	99.84

Garnet chemistry cont.

	Sample ID	River	SiO2	TiO2	Al2O3	Cr2O3	FeO	MnO	MgO	CaO	Na2O	Total
							mass-%					
detection limit			0.016	0.011	0.014	0.013	0.022	0.012	0.009	0.014	0.012	
238	GPS 73	Mpanga	38.59	0.03	21.80	0.07	24.79	0.56	7.19	6.41	0.02	99.45
239	GPS 73	Mpanga	36.75	0.00	21.01	0.00	25.98	13.12	1.46	0.93	0.00	99.26
240	GPS 73	Mpanga	38.16	0.00	21.53	0.13	30.51	0.58	5.83	3.24	0.04	100.03
241	GPS 73	Mpanga	39.06	0.00	22.15	0.19	24.17	0.55	8.20	5.56	0.01	99.89
242	GPS 73	Mpanga	38.68	0.03	21.57	0.10	25.14	0.50	6.48	7.28	0.01	99.79
243	GPS 73	Mpanga	38.21	0.03	21.78	0.04	26.88	1.25	5.50	6.59	0.00	100.28
244	GPS 73	Mpanga	39.57	0.02	22.38	0.09	20.06	0.40	9.62	7.72	0.03	99.89
245	GPS 73	Mpanga	36.61	0.25	17.54	0.02	7.96	29.73	1.39	3.57	0.00	97.06
246	GPS 73	Mpanga	38.22	0.02	21.74	0.08	29.20	0.61	6.73	3.26	0.00	99.87
247	GPS 73	Mpanga	38.85	0.00	22.02	0.07	25.69	0.37	7.37	6.05	0.02	100.45
248	GPS 73	Mpanga	38.51	0.07	21.80	0.13	25.72	0.60	6.84	6.31	0.00	99.99
249	GPS 73	Mpanga	38.60	0.00	21.56	0.02	29.42	0.67	6.46	3.35	0.02	100.10
250	GPS 73	Mpanga	36.67	0.20	20.80	0.01	20.15	20.60	1.05	0.30	0.05	99.83
251	GPS 73	Mpanga	38.75	0.02	21.81	0.05	24.03	0.45	5.69	9.20	0.00	100.00
252	GPS 73	Mpanga	38.36	0.03	21.94	0.09	26.92	0.87	6.13	5.51	0.00	99.85
253	GPS 73	Mpanga	38.41	0.00	21.35	0.14	28.27	0.69	5.92	5.45	0.08	100.31
254	GPS 73	Mpanga	39.24	0.06	22.02	0.14	22.64	0.34	8.84	6.28	0.05	99.61
255	GPS 73	Mpanga	37.50	0.00	21.07	0.03	20.48	17.51	3.01	0.60	0.02	100.21
256	GPS 73	Mpanga	38.09	0.00	21.69	0.04	31.44	1.27	5.16	1.78	0.00	99.47
257	GPS 73	Mpanga	38.33	0.07	21.65	0.10	26.47	0.59	5.91	6.66	0.06	99.83
258	GPS 73	Mpanga	38.29	0.04	21.47	0.00	26.75	0.81	5.54	6.85	0.00	99.75
259	GPS 73	Mpanga	39.64	0.00	22.35	0.11	20.64	0.43	10.83	5.74	0.00	99.74
260	GPS 73	Mpanga	38.54	0.12	21.35	0.04	26.74	0.56	6.20	6.47	0.03	100.05
261	GPS 73	Mpanga	36.30	0.02	20.57	0.11	25.55	0.52	6.83	7.37	0.00	97.27
262	GPS 73	Mpanga	39.00	0.06	21.16	0.02	25.44	0.43	6.34	7.20	0.00	99.66
263	GPS 73	Mpanga	39.65	0.02	22.60	0.09	19.39	0.41	11.13	6.10	0.02	99.40
264	GPS 73	Mpanga	38.31	0.07	21.50	0.15	30.24	0.56	6.24	2.66	0.03	99.76
265	GPS 73	Mpanga	37.84	0.03	21.06	0.02	28.20	1.69	3.98	6.83	0.00	99.64
266	GPS 73	Mpanga	39.64	0.01	22.50	0.07	20.08	0.30	10.78	5.88	0.02	99.28
267	GPS 73	Mpanga	36.34	0.04	20.92	0.05	15.45	25.85	0.29	0.15	0.00	99.10
268	GPS 73	Mpanga	39.50	0.02	22.35	0.02	20.92	0.60	10.10	6.00	0.01	99.51
269	GPS 73	Mpanga	36.22	0.11	20.84	0.01	15.35	26.00	0.32	0.15	0.00	99.00
270	GPS 73	Mpanga	39.02	0.06	21.81	0.02	23.60	0.38	8.05	6.64	0.00	99.58
271	GPS 73	Mpanga	39.57	0.02	22.35	0.20	21.02	0.56	10.20	5.71	0.05	99.67
272	GPS 73	Mpanga	39.11	0.02	21.98	0.06	24.29	0.46	7.66	6.38	0.04	100.00
273	GPS 73	Mpanga	38.16	0.02	21.83	0.04	29.16	0.69	6.22	3.64	0.08	99.84
274	GPS 73	Mpanga	39.20	0.00	21.99	0.09	22.50	0.30	8.52	6.86	0.05	99.51
275	GPS 73	Mpanga	39.63	0.02	21.92	0.08	22.92	0.59	9.01	5.91	0.06	100.13
276	GPS 73	Mpanga	38.54	0.04	21.57	0.00	26.84	0.39	6.21	5.59	0.00	99.18
277	GPS 73	Mpanga	38.74	0.05	22.08	0.09	23.45	0.63	8.57	5.82	0.03	99.46
278	GPS 73	Mpanga	39.19	0.04	22.15	0.15	22.22	0.42	8.57	6.75	0.00	99.49
279	GPS 73	Mpanga	38.67	0.01	21.69	0.01	24.85	0.66	7.78	5.89	0.06	99.63

A3-3 – Zircon U-Pb geochronology

			Isotope ratios								Age estimates								
River name	Sample ID	Analysis No.	$^{207}Pb/^{206}Pb$	±1σ	$^{206}Pb/^{238}U$	±1σ	$^{207}Pb/^{235}U$	±1σ	$^{208}Pb/^{232}Th$	±1σ	$^{207}Pb/^{206}Pb$ [Ma]	±1σ [Ma]	$^{206}Pb/^{238}U$ [Ma]	±1σ [Ma]	$^{207}Pb/^{235}U$ [Ma]	±1σ [Ma]	$^{208}Pb/^{232}Th$ [Ma]	±1σ [Ma]	Concordance [%]
Wambabya (LAB)	GPS 58	~~1~~	~~0.169~~	~~0.005~~	~~0.030~~	~~0.000~~	~~0.641~~	~~0.024~~	~~0.021~~	~~0.002~~	~~2546~~	~~50~~	~~192~~	~~2~~	~~503~~	~~15~~	~~415~~	~~38~~	~~7.5~~
Wambabya (LAB)	GPS 58	~~2~~	~~0.200~~	~~0.003~~	~~0.131~~	~~0.002~~	~~3.515~~	~~0.079~~	~~0.010~~	~~0.000~~	~~2826~~	~~28~~	~~796~~	~~9~~	~~1531~~	~~18~~	~~192~~	~~8~~	~~28.2~~
Wambabya (LAB)	GPS 58	~~3~~	~~0.194~~	~~0.003~~	~~0.130~~	~~0.002~~	~~3.332~~	~~0.076~~	~~0.026~~	~~0.001~~	~~2776~~	~~29~~	~~787~~	~~9~~	~~1489~~	~~18~~	~~528~~	~~24~~	~~28.4~~
Wambabya (LAB)	GPS 58	~~4~~	~~0.183~~	~~0.007~~	~~0.166~~	~~0.002~~	~~4.126~~	~~0.203~~	~~0.124~~	~~0.016~~	~~2677~~	~~63~~	~~989~~	~~13~~	~~1659~~	~~40~~	~~2355~~	~~281~~	~~36.9~~
Wambabya (LAB)	GPS 58	~~5~~	~~0.135~~	~~0.005~~	~~0.136~~	~~0.002~~	~~2.450~~	~~0.108~~	~~0.023~~	~~0.003~~	~~2170~~	~~59~~	~~824~~	~~10~~	~~1257~~	~~32~~	~~453~~	~~50~~	~~38.0~~
Wambabya (LAB)	GPS 58	~~6~~	~~0.205~~	~~0.008~~	~~0.186~~	~~0.003~~	~~5.203~~	~~0.246~~	~~0.111~~	~~0.013~~	~~2865~~	~~59~~	~~1098~~	~~14~~	~~1853~~	~~40~~	~~2122~~	~~242~~	~~38.3~~
Wambabya (LAB)	GPS 58	~~7~~	~~0.161~~	~~0.006~~	~~0.180~~	~~0.002~~	~~3.815~~	~~0.171~~	~~0.063~~	~~0.007~~	~~2463~~	~~59~~	~~1065~~	~~13~~	~~1596~~	~~36~~	~~1242~~	~~137~~	~~43.2~~
Wambabya (LAB)	GPS 58	~~8~~	~~0.149~~	~~0.004~~	~~0.178~~	~~0.002~~	~~3.511~~	~~0.108~~	~~0.013~~	~~0.001~~	~~2335~~	~~41~~	~~1054~~	~~12~~	~~1530~~	~~24~~	~~264~~	~~19~~	~~45.2~~
Wambabya (LAB)	GPS 58	~~9~~	~~0.161~~	~~0.007~~	~~0.192~~	~~0.003~~	~~4.083~~	~~0.226~~	~~0.006~~	~~0.001~~	~~2468~~	~~72~~	~~1134~~	~~15~~	~~1651~~	~~45~~	~~124~~	~~18~~	~~45.9~~
Wambabya (LAB)	GPS 58	~~10~~	~~0.154~~	~~0.010~~	~~0.191~~	~~0.004~~	~~3.859~~	~~0.323~~	~~0.107~~	~~0.024~~	~~2388~~	~~109~~	~~1124~~	~~19~~	~~1605~~	~~67~~	~~2060~~	~~439~~	~~47.1~~
Wambabya (LAB)	GPS 58	~~11~~	~~0.177~~	~~0.006~~	~~0.219~~	~~0.003~~	~~5.363~~	~~0.248~~	~~0.026~~	~~0.003~~	~~2628~~	~~59~~	~~1279~~	~~16~~	~~1879~~	~~40~~	~~515~~	~~59~~	~~48.7~~
Wambabya (LAB)	GPS 58	~~12~~	~~0.144~~	~~0.010~~	~~0.197~~	~~0.004~~	~~4.065~~	~~0.354~~	~~0.045~~	~~0.010~~	~~2276~~	~~115~~	~~1161~~	~~20~~	~~1647~~	~~71~~	~~885~~	~~202~~	~~51.0~~
Wambabya (LAB)	GPS 58	~~13~~	~~0.146~~	~~0.011~~	~~0.202~~	~~0.004~~	~~4.080~~	~~0.382~~	~~0.054~~	~~0.014~~	~~2301~~	~~123~~	~~1187~~	~~22~~	~~1650~~	~~76~~	~~1065~~	~~261~~	~~51.6~~
Wambabya (LAB)	GPS 58	~~14~~	~~0.167~~	~~0.012~~	~~0.227~~	~~0.004~~	~~4.969~~	~~0.447~~	~~0.289~~	~~0.070~~	~~2530~~	~~116~~	~~1317~~	~~23~~	~~1814~~	~~76~~	~~5132~~	~~1097~~	~~52.0~~
Wambabya (LAB)	GPS 58	~~15~~	~~0.165~~	~~0.011~~	~~0.259~~	~~0.005~~	~~5.850~~	~~0.471~~	~~0.139~~	~~0.030~~	~~2511~~	~~104~~	~~1484~~	~~24~~	~~1954~~	~~70~~	~~2623~~	~~529~~	~~59.1~~

Zircon U-Pb geochronology cont.

			Isotope ratios								Age estimates								
River name	Sample ID	Analysis No.	$^{207}Pb/^{206}Pb$	±1σ	$^{206}Pb/^{238}U$	±1σ	$^{207}Pb/^{235}U$	±1σ	$^{208}Pb/^{232}Th$	±1σ	$^{207}Pb/^{206}Pb$ [Ma]	±1σ [Ma]	$^{206}Pb/^{238}U$ [Ma]	±1σ [Ma]	$^{207}Pb/^{235}U$ [Ma]	±1σ [Ma]	$^{208}Pb/^{232}Th$ [Ma]	±1σ [Ma]	Concordance [%]
Wambabya (LAB)	GPS 58	~~16~~	~~0.204~~	~~0.008~~	~~0.299~~	~~0.004~~	~~8.596~~	~~0.437~~	~~0.039~~	~~0.005~~	~~2855~~	~~63~~	~~1688~~	~~21~~	~~2296~~	~~46~~	~~770~~	~~98~~	~~59.1~~
Wambabya (LAB)	GPS 58	~~17~~	~~0.163~~	~~0.003~~	~~0.257~~	~~0.003~~	~~5.731~~	~~0.145~~	~~0.143~~	~~0.008~~	~~2488~~	~~32~~	~~1473~~	~~16~~	~~1936~~	~~22~~	~~2697~~	~~133~~	~~59.2~~
Wambabya (LAB)	GPS 58	~~18~~	~~0.143~~	~~0.009~~	~~0.251~~	~~0.005~~	~~5.013~~	~~0.396~~	~~0.088~~	~~0.019~~	~~2259~~	~~105~~	~~1443~~	~~23~~	~~1822~~	~~67~~	~~1703~~	~~344~~	~~63.9~~
Wambabya (LAB)	GPS 58	~~19~~	~~0.204~~	~~0.014~~	~~0.328~~	~~0.006~~	~~9.202~~	~~0.827~~	~~0.128~~	~~0.030~~	~~2860~~	~~111~~	~~1830~~	~~31~~	~~2358~~	~~82~~	~~2441~~	~~546~~	~~64.0~~
Wambabya (LAB)	GPS 58	~~20~~	~~0.149~~	~~0.003~~	~~0.278~~	~~0.003~~	~~5.788~~	~~0.161~~	~~0.069~~	~~0.004~~	~~2333~~	~~36~~	~~1582~~	~~17~~	~~1945~~	~~24~~	~~1351~~	~~79~~	~~67.8~~
Wambabya (LAB)	GPS 58	~~21~~	~~0.222~~	~~0.009~~	~~0.381~~	~~0.005~~	~~11.782~~	~~0.610~~	~~0.147~~	~~0.020~~	~~2995~~	~~64~~	~~2081~~	~~25~~	~~2587~~	~~48~~	~~2778~~	~~346~~	~~69.5~~
Wambabya (LAB)	GPS 58	~~22~~	~~0.167~~	~~0.008~~	~~0.317~~	~~0.005~~	~~7.781~~	~~0.468~~	~~0.062~~	~~0.009~~	~~2524~~	~~74~~	~~1775~~	~~24~~	~~2206~~	~~54~~	~~1220~~	~~175~~	~~70.3~~
Wambabya (LAB)	GPS 58	~~23~~	~~0.164~~	~~0.012~~	~~0.320~~	~~0.006~~	~~7.291~~	~~0.674~~	~~0.094~~	~~0.023~~	~~2496~~	~~119~~	~~1790~~	~~31~~	~~2148~~	~~83~~	~~1820~~	~~429~~	~~71.7~~
Wambabya (LAB)	GPS 58	~~24~~	~~0.155~~	~~0.010~~	~~0.306~~	~~0.005~~	~~6.426~~	~~0.497~~	~~0.057~~	~~0.012~~	~~2397~~	~~101~~	~~1721~~	~~27~~	~~2036~~	~~68~~	~~1117~~	~~224~~	~~71.8~~
Wambabya (LAB)	GPS 58	~~25~~	~~0.179~~	~~0.008~~	~~0.369~~	~~0.006~~	~~9.220~~	~~0.541~~	~~0.058~~	~~0.009~~	~~2641~~	~~74~~	~~2024~~	~~26~~	~~2360~~	~~54~~	~~1138~~	~~167~~	~~76.7~~
Wambabya (LAB)	GPS 58	~~26~~	~~0.156~~	~~0.003~~	~~0.341~~	~~0.004~~	~~6.959~~	~~0.171~~	~~0.058~~	~~0.003~~	~~2409~~	~~32~~	~~1890~~	~~19~~	~~2106~~	~~22~~	~~1140~~	~~57~~	~~78.5~~
Wambabya (LAB)	GPS 58	~~27~~	~~0.153~~	~~0.006~~	~~0.347~~	~~0.005~~	~~7.395~~	~~0.397~~	~~0.099~~	~~0.014~~	~~2374~~	~~70~~	~~1921~~	~~24~~	~~2160~~	~~48~~	~~1912~~	~~250~~	~~80.9~~
Wambabya (LAB)	GPS 58	~~28~~	~~0.191~~	~~0.005~~	~~0.414~~	~~0.005~~	~~10.823~~	~~0.382~~	~~0.131~~	~~0.010~~	~~2753~~	~~41~~	~~2232~~	~~24~~	~~2508~~	~~33~~	~~2485~~	~~174~~	~~81.1~~
Wambabya (LAB)	GPS 58	~~29~~	~~0.166~~	~~0.005~~	~~0.377~~	~~0.005~~	~~8.453~~	~~0.346~~	~~0.082~~	~~0.008~~	~~2522~~	~~53~~	~~2060~~	~~23~~	~~2281~~	~~37~~	~~1592~~	~~155~~	~~81.7~~
Wambabya (LAB)	GPS 58	~~30~~	~~0.151~~	~~0.006~~	~~0.349~~	~~0.005~~	~~7.377~~	~~0.358~~	~~0.089~~	~~0.011~~	~~2356~~	~~64~~	~~1932~~	~~23~~	~~2158~~	~~43~~	~~1717~~	~~203~~	~~82.0~~
Wambabya (LAB)	GPS 58	~~31~~	~~0.167~~	~~0.004~~	~~0.397~~	~~0.005~~	~~9.316~~	~~0.276~~	~~0.105~~	~~0.007~~	~~2529~~	~~37~~	~~2155~~	~~22~~	~~2370~~	~~27~~	~~2017~~	~~125~~	~~85.2~~
Wambabya (LAB)	GPS 58	~~32~~	~~0.173~~	~~0.011~~	~~0.427~~	~~0.008~~	~~9.734~~	~~0.810~~	~~0.087~~	~~0.019~~	~~2591~~	~~105~~	~~2294~~	~~36~~	~~2410~~	~~77~~	~~1685~~	~~355~~	~~88.5~~
Wambabya (LAB)	GPS 58	~~33~~	~~0.163~~	~~0.004~~	~~0.409~~	~~0.005~~	~~9.258~~	~~0.284~~	~~0.117~~	~~0.008~~	~~2489~~	~~39~~	~~2211~~	~~23~~	~~2364~~	~~28~~	~~2232~~	~~149~~	~~88.9~~
Wambabya (LAB)	GPS 58	~~34~~	~~0.052~~	~~0.002~~	~~0.055~~	~~0.001~~	~~0.396~~	~~0.015~~	~~0.018~~	~~0.001~~	~~290~~	~~69~~	~~344~~	~~4~~	~~338~~	~~11~~	~~351~~	~~28~~	~~118.8~~
Wambabya (LAB)	GPS 58	~~35~~	~~0.850~~	~~0.048~~	~~39.598~~	~~3.373~~	-	-	~~2.185~~	~~0.398~~	~~5008~~	~~78~~	-	~~536~~	-	-	-	~~2526~~	-
Wambabya (LAB)	GPS 58	36	0.112	0.007	0.316	0.006	4.942	0.371	0.087	0.017	1836	104	1772	27	1809	63	1689	321	96.5
Wambabya (LAB)	GPS 58	37	0.114	0.005	0.331	0.005	5.105	0.307	0.096	0.013	1871	78	1845	24	1837	51	1852	248	98.6
Wambabya (LAB)	GPS 58	38	0.158	0.009	0.454	0.008	9.862	0.705	0.127	0.024	2430	92	2415	34	2422	66	2419	423	99.4
Wambabya (LAB)	GPS 58	39	0.166	0.003	0.508	0.006	11.218	0.281	0.123	0.006	2516	30	2648	26	2541	23	2343	106	105.3
Wambabya (LAB)	GPS 58	40	0.168	0.010	0.433	0.007	9.995	0.719	0.104	0.020	2537	92	2319	33	2434	66	1996	361	91.4
Wambabya (LAB)	GPS 58	41	0.168	0.006	0.481	0.006	10.981	0.506	0.139	0.015	2538	55	2531	28	2522	43	2631	259	99.7
Wambabya (LAB)	GPS 58	42	0.169	0.005	0.485	0.006	11.093	0.454	0.135	0.013	2548	50	2551	27	2531	38	2565	231	100.1
Wambabya (LAB)	GPS 58	43	0.169	0.005	0.452	0.006	10.373	0.426	0.127	0.012	2550	52	2404	26	2469	38	2411	224	94.3
Wambabya (LAB)	GPS 58	44	0.169	0.010	0.425	0.007	9.822	0.715	0.061	0.012	2551	94	2284	33	2418	67	1195	225	89.5
Wambabya (LAB)	GPS 58	45	0.169	0.006	0.436	0.006	10.555	0.494	0.127	0.014	2551	56	2334	27	2485	43	2422	245	91.5
Wambabya (LAB)	GPS 58	46	0.170	0.004	0.503	0.006	11.434	0.359	0.129	0.009	2554	38	2628	26	2559	29	2459	155	102.9
Wambabya (LAB)	GPS 58	47	0.170	0.003	0.486	0.006	11.515	0.276	0.112	0.005	2558	28	2554	25	2566	22	2146	87	99.9
Wambabya (LAB)	GPS 58	48	0.171	0.013	0.447	0.009	10.097	0.977	0.103	0.027	2565	124	2383	41	2444	89	1975	491	92.9
Wambabya (LAB)	GPS 58	49	0.171	0.012	0.460	0.009	10.638	0.912	0.121	0.028	2565	109	2439	39	2492	80	2309	498	95.1
Wambabya (LAB)	GPS 58	50	0.172	0.005	0.495	0.006	11.496	0.481	0.136	0.012	2576	48	2592	28	2564	39	2579	218	100.6
Wambabya (LAB)	GPS 58	51	0.173	0.003	0.464	0.006	11.338	0.391	0.141	0.006	2589	32	2455	25	2551	32	2663	113	94.8
Wambabya (LAB)	GPS 58	52	0.174	0.003	0.490	0.006	11.947	0.306	0.123	0.006	2592	31	2571	25	2600	24	2347	109	99.2
Wambabya (LAB)	GPS 58	53	0.174	0.011	0.494	0.009	11.350	0.876	0.114	0.023	2593	97	2589	38	2552	72	2187	419	99.8
Wambabya (LAB)	GPS 58	54	0.176	0.009	0.495	0.008	11.926	0.819	0.143	0.025	2615	86	2590	35	2599	64	2695	448	99.0
Wambabya (LAB)	GPS 58	55	0.176	0.004	0.489	0.006	12.324	0.348	0.123	0.007	2620	33	2567	25	2629	27	2345	125	98.0
Wambabya (LAB)	GPS 58	56	0.177	0.003	0.520	0.006	12.597	0.453	0.125	0.005	2626	30	2698	27	2650	34	2382	95	102.7
Wambabya (LAB)	GPS 58	57	0.179	0.004	0.515	0.006	12.365	0.387	0.124	0.008	2642	36	2676	27	2633	29	2364	140	101.3
Wambabya (LAB)	GPS 58	58	0.182	0.004	0.484	0.006	12.166	0.348	0.094	0.005	2668	34	2543	25	2617	27	1809	101	95.3
Wambabya (LAB)	GPS 58	59	0.183	0.004	0.483	0.006	12.020	0.356	0.101	0.006	2679	33	2542	25	2606	28	1952	102	94.9
Wambabya (LAB)	GPS 58	60	0.187	0.014	0.518	0.011	13.098	1.291	0.144	0.037	2719	121	2689	46	2687	93	2716	651	98.9
trib. Wambabya (LAB)	GPS 59	~~1~~	~~0.072~~	~~0.002~~	~~0.056~~	~~0.001~~	~~0.559~~	~~0.016~~	~~0.016~~	~~0.001~~	~~995~~	~~46~~	~~353~~	~~4~~	~~451~~	~~10~~	~~316~~	~~14~~	~~35.4~~
trib. Wambabya (LAB)	GPS 59	~~2~~	~~0.151~~	~~0.003~~	~~0.150~~	~~0.002~~	~~3.096~~	~~0.075~~	~~0.025~~	~~0.001~~	~~2355~~	~~32~~	~~900~~	~~10~~	~~1432~~	~~19~~	~~508~~	~~21~~	~~38.2~~
trib. Wambabya (LAB)	GPS 59	~~3~~	~~0.170~~	~~0.010~~	~~0.232~~	~~0.004~~	~~5.458~~	~~0.392~~	~~0.025~~	~~0.004~~	~~2555~~	~~92~~	~~1347~~	~~21~~	~~1894~~	~~62~~	~~501~~	~~70~~	~~52.7~~
trib. Wambabya (LAB)	GPS 59	~~4~~	~~0.172~~	~~0.003~~	~~0.245~~	~~0.003~~	~~5.502~~	~~0.144~~	~~0.084~~	~~0.003~~	~~2580~~	~~29~~	~~1411~~	~~15~~	~~1901~~	~~22~~	~~1639~~	~~58~~	~~54.7~~
trib. Wambabya (LAB)	GPS 59	~~5~~	~~0.169~~	~~0.006~~	~~0.256~~	~~0.004~~	~~6.056~~	~~0.270~~	~~0.063~~	~~0.005~~	~~2545~~	~~57~~	~~1472~~	~~18~~	~~1984~~	~~39~~	~~1241~~	~~99~~	~~57.8~~
trib. Wambabya (LAB)	GPS 59	~~6~~	~~0.078~~	~~0.002~~	~~0.108~~	~~0.001~~	~~1.137~~	~~0.041~~	~~0.025~~	~~0.001~~	~~1139~~	~~54~~	~~661~~	~~8~~	~~771~~	~~20~~	~~507~~	~~25~~	~~58.0~~
trib. Wambabya (LAB)	GPS 59	~~7~~	~~0.196~~	~~0.006~~	~~0.288~~	~~0.004~~	~~7.471~~	~~0.331~~	~~0.066~~	~~0.005~~	~~2796~~	~~52~~	~~1634~~	~~20~~	~~2170~~	~~40~~	~~1287~~	~~96~~	~~58.4~~
trib. Wambabya (LAB)	GPS 59	~~8~~	~~0.178~~	~~0.003~~	~~0.271~~	~~0.003~~	~~6.436~~	~~0.157~~	~~0.056~~	~~0.002~~	~~2632~~	~~30~~	~~1545~~	~~16~~	~~2037~~	~~22~~	~~1099~~	~~45~~	~~58.7~~
trib. Wambabya (LAB)	GPS 59	~~9~~	~~0.179~~	~~0.004~~	~~0.311~~	~~0.004~~	~~7.670~~	~~0.227~~	~~0.033~~	~~0.002~~	~~2644~~	~~35~~	~~1745~~	~~19~~	~~2193~~	~~27~~	~~654~~	~~31~~	~~66.0~~
trib. Wambabya (LAB)	GPS 59	~~10~~	~~0.124~~	~~0.003~~	~~0.239~~	~~0.003~~	~~4.116~~	~~0.121~~	~~0.073~~	~~0.003~~	~~2008~~	~~37~~	~~1384~~	~~15~~	~~1657~~	~~24~~	~~1430~~	~~62~~	~~68.9~~
trib. Wambabya (LAB)	GPS 59	~~11~~	~~0.112~~	~~0.002~~	~~0.220~~	~~0.003~~	~~3.470~~	~~0.090~~	~~0.061~~	~~0.002~~	~~1839~~	~~33~~	~~1280~~	~~14~~	~~1520~~	~~20~~	~~1193~~	~~43~~	~~69.6~~
trib. Wambabya (LAB)	GPS 59	~~12~~	~~0.148~~	~~0.005~~	~~0.290~~	~~0.004~~	~~5.759~~	~~0.278~~	~~0.050~~	~~0.004~~	~~2327~~	~~58~~	~~1641~~	~~21~~	~~1940~~	~~42~~	~~986~~	~~76~~	~~70.5~~
trib. Wambabya (LAB)	GPS 59	~~13~~	~~0.171~~	~~0.003~~	~~0.325~~	~~0.004~~	~~7.625~~	~~0.150~~	~~0.062~~	~~0.002~~	~~2571~~	~~24~~	~~1815~~	~~18~~	~~2188~~	~~18~~	~~1219~~	~~36~~	~~70.6~~
trib. Wambabya (LAB)	GPS 59	~~14~~	~~0.089~~	~~0.002~~	~~0.174~~	~~0.002~~	~~2.100~~	~~0.078~~	~~0.055~~	~~0.002~~	~~1411~~	~~47~~	~~1034~~	~~12~~	~~1149~~	~~25~~	~~1080~~	~~38~~	~~73.2~~
trib. Wambabya (LAB)	GPS 59	~~15~~	~~0.094~~	~~0.003~~	~~0.195~~	~~0.003~~	~~2.595~~	~~0.110~~	~~0.059~~	~~0.004~~	~~1510~~	~~55~~	~~1147~~	~~14~~	~~1299~~	~~31~~	~~1149~~	~~68~~	~~76.0~~
trib. Wambabya (LAB)	GPS 59	~~16~~	~~0.081~~	~~0.005~~	~~0.160~~	~~0.003~~	~~1.744~~	~~0.139~~	~~0.041~~	~~0.005~~	~~1225~~	~~111~~	~~957~~	~~17~~	~~1025~~	~~51~~	~~819~~	~~98~~	~~78.1~~
trib. Wambabya (LAB)	GPS 59	~~17~~	~~0.195~~	~~0.010~~	~~0.415~~	~~0.007~~	~~11.442~~	~~0.772~~	~~0.088~~	~~0.012~~	~~2785~~	~~85~~	~~2237~~	~~32~~	~~2560~~	~~63~~	~~1712~~	~~217~~	~~80.3~~
trib. Wambabya (LAB)	GPS 59	~~18~~	~~0.075~~	~~0.002~~	~~0.147~~	~~0.002~~	~~1.568~~	~~0.057~~	~~0.036~~	~~0.002~~	~~1069~~	~~54~~	~~885~~	~~11~~	~~958~~	~~22~~	~~710~~	~~40~~	~~82.7~~
trib. Wambabya (LAB)	GPS 59	~~19~~	~~0.167~~	~~0.008~~	~~0.389~~	~~0.006~~	~~8.809~~	~~0.528~~	~~0.084~~	~~0.010~~	~~2528~~	~~77~~	~~2118~~	~~29~~	~~2318~~	~~55~~	~~1634~~	~~179~~	~~83.8~~
trib. Wambabya (LAB)	GPS 59	~~20~~	~~0.154~~	~~0.008~~	~~0.382~~	~~0.007~~	~~7.668~~	~~0.578~~	~~0.109~~	~~0.014~~	~~2395~~	~~88~~	~~2087~~	~~31~~	~~2193~~	~~68~~	~~2085~~	~~251~~	~~87.1~~
trib. Wambabya (LAB)	GPS 59	~~21~~	~~0.064~~	~~0.003~~	~~0.141~~	~~0.002~~	~~1.222~~	~~0.073~~	~~0.034~~	~~0.004~~	~~727~~	~~96~~	~~848~~	~~13~~	~~811~~	~~33~~	~~673~~	~~73~~	~~116.7~~
trib. Wambabya (LAB)	GPS 59	~~22~~	~~0.625~~	~~0.020~~	~~1.573~~	~~0.047~~	~~395.063~~	~~743.428~~	~~7.349~~	~~0.460~~	~~4568~~	~~46~~	~~6093~~	~~118~~	~~6074~~	~~1906~~	-	~~1114~~	~~133.4~~
trib. Wambabya (LAB)	GPS 59	23	0.069	0.003	0.158	0.003	1.354	0.093	0.040	0.002	906	99	944	14	869	40	793	37	104.3
trib. Wambabya (LAB)	GPS 59	24	0.072	0.004	0.173	0.003	1.737	0.119	0.043	0.006	992	106	1028	16	1022	44	857	109	103.7
trib. Wambabya (LAB)	GPS 59	25	0.072	0.002	0.186	0.003	1.900	0.083	0.046	0.003	993	66	1097	14	1081	29	905	66	110.4
trib. Wambabya (LAB)	GPS 59	26	0.072	0.001	0.172	0.002	1.686	0.046	0.048	0.002	996	40	1025	11	1003	17	947	33	102.9
trib. Wambabya (LAB)	GPS 59	27	0.072	0.004	0.166	0.003	1.664	0.121	0.042	0.006	997	114	990	16	995	46	837	118	99.4
trib. Wambabya (LAB)	GPS 59	28	0.073	0.003	0.174	0.003	1.863	0.113	0.047	0.003	1016	82	1034	15	1068	40	934	65	101.8
trib. Wambabya (LAB)	GPS 59	29	0.074	0.003	0.184	0.003	1.848	0.097	0.046	0.003	1044	73	1088	15	1063	35	911	59	104.2
trib. Wambabya (LAB)	GPS 59	30	0.075	0.003	0.183	0.003	1.917	0.097	0.044	0.004	1059	75	1082	14	1087	34	872	72	102.2

Zircon U-Pb geochronology cont.

			Isotope ratios								Age estimates								
River name	Sample ID	Analysis No.	$^{207}Pb/^{206}Pb$	±1σ	$^{206}Pb/^{238}U$	±1σ	$^{207}Pb/^{235}U$	±1σ	$^{208}Pb/^{232}Th$	±1σ	$^{207}Pb/^{206}Pb$ [Ma]	±1σ [Ma]	$^{206}Pb/^{238}U$ [Ma]	±1σ [Ma]	$^{207}Pb/^{235}U$ [Ma]	±1σ [Ma]	$^{208}Pb/^{232}Th$ [Ma]	±1σ [Ma]	Concordance [%]
trib. Wambabya (LAB)	GPS 59	31	0.077	0.002	0.176	0.002	1.929	0.055	0.039	0.002	1129	41	1045	12	1091	19	774	31	92.6
trib. Wambabya (LAB)	GPS 59	32	0.079	0.002	0.184	0.002	1.997	0.085	0.053	0.003	1166	60	1091	14	1114	29	1036	63	93.6
trib. Wambabya (LAB)	GPS 59	33	0.079	0.003	0.189	0.003	2.132	0.099	0.048	0.003	1183	63	1119	14	1159	32	941	60	94.6
trib. Wambabya (LAB)	GPS 59	34	0.111	0.005	0.340	0.005	5.136	0.300	0.078	0.008	1815	78	1885	25	1842	50	1525	154	103.8
trib. Wambabya (LAB)	GPS 59	35	0.113	0.003	0.339	0.005	5.225	0.214	0.083	0.006	1840	52	1884	22	1857	35	1618	104	102.4
trib. Wambabya (LAB)	GPS 59	36	0.114	0.007	0.349	0.006	5.434	0.422	0.082	0.012	1861	104	1931	31	1890	67	1600	225	103.8
trib. Wambabya (LAB)	GPS 59	37	0.114	0.006	0.329	0.005	5.117	0.321	0.082	0.010	1866	86	1834	26	1839	53	1589	182	98.3
trib. Wambabya (LAB)	GPS 59	38	0.115	0.002	0.338	0.004	5.598	0.185	0.098	0.003	1873	33	1875	20	1916	29	1892	57	100.1
trib. Wambabya (LAB)	GPS 59	39	0.115	0.007	0.303	0.006	4.743	0.376	0.071	0.011	1887	106	1705	28	1775	66	1391	201	90.4
trib. Wambabya (LAB)	GPS 59	40	0.116	0.002	0.346	0.004	5.923	0.187	0.099	0.003	1900	32	1915	20	1965	27	1909	58	100.8
trib. Wambabya (LAB)	GPS 59	41	0.120	0.007	0.351	0.006	5.759	0.413	0.088	0.012	1954	42	1938	29	1940	62	1709	221	99.2
trib. Wambabya (LAB)	GPS 59	42	0.121	0.004	0.351	0.005	6.238	0.314	0.076	0.006	1966	61	1941	24	2010	44	1483	115	98.8
trib. Wambabya (LAB)	GPS 59	43	0.121	0.003	0.376	0.005	6.299	0.246	0.095	0.006	1969	46	2060	23	2018	34	1827	103	104.6
trib. Wambabya (LAB)	GPS 59	44	0.122	0.004	0.378	0.005	6.487	0.312	0.091	0.008	1991	63	2068	25	2044	42	1752	144	103.9
trib. Wambabya (LAB)	GPS 59	45	0.124	0.002	0.384	0.005	6.575	0.164	0.094	0.004	2019	32	2096	21	2056	22	1818	68	103.8
trib. Wambabya (LAB)	GPS 59	46	0.126	0.002	0.365	0.004	6.190	0.197	0.099	0.004	2042	34	2007	21	2003	28	1905	71	98.3
trib. Wambabya (LAB)	GPS 59	47	0.165	0.006	0.471	0.007	10.484	0.545	0.106	0.009	2506	61	2490	30	2479	48	2037	170	99.3
trib. Wambabya (LAB)	GPS 59	48	0.167	0.003	0.462	0.005	10.591	0.233	0.132	0.004	2529	25	2450	24	2488	20	2514	76	96.8
trib. Wambabya (LAB)	GPS 59	49	0.170	0.005	0.491	0.006	11.645	0.456	0.122	0.008	2558	47	2577	28	2576	37	2329	150	100.7
trib. Wambabya (LAB)	GPS 59	50	0.172	0.005	0.485	0.006	11.454	0.482	0.114	0.008	2576	50	2549	28	2561	39	2177	149	98.9
trib. Wambabya (LAB)	GPS 59	51	0.173	0.008	0.503	0.008	12.040	0.706	0.112	0.012	2589	72	2626	33	2608	55	2139	217	101.4
trib. Wambabya (LAB)	GPS 59	52	0.177	0.010	0.528	0.009	12.590	0.905	0.108	0.015	2623	90	2732	39	2650	68	2067	271	104.2
trib. Wambabya (LAB)	GPS 59	53	0.177	0.011	0.474	0.009	11.555	0.914	0.090	0.014	2629	99	2501	39	2569	74	1734	254	95.1
trib. Wambabya (LAB)	GPS 59	54	0.182	0.008	0.472	0.007	11.874	0.693	0.097	0.010	2670	69	2492	32	2595	55	1872	184	93.3
trib. Wambabya (LAB)	GPS 59	55	0.182	0.010	0.509	0.009	12.428	1.040	0.093	0.012	2672	85	2651	39	2637	79	1798	215	99.2
trib. Wambabya (LAB)	GPS 59	56	0.182	0.003	0.514	0.006	13.624	0.345	0.131	0.004	2674	26	2673	26	2724	24	2494	77	100.0
trib. Wambabya (LAB)	GPS 59	57	0.185	0.005	0.511	0.007	13.558	0.530	0.129	0.007	2702	40	2663	28	2719	37	2460	131	98.6
trib. Wambabya (LAB)	GPS 59	58	0.186	0.009	0.464	0.008	11.925	0.837	0.090	0.011	2705	79	2457	34	2599	66	1733	195	90.8
trib. Wambabya (LAB)	GPS 59	59	0.203	0.010	0.573	0.009	16.270	1.172	0.128	0.014	2854	75	2920	39	2893	69	2438	258	102.3
trib. Wambabya (LAB)	GPS 59	60	0.210	0.007	0.574	0.008	16.984	0.808	0.124	0.009	2908	50	2923	32	2934	46	2364	164	100.5
trib. Nkusi (LAB)	GPS 64	~~1~~	~~0.220~~	~~0.004~~	~~0.081~~	~~0.001~~	~~2.433~~	~~0.063~~	~~0.020~~	~~0.001~~	~~2978~~	~~32~~	~~503~~	~~6~~	~~1252~~	~~19~~	~~399~~	~~17~~	~~16.9~~
trib. Nkusi (LAB)	GPS 64	~~2~~	~~0.198~~	~~0.005~~	~~0.135~~	~~0.002~~	~~3.718~~	~~0.134~~	~~0.025~~	~~0.002~~	~~2806~~	~~45~~	~~815~~	~~10~~	~~1575~~	~~29~~	~~504~~	~~33~~	~~29.1~~
trib. Nkusi (LAB)	GPS 64	~~3~~	~~0.179~~	~~0.009~~	~~0.130~~	~~0.002~~	~~3.162~~	~~0.210~~	~~0.065~~	~~0.009~~	~~2643~~	~~84~~	~~787~~	~~12~~	~~1448~~	~~51~~	~~1274~~	~~174~~	~~29.8~~
trib. Nkusi (LAB)	GPS 64	~~4~~	~~0.225~~	~~0.009~~	~~0.157~~	~~0.002~~	~~4.512~~	~~0.221~~	~~0.482~~	~~0.048~~	~~3018~~	~~60~~	~~941~~	~~12~~	~~1733~~	~~41~~	~~7958~~	~~653~~	~~31.2~~
trib. Nkusi (LAB)	GPS 64	~~5~~	~~0.151~~	~~0.005~~	~~0.128~~	~~0.002~~	~~2.672~~	~~0.112~~	~~0.027~~	~~0.002~~	~~2362~~	~~55~~	~~778~~	~~10~~	~~1321~~	~~31~~	~~545~~	~~44~~	~~32.9~~
trib. Nkusi (LAB)	GPS 64	~~6~~	~~0.155~~	~~0.003~~	~~0.132~~	~~0.002~~	~~2.744~~	~~0.078~~	~~0.130~~	~~0.006~~	~~2397~~	~~37~~	~~798~~	~~9~~	~~1341~~	~~21~~	~~2478~~	~~114~~	~~33.3~~
trib. Nkusi (LAB)	GPS 64	~~7~~	~~0.167~~	~~0.011~~	~~0.148~~	~~0.003~~	~~3.315~~	~~0.275~~	~~0.400~~	~~0.073~~	~~2523~~	~~106~~	~~892~~	~~16~~	~~1485~~	~~65~~	~~6798~~	~~1060~~	~~35.4~~
trib. Nkusi (LAB)	GPS 64	~~8~~	~~0.187~~	~~0.007~~	~~0.166~~	~~0.002~~	~~4.291~~	~~0.202~~	~~0.043~~	~~0.004~~	~~2717~~	~~58~~	~~988~~	~~13~~	~~1692~~	~~39~~	~~852~~	~~74~~	~~36.4~~
trib. Nkusi (LAB)	GPS 64	~~9~~	~~0.386~~	~~0.009~~	~~0.252~~	~~0.003~~	~~13.416~~	~~0.408~~	~~0.236~~	~~0.013~~	~~3855~~	~~36~~	~~1450~~	~~15~~	~~2709~~	~~29~~	~~4276~~	~~215~~	~~37.6~~
trib. Nkusi (LAB)	GPS 64	~~10~~	~~0.137~~	~~0.007~~	~~0.142~~	~~0.002~~	~~2.691~~	~~0.172~~	~~0.047~~	~~0.006~~	~~2192~~	~~85~~	~~854~~	~~13~~	~~1326~~	~~47~~	~~928~~	~~122~~	~~39.0~~
trib. Nkusi (LAB)	GPS 64	~~11~~	~~0.202~~	~~0.006~~	~~0.216~~	~~0.003~~	~~6.008~~	~~0.242~~	~~0.058~~	~~0.004~~	~~2843~~	~~49~~	~~1261~~	~~15~~	~~1977~~	~~35~~	~~1137~~	~~83~~	~~44.4~~
trib. Nkusi (LAB)	GPS 64	~~12~~	~~0.162~~	~~0.003~~	~~0.189~~	~~0.002~~	~~4.189~~	~~0.099~~	~~0.042~~	~~0.002~~	~~2475~~	~~30~~	~~1118~~	~~12~~	~~1672~~	~~19~~	~~825~~	~~30~~	~~45.2~~
trib. Nkusi (LAB)	GPS 64	~~13~~	~~0.175~~	~~0.006~~	~~0.215~~	~~0.003~~	~~5.121~~	~~0.235~~	~~0.072~~	~~0.006~~	~~2608~~	~~57~~	~~1257~~	~~15~~	~~1840~~	~~39~~	~~1398~~	~~117~~	~~48.2~~
trib. Nkusi (LAB)	GPS 64	~~14~~	~~0.130~~	~~0.002~~	~~0.172~~	~~0.002~~	~~3.062~~	~~0.068~~	~~0.041~~	~~0.001~~	~~2105~~	~~30~~	~~1021~~	~~11~~	~~1423~~	~~17~~	~~804~~	~~27~~	~~48.5~~
trib. Nkusi (LAB)	GPS 64	~~15~~	~~0.063~~	~~0.003~~	~~0.055~~	~~0.001~~	~~0.479~~	~~0.027~~	~~0.024~~	~~0.003~~	~~705~~	~~94~~	~~345~~	~~5~~	~~397~~	~~19~~	~~488~~	~~55~~	~~48.9~~
trib. Nkusi (LAB)	GPS 64	~~16~~	~~0.091~~	~~0.002~~	~~0.120~~	~~0.001~~	~~1.490~~	~~0.039~~	~~0.021~~	~~0.001~~	~~1449~~	~~39~~	~~733~~	~~8~~	~~926~~	~~16~~	~~422~~	~~18~~	~~50.6~~
trib. Nkusi (LAB)	GPS 64	~~17~~	~~0.183~~	~~0.010~~	~~0.241~~	~~0.004~~	~~6.014~~	~~0.435~~	~~0.028~~	~~0.004~~	~~2680~~	~~90~~	~~1394~~	~~21~~	~~1978~~	~~63~~	~~562~~	~~86~~	~~52.0~~
trib. Nkusi (LAB)	GPS 64	~~18~~	~~0.171~~	~~0.010~~	~~0.256~~	~~0.004~~	~~6.034~~	~~0.452~~	~~0.048~~	~~0.008~~	~~2563~~	~~95~~	~~1470~~	~~23~~	~~1981~~	~~65~~	~~949~~	~~150~~	~~57.3~~
trib. Nkusi (LAB)	GPS 64	~~19~~	~~0.156~~	~~0.009~~	~~0.254~~	~~0.004~~	~~5.498~~	~~0.404~~	~~0.074~~	~~0.012~~	~~2418~~	~~94~~	~~1458~~	~~23~~	~~1900~~	~~63~~	~~1448~~	~~221~~	~~60.3~~
trib. Nkusi (LAB)	GPS 64	~~20~~	~~0.145~~	~~0.005~~	~~0.269~~	~~0.003~~	~~5.433~~	~~0.221~~	~~0.146~~	~~0.011~~	~~2287~~	~~53~~	~~1538~~	~~18~~	~~1890~~	~~35~~	~~2761~~	~~199~~	~~67.2~~
trib. Nkusi (LAB)	GPS 64	~~21~~	~~0.173~~	~~0.004~~	~~0.314~~	~~0.004~~	~~7.485~~	~~0.218~~	~~0.031~~	~~0.002~~	~~2590~~	~~37~~	~~1759~~	~~18~~	~~2171~~	~~26~~	~~616~~	~~31~~	~~67.9~~
trib. Nkusi (LAB)	GPS 64	~~22~~	~~0.183~~	~~0.005~~	~~0.358~~	~~0.005~~	~~9.149~~	~~0.356~~	~~0.097~~	~~0.007~~	~~2682~~	~~48~~	~~1973~~	~~21~~	~~2353~~	~~36~~	~~1875~~	~~130~~	~~73.5~~
trib. Nkusi (LAB)	GPS 64	~~23~~	~~0.178~~	~~0.003~~	~~0.370~~	~~0.004~~	~~9.340~~	~~0.316~~	~~0.100~~	~~0.004~~	~~2636~~	~~31~~	~~2030~~	~~21~~	~~2372~~	~~31~~	~~1918~~	~~66~~	~~77.0~~
trib. Nkusi (LAB)	GPS 64	~~24~~	~~0.154~~	~~0.006~~	~~0.330~~	~~0.005~~	~~7.161~~	~~0.347~~	~~0.069~~	~~0.007~~	~~2388~~	~~62~~	~~1840~~	~~22~~	~~2132~~	~~43~~	~~1352~~	~~123~~	~~77.0~~
trib. Nkusi (LAB)	GPS 64	~~25~~	~~0.164~~	~~0.011~~	~~0.353~~	~~0.007~~	~~7.838~~	~~0.665~~	~~0.062~~	~~0.012~~	~~2492~~	~~108~~	~~1949~~	~~32~~	~~2213~~	~~76~~	~~1210~~	~~220~~	~~78.2~~
trib. Nkusi (LAB)	GPS 64	~~26~~	~~0.163~~	~~0.010~~	~~0.354~~	~~0.006~~	~~7.907~~	~~0.617~~	~~0.071~~	~~0.012~~	~~2483~~	~~98~~	~~1952~~	~~30~~	~~2221~~	~~70~~	~~1388~~	~~222~~	~~78.6~~
trib. Nkusi (LAB)	GPS 64	~~27~~	~~0.206~~	~~0.008~~	~~0.427~~	~~0.006~~	~~12.559~~	~~0.695~~	~~0.154~~	~~0.016~~	~~2876~~	~~64~~	~~2293~~	~~28~~	~~2647~~	~~52~~	~~2893~~	~~282~~	~~79.7~~
trib. Nkusi (LAB)	GPS 64	~~28~~	~~0.168~~	~~0.003~~	~~0.369~~	~~0.004~~	~~8.334~~	~~0.235~~	~~0.071~~	~~0.003~~	~~2537~~	~~34~~	~~2025~~	~~20~~	~~2268~~	~~26~~	~~1378~~	~~61~~	~~79.8~~
trib. Nkusi (LAB)	GPS 64	~~29~~	~~0.153~~	~~0.006~~	~~0.352~~	~~0.005~~	~~7.493~~	~~0.389~~	~~0.146~~	~~0.014~~	~~2380~~	~~64~~	~~1945~~	~~24~~	~~2172~~	~~47~~	~~2753~~	~~250~~	~~81.7~~
trib. Nkusi (LAB)	GPS 64	~~30~~	~~0.171~~	~~0.011~~	~~0.387~~	~~0.007~~	~~9.199~~	~~0.748~~	~~0.099~~	~~0.017~~	~~2571~~	~~102~~	~~2110~~	~~33~~	~~2358~~	~~74~~	~~1901~~	~~320~~	~~82.0~~
trib. Nkusi (LAB)	GPS 64	~~31~~	~~0.156~~	~~0.007~~	~~0.372~~	~~0.005~~	~~7.866~~	~~0.428~~	~~0.094~~	~~0.010~~	~~2410~~	~~70~~	~~2037~~	~~25~~	~~2216~~	~~49~~	~~1822~~	~~193~~	~~84.5~~
trib. Nkusi (LAB)	GPS 64	~~32~~	~~0.167~~	~~0.004~~	~~0.402~~	~~0.005~~	~~9.345~~	~~0.301~~	~~0.095~~	~~0.005~~	~~2532~~	~~39~~	~~2176~~	~~22~~	~~2372~~	~~30~~	~~1832~~	~~95~~	~~86.0~~
trib. Nkusi (LAB)	GPS 64	~~33~~	~~0.158~~	~~0.011~~	~~0.383~~	~~0.007~~	~~8.419~~	~~0.727~~	~~0.089~~	~~0.017~~	~~2431~~	~~110~~	~~2090~~	~~35~~	~~2277~~	~~78~~	~~1718~~	~~315~~	~~86.0~~
trib. Nkusi (LAB)	GPS 64	~~34~~	~~0.167~~	~~0.003~~	~~0.408~~	~~0.005~~	~~9.417~~	~~0.220~~	~~0.067~~	~~0.002~~	~~2525~~	~~27~~	~~2204~~	~~21~~	~~2380~~	~~21~~	~~1308~~	~~39~~	~~87.3~~
trib. Nkusi (LAB)	GPS 64	35	0.161	0.003	0.426	0.005	9.637	0.254	0.090	0.003	2470	29	2289	22	2401	24	1751	58	92.7
trib. Nkusi (LAB)	GPS 64	36	0.162	0.003	0.472	0.005	10.436	0.262	0.099	0.003	2479	28	2492	23	2474	23	1914	60	100.5
trib. Nkusi (LAB)	GPS 64	37	0.164	0.003	0.460	0.005	10.923	0.256	0.086	0.003	2493	27	2439	23	2517	22	1673	51	97.9
trib. Nkusi (LAB)	GPS 64	38	0.164	0.007	0.445	0.006	10.017	0.553	0.112	0.012	2499	68	2371	29	2436	51	2143	219	94.9
trib. Nkusi (LAB)	GPS 64	39	0.166	0.010	0.498	0.009	10.905	0.888	0.117	0.020	2515	101	2605	39	2515	76	2244	366	103.6
trib. Nkusi (LAB)	GPS 64	40	0.167	0.004	0.428	0.005	9.670	0.305	0.107	0.006	2523	38	2297	23	2404	29	2057	102	91.0
trib. Nkusi (LAB)	GPS 64	41	0.168	0.005	0.493	0.006	11.184	0.462	0.112	0.009	2533	52	2584	27	2539	39	2144	161	102.0
trib. Nkusi (LAB)	GPS 64	42	0.168	0.004	0.448	0.005	10.150	0.303	0.091	0.004	2534	35	2388	23	2449	28	1768	80	94.2
trib. Nkusi (LAB)	GPS 64	43	0.168	0.012	0.488	0.010	11.296	1.006	0.112	0.022	2536	111	2563	42	2548	83	2139	397	101.1
trib. Nkusi (LAB)	GPS 64	44	0.168	0.011	0.443	0.008	10.514	0.864	0.112	0.020	2536	104	2365	37	2481	76	2137	365	93.3
trib. Nkusi (LAB)	GPS 64	45	0.169	0.003	0.491	0.006	11.836	0.337	0.104	0.004	2543	31	2573	24	2592	27	2003	73	101.2

			Isotope ratios								Age estimates								
River name	Sample ID	Analysis No.	$^{207}Pb/^{206}Pb$	±1σ	$^{206}Pb/^{238}U$	±1σ	$^{207}Pb/^{235}U$	±1σ	$^{208}Pb/^{232}Th$	±1σ	$^{207}Pb/^{206}Pb$ [Ma]	±1σ [Ma]	$^{206}Pb/^{238}U$ [Ma]	±1σ [Ma]	$^{207}Pb/^{235}U$ [Ma]	±1σ [Ma]	$^{208}Pb/^{232}Th$ [Ma]	±1σ [Ma]	Concordance [%]
trib. Nkusi (LAB)	GPS 64	46	0.169	0.012	0.474	0.010	11.125	1.007	0.127	0.025	2543	113	2500	42	2534	84	2421	455	98.3
trib. Nkusi (LAB)	GPS 64	47	0.169	0.009	0.475	0.008	10.960	0.735	0.094	0.013	2545	83	2504	34	2520	62	1824	241	98.4
trib. Nkusi (LAB)	GPS 64	48	0.169	0.005	0.486	0.006	11.130	0.430	0.100	0.007	2551	47	2553	26	2534	36	1928	125	100.1
trib. Nkusi (LAB)	GPS 64	49	0.170	0.006	0.485	0.007	11.939	0.715	0.116	0.011	2555	61	2550	30	2600	56	2226	193	99.8
trib. Nkusi (LAB)	GPS 64	50	0.170	0.009	0.506	0.009	12.309	0.913	0.113	0.017	2558	89	2641	37	2628	70	2165	304	103.2
trib. Nkusi (LAB)	GPS 64	51	0.171	0.007	0.451	0.006	10.930	0.598	0.086	0.009	2567	65	2399	29	2517	51	1666	163	93.5
trib. Nkusi (LAB)	GPS 64	52	0.172	0.010	0.436	0.007	10.669	0.763	0.104	0.016	2578	89	2331	33	2495	66	2003	288	90.4
trib. Nkusi (LAB)	GPS 64	53	0.172	0.009	0.490	0.008	11.620	0.798	0.112	0.016	2579	86	2570	35	2574	64	2153	295	99.7
trib. Nkusi (LAB)	GPS 64	54	0.173	0.012	0.434	0.009	10.337	0.941	0.026	0.005	2586	114	2323	39	2466	84	525	105	89.8
trib. Nkusi (LAB)	GPS 64	55	0.174	0.005	0.451	0.006	10.644	0.427	0.106	0.007	2592	48	2399	25	2493	37	2032	136	92.5
trib. Nkusi (LAB)	GPS 64	56	0.174	0.005	0.502	0.006	11.717	0.456	0.130	0.009	2594	46	2624	27	2582	36	2465	157	101.2
trib. Nkusi (LAB)	GPS 64	57	0.175	0.003	0.469	0.005	11.279	0.354	0.097	0.003	2603	29	2479	24	2547	29	1878	56	95.2
trib. Nkusi (LAB)	GPS 64	58	0.176	0.011	0.438	0.008	10.661	0.840	0.125	0.021	2616	98	2343	35	2494	73	2377	378	89.6
trib. Nkusi (LAB)	GPS 64	59	0.179	0.004	0.524	0.006	12.921	0.455	0.138	0.006	2639	33	2714	26	2674	33	2618	100	102.8
trib. Nkusi (LAB)	GPS 64	60	0.181	0.004	0.546	0.007	13.667	0.533	0.111	0.005	2666	34	2810	27	2727	37	2120	84	105.4
trib. Nkusi 2 (LAB)	GPS 65	1	~~0.168~~	~~0.011~~	~~0.108~~	~~0.002~~	~~2.423~~	~~0.207~~	~~0.014~~	~~0.003~~	~~2542~~	~~109~~	~~660~~	~~12~~	~~1250~~	~~62~~	~~289~~	~~53~~	~~26.0~~
trib. Nkusi 2 (LAB)	GPS 65	2	~~0.188~~	~~0.003~~	~~0.235~~	~~0.003~~	~~6.004~~	~~0.150~~	~~0.032~~	~~0.001~~	~~2721~~	~~29~~	~~1360~~	~~14~~	~~1977~~	~~22~~	~~630~~	~~22~~	~~50.0~~
trib. Nkusi 2 (LAB)	GPS 65	3	~~0.129~~	~~0.004~~	~~0.180~~	~~0.002~~	~~3.145~~	~~0.137~~	~~0.093~~	~~0.008~~	~~2090~~	~~58~~	~~1067~~	~~13~~	~~1444~~	~~34~~	~~1800~~	~~145~~	~~51.1~~
trib. Nkusi 2 (LAB)	GPS 65	4	~~0.210~~	~~0.008~~	~~0.385~~	~~0.006~~	~~10.937~~	~~0.570~~	~~0.221~~	~~0.022~~	~~2908~~	~~63~~	~~2100~~	~~26~~	~~2518~~	~~48~~	~~4043~~	~~366~~	~~72.2~~
trib. Nkusi 2 (LAB)	GPS 65	5	~~0.196~~	~~0.013~~	~~0.410~~	~~0.008~~	~~11.076~~	~~0.945~~	~~0.092~~	~~0.017~~	~~2792~~	~~105~~	~~2214~~	~~36~~	~~2530~~	~~79~~	~~1785~~	~~309~~	~~79.3~~
trib. Nkusi 2 (LAB)	GPS 65	6	~~0.107~~	~~0.002~~	~~0.255~~	~~0.003~~	~~3.702~~	~~0.082~~	~~0.041~~	~~0.002~~	~~1753~~	~~32~~	~~1462~~	~~15~~	~~1572~~	~~18~~	~~820~~	~~30~~	~~83.4~~
trib. Nkusi 2 (LAB)	GPS 65	7	~~0.100~~	~~0.002~~	~~0.235~~	~~0.003~~	~~3.168~~	~~0.092~~	~~0.040~~	~~0.002~~	~~1621~~	~~42~~	~~1359~~	~~15~~	~~1449~~	~~22~~	~~799~~	~~42~~	~~83.8~~
trib. Nkusi 2 (LAB)	GPS 65	8	~~0.138~~	~~0.002~~	~~0.331~~	~~0.004~~	~~6.254~~	~~0.138~~	~~0.089~~	~~0.003~~	~~2199~~	~~29~~	~~1845~~	~~18~~	~~2012~~	~~19~~	~~1715~~	~~57~~	~~83.9~~
trib. Nkusi 2 (LAB)	GPS 65	9	~~0.104~~	~~0.005~~	~~0.248~~	~~0.004~~	~~3.543~~	~~0.220~~	~~0.074~~	~~0.009~~	~~1704~~	~~86~~	~~1430~~	~~20~~	~~1537~~	~~49~~	~~1439~~	~~172~~	~~83.9~~
trib. Nkusi 2 (LAB)	GPS 65	10	~~0.144~~	~~0.005~~	~~0.346~~	~~0.005~~	~~6.912~~	~~0.343~~	~~0.045~~	~~0.004~~	~~2274~~	~~64~~	~~1917~~	~~23~~	~~2100~~	~~44~~	~~882~~	~~82~~	~~84.3~~
trib. Nkusi 2 (LAB)	GPS 65	11	~~0.145~~	~~0.004~~	~~0.350~~	~~0.004~~	~~7.205~~	~~0.262~~	~~0.040~~	~~0.003~~	~~2290~~	~~45~~	~~1937~~	~~21~~	~~2137~~	~~32~~	~~791~~	~~49~~	~~84.6~~
trib. Nkusi 2 (LAB)	GPS 65	12	~~0.142~~	~~0.006~~	~~0.350~~	~~0.005~~	~~7.194~~	~~0.381~~	~~0.066~~	~~0.007~~	~~2246~~	~~68~~	~~1937~~	~~24~~	~~2136~~	~~47~~	~~1295~~	~~129~~	~~86.2~~
trib. Nkusi 2 (LAB)	GPS 65	13	~~0.117~~	~~0.006~~	~~0.299~~	~~0.005~~	~~4.730~~	~~0.334~~	~~0.069~~	~~0.010~~	~~1916~~	~~96~~	~~1685~~	~~25~~	~~1773~~	~~59~~	~~1341~~	~~188~~	~~88.0~~
trib. Nkusi 2 (LAB)	GPS 65	14	~~0.121~~	~~0.003~~	~~0.313~~	~~0.004~~	~~5.130~~	~~0.176~~	~~0.067~~	~~0.004~~	~~1974~~	~~47~~	~~1753~~	~~19~~	~~1841~~	~~29~~	~~1308~~	~~81~~	~~88.8~~
trib. Nkusi 2 (LAB)	GPS 65	15	~~0.644~~	~~0.033~~	~~1.869~~	~~0.031~~	~~164.937~~	~~12.213~~	~~3.080~~	~~0.418~~	~~4610~~	~~73~~	~~6794~~	~~70~~	~~5190~~	~~75~~	-	~~2070~~	~~147.4~~
trib. Nkusi 2 (LAB)	GPS 65	16	0.110	0.002	0.299	0.003	4.335	0.085	0.080	0.003	1797	28	1687	17	1700	16	1560	48	93.9
trib. Nkusi 2 (LAB)	GPS 65	17	0.111	0.004	0.309	0.004	4.860	0.209	0.063	0.005	1817	59	1738	20	1795	36	1226	97	95.7
trib. Nkusi 2 (LAB)	GPS 65	18	0.112	0.005	0.309	0.005	4.637	0.278	0.068	0.008	1832	83	1736	24	1756	50	1333	156	94.8
trib. Nkusi 2 (LAB)	GPS 65	19	0.114	0.002	0.300	0.004	4.620	0.124	0.066	0.003	1866	38	1693	17	1753	22	1297	62	90.7
trib. Nkusi 2 (LAB)	GPS 65	20	0.122	0.006	0.343	0.006	5.630	0.368	0.077	0.010	1986	87	1900	27	1921	56	1496	187	95.7
trib. Nkusi 2 (LAB)	GPS 65	21	0.123	0.003	0.346	0.004	5.909	0.179	0.082	0.004	1995	40	1913	20	1963	26	1587	80	95.9
trib. Nkusi 2 (LAB)	GPS 65	22	0.123	0.004	0.343	0.005	5.658	0.262	0.083	0.008	2003	63	1903	23	1925	40	1616	141	95.0
trib. Nkusi 2 (LAB)	GPS 65	23	0.123	0.007	0.334	0.006	5.609	0.433	0.066	0.011	2004	104	1859	29	1918	66	1296	204	92.7
trib. Nkusi 2 (LAB)	GPS 65	24	0.123	0.008	0.352	0.007	6.037	0.495	0.080	0.014	2006	110	1945	32	1981	71	1564	261	96.9
trib. Nkusi 2 (LAB)	GPS 65	25	0.124	0.007	0.358	0.006	6.386	0.479	0.088	0.013	2008	97	1973	30	2030	66	1698	242	98.3
trib. Nkusi 2 (LAB)	GPS 65	26	0.124	0.004	0.342	0.004	5.734	0.212	0.058	0.004	2013	50	1894	21	1937	32	1138	77	94.1
trib. Nkusi 2 (LAB)	GPS 65	27	0.124	0.003	0.381	0.004	6.442	0.172	0.087	0.004	2019	36	2080	21	2038	24	1679	77	103.0
trib. Nkusi 2 (LAB)	GPS 65	28	0.127	0.004	0.371	0.005	6.680	0.279	0.105	0.008	2051	56	2034	23	2070	37	2012	152	99.2
trib. Nkusi 2 (LAB)	GPS 65	29	0.128	0.008	0.365	0.007	6.649	0.556	0.063	0.011	2065	111	2006	33	2066	74	1227	211	97.1
trib. Nkusi 2 (LAB)	GPS 65	30	0.128	0.008	0.366	0.007	6.637	0.529	0.094	0.016	2070	105	2012	32	2064	70	1808	287	97.2
trib. Nkusi 2 (LAB)	GPS 65	31	0.128	0.004	0.376	0.005	6.671	0.297	0.092	0.008	2075	60	2057	24	2069	39	1784	147	99.1
trib. Nkusi 2 (LAB)	GPS 65	32	0.128	0.005	0.376	0.005	6.727	0.334	0.099	0.009	2077	64	2059	25	2076	44	1899	168	99.2
trib. Nkusi 2 (LAB)	GPS 65	33	0.129	0.007	0.398	0.007	7.026	0.491	0.117	0.017	2083	92	2161	31	2115	62	2237	301	103.8
trib. Nkusi 2 (LAB)	GPS 65	34	0.129	0.002	0.382	0.004	7.029	0.186	0.085	0.003	2086	32	2084	21	2115	24	1649	63	99.9
trib. Nkusi 2 (LAB)	GPS 65	35	0.129	0.002	0.398	0.005	6.932	0.174	0.093	0.004	2091	33	2159	21	2103	22	1790	72	103.3
trib. Nkusi 2 (LAB)	GPS 65	36	0.131	0.005	0.389	0.006	7.247	0.374	0.099	0.010	2105	67	2117	26	2142	46	1902	177	100.6
trib. Nkusi 2 (LAB)	GPS 65	37	0.131	0.004	0.374	0.005	6.887	0.304	0.106	0.008	2110	53	2046	23	2097	39	2035	143	97.0
trib. Nkusi 2 (LAB)	GPS 65	38	0.131	0.002	0.419	0.005	7.924	0.189	0.095	0.003	2110	29	2255	22	2222	21	1829	61	106.9
trib. Nkusi 2 (LAB)	GPS 65	39	0.131	0.003	0.409	0.005	7.654	0.232	0.105	0.005	2110	36	2209	22	2191	27	2015	90	104.7
trib. Nkusi 2 (LAB)	GPS 65	40	0.132	0.008	0.372	0.007	6.861	0.525	0.090	0.014	2121	101	2041	31	2094	68	1744	265	96.2
trib. Nkusi 2 (LAB)	GPS 65	41	0.132	0.003	0.400	0.005	7.425	0.251	0.112	0.005	2123	35	2169	22	2164	30	2144	86	102.2
trib. Nkusi 2 (LAB)	GPS 65	42	0.132	0.004	0.349	0.005	6.632	0.283	0.089	0.007	2128	55	1932	22	2064	38	1728	129	90.8
trib. Nkusi 2 (LAB)	GPS 65	43	0.133	0.002	0.368	0.004	6.456	0.142	0.094	0.003	2139	28	2020	20	2040	19	1807	55	94.5
trib. Nkusi 2 (LAB)	GPS 65	44	0.133	0.003	0.401	0.005	7.485	0.204	0.104	0.005	2140	34	2173	22	2171	24	1999	83	101.5
trib. Nkusi 2 (LAB)	GPS 65	45	0.134	0.003	0.399	0.005	7.221	0.231	0.099	0.005	2153	39	2163	22	2139	29	1912	93	100.5
trib. Nkusi 2 (LAB)	GPS 65	46	0.135	0.007	0.384	0.006	7.554	0.520	0.096	0.013	2162	90	2094	30	2179	62	1861	247	96.8
trib. Nkusi 2 (LAB)	GPS 65	47	0.136	0.004	0.380	0.005	7.417	0.311	0.068	0.005	2174	53	2074	23	2163	37	1334	98	95.4
trib. Nkusi 2 (LAB)	GPS 65	48	0.136	0.003	0.401	0.005	7.642	0.224	0.107	0.005	2177	35	2176	22	2190	26	2058	89	99.9
trib. Nkusi 2 (LAB)	GPS 65	49	0.136	0.008	0.419	0.007	7.971	0.593	0.108	0.016	2178	97	2258	33	2228	67	2068	299	103.7
trib. Nkusi 2 (LAB)	GPS 65	50	0.136	0.003	0.372	0.004	7.155	0.219	0.105	0.004	2179	32	2037	21	2131	27	2022	72	93.5
trib. Nkusi 2 (LAB)	GPS 65	51	0.136	0.007	0.404	0.006	7.424	0.475	0.102	0.013	2179	83	2189	30	2164	57	1960	237	100.4
trib. Nkusi 2 (LAB)	GPS 65	52	0.137	0.004	0.380	0.005	7.199	0.284	0.090	0.006	2188	50	2078	23	2136	35	1744	120	95.0
trib. Nkusi 2 (LAB)	GPS 65	53	0.137	0.002	0.376	0.004	7.103	0.196	0.114	0.004	2192	30	2059	20	2124	25	2188	69	93.9
trib. Nkusi 2 (LAB)	GPS 65	54	0.144	0.005	0.374	0.005	7.486	0.359	0.099	0.009	2272	60	2050	24	2171	43	1913	161	90.2
trib. Nkusi 2 (LAB)	GPS 65	55	0.151	0.009	0.446	0.008	9.120	0.741	0.100	0.017	2354	104	2377	37	2350	74	1928	312	101.0
trib. Nkusi 2 (LAB)	GPS 65	56	0.154	0.008	0.436	0.007	9.402	0.635	0.101	0.013	2386	85	2335	32	2378	62	1951	247	97.9
trib. Nkusi 2 (LAB)	GPS 65	57	0.157	0.009	0.407	0.007	9.154	0.710	0.098	0.015	2420	96	2202	33	2354	71	1896	281	91.0
trib. Nkusi 2 (LAB)	GPS 65	58	0.164	0.003	0.437	0.005	9.461	0.221	0.107	0.004	2496	29	2335	22	2384	21	2056	76	93.6
trib. Nkusi 2 (LAB)	GPS 65	59	0.174	0.005	0.502	0.006	11.717	0.456	0.130	0.009	2594	46	2624	27	2582	36	2465	157	101.2
trib. Nkusi 2 (LAB)	GPS 65	60	0.179	0.005	0.466	0.006	11.372	0.491	0.120	0.008	2641	46	2466	27	2554	40	2298	144	93.4

Zircon U-Pb geochronology cont.

			Isotope ratios									Age estimates								
River name	Sample ID	Analysis No.	$^{207}Pb/^{206}Pb$	±1σ	$^{206}Pb/^{238}U$	±1σ	$^{207}Pb/^{235}U$	±1σ	$^{208}Pb/^{232}Th$	±1σ	$^{207}Pb/^{206}Pb$ [Ma]	±1σ [Ma]	$^{206}Pb/^{238}U$ [Ma]	±1σ [Ma]	$^{207}Pb/^{235}U$ [Ma]	±1σ [Ma]	$^{208}Pb/^{232}Th$ [Ma]	±1σ [Ma]	Concordance [%]
Muzizi (LAB)	GPS 66	~~1~~	~~0.136~~	~~0.004~~	~~0.156~~	~~0.002~~	~~2.741~~	~~0.103~~	~~0.843~~	~~0.085~~	~~2180~~	~~51~~	~~934~~	~~11~~	~~1340~~	~~28~~	-	~~928~~	~~42.8~~
Muzizi (LAB)	GPS 66	~~2~~	~~0.147~~	~~0.003~~	~~0.202~~	~~0.002~~	~~4.040~~	~~0.110~~	~~0.038~~	~~0.003~~	~~2307~~	~~36~~	~~1187~~	~~13~~	~~1642~~	~~22~~	~~760~~	~~50~~	~~51.4~~
Muzizi (LAB)	GPS 66	~~3~~	~~0.119~~	~~0.007~~	~~0.169~~	~~0.003~~	~~2.756~~	~~0.198~~	~~0.018~~	~~0.003~~	~~1937~~	~~98~~	~~1008~~	~~16~~	~~1344~~	~~54~~	~~352~~	~~54~~	~~52.1~~
Muzizi (LAB)	GPS 66	~~4~~	~~0.151~~	~~0.003~~	~~0.231~~	~~0.003~~	~~4.907~~	~~0.146~~	~~0.019~~	~~0.001~~	~~2361~~	~~39~~	~~1342~~	~~14~~	~~1804~~	~~25~~	~~377~~	~~27~~	~~56.8~~
Muzizi (LAB)	GPS 66	~~5~~	~~0.152~~	~~0.009~~	~~0.246~~	~~0.004~~	~~5.144~~	~~0.379~~	~~0.036~~	~~0.006~~	~~2364~~	~~96~~	~~1419~~	~~22~~	~~1843~~	~~63~~	~~717~~	~~111~~	~~60.0~~
Muzizi (LAB)	GPS 66	~~6~~	~~0.146~~	~~0.003~~	~~0.248~~	~~0.003~~	~~4.925~~	~~0.122~~	~~0.062~~	~~0.003~~	~~2302~~	~~30~~	~~1427~~	~~15~~	~~1807~~	~~21~~	~~1212~~	~~54~~	~~62.0~~
Muzizi (LAB)	GPS 66	~~7~~	~~0.144~~	~~0.003~~	~~0.268~~	~~0.003~~	~~5.343~~	~~0.148~~	~~0.037~~	~~0.002~~	~~2272~~	~~34~~	~~1529~~	~~16~~	~~1876~~	~~24~~	~~742~~	~~44~~	~~67.3~~
Muzizi (LAB)	GPS 66	~~8~~	~~0.152~~	~~0.009~~	~~0.289~~	~~0.005~~	~~5.989~~	~~0.459~~	~~0.056~~	~~0.009~~	~~2369~~	~~100~~	~~1636~~	~~26~~	~~1974~~	~~67~~	~~1108~~	~~173~~	~~69.0~~
Muzizi (LAB)	GPS 66	~~9~~	~~0.139~~	~~0.009~~	~~0.268~~	~~0.005~~	~~4.994~~	~~0.424~~	~~0.047~~	~~0.008~~	~~2217~~	~~112~~	~~1533~~	~~26~~	~~1818~~	~~72~~	~~930~~	~~151~~	~~69.2~~
Muzizi (LAB)	GPS 66	~~10~~	~~0.116~~	~~0.005~~	~~0.228~~	~~0.004~~	~~3.413~~	~~0.213~~	~~0.081~~	~~0.011~~	~~1896~~	~~79~~	~~1324~~	~~18~~	~~1507~~	~~49~~	~~1570~~	~~202~~	~~69.8~~
Muzizi (LAB)	GPS 66	~~11~~	~~0.098~~	~~0.002~~	~~0.191~~	~~0.002~~	~~2.538~~	~~0.071~~	~~0.056~~	~~0.004~~	~~1583~~	~~40~~	~~1126~~	~~12~~	~~1283~~	~~20~~	~~1094~~	~~73~~	~~71.1~~
Muzizi (LAB)	GPS 66	~~12~~	~~0.162~~	~~0.003~~	~~0.321~~	~~0.004~~	~~7.111~~	~~0.179~~	~~0.061~~	~~0.003~~	~~2472~~	~~32~~	~~1794~~	~~18~~	~~2125~~	~~22~~	~~1203~~	~~65~~	~~72.6~~
Muzizi (LAB)	GPS 66	~~13~~	~~0.153~~	~~0.005~~	~~0.309~~	~~0.004~~	~~6.448~~	~~0.259~~	~~0.083~~	~~0.009~~	~~2379~~	~~52~~	~~1734~~	~~20~~	~~2039~~	~~35~~	~~1613~~	~~163~~	~~72.9~~
Muzizi (LAB)	GPS 66	~~14~~	~~0.150~~	~~0.011~~	~~0.304~~	~~0.006~~	~~6.253~~	~~0.559~~	~~0.066~~	~~0.011~~	~~2341~~	~~117~~	~~1710~~	~~30~~	~~2012~~	~~78~~	~~1293~~	~~211~~	~~73.0~~
Muzizi (LAB)	GPS 66	~~15~~	~~0.255~~	~~0.004~~	~~0.454~~	~~0.005~~	~~15.563~~	~~0.375~~	~~0.014~~	~~0.001~~	~~3213~~	~~28~~	~~2415~~	~~23~~	~~2850~~	~~23~~	~~272~~	~~14~~	~~75.2~~
Muzizi (LAB)	GPS 66	~~16~~	~~0.163~~	~~0.010~~	~~0.350~~	~~0.006~~	~~7.542~~	~~0.590~~	~~0.045~~	~~0.007~~	~~2487~~	~~100~~	~~1934~~	~~30~~	~~2178~~	~~70~~	~~893~~	~~141~~	~~77.8~~
Muzizi (LAB)	GPS 66	~~17~~	~~0.114~~	~~0.004~~	~~0.264~~	~~0.004~~	~~4.106~~	~~0.194~~	~~0.078~~	~~0.009~~	~~1859~~	~~66~~	~~1509~~	~~18~~	~~1656~~	~~39~~	~~1518~~	~~177~~	~~81.2~~
Muzizi (LAB)	GPS 66	~~18~~	~~0.164~~	~~0.006~~	~~0.393~~	~~0.005~~	~~8.881~~	~~0.405~~	~~0.070~~	~~0.008~~	~~2493~~	~~58~~	~~2138~~	~~24~~	~~2326~~	~~42~~	~~1374~~	~~155~~	~~85.7~~
Muzizi (LAB)	GPS 66	~~19~~	~~0.148~~	~~0.005~~	~~0.373~~	~~0.005~~	~~7.478~~	~~0.331~~	~~0.080~~	~~0.009~~	~~2319~~	~~57~~	~~2045~~	~~23~~	~~2170~~	~~40~~	~~1562~~	~~169~~	~~88.2~~
Muzizi (LAB)	GPS 66	~~20~~	~~0.165~~	~~0.007~~	~~0.411~~	~~0.006~~	~~9.052~~	~~0.472~~	~~0.087~~	~~0.011~~	~~2507~~	~~65~~	~~2218~~	~~27~~	~~2343~~	~~48~~	~~1686~~	~~207~~	~~88.5~~
Muzizi (LAB)	GPS 66	~~21~~	~~0.160~~	~~0.003~~	~~0.402~~	~~0.005~~	~~8.720~~	~~0.230~~	~~0.137~~	~~0.008~~	~~2458~~	~~32~~	~~2177~~	~~21~~	~~2309~~	~~24~~	~~2602~~	~~141~~	~~88.5~~
Muzizi (LAB)	GPS 66	~~22~~	~~0.169~~	~~0.006~~	~~0.419~~	~~0.006~~	~~9.741~~	~~0.484~~	~~0.054~~	~~0.007~~	~~2543~~	~~62~~	~~2258~~	~~26~~	~~2411~~	~~46~~	~~1069~~	~~128~~	~~88.8~~
Muzizi (LAB)	GPS 66	~~23~~	~~0.068~~	~~0.005~~	~~0.128~~	~~0.002~~	~~1.168~~	~~0.109~~	~~0.030~~	~~0.005~~	~~875~~	~~139~~	~~778~~	~~14~~	~~786~~	~~51~~	~~595~~	~~91~~	~~88.9~~
Muzizi (LAB)	GPS 66	~~24~~	~~0.131~~	~~0.002~~	~~0.340~~	~~0.004~~	~~6.241~~	~~0.151~~	~~0.076~~	~~0.003~~	~~2109~~	~~30~~	~~1885~~	~~19~~	~~2010~~	~~21~~	~~1478~~	~~64~~	~~89.4~~
Muzizi (LAB)	GPS 66	25	0.108	0.007	0.317	0.006	5.021	0.450	0.067	0.011	1764	115	1774	30	1823	76	1312	208	100.6
Muzizi (LAB)	GPS 66	26	0.108	0.008	0.327	0.007	4.871	0.450	0.064	0.011	1771	122	1824	32	1797	78	1256	203	103.0
Muzizi (LAB)	GPS 66	27	0.110	0.008	0.340	0.008	4.921	0.546	0.064	0.011	1797	131	1888	36	1806	94	1250	204	105.1
Muzizi (LAB)	GPS 66	28	0.111	0.007	0.331	0.006	4.996	0.379	0.071	0.011	1814	105	1842	28	1819	64	1389	214	101.6
Muzizi (LAB)	GPS 66	29	0.111	0.003	0.334	0.004	5.434	0.262	0.095	0.008	1818	51	1858	21	1890	41	1841	147	102.2
Muzizi (LAB)	GPS 66	30	0.111	0.004	0.336	0.005	5.027	0.254	0.090	0.011	1819	69	1867	23	1824	43	1733	208	102.6
Muzizi (LAB)	GPS 66	31	0.111	0.004	0.333	0.005	4.884	0.300	0.092	0.010	1821	66	1855	23	1799	52	1775	187	101.9
Muzizi (LAB)	GPS 66	32	0.112	0.006	0.316	0.005	4.606	0.347	0.079	0.012	1825	97	1769	27	1750	63	1534	226	96.9
Muzizi (LAB)	GPS 66	33	0.112	0.003	0.336	0.004	5.346	0.243	0.098	0.008	1827	48	1869	21	1876	39	1895	142	102.3
Muzizi (LAB)	GPS 66	34	0.112	0.005	0.335	0.005	4.873	0.293	0.088	0.012	1828	76	1863	24	1798	51	1695	214	101.9
Muzizi (LAB)	GPS 66	35	0.112	0.002	0.338	0.004	5.211	0.203	0.093	0.005	1832	38	1876	20	1854	33	1790	84	102.4
Muzizi (LAB)	GPS 66	36	0.112	0.003	0.338	0.004	5.203	0.223	0.095	0.009	1833	53	1875	21	1853	37	1827	167	102.3
Muzizi (LAB)	GPS 66	37	0.112	0.004	0.338	0.005	5.098	0.262	0.094	0.010	1834	59	1876	22	1836	44	1811	178	102.3
Muzizi (LAB)	GPS 66	38	0.112	0.004	0.333	0.005	4.965	0.272	0.093	0.011	1838	65	1851	23	1813	46	1796	197	100.7
Muzizi (LAB)	GPS 66	39	0.113	0.006	0.326	0.006	5.048	0.369	0.074	0.011	1841	98	1821	27	1827	62	1443	215	98.9
Muzizi (LAB)	GPS 66	40	0.113	0.002	0.333	0.004	5.276	0.191	0.094	0.004	1851	36	1852	19	1865	31	1815	83	100.0
Muzizi (LAB)	GPS 66	41	0.114	0.004	0.332	0.004	4.990	0.251	0.095	0.009	1856	57	1849	22	1818	42	1842	173	99.6
Muzizi (LAB)	GPS 66	42	0.114	0.005	0.327	0.005	4.485	0.319	0.086	0.011	1858	80	1822	25	1728	59	1671	209	98.1
Muzizi (LAB)	GPS 66	43	0.115	0.003	0.338	0.004	5.265	0.166	0.101	0.006	1887	39	1876	19	1863	27	1938	119	99.4
Muzizi (LAB)	GPS 66	44	0.116	0.003	0.335	0.004	5.393	0.296	0.098	0.008	1891	52	1861	21	1884	47	1892	146	98.4
Muzizi (LAB)	GPS 66	45	0.128	0.005	0.333	0.005	5.637	0.264	0.099	0.012	2064	63	1855	22	1922	40	1903	216	89.9
Muzizi (LAB)	GPS 66	46	0.134	0.007	0.387	0.006	7.524	0.496	0.089	0.013	2150	87	2110	29	2176	59	1716	245	98.1
Muzizi (LAB)	GPS 66	47	0.137	0.009	0.432	0.008	7.992	0.645	0.099	0.016	2195	105	2317	36	2230	73	1915	297	105.5
Muzizi (LAB)	GPS 66	48	0.158	0.007	0.413	0.006	8.785	0.483	0.107	0.015	2440	71	2228	28	2316	50	2059	266	91.3
Muzizi (LAB)	GPS 66	49	0.161	0.011	0.462	0.009	10.080	0.846	0.087	0.014	2463	108	2450	39	2442	78	1690	268	99.5
Muzizi (LAB)	GPS 66	50	0.162	0.008	0.427	0.007	9.172	0.609	0.076	0.011	2480	85	2291	31	2355	61	1482	215	92.4
Muzizi (LAB)	GPS 66	51	0.164	0.012	0.448	0.009	9.935	0.907	0.076	0.013	2495	117	2386	40	2429	84	1480	241	95.6
Muzizi (LAB)	GPS 66	52	0.166	0.011	0.484	0.009	10.693	0.880	0.084	0.014	2515	105	2547	39	2497	76	1632	257	101.2
Muzizi (LAB)	GPS 66	53	0.167	0.004	0.450	0.005	10.205	0.318	0.128	0.010	2526	39	2395	24	2454	29	2432	174	94.8
Muzizi (LAB)	GPS 66	54	0.168	0.007	0.467	0.007	10.930	0.652	0.119	0.016	2533	73	2470	31	2517	55	2280	296	97.5
Muzizi (LAB)	GPS 66	55	0.168	0.006	0.435	0.006	9.830	0.484	0.128	0.014	2543	54	2330	26	2419	45	2440	247	91.6
Muzizi (LAB)	GPS 66	56	0.169	0.003	0.445	0.005	10.503	0.270	0.067	0.004	2552	30	2373	23	2480	24	1310	66	93.0
Muzizi (LAB)	GPS 66	57	0.169	0.004	0.491	0.006	11.484	0.354	0.131	0.009	2552	37	2574	25	2563	29	2483	166	100.9
Muzizi (LAB)	GPS 66	58	0.169	0.010	0.452	0.008	10.787	0.953	0.091	0.014	2552	96	2402	37	2505	82	1769	266	94.1
Muzizi (LAB)	GPS 66	59	0.169	0.003	0.485	0.006	11.250	0.316	0.127	0.008	2552	34	2549	25	2544	26	2417	141	99.9
Muzizi (LAB)	GPS 66	60	0.173	0.003	0.460	0.005	10.941	0.281	0.107	0.006	2587	31	2439	23	2518	24	2064	106	94.3
trib. Dura (LGB)	GPS 72	~~1~~	~~0.152~~	~~0.006~~	~~0.145~~	~~0.002~~	~~2.976~~	~~0.145~~	~~0.096~~	~~0.010~~	~~2370~~	~~63~~	~~873~~	~~11~~	~~1402~~	~~37~~	~~1848~~	~~184~~	~~37~~
trib. Dura (LGB)	GPS 72	~~2~~	~~0.132~~	~~0.004~~	~~0.206~~	~~0.003~~	~~3.737~~	~~0.139~~	~~0.019~~	~~0.001~~	~~2130~~	~~49~~	~~1206~~	~~14~~	~~1579~~	~~30~~	~~374~~	~~28~~	~~57~~
trib. Dura (LGB)	GPS 72	~~3~~	~~0.131~~	~~0.002~~	~~0.216~~	~~0.002~~	~~3.833~~	~~0.083~~	~~0.020~~	~~0.001~~	~~2115~~	~~29~~	~~1260~~	~~13~~	~~1600~~	~~17~~	~~392~~	~~13~~	~~60~~
trib. Dura (LGB)	GPS 72	~~4~~	~~0.143~~	~~0.008~~	~~0.256~~	~~0.004~~	~~4.952~~	~~0.375~~	~~0.103~~	~~0.018~~	~~2259~~	~~98~~	~~1467~~	~~23~~	~~1811~~	~~64~~	~~1988~~	~~331~~	~~65~~
trib. Dura (LGB)	GPS 72	~~5~~	~~0.166~~	~~0.011~~	~~0.294~~	~~0.005~~	~~6.499~~	~~0.541~~	~~0.099~~	~~0.019~~	~~2522~~	~~105~~	~~1660~~	~~27~~	~~2046~~	~~73~~	~~1917~~	~~356~~	~~66~~
trib. Dura (LGB)	GPS 72	~~6~~	~~0.166~~	~~0.003~~	~~0.349~~	~~0.004~~	~~8.298~~	~~0.213~~	~~0.031~~	~~0.001~~	~~2518~~	~~29~~	~~1929~~	~~19~~	~~2264~~	~~23~~	~~625~~	~~21~~	~~77~~
trib. Dura (LGB)	GPS 72	~~7~~	~~0.169~~	~~0.007~~	~~0.360~~	~~0.005~~	~~8.441~~	~~0.457~~	~~0.032~~	~~0.004~~	~~2544~~	~~69~~	~~1981~~	~~25~~	~~2280~~	~~49~~	~~643~~	~~76~~	~~78~~
trib. Dura (LGB)	GPS 72	~~8~~	~~0.125~~	~~0.004~~	~~0.279~~	~~0.004~~	~~4.785~~	~~0.220~~	~~0.054~~	~~0.005~~	~~2031~~	~~62~~	~~1589~~	~~19~~	~~1782~~	~~39~~	~~1072~~	~~103~~	~~78~~
trib. Dura (LGB)	GPS 72	~~9~~	~~0.162~~	~~0.008~~	~~0.360~~	~~0.006~~	~~7.759~~	~~0.533~~	~~0.026~~	~~0.004~~	~~2472~~	~~84~~	~~1984~~	~~28~~	~~2204~~	~~62~~	~~524~~	~~77~~	~~80~~
trib. Dura (LGB)	GPS 72	~~10~~	~~0.173~~	~~0.006~~	~~0.390~~	~~0.005~~	~~9.475~~	~~0.410~~	~~0.039~~	~~0.004~~	~~2583~~	~~54~~	~~2124~~	~~24~~	~~2385~~	~~40~~	~~768~~	~~68~~	~~82~~
trib. Dura (LGB)	GPS 72	~~11~~	~~0.133~~	~~0.004~~	~~0.332~~	~~0.004~~	~~6.170~~	~~0.250~~	~~0.063~~	~~0.005~~	~~2143~~	~~51~~	~~1847~~	~~20~~	~~2000~~	~~35~~	~~1235~~	~~93~~	~~86~~
trib. Dura (LGB)	GPS 72	~~12~~	~~0.166~~	~~0.010~~	~~0.405~~	~~0.007~~	~~9.694~~	~~0.725~~	~~0.078~~	~~0.013~~	~~2519~~	~~94~~	~~2192~~	~~32~~	~~2406~~	~~69~~	~~1509~~	~~249~~	~~87~~
trib. Dura (LGB)	GPS 72	~~13~~	~~0.162~~	~~0.003~~	~~0.407~~	~~0.005~~	~~8.794~~	~~0.229~~	~~0.045~~	~~0.002~~	~~2477~~	~~30~~	~~2202~~	~~21~~	~~2317~~	~~24~~	~~883~~	~~33~~	~~89~~
trib. Dura (LGB)	GPS 72	~~14~~	~~0.128~~	~~0.003~~	~~0.331~~	~~0.004~~	~~5.874~~	~~0.176~~	~~0.046~~	~~0.002~~	~~2071~~	~~39~~	~~1842~~	~~19~~	~~1957~~	~~26~~	~~903~~	~~47~~	~~89~~
trib. Dura (LGB)	GPS 72	~~15~~	~~0.165~~	~~0.007~~	~~0.416~~	~~0.006~~	~~9.253~~	~~0.516~~	~~0.049~~	~~0.006~~	~~2506~~	~~70~~	~~2243~~	~~28~~	~~2363~~	~~51~~	~~964~~	~~115~~	~~89~~

River name	Sample ID	Analysis No.	Isotope ratios								Age estimates								Concordance [%]
			$^{207}Pb/^{206}Pb$	±1σ	$^{206}Pb/^{238}U$	±1σ	$^{207}Pb/^{235}U$	±1σ	$^{208}Pb/^{232}Th$	±1σ	$^{207}Pb/^{206}Pb$ [Ma]	±1σ [Ma]	$^{206}Pb/^{238}U$ [Ma]	±1σ [Ma]	$^{207}Pb/^{235}U$ [Ma]	±1σ [Ma]	$^{208}Pb/^{232}Th$ [Ma]	±1σ [Ma]	
trib. Dura (LGB)	GPS 72	16	0.122	0.005	0.353	0.005	5.960	0.302	0.069	0.008	1980	68	1951	24	1970	44	1354	145	99
trib. Dura (LGB)	GPS 72	17	0.124	0.004	0.345	0.004	5.846	0.236	0.037	0.003	2017	53	1913	21	1953	35	725	57	95
trib. Dura (LGB)	GPS 72	18	0.125	0.003	0.350	0.004	5.850	0.214	0.063	0.005	2027	49	1936	21	1954	32	1229	87	96
trib. Dura (LGB)	GPS 72	19	0.126	0.009	0.369	0.007	6.462	0.596	0.107	0.023	2045	119	2025	34	2041	81	2049	411	99
trib. Dura (LGB)	GPS 72	20	0.126	0.003	0.344	0.004	6.045	0.171	0.085	0.004	2046	36	1904	19	1982	25	1654	74	93
trib. Dura (LGB)	GPS 72	21	0.127	0.003	0.346	0.004	5.798	0.173	0.084	0.005	2053	40	1914	19	1946	26	1622	90	93
trib. Dura (LGB)	GPS 72	22	0.127	0.008	0.376	0.007	6.578	0.511	0.095	0.017	2055	102	2057	31	2057	68	1832	313	100
trib. Dura (LGB)	GPS 72	23	0.128	0.009	0.341	0.007	5.851	0.515	0.102	0.021	2075	116	1889	32	1954	76	1966	387	91
trib. Dura (LGB)	GPS 72	24	0.128	0.009	0.373	0.007	6.633	0.569	0.103	0.020	2077	112	2042	33	2064	76	1973	373	98
trib. Dura (LGB)	GPS 72	25	0.129	0.010	0.380	0.008	6.680	0.640	0.096	0.022	2079	125	2077	36	2070	85	1862	397	100
trib. Dura (LGB)	GPS 72	26	0.129	0.005	0.372	0.005	6.573	0.343	0.094	0.011	2081	69	2038	25	2056	46	1824	198	98
trib. Dura (LGB)	GPS 72	27	0.130	0.008	0.367	0.007	6.545	0.536	0.110	0.021	2104	108	2014	32	2052	72	2102	380	96
trib. Dura (LGB)	GPS 72	28	0.131	0.006	0.382	0.006	6.903	0.393	0.079	0.010	2117	75	2085	26	2099	51	1540	186	98
trib. Dura (LGB)	GPS 72	29	0.133	0.002	0.361	0.004	6.448	0.166	0.048	0.002	2133	31	1988	19	2039	23	938	34	93
trib. Dura (LGB)	GPS 72	30	0.133	0.003	0.383	0.005	7.199	0.229	0.081	0.005	2136	41	2091	21	2136	28	1571	90	98
trib. Dura (LGB)	GPS 72	31	0.135	0.005	0.360	0.005	6.869	0.349	0.055	0.006	2165	66	1984	24	2095	45	1077	113	92
trib. Dura (LGB)	GPS 72	32	0.135	0.003	0.404	0.005	7.285	0.280	0.096	0.004	2169	38	2189	22	2147	34	1859	83	101
trib. Dura (LGB)	GPS 72	33	0.138	0.003	0.362	0.004	6.968	0.201	0.065	0.003	2203	37	1993	20	2107	26	1269	64	90
trib. Dura (LGB)	GPS 72	34	0.144	0.005	0.406	0.005	8.036	0.336	0.080	0.007	2270	54	2197	24	2235	38	1552	127	97
trib. Dura (LGB)	GPS 72	35	0.144	0.008	0.388	0.007	7.143	0.521	0.107	0.018	2277	94	2115	31	2129	65	2063	328	93
trib. Dura (LGB)	GPS 72	36	0.149	0.004	0.451	0.006	9.266	0.348	0.117	0.007	2338	43	2398	25	2365	34	2244	131	103
trib. Dura (LGB)	GPS 72	37	0.150	0.005	0.432	0.006	8.880	0.399	0.097	0.009	2350	57	2313	26	2326	41	1878	167	98
trib. Dura (LGB)	GPS 72	38	0.152	0.006	0.398	0.006	8.135	0.450	0.055	0.006	2372	69	2160	27	2246	50	1076	122	91
trib. Dura (LGB)	GPS 72	39	0.157	0.003	0.456	0.005	9.959	0.221	0.095	0.003	2418	27	2423	22	2431	20	1825	57	100
trib. Dura (LGB)	GPS 72	40	0.159	0.009	0.407	0.007	8.871	0.635	0.086	0.014	2441	91	2200	31	2325	65	1677	264	90
trib. Dura (LGB)	GPS 72	41	0.160	0.003	0.456	0.005	10.054	0.263	0.108	0.004	2451	30	2423	23	2440	24	2073	79	99
trib. Dura (LGB)	GPS 72	42	0.160	0.011	0.442	0.008	9.933	0.864	0.069	0.014	2455	110	2361	38	2429	80	1352	265	96
trib. Dura (LGB)	GPS 72	43	0.163	0.009	0.451	0.007	10.079	0.696	0.074	0.012	2488	87	2400	33	2442	64	1440	217	96
trib. Dura (LGB)	GPS 72	44	0.163	0.009	0.483	0.008	10.636	0.752	0.106	0.017	2490	89	2540	35	2492	66	2037	311	102
trib. Dura (LGB)	GPS 72	45	0.164	0.012	0.439	0.009	9.636	0.909	0.115	0.025	2497	117	2348	40	2401	87	2207	458	94
trib. Dura (LGB)	GPS 72	46	0.164	0.005	0.477	0.006	10.589	0.451	0.104	0.009	2498	51	2514	27	2488	40	2003	158	101
trib. Dura (LGB)	GPS 72	47	0.164	0.006	0.470	0.006	10.442	0.511	0.114	0.012	2501	60	2486	28	2475	45	2182	210	99
trib. Dura (LGB)	GPS 72	48	0.166	0.003	0.466	0.005	10.809	0.328	0.098	0.004	2513	32	2468	24	2507	28	1887	73	98
trib. Dura (LGB)	GPS 72	49	0.166	0.003	0.440	0.005	10.248	0.253	0.042	0.002	2521	31	2351	22	2457	23	824	34	93
trib. Dura (LGB)	GPS 72	50	0.167	0.009	0.442	0.007	10.226	0.692	0.116	0.018	2532	85	2360	32	2455	63	2217	321	93
trib. Dura (LGB)	GPS 72	51	0.168	0.011	0.487	0.009	11.555	0.950	0.112	0.021	2535	101	2559	39	2569	77	2154	381	101
trib. Dura (LGB)	GPS 72	52	0.168	0.003	0.493	0.006	11.426	0.280	0.094	0.004	2537	31	2582	24	2559	23	1813	76	102
trib. Dura (LGB)	GPS 72	53	0.170	0.006	0.490	0.007	11.453	0.517	0.080	0.008	2555	57	2572	28	2561	42	1547	143	101
trib. Dura (LGB)	GPS 72	54	0.170	0.003	0.497	0.006	11.780	0.434	0.104	0.004	2555	31	2602	25	2587	35	2006	71	102
trib. Dura (LGB)	GPS 72	55	0.171	0.011	0.529	0.010	12.362	0.989	0.151	0.028	2571	99	2736	40	2632	75	2846	485	106
trib. Dura (LGB)	GPS 72	56	0.172	0.004	0.489	0.006	11.585	0.338	0.106	0.006	2575	37	2565	25	2571	27	2032	107	100
trib. Dura (LGB)	GPS 72	57	0.173	0.012	0.464	0.009	11.163	1.020	0.039	0.008	2585	114	2458	40	2537	85	781	165	95
trib. Dura (LGB)	GPS 72	58	0.174	0.004	0.497	0.006	12.201	0.363	0.118	0.006	2594	35	2600	25	2620	28	2263	107	100
trib. Dura (LGB)	GPS 72	59	0.177	0.006	0.493	0.007	11.883	0.561	0.116	0.010	2629	54	2586	28	2595	44	2226	185	98
trib. Dura (LGB)	GPS 72	60	0.187	0.004	0.515	0.006	12.900	0.484	0.104	0.005	2716	35	2680	26	2672	35	1992	92	99
Mpanga (LGB)	GPS 73	~~1~~	~~0.171~~	~~0.003~~	~~0.248~~	~~0.003~~	~~5.896~~	~~0.142~~	~~0.058~~	~~0.002~~	~~2565~~	~~31~~	~~1427~~	~~14~~	~~1961~~	~~21~~	~~1136~~	~~46~~	~~55.6~~
Mpanga (LGB)	GPS 73	~~2~~	~~0.166~~	~~0.009~~	~~0.250~~	~~0.004~~	~~5.701~~	~~0.409~~	~~0.046~~	~~0.007~~	~~2517~~	~~91~~	~~1438~~	~~22~~	~~1932~~	~~62~~	~~911~~	~~138~~	~~57.1~~
Mpanga (LGB)	GPS 73	~~3~~	~~0.177~~	~~0.012~~	~~0.266~~	~~0.005~~	~~6.702~~	~~0.592~~	~~0.029~~	~~0.006~~	~~2628~~	~~108~~	~~1523~~	~~26~~	~~2073~~	~~78~~	~~584~~	~~112~~	~~57.9~~
Mpanga (LGB)	GPS 73	~~4~~	~~0.119~~	~~0.007~~	~~0.201~~	~~0.004~~	~~3.270~~	~~0.263~~	~~0.052~~	~~0.009~~	~~1946~~	~~108~~	~~1180~~	~~20~~	~~1474~~	~~63~~	~~1024~~	~~178~~	~~60.6~~
Mpanga (LGB)	GPS 73	~~5~~	~~0.109~~	~~0.004~~	~~0.186~~	~~0.002~~	~~2.796~~	~~0.129~~	~~0.051~~	~~0.005~~	~~1781~~	~~64~~	~~1097~~	~~14~~	~~1354~~	~~35~~	~~997~~	~~91~~	~~61.6~~
Mpanga (LGB)	GPS 73	~~6~~	~~0.155~~	~~0.009~~	~~0.285~~	~~0.005~~	~~6.206~~	~~0.478~~	~~0.078~~	~~0.013~~	~~2401~~	~~97~~	~~1618~~	~~25~~	~~2005~~	~~67~~	~~1524~~	~~244~~	~~67.4~~
Mpanga (LGB)	GPS 73	~~7~~	~~0.134~~	~~0.006~~	~~0.254~~	~~0.004~~	~~4.854~~	~~0.301~~	~~0.075~~	~~0.010~~	~~2147~~	~~81~~	~~1459~~	~~20~~	~~1794~~	~~52~~	~~1456~~	~~181~~	~~67.9~~
Mpanga (LGB)	GPS 73	~~8~~	~~0.177~~	~~0.009~~	~~0.339~~	~~0.005~~	~~8.258~~	~~0.536~~	~~0.042~~	~~0.006~~	~~2627~~	~~82~~	~~1881~~	~~26~~	~~2260~~	~~59~~	~~830~~	~~112~~	~~71.6~~
Mpanga (LGB)	GPS 73	~~9~~	~~0.172~~	~~0.009~~	~~0.343~~	~~0.006~~	~~8.398~~	~~0.604~~	~~0.083~~	~~0.013~~	~~2573~~	~~89~~	~~1902~~	~~28~~	~~2275~~	~~65~~	~~1619~~	~~236~~	~~73.9~~
Mpanga (LGB)	GPS 73	~~10~~	~~0.157~~	~~0.005~~	~~0.338~~	~~0.004~~	~~7.250~~	~~0.271~~	~~0.051~~	~~0.004~~	~~2422~~	~~48~~	~~1875~~	~~20~~	~~2143~~	~~33~~	~~1008~~	~~72~~	~~77.4~~
Mpanga (LGB)	GPS 73	~~11~~	~~0.174~~	~~0.011~~	~~0.371~~	~~0.007~~	~~9.197~~	~~0.760~~	~~0.046~~	~~0.008~~	~~2593~~	~~103~~	~~2035~~	~~32~~	~~2358~~	~~76~~	~~911~~	~~162~~	~~78.5~~
Mpanga (LGB)	GPS 73	~~12~~	~~0.167~~	~~0.003~~	~~0.365~~	~~0.004~~	~~8.439~~	~~0.232~~	~~0.072~~	~~0.003~~	~~2530~~	~~34~~	~~2004~~	~~20~~	~~2279~~	~~25~~	~~1401~~	~~64~~	~~79.2~~
Mpanga (LGB)	GPS 73	~~13~~	~~0.137~~	~~0.008~~	~~0.333~~	~~0.006~~	~~6.301~~	~~0.500~~	~~0.037~~	~~0.006~~	~~2188~~	~~103~~	~~1851~~	~~29~~	~~2019~~	~~69~~	~~725~~	~~124~~	~~84.6~~
Mpanga (LGB)	GPS 73	~~14~~	~~0.144~~	~~0.005~~	~~0.355~~	~~0.005~~	~~7.022~~	~~0.369~~	~~0.095~~	~~0.009~~	~~2276~~	~~64~~	~~1957~~	~~24~~	~~2114~~	~~47~~	~~1838~~	~~169~~	~~86.0~~
Mpanga (LGB)	GPS 73	~~15~~	~~0.166~~	~~0.006~~	~~0.405~~	~~0.006~~	~~9.392~~	~~0.460~~	~~0.074~~	~~0.007~~	~~2521~~	~~62~~	~~2191~~	~~25~~	~~2377~~	~~45~~	~~1434~~	~~136~~	~~86.9~~
Mpanga (LGB)	GPS 73	~~16~~	~~0.176~~	~~0.009~~	~~0.434~~	~~0.007~~	~~10.595~~	~~0.667~~	~~0.086~~	~~0.011~~	~~2618~~	~~79~~	~~2325~~	~~30~~	~~2488~~	~~58~~	~~1662~~	~~210~~	~~88.8~~
Mpanga (LGB)	GPS 73	~~17~~	~~0.184~~	~~0.007~~	~~0.450~~	~~0.006~~	~~10.761~~	~~0.565~~	~~0.150~~	~~0.014~~	~~2694~~	~~58~~	~~2396~~	~~28~~	~~2503~~	~~49~~	~~2832~~	~~242~~	~~89.0~~
Mpanga (LGB)	GPS 73	~~18~~	~~0.168~~	~~0.006~~	~~0.421~~	~~0.006~~	~~9.989~~	~~0.508~~	~~0.082~~	~~0.008~~	~~2536~~	~~63~~	~~2265~~	~~27~~	~~2434~~	~~47~~	~~1585~~	~~154~~	~~89.3~~
Mpanga (LGB)	GPS 73	19	0.117	0.002	0.331	0.004	5.420	0.118	0.098	0.004	1914	30	1843	18	1888	19	1883	65	96.3
Mpanga (LGB)	GPS 73	20	0.132	0.006	0.358	0.005	6.727	0.408	0.080	0.010	2119	80	1974	26	2076	54	1562	189	93.2
Mpanga (LGB)	GPS 73	21	0.132	0.005	0.377	0.005	6.833	0.311	0.090	0.008	2121	59	2064	23	2090	40	1739	148	97.3
Mpanga (LGB)	GPS 73	22	0.132	0.008	0.387	0.007	6.665	0.518	0.108	0.018	2126	102	2111	32	2068	69	2072	335	99.3
Mpanga (LGB)	GPS 73	23	0.136	0.004	0.363	0.005	6.804	0.281	0.105	0.007	2175	49	1997	22	2086	37	2010	134	91.8
Mpanga (LGB)	GPS 73	24	0.137	0.004	0.392	0.005	7.464	0.309	0.100	0.007	2192	50	2134	23	2169	37	1920	132	97.4
Mpanga (LGB)	GPS 73	25	0.150	0.004	0.420	0.005	8.560	0.326	0.119	0.009	2342	50	2259	24	2292	35	2267	162	96.5
Mpanga (LGB)	GPS 73	26	0.163	0.003	0.473	0.005	10.008	0.273	0.092	0.004	2487	31	2496	23	2436	25	1777	70	100.3
Mpanga (LGB)	GPS 73	27	0.164	0.003	0.436	0.005	9.717	0.193	0.045	0.002	2502	26	2332	21	2408	18	888	29	93.2
Mpanga (LGB)	GPS 73	28	0.164	0.009	0.471	0.008	10.858	0.756	0.133	0.019	2502	85	2487	34	2511	65	2519	335	99.4
Mpanga (LGB)	GPS 73	29	0.166	0.006	0.427	0.006	9.717	0.447	0.058	0.005	2522	55	2292	25	2408	42	1139	93	90.9
Mpanga (LGB)	GPS 73	30	0.167	0.003	0.437	0.005	10.106	0.209	0.074	0.002	2523	26	2335	22	2445	19	1447	46	92.6

Zircon U-Pb geochronology cont.

			Isotope ratios								Age estimates								
River name	Sample ID	Analysis No.	$^{207}Pb/^{206}Pb$	±1σ	$^{206}Pb/^{238}U$	±1σ	$^{207}Pb/^{235}U$	±1σ	$^{208}Pb/^{232}Th$	±1σ	$^{207}Pb/^{206}Pb$ [Ma]	±1σ [Ma]	$^{206}Pb/^{238}U$ [Ma]	±1σ [Ma]	$^{207}Pb/^{235}U$ [Ma]	±1σ [Ma]	$^{208}Pb/^{232}Th$ [Ma]	±1σ [Ma]	Concordance [%]
Mpanga (LGB)	GPS 73	31	0.167	0.005	0.459	0.006	10.758	0.378	0.126	0.009	2530	45	2437	25	2503	33	2400	153	96.3
Mpanga (LGB)	GPS 73	32	0.168	0.003	0.429	0.005	9.491	0.221	0.058	0.002	2534	28	2303	22	2387	21	1142	41	90.9
Mpanga (LGB)	GPS 73	33	0.168	0.003	0.453	0.005	10.344	0.379	0.098	0.004	2536	34	2408	24	2466	34	1894	79	94.9
Mpanga (LGB)	GPS 73	34	0.169	0.005	0.511	0.007	11.948	0.540	0.124	0.010	2549	53	2660	28	2600	42	2367	183	104.3
Mpanga (LGB)	GPS 73	35	0.170	0.005	0.477	0.006	11.211	0.459	0.129	0.010	2554	50	2513	26	2541	38	2444	179	98.4
Mpanga (LGB)	GPS 73	36	0.171	0.006	0.496	0.007	12.365	0.618	0.128	0.010	2568	53	2595	28	2633	47	2440	184	101.0
Mpanga (LGB)	GPS 73	37	0.171	0.004	0.514	0.006	12.650	0.484	0.124	0.006	2570	35	2673	26	2654	36	2368	108	104.0
Mpanga (LGB)	GPS 73	38	0.171	0.003	0.483	0.005	11.390	0.240	0.118	0.004	2570	26	2541	23	2556	20	2260	74	98.9
Mpanga (LGB)	GPS 73	39	0.172	0.009	0.464	0.008	11.254	0.775	0.117	0.017	2574	85	2457	34	2544	64	2241	307	95.4
Mpanga (LGB)	GPS 73	40	0.172	0.011	0.466	0.009	10.664	0.912	0.132	0.025	2578	106	2467	39	2494	79	2508	449	95.7
Mpanga (LGB)	GPS 73	41	0.173	0.004	0.475	0.006	11.509	0.344	0.025	0.001	2585	37	2505	24	2565	28	509	27	96.9
Mpanga (LGB)	GPS 73	42	0.173	0.004	0.496	0.006	12.360	0.383	0.098	0.005	2585	35	2597	25	2632	29	1890	91	100.5
Mpanga (LGB)	GPS 73	43	0.174	0.010	0.480	0.008	11.712	0.906	0.148	0.024	2594	93	2526	37	2582	72	2790	414	97.4
Mpanga (LGB)	GPS 73	44	0.174	0.005	0.450	0.006	11.285	0.422	0.103	0.007	2598	43	2396	24	2547	35	1990	121	92.2
Mpanga (LGB)	GPS 73	45	0.174	0.004	0.519	0.007	11.529	0.805	0.027	0.001	2599	40	2697	31	2567	65	541	24	103.8
Mpanga (LGB)	GPS 73	46	0.175	0.011	0.482	0.009	11.510	0.986	0.134	0.025	2601	105	2537	40	2565	80	2536	444	97.5
Mpanga (LGB)	GPS 73	47	0.175	0.003	0.497	0.006	11.678	0.273	0.125	0.005	2601	28	2602	24	2579	22	2379	86	100.0
Mpanga (LGB)	GPS 73	48	0.175	0.004	0.444	0.005	10.957	0.351	0.111	0.006	2606	38	2368	23	2520	30	2131	112	90.9
Mpanga (LGB)	GPS 73	49	0.176	0.007	0.512	0.007	12.379	0.635	0.155	0.016	2612	64	2666	31	2634	48	2910	281	102.1
Mpanga (LGB)	GPS 73	50	0.176	0.007	0.505	0.007	12.388	0.654	0.133	0.014	2612	65	2636	31	2634	50	2520	251	100.9
Mpanga (LGB)	GPS 73	51	0.177	0.003	0.471	0.005	11.378	0.283	0.119	0.005	2627	29	2486	23	2555	23	2271	85	94.6
Mpanga (LGB)	GPS 73	52	0.177	0.005	0.490	0.006	11.970	0.414	0.124	0.008	2627	43	2572	26	2602	32	2360	146	97.9
Mpanga (LGB)	GPS 73	53	0.178	0.003	0.487	0.006	12.217	0.348	0.143	0.006	2630	32	2556	24	2621	27	2700	113	97.2
Mpanga (LGB)	GPS 73	54	0.178	0.006	0.491	0.007	12.094	0.630	0.135	0.012	2635	56	2574	29	2612	49	2568	210	97.7
Mpanga (LGB)	GPS 73	55	0.178	0.003	0.506	0.006	12.752	0.297	0.141	0.005	2639	27	2638	24	2662	22	2674	90	100.0
Mpanga (LGB)	GPS 73	56	0.179	0.010	0.531	0.009	13.089	1.058	0.164	0.027	2644	94	2745	40	2686	76	3068	463	103.8
Mpanga (LGB)	GPS 73	57	0.181	0.004	0.461	0.005	12.852	0.444	0.125	0.006	2664	35	2445	24	2669	33	2387	111	91.8
Mpanga (LGB)	GPS 73	58	0.184	0.010	0.496	0.008	13.016	0.943	0.141	0.021	2688	87	2596	36	2681	68	2672	371	96.6
Mpanga (LGB)	GPS 73	59	0.185	0.009	0.500	0.008	12.768	0.821	0.137	0.018	2696	80	2612	34	2663	61	2591	328	96.9
Mpanga (LGB)	GPS 73	60	0.189	0.004	0.506	0.006	13.149	0.390	0.140	0.007	2734	35	2639	25	2690	28	2656	129	96.5
Dunga (Rwenzori M.)	GPS 92	~~1~~	~~0.866~~	~~0.047~~	~~0.074~~	~~0.003~~	~~15.272~~	~~4.329~~	~~0.017~~	~~0.001~~	~~5035~~	~~31~~	~~459~~	~~25~~	~~2832~~	~~24~~	~~347~~	~~142~~	~~9.1~~
Dunga (Rwenzori M.)	GPS 92	~~2~~	~~0.531~~	~~0.017~~	~~0.255~~	~~0.003~~	~~18.706~~	~~0.752~~	~~0.127~~	~~0.012~~	~~4331~~	~~55~~	~~1465~~	~~31~~	~~3027~~	~~56~~	~~2424~~	~~225~~	~~33.8~~
Dunga (Rwenzori M.)	GPS 92	~~3~~	~~0.168~~	~~0.006~~	~~0.145~~	~~0.002~~	~~3.335~~	~~0.157~~	~~0.012~~	~~0.001~~	~~2534~~	~~59~~	~~875~~	~~21~~	~~1489~~	~~43~~	~~236~~	~~183~~	~~34.5~~
Dunga (Rwenzori M.)	GPS 92	~~4~~	~~0.114~~	~~0.003~~	~~0.163~~	~~0.002~~	~~2.396~~	~~0.085~~	~~0.039~~	~~0.003~~	~~1859~~	~~49~~	~~972~~	~~11~~	~~1242~~	~~23~~	~~774~~	~~21~~	~~52.3~~
Dunga (Rwenzori M.)	GPS 92	~~5~~	~~0.199~~	~~0.003~~	~~0.266~~	~~0.003~~	~~7.268~~	~~0.160~~	~~0.065~~	~~0.003~~	~~2814~~	~~29~~	~~1518~~	~~26~~	~~2145~~	~~30~~	~~1266~~	~~109~~	~~53.9~~
Dunga (Rwenzori M.)	GPS 92	~~6~~	~~0.102~~	~~0.003~~	~~0.151~~	~~0.002~~	~~2.010~~	~~0.070~~	~~0.013~~	~~0.001~~	~~1655~~	~~44~~	~~907~~	~~16~~	~~1119~~	~~30~~	~~254~~	~~80~~	~~54.8~~
Dunga (Rwenzori M.)	GPS 92	~~7~~	~~0.163~~	~~0.004~~	~~0.244~~	~~0.003~~	~~5.667~~	~~0.197~~	~~0.051~~	~~0.004~~	~~2491~~	~~63~~	~~1409~~	~~7~~	~~1926~~	~~17~~	~~1003~~	~~57~~	~~56.5~~
Dunga (Rwenzori M.)	GPS 92	~~8~~	~~0.153~~	~~0.005~~	~~0.232~~	~~0.003~~	~~4.767~~	~~0.212~~	~~0.050~~	~~0.005~~	~~2374~~	~~54~~	~~1345~~	~~19~~	~~1779~~	~~38~~	~~977~~	~~144~~	~~56.6~~
Dunga (Rwenzori M.)	GPS 92	~~9~~	~~0.135~~	~~0.003~~	~~0.220~~	~~0.003~~	~~3.935~~	~~0.100~~	~~0.064~~	~~0.004~~	~~2162~~	~~33~~	~~1280~~	~~21~~	~~1621~~	~~23~~	~~1260~~	~~90~~	~~59.2~~
Dunga (Rwenzori M.)	GPS 92	~~10~~	~~0.176~~	~~0.006~~	~~0.287~~	~~0.004~~	~~6.812~~	~~0.293~~	~~0.082~~	~~0.008~~	~~2620~~	~~54~~	~~1626~~	~~25~~	~~2087~~	~~39~~	~~1596~~	~~185~~	~~62.1~~
Dunga (Rwenzori M.)	GPS 92	~~11~~	~~0.146~~	~~0.006~~	~~0.265~~	~~0.004~~	~~5.186~~	~~0.261~~	~~0.053~~	~~0.005~~	~~2303~~	~~63~~	~~1515~~	~~29~~	~~1850~~	~~46~~	~~1052~~	~~164~~	~~65.8~~
Dunga (Rwenzori M.)	GPS 92	~~12~~	~~0.165~~	~~0.006~~	~~0.304~~	~~0.004~~	~~7.194~~	~~0.349~~	~~0.104~~	~~0.010~~	~~2509~~	~~57~~	~~1712~~	~~25~~	~~2136~~	~~41~~	~~1995~~	~~68~~	~~68.2~~
Dunga (Rwenzori M.)	GPS 92	~~13~~	~~0.153~~	~~0.008~~	~~0.297~~	~~0.005~~	~~6.225~~	~~0.423~~	~~0.028~~	~~0.003~~	~~2384~~	~~85~~	~~1678~~	~~29~~	~~2008~~	~~60~~	~~558~~	~~116~~	~~70.4~~
Dunga (Rwenzori M.)	GPS 92	~~14~~	~~0.175~~	~~0.003~~	~~0.337~~	~~0.004~~	~~7.998~~	~~0.181~~	~~0.103~~	~~0.004~~	~~2603~~	~~27~~	~~1872~~	~~24~~	~~2231~~	~~23~~	~~1978~~	~~96~~	~~71.9~~
Dunga (Rwenzori M.)	GPS 92	~~15~~	~~0.139~~	~~0.005~~	~~0.284~~	~~0.004~~	~~5.122~~	~~0.242~~	~~0.069~~	~~0.007~~	~~2220~~	~~60~~	~~1610~~	~~11~~	~~1840~~	~~37~~	~~1350~~	~~23~~	~~72.5~~
Dunga (Rwenzori M.)	GPS 92	~~16~~	~~0.165~~	~~0.009~~	~~0.350~~	~~0.006~~	~~8.020~~	~~0.535~~	~~0.064~~	~~0.006~~	~~2507~~	~~84~~	~~1936~~	~~37~~	~~2233~~	~~62~~	~~1248~~	~~132~~	~~77.2~~
Dunga (Rwenzori M.)	GPS 92	~~17~~	~~0.150~~	~~0.009~~	~~0.327~~	~~0.006~~	~~6.861~~	~~0.553~~	~~0.045~~	~~0.004~~	~~2344~~	~~101~~	~~1823~~	~~40~~	~~2094~~	~~73~~	~~889~~	~~75~~	~~77.8~~
Dunga (Rwenzori M.)	GPS 92	~~18~~	~~0.144~~	~~0.007~~	~~0.327~~	~~0.005~~	~~6.238~~	~~0.367~~	~~0.060~~	~~0.006~~	~~2273~~	~~98~~	~~1825~~	~~17~~	~~2010~~	~~44~~	~~1173~~	~~66~~	~~80.3~~
Dunga (Rwenzori M.)	GPS 92	~~19~~	~~0.161~~	~~0.009~~	~~0.376~~	~~0.007~~	~~8.478~~	~~0.617~~	~~0.025~~	~~0.002~~	~~2469~~	~~91~~	~~2057~~	~~36~~	~~2284~~	~~67~~	~~497~~	~~52~~	~~83.3~~
Dunga (Rwenzori M.)	GPS 92	~~20~~	~~0.168~~	~~0.003~~	~~0.390~~	~~0.005~~	~~9.174~~	~~0.290~~	~~0.056~~	~~0.003~~	~~2543~~	~~29~~	~~2121~~	~~21~~	~~2356~~	~~21~~	~~1107~~	~~87~~	~~83.4~~
Dunga (Rwenzori M.)	GPS 92	~~21~~	~~0.163~~	~~0.003~~	~~0.381~~	~~0.004~~	~~8.749~~	~~0.225~~	~~0.083~~	~~0.005~~	~~2487~~	~~75~~	~~2083~~	~~17~~	~~2312~~	~~270~~	~~1621~~	~~21~~	~~83.8~~
Dunga (Rwenzori M.)	GPS 92	~~22~~	~~0.167~~	~~0.003~~	~~0.389~~	~~0.004~~	~~8.664~~	~~0.196~~	~~0.096~~	~~0.005~~	~~2526~~	~~30~~	~~2120~~	~~24~~	~~2303~~	~~26~~	~~1852~~	~~109~~	~~83.9~~
Dunga (Rwenzori M.)	GPS 92	~~23~~	~~0.152~~	~~0.008~~	~~0.371~~	~~0.007~~	~~7.967~~	~~0.561~~	~~0.037~~	~~0.003~~	~~2372~~	~~88~~	~~2034~~	~~38~~	~~2227~~	~~65~~	~~726~~	~~130~~	~~85.7~~
Dunga (Rwenzori M.)	GPS 92	~~24~~	~~0.170~~	~~0.006~~	~~0.405~~	~~0.006~~	~~9.482~~	~~0.425~~	~~0.037~~	~~0.003~~	~~2553~~	~~57~~	~~2191~~	~~17~~	~~2386~~	~~37~~	~~726~~	~~90~~	~~85.8~~
Dunga (Rwenzori M.)	GPS 92	~~25~~	~~0.167~~	~~0.005~~	~~0.405~~	~~0.005~~	~~9.242~~	~~0.398~~	~~0.109~~	~~0.010~~	~~2527~~	~~45~~	~~2193~~	~~17~~	~~2362~~	~~39~~	~~2086~~	~~210~~	~~86.8~~
Dunga (Rwenzori M.)	GPS 92	~~26~~	~~0.162~~	~~0.005~~	~~0.400~~	~~0.005~~	~~9.280~~	~~0.373~~	~~0.043~~	~~0.004~~	~~2473~~	~~50~~	~~2170~~	~~26~~	~~2366~~	~~41~~	~~847~~	~~270~~	~~87.7~~
Dunga (Rwenzori M.)	GPS 92	27	0.153	0.009	0.457	0.009	9.672	0.769	0.059	0.005	2385	100	2426	43	2404	78	1153	115	101.7
Dunga (Rwenzori M.)	GPS 92	28	0.158	0.010	0.515	0.010	11.164	0.934	0.064	0.006	2439	97	2676	41	2537	72	1261	104	109.7
Dunga (Rwenzori M.)	GPS 92	29	0.159	0.008	0.406	0.007	8.791	0.571	0.048	0.005	2444	80	2195	36	2317	61	940	143	89.8
Dunga (Rwenzori M.)	GPS 92	30	0.159	0.009	0.503	0.010	10.748	0.830	0.059	0.005	2448	96	2628	37	2502	70	1150	94	107.3
Dunga (Rwenzori M.)	GPS 92	31	0.160	0.010	0.460	0.009	10.119	0.804	0.042	0.004	2454	101	2439	39	2446	73	835	104	99.4
Dunga (Rwenzori M.)	GPS 92	32	0.160	0.009	0.447	0.008	10.000	0.758	0.052	0.005	2457	94	2382	40	2435	71	1025	117	96.9
Dunga (Rwenzori M.)	GPS 92	33	0.160	0.009	0.505	0.009	11.324	0.792	0.073	0.007	2457	87	2633	26	2550	59	1416	53	107.2
Dunga (Rwenzori M.)	GPS 92	34	0.161	0.009	0.443	0.008	10.119	0.730	0.028	0.003	2470	90	2363	31	2446	64	558	68	95.7
Dunga (Rwenzori M.)	GPS 92	35	0.162	0.009	0.505	0.009	11.247	0.860	0.065	0.006	2475	92	2635	32	2544	66	1281	46	106.4
Dunga (Rwenzori M.)	GPS 92	36	0.163	0.008	0.533	0.009	12.506	0.847	0.078	0.008	2485	78	2753	34	2643	60	1517	148	110.5
Dunga (Rwenzori M.)	GPS 92	37	0.164	0.006	0.453	0.007	10.264	0.513	0.091	0.009	2497	62	2411	32	2459	50	1759	200	96.5
Dunga (Rwenzori M.)	GPS 92	38	0.164	0.008	0.477	0.008	11.401	0.722	0.042	0.004	2497	77	2513	25	2557	52	825	111	100.6
Dunga (Rwenzori M.)	GPS 92	39	0.164	0.008	0.523	0.009	11.886	0.788	0.073	0.007	2502	83	2711	31	2596	59	1421	89	108.3
Dunga (Rwenzori M.)	GPS 92	40	0.165	0.008	0.483	0.008	11.431	0.730	0.081	0.008	2511	77	2539	34	2559	59	1580	80	101.1
Dunga (Rwenzori M.)	GPS 92	41	0.168	0.004	0.477	0.006	11.281	0.343	0.144	0.010	2542	38	2512	27	2547	37	2725	185	98.8
Dunga (Rwenzori M.)	GPS 92	42	0.168	0.003	0.504	0.006	11.631	0.297	0.149	0.008	2542	33	2632	22	2575	29	2807	56	103.5
Dunga (Rwenzori M.)	GPS 92	43	0.170	0.008	0.514	0.009	12.304	0.795	0.079	0.008	2553	80	2674	37	2628	64	1530	143	104.7
Dunga (Rwenzori M.)	GPS 92	44	0.170	0.006	0.515	0.007	12.331	0.729	0.138	0.013	2558	50	2677	24	2630	37	2618	75	104.6
Dunga (Rwenzori M.)	GPS 92	45	0.173	0.007	0.512	0.007	12.294	0.654	0.114	0.011	2585	62	2665	20	2627	40	2180	126	103.1

Zircon U-Pb geochronology cont.

			Isotope ratios								Age estimates								
River name	Sample ID	Analysis No.	$^{207}Pb/^{206}Pb$	±1σ	$^{206}Pb/^{238}U$	±1σ	$^{207}Pb/^{235}U$	±1σ	$^{208}Pb/^{232}Th$	±1σ	$^{207}Pb/^{206}Pb$ [Ma]	±1σ [Ma]	$^{206}Pb/^{238}U$ [Ma]	±1σ [Ma]	$^{207}Pb/^{235}U$ [Ma]	±1σ [Ma]	$^{208}Pb/^{232}Th$ [Ma]	±1σ [Ma]	Concordance [%]
Dunga (Rwenzori M.)	GPS 92	46	0.173	0.005	0.434	0.006	10.576	0.467	0.176	0.016	2587	48	2324	28	2487	38	3277	201	89.9
Dunga (Rwenzori M.)	GPS 92	47	0.174	0.004	0.508	0.006	12.427	0.345	0.150	0.010	2594	36	2648	25	2637	32	2826	170	102.1
Dunga (Rwenzori M.)	GPS 92	48	0.175	0.005	0.509	0.007	12.380	0.499	0.129	0.011	2603	47	2652	27	2634	38	2444	170	101.9
Dunga (Rwenzori M.)	GPS 92	49	0.175	0.005	0.474	0.006	12.049	0.488	0.108	0.009	2606	49	2500	11	2608	25	2074	64	95.9
Dunga (Rwenzori M.)	GPS 92	50	0.175	0.004	0.528	0.007	12.654	0.457	0.162	0.012	2608	38	2733	25	2654	28	3040	180	104.8
Dunga (Rwenzori M.)	GPS 92	51	0.175	0.003	0.479	0.006	11.740	0.329	0.129	0.006	2609	30	2525	26	2584	29	2448	123	96.8
Dunga (Rwenzori M.)	GPS 92	52	0.176	0.007	0.490	0.007	11.673	0.655	0.105	0.010	2611	66	2569	20	2579	43	2021	100	98.4
Dunga (Rwenzori M.)	GPS 92	53	0.176	0.003	0.494	0.006	12.504	0.401	0.130	0.005	2612	26	2590	23	2643	23	2469	83	99.2
Dunga (Rwenzori M.)	GPS 92	54	0.176	0.004	0.462	0.006	11.198	0.327	0.130	0.009	2612	35	2447	26	2540	26	2462	169	93.7
Dunga (Rwenzori M.)	GPS 92	55	0.176	0.004	0.502	0.006	12.318	0.480	0.153	0.011	2614	36	2624	24	2629	27	2879	154	100.4
Dunga (Rwenzori M.)	GPS 92	56	0.177	0.004	0.457	0.006	10.776	0.373	0.156	0.010	2627	35	2425	14	2504	21	2923	73	92.3
Dunga (Rwenzori M.)	GPS 92	57	0.180	0.003	0.516	0.006	13.054	0.395	0.153	0.007	2657	27	2681	15	2684	20	2880	53	100.9
Dunga (Rwenzori M.)	GPS 92	58	0.181	0.003	0.456	0.005	11.269	0.277	0.130	0.005	2658	46	2422	7	2546	12	2465	35	91.1
Dunga (Rwenzori M.)	GPS 92	59	0.181	0.003	0.489	0.006	12.798	0.315	0.139	0.005	2663	28	2568	25	2665	30	2632	89	96.5
Dunga (Rwenzori M.)	GPS 92	60	0.184	0.003	0.512	0.006	12.950	0.413	0.146	0.006	2693	27	2667	18	2676	20	2763	75	99.0
Mubuku (Rwenzori M.)	GPS 96	~~1~~	~~0.464~~	~~0.123~~	~~0.061~~	~~0.011~~	~~4.380~~	~~3.360~~	~~-0.013~~	~~0.090~~	~~4129~~	~~345~~	~~382~~	~~65~~	~~1709~~	~~634~~	~~-262~~	~~1833~~	~~9.3~~
Mubuku (Rwenzori M.)	GPS 96	~~2~~	~~0.190~~	~~1.283~~	~~0.041~~	~~0.052~~	~~-0.447~~	~~3.136~~	~~0.155~~	~~0.083~~	~~2744~~	~~3032~~	~~262~~	~~319~~	~~-601~~	~~5753~~	~~2916~~	~~1449~~	~~9.5~~
Mubuku (Rwenzori M.)	GPS 96	~~3~~	~~1.370~~	~~1.457~~	~~0.313~~	~~0.280~~	~~16.860~~	~~103.549~~	~~-30.735~~	~~192.965~~	~~5676~~	~~985~~	~~1757~~	~~1373~~	~~2927~~	~~5887~~	~~-~~	~~-~~	~~30.9~~
Mubuku (Rwenzori M.)	GPS 96	~~4~~	~~0.299~~	~~0.039~~	~~0.197~~	~~0.011~~	~~5.897~~	~~2.267~~	~~0.263~~	~~0.028~~	~~3467~~	~~187~~	~~1159~~	~~57~~	~~1961~~	~~334~~	~~4719~~	~~451~~	~~33.4~~
Mubuku (Rwenzori M.)	GPS 96	~~5~~	~~0.185~~	~~0.019~~	~~0.159~~	~~0.005~~	~~4.112~~	~~1.197~~	~~0.170~~	~~0.021~~	~~2696~~	~~162~~	~~953~~	~~27~~	~~1657~~	~~238~~	~~3174~~	~~367~~	~~35.3~~
Mubuku (Rwenzori M.)	GPS 96	~~6~~	~~0.311~~	~~0.093~~	~~0.226~~	~~0.022~~	~~8.694~~	~~13.569~~	~~0.216~~	~~0.055~~	~~3526~~	~~399~~	~~1314~~	~~115~~	~~2306~~	~~1421~~	~~3946~~	~~914~~	~~37.3~~
Mubuku (Rwenzori M.)	GPS 96	~~7~~	~~0.157~~	~~0.023~~	~~0.203~~	~~0.006~~	~~7.862~~	~~5.025~~	~~0.230~~	~~0.022~~	~~2425~~	~~226~~	~~1194~~	~~35~~	~~2215~~	~~576~~	~~4179~~	~~366~~	~~49.2~~
Mubuku (Rwenzori M.)	GPS 96	~~8~~	~~0.157~~	~~0.049~~	~~0.210~~	~~0.012~~	~~3.386~~	~~1.660~~	~~0.164~~	~~0.028~~	~~2419~~	~~450~~	~~1231~~	~~61~~	~~1501~~	~~384~~	~~3076~~	~~491~~	~~50.9~~
Mubuku (Rwenzori M.)	GPS 96	~~9~~	~~0.185~~	~~0.018~~	~~0.270~~	~~0.007~~	~~3.899~~	~~0.726~~	~~0.211~~	~~0.027~~	~~2695~~	~~156~~	~~1538~~	~~37~~	~~1614~~	~~150~~	~~3872~~	~~451~~	~~57.1~~
Mubuku (Rwenzori M.)	GPS 96	~~10~~	~~0.160~~	~~0.004~~	~~0.293~~	~~0.004~~	~~6.451~~	~~0.188~~	~~0.091~~	~~0.006~~	~~2455~~	~~38~~	~~1656~~	~~18~~	~~2039~~	~~26~~	~~1768~~	~~111~~	~~67.4~~
Mubuku (Rwenzori M.)	GPS 96	~~11~~	~~0.240~~	~~0.014~~	~~0.399~~	~~0.010~~	~~37.502~~	~~52.179~~	~~0.226~~	~~0.024~~	~~3121~~	~~89~~	~~2164~~	~~45~~	~~3707~~	~~1376~~	~~4113~~	~~399~~	~~69.4~~
Mubuku (Rwenzori M.)	GPS 96	~~12~~	~~0.125~~	~~0.007~~	~~0.255~~	~~0.004~~	~~4.416~~	~~0.310~~	~~0.083~~	~~0.013~~	~~2029~~	~~94~~	~~1466~~	~~22~~	~~1715~~	~~58~~	~~1610~~	~~248~~	~~72.2~~
Mubuku (Rwenzori M.)	GPS 96	~~13~~	~~0.148~~	~~0.009~~	~~0.322~~	~~0.006~~	~~6.663~~	~~0.523~~	~~0.104~~	~~0.018~~	~~2323~~	~~103~~	~~1799~~	~~29~~	~~2068~~	~~69~~	~~1991~~	~~332~~	~~77.4~~
Mubuku (Rwenzori M.)	GPS 96	~~14~~	~~0.156~~	~~0.003~~	~~0.339~~	~~0.004~~	~~7.499~~	~~0.199~~	~~0.143~~	~~0.007~~	~~2408~~	~~31~~	~~1880~~	~~19~~	~~2173~~	~~24~~	~~2699~~	~~117~~	~~78.1~~
Mubuku (Rwenzori M.)	GPS 96	~~15~~	~~0.163~~	~~0.012~~	~~0.372~~	~~0.008~~	~~8.154~~	~~0.748~~	~~0.091~~	~~0.018~~	~~2487~~	~~117~~	~~2037~~	~~36~~	~~2248~~	~~83~~	~~1759~~	~~326~~	~~81.9~~
Mubuku (Rwenzori M.)	GPS 96	~~16~~	~~0.151~~	~~0.006~~	~~0.368~~	~~0.005~~	~~7.637~~	~~0.392~~	~~0.129~~	~~0.016~~	~~2359~~	~~67~~	~~2020~~	~~25~~	~~2189~~	~~46~~	~~2448~~	~~282~~	~~85.6~~
Mubuku (Rwenzori M.)	GPS 96	~~17~~	~~0.173~~	~~0.010~~	~~0.418~~	~~0.007~~	~~10.056~~	~~0.737~~	~~0.123~~	~~0.020~~	~~2584~~	~~92~~	~~2252~~	~~33~~	~~2440~~	~~68~~	~~2344~~	~~366~~	~~87.2~~
Mubuku (Rwenzori M.)	GPS 96	~~18~~	~~-0.145~~	~~1.141~~	~~0.068~~	~~0.068~~	~~-0.119~~	~~0.925~~	~~-0.481~~	~~0.305~~	~~0~~	~~5232~~	~~422~~	~~412~~	~~-128~~	~~1066~~	~~-~~	~~-~~	~~21900.~~
Mubuku (Rwenzori M.)	GPS 96	~~19~~	~~-4.322~~	~~15.044~~	~~0.333~~	~~1.112~~	~~9.318~~	~~49.526~~	~~0.918~~	~~0.794~~	~~0~~	~~8000~~	~~1853~~	~~5379~~	~~2370~~	~~4874~~	~~-~~	~~8370~~	~~153300~~
Mubuku (Rwenzori M.)	GPS 96	~~20~~	~~-0.439~~	~~0.781~~	~~1.703~~	~~0.766~~	~~-0.967~~	~~1.794~~	~~0.917~~	~~0.836~~	~~0~~	~~3672~~	~~6411~~	~~1826~~	~~-~~	~~-~~	~~-~~	~~8816~~	~~110900~~
Mubuku (Rwenzori M.)	GPS 96	~~21~~	~~-0.544~~	~~0.861~~	~~-1.660~~	~~1.660~~	~~0.456~~	~~0.646~~	~~0.838~~	~~1.369~~	~~0~~	~~3557~~	~~-~~	~~-~~	~~382~~	~~451~~	~~-~~	~~-~~	~~-~~
Mubuku (Rwenzori M.)	GPS 96	~~22~~	~~1.961~~	~~10.252~~	~~-~~	~~-~~	~~-0.822~~	~~2.041~~	~~-0.282~~	~~1.418~~	~~6168~~	~~1832~~	~~-~~	~~-~~	~~-~~	~~-~~	~~-~~	~~-~~	~~-~~
Mubuku (Rwenzori M.)	GPS 96	~~23~~	~~1.015~~	~~0.058~~	~~-~~	~~209.809~~	~~-~~	~~-~~	~~967.408~~	~~997.936~~	~~5259~~	~~78~~	~~-~~	~~-~~	~~7040~~	~~1752~~	~~-~~	~~-~~	~~-~~
Mubuku (Rwenzori M.)	GPS 96	24	0.128	0.002	0.370	0.004	6.263	0.133	0.127	0.005	2069	28	2031	20	2013	19	2414	87	98.1
Mubuku (Rwenzori M.)	GPS 96	25	0.129	0.010	0.379	0.008	6.641	0.649	0.085	0.017	2087	131	2069	39	2065	86	1643	318	99.2
Mubuku (Rwenzori M.)	GPS 96	26	0.132	0.010	0.382	0.008	6.696	0.656	0.081	0.016	2123	128	2088	39	2072	87	1580	304	98.4
Mubuku (Rwenzori M.)	GPS 96	27	0.135	0.010	0.388	0.008	7.209	0.701	0.110	0.021	2162	121	2114	38	2138	87	2112	385	97.8
Mubuku (Rwenzori M.)	GPS 96	28	0.137	0.009	0.379	0.007	7.003	0.595	0.134	0.025	2196	112	2069	35	2112	75	2533	439	94.3
Mubuku (Rwenzori M.)	GPS 96	29	0.141	0.003	0.405	0.005	7.834	0.246	0.103	0.008	2242	42	2194	23	2212	28	1978	138	97.9
Mubuku (Rwenzori M.)	GPS 96	30	0.142	0.009	0.408	0.008	7.978	0.641	0.110	0.020	2250	105	2207	35	2229	72	2110	356	98.1
Mubuku (Rwenzori M.)	GPS 96	31	0.143	0.009	0.400	0.008	7.748	0.646	0.101	0.018	2261	109	2170	35	2202	75	1949	339	96.0
Mubuku (Rwenzori M.)	GPS 96	32	0.146	0.011	0.437	0.009	8.637	0.815	0.114	0.023	2295	123	2338	42	2301	86	2185	410	101.8
Mubuku (Rwenzori M.)	GPS 96	33	0.153	0.011	0.393	0.008	8.270	0.767	0.072	0.014	2381	120	2136	38	2261	84	1401	265	89.7
Mubuku (Rwenzori M.)	GPS 96	34	0.155	0.006	0.427	0.006	9.089	0.491	0.132	0.017	2398	70	2291	28	2347	49	2505	301	95.6
Mubuku (Rwenzori M.)	GPS 96	35	0.155	0.007	0.433	0.006	9.329	0.512	0.139	0.018	2406	71	2318	29	2371	50	2631	322	96.3
Mubuku (Rwenzori M.)	GPS 96	36	0.156	0.009	0.429	0.008	9.261	0.714	0.113	0.020	2416	100	2302	35	2364	71	2167	355	95.3
Mubuku (Rwenzori M.)	GPS 96	37	0.158	0.003	0.437	0.005	9.467	0.220	0.099	0.004	2431	28	2336	23	2384	21	1915	75	96.1
Mubuku (Rwenzori M.)	GPS 96	38	0.161	0.011	0.435	0.009	9.663	0.860	0.120	0.023	2465	113	2327	39	2403	82	2294	410	94.4
Mubuku (Rwenzori M.)	GPS 96	39	0.161	0.009	0.424	0.007	9.339	0.667	0.048	0.008	2466	92	2278	33	2372	66	941	150	92.4
Mubuku (Rwenzori M.)	GPS 96	40	0.161	0.003	0.457	0.006	10.108	0.305	0.139	0.008	2468	35	2426	24	2445	28	2636	145	98.3
Mubuku (Rwenzori M.)	GPS 96	41	0.162	0.003	0.443	0.005	10.238	0.303	0.112	0.006	2475	34	2364	24	2457	27	2141	110	95.5
Mubuku (Rwenzori M.)	GPS 96	42	0.163	0.007	0.469	0.007	10.435	0.550	0.133	0.017	2482	67	2481	30	2474	49	2523	296	99.9
Mubuku (Rwenzori M.)	GPS 96	43	0.163	0.003	0.465	0.005	10.437	0.261	0.113	0.006	2483	31	2462	24	2474	23	2157	102	99.1
Mubuku (Rwenzori M.)	GPS 96	44	0.164	0.003	0.463	0.005	10.551	0.259	0.129	0.005	2497	28	2451	24	2484	23	2444	98	98.1
Mubuku (Rwenzori M.)	GPS 96	45	0.164	0.004	0.477	0.006	11.010	0.348	0.138	0.010	2501	40	2513	26	2524	29	2610	173	100.5
Mubuku (Rwenzori M.)	GPS 96	46	0.165	0.003	0.462	0.005	10.489	0.226	0.121	0.004	2507	25	2450	24	2479	20	2311	77	97.7
Mubuku (Rwenzori M.)	GPS 96	47	0.167	0.011	0.481	0.009	11.237	0.926	0.125	0.022	2528	104	2533	40	2543	77	2375	403	100.2
Mubuku (Rwenzori M.)	GPS 96	48	0.168	0.010	0.490	0.009	11.390	0.859	0.048	0.008	2535	95	2572	38	2556	70	948	155	101.5
Mubuku (Rwenzori M.)	GPS 96	49	0.168	0.003	0.468	0.006	10.612	0.271	0.071	0.004	2538	32	2476	24	2490	24	1382	69	97.6
Mubuku (Rwenzori M.)	GPS 96	50	0.169	0.008	0.451	0.007	10.551	0.643	0.115	0.016	2544	76	2401	31	2484	57	2208	290	94.4
Mubuku (Rwenzori M.)	GPS 96	51	0.169	0.012	0.478	0.009	11.166	0.970	0.119	0.022	2545	110	2518	41	2537	81	2276	402	98.9
Mubuku (Rwenzori M.)	GPS 96	52	0.171	0.007	0.501	0.007	11.684	0.582	0.142	0.017	2565	62	2619	30	2579	47	2675	292	102.1
Mubuku (Rwenzori M.)	GPS 96	53	0.172	0.003	0.471	0.006	11.475	0.308	0.136	0.008	2577	33	2489	25	2563	25	2582	137	96.6
Mubuku (Rwenzori M.)	GPS 96	54	0.172	0.010	0.501	0.009	11.939	0.911	0.128	0.022	2579	96	2617	39	2600	71	2438	391	101.5
Mubuku (Rwenzori M.)	GPS 96	55	0.173	0.008	0.470	0.007	11.581	0.673	0.123	0.017	2589	73	2484	31	2571	54	2342	301	95.9
Mubuku (Rwenzori M.)	GPS 96	56	0.174	0.004	0.496	0.006	12.648	0.460	0.140	0.010	2596	39	2595	27	2654	34	2650	170	100.0
Mubuku (Rwenzori M.)	GPS 96	57	0.174	0.007	0.475	0.007	12.087	0.611	0.115	0.014	2598	64	2507	30	2611	47	2207	250	96.5
Mubuku (Rwenzori M.)	GPS 96	58	0.175	0.008	0.468	0.007	11.713	0.683	0.138	0.018	2602	72	2473	31	2582	55	2618	327	95.1
Mubuku (Rwenzori M.)	GPS 96	59	0.178	0.004	0.511	0.006	12.661	0.448	0.180	0.011	2635	37	2663	27	2655	33	3339	196	101.0
Mubuku (Rwenzori M.)	GPS 96	60	0.180	0.004	0.493	0.006	12.066	0.347	0.156	0.009	2654	35	2584	26	2610	27	2922	166	97.4

A3-4 – Zircon morphology

River name		Wambabya	trib. Wambabya	trib. Nkusi	trib. Nkusi 2	Muzizi
Sample ID		GPS 58	GPS 59	GPS 64	GPS 65	GPS 66
Morphology	irregular, patchy, diffuse (auroral-light)	37	59	41	38	40
	homogeneous, locally fractured	5	5	9	2	3
	nearly homogeneous, concentric zoning recognizable	19	18	26	23	21
	irregular oscillatory zoning, locally with zones of recrystallization	7	3	9	11	14
	irregular sector zoning	5	3	3	2	3
	xenocrystic core surrounded by large thick homogenous bands or mantle	28	8	10	20	17
	light core and dark rim	0	0	0	0	0
	regular oscillatory zoning (magmatic zircon)	0	4	1	4	4
Color	pink	8	11	15	7	7
	transparent	45	66	47	52	65
	white/milky	28	13	15	19	17
	yellow/brown	19	10	23	20	11
Length/width ratio	short stubby	12	11	18	29	14
	long stubby	29	43	40	29	27
	short stalky	30	33	32	21	26
	long stalky	13	3	8	9	16
	short prismatic	7	4	0	4	11
	long prismatic	2	0	0	0	0
	needlelike	0	0	0	0	0
	broken	7	5	3	9	7

River name		Dura	trib. Dura 2	Mpanga	Dunga	Mubuku
Sample ID		GPS 70	GPS 72	GPS 73	GPS 92	GPS 96
Morphology	irregular, patchy, diffuse (auroral-light)	36	39	32	32	43
	homogeneous, locally fractured	14	1	3	13	0
	nearly homogeneous, concentric zoning recognizable	23	29	27	16	31
	irregular oscillatory zoning, locally with zones of recrystallization	15	9	4	10	14
	irregular sector zoning	2	1	1	0	0
	xenocrystic core surrounded by large thick homogenous bands or mantle	8	21	29	17	7
	light core and dark rim	2	0	4	7	4
	regular oscillatory zoning (magmatic zircon)	0	0	0	6	0
Color	pink	19	23	21	45	60
	transparent	54	25	46	35	29
	white/milky	16	15	15	12	6
	yellow/brown	11	10	18	8	5
Length/width ratio	short stubby	14	11	20	8	3
	long stubby	37	45	40	22	25
	short stalky	25	30	25	47	56
	long stalky	7	3	10	12	9
	short prismatic	3	1	2	3	1
	long prismatic	0	0	0	0	0
	needlelike	0	0	0	0	0
	broken	14	9	4	9	6

All data in percent (%)

Appendix – Chapter 4

A4-1 – Framework petrography (point-counting results)

Sample ID	Formation	MQ	PQ	Plag	K-fsp	Chert	Lmp	Lmf	Lmb	Musc	Biot	HM/Op	Total	Q_{total}	F	R
SEM 201-1	Kisegi	55	18	5	15	0	0	6	0	1	0	0	100	73	20	6
SEM 200-1	Kisegi	58	11	9	12	0	0	10	0	0	0	0	100	69	21	10
SEM 200-2	Kisegi	53	10	8	14	1	0	13	0	1	0	0	100	64	22	14
SEM 200-3	Kisegi	56	17	6	8	1	0	12	0	0	0	0	100	74	14	13
SEM 136-1	Kisegi	58	9	5	19	0	0	9	0	0	0	0	100	67	24	9
SEM 139-2	Kisegi	56	11	6	20	0	0	7	0	0	0	0	100	67	26	7
SEM 140-1	Kisegi	56	17	7	12	0	0	8	0	0	0	0	100	73	19	8
SEM 131-2	Kisegi	61	12	6	15	0	0	6	0	0	0	0	100	73	21	6
SEM 149-1	Kisegi	53	13	6	19	0	0	9	0	0	0	0	100	66	25	9
SEM 130-1	Kisegi	52	26	3	16	0	0	3	0	0	0	0	100	78	19	3
SEM 122-2	Kisegi	55	13	3	18	0	0	11	0	0	0	0	100	68	21	11
SEM 119-1	Kakara	62	19	5	7	1	0	6	0	0	0	0	100	82	12	6
SEM 87-1	Kakara	65	17	2	12	0	0	4	0	0	0	0	100	82	14	4
SEM 79-2	Oluka	52	22	5	17	0	0	4	0	0	0	0	100	74	22	4
LB-2	Oluka	67	12	5	13	0	0	2	0	1	0	0	100	79	18	2
LB-5	Oluka	71	15	5	7	1	0	1	0	1	0	0	100	87	12	1
NG1	Nyaburogo	58	17	9	11	0	0	5	0	0	0	0	100	75	20	5
GH10-1	Nyakabingo	53	7	13	14	0	0	5	0	1	1	6	100	60	27	5
GH10-2	Nyakabingo	58	15	10	9	0	0	4	0	1	1	2	100	73	19	4
GH12-3	Nyakabingo	57	7	16	11	0	0	4	1	0	0	4	100	64	27	4
D-1	Katorogo	41	41	6	8	0	0	2	0	0	1	1	100	82	15	2
D-2	Katorogo	42	43	5	8	0	0	1	0	0	0	0	100	85	13	1
D-3	Katorogo	39	40	5	11	0	0	3	0	0	0	1	100	79	16	3
JK-1	Nyabusosi	38	18	6	9	0	0	6	1	19	2	1	100	56	15	7
JK-4	Nyabusosi	56	29	6	5	0	0	1	0	2	0	1	100	85	11	1
Ameise 4	Nyabusosi	41	16	7	8	0	0	12	0	11	4	0	100	57	15	12
143-1	Nyabusosi	50	14	10	13	0	0	6	2	2	0	3	100	64	23	8
143-5	Nyabusosi	45	17	9	8	0	0	11	2	2	1	5	100	62	17	13
144-2	Nyabusosi	43	13	14	9	0	1	8	3	4	2	3	100	56	23	12

MQ = monocrystalline quartz, QP = polycrystalline quartz, Plag = plagioclase, K-fsp = potassium feldspar, Lmp = metapelite grains, Lmf = metafelsite grains, Lmb = metabasite grains, Musc = white mica, Biot = biotite, HM/Op = heavy mineral and opaques, Q_{tot} = mono- and polycrystalline quartz + chert, F = feldspar, R = rock fragments.

A4-2 – Heavy mineral analysis (point-counting results)

Sample-ID	Formation	Epidote	Amphibole	Zircon	Tourmaline	Rutile	Garnet	Sillimanite	Kyanite	Titanite	Monazite	Andalusite	Apatite	Pyroxene	Klinozoisite	Zoisite	Staurolite	ZTR	GZi	RuZi
SEM 201-1	Kisegi	9	0	41	2	9	34	1	3	1	0	0	0	0	0	0	0	52	45	18
SEM 200-1	Kisegi	6	1	58	3	7	20	2	2	0	0	0	1	0	0	0	0	68	26	11
SEM 200-2	Kisegi	6	1	69	2	9	12	0	0	1	0	0	0	0	0	0	0	80	15	12
SEM 136-1	Kisegi	7	0	73	3	10	1	1	2	<1	0	0	2	0	<1	0	0	86	1	12
SEM 149-1	Kisegi	2	4	62	2	9	15	0	5	0	1	0	0	<1	1	0	0	73	19	13
SEM 130-2	Kisegi	33	9	35	3	6	9	1	2	0	0	0	0	0	2	0	0	44	20	15
SEM 122-2	Kisegi	12	1	60	1	16	4	0	2	1	0	0	1	0	2	0	<1	77	6	21
SEM 119-1	Kakara	12	5	30	0	10	42	0	0	0	0	0	0	<1	1	0	0	40	58	25
SEM 92-1	Kakara	8	0	24	1	7	58	0	1	1	0	0	0	0	0	0	0	32	71	23
SEM 87-1	Oluka	2	1	68	5	14	2	1	5	0	1	0	0	0	0	0	1	87	3	17
SEM 78-8	Oluka	3	5	43	19	18	1	1	3	<1	0	<1	2	0	4	0	<1	80	2	30
LB-5	Oluka	15	1	33	6	9	23	9	1	0	0	0	0	0	2	1	<1	48	41	21
NG1	Nyaburogo	35	44	2	2	2	10	4	0	0	0	1	0	0	0	0	0	6	83	50
GH10-1	Nyakabingo	16	41	14	2	4	16	4	0	2	<1	0	1	<1	<1	0	0	20	53	22
FeKR-1	Nyakabingo	35	38	4	2	1	11	5	<1	1	0	0	<1	0	2	0	1	7	73	20
GH12-3	Nyakabingo	28	40	9	1	2	11	7	<1	1	0	0	0	0	1	<1	0	12	55	18
D-1	Katorogo	82	5	4	3	1	2	2	<1	0	0	0	0	0	1	0	0	8	33	20
D-2	Katorogo	78	2	10	4	1	1	2	0	<1	0	0	0	0	2	0	<1	15	9	9
D-3	Katorogo	74	6	4	5	<1	1	1	<1	0	0	0	<1	0	8	0	0	10	20	0
JK-1	Nyabusosi	62	19	6	5	1	2	2	2	1	0	0	0	0	0	0	0	12	25	14
JK-3	Nyabusosi	70	4	10	4	2	<1	5	1	1	0	0	0	0	<1	0	2	16	9	17
JK-4	Nyabusosi	62	8	4	8	<1	1	10	0	<1	0	0	0	0	6	0	0	13	20	20
Ameise 4	Nyabusosi	48	37	2	3	1	1	4	0	2	0	0	0	<1	2	0	0	6	33	33
143-1	Nyabusosi	47	28	4	5	2	2	3	1	0	0	1	2	1	4	0	0	11	33	33
143-5	Nyabusosi	49	42	2	3	0	1	2	0	0	0	0	0	0	0	0	1	5	33	0
144-1	Nyabusosi	48	32	3	4	2	1	6	0	0	0	0	0	0	4	0	0	9	25	40
144-2	Nyabusosi	47	34	2	3	2	1	2	2	<1	0	2	0	<1	4	1	0	7	33	50
144-4	Nyabusosi	44	29	4	4	3	3	4	1	1	0	<1	0	0	6	0	1	11	43	43

ZTR = zircon-tourmaline-rutile index, GZi = garnet:zircon index, RuZi = rutile:zircon index

A4-3 – Garnet chemistry (Jeol JXA-2800, Johannes Gutenberg University of Mainz)

	Sample ID	Formation	SiO_2	TiO_2	Al_2O_3	Cr_2O_3	FeO	MnO	MgO	CaO	Na_2O	Total
							mass-%					
detection limit			0.016	0.011	0.014	0.013	0.022	0.012	0.009	0.014	0.012	
1	SEM 201-1	Kisegi	38.38	0.02	20.57	0.06	14.86	13.75	2.58	7.74	0.02	97.97
2	SEM 201-1	Kisegi	37.23	0.01	20.18	0.02	24.15	14.19	1.77	0.55	0.00	98.10
3	SEM 201-1	Kisegi	38.07	0.00	20.84	0.00	29.68	1.35	6.39	1.80	0.00	98.13
4	SEM 201-1	Kisegi	38.60	0.05	20.89	0.15	24.67	1.27	6.45	6.12	0.00	98.20
5	SEM 201-1	Kisegi	39.69	0.00	21.40	0.05	23.80	0.93	11.00	1.33	0.00	98.21
6	SEM 201-1	Kisegi	39.50	0.02	21.41	0.02	23.67	0.52	10.01	3.17	0.00	98.33
7	SEM 201-1	Kisegi	37.35	0.06	20.08	0.05	17.26	21.30	0.84	1.41	0.04	98.40
8	SEM 201-1	Kisegi	40.47	0.03	21.86	0.11	17.62	1.08	13.23	4.07	0.00	98.46
9	SEM 201-1	Kisegi	39.42	0.05	21.04	0.06	23.06	0.76	7.49	6.60	0.00	98.49
10	SEM 201-1	Kisegi	38.74	0.01	21.02	0.06	28.84	0.42	8.22	1.13	0.08	98.52
11	SEM 201-1	Kisegi	40.08	0.04	21.44	0.00	23.81	0.33	11.64	1.21	0.00	98.54
12	SEM 201-1	Kisegi	37.16	0.00	20.01	0.02	25.91	14.02	0.33	1.06	0.08	98.58
13	SEM201-1	Kisegi	38.63	0.06	20.76	0.07	25.78	0.69	5.74	6.82	0.05	98.60
14	SEM201-1	Kisegi	37.18	0.00	20.06	0.02	22.99	17.65	0.43	0.27	0.02	98.61
15	SEM201-1	Kisegi	37.96	0.01	20.72	0.00	26.18	5.30	4.52	3.88	0.09	98.65
16	SEM201-1	Kisegi	40.23	0.00	21.72	0.12	22.05	0.40	13.07	1.03	0.04	98.66
17	SEM201-1	Kisegi	39.83	0.02	21.70	0.16	22.88	0.41	12.58	1.04	0.04	98.67
18	SEM201-1	Kisegi	40.13	0.00	21.67	0.09	22.46	0.42	13.08	0.87	0.04	98.76
19	SEM201-1	Kisegi	38.75	0.00	21.12	0.05	28.01	0.87	8.53	1.43	0.01	98.77
20	SEM201-1	Kisegi	38.23	0.01	19.70	0.04	25.51	2.97	2.24	10.11	0.06	98.86
21	SEM201-1	Kisegi	38.87	0.02	21.31	0.04	28.77	0.35	8.26	1.22	0.03	98.87
22	SEM201-1	Kisegi	38.79	0.11	20.79	0.04	23.25	1.64	4.39	9.86	0.00	98.88
23	SEM201-1	Kisegi	39.42	0.01	21.10	0.07	22.96	1.76	7.59	5.96	0.04	98.91
24	SEM201-1	Kisegi	38.96	0.05	22.51	0.10	22.17	0.45	12.76	2.00	0.00	99.01
25	SEM201-1	Kisegi	37.93	0.03	21.74	0.01	23.21	1.69	3.13	11.23	0.04	99.02
26	SEM201-1	Kisegi	38.03	0.11	21.89	0.10	25.39	0.59	6.82	6.10	0.00	99.03
27	SEM201-1	Kisegi	38.71	0.02	22.47	0.10	24.31	0.82	10.56	2.08	0.00	99.07
28	SEM201-1	Kisegi	37.41	0.10	21.12	0.02	28.36	0.65	3.53	7.90	0.00	99.09
29	SEM201-1	Kisegi	39.87	0.02	21.66	0.05	21.34	0.51	9.53	6.08	0.03	99.09
30	SEM201-1	Kisegi	38.48	0.03	22.20	0.00	24.75	1.47	10.70	1.48	0.03	99.15
31	SEM201-1	Kisegi	39.81	0.03	21.71	0.02	23.68	0.68	11.29	1.91	0.05	99.17
32	SEM201-1	Kisegi	39.89	0.08	21.65	0.12	23.14	0.49	11.00	2.85	0.01	99.23
33	SEM201-1	Kisegi	36.71	0.06	19.79	0.00	15.00	26.83	0.28	0.56	0.02	99.25
34	SEM201-1	Kisegi	38.50	0.15	20.70	0.03	28.23	0.73	4.56	6.37	0.00	99.27
35	SEM201-1	Kisegi	38.69	0.02	20.90	0.12	21.64	0.87	2.28	14.73	0.04	99.29
36	SEM201-1	Kisegi	38.12	0.06	20.65	0.04	29.12	2.13	4.07	5.15	0.06	99.39
37	SEM201-1	Kisegi	40.25	0.02	21.92	0.04	22.81	0.66	12.42	1.28	0.01	99.41
38	SEM201-1	Kisegi	38.98	0.00	22.54	0.12	23.69	0.74	10.68	2.68	0.00	99.43
39	SEM201-1	Kisegi	39.65	0.01	21.64	0.03	25.60	0.50	9.93	2.08	0.00	99.45
40	SEM201-1	Kisegi	38.85	0.00	21.17	0.04	29.74	1.18	6.26	2.18	0.04	99.46
41	SEM201-1	Kisegi	40.55	0.00	21.91	0.05	19.52	1.21	11.73	4.54	0.00	99.52
42	SEM201-1	Kisegi	38.72	0.02	22.43	0.02	25.42	0.44	9.44	3.04	0.01	99.55
43	SEM201-1	Kisegi	39.83	0.02	21.51	0.08	25.96	0.45	10.07	1.64	0.01	99.57
44	SEM201-1	Kisegi	40.55	0.00	21.85	0.14	21.57	0.46	12.39	2.58	0.06	99.59
45	SEM201-1	Kisegi	38.16	0.02	22.28	0.10	26.41	0.67	7.72	4.25	0.01	99.62
46	SEM201-1	Kisegi	39.62	0.00	21.54	0.06	27.07	0.34	9.89	1.02	0.09	99.63
47	SEM201-1	Kisegi	37.42	0.09	21.60	0.06	28.44	0.50	3.56	7.92	0.06	99.64
48	SEM201-1	Kisegi	38.34	0.06	20.59	0.03	30.10	1.01	2.69	6.80	0.04	99.66
49	SEM201-1	Kisegi	38.83	0.00	22.52	0.03	25.15	1.11	10.77	1.26	0.00	99.68
50	SEM201-1	Kisegi	37.54	0.00	21.20	0.07	29.60	0.87	3.64	6.87	0.00	99.80
51	SEM201-1	Kisegi	38.91	0.05	22.51	0.10	25.83	0.60	10.93	1.00	0.00	99.92
52	SEM201-1	Kisegi	39.47	0.12	21.20	0.03	25.29	0.68	6.90	6.33	0.03	100.05
53	SEM201-1	Kisegi	38.33	0.02	22.13	0.10	28.98	0.40	7.73	2.45	0.04	100.17
54	SEM92-1	Kakara	38.37	0.00	22.86	0.11	20.72	0.59	12.77	2.11	0.04	97.57
55	SEM92-1	Kakara	38.27	0.00	22.48	0.10	22.40	0.94	11.70	1.83	0.03	97.75
56	SEM92-1	Kakara	37.40	0.04	21.44	0.04	23.48	6.93	5.01	3.83	0.02	98.18
57	SEM92-1	Kakara	37.31	0.02	21.30	0.09	28.23	1.46	3.39	6.69	0.00	98.49
58	SEM92-1	Kakara	38.72	0.01	22.40	0.08	23.59	0.44	10.61	2.68	0.00	98.53
59	SEM92-1	Kakara	37.09	0.00	21.80	0.02	27.38	1.10	4.35	6.84	0.01	98.59
60	SEM92-1	Kakara	39.22	0.04	22.40	0.12	21.87	0.37	12.86	1.72	0.00	98.59
61	SEM92-1	Kakara	37.87	0.06	22.41	0.07	27.63	0.30	9.08	1.18	0.00	98.60
62	SEM92-1	Kakara	37.52	0.00	21.63	0.05	26.91	1.21	5.00	6.32	0.00	98.64
63	SEM92-1	Kakara	38.00	0.01	22.62	0.08	25.19	0.54	8.53	3.63	0.05	98.66
64	SEM92-1	Kakara	38.32	0.06	22.56	0.14	24.46	0.48	11.31	1.33	0.02	98.69
65	SEM92-1	Kakara	38.11	0.00	22.31	0.00	26.83	0.80	8.93	1.72	0.00	98.71
66	SEM92-1	Kakara	37.88	0.02	22.32	0.00	27.03	0.75	8.95	1.73	0.03	98.71
67	SEM92-1	Kakara	37.95	0.00	22.24	0.03	26.03	2.00	8.64	1.80	0.03	98.72
68	SEM92-1	Kakara	38.69	0.06	22.68	0.10	20.14	0.64	10.62	5.77	0.02	98.72
69	SEM92-1	Kakara	38.22	0.09	22.52	0.00	25.60	0.50	9.41	2.43	0.01	98.78
70	SEM92-1	Kakara	37.98	0.02	22.44	0.07	26.47	1.02	8.94	1.85	0.07	98.85

Garnet chemistry cont.

	Sample ID	Formation	SiO_2	TiO_2	Al_2O_3	Cr_2O_3	FeO	MnO	MgO	CaO	Na_2O	Total
							mass-%					
detection limit			0.016	0.011	0.014	0.013	0.022	0.012	0.009	0.014	0.012	
71	SEM92-1	Kakara	37.91	0.06	21.92	0.11	23.86	1.96	6.63	6.40	0.00	98.85
72	SEM92-1	Kakara	38.10	0.05	22.22	0.17	13.31	12.18	6.58	6.23	0.02	98.86
73	SEM92-1	Kakara	37.65	0.00	22.11	0.00	26.39	0.61	5.84	6.25	0.01	98.86
74	SEM92-1	Kakara	38.59	0.02	22.61	0.14	24.43	0.62	9.94	2.42	0.10	98.86
75	SEM92-1	Kakara	37.03	0.00	21.90	0.01	27.67	1.03	4.24	6.98	0.02	98.88
76	SEM92-1	Kakara	39.25	0.01	22.83	0.12	22.37	0.57	12.71	1.06	0.00	98.92
77	SEM92-1	Kakara	38.02	0.00	21.95	0.04	28.74	0.97	7.87	1.26	0.08	98.93
78	SEM92-1	Kakara	37.44	0.00	22.21	0.03	30.38	0.54	7.44	0.91	0.00	98.95
79	SEM92-1	Kakara	38.87	0.03	23.03	0.13	22.95	0.40	12.45	1.04	0.06	98.95
80	SEM92-1	Kakara	39.11	0.00	22.92	0.09	21.74	0.35	12.08	2.71	0.00	98.99
81	SEM92-1	Kakara	38.37	0.01	22.59	0.06	24.61	0.67	10.34	2.29	0.07	99.00
82	SEM92-1	Kakara	38.32	0.00	21.16	0.04	22.23	4.41	5.21	7.65	0.00	99.02
83	SEM92-1	Kakara	37.49	0.04	21.94	0.08	26.96	0.65	6.13	5.74	0.00	99.02
84	SEM92-1	Kakara	38.78	0.01	22.38	0.03	23.54	1.03	8.35	4.90	0.01	99.03
85	SEM92-1	Kakara	37.15	0.03	21.71	0.01	27.68	1.28	4.37	6.77	0.03	99.03
86	SEM92-1	Kakara	37.73	0.05	21.85	0.10	26.76	0.62	6.16	5.75	0.02	99.03
87	SEM92-1	Kakara	38.91	0.01	22.47	0.03	24.28	0.49	10.99	1.86	0.00	99.04
88	SEM92-1	Kakara	38.50	0.02	22.30	0.02	23.43	0.46	8.05	6.27	0.00	99.05
89	SEM92-1	Kakara	39.09	0.01	22.45	0.18	21.52	0.51	9.25	6.04	0.01	99.05
90	SEM92-1	Kakara	38.74	0.01	22.55	0.21	23.64	0.44	10.93	2.53	0.00	99.06
91	SEM92-1	Kakara	37.86	0.00	21.69	0.02	27.00	0.81	5.23	6.42	0.04	99.07
92	SEM92-1	Kakara	37.98	0.00	22.07	0.10	26.87	0.68	7.66	3.73	0.02	99.10
93	SEM92-1	Kakara	37.98	0.03	22.68	0.01	25.89	1.37	9.39	1.67	0.08	99.10
94	SEM92-1	Kakara	36.43	0.04	20.99	0.03	31.01	0.67	1.51	8.36	0.07	99.10
95	SEM92-1	Kakara	39.02	0.01	22.68	0.08	23.72	0.45	11.20	1.96	0.00	99.12
96	SEM92-1	Kakara	38.82	0.01	22.72	0.08	23.96	0.50	11.28	1.70	0.07	99.13
97	SEM92-1	Kakara	37.71	0.10	21.63	0.07	27.54	0.53	5.08	6.47	0.00	99.13
98	SEM92-1	Kakara	38.32	0.03	22.58	0.02	25.22	0.45	9.80	2.69	0.02	99.13
99	SEM92-1	Kakara	38.90	0.00	22.92	0.01	23.23	0.84	11.89	1.30	0.06	99.15
100	SEM92-1	Kakara	39.09	0.02	22.92	0.26	22.39	0.46	12.45	1.47	0.09	99.15
101	SEM92-1	Kakara	38.65	0.01	22.92	0.06	24.62	0.34	10.50	2.01	0.04	99.15
102	SEM92-1	Kakara	38.33	0.01	21.80	0.24	28.02	0.61	8.13	1.99	0.02	99.15
103	SEM92-1	Kakara	37.92	0.07	21.81	0.03	26.38	0.71	5.86	6.35	0.03	99.16
104	SEM92-1	Kakara	39.32	0.04	22.85	0.07	22.00	0.60	12.28	1.99	0.02	99.17
105	SEM92-1	Kakara	38.91	0.05	22.73	0.05	23.52	0.59	12.04	1.28	0.01	99.18
106	SEM92-1	Kakara	37.51	0.06	21.83	0.00	27.87	0.79	4.06	7.03	0.03	99.18
107	SEM92-1	Kakara	39.43	0.01	22.74	0.08	21.76	0.27	12.22	2.67	0.01	99.19
108	SEM92-1	Kakara	39.48	0.00	22.82	0.08	21.45	0.15	12.86	2.36	0.00	99.20
109	SEM92-1	Kakara	37.30	0.03	21.55	0.03	26.96	1.73	2.81	8.74	0.05	99.21
110	SEM92-1	Kakara	37.97	0.02	22.56	0.04	27.16	0.50	9.40	1.54	0.02	99.21
111	SEM92-1	Kakara	37.82	0.05	22.35	0.04	28.34	0.61	7.87	2.14	0.00	99.21
112	SEM92-1	Kakara	37.48	0.02	21.33	0.00	28.10	0.75	4.76	6.73	0.05	99.22
113	SEM92-1	Kakara	38.19	0.02	22.03	0.10	28.61	0.91	7.72	1.65	0.00	99.23
114	SEM92-1	Kakara	38.87	0.05	22.52	0.04	24.91	0.40	10.59	1.87	0.00	99.24
115	SEM92-1	Kakara	38.27	0.03	22.16	0.09	27.36	0.63	9.11	1.59	0.00	99.24
116	SEM92-1	Kakara	37.47	0.04	21.99	0.03	27.39	0.86	5.03	6.43	0.00	99.25
117	SEM92-1	Kakara	38.82	0.08	22.21	0.00	23.13	1.00	7.51	6.46	0.04	99.25
118	SEM92-1	Kakara	37.64	0.00	21.76	0.08	31.50	0.91	6.19	1.18	0.00	99.25
119	SEM92-1	Kakara	38.07	0.07	21.97	0.20	25.91	0.87	6.84	5.28	0.04	99.26
120	SEM92-1	Kakara	38.41	0.06	22.00	0.07	25.08	0.74	6.75	6.17	0.00	99.28
121	SEM92-1	Kakara	39.26	0.00	22.74	0.09	23.80	0.30	11.84	1.23	0.03	99.29
122	SEM92-1	Kakara	38.90	0.03	22.77	0.08	23.33	0.66	11.90	1.54	0.09	99.29
123	SEM92-1	Kakara	39.02	0.00	22.71	0.01	25.45	0.28	10.32	1.50	0.00	99.30
124	SEM92-1	Kakara	38.00	0.09	22.13	0.00	25.12	0.62	6.64	6.67	0.03	99.30
125	SEM92-1	Kakara	37.84	0.00	21.97	0.21	30.11	0.88	6.47	1.81	0.00	99.30
126	SEM92-1	Kakara	38.02	0.05	22.33	0.07	28.03	0.73	9.07	1.01	0.00	99.30
127	SEM92-1	Kakara	37.07	0.05	21.41	0.03	30.07	0.79	3.06	6.83	0.00	99.31
128	SEM92-1	Kakara	37.92	0.00	22.35	0.04	28.46	0.31	8.86	1.33	0.04	99.31
129	SEM92-1	Kakara	38.70	0.00	22.41	0.05	25.27	0.40	9.84	2.64	0.00	99.31
130	SEM92-1	Kakara	37.98	0.04	22.36	0.05	29.29	0.30	8.06	1.16	0.08	99.32
131	SEM92-1	Kakara	38.62	0.00	22.62	0.10	25.94	0.39	9.97	1.69	0.00	99.33
132	SEM92-1	Kakara	38.86	0.00	22.78	0.11	23.58	0.53	10.95	2.52	0.00	99.33
133	SEM92-1	Kakara	36.89	0.03	21.82	0.10	30.33	3.42	3.73	3.01	0.00	99.34
134	SEM92-1	Kakara	38.48	0.00	22.55	0.05	26.82	0.28	9.96	1.21	0.00	99.35
135	SEM92-1	Kakara	37.70	0.03	21.76	0.02	27.42	0.69	5.19	6.55	0.00	99.35
136	SEM92-1	Kakara	38.36	0.05	22.25	0.09	28.05	0.45	8.75	1.35	0.00	99.35
137	SEM92-1	Kakara	38.08	0.00	21.74	0.14	27.62	1.34	7.31	3.13	0.00	99.36
138	SEM92-1	Kakara	39.32	0.00	22.58	0.08	23.08	0.93	12.13	1.20	0.04	99.36
139	SEM92-1	Kakara	38.76	0.00	22.89	0.08	23.38	0.37	11.00	2.83	0.07	99.38
140	SEM92-1	Kakara	37.93	0.06	22.18	0.10	26.24	0.72	6.80	5.32	0.03	99.38

Garnet chemistry cont.

	Sample ID	Formation	SiO_2	TiO_2	Al_2O_3	Cr_2O_3	FeO	MnO	MgO	CaO	Na_2O	Total
							mass-%					
detection limit			**0.016**	**0.011**	**0.014**	**0.013**	**0.022**	**0.012**	**0.009**	**0.014**	**0.012**	
141	SEM92-1	Kakara	36.99	0.00	21.41	0.04	28.87	5.17	1.51	5.39	0.00	99.38
142	SEM92-1	Kakara	39.28	0.00	22.88	0.24	22.49	0.44	12.56	1.48	0.00	99.38
143	SEM92-1	Kakara	38.67	0.00	22.81	0.04	24.65	0.65	10.48	2.03	0.06	99.38
144	SEM92-1	Kakara	39.11	0.03	22.69	0.05	22.87	0.36	11.94	2.34	0.00	99.39
145	SEM92-1	Kakara	38.15	0.02	22.05	0.02	28.67	0.70	7.45	2.34	0.00	99.40
146	SEM92-1	Kakara	37.90	0.07	22.03	0.03	27.71	0.85	5.76	5.05	0.00	99.40
147	SEM92-1	Kakara	38.26	0.00	22.32	0.03	26.90	0.59	8.94	2.35	0.02	99.41
148	SEM92-1	Kakara	37.59	0.08	21.84	0.00	28.08	0.56	4.46	6.82	0.01	99.44
149	SEM92-1	Kakara	38.45	0.05	22.38	0.03	23.89	0.89	7.48	6.23	0.03	99.44
150	SEM92-1	Kakara	38.58	0.07	21.96	0.02	25.43	0.63	6.15	6.61	0.00	99.45
151	SEM92-1	Kakara	37.41	0.05	21.50	0.06	28.40	0.66	3.08	8.29	0.00	99.45
152	SEM92-1	Kakara	38.08	0.08	21.92	0.02	25.55	0.78	6.49	6.46	0.11	99.48
153	SEM92-1	Kakara	38.69	0.07	22.15	0.04	22.24	1.06	6.78	8.42	0.03	99.48
154	SEM92-1	Kakara	38.42	0.05	22.56	0.06	26.58	0.35	10.11	1.30	0.05	99.49
155	SEM92-1	Kakara	37.81	0.03	22.27	0.01	25.30	0.63	5.99	7.44	0.00	99.49
156	SEM92-1	Kakara	38.55	0.00	22.10	0.00	27.61	0.64	9.52	1.09	0.00	99.51
157	SEM92-1	Kakara	38.03	0.09	22.17	0.06	25.08	0.61	7.06	6.40	0.00	99.51
158	SEM92-1	Kakara	38.36	0.05	22.27	0.07	22.85	0.67	6.38	8.86	0.00	99.51
159	SEM92-1	Kakara	38.77	0.04	22.35	0.13	24.78	0.54	8.59	4.27	0.06	99.54
160	SEM92-1	Kakara	39.59	0.08	22.88	0.10	19.28	0.66	10.57	6.39	0.00	99.55
161	SEM92-1	Kakara	39.40	0.00	22.75	0.12	21.59	0.71	10.08	4.89	0.01	99.55
162	SEM92-1	Kakara	38.06	0.04	22.31	0.11	27.71	1.47	8.00	1.81	0.05	99.55
163	SEM92-1	Kakara	37.55	0.05	22.10	0.08	30.09	0.75	6.11	2.79	0.04	99.56
164	SEM92-1	Kakara	37.66	0.04	22.37	0.03	28.77	0.60	8.23	1.85	0.01	99.56
165	SEM92-1	Kakara	38.42	0.07	22.13	0.09	25.36	0.76	6.88	5.86	0.00	99.57
166	SEM92-1	Kakara	37.37	0.04	22.19	0.04	29.98	0.91	5.41	3.55	0.08	99.57
167	SEM92-1	Kakara	39.55	0.04	22.92	0.00	22.55	0.65	12.64	1.17	0.05	99.57
168	SEM92-1	Kakara	39.09	0.06	22.45	0.02	25.49	0.35	10.81	1.26	0.05	99.57
169	SEM92-1	Kakara	38.57	0.00	23.00	0.06	24.63	0.57	10.82	1.92	0.00	99.58
170	SEM92-1	Kakara	37.64	0.02	21.68	0.07	28.92	0.60	3.84	6.76	0.05	99.58
171	SEM92-1	Kakara	37.36	0.08	21.69	0.09	28.98	0.65	4.26	6.44	0.04	99.59
172	SEM92-1	Kakara	38.05	0.07	21.95	0.00	26.36	0.69	5.82	6.60	0.06	99.59
173	SEM92-1	Kakara	37.02	0.10	21.16	0.02	31.10	0.95	2.22	7.01	0.01	99.59
174	SEM92-1	Kakara	38.91	0.03	22.64	0.10	23.97	0.39	11.00	2.50	0.05	99.59
175	SEM92-1	Kakara	38.29	0.00	22.13	0.05	27.25	0.86	8.74	2.28	0.00	99.60
176	SEM92-1	Kakara	39.36	0.00	22.80	0.04	23.49	0.55	11.84	1.54	0.00	99.62
177	SEM92-1	Kakara	38.81	0.00	22.63	0.00	22.06	0.44	9.19	6.48	0.01	99.62
178	SEM92-1	Kakara	38.24	0.05	22.21	0.18	24.57	0.58	7.09	6.72	0.00	99.64
179	SEM92-1	Kakara	38.39	0.09	22.36	0.07	27.26	0.57	8.82	2.11	0.00	99.66
180	SEM92-1	Kakara	37.78	0.00	22.31	0.08	30.84	0.54	7.21	0.88	0.04	99.67
181	SEM92-1	Kakara	38.27	0.00	22.39	0.04	28.17	0.45	8.72	1.59	0.04	99.68
182	SEM92-1	Kakara	37.74	0.09	21.74	0.04	27.22	0.55	4.07	8.19	0.04	99.68
183	SEM92-1	Kakara	39.60	0.00	22.55	0.03	23.94	0.58	11.35	1.63	0.00	99.68
184	SEM92-1	Kakara	39.42	0.04	23.16	0.05	22.42	0.31	12.83	1.46	0.00	99.68
185	SEM92-1	Kakara	38.15	0.05	21.83	0.06	26.47	0.89	5.89	6.34	0.02	99.70
186	SEM92-1	Kakara	38.79	0.00	22.38	0.11	24.49	0.31	8.63	4.99	0.01	99.70
187	SEM92-1	Kakara	38.42	0.01	22.49	0.05	27.20	0.66	8.33	2.51	0.03	99.70
188	SEM92-1	Kakara	37.34	0.04	21.02	0.01	31.21	0.92	2.07	7.06	0.04	99.71
189	SEM92-1	Kakara	39.58	0.00	22.77	0.09	20.21	0.58	10.40	6.01	0.06	99.71
190	SEM92-1	Kakara	37.28	0.03	21.42	0.01	30.88	0.57	2.52	7.00	0.00	99.71
191	SEM92-1	Kakara	38.09	0.06	22.33	0.10	29.09	0.81	8.03	1.19	0.02	99.72
192	SEM92-1	Kakara	37.99	0.01	21.35	0.04	27.43	1.03	5.59	6.28	0.02	99.73
193	SEM92-1	Kakara	38.84	0.05	22.31	0.19	25.93	0.76	9.67	1.99	0.02	99.75
194	SEM92-1	Kakara	38.60	0.00	22.43	0.02	27.64	0.51	9.36	1.20	0.00	99.76
195	SEM92-1	Kakara	38.97	0.02	22.51	0.08	25.54	0.46	10.55	1.57	0.06	99.76
196	SEM92-1	Kakara	39.08	0.00	22.86	0.03	24.74	0.47	10.75	1.83	0.01	99.77
197	SEM92-1	Kakara	38.42	0.00	22.46	0.00	27.00	0.65	9.01	2.24	0.00	99.78
198	SEM92-1	Kakara	39.14	0.00	22.25	0.04	25.93	0.58	9.97	1.87	0.00	99.78
199	SEM92-1	Kakara	38.53	0.04	22.41	0.07	26.65	0.53	8.58	2.93	0.05	99.79
200	SEM92-1	Kakara	38.80	0.02	22.56	0.06	26.18	0.55	10.53	1.12	0.00	99.82
201	SEM92-1	Kakara	38.61	0.09	21.98	0.09	24.97	0.87	6.83	6.37	0.01	99.82
202	SEM92-1	Kakara	38.11	0.00	21.90	0.04	30.38	0.63	7.15	1.58	0.02	99.82
203	SEM92-1	Kakara	37.27	0.00	21.62	0.01	30.76	0.62	2.48	7.05	0.03	99.84
204	SEM92-1	Kakara	37.59	0.01	21.36	0.04	30.16	0.76	2.69	7.17	0.06	99.84
205	SEM92-1	Kakara	37.86	0.00	21.76	0.09	30.75	1.51	5.58	2.33	0.02	99.90
206	SEM92-1	Kakara	38.13	0.00	22.45	0.08	29.90	0.24	8.04	1.04	0.02	99.90
207	SEM92-1	Kakara	38.94	0.01	22.33	0.05	26.12	0.79	9.16	2.49	0.01	99.90
208	SEM92-1	Kakara	39.12	0.00	22.53	0.06	24.88	0.42	10.35	2.51	0.03	99.91
209	SEM92-1	Kakara	37.83	0.01	21.87	0.08	29.88	1.70	5.40	3.15	0.04	99.97
210	SEM92-1	Kakara	39.19	0.00	22.48	0.01	25.70	0.56	10.94	1.08	0.01	99.97

Garnet chemistry cont.

	Sample ID	Formation	SiO_2	TiO_2	Al_2O_3	Cr_2O_3	FeO	MnO	MgO	CaO	Na_2O	Total
							mass-%					
detection limit			**0.016**	**0.011**	**0.014**	**0.013**	**0.022**	**0.012**	**0.009**	**0.014**	**0.012**	
211	SEM92-1	Kakara	38.94	0.00	22.59	0.03	24.60	0.50	8.46	4.85	0.00	99.97
212	SEM92-1	Kakara	38.90	0.12	21.64	0.07	25.74	0.81	5.81	6.87	0.02	99.98
213	SEM92-1	Kakara	38.66	0.00	22.46	0.12	27.34	0.59	9.76	1.01	0.03	99.98
214	SEM92-1	Kakara	38.27	0.00	22.10	0.09	29.39	1.11	7.35	1.67	0.00	99.99
215	SEM92-1	Kakara	37.74	0.07	22.17	0.00	26.94	1.18	5.49	6.40	0.00	99.99
216	SEM92-1	Kakara	38.75	0.00	22.30	0.08	27.36	0.80	8.82	1.85	0.04	100.00
217	SEM92-1	Kakara	38.38	0.00	22.44	0.06	27.56	1.06	6.69	3.80	0.00	100.00
218	SEM92-1	Kakara	38.57	0.01	22.63	0.00	27.31	0.38	9.61	1.44	0.05	100.00
219	SEM92-1	Kakara	39.05	0.03	22.55	0.07	25.27	0.66	11.11	1.24	0.03	100.01
220	SEM92-1	Kakara	38.37	0.00	21.76	0.00	27.07	2.52	5.62	4.71	0.00	100.05
221	SEM92-1	Kakara	38.99	0.00	22.18	0.07	26.27	0.98	9.87	1.71	0.00	100.06
222	SEM92-1	Kakara	38.70	0.00	22.27	0.10	28.73	0.52	8.48	1.22	0.04	100.07
223	SEM92-1	Kakara	37.60	0.07	21.64	0.08	29.38	0.71	3.94	6.72	0.00	100.14
224	SEM92-1	Kakara	39.09	0.00	22.63	0.14	25.43	0.40	10.79	1.64	0.04	100.16
225	SEM92-1	Kakara	37.82	0.05	21.64	0.01	28.20	0.99	3.19	8.30	0.07	100.27
226	SEM92-1	Kakara	37.40	0.04	21.39	0.07	31.44	0.69	1.95	7.29	0.02	100.29
227	SEM92-1	Kakara	38.39	0.02	22.20	0.04	28.54	0.66	8.37	2.09	0.05	100.36
228	LB-5	Oluka	37.90	0.02	20.54	0.05	25.33	6.15	2.71	5.22	0.00	97.92
229	LB-5	Oluka	38.22	0.00	20.37	0.00	25.83	2.27	1.40	10.26	0.00	98.35
230	LB-5	Oluka	38.09	0.02	20.81	0.05	23.09	1.99	2.19	12.11	0.02	98.37
231	LB-5	Oluka	39.19	0.03	21.70	0.08	24.17	0.91	9.50	2.87	0.01	98.45
232	LB-5	Oluka	38.03	0.00	20.53	0.03	22.00	9.08	3.89	5.00	0.00	98.56
233	LB-5	Oluka	38.24	0.03	19.87	0.04	22.99	3.11	2.64	11.62	0.05	98.59
234	LB-5	Oluka	38.71	0.08	20.47	0.03	24.59	0.76	5.33	8.64	0.00	98.61
235	LB-5	Oluka	39.98	0.02	22.02	0.03	21.95	0.42	11.55	2.91	0.00	98.88
236	LB-5	Oluka	38.64	0.02	20.81	0.05	17.30	5.69	1.70	14.62	0.05	98.88
237	LB-5	Oluka	38.02	0.06	20.42	0.00	21.12	7.85	2.48	8.93	0.03	98.92
238	LB-5	Oluka	38.30	0.02	20.39	0.00	29.22	0.86	3.41	6.73	0.01	98.93
239	LB-5	Oluka	39.25	0.01	21.20	0.08	21.32	0.89	7.23	8.95	0.00	98.93
240	LB-5	Oluka	38.03	0.07	20.60	0.00	29.83	0.81	2.74	6.86	0.01	98.95
241	LB-5	Oluka	38.55	0.09	20.29	0.01	27.55	0.97	4.74	6.87	0.03	99.09
242	LB-5	Oluka	38.58	0.05	20.51	0.00	27.02	0.94	5.22	6.74	0.05	99.11
243	LB-5	Oluka	39.18	0.01	21.26	0.10	24.41	1.09	6.79	6.31	0.06	99.21
244	LB-5	Oluka	40.09	0.03	22.28	0.03	21.70	1.34	12.49	1.21	0.05	99.22
245	LB-5	Oluka	40.30	0.00	21.84	0.00	22.00	1.43	12.42	1.23	0.03	99.25
246	LB-5	Oluka	39.61	0.03	21.98	0.08	24.08	0.63	10.57	2.27	0.03	99.28
247	LB-5	Oluka	39.15	0.01	21.27	0.04	22.27	0.85	6.15	9.51	0.06	99.31
248	LB-5	Oluka	39.00	0.03	20.74	0.01	25.84	0.66	6.77	6.26	0.00	99.31
249	LB-5	Oluka	39.87	0.11	21.50	0.30	21.89	0.61	8.86	6.16	0.01	99.32
250	LB-5	Oluka	39.28	0.05	21.02	0.01	25.20	0.82	6.44	6.50	0.02	99.33
251	LB-5	Oluka	39.21	0.00	22.75	0.05	24.61	0.42	11.23	1.08	0.03	99.37
252	LB-5	Oluka	39.88	0.00	21.50	0.06	22.55	0.85	8.19	6.31	0.03	99.37
253	LB-5	Oluka	39.97	0.07	21.23	0.09	22.92	0.57	9.60	4.92	0.01	99.37
254	LB-5	Oluka	39.60	0.02	21.24	0.08	26.84	0.43	9.75	1.35	0.09	99.39
255	LB-5	Oluka	38.49	0.06	21.00	0.08	25.66	1.26	4.42	8.42	0.00	99.39
256	LB-5	Oluka	40.75	0.03	22.04	0.18	20.85	0.33	14.09	1.12	0.04	99.42
257	LB-5	Oluka	39.37	0.01	22.79	0.05	22.59	0.49	11.09	3.05	0.00	99.44
258	LB-5	Oluka	40.19	0.01	21.57	0.09	24.18	0.39	11.15	1.87	0.04	99.48
259	LB-5	Oluka	39.34	0.09	21.38	0.09	23.89	0.47	7.80	6.43	0.00	99.49
260	LB-5	Oluka	40.10	0.01	22.04	0.06	22.84	0.43	12.08	1.96	0.01	99.53
261	LB-5	Oluka	39.19	0.02	21.42	0.02	28.20	0.55	9.09	1.04	0.02	99.55
262	LB-5	Oluka	37.55	0.00	21.80	0.06	29.81	3.32	5.19	1.81	0.03	99.58
263	LB-5	Oluka	38.12	0.00	20.94	0.00	24.26	5.32	2.25	8.65	0.05	99.59
264	LB-5	Oluka	40.16	0.02	21.80	0.05	24.42	0.66	11.14	1.36	0.00	99.60
265	LB-5	Oluka	39.35	0.00	22.46	0.00	24.25	1.13	10.65	1.70	0.10	99.65
266	LB-5	Oluka	39.35	0.08	22.22	0.00	26.05	0.88	9.70	1.35	0.01	99.65
267	LB-5	Oluka	40.77	0.00	22.25	0.11	20.50	0.26	13.79	1.93	0.05	99.66
268	LB-5	Oluka	39.16	0.06	21.41	0.06	24.12	0.59	5.10	9.15	0.02	99.67
269	LB-5	Oluka	39.45	0.04	21.50	0.05	24.47	0.67	7.30	6.21	0.00	99.69
270	LB-5	Oluka	39.33	0.01	22.45	0.07	24.21	0.84	10.51	2.26	0.04	99.72
271	LB-5	Oluka	38.45	0.01	20.78	0.08	25.63	7.74	4.85	2.22	0.01	99.76
272	LB-5	Oluka	39.66	0.06	21.48	0.08	23.74	0.59	7.81	6.30	0.05	99.77
273	LB-5	Oluka	39.56	0.07	22.64	0.12	20.44	0.74	9.97	6.19	0.06	99.78
274	LB-5	Oluka	38.77	0.00	21.05	0.05	31.14	1.55	5.85	1.34	0.06	99.81
275	LB-5	Oluka	39.44	0.10	21.23	0.06	25.13	0.59	6.70	6.53	0.05	99.84
276	LB-5	Oluka	37.38	0.09	20.87	0.00	32.46	1.00	1.28	6.70	0.05	99.84
277	LB-5	Oluka	40.33	0.02	21.63	0.09	22.91	0.61	11.42	2.79	0.05	99.85
278	LB-5	Oluka	38.12	0.00	21.35	0.04	27.16	2.30	3.26	7.63	0.00	99.86
279	LB-5	Oluka	37.76	0.04	21.09	0.05	24.89	5.28	1.74	9.01	0.02	99.88
280	LB-5	Oluka	37.71	0.09	21.18	0.06	30.33	0.64	2.32	7.54	0.01	99.88

Garnet chemistry cont.

	Sample ID	Formation	SiO_2	TiO_2	Al_2O_3	Cr_2O_3	FeO	MnO	MgO	CaO	Na_2O	Total
							mass-%					
detection limit			**0.016**	**0.011**	**0.014**	**0.013**	**0.022**	**0.012**	**0.009**	**0.014**	**0.012**	
281	LB-5	Oluka	38.86	0.00	21.12	0.05	27.62	1.96	4.97	5.36	0.00	99.94
282	LB-5	Oluka	38.41	0.10	22.00	0.04	24.95	1.06	5.73	7.62	0.02	99.94
283	LB-5	Oluka	39.28	0.02	21.54	0.00	23.57	4.55	6.26	4.76	0.00	99.98
284	LB-5	Oluka	39.13	0.00	20.82	0.10	26.45	1.46	3.47	8.55	0.00	99.98
285	LB-5	Oluka	38.28	0.05	20.93	0.03	21.93	6.67	2.91	9.21	0.00	100.01
286	LB-5	Oluka	40.43	0.00	21.93	0.06	23.17	0.55	12.25	1.62	0.01	100.02
287	LB-5	Oluka	37.86	0.02	21.49	0.05	30.36	0.85	2.72	6.68	0.00	100.03
288	LB-5	Oluka	38.34	0.01	22.37	0.04	29.46	0.46	8.02	1.31	0.02	100.03
289	LB-5	Oluka	38.58	0.04	22.26	0.04	25.77	0.81	6.37	6.17	0.00	100.03
290	LB-5	Oluka	37.77	0.08	21.04	0.04	26.69	2.31	0.96	11.15	0.01	100.06
291	LB-5	Oluka	39.33	0.00	22.64	0.07	25.26	0.41	10.88	1.50	0.05	100.14
292	LB-5	Oluka	39.71	0.02	22.73	0.00	23.97	0.46	11.16	2.24	0.00	100.29
293	LB-5	Oluka	38.16	0.01	21.93	0.02	27.10	1.32	5.52	6.25	0.00	100.30
294	LB-5	Oluka	39.41	0.00	22.35	0.07	23.51	0.79	8.92	5.23	0.04	100.32
295	LB-5	Oluka	38.26	0.00	21.45	0.03	27.40	1.79	2.44	9.08	0.02	100.47
296	LB-5	Oluka	39.53	0.03	22.11	0.25	23.07	0.75	8.66	6.28	0.06	100.74
297	NG-1	Nyaburogo	37.50	0.05	20.59	0.01	22.22	7.74	1.82	9.36	0.00	99.29
298	NG-1	Nyaburogo	38.07	0.04	21.31	0.05	22.87	1.36	3.44	12.29	0.00	99.44
299	NG-1	Nyaburogo	38.89	0.07	21.59	0.13	24.52	0.72	7.70	5.95	0.05	99.62
300	NG-1	Nyaburogo	37.36	0.08	20.83	0.06	31.41	0.72	2.04	7.33	0.00	99.84
301	NG-1	Nyaburogo	38.00	0.03	21.34	0.01	26.69	0.84	3.51	9.41	0.00	99.84
302	NG-1	Nyaburogo	38.32	0.08	21.27	0.04	25.95	0.90	6.68	6.62	0.00	99.86
303	NG-1	Nyaburogo	37.93	0.04	21.24	0.01	29.24	0.87	3.20	7.34	0.00	99.87
304	NG-1	Nyaburogo	37.57	0.08	21.09	0.02	23.08	4.54	1.11	12.38	0.00	99.87
305	NG-1	Nyaburogo	38.03	0.01	22.03	0.04	25.21	0.73	4.84	9.10	0.00	100.00
306	NG-1	Nyaburogo	37.91	0.12	21.30	0.00	27.90	1.06	4.16	7.56	0.01	100.01
307	NG-1	Nyaburogo	38.59	0.08	21.78	0.08	25.89	1.17	5.77	6.65	0.02	100.03
308	NG-1	Nyaburogo	38.27	0.06	21.29	0.00	28.06	1.03	4.63	6.68	0.02	100.04
309	NG-1	Nyaburogo	37.19	0.00	20.97	0.02	24.24	10.87	1.66	5.09	0.01	100.04
310	NG-1	Nyaburogo	38.38	0.05	21.68	0.06	27.49	2.34	5.51	4.54	0.05	100.10
311	NG-1	Nyaburogo	37.66	0.00	21.07	0.03	31.41	0.83	1.94	7.13	0.03	100.10
312	NG-1	Nyaburogo	38.00	0.04	21.17	0.00	29.39	0.81	3.55	7.14	0.06	100.16
313	NG-1	Nyaburogo	37.90	0.03	20.77	0.07	29.31	2.57	2.28	7.24	0.00	100.16
314	NG-1	Nyaburogo	37.47	0.04	21.37	0.06	30.61	0.87	2.69	7.06	0.01	100.18
315	NG-1	Nyaburogo	37.64	0.03	20.93	0.05	31.50	0.79	1.79	7.46	0.01	100.19
316	NG-1	Nyaburogo	37.51	0.04	21.01	0.00	32.05	0.93	1.41	7.25	0.00	100.20
317	NG-1	Nyaburogo	37.67	0.00	21.04	0.02	30.38	0.53	2.08	8.46	0.02	100.21
318	NG-1	Nyaburogo	38.25	0.01	21.83	0.07	24.78	1.95	3.79	9.53	0.01	100.22
319	NG-1	Nyaburogo	38.10	0.06	21.54	0.05	28.13	0.90	4.69	6.71	0.04	100.22
320	NG-1	Nyaburogo	37.67	0.02	19.96	0.03	22.70	5.85	1.59	12.45	0.00	100.26
321	NG-1	Nyaburogo	38.02	0.03	21.57	0.02	28.31	1.14	4.38	6.79	0.01	100.27
322	NG-1	Nyaburogo	37.64	0.02	21.34	0.00	29.82	0.77	1.80	8.84	0.03	100.27
323	NG-1	Nyaburogo	38.48	0.03	21.57	0.01	25.81	0.98	4.89	8.50	0.00	100.27
324	NG-1	Nyaburogo	38.44	0.05	21.63	0.03	24.93	2.07	3.66	9.47	0.00	100.28
325	NG-1	Nyaburogo	37.93	0.00	21.43	0.06	26.14	3.07	3.47	8.10	0.08	100.28
326	NG-1	Nyaburogo	37.87	0.07	21.22	0.00	30.53	0.83	3.67	6.08	0.01	100.28
327	NG-1	Nyaburogo	38.45	0.00	21.48	0.00	27.67	1.29	4.94	6.44	0.02	100.29
328	NG-1	Nyaburogo	37.48	0.05	20.82	0.04	32.00	0.93	1.42	7.55	0.03	100.32
329	NG-1	Nyaburogo	37.36	0.05	20.48	0.00	32.95	0.89	1.20	7.40	0.00	100.33
330	NG-1	Nyaburogo	37.63	0.02	20.73	0.06	29.38	2.70	2.38	7.46	0.00	100.36
331	NG-1	Nyaburogo	38.81	0.04	21.87	0.05	23.15	0.95	5.65	9.82	0.01	100.36
332	NG-1	Nyaburogo	38.70	0.01	21.98	0.06	25.96	0.69	6.54	6.44	0.00	100.39
333	NG-1	Nyaburogo	38.61	0.00	21.29	0.05	25.24	0.79	4.44	9.98	0.00	100.40
334	NG-1	Nyaburogo	38.20	0.03	21.25	0.00	30.14	0.71	3.49	6.58	0.00	100.40
335	NG-1	Nyaburogo	38.50	0.02	21.77	0.03	24.72	0.38	4.88	10.11	0.00	100.41
336	NG-1	Nyaburogo	37.74	0.00	20.77	0.00	31.94	0.63	1.34	8.00	0.00	100.42
337	NG-1	Nyaburogo	37.50	0.00	20.92	0.06	32.04	1.03	1.67	7.21	0.00	100.43
338	NG-1	Nyaburogo	38.46	0.07	21.52	0.01	25.78	0.67	5.32	8.60	0.00	100.43
339	NG-1	Nyaburogo	39.04	0.01	22.03	0.06	25.35	0.76	6.87	6.31	0.00	100.44
340	NG-1	Nyaburogo	38.11	0.00	21.04	0.03	30.97	0.83	2.60	6.86	0.00	100.45
341	NG-1	Nyaburogo	38.56	0.04	21.82	0.02	27.91	0.64	4.92	6.55	0.00	100.46
342	NG-1	Nyaburogo	38.33	0.01	21.36	0.08	29.25	1.46	4.47	5.50	0.01	100.47
343	NG-1	Nyaburogo	37.62	0.06	20.82	0.01	31.97	1.27	1.97	6.74	0.00	100.47
344	NG-1	Nyaburogo	37.58	0.05	21.14	0.01	32.10	1.09	1.34	7.16	0.00	100.48
345	NG-1	Nyaburogo	38.25	0.03	21.11	0.02	29.26	0.80	4.01	7.00	0.00	100.48
346	NG-1	Nyaburogo	37.62	0.00	20.82	0.00	32.35	0.97	1.49	7.23	0.00	100.48
347	NG-1	Nyaburogo	38.78	0.00	21.91	0.08	26.22	1.50	5.79	6.17	0.04	100.49
348	NG-1	Nyaburogo	38.23	0.01	21.51	0.05	27.34	2.86	4.64	5.84	0.03	100.51
349	NG-1	Nyaburogo	38.95	0.01	21.76	0.04	25.53	1.36	6.28	6.60	0.00	100.52
350	NG-1	Nyaburogo	37.47	0.08	21.01	0.02	32.38	0.78	1.22	7.58	0.00	100.53
351	NG-1	Nyaburogo	38.20	0.06	21.38	0.00	28.74	0.69	3.68	7.79	0.00	100.54

Garnet chemistry cont.

	Sample ID	Formation	SiO_2	TiO_2	Al_2O_3	Cr_2O_3	FeO	MnO	MgO	CaO	Na_2O	Total
							mass-%					
detection limit			0.016	0.011	0.014	0.013	0.022	0.012	0.009	0.014	0.012	
352	NG-1	Nyaburogo	37.38	0.05	20.89	0.00	32.90	0.73	1.25	7.33	0.05	100.58
353	NG-1	Nyaburogo	37.71	0.08	21.16	0.00	31.75	0.98	2.10	6.80	0.00	100.58
354	NG-1	Nyaburogo	37.92	0.00	21.29	0.02	30.37	0.78	2.47	7.73	0.03	100.61
355	NG-1	Nyaburogo	38.03	0.01	21.35	0.01	27.05	0.87	2.58	10.69	0.03	100.62
356	NG-1	Nyaburogo	37.96	0.00	21.14	0.05	28.85	2.89	3.42	6.32	0.00	100.63
357	NG-1	Nyaburogo	38.18	0.00	21.48	0.03	25.47	2.19	4.03	9.26	0.00	100.64
358	NG-1	Nyaburogo	38.17	0.13	20.91	0.06	25.21	1.09	2.72	12.31	0.04	100.65
359	NG-1	Nyaburogo	38.46	0.04	21.44	0.02	24.58	1.86	3.86	10.33	0.06	100.65
360	NG-1	Nyaburogo	38.82	0.00	21.72	0.01	26.05	1.12	5.79	7.14	0.00	100.65
361	NG-1	Nyaburogo	38.70	0.11	21.64	0.08	26.76	0.94	5.53	6.83	0.08	100.67
362	NG-1	Nyaburogo	38.31	0.10	21.44	0.06	27.03	1.40	3.48	8.86	0.02	100.71
363	NG-1	Nyaburogo	38.82	0.05	21.70	0.06	24.23	0.96	4.37	10.55	0.00	100.74
364	NG-1	Nyaburogo	38.17	0.08	21.34	0.05	28.96	0.96	3.54	7.65	0.00	100.75
365	NG-1	Nyaburogo	38.16	0.00	21.60	0.01	29.84	0.94	3.92	6.31	0.00	100.78
366	NG-1	Nyaburogo	37.37	0.01	21.00	0.06	32.62	1.47	0.83	7.44	0.05	100.85
367	NG-1	Nyaburogo	38.10	0.01	21.41	0.03	28.11	1.26	3.06	8.86	0.02	100.86
368	NG-1	Nyaburogo	38.42	0.25	21.41	0.06	27.28	0.66	4.22	8.52	0.04	100.87
369	NG-1	Nyaburogo	38.03	0.00	21.20	0.00	31.37	0.87	2.55	6.84	0.00	100.87
370	NG-1	Nyaburogo	38.58	0.07	21.31	0.02	27.68	1.70	4.34	7.19	0.00	100.89
371	NG-1	Nyaburogo	37.87	0.00	21.70	0.03	34.10	0.54	4.22	2.45	0.00	100.90
372	NG-1	Nyaburogo	38.70	0.04	21.74	0.05	26.52	0.92	6.29	6.65	0.00	100.91
373	NG-1	Nyaburogo	37.74	0.09	20.99	0.01	31.86	1.16	2.22	6.87	0.00	100.94
374	NG-1	Nyaburogo	37.71	0.05	20.83	0.07	32.51	0.96	1.38	7.44	0.01	100.95
375	NG-1	Nyaburogo	38.46	0.07	21.43	0.04	28.39	1.36	3.56	7.69	0.00	101.00
376	NG-1	Nyaburogo	38.68	0.05	21.21	0.12	28.57	1.45	4.43	6.60	0.00	101.11
377	NG-1	Nyaburogo	37.94	0.09	21.04	0.08	31.32	0.79	2.28	7.59	0.10	101.23
378	GH-10	Nyakabingo	37.45	0.03	22.02	0.04	27.48	0.40	9.13	1.45	0.00	98.00
379	GH-10	Nyakabingo	37.48	0.01	21.82	0.07	23.81	1.11	6.07	7.84	0.00	98.21
380	GH-10	Nyakabingo	39.58	0.02	23.07	0.07	19.35	0.28	14.58	1.48	0.00	98.42
381	GH-10	Nyakabingo	37.80	0.08	21.96	0.01	24.29	0.59	7.01	6.72	0.02	98.47
382	GH-10	Nyakabingo	36.56	0.06	21.03	0.07	25.85	3.88	2.54	8.51	0.00	98.50
383	GH-10	Nyakabingo	37.67	0.03	21.64	0.05	24.88	0.69	4.42	9.14	0.00	98.52
384	GH-10	Nyakabingo	37.68	0.05	22.19	0.12	26.57	0.43	7.87	3.64	0.00	98.54
385	GH-10	Nyakabingo	36.67	0.09	20.75	0.07	30.74	0.82	3.04	6.42	0.01	98.60
386	GH-10	Nyakabingo	37.75	0.05	20.97	0.04	21.02	1.23	1.73	15.82	0.00	98.61
387	GH-10	Nyakabingo	37.98	0.04	22.15	0.08	26.14	0.59	7.75	3.96	0.00	98.68
388	GH-10	Nyakabingo	37.82	0.01	21.59	0.03	24.71	2.33	5.84	6.35	0.00	98.69
389	GH-10	Nyakabingo	37.33	0.04	21.59	0.08	27.13	0.60	4.42	7.51	0.00	98.69
390	GH-10	Nyakabingo	38.53	0.07	22.35	0.05	20.79	0.56	9.28	7.08	0.03	98.75
391	GH-10	Nyakabingo	38.02	0.00	22.25	0.08	27.41	0.53	9.16	1.34	0.00	98.79
392	GH-10	Nyakabingo	37.60	0.04	22.04	0.02	24.73	1.31	4.96	8.11	0.04	98.85
393	GH-10	Nyakabingo	38.20	0.01	22.08	0.28	24.34	0.73	7.22	5.99	0.00	98.85
394	GH-10	Nyakabingo	37.60	0.02	21.93	0.06	25.06	1.78	5.44	6.92	0.05	98.86
395	GH-10	Nyakabingo	37.72	0.14	21.63	0.07	25.40	0.50	6.76	6.64	0.00	98.87
396	GH-10	Nyakabingo	39.71	0.03	23.19	0.07	19.13	1.12	14.23	1.40	0.00	98.88
397	GH-10	Nyakabingo	38.84	0.07	22.49	0.18	20.89	0.43	10.11	5.91	0.04	98.95
398	GH-10	Nyakabingo	39.31	0.06	22.74	0.09	19.14	0.41	11.58	5.63	0.00	98.96
399	GH-10	Nyakabingo	37.41	0.00	21.93	0.02	26.05	1.03	5.47	7.07	0.00	98.98
400	GH-10	Nyakabingo	37.32	0.03	21.60	0.01	25.76	2.19	4.22	7.80	0.06	98.99
401	GH-10	Nyakabingo	37.97	0.02	22.08	0.14	28.27	0.54	8.37	1.62	0.01	99.02
402	GH-10	Nyakabingo	37.74	0.03	21.47	0.00	25.88	1.14	3.75	9.02	0.00	99.03
403	GH-10	Nyakabingo	37.80	0.02	21.67	0.02	27.25	0.79	5.06	6.43	0.00	99.03
404	GH-10	Nyakabingo	36.98	0.06	21.09	0.00	30.24	0.70	3.03	6.94	0.00	99.04
405	GH-10	Nyakabingo	38.31	0.01	22.12	0.04	24.70	0.68	7.54	5.59	0.06	99.05
406	GH-10	Nyakabingo	37.08	0.01	21.94	0.02	28.08	2.30	3.70	5.91	0.02	99.06
407	GH-10	Nyakabingo	38.59	0.00	22.29	0.01	22.38	0.42	7.38	7.95	0.05	99.07
408	GH-10	Nyakabingo	38.57	0.00	22.45	0.00	25.33	0.47	10.80	1.48	0.00	99.10
409	GH-10	Nyakabingo	38.20	0.02	22.14	0.00	24.83	0.72	6.98	6.22	0.00	99.11
410	GH-10	Nyakabingo	37.94	0.00	21.64	0.00	24.43	0.64	4.40	10.06	0.00	99.11
411	GH-10	Nyakabingo	39.38	0.00	23.02	0.06	21.33	0.41	12.96	1.92	0.04	99.12
412	GH-10	Nyakabingo	37.45	0.06	21.68	0.04	27.50	1.02	4.42	6.94	0.00	99.13
413	GH-10	Nyakabingo	36.26	0.00	21.39	0.05	31.30	4.57	3.04	2.43	0.09	99.13
414	GH-10	Nyakabingo	38.93	0.00	22.72	0.07	23.59	0.18	11.83	1.78	0.03	99.13
415	GH-10	Nyakabingo	37.79	0.06	21.63	0.04	25.25	0.86	4.78	8.70	0.04	99.15
416	GH-10	Nyakabingo	38.21	0.09	21.76	0.07	26.16	0.70	5.44	6.71	0.02	99.16
417	GH-10	Nyakabingo	37.24	0.02	21.86	0.05	27.45	0.78	4.42	7.29	0.07	99.19
418	GH-10	Nyakabingo	38.20	0.02	22.09	0.03	25.22	0.63	7.12	5.82	0.07	99.20
419	GH-10	Nyakabingo	37.91	0.02	22.05	0.01	28.58	0.74	7.30	2.59	0.00	99.20
420	GH-10	Nyakabingo	39.72	0.00	23.28	0.04	19.93	0.27	14.27	1.66	0.03	99.21

Garnet chemistry cont.

	Sample ID	Formation	SiO_2	TiO_2	Al_2O_3	Cr_2O_3	FeO	MnO	MgO	CaO	Na_2O	Total
							mass-%					
detection limit			**0.016**	**0.011**	**0.014**	**0.013**	**0.022**	**0.012**	**0.009**	**0.014**	**0.012**	
421	GH-10	Nyakabingo	38.02	0.00	22.13	0.02	25.09	0.58	6.87	6.44	0.06	99.21
422	GH-10	Nyakabingo	37.74	0.09	21.81	0.00	25.19	0.50	4.54	9.30	0.05	99.23
423	GH-10	Nyakabingo	37.49	0.13	21.05	0.05	29.24	1.35	3.61	6.31	0.00	99.23
424	GH-10	Nyakabingo	38.15	0.04	21.71	0.09	24.01	0.72	4.96	9.51	0.04	99.24
425	GH-10	Nyakabingo	38.39	0.05	21.80	0.02	24.28	0.47	7.69	6.53	0.02	99.24
426	GH-10	Nyakabingo	38.44	0.02	22.24	0.05	27.73	0.37	8.71	1.69	0.00	99.25
427	GH-10	Nyakabingo	37.85	0.00	21.88	0.02	24.99	0.68	3.95	9.87	0.02	99.25
428	GH-10	Nyakabingo	36.49	0.00	21.31	0.02	31.86	0.79	1.61	7.11	0.08	99.26
429	GH-10	Nyakabingo	37.97	0.00	21.67	0.03	24.38	0.58	4.55	10.05	0.04	99.27
430	GH-10	Nyakabingo	37.56	0.01	21.46	0.04	24.69	1.31	3.03	11.18	0.00	99.28
431	GH-10	Nyakabingo	37.30	0.01	21.69	0.05	31.40	0.93	4.46	3.43	0.02	99.29
432	GH-10	Nyakabingo	37.65	0.04	21.89	0.07	23.71	8.99	4.82	2.04	0.09	99.31
433	GH-10	Nyakabingo	38.37	0.03	22.23	0.05	24.40	0.68	6.43	7.10	0.03	99.31
434	GH-10	Nyakabingo	37.66	0.07	21.81	0.03	27.74	0.67	4.99	6.34	0.00	99.31
435	GH-10	Nyakabingo	37.47	0.05	21.73	0.04	31.05	0.71	6.60	1.68	0.00	99.32
436	GH-10	Nyakabingo	37.60	0.04	21.94	0.09	25.16	0.66	4.01	9.83	0.00	99.33
437	GH-10	Nyakabingo	38.45	0.00	22.45	0.06	27.36	0.34	9.53	1.15	0.00	99.33
438	GH-10	Nyakabingo	38.50	0.04	22.44	0.04	27.17	0.39	9.60	1.14	0.02	99.34
439	GH-10	Nyakabingo	37.36	0.04	22.23	0.05	31.42	0.50	6.60	1.13	0.04	99.36
440	GH-10	Nyakabingo	36.81	0.07	20.99	0.00	32.44	0.90	1.74	6.40	0.01	99.36
441	GH-10	Nyakabingo	38.09	0.08	21.80	0.17	22.22	1.86	4.86	10.22	0.06	99.36
442	GH-10	Nyakabingo	38.36	0.00	22.44	0.12	26.13	0.60	9.74	1.94	0.03	99.37
443	GH-10	Nyakabingo	38.56	0.09	22.01	0.01	25.08	0.65	6.92	6.06	0.00	99.38
444	GH-10	Nyakabingo	38.30	0.00	22.38	0.08	27.71	0.55	8.31	2.06	0.00	99.39
445	GH-10	Nyakabingo	37.67	0.03	21.57	0.06	28.11	1.16	4.57	6.18	0.05	99.40
446	GH-10	Nyakabingo	38.40	0.02	22.06	0.05	26.09	1.06	8.23	3.50	0.00	99.41
447	GH-10	Nyakabingo	38.58	0.03	22.18	0.04	24.19	0.79	7.39	6.23	0.00	99.42
448	GH-10	Nyakabingo	38.42	0.10	22.11	0.01	21.10	0.44	4.65	12.56	0.02	99.42
449	GH-10	Nyakabingo	37.97	0.01	21.81	0.04	27.11	0.96	4.22	7.30	0.01	99.43
450	GH-10	Nyakabingo	37.51	0.04	21.64	0.07	28.27	0.97	3.97	6.98	0.00	99.44
451	GH-10	Nyakabingo	36.66	0.05	21.08	0.05	32.34	0.77	1.32	7.14	0.04	99.45
452	GH-10	Nyakabingo	38.13	0.04	22.05	0.00	24.65	0.62	5.69	8.29	0.00	99.47
453	GH-10	Nyakabingo	38.71	0.00	22.67	0.00	25.87	0.71	10.01	1.51	0.00	99.48
454	GH-10	Nyakabingo	37.05	0.16	21.31	0.01	30.97	0.97	2.31	6.70	0.00	99.49
455	GH-10	Nyakabingo	38.17	0.02	21.95	0.02	25.16	0.70	6.12	7.37	0.01	99.53
456	GH-10	Nyakabingo	36.85	0.02	20.80	0.00	32.87	0.96	1.19	6.84	0.00	99.54
457	GH-10	Nyakabingo	37.70	0.03	21.68	0.04	27.40	1.14	4.89	6.67	0.00	99.55
458	GH-10	Nyakabingo	38.87	0.02	22.44	0.04	23.07	0.64	8.36	6.13	0.00	99.58
459	GH-10	Nyakabingo	37.76	0.07	21.80	0.17	26.97	1.06	5.93	5.81	0.02	99.58
460	GH-10	Nyakabingo	39.10	0.03	22.56	0.00	25.08	0.52	10.14	2.13	0.05	99.61
461	GH-10	Nyakabingo	37.99	0.05	21.90	0.01	26.35	1.24	5.70	6.33	0.05	99.62
462	GH-10	Nyakabingo	37.74	0.05	21.79	0.07	26.43	0.51	3.91	9.12	0.02	99.64
463	GH-10	Nyakabingo	37.71	0.03	21.36	0.07	26.83	0.93	2.86	9.86	0.00	99.65
464	GH-10	Nyakabingo	38.24	0.06	22.31	0.00	28.08	0.63	8.99	1.29	0.06	99.66
465	GH-10	Nyakabingo	38.13	0.12	22.04	0.07	24.54	1.24	5.94	7.54	0.05	99.66
466	GH-10	Nyakabingo	38.00	0.03	21.88	0.03	25.52	2.56	5.43	6.27	0.00	99.72
467	GH-10	Nyakabingo	38.18	0.17	21.86	0.06	26.03	0.64	6.14	6.63	0.01	99.72
468	GH-10	Nyakabingo	36.81	0.09	21.08	0.05	32.14	0.86	1.63	7.06	0.00	99.72
469	GH-10	Nyakabingo	37.65	0.04	22.20	0.06	30.44	0.98	7.11	1.18	0.06	99.73
470	GH-10	Nyakabingo	38.47	0.00	22.13	0.06	27.47	0.42	8.06	3.09	0.03	99.73
471	GH-10	Nyakabingo	37.76	0.05	21.44	0.02	28.02	1.06	4.53	6.79	0.08	99.74
472	GH-10	Nyakabingo	38.19	0.03	21.56	0.04	25.68	2.01	5.42	6.81	0.00	99.74
473	GH-10	Nyakabingo	37.81	0.00	21.75	0.05	29.30	1.61	3.77	5.43	0.03	99.75
474	GH-10	Nyakabingo	37.21	0.09	21.12	0.00	31.32	0.62	1.79	7.63	0.01	99.79
475	GH-10	Nyakabingo	37.99	0.11	22.08	0.01	26.99	0.75	5.74	6.10	0.04	99.81
476	GH-10	Nyakabingo	37.12	0.05	21.41	0.03	29.04	0.90	0.98	10.34	0.00	99.87
477	GH-10	Nyakabingo	37.80	0.03	21.73	0.00	29.16	0.78	4.02	6.48	0.00	100.00
478	GH-10	Nyakabingo	37.46	0.00	22.16	0.05	30.73	1.10	6.28	2.20	0.05	100.03
479	GH-10	Nyakabingo	37.45	0.10	21.78	0.03	28.87	1.11	3.68	6.99	0.03	100.05
480	GH-10	Nyakabingo	38.31	0.05	21.84	0.05	26.26	0.59	3.66	9.67	0.01	100.44
481	143-5	Nyabusosi	36.88	0.00	20.48	0.04	22.38	14.68	2.00	0.95	0.03	97.43
482	143-5	Nyabusosi	37.68	0.09	19.51	0.11	18.66	17.20	2.94	1.20	0.06	97.44
483	143-5	Nyabusosi	37.51	0.09	20.22	0.00	14.85	21.13	1.02	3.00	0.03	97.85
484	143-5	Nyabusosi	37.24	0.08	20.05	0.02	13.95	23.70	2.49	0.31	0.08	97.91
485	143-5	Nyabusosi	37.79	0.06	20.55	0.03	22.82	12.35	3.00	1.60	0.02	98.22
486	143-5	Nyabusosi	37.60	0.00	20.06	0.06	16.57	20.51	2.47	1.01	0.02	98.30
487	143-5	Nyabusosi	38.01	0.05	20.32	0.00	20.44	15.34	3.23	1.06	0.02	98.46
488	143-5	Nyabusosi	37.76	0.08	20.32	0.04	7.12	27.09	0.41	5.73	0.06	98.61
489	143-5	Nyabusosi	37.52	0.08	20.31	0.00	20.49	15.99	3.23	1.05	0.00	98.67
490	143-5	Nyabusosi	37.74	0.00	20.76	0.07	13.74	23.77	2.66	0.23	0.00	98.97

Garnet chemistry cont.

	Sample ID	Formation	SiO_2	TiO_2	Al_2O_3	Cr_2O_3	FeO	MnO	MgO	CaO	Na_2O	Total
							mass-%					
detection limit			0.016	0.011	0.014	0.013	0.022	0.012	0.009	0.014	0.012	
491	143-5	Nyabusosi	37.93	0.01	20.47	0.08	23.81	13.39	2.43	0.93	0.00	99.05
492	143-5	Nyabusosi	37.87	0.00	20.51	0.05	25.21	11.46	2.75	1.18	0.04	99.07
493	143-5	Nyabusosi	37.96	0.03	20.45	0.08	24.05	12.07	3.15	1.24	0.05	99.09
494	143-5	Nyabusosi	38.17	0.00	20.50	0.08	31.67	1.40	4.53	2.66	0.08	99.09
495	143-5	Nyabusosi	37.69	0.02	20.30	0.11	29.05	3.53	2.72	5.61	0.07	99.10
496	143-5	Nyabusosi	38.27	0.02	20.99	0.06	29.99	1.95	5.11	2.67	0.05	99.11
497	143-5	Nyabusosi	38.51	0.02	20.68	0.05	27.37	0.99	4.42	7.09	0.00	99.13
498	143-5	Nyabusosi	37.70	0.04	20.62	0.08	30.00	6.00	2.21	2.55	0.03	99.22
499	143-5	Nyabusosi	37.73	0.01	20.43	0.00	20.11	17.89	1.80	1.25	0.00	99.22
500	143-5	Nyabusosi	37.48	0.08	20.57	0.04	25.43	11.97	1.60	2.03	0.07	99.27
501	143-5	Nyabusosi	39.03	0.02	20.87	0.04	26.26	1.07	5.34	6.68	0.02	99.33
502	143-5	Nyabusosi	38.52	0.01	21.09	0.04	24.26	6.53	5.40	3.46	0.05	99.35
503	143-5	Nyabusosi	37.86	0.00	20.80	0.00	24.45	11.37	3.34	1.56	0.00	99.38
504	143-5	Nyabusosi	37.17	0.00	21.62	0.05	17.95	17.87	2.80	1.99	0.03	99.48
505	143-5	Nyabusosi	38.10	0.00	20.19	0.05	17.16	18.76	3.98	1.20	0.05	99.49
506	143-5	Nyabusosi	37.91	0.01	20.83	0.03	11.21	24.09	2.78	2.65	0.00	99.51
507	143-5	Nyabusosi	39.06	0.03	20.93	0.02	26.22	0.81	5.43	7.00	0.05	99.55
508	143-5	Nyabusosi	38.74	0.04	21.18	0.05	26.27	1.19	5.52	6.57	0.00	99.55
509	143-5	Nyabusosi	38.57	0.02	20.98	0.04	31.25	0.94	5.43	2.44	0.00	99.66
510	143-5	Nyabusosi	37.86	0.00	20.63	0.03	34.37	0.80	2.88	3.04	0.06	99.67
511	143-5	Nyabusosi	38.30	0.03	20.72	0.09	30.52	0.95	2.38	6.70	0.00	99.69
512	143-5	Nyabusosi	37.76	0.02	20.45	0.08	33.22	4.04	2.50	1.58	0.07	99.72
513	143-5	Nyabusosi	38.01	0.00	20.84	0.00	24.14	12.63	3.07	1.03	0.00	99.72
514	143-5	Nyabusosi	37.16	0.15	20.85	0.05	14.90	23.75	1.53	1.32	0.03	99.73
515	143-5	Nyabusosi	38.48	0.00	20.97	0.12	29.60	0.94	4.58	5.08	0.00	99.77
516	143-5	Nyabusosi	37.73	0.00	20.48	0.03	32.98	1.85	2.11	4.60	0.00	99.78
517	143-5	Nyabusosi	38.61	0.02	20.75	0.05	27.94	1.69	3.20	7.50	0.06	99.82
518	143-5	Nyabusosi	38.01	0.08	20.39	0.00	30.90	1.14	2.38	6.96	0.01	99.88
519	143-5	Nyabusosi	37.96	0.00	20.76	0.08	31.00	4.19	2.97	3.04	0.01	100.01
520	143-5	Nyabusosi	37.61	0.00	20.80	0.05	19.67	18.89	2.38	0.61	0.08	100.09
521	143-5	Nyabusosi	38.63	0.00	20.99	0.16	30.03	0.75	4.07	5.47	0.00	100.09
522	143-5	Nyabusosi	37.15	0.01	21.77	0.03	24.99	11.67	2.88	1.56	0.07	100.13
523	143-5	Nyabusosi	36.89	0.01	21.62	0.06	24.39	12.56	2.99	1.69	0.02	100.23
524	143-5	Nyabusosi	37.76	0.00	20.77	0.00	20.21	17.97	2.43	1.12	0.00	100.27
525	143-5	Nyabusosi	37.76	0.01	20.75	0.00	33.57	4.16	2.49	1.60	0.03	100.37
526	143-5	Nyabusosi	37.08	0.00	21.42	0.10	36.06	0.39	2.07	3.50	0.00	100.62
527	143-5	Nyabusosi	37.80	0.00	21.72	0.02	30.42	2.54	3.61	4.58	0.00	100.69
528	143-5	Nyabusosi	37.53	0.00	21.81	0.06	26.88	4.32	1.98	8.11	0.06	100.75

A4-4 – Rutile chemistry (Jeol JXA-2800, Johannes Gutenberg University of Mainz)

	Sample ID	Formation	Al	Si	Nb	Cr	Fe	Ti	V	Zr	Total
			ppm	ppm	ppm	ppm	ppm	ppm	ppm	ppm	
Detection limit			0.001	0.003	0.004	0.0017	0.002	0.02	0.002	0.027	
1	143-5	Nyabusosi	85	97	451	219	3176	608083	109	326	99.21
2	143-5	Nyabusosi	102	115	2816	919	1507	611081	415	421	98.31
3	143-5	Nyabusosi	52	132	3586	1698	3255	615877	315	390	98.68
4	143-5	Nyabusosi	174	116	1571	521	965	612220	935	576	100.70
5	143-5	Nyabusosi	34	132	3467	257	5150	616896	0	409	100.25
6	143-5	Nyabusosi	34	136	646	2048	2686	618514	0	778	98.73
7	143-5	Nyabusosi	57	160	1504	90	3066	611800	517	113	100.58
8	143-5	Nyabusosi	49	134	7872	159	6931	622171	0	480	100.80
9	143-5	Nyabusosi	33	130	2682	712	4103	608802	0	81	99.58
10	143-5	Nyabusosi	39	110	2245	510	1513	622112	1249	294	100.83
11	143-5	Nyabusosi	141	113	12443	363	11271	599510	86	543	98.52
12	143-5	Nyabusosi	34	92	2008	527	3602	620553	472	144	99.39
13	143-5	Nyabusosi	91	99	930	1853	576	620493	755	1414	98.53
14	143-5	Nyabusosi	87	129	1187	727	428	627207	1943	890	99.50
15	143-5	Nyabusosi	31	144	2018	1568	3971	607184	670	640	99.72

Rutile chemistry cont.

	Sample ID	Formation	Al ppm	Si ppm	Nb ppm	Cr ppm	Fe ppm	Ti ppm	V ppm	Zr ppm	Total
Detection limit			0.001	0.003	0.004	0.0017	0.002	0.02	0.002	0.027	
16	143-5	Nyabusosi	221	151	5679	686	3342	617675	193	492	98.63
17	143-5	Nyabusosi	80	123	7143	225	6236	605625	0	410	99.11
18	143-5	Nyabusosi	47	151	1237	259	2808	621212	162	151	99.57
19	143-5	Nyabusosi	42	130	8379	4894	1110	622291	769	238	100.00
20	143-5	Nyabusosi	61	129	5169	679	5545	613059	40	116	98.63
21	143-5	Nyabusosi	46	154	517	358	3028	618395	44	156	99.42
22	143-5	Nyabusosi	58	134	8005	354	7829	612040	0	232	99.79
23	143-5	Nyabusosi	131	141	10905	906	6159	599630	154	449	100.66
24	143-5	Nyabusosi	60	161	5178	229	7270	612100	0	240	100.52
25	143-5	Nyabusosi	48	154	2702	116	3970	619713	0	224	100.53
26	143-5	Nyabusosi	175	255	7025	269	3862	603107	469	664	99.06
27	143-5	Nyabusosi	3150	1339	312	499	3440	465520	195	104	99.54
28	143-5	Nyabusosi	1552	5525	493	361	2951	597771	145	261	99.28
29	143-5	Nyabusosi	132	130	10695	203	6181	608742	351	447	100.84
30	143-5	Nyabusosi	155	118	5245	751	2707	608143	164	416	99.83
31	143-5	Nyabusosi	65	127	3932	399	2347	624629	865	180	100.06
32	143-5	Nyabusosi	37	139	542	104	713	619174	155	708	100.56
33	143-5	Nyabusosi	439	537	6419	1134	4577	620972	0	155	99.32
34	143-5	Nyabusosi	35	151	10625	2587	4302	605085	164	135	99.73
35	143-5	Nyabusosi	258	171	239	177	2985	618095	2156	168	100.10
36	143-5	Nyabusosi	327	180	1136	1175	1039	608023	1101	144	100.98
37	143-5	Nyabusosi	303	673	2342	760	4372	582604	583	104	100.83
38	143-5	Nyabusosi	260	153	3942	278	4308	580685	1416	382	100.84
39	143-5	Nyabusosi	313	212	5394	415	3665	575230	1364	462	99.83
40	143-5	Nyabusosi	245	169	1213	64	4101	596992	1084	420	100.06
41	143-5	Nyabusosi	259	144	3604	372	4144	579247	1555	334	100.56
42	143-5	Nyabusosi	319	209	3485	1875	1763	580745	1133	133	99.32
43	143-5	Nyabusosi	246	148	779	308	3003	597352	974	150	99.73
44	143-5	Nyabusosi	246	201	1718	1086	2389	590817	1269	181	100.10
45	143-5	Nyabusosi	1835	371	598	395	2100	587820	1867	508	100.98
46	143-5	Nyabusosi	231	167	7722	836	5473	595793	837	95	100.83
47	143-5	Nyabusosi	304	182	2301	2257	232	597232	2015	961	100.84
48	143-5	Nyabusosi	259	171	3355	4238	1150	595433	2366	661	99.37
49	143-5	Nyabusosi	304	175	2012	3604	1741	581525	1438	281	99.85
50	143-5	Nyabusosi	278	179	12653	231	8362	579127	1536	583	100.30
51	GH-10	Nyakabingo	60	100	2649	783	427	606404	2530	1101	100.74
52	GH-10	Nyakabingo	77	92	1456	687	714	603227	3206	1096	99.36
53	GH-10	Nyakabingo	49	112	1253	1487	111	589858	7059	1441	99.09
54	GH-10	Nyakabingo	58	103	94	32	3208	606225	1318	426	99.32
55	GH-10	Nyakabingo	84	75	1151	809	634	600949	2381	816	99.83
56	GH-10	Nyakabingo	142	94	1799	759	1011	591357	2445	1268	98.59
57	GH-10	Nyakabingo	39	144	2795	639	923	595793	2928	1002	101.00
58	GH-10	Nyakabingo	75	130	931	613	571	607903	1595	884	100.46
59	GH-10	Nyakabingo	49	137	6913	637	8152	585601	1213	184	100.00
60	GH-10	Nyakabingo	229	106	5929	668	4097	610061	1101	451	97.86
61	GH-10	Nyakabingo	29	84	419	809	1810	602687	868	370	99.42
62	GH-10	Nyakabingo	95	100	2146	506	157	603467	3193	1050	98.41
63	GH-10	Nyakabingo	160	137	3587	600	1125	601728	1924	831	98.64
64	GH-10	Nyakabingo	98	85	4056	1808	1418	612939	2011	1726	99.14
65	GH-10	Nyakabingo	80	154	3701	341	3347	606524	1707	520	97.90
66	GH-10	Nyakabingo	92	110	582	482	708	605685	1856	1349	98.31
67	GH-10	Nyakabingo	79	96	1768	371	1658	598071	3418	1354	98.68
68	GH-10	Nyakabingo	44	105	645	840	255	611620	5336	973	99.00
69	GH-10	Nyakabingo	40	187	1253	366	3471	597711	905	247	99.36
70	GH-10	Nyakabingo	46	87	1965	450	3462	598551	670	470	98.41
71	GH-10	Nyakabingo	149	99	2335	365	1486	605205	1198	752	100.92
72	GH-10	Nyakabingo	56	105	2911	1520	240	611680	4455	988	98.78
73	GH-10	Nyakabingo	74	107	2069	783	7398	600769	2306	1201	100.34
74	GH-10	Nyakabingo	95	72	405	405	602	612759	3319	2426	99.33
75	GH-10	Nyakabingo	77	91	3097	1329	657	617915	1631	1417	99.56
76	GH-10	Nyakabingo	144	74	11	534	2342	621572	426	807	100.06
77	GH-10	Nyakabingo	42	74	2453	259	5088	617975	975	378	98.82
78	GH-10	Nyakabingo	126	103	1882	862	402	614917	3697	1361	99.23
79	GH-10	Nyakabingo	67	155	489	1468	309	614917	2393	153	99.60
80	GH-10	Nyakabingo	35	125	630	77	1330	612699	979	255	100.48

Rutile chemistry cont.

	Sample ID	Formation	Al ppm	Si ppm	Nb ppm	Cr ppm	Fe ppm	Ti ppm	V ppm	Zr ppm	Total
Detection limit			0.001	0.003	0.004	0.0017	0.002	0.02	0.002	0.027	
81	GH-10	Nyakabingo	117	109	510	490	3126	612100	871	377	100.33
82	GH-10	Nyakabingo	281	171	1248	184	3227	621512	350	314	100.34
83	GH-10	Nyakabingo	62	117	580	1325	263	596872	7340	3521	98.87
84	GH-10	Nyakabingo	84	104	213	2283	569	626608	1495	1542	99.35
85	GH-10	Nyakabingo	66	121	924	946	421	607663	2092	591	99.80
86	GH-10	Nyakabingo	87	103	2136	426	798	609342	2015	623	100.24
87	GH-10	Nyakabingo	126	98	2419	1833	884	612459	1797	1837	98.86
88	GH-10	Nyakabingo	149	84	2572	580	1237	600709	2423	1314	99.66
89	GH-10	Nyakabingo	51	81	2900	1084	927	621932	2756	1127	100.02
90	GH-10	Nyakabingo	60	124	472	168	2027	621692	1445	491	100.90
91	GH-10	Nyakabingo	89	94	1971	244	3364	623251	970	348	100.75
92	GH-10	Nyakabingo	108	91	2823	884	690	598910	2922	1494	100.77
93	GH-10	Nyakabingo	121	107	7322	1078	1456	604546	2565	657	99.29
94	GH-10	Nyakabingo	60	98	114	1026	1534	608503	1697	626	99.77
95	GH-10	Nyakabingo	49	84	2516	991	940	617315	3204	1503	100.23
96	GH-10	Nyakabingo	177	103	3490	874	1087	601788	2287	680	100.66
97	GH-10	Nyakabingo	104	94	211	600	488	615877	2049	615	99.29
98	GH-10	Nyakabingo	37	105	910	580	2740	630565	468	364	98.66
99	GH-10	Nyakabingo	82	89	2504	641	543	616776	1963	1480	100.18
100	GH-10	Nyakabingo	49	100	1992	1634	1492	594774	2005	1370	100.66
101	GH-10	Nyakabingo	102	86	696	354	280	626668	1882	1324	100.52
102	GH-10	Nyakabingo	96	115	921	1012	731	625709	2332	308	98.42
103	GH-10	Nyakabingo	83	119	103	959	1053	604906	1652	238	99.32
104	NG-1	Nyaburogo	303	197	1950	1885	939	584822	2456	640	100.75
105	NG-1	Nyaburogo	297	174	1501	719	904	586680	2276	801	100.77
106	NG-1	Nyaburogo	239	171	2181	606	3216	591177	981	548	99.29
107	NG-1	Nyaburogo	408	217	1492	1607	964	598491	2072	1563	98.88
108	NG-1	Nyaburogo	338	200	367	970	1108	606045	1896	1705	100.97
109	NG-1	Nyaburogo	276	189	234	1219	1170	594834	1926	312	99.99
110	NG-1	Nyaburogo	274	179	5835	1033	3531	581944	1303	372	100.43
111	NG-1	Nyaburogo	272	175	948	668	431	587160	3831	2171	99.05
112	NG-1	Nyaburogo	268	220	2382	2074	941	596692	3092	1402	98.42
113	NG-1	Nyaburogo	274	197	1151	248	1322	606404	1199	930	99.94
114	NG-1	Nyaburogo	416	309	395	1203	696	607483	2027	381	98.63
115	NG-1	Nyaburogo	389	202	1903	545	972	601968	1271	865	99.11
116	NG-1	Nyaburogo	273	167	1192	5394	495	592915	2733	1494	99.57
117	NG-1	Nyaburogo	242	189	1629	688	423	591417	3198	2430	100.00
118	NG-1	Nyaburogo	281	196	2108	3265	610	600829	1419	1579	98.63
119	NG-1	Nyaburogo	417	178	9947	117	3875	593515	1410	1061	100.34
120	NG-1	Nyaburogo	294	168	1907	1070	1922	605565	650	381	99.33
121	NG-1	Nyaburogo	266	429	1100	2046	288	589558	6700	828	99.56
122	NG-1	Nyaburogo	286	205	2212	954	1407	600229	1386	1000	100.06
123	NG-1	Nyaburogo	227	187	4723	2802	2755	578107	922	267	98.82
124	NG-1	Nyaburogo	358	188	2922	701	1073	584282	3844	1564	99.23
125	NG-1	Nyaburogo	214	158	2622	516	1604	590637	1050	457	99.60
126	NG-1	Nyaburogo	354	198	2096	126	2087	581585	2293	421	100.48
127	NG-1	Nyaburogo	219	163	1084	1018	144	581824	7657	1418	100.33
128	NG-1	Nyaburogo	247	179	1283	1179	815	607124	3433	634	100.34
129	NG-1	Nyaburogo	296	198	2277	1347	648	595973	4222	1800	98.87
130	NG-1	Nyaburogo	245	153	233	410	171	607304	4385	1413	99.35
131	NG-1	Nyaburogo	283	182	356	275	974	585002	2455	765	99.80
132	NG-1	Nyaburogo	294	182	1183	1700	941	580745	1101	809	100.24
133	NG-1	Nyaburogo	2015	2243	1905	584	1157	594174	2001	1298	98.86
134	NG-1	Nyaburogo	220	185	5266	205	4361	580985	1438	396	100.68
135	NG-1	Nyaburogo	276	203	1288	634	313	609702	2119	346	98.55
136	NG-1	Nyaburogo	278	163	977	942	4385	579786	714	529	100.10
137	NG-1	Nyaburogo	313	185	1293	2835	1851	600229	398	165	99.09
138	NG-1	Nyaburogo	252	201	1675	1182	344	594054	6034	3169	99.32
139	NG-1	Nyaburogo	276	184	575	239	335	587760	1984	1092	99.83
140	NG-1	Nyaburogo	260	186	150	347	1855	606644	1125	191	98.59
141	NG-1	Nyaburogo	332	194	385	355	1262	581884	2224	1325	99.00
142	NG-1	Nyaburogo	299	195	3165	577	1058	580206	2818	1545	99.36
143	NG-1	Nyaburogo	265	170	1775	610	762	603647	2278	1518	100.24
144	NG-1	Nyaburogo	263	168	1902	1262	167	582184	4566	1438	100.10
145	NG-1	Nyaburogo	255	190	69904	357	264	592196	3785	244	100.11

Rutile chemistry cont.

	Sample ID	Formation	Al ppm	Si ppm	Nb ppm	Cr ppm	Fe ppm	Ti ppm	V ppm	Zr ppm	Total
Detection limit			0.001	0.003	0.004	0.0017	0.002	0.02	0.002	0.027	
146	NG-1	Nyaburogo	261	182	1422	380	3433	595913	443	264	98.63
147	NG-1	Nyaburogo	292	184	16847	2547	7622	584342	1262	364	99.11
148	NG-1	Nyaburogo	279	188	2416	1184	532	599930	4951	1686	99.57
149	NG-1	Nyaburogo	283	165	3163	1102	936	589079	2072	701	100.00
150	NG-1	Nyaburogo	323	169	1552	1192	526	577928	3964	1418	98.63
151	NG-1	Nyaburogo	294	208	1451	606	167	586381	3421	899	99.42
152	NG-1	Nyaburogo	274	136	2126	1173	324	597112	4484	1846	99.79
153	LB-5	Oluka	275	187	4756	257	4547	595673	622	261	100.66
154	LB-5	Oluka	337	160	4670	2827	1913	594174	1987	736	100.52
155	LB-5	Oluka	283	249	1924	1229	1178	600469	2966	1032	100.53
156	LB-5	Oluka	312	160	2737	286	1029	596572	2469	1222	99.06
157	LB-5	Oluka	257	258	164	322	1499	597831	950	203	99.54
158	LB-5	Oluka	311	198	3252	958	2327	594774	1145	1474	99.99
159	LB-5	Oluka	314	173	3023	1128	964	592316	6010	2443	100.43
160	LB-5	Oluka	267	169	2115	661	1096	589618	1403	1559	99.05
161	LB-5	Oluka	968	3353	394	393	756	575470	1977	2265	98.42
162	LB-5	Oluka	304	134	1961	608	1618	600229	3702	775	99.94
163	LB-5	Oluka	473	174	4428	692	1241	600769	1867	1468	98.63
164	LB-5	Oluka	304	188	309	744	776	596632	1663	1302	99.11
165	LB-5	Oluka	376	190	1848	937	895	587939	2312	1125	99.57
166	LB-5	Oluka	396	158	4700	1048	2669	585721	2009	1324	100.00
167	LB-5	Oluka	356	323	1925	488	674	600169	2119	1160	98.63
168	LB-5	Oluka	282	160	487	323	1121	589678	2257	2499	98.00
169	LB-5	Oluka	255	141	1221	1909	534	600829	2478	362	100.52
170	LB-5	Oluka	235	178	40	1552	678	599330	4195	1001	100.51
171	LB-5	Oluka	307	169	2221	930	542	601908	2234	818	98.37
172	LB-5	Oluka	265	148	859	711	405	591477	2815	1198	99.93
173	LB-5	Oluka	275	199	1328	795	480	596932	3142	2551	98.92
174	LB-5	Oluka	341	173	1430	294	1359	592016	1829	2104	99.15
175	LB-5	Oluka	453	648	1764	1359	1516	592316	1188	1575	99.65
176	LB-5	Oluka	592	152	4763	1438	1076	584402	2746	1943	98.41
177	LB-5	Oluka	316	185	2359	952	1802	592736	1519	1461	98.82
178	LB-5	Oluka	287	194	388	298	194	600769	1939	861	99.19
179	LB-5	Oluka	266	143	2965	1396	398	589738	3417	1606	100.07
180	LB-5	Oluka	322	166	4437	1169	794	591177	6235	1541	99.92
181	LB-5	Oluka	294	158	1466	1348	414	603047	4694	700	99.93
182	LB-5	Oluka	320	165	566	266	3444	595014	876	531	98.46
183	LB-5	Oluka	281	149	0	754	377	595793	5579	96	98.94
184	LB-5	Oluka	347	172	2571	1072	921	600229	1450	508	99.39
185	LB-5	Oluka	283	184	3713	151	3143	602987	1181	140	99.83
186	SEM 78-8	Oluka	364	149	4738	1898	977	594654	2676	997	98.45
187	SEM 78-8	Oluka	356	157	3733	1341	330	604126	2291	954	99.24
188	SEM 78-8	Oluka	361	161	4530	707	1464	594594	2843	2135	99.61
189	SEM 78-8	Oluka	257	186	990	462	456	607723	5269	1689	100.49
190	SEM 78-8	Oluka	255	145	971	684	249	594834	2933	1301	100.34
191	SEM 78-8	Oluka	252	186	4001	498	3385	589438	1374	471	100.35
192	SEM 78-8	Oluka	205	173	126	859	283	589738	5502	1020	98.88
193	SEM 78-8	Oluka	338	146	14330	181	8162	577928	1132	289	99.36
194	SEM 78-8	Oluka	261	182	468	261	1888	595134	1008	431	99.82
195	SEM 78-8	Oluka	342	201	7613	1992	1412	593215	2591	312	100.25
196	SEM 78-8	Oluka	229	154	1067	4931	236	588539	4613	426	98.87
197	SEM 78-8	Oluka	360	220	1089	405	812	594714	1841	1743	98.25
198	SEM 78-8	Oluka	325	164	3292	413	1594	603227	1228	1076	99.77
199	SEM 78-8	Oluka	325	208	1217	1215	864	582124	6455	3223	98.46
200	SEM 78-8	Oluka	303	173	1168	1117	325	602508	5267	794	98.94
201	SEM 78-8	Oluka	316	170	2411	374	753	598671	1987	1266	99.39
202	SEM 78-8	Oluka	266	145	449	251	230	601728	3862	490	99.83
203	SEM 78-8	Oluka	316	168	226	142	944	601728	1294	1137	98.45
204	SEM 78-8	Oluka	255	153	3290	356	3290	585961	1218	486	97.82
205	SEM 78-8	Oluka	353	176	2835	500	1164	593755	2563	1651	100.35
206	SEM 78-8	Oluka	259	144	548	2059	187	589618	4681	2738	99.05
207	SEM 78-8	Oluka	290	154	1168	457	239	582004	5046	1289	98.42
208	SEM 78-8	Oluka	307	151	2545	919	505	600229	2342	1172	99.94
209	SEM 78-8	Oluka	279	179	1237	541	1607	597292	1222	361	98.63
210	SEM 78-8	Oluka	251	129	1262	1278	747	595373	2131	140	99.11

Rutile chemistry cont.

	Sample ID	Formation	Al ppm	Si ppm	Nb ppm	Cr ppm	Fe ppm	Ti ppm	V ppm	Zr ppm	Total
Detection limit			0.001	0.003	0.004	0.0017	0.002	0.02	0.002	0.027	
211	SEM 78-8	Oluka	215	155	1035	806	119	592496	5407	993	98.55
212	SEM 78-8	Oluka	260	149	798	639	703	603167	1383	482	100.10
213	SEM 78-8	Oluka	303	158	2322	950	578	591537	5946	1578	99.09
214	SEM 78-8	Oluka	393	182	5102	977	2100	586201	1961	677	99.32
215	SEM 78-8	Oluka	288	163	2359	3565	528	583623	1957	951	99.83
216	SEM 78-8	Oluka	248	198	1316	933	107	580206	9139	1871	98.59
217	SEM 78-8	Oluka	245	158	723	881	89	595553	8175	1087	99.00
218	SEM 78-8	Oluka	267	171	1956	521	532	586441	2512	1953	99.36
219	SEM 78-8	Oluka	270	158	3532	761	2308	603227	697	458	100.24
220	SEM 78-8	Oluka	323	148	2198	1060	1507	590697	4009	2550	100.10
221	SEM 78-8	Oluka	266	168	500	1674	330	598071	2228	700	100.11
222	SEM 78-8	Oluka	361	187	4477	824	1432	596452	2315	1094	98.63
223	SEM 78-8	Oluka	254	140	1469	1563	389	587999	3874	614	99.11
224	SEM 78-8	Oluka	367	166	2315	931	691	603767	1931	987	99.57
225	SEM 78-8	Oluka	294	132	933	596	1081	590397	2808	610	100.00
226	SEM 78-8	Oluka	320	214	691	659	575	589438	3351	2054	98.63
227	SEM 78-8	Oluka	350	155	821	712	421	591776	5015	1082	99.42
228	SEM 78-8	Oluka	292	167	1145	763	767	602927	2345	1437	99.79
229	SEM 78-8	Oluka	274	169	1859	910	812	601848	3082	1053	100.66
230	SEM 78-8	Oluka	331	144	29	1711	1381	600709	1787	600	100.52
231	SEM 78-8	Oluka	283	142	1648	465	1069	598191	1849	760	100.53
232	SEM 78-8	Oluka	312	184	1795	537	644	584822	2669	897	99.06
233	SEM 78-8	Oluka	247	154	671	1036	675	588719	2084	257	99.54
234	SEM 78-8	Oluka	249	171	6730	3894	1234	585062	1553	535	99.99
235	SEM 78-8	Oluka	242	173	6618	3979	1300	583623	1577	463	100.43
236	SEM 92-1	Kakara	75	143	3601	1302	328	586920	2179	1447	99.05
237	SEM 92-1	Kakara	35	138	982	970	381	596872	3271	1806	98.42
238	SEM 92-1	Kakara	56	117	6224	209	5931	595613	0	640	99.94
239	SEM 92-1	Kakara	86	102	1130	818	236	599090	2709	907	98.63
240	SEM 92-1	Kakara	68	105	384	1287	154	590817	3077	2097	99.11
241	SEM 92-1	Kakara	170	94	3947	650	1534	583623	803	1064	99.57
242	SEM 92-1	Kakara	84	118	2682	998	1177	588839	1258	2724	100.00
243	SEM 92-1	Kakara	62	94	2916	3164	1299	590577	472	432	98.63
244	SEM 92-1	Kakara	55	119	1169	393	734	599210	891	1622	98.00
245	SEM 92-1	Kakara	98	96	796	724	676	611500	688	646	100.52
246	SEM 92-1	Kakara	157	113	366	313	714	595134	517	602	99.46
247	SEM 92-1	Kakara	48	121	1453	830	199	599810	2305	1524	98.45
248	SEM 92-1	Kakara	60	94	1457	503	772	608922	1714	1113	98.68
249	SEM 92-1	Kakara	60	120	552	858	92	606344	3303	730	99.18
250	SEM 92-1	Kakara	76	100	238	419	976	602448	1074	389	97.94
251	SEM 92-1	Kakara	53	90	2642	1335	462	594114	2932	2646	98.35
252	SEM 92-1	Kakara	153	99	3042	1089	776	603587	1160	2539	98.72
253	SEM 92-1	Kakara	129	110	3146	1039	763	610541	1184	2491	99.60
254	SEM 92-1	Kakara	115	116	3790	669	1595	587760	975	1527	99.45
255	SEM 92-1	Kakara	87	136	2311	1466	3724	596033	0	545	99.46
256	SEM 92-1	Kakara	90	101	1266	825	770	591057	1822	3226	97.99
257	SEM 92-1	Kakara	76	115	1685	5567	618	595913	1515	1344	98.47
258	SEM 92-1	Kakara	248	662	1798	1257	1030	598731	222	1315	98.93
259	SEM 92-1	Kakara	17	75	46	2184	1726	591057	794	705	99.36
260	SEM 92-1	Kakara	144	99	1427	2758	792	595553	58	1465	97.98
261	SEM 92-1	Kakara	140	82	3451	870	954	589798	764	615	98.41
262	SEM 92-1	Kakara	162	101	2812	850	1140	608203	1398	1644	98.89
263	SEM 92-1	Kakara	66	95	873	1990	505	600349	1279	1156	99.37
264	SEM 92-1	Kakara	135	117	1999	785	850	608083	1892	1623	98.88
265	SEM 92-1	Kakara	248	95	11744	809	4065	601069	382	1014	99.36
266	SEM 92-1	Kakara	84	74	2260	919	413	605985	2331	1112	99.82
267	SEM 92-1	Kakara	45	95	3800	1781	501	598311	2812	368	100.25
268	SEM 92-1	Kakara	44	117	217	751	124	604786	1494	456	98.87
269	SEM 92-1	Kakara	75	99	2743	837	1078	602508	1247	1741	98.25
270	SEM 92-1	Kakara	75	110	1592	735	264	607004	2196	930	99.77
271	SEM 92-1	Kakara	168	84	7926	551	3635	593815	122	894	98.46
272	SEM 92-1	Kakara	156	87	1663	485	551	602268	751	641	98.94
273	SEM 92-1	Kakara	67	97	106	715	1197	612699	548	452	99.39
274	SEM 92-1	Kakara	112	100	1673	571	618	615457	1137	708	99.83
275	SEM 92-1	Kakara	25	81	1180	1376	1024	599810	6431	1732	98.45

Rutile chemistry cont.

	Sample ID	Formation	Al ppm	Si ppm	Nb ppm	Cr ppm	Fe ppm	Ti ppm	V ppm	Zr ppm	Total
Detection limit			0.001	0.003	0.004	0.0017	0.002	0.02	0.002	0.027	
276	SEM 92-1	Kakara	86	112	1559	870	665	611260	2718	1318	97.82
277	SEM 92-1	Kakara	102	95	1430	897	684	604426	2720	1265	100.35
278	SEM 92-1	Kakara	61	102	34	2003	602	605685	954	514	98.93
279	SEM 92-1	Kakara	55	108	793	1164	2136	608802	664	774	99.36
280	SEM 92-1	Kakara	135	108	1504	1535	523	607483	2078	1074	97.98
281	SEM 92-1	Kakara	52	124	1193	454	3119	608083	0	505	97.36
282	SEM 92-1	Kakara	73	110	988	872	249	617675	3079	1103	99.88
283	SEM 92-1	Kakara	104	99	120	1272	201	620553	424	882	97.78
284	SEM 92-1	Kakara	79	109	1557	779	190	611260	1247	678	99.30
285	SEM201-1	Kisegi	117	88	3346	1631	696	616536	1257	2888	97.99
286	SEM201-1	Kisegi	115	124	196	1810	421	614738	2444	1416	98.47
287	SEM201-1	Kisegi	241	112	5557	675	1913	608503	534	905	100.51
288	SEM201-1	Kisegi	96	124	161	1340	766	615637	827	374	98.37
289	SEM201-1	Kisegi	49	119	4656	303	5217	614078	29	419	99.93
290	SEM201-1	Kisegi	133	124	3603	764	2511	591716	1354	1312	98.92
291	SEM201-1	Kisegi	75	122	2830	2402	410	579067	2679	2626	99.15
292	SEM201-1	Kisegi	140	135	4226	2438	672	597352	724	4303	99.65
293	SEM201-1	Kisegi	39	122	387	254	844	588719	320	1013	98.41
294	SEM201-1	Kisegi	123	114	8430	96	6486	587939	0	443	98.82
295	SEM201-1	Kisegi	75	126	2194	564	673	594714	1667	418	99.19
296	SEM201-1	Kisegi	118	173	8493	136	6509	587160	0	408	100.07
297	SEM201-1	Kisegi	139	75	733	1412	854	595253	1075	1529	99.92
298	SEM201-1	Kisegi	3711	265	8307	81	5346	507126	63	1766	99.93
299	SEM201-1	Kisegi	84	112	2939	91	3601	604246	0	601	98.46
300	SEM201-1	Kisegi	789	4203	147	132	2013	296697	307	170	98.94
301	SEM201-1	Kisegi	69	73	444	361	3688	597891	0	640	99.39
302	SEM201-1	Kisegi	153	115	3769	103	3087	607963	0	190	99.83
303	SEM201-1	Kisegi	133	89	889	461	855	605325	542	1092	98.45
304	SEM201-1	Kisegi	77	109	502	1184	368	601668	2676	685	99.24
305	SEM201-1	Kisegi	46	108	290	1276	211	602328	2633	1035	99.61
306	SEM201-1	Kisegi	80	126	2631	1693	438	590337	1122	1089	100.49
307	SEM201-1	Kisegi	89	117	2878	2698	527	596992	3623	2824	100.34
308	SEM201-1	Kisegi	46	112	1052	1622	630	592616	1179	602	100.35

Appendix – Chapter 5

A5-1 – Framework petrography (point-counting results)

Sample ID	Formation	MQ	PQ	Plag	K-fsp	Chert	Lmp	Lmf	Lmb	Musc	Biot	HM/Op	Q_{total}	F	R	ln Q/F	ln Q/R
							in %										
MB-1	Museta Beds	57	25	6	9	0	0	2	1	0	0	1	82	15	2	2	4
MB-2	Museta Beds	63	19	5	10	0	0	0	0	0	0	2	82	15	1	2	5
MB-3	Museta Beds	68	16	5	9	0	0	1	0	0	0	2	84	14	1	2	4
KAI 51-1	Kaiso Village	75	11	1	11	0	0	2	0	0	0	0	86	12	2	2	4
KAI 52-1	Kaiso Village	83	10	1	5	0	0	1	0	0	0	0	93	6	1	3	4
KV-4	Kaiso Village	77	5	7	10	0	0	1	0	0	0	1	82	17	1	2	4
Kyeoro -1	Kyeoro	70	14	4	9	1	0	2	0	0	0	1	85	13	2	2	4
Kyeoro -2	Kyeoro	65	5	8	12	0	1	4	0	1	2	2	70	20	5	1	3
Cl 6m40	Warwire	54	15	10	15	0	0	0	0	1	1	1	69	25	1	1	5
Cl 9m15	Warwire	51	7	15	14	0	1	5	0	2	3	2	58	29	6	1	2
Cl 14m30	Warwire	62	7	10	14	0	0	1	0	0	0	6	69	24	1	1	4
Cl 2-1	Warwire	63	3	12	15	0	0	3	0	1	0	3	66	27	4	1	3
Cl 2-4	Warwire	53	8	14	12	0	0	6	0	0	0	5	61	26	7	1	2
SC 1/1m10	Warwire	54	13	13	12	0	0	5	0	0	0	3	67	25	5	1	3
SC 2/0m40	Warwire	56	9	15	12	0	0	3	0	1	1	3	65	27	3	1	3
SC 3/3m70	Warwire	53	10	11	15	0	0	8	1	0	0	2	63	26	9	1	2
SC 4/3m50	Warwire	45	16	14	15	0	0	6	0	1	2	0	61	29	6	1	2
SN-1	Warwire	58	13	12	9	0	0	3	1	0	2	2	71	21	4	1	3
SV1m30	Warwire	56	18	6	15	0	0	4	0	0	0	1	74	21	4	1	3
SV7m35	Warwire	71	10	6	12	0	0	1	0	0	0	0	81	18	1	2	4
SG2	Warwire	54	13	10	15	0	0	4	0	0	1	3	67	25	4	1	3
Nk-Fe-2	Nkondo	62	13	8	11	0	0	1	0	1	1	3	75	19	1	1	4
NV2-3	Nkondo	56	20	5	15	0	0	3	1	0	0	0	76	20	4	1	3
NV3-1	Nkondo	64	9	8	11	0	0	2	0	1	1	3	73	19	2	1	3
NV3-2	Nkondo	58	10	11	15	0	0	2	0	1	0	3	68	26	2	1	3

MQ = monocrystalline quartz, QP = polycrystalline quartz, Plag = plagioclase, K-fsp = potassium feldspar, Lmp = metapelite grains, Lmf = metafelsite grains, Lmb = metabasite grains, Musc = white mica, Biot = biotite, HM/Op = heavy mineral and opaques, Q_{tot} = mono- and polycrystalline quartz + chert, F = feldspar, R = rock fragments.

A5-2 – Heavy mineral analysis (point-counting results)

				transparent HM																		
Sample-ID	Formation	transparent HM (%)	Opaque minerals (%)	Epidote (%)	Amphibole (%)	Zircon (%)	Tourmaline (%)	Rutile (%)	Garnet (%)	Sillimanite (%)	Kyanite (%)	Titanite (%)	Monazite (%)	Andalusite (%)	Apatite (%)	Pyroxene (%)	Klinozoisite (%)	Zoisite (%)	Staurolite (%)	ZTR	GZi	RuZi
MB-1	Museta Beds	51	49	47	3	40	0	3	3	2	1	0	0	0	0	0	1	0	0	43	7	7
MB-2	Museta Beds	47	53	57	5	24	0	3	2	7	1	1	0	0	0	0	0	0	0	27	8	11
KAI 47-1	Kaiso Village	58	42	18	1	63	6	2	1	3	0	0	0	3	2	1	0	0	0	71	2	3
KAI 51-1	Kaiso Village	31	69	33	1	42	20	1	0	1	0	0	0	0	0	0	2	0	0	63	0	2
KAI 52-1	Kaiso Village	47	53	36	0	48	11	2	0	1	0	0	0	0	0	0	2	0	0	61	0	4
KV-4	Kaiso Village	39	61	63	2	13	4	2	6	7	1	0	0	0	1	0	0	0	1	19	32	13
Kyeoro -1	Kyeoro	71	29	46	11	5	1	3	18	8	1	1	0	2	2	0	2	0	0	9	78	38
Kyeoro -2	Kyeoro	81	19	35	38	1	1	1	10	5	2	1	0	0	3	1	2	0	0	3	91	50
Cl 6m40	Warwire	83	17	36	38	5	1	3	6	2	1	2	1	0	0	0	5	0	0	9	55	38
Cl 14m30	Warwire	88	13	29	52	3	2	1	6	3	0	2	0	0	2	0	0	0	0	6	67	25
Cl 23m75	Warwire	74	26	32	40	4	1	2	8	5	0	3	0	0	1	0	4	0	0	7	67	33
Cl 2-1	Warwire	84	16	26	45	4	1	2	12	4	1	0	0	0	1	0	4	0	0	7	75	33
Cl 2-4	Warwire	75	25	14	40	16	1	2	19	3	0	1	0	1	0	0	2	0	1	19	54	11
SC 1/1m10	Warwire	80	20	19	41	12	1	3	14	2	0	2	0	0	0	2	3	1	0	16	54	20
SC 2/0m40	Warwire	83	17	22	48	10	1	2	10	5	0	0	0	0	1	1	0	0	0	13	50	17
SC 3/3m70	Warwire	78	22	21	46	5	2	3	12	4	1	2	0	0	2	0	1	1	0	10	71	38
SC 4/3m50	Warwire	94	6	18	61	2	2	1	5	3	1	0	0	0	1	1	4	1	0	5	71	33
SN-1	Warwire	85	15	31	45	2	0	1	6	4	2	2	0	2	2	0	3	0	0	3	75	33
SG2	Warwire	59	41	33	39	4	2	2	14	5	0	0	0	0	0	0	0	1	0	8	78	33
SV7m30	Warwire	73	27	32	43	5	1	1	12	4	1	0	0	0	0	0	1	0	0	7	71	17
SV1m30	Warwire	72	28	43	32	4	0	2	12	5	0	1	0	0	0	0	1	0	0	6	75	33
LA-1	Nkondo	82	18	44	31	10	1	5	3	2	1	1	0	0	0	0	2	0	0	16	23	33
Nk-Fe-2	Nkondo	85	15	36	43	8	2	2	4	0	0	0	0	0	0	0	3	0	0	12	33	20
NV2-3	Nkondo	52	48	48	26	15	1	2	4	4	0	0	0	0	0	0	0	0	0	18	21	12
NV3-1	Nkondo	65	35	42	26	8	1	2	9	4	2	2	0	0	2	1	1	0	0	11	53	20

ZTR = zircon-tourmaline-rutile index, GZi = garnet:zircon index, RuZi = rutile:zircon index

A5-3 – Garnet chemistry (Jeol JXA-2800, Johannes Gutenberg University of Mainz)

	Sample ID	Formation	SiO2	TiO2	Al2O3	Cr2O3	FeO	MnO	MgO	CaO	Na2O	Total
							mass-%					
detection limit			0,016	0,011	0,014	0,013	0,022	0,012	0,009	0,014	0,012	
1	NV3-2	Nkondo	38,15	0,01	20,01	0,03	24,37	1,31	2,66	12,06	0,00	98,59
2	NV3-2	Nkondo	37,72	0,02	20,41	0,01	31,65	1,33	3,86	3,60	0,00	98,60
3	NV3-2	Nkondo	39,11	0,02	21,02	0,19	23,79	0,57	7,65	6,22	0,07	98,63
4	NV3-2	Nkondo	38,21	0,01	20,22	0,04	19,95	5,40	2,53	12,27	0,02	98,66
5	NV3-2	Nkondo	38,73	0,04	20,60	0,10	25,79	1,11	6,17	6,16	0,04	98,73
6	NV3-2	Nkondo	37,63	0,07	19,95	0,05	31,76	0,79	1,51	7,02	0,00	98,78
7	NV3-2	Nkondo	37,94	0,14	20,25	0,08	24,88	3,08	1,52	10,90	0,01	98,80
8	NV3-2	Nkondo	38,18	0,22	20,09	0,03	26,56	2,66	3,85	7,30	0,00	98,89
9	NV3-2	Nkondo	37,17	0,03	19,84	0,06	32,17	1,14	1,10	7,34	0,05	98,90
10	NV3-2	Nkondo	37,80	0,03	20,03	0,00	31,53	1,49	1,60	6,47	0,00	98,95
11	NV3-2	Nkondo	39,07	0,01	21,12	0,04	24,24	0,85	7,41	6,25	0,02	99,01
12	NV3-2	Nkondo	37,88	0,00	20,77	0,02	31,83	0,96	4,27	3,28	0,00	99,01
13	NV3-2	Nkondo	38,23	0,10	19,12	0,04	22,45	1,57	1,31	16,17	0,05	99,04
14	NV3-2	Nkondo	38,69	0,07	20,15	0,08	26,44	0,93	5,28	7,42	0,00	99,06
15	NV3-2	Nkondo	39,10	0,01	21,43	0,05	27,16	0,33	9,90	1,12	0,00	99,11
16	NV3-2	Nkondo	39,53	0,23	20,83	0,11	22,71	0,89	7,16	7,71	0,02	99,18
17	NV3-2	Nkondo	39,29	0,00	21,56	0,00	19,86	1,25	7,62	9,58	0,03	99,19
18	NV3-2	Nkondo	38,38	0,01	20,90	0,07	29,30	0,73	5,20	4,61	0,00	99,20
19	NV3-2	Nkondo	38,54	0,02	20,94	0,08	23,03	0,85	2,95	12,85	0,00	99,26
20	NV3-2	Nkondo	38,16	0,04	20,29	0,01	30,29	0,76	2,63	7,07	0,03	99,29
21	NV3-2	Nkondo	38,03	0,07	20,89	0,01	29,09	0,72	3,29	7,20	0,00	99,30
22	NV3-2	Nkondo	38,31	0,04	20,41	0,01	28,45	0,86	4,08	7,16	0,00	99,32
23	NV3-2	Nkondo	39,65	0,01	21,66	0,16	25,84	0,46	10,40	1,12	0,03	99,33
24	NV3-2	Nkondo	38,02	0,10	20,05	0,01	31,63	0,87	1,56	7,09	0,02	99,35
25	NV3-2	Nkondo	38,39	0,00	20,76	0,04	30,05	0,94	5,14	4,06	0,00	99,37
26	NV3-2	Nkondo	39,78	0,03	21,73	0,12	23,83	0,78	11,32	1,80	0,00	99,39
27	NV3-2	Nkondo	39,15	0,08	21,12	0,07	22,89	0,58	4,27	11,20	0,03	99,39
28	NV3-2	Nkondo	39,66	0,04	21,44	0,03	24,13	0,65	7,42	6,04	0,02	99,42
29	NV3-2	Nkondo	39,56	0,00	21,40	0,07	25,94	0,47	10,01	1,99	0,00	99,44
30	NV3-2	Nkondo	38,59	0,05	20,81	0,01	26,70	0,68	4,50	8,12	0,00	99,46
31	NV3-2	Nkondo	38,50	0,08	20,49	0,05	28,74	0,81	3,83	7,02	0,00	99,52
32	NV3-2	Nkondo	38,62	0,04	21,15	0,06	27,15	1,06	5,91	5,53	0,03	99,54
33	NV3-2	Nkondo	39,37	0,00	21,15	0,04	27,14	1,23	9,09	1,54	0,00	99,56
34	NV3-2	Nkondo	38,41	0,03	20,63	0,03	26,12	1,04	3,52	9,73	0,05	99,56
35	NV3-2	Nkondo	39,04	0,00	21,14	0,09	26,04	0,91	6,56	5,78	0,01	99,57
36	NV3-2	Nkondo	37,67	0,07	19,83	0,03	32,39	1,16	1,08	7,35	0,01	99,59
37	NV3-2	Nkondo	38,17	0,08	20,65	0,00	29,78	0,72	3,58	6,61	0,00	99,59
38	NV3-2	Nkondo	39,33	0,00	21,40	0,04	26,77	1,34	8,86	1,85	0,01	99,60
39	NV3-2	Nkondo	39,70	0,06	21,02	0,04	21,96	0,41	6,60	9,79	0,03	99,61
40	NV3-2	Nkondo	38,24	0,01	20,19	0,10	25,83	2,08	1,87	11,25	0,04	99,62
41	NV3-2	Nkondo	38,68	0,10	20,73	0,04	27,48	0,91	4,76	6,92	0,00	99,62
42	NV3-2	Nkondo	38,69	0,04	20,76	0,00	25,88	1,71	4,36	8,20	0,01	99,65
43	NV3-2	Nkondo	38,78	0,05	21,09	0,00	27,13	0,91	4,88	6,78	0,03	99,66
44	NV3-2	Nkondo	39,09	0,00	21,46	0,09	28,53	0,83	8,22	1,44	0,00	99,66
45	NV3-2	Nkondo	38,96	0,05	21,01	0,07	23,74	0,74	4,55	10,54	0,02	99,67
46	NV3-2	Nkondo	37,99	0,03	20,24	0,03	31,68	0,96	1,29	7,47	0,00	99,69
47	NV3-2	Nkondo	37,82	0,03	20,18	0,01	32,24	0,73	1,41	7,28	0,00	99,69
48	NV3-2	Nkondo	38,91	0,08	21,02	0,08	26,33	1,01	5,67	6,59	0,00	99,70
49	NV3-2	Nkondo	39,18	0,02	21,57	0,05	23,84	0,70	7,55	6,77	0,05	99,73
50	NV3-2	Nkondo	39,96	0,02	21,66	0,07	25,09	0,32	11,07	1,54	0,02	99,75
51	NV3-2	Nkondo	38,30	0,11	20,52	0,04	29,54	0,67	3,61	6,90	0,06	99,75
52	NV3-2	Nkondo	38,33	0,02	20,81	0,04	29,05	1,50	3,22	6,71	0,08	99,76
53	NV3-2	Nkondo	40,23	0,05	21,79	0,02	24,64	0,32	10,08	2,60	0,04	99,78
54	NV3-2	Nkondo	38,93	0,00	21,12	0,06	23,56	0,63	3,83	11,66	0,01	99,80
55	NV3-2	Nkondo	39,20	0,05	21,21	0,02	24,37	0,72	7,08	7,11	0,06	99,82
56	NV3-2	Nkondo	37,86	0,03	20,48	0,01	32,26	1,06	0,98	7,15	0,02	99,85
57	NV3-2	Nkondo	39,18	0,06	21,39	0,07	28,11	0,90	8,26	1,88	0,00	99,86
58	NV3-2	Nkondo	38,75	0,08	20,73	0,05	27,91	0,90	5,09	6,36	0,03	99,90
59	NV3-2	Nkondo	39,97	0,01	21,75	0,09	24,51	0,51	11,05	1,97	0,03	99,90
60	NV3-2	Nkondo	38,98	0,05	20,98	0,00	27,13	0,61	5,33	6,82	0,01	99,91
61	NV3-2	Nkondo	39,04	0,06	21,10	0,03	27,16	0,65	5,39	6,49	0,01	99,92
62	NV3-2	Nkondo	40,10	0,00	21,90	0,08	23,95	0,46	11,54	1,90	0,00	99,92
63	NV3-2	Nkondo	39,38	0,02	20,71	0,08	26,55	1,11	6,91	5,16	0,01	99,93
64	NV3-2	Nkondo	37,49	0,00	20,46	0,00	35,30	0,27	1,10	5,34	0,00	99,95
65	NV3-2	Nkondo	38,56	0,03	20,55	0,02	27,96	0,70	1,51	10,64	0,00	99,98
66	NV3-2	Nkondo	39,97	0,01	21,85	0,12	24,64	0,53	10,23	2,57	0,07	99,98
67	NV3-2	Nkondo	38,46	0,05	21,09	0,00	28,02	0,66	4,58	7,09	0,03	99,99
68	NV3-2	Nkondo	39,18	0,10	20,81	0,04	24,92	1,02	4,52	9,40	0,00	99,99
69	NV3-2	Nkondo	39,41	0,00	21,65	0,05	27,55	0,36	10,03	0,93	0,02	100,00
70	NV3-2	Nkondo	38,04	0,07	20,91	0,03	29,83	1,07	3,36	6,69	0,00	100,00

Garnet chemistry cont.

	Sample ID	Formation	SiO2	TiO2	Al2O3	Cr2O3	FeO	MnO	MgO	CaO	Na2O	Total
							mass-%					
detection limit			0,016	0,011	0,014	0,013	0,022	0,012	0,009	0,014	0,012	
71	NV3-2	Nkondo	39,43	0,07	21,41	0,03	27,24	0,67	9,20	1,93	0,03	100,01
72	NV3-2	Nkondo	38,67	0,03	21,21	0,04	30,51	1,39	5,48	2,72	0,01	100,06
73	NV3-2	Nkondo	39,13	0,01	21,26	0,07	27,14	1,44	6,56	4,46	0,02	100,10
74	NV3-2	Nkondo	38,13	0,00	20,51	0,02	31,66	0,86	1,88	7,03	0,01	100,10
75	NV3-2	Nkondo	40,19	0,00	21,87	0,07	22,62	2,39	11,82	1,08	0,06	100,11
76	NV3-2	Nkondo	38,02	0,00	20,63	0,03	31,70	0,83	1,72	7,11	0,07	100,12
77	NV3-2	Nkondo	38,74	0,08	20,85	0,06	26,58	0,69	2,67	10,38	0,06	100,12
78	NV3-2	Nkondo	38,78	0,19	20,75	0,08	23,46	5,63	2,81	8,46	0,01	100,17
79	NV3-2	Nkondo	40,40	0,01	21,97	0,09	23,83	0,37	11,76	1,77	0,01	100,20
80	NV3-2	Nkondo	38,60	0,05	20,69	0,03	28,86	0,72	3,48	7,78	0,00	100,22
81	NV3-2	Nkondo	39,42	0,02	21,37	0,07	25,23	0,76	6,34	7,02	0,07	100,30
82	NV3-2	Nkondo	38,96	0,00	21,08	0,04	24,53	5,03	5,25	5,43	0,00	100,32
83	NV3-2	Nkondo	38,78	0,03	21,03	0,07	28,15	0,70	3,27	8,39	0,03	100,44
84	NV3-2	Nkondo	39,11	0,01	21,47	0,02	29,90	0,84	7,47	1,64	0,04	100,49
85	NV3-2	Nkondo	40,01	0,07	21,50	0,04	26,05	0,77	9,44	2,61	0,01	100,50
86	SC1-1m10	Warwire	38,92	0,01	22,35	0,09	22,81	0,36	8,68	6,44	0,01	99,67
87	SC1-1m10	Warwire	38,36	0,05	21,36	0,00	24,74	0,71	5,32	8,48	0,00	99,02
88	SC1-1m10	Warwire	37,88	0,00	21,08	0,00	26,14	1,40	5,43	7,04	0,06	99,03
89	SC1-1m10	Warwire	37,86	0,04	21,95	0,02	25,41	0,51	4,95	8,34	0,04	99,12
90	SC1-1m10	Warwire	38,62	0,07	22,12	0,00	22,64	0,71	8,28	6,72	0,00	99,15
91	SC1-1m10	Warwire	40,13	0,03	23,01	0,09	19,80	0,36	13,92	1,90	0,00	99,24
92	SC1-1m10	Warwire	37,86	0,19	21,45	0,00	23,59	1,22	3,76	11,23	0,00	99,29
93	SC1-1m10	Warwire	38,21	0,05	21,26	0,07	21,61	1,66	1,98	14,47	0,02	99,32
94	SC1-1m10	Warwire	37,52	0,02	21,07	0,03	28,48	2,14	3,61	6,37	0,11	99,34
95	SC1-1m10	Warwire	37,69	0,01	21,58	0,01	26,15	0,99	3,09	9,81	0,04	99,37
96	SC1-1m10	Warwire	38,22	0,00	21,58	0,01	24,77	1,13	3,76	9,93	0,00	99,40
97	SC1-1m10	Warwire	36,98	0,03	21,25	0,07	31,63	0,68	1,89	6,86	0,01	99,40
98	SC1-1m10	Warwire	37,88	0,02	20,84	0,00	21,40	9,50	2,28	7,45	0,06	99,42
99	SC1-1m10	Warwire	39,39	0,02	22,85	0,10	22,72	0,37	11,92	2,02	0,05	99,45
100	SC1-1m10	Warwire	38,10	0,00	21,26	0,07	26,16	0,85	4,56	8,44	0,01	99,45
101	SC1-1m10	Warwire	38,43	0,04	21,75	0,04	26,61	0,62	5,47	6,52	0,00	99,48
102	SC1-1m10	Warwire	37,89	0,07	21,38	0,00	26,44	0,89	4,90	7,92	0,00	99,49
103	SC1-1m10	Warwire	38,19	0,04	21,85	0,06	26,38	0,72	6,16	6,09	0,01	99,50
104	SC1-1m10	Warwire	37,89	0,02	21,23	0,06	26,90	0,91	5,24	7,25	0,00	99,50
105	SC1-1m10	Warwire	39,90	0,06	22,77	0,07	18,25	0,49	10,23	7,75	0,00	99,52
106	SC1-1m10	Warwire	37,15	0,01	21,06	0,07	31,11	0,98	2,45	6,65	0,03	99,52
107	SC1-1m10	Warwire	37,22	0,02	21,28	0,03	30,80	0,81	2,27	7,02	0,07	99,52
108	SC1-1m10	Warwire	37,98	0,00	21,58	0,04	26,71	0,94	4,17	8,09	0,05	99,56
109	SC1-1m10	Warwire	38,47	0,00	22,01	0,05	28,33	0,91	8,25	1,53	0,03	99,58
110	SC1-1m10	Warwire	37,91	0,00	21,61	0,07	27,74	0,57	3,62	8,07	0,00	99,58
111	SC1-1m10	Warwire	38,68	0,02	22,20	0,05	24,31	0,56	7,52	6,26	0,00	99,60
112	SC1-1m10	Warwire	37,93	0,03	21,48	0,01	29,95	0,73	5,05	4,41	0,02	99,61
113	SC1-1m10	Warwire	36,82	0,07	21,00	0,00	32,51	0,73	0,91	7,52	0,07	99,63
114	SC1-1m10	Warwire	38,05	0,07	21,78	0,07	27,31	1,18	4,96	6,17	0,04	99,63
115	SC1-1m10	Warwire	38,76	0,02	22,16	0,12	24,28	0,68	7,47	6,11	0,03	99,64
116	SC1-1m10	Warwire	37,79	0,10	21,32	0,02	29,52	1,06	3,16	6,59	0,08	99,64
117	SC1-1m10	Warwire	38,31	0,07	21,70	0,08	27,03	0,74	5,02	6,70	0,00	99,65
118	SC1-1m10	Warwire	39,96	0,00	22,82	0,06	21,99	0,37	13,05	1,44	0,00	99,69
119	SC1-1m10	Warwire	38,17	0,05	21,44	0,00	25,73	1,69	4,07	8,52	0,06	99,73
120	SC1-1m10	Warwire	38,38	0,00	21,40	0,01	26,90	1,20	4,44	7,40	0,01	99,74
121	SC1-1m10	Warwire	37,96	0,04	21,53	0,06	27,72	0,53	5,43	6,39	0,07	99,74
122	SC1-1m10	Warwire	39,14	0,00	22,46	0,24	23,97	0,74	9,47	3,72	0,00	99,74
123	SC1-1m10	Warwire	38,23	0,11	20,95	0,03	25,89	0,34	3,30	10,84	0,05	99,74
124	SC1-1m10	Warwire	37,60	0,03	20,94	0,03	28,50	2,72	2,15	7,78	0,00	99,75
125	SC1-1m10	Warwire	39,78	0,01	22,82	0,01	23,48	0,31	11,93	1,44	0,04	99,82
126	SC1-1m10	Warwire	38,61	0,03	22,22	0,02	24,90	0,55	7,32	6,19	0,00	99,84
127	SC1-1m10	Warwire	38,63	0,00	21,53	0,00	25,46	1,38	5,58	7,24	0,02	99,84
128	SC1-1m10	Warwire	38,70	0,05	22,20	0,05	23,13	0,89	6,88	7,92	0,05	99,86
129	SC1-1m10	Warwire	37,66	0,01	22,04	0,06	28,81	1,63	5,74	3,85	0,06	99,86
130	SC1-1m10	Warwire	38,05	0,13	21,59	0,01	27,66	1,08	3,50	7,85	0,00	99,87
131	SC1-1m10	Warwire	38,36	0,02	21,86	0,09	26,33	0,64	6,27	6,31	0,00	99,89
132	SC1-1m10	Warwire	39,16	0,04	22,45	0,10	24,90	0,51	10,88	1,81	0,05	99,90
133	SC1-1m10	Warwire	39,08	0,00	22,44	0,17	25,21	0,48	9,84	2,69	0,00	99,91
134	SC1-1m10	Warwire	38,35	0,07	21,76	0,05	27,06	0,73	4,98	6,92	0,01	99,94
135	SC1-1m10	Warwire	38,60	0,08	21,38	0,00	26,32	0,54	4,36	8,66	0,00	99,95
136	SC1-1m10	Warwire	39,76	0,03	22,80	0,08	21,97	0,51	12,72	2,05	0,04	99,96
137	SC1-1m10	Warwire	38,70	0,00	22,27	0,06	27,12	0,77	8,05	3,01	0,00	99,98
138	SC1-1m10	Warwire	38,14	0,03	21,35	0,05	30,56	0,78	3,87	5,13	0,10	100,00
139	SC1-1m10	Warwire	39,98	0,02	22,55	0,13	22,23	0,62	11,08	3,39	0,00	100,01
140	SC1-1m10	Warwire	38,86	0,00	22,46	0,02	24,36	0,57	7,65	6,09	0,00	100,01

Garnet chemistry cont.

	Sample ID	Formation	SiO2	TiO2	Al2O3	Cr2O3	FeO	MnO	MgO	CaO	Na2O	Total
							mass-%					
detection limit			0,016	0,011	0,014	0,013	0,022	0,012	0,009	0,014	0,012	
141	SC1-1m10	Warwire	38,39	0,07	21,72	0,00	27,19	0,74	5,13	6,72	0,05	100,01
142	SC1-1m10	Warwire	39,27	0,00	22,40	0,13	23,79	0,93	10,10	3,34	0,06	100,02
143	SC1-1m10	Warwire	37,98	0,00	21,46	0,05	28,44	1,45	5,43	5,21	0,00	100,02
144	SC1-1m10	Warwire	38,92	0,01	22,28	0,03	24,91	0,52	7,14	6,22	0,00	100,03
145	SC1-1m10	Warwire	38,42	0,00	21,41	0,08	26,63	1,43	3,63	8,41	0,02	100,03
146	SC1-1m10	Warwire	38,40	0,02	21,40	0,01	27,58	0,92	5,23	6,40	0,07	100,03
147	SC1-1m10	Warwire	38,11	0,08	21,21	0,01	23,65	2,00	3,28	11,69	0,00	100,03
148	SC1-1m10	Warwire	39,31	0,00	22,59	0,08	23,86	0,51	10,20	3,41	0,07	100,04
149	SC1-1m10	Warwire	38,34	0,00	21,92	0,00	29,79	0,40	6,83	2,74	0,04	100,06
150	SC1-1m10	Warwire	38,66	0,00	22,44	0,07	27,01	1,10	9,35	1,45	0,00	100,08
151	SC1-1m10	Warwire	38,81	0,05	22,16	0,06	24,80	0,76	7,33	6,11	0,01	100,09
152	SC1-1m10	Warwire	38,43	0,01	21,71	0,01	27,44	0,87	5,08	6,48	0,06	100,09
153	SC1-1m10	Warwire	39,21	0,00	22,47	0,06	24,98	0,66	10,69	2,01	0,03	100,11
154	SC1-1m10	Warwire	37,30	0,03	20,91	0,05	32,87	1,50	0,99	6,47	0,00	100,13
155	SC1-1m10	Warwire	38,54	0,00	21,88	0,08	26,93	0,81	7,11	4,69	0,09	100,14
156	SC1-1m10	Warwire	38,60	0,00	21,34	0,00	27,39	2,22	4,37	6,21	0,01	100,14
157	SC1-1m10	Warwire	38,65	0,10	22,08	0,13	25,21	0,82	6,80	6,38	0,00	100,16
158	SC1-1m10	Warwire	38,73	0,00	21,96	0,02	24,91	0,75	5,40	8,40	0,00	100,17
159	SC1-1m10	Warwire	38,80	0,00	22,03	0,04	27,32	0,79	7,36	3,76	0,08	100,18
160	SC1-1m10	Warwire	37,81	0,01	21,48	0,06	30,09	0,55	3,19	6,93	0,06	100,18
161	SC1-1m10	Warwire	37,97	0,03	21,43	0,04	27,92	0,45	4,21	8,14	0,00	100,19
162	SC1-1m10	Warwire	38,22	0,05	21,78	0,06	27,77	1,98	4,21	6,12	0,00	100,19
163	SC1-1m10	Warwire	39,27	0,00	22,39	0,06	25,84	0,89	10,40	1,31	0,05	100,21
164	SC1-1m10	Warwire	38,63	0,07	21,44	0,00	26,98	0,79	4,53	7,74	0,03	100,22
165	SC1-1m10	Warwire	38,62	0,02	22,08	0,07	26,34	0,74	5,97	6,38	0,00	100,22
166	SC1-1m10	Warwire	38,03	0,00	21,37	0,00	29,24	1,08	3,69	6,83	0,01	100,25
167	SC1-1m10	Warwire	38,75	0,00	21,78	0,00	28,55	0,96	7,06	3,12	0,06	100,28
168	SC1-1m10	Warwire	38,50	0,00	21,94	0,08	26,65	1,41	5,46	6,22	0,04	100,30
169	SC1-1m10	Warwire	39,85	0,00	22,90	0,08	23,14	0,31	11,85	2,17	0,00	100,30
170	SC1-1m10	Warwire	37,62	0,04	20,95	0,08	31,55	0,89	2,12	7,06	0,00	100,30
171	SC1-1m10	Warwire	38,83	0,07	21,78	0,05	25,19	0,51	7,28	6,59	0,00	100,30
172	SC1-1m10	Warwire	38,47	0,05	21,83	0,07	27,10	1,19	5,45	6,14	0,01	100,31
173	SC1-1m10	Warwire	38,14	0,02	21,56	0,00	27,56	2,67	5,00	5,29	0,07	100,32
174	SC1-1m10	Warwire	39,03	0,00	22,36	0,10	27,98	0,39	9,20	1,28	0,00	100,33
175	SC1-1m10	Warwire	39,44	0,03	22,39	0,04	25,72	0,78	10,77	1,18	0,00	100,34
176	SC1-1m10	Warwire	38,59	0,00	22,02	0,01	30,30	1,00	6,83	1,59	0,00	100,34
177	SC1-1m10	Warwire	37,52	0,05	20,94	0,02	32,36	0,84	1,73	6,87	0,02	100,35
178	SC1-1m10	Warwire	39,31	0,00	21,98	0,04	23,43	0,58	7,04	8,00	0,00	100,38
179	SC1-1m10	Warwire	37,69	0,09	21,10	0,08	31,34	0,73	2,62	6,73	0,00	100,39
180	SC1-1m10	Warwire	38,81	0,09	21,72	0,06	25,07	0,54	5,34	8,75	0,02	100,39
181	SC1-1m10	Warwire	38,35	0,01	21,43	0,07	28,21	0,65	4,51	7,19	0,00	100,43
182	SC1-1m10	Warwire	38,53	0,00	21,76	0,08	26,88	1,92	4,56	6,71	0,00	100,44
183	SC1-1m10	Warwire	37,63	0,03	21,41	0,02	31,06	0,81	2,39	7,03	0,05	100,44
184	SC1-1m10	Warwire	39,32	0,05	22,45	0,09	25,79	0,35	9,74	2,65	0,00	100,44
185	SC1-1m10	Warwire	38,76	0,01	21,52	0,09	27,05	0,98	5,49	6,55	0,00	100,45
186	SC1-1m10	Warwire	38,18	0,09	21,84	0,07	27,27	0,48	4,00	8,55	0,00	100,48
187	SC1-1m10	Warwire	38,35	0,04	21,54	0,04	26,39	2,17	3,54	8,39	0,02	100,48
188	SC1-1m10	Warwire	39,01	0,01	21,89	0,02	27,52	0,99	7,99	3,01	0,05	100,48
189	SC1-1m10	Warwire	39,45	0,03	22,38	0,08	26,84	0,57	9,35	1,76	0,03	100,50
190	SC1-1m10	Warwire	37,85	0,05	21,29	0,04	28,51	2,28	2,34	8,15	0,01	100,52
191	SC1-1m10	Warwire	37,94	0,04	21,88	0,08	30,19	1,23	4,92	4,23	0,02	100,53
192	SC1-1m10	Warwire	38,74	0,00	22,30	0,06	29,01	0,56	8,16	1,67	0,03	100,53
193	SC1-1m10	Warwire	38,25	0,02	21,84	0,07	24,51	0,75	2,04	13,04	0,02	100,53
194	SC1-1m10	Warwire	40,05	0,00	22,65	0,04	23,51	0,38	12,16	1,73	0,04	100,56
195	SC1-1m10	Warwire	38,04	0,00	21,86	0,05	32,50	0,96	5,99	1,20	0,00	100,59
196	SC1-1m10	Warwire	38,35	0,02	22,28	0,04	30,33	0,91	6,54	2,08	0,03	100,59
197	SC1-1m10	Warwire	38,91	0,05	22,49	0,08	29,06	0,52	8,63	0,86	0,00	100,60
198	SC1-1m10	Warwire	39,62	0,00	22,94	0,02	24,34	0,47	11,40	1,80	0,01	100,60
199	SC1-1m10	Warwire	39,11	0,00	22,54	0,08	26,87	0,74	9,23	2,03	0,03	100,63
200	SC1-1m10	Warwire	37,70	0,04	21,06	0,02	31,75	0,68	2,26	7,11	0,02	100,64
201	SC1-1m10	Warwire	38,16	0,01	21,27	0,03	30,48	1,85	2,98	5,87	0,01	100,66
202	SC1-1m10	Warwire	38,30	0,02	21,16	0,03	29,84	1,13	3,32	6,76	0,10	100,66
203	SC1-1m10	Warwire	38,79	0,01	22,14	0,11	29,11	0,50	8,00	1,96	0,05	100,67
204	SC1-1m10	Warwire	38,08	0,07	20,98	0,10	29,04	2,46	2,39	7,63	0,04	100,78
205	SC1-1m10	Warwire	38,22	0,00	21,94	0,04	32,67	1,25	5,34	1,40	0,00	100,87
206	SC1-1m10	Warwire	38,31	0,02	21,84	0,00	32,68	0,95	5,20	2,07	0,07	101,14
207	MB-2	Museta beds	38,12	0,00	21,78	0,11	31,09	0,54	4,89	3,92	0,00	100,45
208	MB-2	Museta beds	37,86	0,04	21,42	0,00	27,55	1,10	4,19	6,81	0,03	99,00
209	MB-2	Museta beds	38,54	0,04	21,57	0,00	26,84	0,39	6,21	5,59	0,00	99,18
210	MB-2	Museta beds	39,01	0,00	22,44	0,07	24,74	1,08	10,41	1,55	0,04	99,34

Garnet chemistry cont.

	Sample ID	Formation	SiO2	TiO2	Al2O3	Cr2O3	FeO	MnO	MgO	CaO	Na2O	Total
							mass-%					
detection limit			0,016	0,011	0,014	0,013	0,022	0,012	0,009	0,014	0,012	
211	MB-2	Museta beds	38,76	0,05	22,19	0,06	24,31	0,51	7,17	6,31	0,00	99,37
212	MB-2	Museta beds	37,51	0,03	21,39	0,00	30,76	1,08	3,73	4,88	0,00	99,38
213	MB-2	Museta beds	38,74	0,05	22,08	0,09	23,45	0,63	8,57	5,82	0,03	99,46
214	MB-2	Museta beds	39,19	0,04	22,15	0,15	22,22	0,42	8,57	6,75	0,00	99,49
215	MB-2	Museta beds	37,85	0,02	21,45	0,00	27,65	1,05	4,52	6,92	0,03	99,49
216	MB-2	Museta beds	39,20	0,00	21,99	0,09	22,50	0,30	8,52	6,86	0,05	99,51
217	MB-2	Museta beds	39,37	0,01	22,23	0,19	23,53	0,40	10,87	2,86	0,06	99,52
218	MB-2	Museta beds	37,19	0,04	21,05	0,00	31,42	0,89	1,65	7,28	0,05	99,56
219	MB-2	Museta beds	37,74	0,01	21,71	0,01	30,91	1,01	5,35	2,88	0,00	99,61
220	MB-2	Museta beds	37,31	0,05	20,81	0,01	31,90	1,18	0,92	7,44	0,00	99,62
221	MB-2	Museta beds	38,67	0,01	21,69	0,01	24,85	0,66	7,78	5,89	0,06	99,63
222	MB-2	Museta beds	37,85	0,04	21,46	0,00	27,78	1,48	4,33	6,67	0,05	99,66
223	MB-2	Museta beds	39,57	0,02	22,35	0,20	21,02	0,56	10,20	5,71	0,05	99,67
224	MB-2	Museta beds	37,88	0,06	21,39	0,02	27,55	1,56	4,31	6,91	0,00	99,68
225	MB-2	Museta beds	38,22	0,04	21,89	0,00	25,97	0,90	5,64	7,03	0,00	99,69
226	MB-2	Museta beds	37,82	0,07	21,67	0,02	27,15	1,26	3,76	7,94	0,02	99,72
227	MB-2	Museta beds	38,01	0,09	21,17	0,08	27,65	0,88	4,98	6,87	0,00	99,73
228	MB-2	Museta beds	38,89	0,00	22,20	0,13	28,25	0,81	8,54	0,97	0,00	99,79
229	MB-2	Museta beds	38,16	0,02	21,83	0,04	29,16	0,69	6,22	3,64	0,08	99,84
230	MB-2	Museta beds	38,02	0,04	21,79	0,08	23,51	1,34	3,22	11,82	0,02	99,84
231	MB-2	Museta beds	38,32	0,11	21,39	0,05	23,45	0,76	4,42	11,35	0,00	99,85
232	MB-2	Museta beds	36,94	0,08	21,25	0,08	31,98	0,90	1,50	7,13	0,00	99,85
233	MB-2	Museta beds	38,85	0,08	22,05	0,20	24,30	0,72	7,72	5,95	0,00	99,86
234	MB-2	Museta beds	38,34	0,05	21,69	0,06	24,68	0,54	4,81	9,64	0,07	99,88
235	MB-2	Museta beds	37,90	0,00	21,44	0,05	25,68	2,50	3,53	8,76	0,02	99,88
236	MB-2	Museta beds	37,79	0,00	21,73	0,02	31,95	0,62	5,57	2,25	0,00	99,94
237	MB-2	Museta beds	37,95	0,05	21,76	0,04	27,51	1,54	4,09	7,04	0,00	99,98
238	MB-2	Museta beds	39,11	0,02	21,98	0,06	24,29	0,46	7,66	6,38	0,04	100,00
239	MB-2	Museta beds	37,45	0,00	21,40	0,10	31,98	1,11	3,58	4,38	0,00	100,00
240	MB-2	Museta beds	38,10	0,03	21,84	0,00	30,71	1,26	6,19	1,95	0,00	100,07
241	MB-2	Museta beds	37,77	0,06	21,70	0,02	31,90	0,71	5,56	2,30	0,08	100,10
242	MB-2	Museta beds	38,84	0,01	22,25	0,01	25,37	0,38	6,91	6,36	0,00	100,13
243	MB-2	Museta beds	38,41	0,03	21,78	0,02	27,16	0,58	5,44	6,66	0,05	100,13
244	MB-2	Museta beds	39,63	0,02	21,92	0,08	22,92	0,59	9,01	5,91	0,06	100,13
245	MB-2	Museta beds	37,58	0,05	21,08	0,07	30,75	0,64	3,01	6,91	0,06	100,15
246	MB-2	Museta beds	37,94	0,08	21,53	0,02	28,08	1,48	4,01	6,98	0,03	100,16
247	MB-2	Museta beds	38,75	0,06	21,52	0,02	24,33	1,60	4,75	9,15	0,00	100,18
248	MB-2	Museta beds	38,25	0,00	21,91	0,01	27,70	1,57	5,49	5,29	0,00	100,22
249	MB-2	Museta beds	38,14	0,00	21,97	0,02	27,66	1,52	5,51	5,41	0,02	100,25
250	MB-2	Museta beds	37,84	0,04	21,15	0,01	30,27	0,90	3,09	6,97	0,00	100,27
251	MB-2	Museta beds	38,16	0,06	21,49	0,08	27,00	1,65	4,89	6,91	0,04	100,29
252	MB-2	Museta beds	37,66	0,03	21,55	0,03	32,63	0,63	4,25	3,55	0,00	100,33

A5-4 – Rutile chemistry (Jeol JXA-2800, Johannes Gutenberg University of Mainz)

	Sample ID	Formation	Al	Si	Nb	Cr	Fe	Ti	V	Zr	Total
			ppm	ppm	ppm	ppm	ppm	ppm	ppm	ppm	
Detection limits			0,001	0,003	0,004	0,0017	0,002	0,02	0,002	0,027	
1	MB-2	Museta beds	322	172	605	600	903	607483	3432	1055	99,21
2	MB-2	Museta beds	265	158	439	2017	105	607364	1998	882	98,31
3	MB-2	Museta beds	310	193	274	212	3133	617136	689	615	98,68
4	MB-2	Museta beds	307	213	1144	536	3279	613359	533	270	100,70
5	MB-2	Museta beds	304	192	141	350	4215	614738	849	458	100,25
6	MB-2	Museta beds	306	217	332	817	209	614498	3896	1096	98,73
7	MB-2	Museta beds	374	155	1644	1619	428	604726	3953	1928	100,58
8	MB-2	Museta beds	312	161	510	861	1162	623970	1989	2469	100,80
9	MB-2	Museta beds	265	158	2201	1121	680	616956	2788	500	99,58
10	MB-2	Museta beds	349	184	1337	570	670	618694	2576	1407	100,83

Geochemical analyses of rutile cont.

	Sample ID	Formation	Al	Si	Nb	Cr	Fe	Ti	V	Zr	Total
			ppm	ppm	ppm	ppm	ppm	ppm	ppm	ppm	
Detection limits			0,001	0,003	0,004	0,0017	0,002	0,02	0,002	0,027	
11	MB-2	Museta beds	226	192	12	80	3084	606524	1067	267	98,52
12	MB-2	Museta beds	288	208	484	504	632	617495	1941	773	99,39
13	MB-2	Museta beds	298	184	2779	547	612	617196	2591	1159	98,53
14	MB-2	Museta beds	280	176	6948	386	5574	624030	832	592	99,50
15	MB-2	Museta beds	277	177	989	970	2137	606225	3978	959	99,72
16	MB-2	Museta beds	360	179	2117	738	840	605685	2738	1745	98,63
17	MB-2	Museta beds	252	188	823	3303	411	616236	2408	744	99,11
18	MB-2	Museta beds	285	235	108	3006	308	614198	2940	2487	99,57
19	MB-2	Museta beds	334	193	1776	232	1406	615217	2270	1532	100,00
20	MB-2	Museta beds	285	185	935	285	2884	614438	844	626	98,63
21	MB-2	Museta beds	265	171	1095	731	124	620073	2669	1605	99,42
22	MB-2	Museta beds	355	341	919	216	3188	609462	909	595	99,79
23	MB-2	Museta beds	335	208	632	146	1792	621092	2164	534	100,66
24	MB-2	Museta beds	322	158	3248	1670	405	600589	4454	2354	100,52
25	MB-2	Museta beds	402	149	4989	1043	1485	614438	1640	1401	100,53
26	MB-2	Museta beds	352	156	352	360	1778	622591	1924	811	99,06
27	MB-2	Museta beds	304	184	1489	499	3339	605325	908	415	99,54
28	MB-2	Museta beds	419	174	4485	750	1449	598551	1692	948	99,28
29	MB-2	Museta beds	321	199	2569	366	11349	602328	801	567	100,84
30	MB-2	Museta beds	306	180	809	521	296	605205	3045	1749	99,83
31	MB-2	Museta beds	328	163	942	573	817	607543	3689	570	100,06
32	MB-2	Museta beds	369	179	3178	710	1145	598491	2281	2069	100,56
33	MB-2	Museta beds	1634	192	1973	2611	5250	595973	5348	1078	99,32
34	MB-2	Museta beds	306	153	3847	770	1026	602867	3096	1669	100,24
35	MB-2	Museta beds	274	181	3607	2253	446	605805	3083	799	99,83
36	MB-2	Museta beds	245	208	1563	633	435	624929	2471	1740	98,59
37	MB-2	Museta beds	252	257	996	736	166	599150	4989	1145	99,00
38	MB-2	Museta beds	205	204	1498	1675	154	606584	3997	1446	99,36
39	MB-2	Museta beds	274	138	802	1909	98	582724	3075	729	100,24
40	MB-2	Museta beds	333	208	189	703	469	592915	2351	803	100,10
41	MB-2	Museta beds	257	200	1945	2146	92	591776	3986	1336	98,63
42	MB-2	Museta beds	275	220	1581	467	1457	605925	1311	371	99,42
43	MB-2	Museta beds	246	212	196	737	2923	597232	812	474	99,79
44	MB-2	Museta beds	272	131	163	1516	297	608263	1956	813	100,66
45	MB-2	Museta beds	285	180	5950	271	1579	590038	2143	657	100,52
46	KAI 52-1	Kaiso Village	265	191	1147	276	365	560062	2296	1379	100,53
47	KAI 52-1	Kaiso Village	267	187	1620	1388	278	571033	1617	1400	99,06
48	KAI 52-1	Kaiso Village	285	164	4228	611	2105	570614	755	1025	99,54
49	KAI 52-1	Kaiso Village	296	213	1611	1512	379	573851	1479	1211	99,99
50	KAI 52-1	Kaiso Village	239	176	1905	1205	428	572712	1741	1666	100,43
51	KAI 52-1	Kaiso Village	374	221	5093	744	2756	577088	1126	4427	99,05
52	KAI 52-1	Kaiso Village	300	215	1448	1962	289	575290	2060	1365	98,42
53	KAI 52-1	Kaiso Village	350	192	1675	574	756	573012	2465	603	99,94
54	KAI 52-1	Kaiso Village	266	189	2346	531	1150	593755	2618	1062	99,32
55	KAI 52-1	Kaiso Village	287	180	3696	1322	5065	568395	1101	626	99,83
56	KAI 52-1	Kaiso Village	251	187	721	1188	157	583803	2266	804	98,59
57	KAI 52-1	Kaiso Village	267	212	1685	1637	157	570674	2635	2801	101,00
58	KAI 52-1	Kaiso Village	256	143	1454	1437	173	611380	2446	1156	100,46
59	KAI 52-1	Kaiso Village	292	194	3865	543	2126	593455	1309	735	100,00
60	KAI 52-1	Kaiso Village	249	145	2281	703	1768	589019	1248	1111	97,86
61	KAI 52-1	Kaiso Village	227	133	2156	1568	2364	573551	763	474	99,42
62	KAI 52-1	Kaiso Village	228	178	233	714	1970	586261	1252	1068	98,41
63	KAI 52-1	Kaiso Village	285	256	1636	1708	626	591716	1328	874	98,64
64	SC1-1m10	Warwire	0	108	1799	3709	309	599690	919	629	99,14
65	SC1-1m10	Warwire	22	191	784	1892	241	599510	3637	1183	97,90
66	SC1-1m10	Warwire	34	121	1120	1013	1873	583263	1371	573	98,31
67	SC1-1m10	Warwire	49	111	1683	1179	611	580326	2654	679	98,68
68	SC1-1m10	Warwire	53	83	2838	1529	579	583443	1406	1088	99,00
69	SC1-1m10	Warwire	58	108	764	3823	241	583503	1440	1584	99,36
70	SC1-1m10	Warwire	40	391	1999	1903	276	598311	3320	1090	98,41
71	SC1-1m10	Warwire	46	123	1574	2270	113	588239	3473	480	100,92
72	SC1-1m10	Warwire	53	134	744	304	450	593035	2092	572	98,78
73	SC1-1m10	Warwire	56	130	1859	2150	152	594294	1928	1375	100,34
74	SC1-1m10	Warwire	29	112	5	1552	169	602687	2374	937	99,33
75	SC1-1m10	Warwire	29	154	138	694	1152	593695	1041	269	99,56

Geochemical analyses of rutile cont.

	Sample ID	Formation	Al	Si	Nb	Cr	Fe	Ti	V	Zr	Total
			ppm	ppm	ppm	ppm	ppm	ppm	ppm	ppm	
Detection limits			0,001	0,003	0,004	0,0017	0,002	0,02	0,002	0,027	
76	SC1-1m10	Warwire	46	131	1763	2053	196	597891	1935	1366	100,06
77	SC1-1m10	Warwire	84	139	1560	2442	160	594234	2289	699	98,82
78	SC1-1m10	Warwire	82	118	679	1827	223	588719	5004	1273	99,23
79	SC1-1m10	Warwire	74	128	573	1889	238	591237	4864	1264	99,60
80	SC1-1m10	Warwire	281	161	3151	385	3373	593155	829	622	100,48
81	SC1-1m10	Warwire	394	157	4356	586	1513	599750	1879	1204	100,33
82	SC1-1m10	Warwire	287	159	3356	581	1610	594774	1377	802	100,34
83	SC1-1m10	Warwire	302	185	3441	152	3852	578527	830	352	98,87
84	SC1-1m10	Warwire	350	161	4724	725	2604	597951	2236	1372	99,35
85	SC1-1m10	Warwire	305	146	4234	892	923	595733	3172	1025	99,80
86	SC1-1m10	Warwire	242	165	439	92	2805	585541	1285	197	100,24
87	SC1-1m10	Warwire	257	225	62	630	1267	595194	1320	113	98,86
88	SC1-1m10	Warwire	228	164	122	1064	1723	598071	1635	508	99,66
89	SC1-1m10	Warwire	361	220	2639	681	1370	593755	1817	1141	100,02
90	SC1-1m10	Warwire	246	179	1551	177	3339	599030	763	190	100,90
91	SC1-1m10	Warwire	246	153	1746	1526	129	578587	7926	2689	100,75
92	SC1-1m10	Warwire	239	136	1490	803	73	584642	3297	830	100,77
93	SC1-1m10	Warwire	312	175	10905	431	9208	584043	832	695	99,29
94	SC1-1m10	Warwire	239	237	1571	1333	149	578467	6288	991	99,77
95	SC1-1m10	Warwire	393	184	1866	1615	2993	594114	2106	600	100,23
96	SC1-1m10	Warwire	269	130	2640	79	4389	594534	854	595	100,66
97	SC1-1m10	Warwire	314	206	5875	1794	2010	603587	658	706	99,29
98	SC1-1m10	Warwire	288	137	1488	1301	237	584822	5930	857	98,66
99	SC1-1m10	Warwire	302	156	9	746	853	599390	1461	233	100,18
100	SC1-1m10	Warwire	327	165	111	163	1314	593755	1476	545	100,66
101	SC1-1m10	Warwire	316	136	5483	483	2935	592795	1406	1002	100,52
102	SC1-1m10	Warwire	318	173	1818	1033	467	583203	4768	1608	98,42
103	SC1-1m10	Warwire	299	160	2009	1305	997	595253	2955	625	99,32
104	SC1-1m10	Warwire	323	165	2245	407	912	603107	1992	1204	100,75
105	SC1-1m10	Warwire	282	178	3803	224	3929	585901	967	337	100,77
106	SC1-1m10	Warwire	377	191	7987	237	3611	576249	1478	472	99,29
107	SC1-1m10	Warwire	375	135	6756	1104	2301	600169	1035	316	98,88
108	SC1-1m10	Warwire	292	143	40	854	1163	596992	1329	1665	100,97
109	SC1-1m10	Warwire	372	256	6823	1139	2434	603826	1117	301	99,99
110	SC1-1m10	Warwire	605	155	14470	1037	5467	575949	2037	1563	100,43
111	SC1-1m10	Warwire	272	171	589	486	720	611320	2096	1388	99,05
112	SC1-1m10	Warwire	290	163	1161	193	1600	584163	2027	652	98,42
113	SC1-1m10	Warwire	256	151	538	462	623	603946	2173	1407	99,94
114	SC1-1m10	Warwire	591	233	14330	1056	5443	575530	2015	1561	98,63
115	SC1-1m10	Warwire	273	177	11	556	849	591417	2191	197	99,11
116	SC1-1m10	Warwire	396	165	4166	794	1341	601309	2807	1994	99,57
117	SC1-1m10	Warwire	290	184	2786	1381	4773	593335	910	470	100,00
118	SC1-1m10	Warwire	288	183	193	445	519	604066	3106	682	98,63
119	SC1-1m10	Warwire	293	180	1244	3293	402	582604	3126	641	100,34
120	SC1-1m10	Warwire	273	328	322	484	503	603347	3057	664	99,33
121	SC1-1m10	Warwire	285	179	1588	1048	362	596752	2460	335	99,56
122	SC1-1m10	Warwire	288	169	2398	591	947	600229	2052	723	101,00
123	SC1-1m10	Warwire	364	187	3381	746	941	578347	2446	1094	100,46
124	SC1-1m10	Warwire	321	177	291	838	592	599030	3077	1504	100,00
125	SC1-1m10	Warwire	304	154	2273	2095	489	582664	4735	2362	97,86
126	SC1-1m10	Warwire	304	162	556	1234	832	600229	2533	458	99,42
127	SC1-1m10	Warwire	256	161	466	478	405	601728	1794	1481	98,41
128	SC1-1m10	Warwire	282	165	1186	594	330	599270	1901	680	98,64
129	NV3-2	Nkondo	80	113	628	2527	322	601428	629	820	99,14
130	NV3-2	Nkondo	78	118	524	2545	352	612999	533	834	97,90
131	NV3-2	Nkondo	67	135	1379	953	287	616056	2063	1196	99,80
132	NV3-2	Nkondo	62	93	22	1436	464	600110	1292	1204	100,24
133	NV3-2	Nkondo	80	118	849	942	301	623191	1553	781	98,86
134	NV3-2	Nkondo	77	111	839	932	351	609222	1525	785	100,68
135	NV3-2	Nkondo	88	101	1506	649	372	605445	1192	962	98,55
136	NV3-2	Nkondo	48	122	394	1282	1847	597771	686	4722	100,10
137	NV3-2	Nkondo	56	136	567	2645	464	618514	491	869	99,09
138	NV3-2	Nkondo	74	112	353	2521	269	594534	1831	2515	99,32
139	NV3-2	Nkondo	131	133	336	158	1590	618335	140	812	99,83
140	NV3-2	Nkondo	71	114	89	998	686	618814	1172	2534	98,59

Geochemical analyses of rutile cont.

	Sample ID	Formation	Al	Si	Nb	Cr	Fe	Ti	V	Zr	Total
			ppm	ppm	ppm	ppm	ppm	ppm	ppm	ppm	
Detection limits			0,001	0,003	0,004	0,0017	0,002	0,02	0,002	0,027	
141	**NV3-2**	**Nkondo**	84	120	3611	1137	1531	625769	633	554	99,00
142	**NV3-2**	**Nkondo**	116	113	1768	343	916	609582	1739	1487	99,36
143	**NV3-2**	**Nkondo**	71	107	1854	219	3649	600649	355	431	100,24
144	**NV3-2**	**Nkondo**	45	94	373	3106	499	604186	686	2996	100,10
145	**NV3-2**	**Nkondo**	62	96	84	1009	516	605985	1026	931	100,11
146	**NV3-2**	**Nkondo**	174	121	1661	153	1900	608383	830	683	98,63
147	**NV3-2**	**Nkondo**	53	99	756	246	1543	614258	752	926	99,11
148	**NV3-2**	**Nkondo**	74	126	1348	964	171	602867	2370	1241	99,57
149	**NV3-2**	**Nkondo**	73	92	1004	414	200	615577	585	814	100,00
150	**NV3-2**	**Nkondo**	101	112	9059	685	5357	606105	26	529	98,63
151	**NV3-2**	**Nkondo**	70	115	7591	595	20055	585302	0	369	99,42
152	**NV3-2**	**Nkondo**	52	119	1345	1074	4173	611320	526	1119	99,79
153	**NV3-2**	**Nkondo**	47	183	6310	209	5883	609042	0	274	100,66
154	**NV3-2**	**Nkondo**	41	121	2523	725	822	605085	680	842	100,52
155	**NV3-2**	**Nkondo**	86	111	1310	466	833	611440	395	839	100,53
156	**NV3-2**	**Nkondo**	45	108	856	506	4091	613958	0	349	99,06
157	**NV3-2**	**Nkondo**	34	104	809	838	93	604846	5095	1442	99,54
158	**NV3-2**	**Nkondo**	111	165	1501	1158	634	611021	3051	1851	99,99
159	**NV3-2**	**Nkondo**	124	151	1330	1166	658	612759	3047	1897	100,43
160	**NV3-2**	**Nkondo**	37	114	555	597	44	610301	2944	719	99,05
161	**NV3-2**	**Nkondo**	217	104	3662	588	1437	608862	342	1072	99,28
162	**NV3-2**	**Nkondo**	42	100	474	3007	138	621152	1974	933	100,56
163	**NV3-2**	**Nkondo**	37	113	1626	900	758	617735	2225	862	99,73
164	**NV3-2**	**Nkondo**	102	112	3074	914	1188	607963	1068	1105	100,98
165	**NV3-2**	**Nkondo**	100	129	964	715	3120	619893	0	292	100,84
166	**NV3-2**	**Nkondo**	91	107	1718	68	3251	613299	52	537	99,37
167	**NV3-2**	**Nkondo**	78	117	1680	1199	484	623191	2911	1542	100,30
168	**NV3-2**	**Nkondo**	86	95	1225	1157	931	608802	137	3565	99,36
169	**NV3-2**	**Nkondo**	44	109	1730	200	3335	615757	0	874	102,60
170	**NV3-2**	**Nkondo**	410	109	1837	794	370	607723	2434	1572	101,00
171	**NV3-2**	**Nkondo**	68	88	41	662	944	625709	0	106	98,37
172	**NV3-2**	**Nkondo**	41	97	287	1728	2224	609042	1408	354	99,93
173	**NV3-2**	**Nkondo**	49	96	1184	1349	2545	607364	0	397	98,92
174	**NV3-2**	**Nkondo**	73	93	9	740	901	623970	0	210	99,15
175	**NV3-2**	**Nkondo**	22	92	825	876	84	607543	3824	1028	99,65

Appendix – Chapter 6

A6-1 – Bulk rock geochemistry (Kisegi-Nyabusosi area)

	Sample ID	144-2	143-1	Ameise 4	D-1	D-3	Fekr-1	GH10-1	GH12-3
	Formation	Nyabusosi	Nyabusosi	Nyabusosi	Katorogo	Katorogo	Nyakabingo	Nyakabingo	Nyakabingo
SiO_2	%	63.43	76.54	72.11	83.51	77.15	74.14	74.23	77.70
Al_2O_3	%	15.35	10.18	12.56	6.89	9.67	11.11	10.74	8.91
Fe_2O_3	%	5.83	3.43	3.63	2.02	2.63	3.78	3.33	3.42
CaO	%	1.48	1.23	1.57	0.54	1.33	1.89	2.27	1.61
MgO	%	1.11	0.72	1.08	0.36	0.40	0.56	0.62	0.50
Na_2O	%	1.79	1.62	2.01	0.94	1.92	2.08	2.10	1.84
K_2O	%	1.72	1.73	1.91	1.40	1.67	2.08	2.02	1.89
Cr_2O3	%	0.01	0.01	0.03	0.07	0.03	0.08	0.06	0.04
TiO_2	%	0.79	0.76	0.69	0.31	0.46	0.79	0.92	0.66
MnO	%	0.12	0.04	0.05	0.01	0.02	0.07	0.08	0.06
P_2O_5	%	0.08	0.07	0.04	0.02	0.04	0.07	0.06	0.15
Sc	ppm	15.01	10.02	11.24	3.05	5.00	6.09	6.05	4.02
Be	ppm	3.00	2.00	0.00	0.00	0.00	0.00	0.00	0.00
V	ppm	104.06	61.10	78.65	30.52	42.97	46.65	48.41	42.22
Cr	ppm	211.98	154.34	194.08	427.22	179.87	436.11	363.09	241.23
Co	ppm	18.71	12.32	8.17	7.12	12.99	10.14	15.13	7.04
Ni	ppm	24.31	11.12	23.49	24.41	23.98	19.27	22.19	16.08
Cu	ppm	22.81	6.21	30.64	10.17	10.99	11.16	8.07	6.03
Zn	ppm	44.03	30.05	89.89	28.48	51.96	42.60	38.33	30.15
Ga	ppm	19.81	12.32	40.25	49.33	50.66	51.01	12.61	45.63
Ge	ppm	0.00	0.00	0.00	0.00	0.00	0.00	0.00	0.00
As	ppm	0.70	-	1.23	0.41	0.50	1.22	1.82	2.31
Rb	ppm	84.65	62.21	67.21	34.79	43.97	51.32	49.92	45.63
Sr	ppm	260.46	155.16	166.50	107.31	201.86	346.86	389.31	357.82
Y	ppm	26.82	24.14	25.54	8.65	19.59	18.26	18.56	28.95
Zr	ppm	283.97	341.48	261.49	185.13	312.78	515.21	594.05	534.73
Nb	ppm	32.52	28.55	19.92	9.46	15.59	25.15	22.69	21.21
Mo	ppm	0.30	0.10	5.11	8.14	5.00	8.11	6.05	6.03
Ag	ppm	-	-	-	-	-	-	-	-
In	ppm	0.00	0.00	0.00	0.00	0.00	0.00	0.00	0.00
Sn	ppm	2.00	2.00	2.04	2.03	2.00	2.03	1.01	2.01
Sb	ppm	-	-	0.76	0.07	-	0.06	-	0.05
Cs	ppm	3.00	2.30	2.63	1.01	1.45	0.63	0.65	0.71
Ba	ppm	659.40	445.76	476.00	376.36	531.63	796.15	750.38	718.67
La	ppm	42.93	37.36	45.76	14.44	38.27	31.14	35.00	62.32
Ce	ppm	97.46	71.62	83.25	24.11	73.55	59.33	66.06	129.66
Pr	ppm	10.76	9.21	9.40	2.90	8.68	6.69	7.54	13.67
Nd	ppm	38.52	32.25	35.34	11.80	33.58	26.27	29.45	48.25
Sm	ppm	5.92	5.18	6.52	2.42	6.25	4.54	4.86	8.70
Eu	ppm	1.41	1.14	1.38	0.51	1.28	1.16	1.17	1.89
Gd	ppm	5.61	4.92	5.36	1.87	4.96	4.17	4.32	8.16
Tb	ppm	0.94	0.85	0.77	0.29	0.77	0.64	0.58	1.07
Dy	ppm	4.93	4.69	4.89	1.63	4.95	3.84	3.30	6.52
Ho	ppm	0.99	0.92	1.03	0.34	0.75	0.71	0.69	1.21
Er	ppm	3.05	2.81	2.88	1.05	1.84	1.94	2.12	3.39
Tm	ppm	0.47	0.45	0.39	0.15	0.29	0.31	0.31	0.42
Yb	ppm	2.83	2.74	2.83	0.83	1.62	1.82	1.92	3.15
Lu	ppm	0.44	0.43	0.42	0.13	0.32	0.35	0.32	0.44
Hf	ppm	8.20	10.22	6.64	4.88	7.49	12.47	14.83	13.37
Ta	ppm	1.80	1.80	1.63	1.02	1.30	1.93	1.71	1.71
W	ppm	2.00	2.50	2.04	3.05	1.00	3.04	3.03	1.01
Tl	ppm	0.10	0.10	0.61	-	0.60	0.51	-	0.50
Pb	ppm	9.51	5.51	43.92	10.17	13.99	11.16	11.09	15.08
Bi	ppm	-	-	0.21	0.06	0.06	0.05	0.05	0.04
Th	ppm	13.51	12.72	8.05	4.31	7.89	8.16	10.79	7.88
U	ppm	3.00	3.01	2.47	1.19	1.49	1.93	2.48	2.52
LOI	ppm	8.30	3.71	4.28	3.83	4.60	3.32	3.46	3.12
Total	%	100	100	100	100	100	100	100	100

Bulk rock geochemistry (Kisegi-Nyabusosi area) cont.

	Sample ID	NG-1	LB-5	SEM 79-2	SEM 78-8	SEM 91-1	SEM 92-1	SEM 89-1
	Formation	Nyaburogo	Oluka	Oluka	Oluka	Kakara	Kakara	Kakara
SiO_2	%	90.24	87.23	94.85	72.72	79.97	83.67	87.80
Al_2O_3	%	4.66	5.20	2.03	11.09	6.65	6.61	4.56
Fe_2O_3	%	1.10	2.07	0.65	3.41	2.42	1.47	1.24
CaO	%	0.49	0.49	0.13	0.68	0.91	0.76	0.43
MgO	%	0.11	0.14	0.03	0.52	0.19	0.17	0.08
Na_2O	%	0.83	0.81	0.20	1.29	1.43	1.33	0.83
K_2O	%	1.67	1.69	1.18	2.94	2.13	2.15	1.73
Cr_2O3	%	0.00	0.08	0.00	0.00	0.00	0.00	0.00
TiO_2	%	0.13	0.35	0.08	0.86	1.13	0.36	0.42
MnO	%	0.01	0.05	-	0.02	0.04	0.01	0.01
P_2O_5	%	-	-	-	0.09	0.08	0.05	-
Sc	ppm	1.98	0.99	1.02	6.08	3.98	3.07	1.98
Be	ppm	-	0.00	0.00	0.00	0.00	0.00	0.00
V	ppm	12.87	22.77	5.08	73.94	59.68	38.92	21.83
Cr	ppm	118.81	475.25	264.31	324.12	169.09	163.87	208.33
Co	ppm	2.97	5.94	-	4.05	4.97	2.05	3.97
Ni	ppm	-	11.88	5.08	14.18	8.95	6.15	5.95
Cu	ppm	-	5.94	3.05	28.36	4.97	4.10	2.98
Zn	ppm	-	17.82	4.07	42.54	22.88	12.29	13.89
Ga	ppm	4.95	22.77	3.76	15.09	14.22	13.62	7.84
Ge	ppm	0.79	0.00	0.00	0.00	0.00	0.00	0.00
As	ppm	-	0.50	2.24	0.51	7.86	2.36	5.46
Rb	ppm	38.61	39.31	34.87	96.73	57.99	65.44	49.40
Sr	ppm	146.53	165.84	93.32	389.95	239.71	236.58	154.76
Y	ppm	3.76	5.05	7.01	27.55	21.38	6.76	8.53
Zr	ppm	72.28	289.11	101.66	374.76	925.00	174.11	238.10
Nb	ppm	4.65	18.51	4.47	46.90	41.58	16.80	14.48
Mo	ppm	1.98	6.93	4.07	2.03	7.96	3.07	5.95
Ag	ppm	-	-	-	-	-	-	-
In	ppm	-	0.00	0.00	0.00	0.00	0.00	0.00
Sn	ppm	-	1.98	-	1.01	0.99	-	-
Sb	ppm	0.50	0.05	-	0.07	-	-	-
Cs	ppm	0.40	0.33	0.22	2.21	1.21	1.42	0.69
Ba	ppm	541.58	598.02	435.09	1311.66	763.88	792.71	611.11
La	ppm	9.30	16.44	8.44	60.16	53.91	20.79	22.42
Ce	ppm	18.91	24.26	16.77	112.43	105.93	40.35	47.72
Pr	ppm	1.96	2.48	1.97	12.00	11.74	4.28	4.97
Nd	ppm	7.27	8.91	7.83	40.01	42.17	15.16	17.56
Sm	ppm	1.32	1.60	1.65	7.16	7.11	2.29	3.13
Eu	ppm	0.35	0.38	0.43	1.75	1.39	0.70	0.78
Gd	ppm	0.96	0.99	1.36	6.06	5.11	1.75	2.22
Tb	ppm	0.15	0.13	0.21	0.89	0.72	0.25	0.32
Dy	ppm	0.79	0.92	1.19	4.71	3.69	1.24	1.55
Ho	ppm	0.15	0.20	0.22	0.89	0.72	0.24	0.29
Er	ppm	0.43	0.76	0.70	2.70	2.23	0.72	0.88
Tm	ppm	0.06	0.10	0.13	0.45	0.40	0.13	0.17
Yb	ppm	0.44	0.69	0.68	2.51	2.35	0.75	0.88
Lu	ppm	0.07	0.14	0.10	0.38	0.37	0.12	0.15
Hf	ppm	1.68	6.83	2.64	9.12	21.58	4.20	5.56
Ta	ppm	0.30	1.29	0.30	3.04	2.98	1.13	1.09
W	ppm	1.19	3.96	1.02	3.04	4.97	2.05	2.98
Tl	ppm	0.19	-	-	-	-	-	-
Pb	ppm	9.90	8.91	6.10	19.24	10.94	8.19	7.94
Bi	ppm	-	0.04	0.01	0.03	0.02	0.01	0.01
Th	ppm	1.93	3.97	2.52	11.75	17.70	4.42	5.01
U	ppm	0.55	1.85	1.02	2.62	4.80	1.67	3.02
LOI	ppm	0.73	1.84	0.76	6.16	4.92	3.28	2.80
Total	%	100	100	100	100	100	100	100

Bulk rock geochemistry (Kisegi-Nyabusosi area) cont.

	Sample ID	SEM 88-1	SEM 87-1	SEM 119-1	SEM 126-1	SEM 122-2	SEM 130-2	SEM 130-1
	Formation	Kakara	Kakara	Kakara	Kisegi	Kisegi	Kisegi	Kisegi
SiO_2	%	91.30	87.39	89.51	88.58	87.47	88.87	92.30
Al_2O_3	%	3.29	4.56	4.86	5.10	5.45	3.38	3.35
Fe_2O_3	%	0.63	1.09	0.64	1.03	1.08	2.07	0.64
CaO	%	0.26	0.28	0.44	0.42	0.45	0.16	0.23
MgO	%	0.03	0.20	0.05	0.03	0.03	-	0.05
Na_2O	%	0.47	0.48	1.00	1.05	1.16	0.61	0.58
K_2O	%	1.37	1.62	1.58	1.74	1.81	1.22	1.21
Cr_2O3	%	0.00	0.00	0.00	0.00	0.00	0.00	0.00
TiO_2	%	0.24	0.25	0.33	0.74	0.44	0.26	0.14
MnO	%	0.01	0.03	0.02	0.01	0.01	0.01	-
P_2O_5	%	-	0.11	0.02	0.03	-	0.06	-
Sc	ppm	1.99	2.99	1.01	2.02	2.06	3.04	1.02
Be	ppm	0.00	0.00	0.00	0.00	0.00	0.00	0.00
V	ppm	14.90	32.85	23.24	33.29	23.70	66.96	22.54
Cr	ppm	218.56	159.25	232.37	312.75	185.45	294.21	184.39
Co	ppm	1.99	10.95	2.02	2.02	2.06	2.03	2.05
Ni	ppm	4.97	15.93	5.05	11.10	4.12	6.09	9.22
Cu	ppm	2.98	5.97	3.03	9.08	5.15	8.12	9.22
Zn	ppm	7.95	36.83	8.08	18.16	8.24	9.13	12.29
Ga	ppm	5.36	9.65	6.47	7.97	8.04	6.09	5.74
Ge	ppm	0.00	0.00	0.00	0.00	0.00	0.00	0.00
As	ppm	3.48	4.28	0.61	0.50	0.31	0.71	0.41
Rb	ppm	38.74	49.07	42.33	47.72	51.10	38.96	36.78
Sr	ppm	102.32	142.83	177.81	204.80	208.12	130.36	97.83
Y	ppm	6.36	11.84	6.87	6.66	6.39	6.49	5.33
Zr	ppm	149.02	99.53	131.34	252.22	216.36	152.18	92.19
Nb	ppm	8.94	13.54	13.13	38.34	21.02	14.20	6.25
Mo	ppm	7.95	3.98	3.03	6.05	2.06	5.07	3.07
Ag	ppm	-	-	-	-	-	-	-
In	ppm	0.00	0.00	0.00	0.00	0.00	0.00	0.00
Sn	ppm	-	-	-	1.01	-	1.01	-
Sb	ppm	-	-	-	-	-	-	-
Cs	ppm	0.57	1.79	1.32	0.65	0.78	1.10	0.76
Ba	ppm	483.81	542.45	613.26	613.40	702.66	443.34	404.63
La	ppm	25.13	24.39	16.16	27.95	22.77	39.87	11.47
Ce	ppm	52.16	53.55	30.61	48.73	42.04	94.65	20.69
Pr	ppm	5.11	6.48	3.31	4.89	4.27	8.51	2.32
Nd	ppm	17.48	26.67	11.82	16.04	13.91	27.70	8.09
Sm	ppm	2.97	3.83	2.21	2.42	2.12	3.68	1.41
Eu	ppm	0.70	0.88	0.60	0.66	0.65	0.81	0.36
Gd	ppm	2.03	2.54	1.68	1.67	1.47	2.16	1.10
Tb	ppm	0.27	0.40	0.23	0.23	0.21	0.26	0.15
Dy	ppm	1.36	2.14	1.20	1.21	1.12	1.31	0.87
Ho	ppm	0.24	0.41	0.22	0.23	0.22	0.24	0.17
Er	ppm	0.68	1.16	0.67	0.73	0.66	0.72	0.56
Tm	ppm	0.13	0.20	0.13	0.14	0.13	0.14	0.11
Yb	ppm	0.68	1.01	0.69	0.79	0.69	0.80	0.67
Lu	ppm	0.11	0.15	0.10	0.12	0.10	0.12	0.10
Hf	ppm	3.48	2.79	3.13	5.45	4.84	3.35	2.36
Ta	ppm	0.70	1.00	0.91	3.03	1.55	0.91	0.41
W	ppm	1.99	1.99	2.02	4.04	3.09	3.04	1.02
Tl	ppm	-	-	-	-	-	-	-
Pb	ppm	5.96	7.96	8.08	14.12	9.27	14.20	8.20
Bi	ppm	0.01	0.01	0.01	0.01	0.01	0.03	0.04
Th	ppm	5.55	4.67	3.92	6.30	5.02	4.63	3.14
U	ppm	2.15	1.98	0.80	1.18	1.26	2.06	1.30
LOI	ppm	2.32	3.89	1.43	1.15	1.98	3.28	1.43
Total	%	100	100	100	100	100	100	100

Bulk rock geochemistry (Kisegi-Nyabusosi area) cont.

	Sample ID	SEM 149-1	SEM 131-2	SEM 140-1	SEM 139-2	SEM 136-1	SEM 200-2	SEM 201-1
	Formation	Kisegi	Kisegi	Kisegi	Kisegi	Kisegi	Kisegi	Kisegi
SiO_2	%	81.61	83.56	86.34	75.14	77.99	80.06	73.74
Al_2O_3	%	7.60	5.83	6.34	7.08	6.96	6.20	4.98
Fe_2O_3	%	1.60	1.87	0.72	5.16	3.14	2.42	6.22
CaO	%	0.87	0.92	0.63	0.54	0.58	1.00	0.32
MgO	%	0.18	0.05	0.09	0.26	0.29	0.13	0.23
Na_2O	%	1.68	1.46	1.40	1.64	1.37	1.31	0.53
K_2O	%	2.19	1.83	2.08	2.50	1.97	2.57	2.53
Cr_2O3	%	0.00	0.00	0.00	0.00	0.00	0.13	0.01
TiO_2	%	0.72	0.59	0.60	1.02	1.11	1.49	0.98
MnO	%	0.03	0.01	0.01	0.02	0.01	0.01	0.01
P_2O_5	%	0.08	0.08	0.02	0.15	0.20	0.05	0.33
Sc	ppm	3.03	3.00	2.03	5.00	5.08	2.99	4.05
Be	ppm	0.00	0.00	0.00	0.00	0.00	0.00	0.00
V	ppm	58.58	42.03	32.50	141.07	90.50	66.71	99.13
Cr	ppm	141.40	300.21	223.46	190.10	132.19	726.87	50.58
Co	ppm	6.06	-	1.02	4.00	4.07	3.98	382.36
Ni	ppm	7.07	6.00	5.08	4.00	4.07	13.94	5.06
Cu	ppm	9.09	4.00	6.09	10.01	21.35	22.90	20.23
Zn	ppm	20.20	4.00	7.11	16.01	30.51	7.97	38.44
Ga	ppm	13.33	10.41	11.99	23.21	19.22	19.91	11.94
Ge	ppm	0.00	0.00	0.00	0.00	0.00	0.00	0.00
As	ppm	0.71	7.10	3.15	17.11	1.73	12.45	-
Rb	ppm	69.49	55.14	63.48	105.05	73.42	66.91	66.46
Sr	ppm	250.48	249.17	207.21	246.12	684.36	213.08	176.01
Y	ppm	13.33	6.70	6.70	9.20	18.51	10.46	6.88
Zr	ppm	353.50	110.08	233.62	260.13	467.76	379.37	181.06
Nb	ppm	46.86	37.73	44.29	69.13	85.01	94.79	67.47
Mo	ppm	2.02	8.01	5.08	19.01	5.08	24.89	1.01
Ag	ppm	-	-	-	-	-	-	-
In	ppm	0.00	0.00	0.00	0.00	0.00	0.00	0.00
Sn	ppm	1.01	-	-	1.00	1.02	1.99	2.02
Sb	ppm	-	-	-	-	-	0.54	0.33
Cs	ppm	2.01	0.86	2.71	3.38	2.52	0.69	1.41
Ba	ppm	760.53	621.44	656.17	747.37	734.19	651.20	641.31
La	ppm	50.70	36.03	34.03	85.54	79.72	66.61	57.15
Ce	ppm	97.77	68.55	63.79	164.08	154.06	119.98	125.43
Pr	ppm	10.81	7.98	6.23	16.86	17.49	13.44	14.97
Nd	ppm	39.09	28.82	20.01	42.52	63.45	47.99	55.33
Sm	ppm	6.43	4.26	3.21	4.83	7.71	6.86	8.56
Eu	ppm	1.56	1.11	0.81	1.27	1.61	1.46	1.86
Gd	ppm	4.34	2.44	1.94	3.13	4.19	4.06	4.14
Tb	ppm	0.56	0.32	0.26	0.40	0.56	0.51	0.47
Dy	ppm	2.70	1.53	1.32	1.88	2.93	2.87	2.42
Ho	ppm	0.46	0.27	0.24	0.33	0.57	0.42	0.43
Er	ppm	1.36	0.74	0.76	0.93	1.77	1.42	0.96
Tm	ppm	0.25	0.13	0.16	0.17	0.32	0.16	0.14
Yb	ppm	1.34	0.72	0.90	0.90	1.80	1.15	0.78
Lu	ppm	0.21	0.10	0.15	0.14	0.28	0.22	0.11
Hf	ppm	7.88	2.70	5.59	6.30	10.58	9.06	3.94
Ta	ppm	3.03	2.70	2.74	4.00	4.98	5.28	6.47
W	ppm	6.06	8.01	4.06	12.01	13.22	15.93	999.39
Tl	ppm	-	-	-	-	-	0.50	0.51
Pb	ppm	12.12	10.01	8.13	13.01	13.22	8.96	17.20
Bi	ppm	0.02	0.01	0.02	0.02	0.03	0.13	0.90
Th	ppm	9.35	4.60	6.63	12.51	11.03	10.95	11.68
U	ppm	1.97	1.87	3.80	3.57	9.63	5.77	1.81
LOI	ppm	3.32	3.66	1.65	6.35	6.18	4.52	10.03
Total	%	100	100	100	100	100	100	100

A6-2 – Bulk rock geochemistry (Nkondo-Kaiso area)

	Sample ID	MB-2	MB-3	KAI 47-1	KAI 51-1	KAI 52-1	KV-4	Kyeoro 1
	Formation	Museta beds	Museta beds	Kaiso Village	Kaiso Village	Kaiso Village	Kaiso Village	Kyeoro
SiO_2	%	76.48	70.75	82.98	83.91	82.06	76.95	67.18
Al_2O_3	%	7.79	8.82	6.82	7.33	6.61	5.62	13.00
Fe_2O_3	%	4.42	4.66	2.44	2.23	2.99	8.01	4.65
CaO	%	0.95	2.23	0.35	0.12	0.42	0.89	1.85
MgO	%	0.52	0.66	0.27	0.25	0.58	0.32	0.72
Na_2O	%	0.76	1.04	0.45	0.21	0.28	0.84	2.27
K_2O	%	1.25	1.44	1.50	0.93	0.82	1.15	2.08
Cr_2O3	%	0.09	0.04	0.00	0.00	0.00	0.09	0.03
TiO_2	%	1.14	1.18	0.72	0.77	0.71	0.54	0.97
MnO	%	0.13	0.18	0.02	0.02	0.03	0.16	0.07
P_2O_5	%	0.07	0.12	0.01	0.02	0.03	0.19	0.09
Sc	ppm	6.00	7.02	4.93	7.95	6.09	4.00	9.04
Be	ppm	0.00	0.00	0.00	0.00	0.00	0.00	0.00
V	ppm	64.99	76.27	55.19	67.61	67.96	56.97	81.33
Cr	ppm	509.90	240.84	118.26	109.37	101.43	539.68	160.66
Co	ppm	17.00	18.06	6.90	3.98	8.11	18.99	13.05
Ni	ppm	24.00	24.08	15.77	12.93	17.24	23.99	22.09
Cu	ppm	19.00	24.08	11.83	10.94	13.19	9.99	19.08
Zn	ppm	45.99	53.19	40.41	31.82	33.47	46.97	67.28
Ga	ppm	26.29	25.79	11.04	11.53	9.23	38.58	43.78
Ge	ppm	0.00	0.00	0.00	0.00	0.00	0.00	0.00
As	ppm	0.60	1.00	0.30	0.99	0.51	5.20	0.20
Rb	ppm	32.89	40.14	45.92	45.24	30.73	26.58	65.47
Sr	ppm	152.47	248.87	117.77	45.54	84.39	138.92	305.25
Y	ppm	24.30	27.50	21.78	32.61	21.91	16.69	19.38
Zr	ppm	473.91	523.83	364.64	308.21	324.58	338.80	450.85
Nb	ppm	30.49	34.22	22.17	15.21	17.34	16.19	39.56
Mo	ppm	9.00	3.01	0.99	-	-	8.99	3.01
Ag	ppm	-	-	-	-	-	-	-
In	ppm	0.00	0.00	0.00	0.00	0.00	0.00	0.00
Sn	ppm	2.00	3.01	0.99	0.99	1.01	1.00	3.01
Sb	ppm	-	-	-	0.08	-	0.08	-
Cs	ppm	0.65	0.67	1.13	1.97	1.25	0.52	1.49
Ba	ppm	667.87	1279.48	742.09	353.95	365.15	531.68	761.12
La	ppm	56.89	62.72	45.53	97.83	47.06	34.78	42.37
Ce	ppm	104.48	122.93	86.82	217.74	93.01	72.16	84.25
Pr	ppm	12.05	13.30	9.90	23.56	10.45	7.85	9.42
Nd	ppm	45.19	51.18	35.58	83.22	37.93	30.28	35.55
Sm	ppm	7.79	9.08	6.25	14.17	6.63	5.33	6.37
Eu	ppm	1.48	1.92	1.35	3.01	1.24	1.18	1.64
Gd	ppm	6.14	6.86	4.91	10.59	4.68	4.81	5.14
Tb	ppm	0.78	0.83	0.74	1.47	0.66	0.66	0.67
Dy	ppm	4.83	6.08	3.96	6.99	3.99	3.77	4.04
Ho	ppm	0.82	1.00	0.75	1.19	0.79	0.72	0.76
Er	ppm	2.69	3.01	2.19	3.14	2.15	2.41	2.29
Tm	ppm	0.35	0.42	0.36	0.50	0.32	0.28	0.31
Yb	ppm	2.39	2.59	2.04	2.55	2.08	1.91	1.95
Lu	ppm	0.34	0.44	0.31	0.37	0.32	0.31	0.33
Hf	ppm	11.30	12.44	8.38	7.26	7.81	8.10	11.35
Ta	ppm	1.70	2.11	1.38	0.99	1.12	1.20	2.51
W	ppm	10.00	2.01	0.99	0.99	1.01	4.00	1.00
Tl	ppm	0.50	0.70	-	-	-	0.60	0.60
Pb	ppm	13.00	16.06	9.86	12.93	9.13	12.99	16.07
Bi	ppm	0.05	0.06	0.03	0.04	0.03	0.06	0.06
Th	ppm	12.25	12.09	9.43	9.77	9.81	6.60	10.74
U	ppm	2.27	2.48	1.84	2.23	1.99	2.11	1.96
LOI	ppm	6.29	8.71	4.33	4.15	5.41	5.19	6.94
Total	%	100	100	100	100	100	100	100

Bulk rock geochemistry (Nkondo-Kaiso area) cont.

		Kyeoro 2 Kyeoro	CL2-1 Warwire	CL2-4 Warwire	CL23m70 Warwire	CL9m10 Warwire	CL6m40 Warwire	SC1/1m10 Warwire
SiO_2	%	74.65	80.44	78.17	75.54	78.08	77.02	86.64
Al_2O_3	%	11.21	7.39	10.03	11.41	10.53	11.43	6.74
Fe_2O_3	%	3.01	4.19	2.41	2.60	2.27	2.11	1.14
CaO	%	1.93	1.34	2.00	2.00	2.37	2.28	0.96
MgO	%	0.41	0.37	0.39	0.61	0.61	0.53	0.20
Na_2O	%	2.27	1.56	2.14	2.37	2.39	2.52	1.40
K_2O	%	2.30	1.72	2.30	2.42	2.15	2.39	2.05
Cr_2O3	%	0.03	0.00	0.00	0.00	0.00	0.00	0.00
TiO_2	%	0.65	0.28	0.55	0.48	0.62	0.44	0.14
MnO	%	0.15	0.04	0.05	0.03	0.04	0.03	0.01
P_2O_5	%	0.19	0.01	0.13	0.04	0.07	0.07	0.01
Sc	ppm	5.07	3.04	3.97	4.97	5.96	4.97	1.98
Be	ppm	0.00	1.01	0.99	1.99	-	0.99	-
V	ppm	44.63	32.43	30.75	40.71	40.71	38.77	15.84
Cr	ppm	192.72	70.94	79.37	119.17	89.37	89.46	158.42
Co	ppm	7.10	15.20	7.94	7.94	5.96	7.95	3.96
Ni	ppm	16.23	-	-	-	-	-	-
Cu	ppm	7.10	-	-	-	-	-	-
Zn	ppm	30.43	40.54	-	39.72	-	-	-
Ga	ppm	35.70	8.11	10.91	13.90	10.92	11.93	6.93
Ge	ppm	0.00	1.01	1.09	1.09	0.99	1.29	0.99
As	ppm	0.81	-	-	-	-	-	-
Rb	ppm	56.70	37.49	47.62	58.59	43.69	55.67	43.56
Sr	ppm	386.45	283.75	364.09	383.32	407.15	430.42	243.56
Y	ppm	12.78	14.19	24.80	14.30	12.12	9.94	5.15
Zr	ppm	407.75	171.26	302.58	199.60	421.05	178.93	66.34
Nb	ppm	21.91	8.82	22.32	20.75	14.60	14.21	5.35
Mo	ppm	5.07	-	-	-	-	-	2.97
Ag	ppm	-	0.61	1.19	0.79	1.69	0.70	-
In	ppm	0.00	-	-	-	-	-	-
Sn	ppm	2.03	-	-	0.99	-	-	-
Sb	ppm	-	0.61	0.69	0.60	0.60	0.60	0.59
Cs	ppm	0.75	0.41	0.50	0.70	0.40	0.50	0.30
Ba	ppm	878.39	680.99	860.12	884.81	857.99	914.51	699.01
La	ppm	23.73	20.77	29.37	24.53	18.77	19.18	12.57
Ce	ppm	46.15	47.63	57.74	48.86	37.84	39.36	26.63
Pr	ppm	5.21	4.58	6.40	5.30	4.27	4.17	2.64
Nd	ppm	19.98	17.33	25.40	20.36	16.58	15.61	9.84
Sm	ppm	3.89	3.44	4.92	3.72	3.23	2.90	1.72
Eu	ppm	0.86	0.86	1.21	0.98	0.94	0.88	0.51
Gd	ppm	3.28	3.08	4.64	3.15	2.67	2.46	1.41
Tb	ppm	0.43	0.51	0.75	0.50	0.41	0.38	0.19
Dy	ppm	2.34	2.82	4.53	2.79	2.26	1.98	1.01
Ho	ppm	0.54	0.56	0.89	0.54	0.44	0.37	0.20
Er	ppm	1.46	1.63	2.68	1.54	1.33	1.06	0.56
Tm	ppm	0.15	0.25	0.39	0.23	0.21	0.16	0.08
Yb	ppm	1.51	1.64	2.52	1.57	1.41	1.06	0.53
Lu	ppm	0.30	0.25	0.40	0.25	0.24	0.17	0.09
Hf	ppm	10.14	3.75	7.04	4.47	9.43	4.08	1.49
Ta	ppm	1.62	0.55	1.19	1.14	0.93	0.83	0.33
W	ppm	2.03	0.71	1.19	0.89	0.99	1.09	-
Tl	ppm	0.61	0.19	0.21	0.24	0.18	0.24	0.19
Pb	ppm	8.11	16.21	17.86	17.87	15.89	16.90	11.88
Bi	ppm	0.04	-	-	-	-	-	-
Th	ppm	6.15	2.46	5.20	4.46	4.51	3.67	1.87
U	ppm	1.52	0.79	1.33	0.95	1.26	0.89	0.44
LOI	ppm	3.00	2.66	1.80	2.52	0.89	1.23	0.66
Total	%	100	100	100	100	100	100	100

Bulk rock geochemistry (Nkondo-Kaiso area) cont.

		SC3/3m70 Warwire	SC4/3m30 Warwire	SV1m30 Warwire	SV5m70 Warwire	SV7m30 Warwire	LA-1 Nkondo	NK-Fe-2 Nkondo
SiO_2	%	78.20	77.07	85.39	70.18	78.79	73.96	71.20
Al_2O_3	%	10.20	10.77	7.31	11.63	6.89	11.49	8.30
Fe_2O_3	%	2.77	2.42	1.41	4.99	5.40	2.96	9.47
CaO	%	1.88	1.99	1.13	1.88	1.26	1.54	1.29
MgO	%	0.39	0.53	0.16	0.58	0.42	0.44	0.47
Na_2O	%	2.37	2.26	1.50	2.02	1.08	2.05	1.29
K_2O	%	2.21	2.42	1.98	2.24	1.59	2.91	1.94
Cr_2O3	%	0.00	0.00	0.00	0.00	0.00	0.03	0.05
TiO_2	%	0.35	0.46	0.31	0.63	0.57	1.10	0.61
MnO	%	0.03	0.03	0.02	0.03	0.05	0.04	0.13
P_2O_5	%	0.07	0.04	0.02	0.04	0.05	0.07	0.09
Sc	ppm	3.98	4.98	1.99	7.10	3.98	6.00	5.01
Be	ppm	-	1.00	-	2.03	1.00	0.00	0.00
V	ppm	30.82	38.84	19.86	54.74	53.73	53.97	74.21
Cr	ppm	89.46	89.64	148.96	91.24	119.40	189.89	290.81
Co	ppm	6.96	6.97	4.97	12.17	16.92	8.00	23.06
Ni	ppm	-	-	-	-	19.90	13.99	25.07
Cu	ppm	-	-	-	10.14	-	23.99	14.04
Zn	ppm	-	-	-	40.55	49.75	42.97	77.22
Ga	ppm	9.94	11.95	6.95	14.19	7.96	33.78	21.26
Ge	ppm	0.99	1.10	0.89	1.32	1.39	0.00	0.00
As	ppm	-	-	-	-	4.98	1.30	2.31
Rb	ppm	45.73	56.77	41.71	54.74	36.82	68.06	64.68
Sr	ppm	377.73	385.46	276.07	353.81	217.91	359.78	221.62
Y	ppm	8.75	9.26	6.55	15.71	19.20	26.78	19.55
Zr	ppm	128.23	157.37	174.78	295.01	439.80	973.42	482.35
Nb	ppm	9.15	15.34	6.95	19.16	18.61	45.67	23.27
Mo	ppm	-	-	1.99	-	-	4.00	5.01
Ag	ppm	0.50	0.60	0.70	1.12	1.69	-	-
In	ppm	-	-	-	-	-	0.00	0.00
Sn	ppm	-	-	-	1.01	-	3.00	1.00
Sb	ppm	0.60	0.60	0.60	0.61	0.70	0.44	0.06
Cs	ppm	0.40	0.60	0.30	0.81	0.40	0.72	1.60
Ba	ppm	868.79	951.20	786.49	875.91	636.82	1099.34	830.32
La	ppm	16.10	19.42	14.80	28.49	37.01	50.07	35.10
Ce	ppm	32.80	38.15	28.10	55.35	76.22	95.34	67.79
Pr	ppm	3.47	4.13	3.08	6.03	8.17	10.64	8.44
Nd	ppm	12.92	15.54	11.52	22.81	31.34	39.88	31.69
Sm	ppm	2.47	2.86	2.07	4.21	5.85	7.75	5.96
Eu	ppm	0.77	0.85	0.59	1.13	1.20	1.52	1.25
Gd	ppm	2.04	2.37	1.64	3.68	5.12	6.19	4.55
Tb	ppm	0.30	0.35	0.24	0.55	0.80	0.85	0.60
Dy	ppm	1.67	1.88	1.26	3.00	4.32	5.45	4.23
Ho	ppm	0.32	0.36	0.25	0.59	0.81	1.03	0.82
Er	ppm	0.94	1.03	0.72	1.73	2.27	3.20	2.44
Tm	ppm	0.14	0.15	0.11	0.26	0.33	0.49	0.34
Yb	ppm	0.94	0.99	0.75	1.76	2.22	2.91	2.33
Lu	ppm	0.15	0.15	0.12	0.29	0.35	0.44	0.41
Hf	ppm	2.88	3.59	3.97	6.69	9.65	22.59	11.73
Ta	ppm	0.60	0.90	0.47	1.14	1.02	2.80	1.60
W	ppm	0.70	0.90	1.29	0.71	0.70	2.00	5.01
Tl	ppm	0.20	0.24	0.17	0.25	0.16	-	0.60
Pb	ppm	14.91	16.93	12.91	19.26	19.90	21.99	7.02
Bi	ppm	-	-	-	-	-	0.15	0.08
Th	ppm	2.53	3.47	2.92	5.65	6.27	12.74	7.99
U	ppm	0.92	0.89	0.66	1.32	1.21	3.26	2.04
LOI	ppm	1.49	2.04	0.79	5.78	3.89	3.23	5.08
Total	%	100	100	100	100	100	100	100

Bulk rock geochemistry (Nkondo-Kaiso area) cont.

		NV3-1 Nkondo	NV3-2 Nkondo
SiO_2	%	70.72	78.59
Al_2O_3	%	10.05	8.85
Fe_2O_3	%	5.26	2.90
CaO	%	1.53	1.13
MgO	%	0.56	0.41
Na_2O	%	1.72	1.39
K_2O	%	2.52	2.07
Cr_2O3	%	0.01	0.10
TiO_2	%	1.67	0.55
MnO	%	0.15	0.09
P_2O_5	%	0.26	0.09
Sc	ppm	6.04	4.00
Be	ppm	0.00	0.00
V	ppm	78.58	35.00
Cr	ppm	50.37	579.94
Co	ppm	165.22	10.00
Ni	ppm	28.21	20.00
Cu	ppm	25.19	13.00
Zn	ppm	65.48	38.00
Ga	ppm	19.44	19.20
Ge	ppm	0.00	0.00
As	ppm	2.92	0.60
Rb	ppm	67.40	54.09
Sr	ppm	293.17	232.98
Y	ppm	45.54	10.90
Zr	ppm	567.20	281.97
Nb	ppm	62.16	18.90
Mo	ppm	-	11.00
Ag	ppm	-	-
In	ppm	0.00	0.00
Sn	ppm	2.01	1.00
Sb	ppm	0.07	0.07
Cs	ppm	1.01	0.65
Ba	ppm	1032.64	737.93
La	ppm	71.03	25.80
Ce	ppm	133.99	50.99
Pr	ppm	14.91	5.55
Nd	ppm	55.81	21.60
Sm	ppm	10.68	3.86
Eu	ppm	2.21	0.99
Gd	ppm	8.83	2.68
Tb	ppm	1.34	0.41
Dy	ppm	8.35	2.68
Ho	ppm	1.75	0.45
Er	ppm	5.00	1.36
Tm	ppm	0.70	0.18
Yb	ppm	4.67	1.02
Lu	ppm	0.72	0.22
Hf	ppm	13.30	7.20
Ta	ppm	5.44	1.30
W	ppm	890.59	5.00
Tl	ppm	0.71	0.50
Pb	ppm	23.17	14.00
Bi	ppm	0.10	0.05
Th	ppm	14.56	6.07
U	ppm	3.20	1.17
LOI	ppm	5.36	3.69
Total	%	100	100

A6-3 Zircon U-Pb geochronology (Kisegi-Nyabusosi area)

			Isotope ratios								Age estimates								
Formation	Sample ID	Analysis No.	$^{207}Pb/^{206}Pb$	±1σ	$^{206}Pb/^{238}U$	±1σ	$^{207}Pb/^{235}U$	±1σ	$^{208}Pb/^{232}Th$	±1σ	$^{207}Pb/^{206}Pb$ [Ma]	±1σ [Ma]	$^{206}Pb/^{238}U$ [Ma]	±1σ [Ma]	$^{207}Pb/^{235}U$ [Ma]	±1σ [Ma]	$^{208}Pb/^{232}Th$ [Ma]	±1σ [Ma]	Concordance [%]
Kisegi	SEM-200-2	1	~~0.162~~	~~0.002~~	~~0.093~~	~~0.001~~	~~2.130~~	~~0.041~~	~~0.021~~	~~0.001~~	~~2477~~	~~23~~	~~571~~	~~7~~	~~1159~~	~~13~~	~~416~~	~~13~~	~~23~~
Kisegi	SEM-200-2	2	~~0.132~~	~~0.002~~	~~0.104~~	~~0.001~~	~~1.938~~	~~0.039~~	~~0.018~~	~~0.001~~	~~2119~~	~~25~~	~~639~~	~~7~~	~~1094~~	~~14~~	~~360~~	~~14~~	~~30~~
Kisegi	SEM-200-2	3	~~0.158~~	~~0.002~~	~~0.135~~	~~0.002~~	~~3.030~~	~~0.057~~	~~0.031~~	~~0.001~~	~~2435~~	~~23~~	~~817~~	~~9~~	~~1415~~	~~14~~	~~619~~	~~21~~	~~34~~
Kisegi	SEM-200-2	4	~~0.147~~	~~0.002~~	~~0.128~~	~~0.002~~	~~2.641~~	~~0.049~~	~~0.026~~	~~0.001~~	~~2306~~	~~23~~	~~778~~	~~9~~	~~1312~~	~~14~~	~~525~~	~~17~~	~~34~~
Kisegi	SEM-200-2	5	~~0.167~~	~~0.003~~	~~0.149~~	~~0.002~~	~~3.511~~	~~0.100~~	~~0.024~~	~~0.001~~	~~2528~~	~~32~~	~~895~~	~~11~~	~~1530~~	~~23~~	~~478~~	~~29~~	~~35~~
Kisegi	SEM-200-2	6	~~4.889~~	~~0.089~~	~~0.527~~	~~0.007~~	~~351.186~~	~~11.699~~	~~0.134~~	~~0.008~~	~~7390~~	~~24~~	~~2729~~	~~29~~	~~5954~~	~~34~~	~~2550~~	~~140~~	~~37~~
Kisegi	SEM-200-2	7	~~0.152~~	~~0.002~~	~~0.173~~	~~0.002~~	~~3.741~~	~~0.075~~	~~0.038~~	~~0.001~~	~~2366~~	~~23~~	~~1029~~	~~12~~	~~1580~~	~~16~~	~~763~~	~~24~~	~~44~~
Kisegi	SEM-200-2	8	~~0.163~~	~~0.002~~	~~0.187~~	~~0.002~~	~~4.299~~	~~0.088~~	~~0.003~~	~~0.000~~	~~2485~~	~~23~~	~~1105~~	~~12~~	~~1693~~	~~17~~	~~57~~	~~2~~	~~44~~
Kisegi	SEM-200-2	9	~~0.151~~	~~0.002~~	~~0.190~~	~~0.002~~	~~4.121~~	~~0.107~~	~~0.037~~	~~0.001~~	~~2359~~	~~26~~	~~1121~~	~~13~~	~~1658~~	~~21~~	~~735~~	~~26~~	~~48~~
Kisegi	SEM-200-2	10	~~0.161~~	~~0.002~~	~~0.210~~	~~0.003~~	~~4.733~~	~~0.111~~	~~0.025~~	~~0.001~~	~~2466~~	~~26~~	~~1230~~	~~14~~	~~1773~~	~~20~~	~~502~~	~~22~~	~~50~~
Kisegi	SEM-200-2	11	~~0.156~~	~~0.002~~	~~0.212~~	~~0.003~~	~~4.531~~	~~0.108~~	~~0.043~~	~~0.002~~	~~2409~~	~~27~~	~~1238~~	~~14~~	~~1737~~	~~20~~	~~844~~	~~37~~	~~51~~
Kisegi	SEM-200-2	12	~~0.166~~	~~0.002~~	~~0.223~~	~~0.003~~	~~5.189~~	~~0.107~~	~~0.026~~	~~0.001~~	~~2516~~	~~23~~	~~1296~~	~~14~~	~~1851~~	~~18~~	~~520~~	~~17~~	~~52~~
Kisegi	SEM-200-2	13	~~0.065~~	~~0.001~~	~~0.070~~	~~0.001~~	~~0.637~~	~~0.016~~	~~0.020~~	~~0.001~~	~~784~~	~~38~~	~~435~~	~~5~~	~~501~~	~~10~~	~~406~~	~~19~~	~~55~~
Kisegi	SEM-200-2	14	~~0.158~~	~~0.003~~	~~0.239~~	~~0.003~~	~~5.122~~	~~0.156~~	~~0.065~~	~~0.004~~	~~2437~~	~~32~~	~~1382~~	~~16~~	~~1840~~	~~26~~	~~1265~~	~~70~~	~~57~~
Kisegi	SEM-200-2	15	~~0.177~~	~~0.003~~	~~0.291~~	~~0.004~~	~~7.092~~	~~0.165~~	~~0.081~~	~~0.003~~	~~2620~~	~~24~~	~~1646~~	~~18~~	~~2123~~	~~21~~	~~1577~~	~~55~~	~~63~~
Kisegi	SEM-200-2	16	~~0.169~~	~~0.003~~	~~0.286~~	~~0.004~~	~~6.762~~	~~0.199~~	~~0.036~~	~~0.002~~	~~2550~~	~~31~~	~~1621~~	~~19~~	~~2081~~	~~26~~	~~710~~	~~41~~	~~64~~
Kisegi	SEM-200-2	17	~~0.164~~	~~0.003~~	~~0.283~~	~~0.004~~	~~6.402~~	~~0.193~~	~~0.067~~	~~0.002~~	~~2499~~	~~26~~	~~1607~~	~~18~~	~~2033~~	~~26~~	~~1305~~	~~47~~	~~64~~
Kisegi	SEM-200-2	18	~~0.184~~	~~0.003~~	~~0.315~~	~~0.004~~	~~8.040~~	~~0.228~~	~~0.073~~	~~0.004~~	~~2690~~	~~30~~	~~1767~~	~~20~~	~~2236~~	~~26~~	~~1419~~	~~79~~	~~66~~
Kisegi	SEM-200-2	19	~~0.177~~	~~0.003~~	~~0.312~~	~~0.004~~	~~7.803~~	~~0.240~~	~~0.091~~	~~0.005~~	~~2623~~	~~31~~	~~1751~~	~~20~~	~~2209~~	~~28~~	~~1752~~	~~100~~	~~67~~
Kisegi	SEM-200-2	20	~~0.166~~	~~0.003~~	~~0.345~~	~~0.005~~	~~7.778~~	~~0.231~~	~~0.083~~	~~0.005~~	~~2520~~	~~32~~	~~1909~~	~~22~~	~~2206~~	~~27~~	~~1618~~	~~96~~	~~76~~
Kisegi	SEM-200-2	21	~~0.171~~	~~0.002~~	~~0.367~~	~~0.004~~	~~8.845~~	~~0.174~~	~~0.037~~	~~0.001~~	~~2569~~	~~22~~	~~2017~~	~~21~~	~~2322~~	~~18~~	~~731~~	~~24~~	~~79~~
Kisegi	SEM-200-2	22	~~0.170~~	~~0.003~~	~~0.371~~	~~0.005~~	~~8.860~~	~~0.278~~	~~0.090~~	~~0.006~~	~~2556~~	~~33~~	~~2034~~	~~23~~	~~2324~~	~~29~~	~~1749~~	~~105~~	~~80~~
Kisegi	SEM-200-2	23	~~0.174~~	~~0.003~~	~~0.382~~	~~0.005~~	~~9.289~~	~~0.234~~	~~0.088~~	~~0.004~~	~~2597~~	~~25~~	~~2085~~	~~22~~	~~2367~~	~~23~~	~~1709~~	~~69~~	~~80~~
Kisegi	SEM-200-2	24	~~0.122~~	~~0.002~~	~~0.280~~	~~0.004~~	~~4.531~~	~~0.140~~	~~0.077~~	~~0.004~~	~~1983~~	~~32~~	~~1593~~	~~18~~	~~1737~~	~~26~~	~~1506~~	~~76~~	~~80~~
Kisegi	SEM-200-2	25	~~0.067~~	~~0.002~~	~~0.111~~	~~0.002~~	~~1.141~~	~~0.060~~	~~0.034~~	~~0.002~~	~~834~~	~~68~~	~~681~~	~~10~~	~~773~~	~~28~~	~~676~~	~~31~~	~~82~~
Kisegi	SEM-200-2	26	~~0.181~~	~~0.003~~	~~0.403~~	~~0.005~~	~~9.893~~	~~0.344~~	~~0.111~~	~~0.004~~	~~2658~~	~~25~~	~~2185~~	~~24~~	~~2425~~	~~32~~	~~2121~~	~~74~~	~~82~~
Kisegi	SEM-200-2	27	~~0.176~~	~~0.004~~	~~0.402~~	~~0.005~~	~~9.944~~	~~0.320~~	~~0.112~~	~~0.007~~	~~2612~~	~~33~~	~~2179~~	~~24~~	~~2430~~	~~30~~	~~2137~~	~~132~~	~~83~~
Kisegi	SEM-200-2	28	~~0.170~~	~~0.003~~	~~0.401~~	~~0.005~~	~~9.550~~	~~0.254~~	~~0.095~~	~~0.005~~	~~2554~~	~~28~~	~~2174~~	~~23~~	~~2392~~	~~24~~	~~1838~~	~~90~~	~~85~~
Kisegi	SEM-200-2	29	~~0.174~~	~~0.003~~	~~0.418~~	~~0.005~~	~~10.018~~	~~0.233~~	~~0.111~~	~~0.005~~	~~2601~~	~~25~~	~~2250~~	~~24~~	~~2436~~	~~21~~	~~2133~~	~~86~~	~~87~~
Kisegi	SEM-200-2	30	~~0.060~~	~~0.002~~	~~0.083~~	~~0.001~~	~~0.698~~	~~0.031~~	~~0.011~~	~~0.002~~	~~597~~	~~66~~	~~517~~	~~7~~	~~538~~	~~18~~	~~218~~	~~32~~	~~87~~
Kisegi	SEM-200-2	31	~~0.171~~	~~0.003~~	~~0.423~~	~~0.005~~	~~10.196~~	~~0.259~~	~~0.110~~	~~0.005~~	~~2570~~	~~27~~	~~2275~~	~~24~~	~~2453~~	~~23~~	~~2115~~	~~97~~	~~89~~
Kisegi	SEM-200-2	32	~~0.177~~	~~0.003~~	~~0.439~~	~~0.006~~	~~10.844~~	~~0.271~~	~~0.097~~	~~0.004~~	~~2622~~	~~26~~	~~2344~~	~~25~~	~~2510~~	~~23~~	~~1867~~	~~82~~	~~89~~
Kisegi	SEM-200-2	33	~~-0.220~~	~~0.581~~	~~177.821~~	~~177.821~~	~~-0.234~~	~~0.619~~	~~0.224~~	~~0.421~~	~~0~~	~~3754~~	~~177.821~~	~~177.821~~	~~-270~~	~~821~~	~~4090~~	~~6955~~	~~177.821~~
Kisegi	SEM-200-2	34	~~0.847~~	~~0.076~~	~~35.685~~	~~8.528~~	~~54.235~~	~~17.740~~	~~54.751~~	~~21.033~~	~~5003~~	~~122~~	~~177.821~~	~~1498~~	~~4073~~	~~326~~	~~177.821~~	~~7625~~	~~177.821~~
Kisegi	SEM-200-2	35	~~0.293~~	~~0.564~~	~~-0.629~~	~~0.502~~	~~0.397~~	~~0.769~~	~~177.821~~	~~177.821~~	~~3435~~	~~1585~~	~~177.821~~	~~8729~~	~~339~~	~~559~~	~~177.821~~	~~177.821~~	~~177.821~~
Kisegi	SEM-200-2	36	0.061	0.002	0.111	0.002	0.916	0.044	0.032	0.002	625	68	680	10	660	23	630	41	109
Kisegi	SEM-200-2	37	0.061	0.002	0.115	0.002	0.979	0.037	0.032	0.001	653	54	701	9	693	19	627	28	107
Kisegi	SEM-200-2	38	0.062	0.001	0.107	0.001	0.921	0.030	0.031	0.001	678	47	654	8	663	16	620	25	96
Kisegi	SEM-200-2	39	0.062	0.002	0.105	0.002	0.939	0.039	0.029	0.002	684	59	643	9	673	20	582	38	94
Kisegi	SEM-200-2	40	0.067	0.002	0.124	0.002	1.109	0.041	0.035	0.001	834	49	755	10	758	20	705	26	91
Kisegi	SEM-200-2	41	0.067	0.001	0.139	0.002	1.291	0.036	0.034	0.002	853	39	839	10	842	16	683	29	98
Kisegi	SEM-200-2	42	0.069	0.002	0.143	0.002	1.372	0.054	0.032	0.002	905	51	859	11	877	23	630	44	95
Kisegi	SEM-200-2	43	0.070	0.001	0.148	0.002	1.436	0.039	0.044	0.002	940	37	888	11	904	16	863	43	94
Kisegi	SEM-200-2	44	0.126	0.003	0.367	0.005	6.546	0.281	0.104	0.007	2040	39	2017	24	2052	38	2006	129	99
Kisegi	SEM-200-2	45	0.169	0.003	0.481	0.006	11.338	0.311	0.126	0.006	2550	26	2530	26	2551	26	2407	100	99
Kisegi	SEM-200-2	46	0.169	0.003	0.443	0.006	10.848	0.355	0.112	0.007	2552	33	2365	26	2510	30	2143	131	93
Kisegi	SEM-200-2	47	0.173	0.003	0.497	0.007	11.486	0.393	0.127	0.008	2589	32	2602	28	2564	32	2418	141	101
Kisegi	SEM-200-2	48	0.173	0.003	0.481	0.006	11.684	0.320	0.150	0.007	2591	27	2530	26	2579	26	2827	127	98
Kisegi	SEM-200-2	49	0.174	0.003	0.453	0.006	10.909	0.299	0.105	0.005	2598	28	2410	26	2515	25	2024	96	93
Kisegi	SEM-200-2	50	0.175	0.003	0.520	0.007	12.503	0.351	0.133	0.007	2604	29	2697	28	2643	26	2525	131	104
Kisegi	SEM-200-2	51	0.177	0.002	0.515	0.006	13.012	0.322	0.136	0.005	2623	23	2680	27	2681	23	2574	84	102
Kisegi	SEM-200-2	52	0.177	0.003	0.519	0.007	12.984	0.460	0.127	0.006	2627	28	2695	29	2679	33	2418	108	103
Kisegi	SEM-200-2	53	0.178	0.003	0.511	0.006	12.657	0.293	0.129	0.005	2635	23	2661	27	2654	22	2459	85	101
Kisegi	SEM-200-2	54	0.179	0.003	0.504	0.006	12.812	0.327	0.129	0.005	2647	25	2633	27	2666	24	2444	94	99
Kisegi	SEM-200-2	55	0.179	0.003	0.487	0.006	12.017	0.342	0.133	0.006	2647	23	2558	26	2606	27	2530	102	97
Kisegi	SEM-200-2	56	0.181	0.003	0.474	0.006	11.780	0.320	0.123	0.006	2665	27	2502	26	2587	25	2336	108	94
Kisegi	SEM-200-2	57	0.186	0.003	0.465	0.006	11.223	0.372	0.116	0.005	2709	25	2460	26	2542	31	2217	82	91
Kisegi	SEM-200-2	58	0.189	0.004	0.507	0.007	13.164	0.454	0.126	0.007	2738	30	2643	28	2692	33	2398	127	97
Kisegi	SEM-200-2	59	0.250	0.004	0.660	0.008	23.045	0.541	0.166	0.007	3184	24	3268	32	3229	23	3102	128	103
Kisegi	SEM-200-2	60	0.259	0.004	0.617	0.008	22.059	0.603	0.160	0.006	3243	22	3099	31	3186	27	2998	106	96
Kakara	SEM-92-1	1	~~0.090~~	~~0.003~~	~~0.058~~	~~0.001~~	~~0.739~~	~~0.040~~	~~0.032~~	~~0.004~~	~~1435~~	~~69~~	~~363~~	~~6~~	~~562~~	~~23~~	~~644~~	~~75~~	~~25~~
Kakara	SEM-92-1	2	~~0.586~~	~~0.031~~	~~0.226~~	~~0.005~~	~~19.941~~	~~2.322~~	~~0.265~~	~~0.039~~	~~4473~~	~~74~~	~~1315~~	~~28~~	~~3089~~	~~113~~	~~4752~~	~~619~~	~~29~~
Kakara	SEM-92-1	3	~~0.171~~	~~0.007~~	~~0.152~~	~~0.003~~	~~3.579~~	~~0.206~~	~~0.018~~	~~0.002~~	~~2564~~	~~64~~	~~910~~	~~14~~	~~1545~~	~~46~~	~~360~~	~~44~~	~~35~~
Kakara	SEM-92-1	4	~~0.163~~	~~0.008~~	~~0.192~~	~~0.003~~	~~4.372~~	~~0.295~~	~~0.033~~	~~0.005~~	~~2485~~	~~76~~	~~1134~~	~~19~~	~~1707~~	~~56~~	~~653~~	~~90~~	~~46~~
Kakara	SEM-92-1	5	~~0.093~~	~~0.004~~	~~0.116~~	~~0.002~~	~~1.434~~	~~0.087~~	~~0.105~~	~~0.013~~	~~1490~~	~~75~~	~~708~~	~~12~~	~~903~~	~~36~~	~~2025~~	~~239~~	~~47~~
Kakara	SEM-92-1	6	~~0.071~~	~~0.003~~	~~0.075~~	~~0.001~~	~~0.744~~	~~0.048~~	~~0.022~~	~~0.003~~	~~956~~	~~88~~	~~467~~	~~8~~	~~565~~	~~28~~	~~437~~	~~57~~	~~49~~
Kakara	SEM-92-1	7	~~0.083~~	~~0.005~~	~~0.107~~	~~0.002~~	~~1.239~~	~~0.107~~	~~0.023~~	~~0.003~~	~~1261~~	~~110~~	~~657~~	~~13~~	~~818~~	~~49~~	~~453~~	~~69~~	~~52~~
Kakara	SEM-92-1	8	~~0.084~~	~~0.004~~	~~0.123~~	~~0.002~~	~~1.472~~	~~0.097~~	~~0.036~~	~~0.005~~	~~1302~~	~~83~~	~~748~~	~~13~~	~~919~~	~~40~~	~~707~~	~~90~~	~~57~~
Kakara	SEM-92-1	9	~~0.077~~	~~0.003~~	~~0.105~~	~~0.002~~	~~1.150~~	~~0.061~~	~~0.030~~	~~0.003~~	~~1121~~	~~71~~	~~646~~	~~10~~	~~777~~	~~29~~	~~591~~	~~68~~	~~58~~
Kakara	SEM-92-1	10	~~0.176~~	~~0.009~~	~~0.263~~	~~0.005~~	~~6.233~~	~~0.440~~	~~0.150~~	~~0.022~~	~~2612~~	~~78~~	~~1507~~	~~25~~	~~2009~~	~~62~~	~~2824~~	~~382~~	~~58~~

Zircon U-Pb geochronology (Kisegi-Nyabusosi area) cont.

			Isotope ratios									Age estimates								
Formation	Sample ID	Analysis No.	$^{207}Pb/^{206}Pb$	±1σ	$^{206}Pb/^{238}U$	±1σ	$^{207}Pb/^{235}U$	±1σ	$^{208}Pb/^{232}Th$	±1σ	$^{207}Pb/^{206}Pb$ [Ma]	±1σ [Ma]	$^{206}Pb/^{238}U$ [Ma]	±1σ [Ma]	$^{207}Pb/^{235}U$ [Ma]	±1σ [Ma]	$^{208}Pb/^{232}Th$ [Ma]	±1σ [Ma]	Concordance [%]
Kakara	SEM-92-1	11	0.073	0.004	0.098	0.002	0.980	0.073	0.027	0.004	1016	102	600	11	694	38	544	81	59
Kakara	SEM-92-1	12	0.152	0.005	0.249	0.004	5.202	0.272	0.069	0.008	2367	58	1432	20	1853	44	1358	148	60
Kakara	SEM-92-1	13	0.159	0.007	0.265	0.005	5.810	0.369	0.027	0.004	2440	72	1514	24	1948	55	544	72	62
Kakara	SEM-92-1	14	0.211	0.009	0.353	0.006	10.102	0.675	0.136	0.017	2911	64	1950	29	2444	62	2581	308	67
Kakara	SEM-92-1	15	0.175	0.006	0.318	0.005	7.674	0.430	0.027	0.003	2606	60	1779	25	2194	50	533	62	68
Kakara	SEM-92-1	16	0.165	0.008	0.309	0.006	7.067	0.514	0.026	0.004	2507	82	1734	29	2120	65	518	76	69
Kakara	SEM-92-1	17	0.162	0.007	0.307	0.005	6.945	0.440	0.054	0.007	2476	70	1727	26	2104	56	1068	138	70
Kakara	SEM-92-1	18	0.169	0.006	0.327	0.005	7.768	0.432	0.090	0.011	2547	61	1826	26	2205	50	1745	200	72
Kakara	SEM-92-1	19	0.171	0.006	0.344	0.005	8.107	0.430	0.095	0.011	2569	58	1907	26	2243	48	1837	202	74
Kakara	SEM-92-1	20	0.162	0.007	0.330	0.006	7.524	0.497	0.050	0.007	2473	74	1837	29	2176	59	981	132	74
Kakara	SEM-92-1	21	0.067	0.003	0.106	0.002	0.957	0.072	0.035	0.005	844	105	650	12	682	37	693	102	77
Kakara	SEM-92-1	22	0.170	0.007	0.361	0.006	8.324	0.510	0.090	0.011	2562	66	1988	29	2267	55	1743	212	78
Kakara	SEM-92-1	23	0.204	0.010	0.419	0.008	12.186	0.855	0.069	0.010	2861	76	2255	35	2619	66	1355	188	79
Kakara	SEM-92-1	24	0.163	0.006	0.358	0.006	8.071	0.423	0.095	0.011	2483	56	1972	27	2239	47	1831	194	79
Kakara	SEM-92-1	25	0.170	0.008	0.371	0.007	8.658	0.627	0.058	0.008	2562	81	2036	33	2303	66	1132	162	79
Kakara	SEM-92-1	26	0.171	0.006	0.375	0.006	8.801	0.483	0.034	0.004	2569	59	2054	28	2318	50	681	78	80
Kakara	SEM-92-1	27	0.065	0.003	0.101	0.002	0.871	0.057	0.109	0.015	769	92	622	11	636	31	2086	279	81
Kakara	SEM-92-1	28	0.071	0.003	0.128	0.002	1.253	0.068	0.031	0.004	955	73	779	12	825	31	611	70	82
Kakara	SEM-92-1	29	0.070	0.003	0.124	0.002	1.194	0.083	0.023	0.003	916	95	753	13	798	39	460	65	82
Kakara	SEM-92-1	30	0.177	0.007	0.409	0.007	10.015	0.586	0.085	0.011	2628	64	2208	31	2436	54	1654	199	84
Kakara	SEM-92-1	31	0.070	0.003	0.128	0.002	1.266	0.078	0.037	0.005	914	84	777	13	830	35	734	93	85
Kakara	SEM-92-1	32	0.168	0.009	0.408	0.008	9.587	0.715	0.100	0.015	2534	84	2204	36	2396	69	1932	276	87
Kakara	SEM-92-1	33	0.158	0.007	0.402	0.007	8.930	0.576	0.082	0.011	2439	72	2179	33	2331	59	1599	207	89
Kakara	SEM-92-1	34	0.129	0.006	0.336	0.006	6.011	0.429	0.136	0.019	2084	81	1869	30	1978	62	2578	344	90
Kakara	SEM-92-1	35	0.061	0.003	0.148	0.003	1.208	0.104	0.034	0.005	629	118	891	17	804	48	670	99	142
Kakara	SEM-92-1	36	1.632	0.699	5.525	3.826	-33.499	131.522	6.493	4.873	5917	485	177.821	3780	177.821	177.821	177.821	177.821	177.821
Kakara	SEM-92-1	37	0.814	0.041	5.556	0.221	230.341	80.673	11.601	1.838	4947	70	177.821	218	5528	354	177.821	2949	177.821
Kakara	SEM-92-1	38	0.959	0.052	10.476	0.419	522.905	187.069	41.535	7.474	5179	74	177.821	236	6358	363	177.821	3552	177.821
Kakara	SEM-92-1	39	0.059	0.002	0.096	0.002	0.787	0.046	0.027	0.003	550	86	593	10	589	26	534	69	108
Kakara	SEM-92-1	40	0.063	0.002	0.117	0.002	0.964	0.045	0.031	0.003	707	66	712	10	685	23	609	54	101
Kakara	SEM-92-1	41	0.064	0.002	0.131	0.002	1.129	0.064	0.035	0.003	756	76	796	12	767	30	698	63	105
Kakara	SEM-92-1	42	0.066	0.003	0.146	0.002	1.280	0.074	0.037	0.004	815	77	877	14	837	33	732	79	108
Kakara	SEM-92-1	43	0.067	0.002	0.148	0.002	1.384	0.075	0.038	0.004	844	72	889	13	882	32	759	80	105
Kakara	SEM-92-1	44	0.069	0.003	0.145	0.002	1.409	0.080	0.038	0.004	897	74	871	13	893	34	750	78	97
Kakara	SEM-92-1	34	0,129	0,006	0,336	0,006	6,011	0,429	0,136	0,019	2084	81	1869	30	1978	62	2578	344	90
Kakara	SEM-92-1	45	0.165	0.007	0.427	0.007	9.837	0.620	0.089	0.012	2506	68	2293	33	2420	58	1714	214	92
Kakara	SEM-92-1	46	0.168	0.006	0.467	0.007	10.680	0.568	-0.249	0.028	2540	57	2471	32	2496	49	177.821	757	97
Kakara	SEM-92-1	47	0.171	0.008	0.502	0.009	11.707	0.766	0.106	0.014	2564	72	2622	38	2581	61	2041	264	102
Kakara	SEM-92-1	48	0.171	0.007	0.435	0.007	10.576	0.612	0.072	0.009	2567	64	2329	33	2487	54	1396	169	91
Kakara	SEM-92-1	49	0.171	0.008	0.491	0.009	11.444	0.828	0.101	0.015	2570	80	2576	40	2560	68	1951	271	100
Kakara	SEM-92-1	50	0.172	0.009	0.499	0.010	11.880	0.889	0.097	0.014	2581	83	2609	41	2595	70	1871	267	101
Kakara	SEM-92-1	51	0.173	0.008	0.487	0.009	12.300	0.861	0.103	0.014	2584	72	2558	38	2628	66	1988	257	99
Kakara	SEM-92-1	52	0.174	0.006	0.511	0.008	11.904	0.676	0.117	0.013	2599	55	2663	35	2597	53	2238	233	102
Kakara	SEM-92-1	53	0.174	0.008	0.474	0.008	11.192	0.712	0.105	0.014	2601	70	2501	36	2539	59	2018	256	96
Kakara	SEM-92-1	54	0.175	0.006	0.506	0.008	12.220	0.630	0.112	0.012	2606	54	2638	34	2621	48	2140	220	101
Kakara	SEM-92-1	55	0.175	0.006	0.507	0.008	12.241	0.637	0.120	0.013	2609	56	2643	34	2623	49	2283	242	101
Kakara	SEM-92-1	56	0.175	0.009	0.502	0.010	12.219	0.907	0.102	0.015	2609	80	2622	41	2621	70	1960	274	100
Kakara	SEM-92-1	57	0.176	0.007	0.483	0.008	11.592	0.745	0.100	0.013	2619	69	2541	37	2572	60	1934	242	97
Kakara	SEM-92-1	58	0.177	0.007	0.504	0.009	11.977	0.766	0.094	0.012	2622	67	2631	37	2603	60	1822	225	100
Kakara	SEM-92-1	59	0.179	0.006	0.488	0.008	12.089	0.644	0.099	0.011	2645	55	2564	33	2611	50	1917	202	97
Kakara	SEM-92-1	60	0.185	0.007	0.491	0.008	12.503	0.710	0.151	0.017	2698	57	2574	34	2643	53	2836	302	95
Oluka	LB-5	1	0.139	0.006	0.117	0.002	2.295	0.131	0.019	0.002	2217	67	715	11	1211	40	382	49	32
Oluka	LB-5	2	0.137	0.007	0.129	0.002	2.426	0.166	0.023	0.004	2190	81	779	14	1250	49	457	72	36
Oluka	LB-5	3	0.189	0.007	0.171	0.003	4.367	0.261	0.021	0.002	2737	57	1017	16	1706	49	424	44	37
Oluka	LB-5	4	0.144	0.005	0.144	0.002	2.906	0.158	0.005	0.001	2281	63	865	13	1384	41	102	12	38
Oluka	LB-5	5	0.156	0.006	0.153	0.003	3.331	0.193	0.015	0.002	2415	67	918	14	1488	45	300	39	38
Oluka	LB-5	6	0.130	0.004	0.146	0.002	2.607	0.116	0.004	0.000	2104	53	879	12	1303	33	86	8	42
Oluka	LB-5	7	0.105	0.004	0.178	0.003	2.576	0.128	0.066	0.007	1708	62	1058	15	1294	36	1290	137	62
Oluka	LB-5	8	0.329	0.128	0.428	0.082	79.898	177.821	0.254	0.107	3612	497	2298	372	177.821	177.821	4578	1725	64
Oluka	LB-5	9	0.166	0.008	0.286	0.005	6.571	0.472	0.027	0.005	2522	81	1621	27	2056	63	548	91	64
Oluka	LB-5	10	0.210	0.008	0.344	0.006	10.014	0.569	0.071	0.009	2908	61	1906	27	2436	52	1386	167	66
Oluka	LB-5	11	0.156	0.005	0.302	0.004	6.509	0.286	0.077	0.007	2417	50	1699	22	2047	39	1507	138	70
Oluka	LB-5	12	0.157	0.006	0.304	0.005	6.388	0.341	0.066	0.008	2421	61	1710	24	2031	47	1283	147	71
Oluka	LB-5	13	0.170	0.008	0.325	0.006	7.743	0.559	0.075	0.012	2561	80	1815	30	2202	65	1458	232	71
Oluka	LB-5	14	0.165	0.009	0.327	0.006	7.319	0.546	0.072	0.013	2510	84	1824	31	2151	67	1405	238	73
Oluka	LB-5	15	0.152	0.005	0.308	0.005	6.513	0.309	0.072	0.008	2365	55	1729	23	2048	42	1399	142	73
Oluka	LB-5	16	0.175	0.006	0.345	0.005	8.479	0.423	0.072	0.008	2606	55	1911	26	2284	45	1414	146	73
Oluka	LB-5	17	0.174	0.007	0.357	0.006	8.693	0.517	0.106	0.014	2599	67	1968	29	2306	54	2037	261	76
Oluka	LB-5	18	0.235	0.007	0.446	0.007	14.463	0.682	0.077	0.008	3085	49	2379	30	2781	45	1492	142	77
Oluka	LB-5	19	0.176	0.009	0.376	0.007	9.046	0.695	0.041	0.007	2619	86	2059	35	2343	70	819	145	79
Oluka	LB-5	20	0.177	0.007	0.389	0.007	9.455	0.569	0.030	0.004	2629	66	2119	31	2383	55	605	80	81

Zircon U-Pb geochronology (Kisegi-Nyabusosi area) cont.

			Isotope ratios									Age estimates								
Formation	Sample ID	Analysis No.	$^{207}Pb/^{206}Pb$	±1σ	$^{206}Pb/^{238}U$	±1σ	$^{207}Pb/^{235}U$	±1σ	$^{208}Pb/^{232}Th$	±1σ	$^{207}Pb/^{206}Pb$ [Ma]	±1σ [Ma]	$^{206}Pb/^{238}U$ [Ma]	±1σ [Ma]	$^{207}Pb/^{235}U$ [Ma]	±1σ [Ma]	$^{208}Pb/^{232}Th$ [Ma]	±1σ [Ma]	Concordance [%]
Oluka	LB-5	21	0.165	0.006	0.371	0.006	8.578	0.461	0.093	0.011	2509	60	2036	28	2294	49	1793	201	81
Oluka	LB-5	22	0.173	0.008	0.397	0.007	9.250	0.628	0.064	0.010	2587	76	2156	34	2363	62	1249	189	83
Oluka	LB-5	23	0.068	0.003	0.123	0.002	1.173	0.066	0.036	0.003	859	75	745	11	788	31	718	65	87
Oluka	LB-5	24	0.178	0.009	0.426	0.008	10.138	0.753	0.098	0.017	2631	81	2288	37	2447	69	1885	306	87
Oluka	LB-5	25	0.067	0.003	0.125	0.002	1.121	0.076	0.032	0.005	848	95	758	13	763	36	642	96	89
Oluka	LB-5	26	0.793	0.025	2.723	0.067	278.582	66.863	5.166	0.502	4909	44	8474	115	5720	243	177.821	1646	173
Oluka	LB-5	27	0.074	0.002	0.760	0.012	7.624	0.390	0.090	0.009	1041	65	3645	43	2188	46	1750	174	350
Oluka	LB-5	28	0.755	0.030	14.451	0.269	177.821	135.689	1.797	0.234	4839	56	177.821	112	7239	110	177.821	1692	177.821
Oluka	LB-5	29	0.060	0.003	0.107	0.002	0.892	0.054	0.031	0.004	615	88	657	11	648	29	608	73	107
Oluka	LB-5	30	0.062	0.002	0.117	0.002	1.050	0.051	0.032	0.003	675	67	711	10	729	25	633	53	105
Oluka	LB-5	31	0.064	0.002	0.133	0.002	1.200	0.050	0.034	0.003	753	58	805	11	800	23	669	56	107
Oluka	LB-5	32	0.065	0.002	0.113	0.002	1.024	0.053	0.034	0.003	771	73	691	10	716	27	674	65	90
Oluka	LB-5	33	0.065	0.003	0.126	0.002	1.179	0.072	0.035	0.004	777	85	767	12	791	33	686	84	99
Oluka	LB-5	34	0.112	0.003	0.357	0.005	5.435	0.265	0.090	0.008	1827	52	1968	25	1890	42	1733	147	108
Oluka	LB-5	35	0.159	0.005	0.424	0.006	9.373	0.410	0.087	0.008	2443	49	2279	28	2375	40	1690	152	93
Oluka	LB-5	36	0.169	0.007	0.479	0.008	11.287	0.654	0.127	0.016	2548	64	2524	35	2547	54	2412	290	99
Oluka	LB-5	37	0.170	0.007	0.434	0.007	10.360	0.636	0.080	0.011	2555	68	2326	34	2468	57	1557	206	91
Oluka	LB-5	38	0.170	0.007	0.490	0.008	11.362	0.645	0.121	0.015	2559	63	2570	35	2553	53	2308	275	100
Oluka	LB-5	39	0.171	0.006	0.439	0.007	10.351	0.544	0.104	0.012	2563	59	2344	31	2467	49	1999	220	91
Oluka	LB-5	40	0.171	0.007	0.453	0.008	10.335	0.683	0.125	0.018	2563	70	2407	35	2465	61	2386	317	94
Oluka	LB-5	41	0.171	0.005	0.440	0.007	10.296	0.476	0.084	0.008	2565	51	2349	30	2462	43	1623	153	92
Oluka	LB-5	42	0.171	0.006	0.462	0.008	10.775	0.593	0.079	0.010	2566	62	2447	33	2504	51	1534	180	95
Oluka	LB-5	43	0.171	0.009	0.457	0.009	10.453	0.778	0.117	0.019	2569	81	2425	39	2476	69	2232	352	94
Oluka	LB-5	44	0.172	0.006	0.437	0.007	9.956	0.496	0.096	0.010	2577	55	2337	30	2431	46	1846	191	91
Oluka	LB-5	45	0.173	0.009	0.464	0.009	10.808	0.803	0.120	0.021	2584	83	2459	39	2507	69	2282	374	95
Oluka	LB-5	46	0.173	0.006	0.484	0.007	11.333	0.572	0.118	0.012	2588	52	2545	32	2551	47	2254	214	98
Oluka	LB-5	47	0.173	0.009	0.487	0.010	11.532	0.898	0.126	0.023	2589	87	2559	42	2567	73	2404	414	99
Oluka	LB-5	48	0.174	0.007	0.456	0.008	10.877	0.677	0.058	0.008	2594	70	2424	35	2513	58	1144	158	93
Oluka	LB-5	49	0.174	0.005	0.474	0.007	11.345	0.489	0.083	0.008	2597	48	2502	30	2552	40	1619	144	96
Oluka	LB-5	50	0.175	0.006	0.475	0.008	11.323	0.629	0.109	0.012	2605	55	2505	33	2550	52	2086	211	96
Oluka	LB-5	51	0.177	0.008	0.441	0.008	10.733	0.749	0.104	0.016	2621	77	2354	36	2500	65	2006	302	90
Oluka	LB-5	52	0.177	0.006	0.501	0.008	11.881	0.615	0.125	0.013	2627	52	2616	33	2595	49	2381	228	100
Oluka	LB-5	53	0.179	0.009	0.495	0.010	11.773	0.926	0.134	0.024	2640	85	2592	42	2587	74	2547	429	98
Oluka	LB-5	54	0.179	0.008	0.508	0.009	12.122	0.833	0.124	0.019	2641	73	2649	39	2614	64	2368	335	100
Oluka	LB-5	55	0.179	0.009	0.502	0.010	12.310	0.913	0.127	0.022	2644	82	2620	41	2628	70	2417	391	99
Oluka	LB-5	56	0.182	0.005	0.518	0.008	12.799	0.588	0.045	0.005	2673	47	2691	32	2665	43	885	95	101
Oluka	LB-5	57	0.191	0.008	0.498	0.009	13.468	0.851	0.133	0.018	2751	68	2606	37	2713	60	2521	330	95
Oluka	LB-5	58	0.193	0.010	0.510	0.010	14.185	1.124	0.114	0.019	2772	78	2657	42	2762	75	2183	338	96
Oluka	LB-5	59	0.208	0.011	0.553	0.011	15.817	1.225	0.126	0.022	2891	82	2839	45	2866	74	2394	400	98
Oluka	LB-5	60	0.222	0.009	0.542	0.009	16.182	0.981	0.138	0.019	2993	65	2792	39	2888	58	2608	333	93
Nyakabingo	GH-10	1	0.820	0.059	0.046	0.002	4.824	0.630	0.017	0.002	4956	79	287	31	1789	57	331	191	5.8
Nyakabingo	GH-10	2	0.688	0.045	0.045	0.002	4.555	0.638	0.013	0.001	4706	64	281	32	1741	155	268	115	6.0
Nyakabingo	GH-10	3	0.762	0.036	0.050	0.002	5.302	0.532	0.022	0.001	4852	68	317	21	1869	146	447	20	6.5
Nyakabingo	GH-10	4	0.810	0.041	0.078	0.003	8.190	1.209	0.028	0.001	4940	88	486	24	2252	331	561	31	9.8
Nyakabingo	GH-10	5	0.802	0.050	0.083	0.003	11.268	1.944	0.027	0.003	4926	83	511	20	2546	156	531	31	10.4
Nyakabingo	GH-10	6	0.720	0.040	0.089	0.003	11.336	2.447	0.015	0.001	4772	35	547	21	2551	25	298	76	11.5
Nyakabingo	GH-10	7	0.777	0.054	0.091	0.004	9.111	2.080	0.024	0.001	4881	63	563	22	2349	168	487	55	11.5
Nyakabingo	GH-10	8	0.793	0.051	0.095	0.004	15.148	5.265	0.034	0.002	4909	27	587	24	2825	23	682	83	12.0
Nyakabingo	GH-10	9	0.826	0.041	0.097	0.003	13.705	2.539	0.032	0.002	4967	41	595	19	2730	30	631	23	12.0
Nyakabingo	GH-10	10	0.822	0.055	0.098	0.004	11.296	2.455	0.015	0.001	4960	62	602	22	2548	48	294	107	12.1
Nyakabingo	GH-10	11	0.810	0.049	0.111	0.004	12.899	2.133	0.013	0.002	4940	95	676	15	2672	43	255	119	13.7
Nyakabingo	GH-10	12	0.756	0.037	0.109	0.004	9.564	1.520	0.019	0.001	4840	68	666	25	2394	139	389	71	13.8
Nyakabingo	GH-10	13	0.923	0.050	0.121	0.003	15.365	1.697	0.073	0.009	5125	86	734	16	2838	161	1425	66	14.3
Nyakabingo	GH-10	14	0.803	0.035	0.121	0.004	14.249	2.572	0.046	0.002	4927	35	737	343	2767	2010	918	89	15.0
Nyakabingo	GH-10	15	0.795	0.036	0.124	0.004	13.231	2.348	0.063	0.003	4913	29	755	18	2696	21	1227	69	15.4
Nyakabingo	GH-10	16	0.774	0.044	0.126	0.004	13.023	2.460	0.021	0.002	4876	55	764	29	2681	41	426	200	15.7
Nyakabingo	GH-10	17	0.765	0.037	0.133	0.004	10.666	1.602	0.077	0.004	4857	95	803	25	2495	209	1502	25	16.5
Nyakabingo	GH-10	18	0.801	0.059	0.147	0.005	15.300	3.154	0.027	0.005	4924	95	884	35	2834	70	544	323	17.9
Nyakabingo	GH-10	19	0.838	0.052	0.150	0.004	15.874	2.509	0.020	0.003	4988	82	899	32	2869	59	403	270	18.0
Nyakabingo	GH-10	20	0.788	0.032	0.185	0.005	20.737	4.391	0.040	0.001	4900	25	1094	16	3126	18	788	5	22.3
Nyakabingo	GH-10	21	0.775	0.036	0.200	0.006	14.858	2.427	0.090	0.006	4877	69	1175	18	2806	175	1747	42	24.1
Nyakabingo	GH-10	22	0.164	0.004	0.212	0.003	4.705	0.132	0.061	0.003	2492	36	1240	26	1768	28	1205	127	49.7
Nyakabingo	GH-10	23	0.162	0.006	0.233	0.003	5.212	0.263	0.067	0.007	2477	65	1353	28	1855	53	1314	231	54.6
Nyakabingo	GH-10	24	0.732	0.057	0.509	0.023	24.755	8.581	0.186	0.029	4794	94	2652	28	3299	63	3454	124	55.3
Nyakabingo	GH-10	25	0.862	0.035	0.617	0.014	55.152	10.263	0.100	0.009	5027	78	3097	24	4090	178	1930	39	61.6
Nyakabingo	GH-10	26	0.182	0.003	0.296	0.003	7.484	0.153	0.009	0.000	2675	44	1672	7	2171	11	179	30	62.5
Nyakabingo	GH-10	27	0.180	0.004	0.330	0.004	8.132	0.266	0.018	0.001	2649	60	1840	7	2246	16	361	42	69.4
Nyakabingo	GH-10	28	0.158	0.006	0.309	0.004	6.773	0.368	0.059	0.006	2436	56	1736	55	2082	186	1164	170	71.3
Nyakabingo	GH-10	29	0.171	0.003	0.329	0.004	7.577	0.178	0.092	0.004	2564	29	1832	22	2182	23	1780	59	71.4
Nyakabingo	GH-10	30	0.169	0.006	0.350	0.005	8.067	0.342	0.045	0.004	2547	52	1937	27	2239	39	889	173	76.0

Zircon U-Pb geochronology Nyabusosi area) cont.

			Isotope ratios								Age estimates								
Formation	Sample ID	Analysis No.	$^{207}Pb/^{206}Pb$	±1σ	$^{206}Pb/^{238}U$	±1σ	$^{207}Pb/^{235}U$	±1σ	$^{208}Pb/^{232}Th$	±1σ	$^{207}Pb/^{206}Pb$ [Ma]	±1σ [Ma]	$^{206}Pb/^{238}U$ [Ma]	±1σ [Ma]	$^{207}Pb/^{235}U$ [Ma]	±1σ [Ma]	$^{208}Pb/^{232}Th$ [Ma]	±1σ [Ma]	Concordance [%]
Nyakabingo	GH-10	31	0.171	0.005	0.389	0.005	9.099	0.351	0.079	0.006	2572	47	2116	27	2348	34	1546	128	82.3
Nyakabingo	GH-10	32	0.168	0.009	0.383	0.006	8.708	0.596	0.016	0.002	2538	85	2089	34	2308	62	317	273	82.3
Nyakabingo	GH-10	33	0.173	0.009	0.401	0.007	9.610	0.669	0.113	0.017	2589	87	2175	30	2398	62	2163	46	84.0
Nyakabingo	GH-10	34	0.187	0.012	0.428	0.008	10.625	0.947	0.073	0.013	2712	104	2296	39	2491	78	1417	449	84.7
Nyakabingo	GH-10	35	0.169	0.007	0.405	0.006	8.855	0.516	0.126	0.013	2543	61	2194	28	2323	44	2403	123	86.3
Nyakabingo	GH-10	36	0.137	0.008	0.344	0.006	6.364	0.455	0.042	0.006	2184	88	1906	31	2027	64	835	305	87.3
Nyakabingo	GH-10	37	0.136	0.004	0.347	0.004	6.453	0.258	0.053	0.004	2182	190	1921	1645	2040	545	1041	2529	88.0
Nyakabingo	GH-10	38	0.168	0.003	0.420	0.005	10.214	0.217	0.083	0.003	2538	61	2261	21	2454	171	1608	34	89.1
Nyakabingo	GH-10	39	0.863	0.022	13.255	0.759	792.292	********	0.152	0.005	5029	56	******	29	6779	205	2859	28	********
Nyakabingo	GH-10	40	0.631	0.089	6.903	2.017	7.407	3.440	3.311	0.540	4580	49	******	23	********	35	******	114	********
Nyakabingo	GH-10	41	0.152	0.003	0.399	0.005	8.229	0.223	0.083	0.004	2374	66	2163	10	2257	86	1614	23	91.1
Nyakabingo	GH-10	42	0.161	0.003	0.419	0.005	9.350	0.230	0.080	0.003	2471	30	2254	24	2373	29	1564	83	91.2
Nyakabingo	GH-10	43	0.168	0.008	0.445	0.007	10.285	0.633	0.078	0.010	2539	74	2372	17	2461	105	1513	177	93.4
Nyakabingo	GH-10	44	0.168	0.003	0.501	0.006	11.889	0.296	0.134	0.005	2541	26	2617	21	2596	20	2537	52	103.0
Nyakabingo	GH-10	45	0.169	0.006	0.447	0.006	9.919	0.471	0.065	0.006	2543	91	2383	24	2427	203	1281	29	93.7
Nyakabingo	GH-10	46	0.170	0.005	0.458	0.006	10.825	0.455	0.115	0.010	2553	53	2433	21	2508	35	2196	82	95.3
Nyakabingo	GH-10	47	0.171	0.009	0.480	0.008	11.145	0.743	0.105	0.015	2564	85	2529	25	2535	151	2012	56	98.6
Nyakabingo	GH-10	48	0.171	0.005	0.489	0.006	11.086	0.408	0.093	0.007	2565	47	2567	25	2530	35	1796	175	100.1
Nyakabingo	GH-10	49	0.171	0.005	0.445	0.006	10.290	0.385	0.136	0.010	2569	45	2371	26	2461	33	2573	150	92.3
Nyakabingo	GH-10	50	0.171	0.006	0.501	0.007	11.667	0.512	0.128	0.011	2569	54	2617	22	2578	38	2437	74	101.9
Nyakabingo	GH-10	51	0.171	0.009	0.446	0.007	10.480	0.672	0.108	0.015	2571	99	2378	11	2478	110	2078	45	92.5
Nyakabingo	GH-10	52	0.172	0.004	0.509	0.006	11.890	0.350	0.136	0.007	2572	77	2653	19	2596	201	2584	16	103.1
Nyakabingo	GH-10	53	0.172	0.003	0.458	0.005	10.480	0.326	0.120	0.005	2574	71	2431	17	2478	134	2283	24	94.5
Nyakabingo	GH-10	54	0.172	0.005	0.485	0.006	11.424	0.404	0.118	0.008	2578	91	2548	11	2558	117	2247	19	98.8
Nyakabingo	GH-10	55	0.173	0.010	0.446	0.008	10.534	0.792	0.110	0.018	2587	93	2377	37	2483	69	2103	288	91.9
Nyakabingo	GH-10	56	0.173	0.011	0.467	0.009	10.969	0.872	0.096	0.017	2587	99	2470	38	2521	74	1853	401	95.5
Nyakabingo	GH-10	57	0.176	0.010	0.486	0.008	11.869	0.879	0.099	0.016	2615	107	2553	98	2594	338	1903	501	97.7
Nyakabingo	GH-10	58	0.178	0.012	0.476	0.009	11.722	0.977	0.141	0.025	2637	102	2511	37	2582	77	2673	261	95.2
Nyakabingo	GH-10	59	0.179	0.011	0.492	0.009	11.994	0.946	0.133	0.022	2640	102	2578	29	2604	196	2526	89	97.7
Nyakabingo	GH-10	60	0.179	0.011	0.452	0.008	11.004	0.904	0.079	0.014	2644	101	2403	37	2523	74	1541	305	90.9
Nyabusosi	143-5	1	0.140	0.003	0.093	0.001	1.850	0.057	0.008	0.001	2228	36	571	7	1063	20	167	11	26
Nyabusosi	143-5	2	0.173	0.003	0.135	0.002	3.408	0.070	0.043	0.002	2590	25	818	10	1506	16	845	35	32
Nyabusosi	143-5	3	0.174	0.003	0.140	0.002	3.495	0.089	0.022	0.001	2599	29	843	10	1526	20	430	23	32
Nyabusosi	143-5	4	0.121	0.002	0.107	0.001	1.862	0.037	0.042	0.002	1978	26	655	8	1068	13	826	32	33
Nyabusosi	143-5	5	0.165	0.004	0.145	0.002	3.325	0.109	0.024	0.002	2507	37	871	11	1487	26	475	33	35
Nyabusosi	143-5	6	0.169	0.004	0.190	0.003	4.596	0.151	0.081	0.006	2547	36	1124	14	1749	27	1572	104	44
Nyabusosi	143-5	7	0.160	0.002	0.191	0.002	4.258	0.090	0.012	0.000	2457	24	1127	13	1685	17	242	9	46
Nyabusosi	143-5	8	0.098	0.002	0.161	0.002	2.192	0.053	0.015	0.001	1578	31	961	11	1178	17	291	14	61
Nyabusosi	143-5	9	0.162	0.003	0.292	0.004	6.599	0.203	0.078	0.003	2481	28	1650	19	2059	27	1526	63	67
Nyabusosi	143-5	10	0.166	0.002	0.300	0.004	7.089	0.152	0.062	0.003	2513	24	1692	19	2123	19	1214	48	67
Nyabusosi	143-5	11	0.158	0.003	0.304	0.004	6.881	0.215	0.076	0.005	2438	35	1709	20	2096	28	1485	94	70
Nyabusosi	143-5	12	0.173	0.004	0.328	0.004	8.068	0.283	0.058	0.004	2589	37	1827	22	2239	32	1134	80	71
Nyabusosi	143-5	13	0.173	0.003	0.344	0.004	8.339	0.218	0.061	0.002	2590	25	1907	21	2269	24	1199	46	74
Nyabusosi	143-5	14	0.159	0.003	0.354	0.005	7.925	0.199	0.091	0.005	2446	29	1956	21	2223	23	1766	86	80
Nyabusosi	143-5	15	0.174	0.003	0.397	0.005	9.534	0.253	0.026	0.001	2597	25	2154	23	2391	24	521	21	83
Nyabusosi	143-5	16	0.152	0.003	0.369	0.005	7.825	0.255	0.096	0.006	2373	34	2023	23	2211	29	1860	112	85
Nyabusosi	143-5	17	0.165	0.002	0.395	0.005	9.222	0.183	0.085	0.003	2504	23	2146	23	2360	18	1652	60	86
Nyabusosi	143-5	18	0.159	0.003	0.396	0.005	9.084	0.251	0.094	0.006	2445	31	2151	24	2347	25	1824	103	88
Nyabusosi	143-5	19	0.183	0.003	0.441	0.006	11.056	0.445	0.084	0.004	2679	27	2357	26	2528	37	1625	68	88
Nyabusosi	143-5	20	0.167	0.003	0.419	0.005	9.878	0.270	0.095	0.005	2530	28	2255	24	2424	25	1825	85	89
Nyabusosi	143-5	21	0.818	0.020	1.733	0.034	177.821	28.859	2.650	0.198	4953	35	6482	80	5266	164	177.821	1098	131
Nyabusosi	143-5	22	0.855	0.016	62.508	1.726	177.821	177.821	106.517	7.457	5017	26	178	175	9228	444	177.821	1402	177.821
Nyabusosi	143-5	23	0.656	0.017	1.126	0.027	134.008	40.770	2.711	0.184	4638	37	4863	81	4981	307	177.821	1000	105
Nyabusosi	143-5	24	0.135	0.002	0.440	0.006	8.108	0.256	0.115	0.006	2167	31	2350	26	2243	28	2201	109	108
Nyabusosi	143-5	25	0.146	0.013	0.433	0.017	6.298	1.890	0.108	0.016	2299	143	2318	75	2018	263	2067	291	101
Nyabusosi	143-5	26	0.160	0.003	0.481	0.007	11.786	0.579	0.121	0.007	2453	35	2533	29	2588	46	2301	125	103
Nyabusosi	143-5	27	0.165	0.002	0.430	0.005	9.969	0.188	0.108	0.004	2509	22	2304	24	2432	17	2074	72	92
Nyabusosi	143-5	28	0.167	0.004	0.456	0.006	11.153	0.346	0.118	0.008	2533	35	2424	27	2536	29	2253	144	96
Nyabusosi	143-5	29	0.168	0.003	0.498	0.007	11.680	0.350	0.129	0.008	2539	33	2604	28	2579	28	2454	148	103
Nyabusosi	143-5	30	0.168	0.003	0.506	0.007	12.060	0.383	0.129	0.008	2541	33	2637	29	2609	30	2451	146	104
Nyabusosi	143-5	31	0.168	0.003	0.493	0.006	11.384	0.281	0.131	0.005	2542	25	2582	27	2555	23	2495	96	102
Nyabusosi	143-5	32	0.169	0.004	0.446	0.006	10.178	0.338	0.119	0.008	2545	35	2376	27	2451	31	2277	143	93
Nyabusosi	143-5	33	0.169	0.002	0.473	0.006	10.875	0.282	0.127	0.005	2546	24	2497	26	2513	24	2419	82	98
Nyabusosi	143-5	34	0.169	0.004	0.456	0.006	10.708	0.374	0.101	0.007	2549	37	2423	27	2498	32	1953	132	95
Nyabusosi	143-5	35	0.169	0.003	0.431	0.006	9.886	0.273	0.108	0.005	2552	28	2312	25	2424	25	2072	97	91
Nyabusosi	143-5	36	0.170	0.002	0.478	0.006	11.698	0.247	0.128	0.005	2555	23	2519	26	2581	20	2439	84	99
Nyabusosi	143-5	37	0.170	0.003	0.503	0.006	12.201	0.380	0.125	0.006	2556	28	2627	28	2620	29	2378	106	103
Nyabusosi	143-5	38	0.170	0.004	0.501	0.007	12.062	0.468	0.119	0.009	2558	38	2620	30	2609	36	2275	159	102
Nyabusosi	143-5	39	0.170	0.002	0.493	0.006	11.563	0.279	0.128	0.005	2559	24	2586	27	2570	23	2443	87	101
Nyabusosi	143-5	40	0.170	0.003	0.469	0.006	11.263	0.325	0.120	0.006	2562	28	2477	26	2545	27	2298	108	97

Zircon U-Pb geochronology (Kisegi-Nyabusosi area) cont.

			Isotope ratios								Age estimates								
Formation	Sample ID	Analysis No.	$^{207}Pb/^{206}Pb$	±1σ	$^{206}Pb/^{238}U$	±1σ	$^{207}Pb/^{235}U$	±1σ	$^{208}Pb/^{232}Th$	±1σ	$^{207}Pb/^{206}Pb$ [Ma]	±1σ [Ma]	$^{206}Pb/^{238}U$ [Ma]	±1σ [Ma]	$^{207}Pb/^{235}U$ [Ma]	±1σ [Ma]	$^{208}Pb/^{232}Th$ [Ma]	±1σ [Ma]	Concordance [%]
Nyabusosi	143-5	41	0.171	0.002	0.436	0.005	10.406	0.243	0.138	0.006	2567	24	2334	24	2472	22	2611	98	91
Nyabusosi	143-5	42	0.171	0.004	0.522	0.007	12.485	0.447	0.127	0.009	2569	38	2707	30	2642	34	2408	169	105
Nyabusosi	143-5	43	0.171	0.003	0.473	0.006	11.292	0.318	0.148	0.006	2570	24	2498	26	2548	26	2795	106	97
Nyabusosi	143-5	44	0.172	0.003	0.455	0.006	10.963	0.298	0.112	0.006	2575	30	2419	26	2520	25	2146	111	94
Nyabusosi	143-5	45	0.172	0.003	0.491	0.006	11.694	0.319	0.122	0.006	2576	29	2576	27	2580	25	2333	115	100
Nyabusosi	143-5	46	0.172	0.003	0.474	0.006	11.365	0.283	0.127	0.006	2576	26	2502	26	2554	23	2424	104	97
Nyabusosi	143-5	47	0.172	0.002	0.431	0.005	10.463	0.259	0.045	0.002	2578	24	2310	24	2477	23	888	35	90
Nyabusosi	143-5	48	0.172	0.003	0.497	0.006	12.015	0.326	0.125	0.006	2579	27	2603	27	2606	25	2387	107	101
Nyabusosi	143-5	49	0.172	0.003	0.502	0.006	12.213	0.375	0.125	0.006	2581	29	2623	28	2621	29	2386	115	102
Nyabusosi	143-5	50	0.173	0.004	0.521	0.007	12.571	0.433	0.128	0.009	2585	35	2704	30	2648	32	2443	157	105
Nyabusosi	143-5	51	0.173	0.003	0.482	0.006	11.864	0.362	0.121	0.007	2585	31	2535	27	2594	29	2313	126	98
Nyabusosi	143-5	52	0.174	0.003	0.495	0.006	11.919	0.325	0.126	0.006	2599	27	2591	27	2598	26	2390	104	100
Nyabusosi	143-5	53	0.174	0.002	0.502	0.006	5.920	0.117	0.113	0.004	2601	23	2625	27	1964	17	2160	74	101
Nyabusosi	143-5	54	0.179	0.003	0.510	0.006	12.377	0.326	0.141	0.005	2643	23	2656	27	2633	25	2673	90	100
Nyabusosi	143-5	55	0.180	0.003	0.518	0.007	12.744	0.466	0.117	0.006	2648	31	2691	29	2661	34	2235	115	102

A6-4 Zircon U-Pb geochronology (Nkondo-Kaiso area)

			Isotope ratios								Age estimates								
Formation	Sample ID	Analysis No.	$^{207}Pb/^{206}Pb$	±1σ	$^{206}Pb/^{238}U$	±1σ	$^{207}Pb/^{235}U$	±1σ	$^{208}Pb/^{232}Th$	±1σ	$^{207}Pb/^{206}Pb$ [Ma]	±1σ [Ma]	$^{206}Pb/^{238}U$ [Ma]	±1σ [Ma]	$^{207}Pb/^{235}U$ [Ma]	±1σ [Ma]	$^{208}Pb/^{232}Th$ [Ma]	±1σ [Ma]	Concordance [%]
Nkondo	NV3-2	1	0.160	0.003	0.141	0.002	3.255	0.093	0.034	0.002	2453	32	852	10	1470	22	684	33	35
Nkondo	NV3-2	2	0.167	0.003	0.158	0.002	3.803	0.101	0.014	0.001	2523	29	946	11	1593	21	286	12	37
Nkondo	NV3-2	3	0.184	0.005	0.171	0.002	4.527	0.185	0.018	0.002	2691	45	1018	13	1736	34	353	30	38
Nkondo	NV3-2	4	0.179	0.003	0.180	0.002	4.639	0.129	0.006	0.000	2648	31	1070	13	1756	23	118	6	40
Nkondo	NV3-2	5	0.158	0.004	0.192	0.003	4.382	0.166	0.030	0.002	2433	43	1131	14	1709	31	595	46	46
Nkondo	NV3-2	6	0.167	0.004	0.218	0.003	5.268	0.172	0.016	0.001	2528	36	1270	15	1864	28	317	19	50
Nkondo	NV3-2	7	0.182	0.005	0.244	0.003	6.285	0.244	0.046	0.004	2673	42	1406	17	2016	34	912	70	53
Nkondo	NV3-2	8	0.150	0.003	0.212	0.003	4.646	0.141	0.049	0.003	2350	34	1238	15	1758	25	965	53	53
Nkondo	NV3-2	9	0.163	0.005	0.227	0.003	5.351	0.230	0.043	0.004	2491	48	1320	17	1877	37	846	74	53
Nkondo	NV3-2	10	0.154	0.003	0.217	0.003	4.747	0.135	0.060	0.003	2386	33	1268	15	1776	24	1170	61	53
Nkondo	NV3-2	11	0.190	0.005	0.255	0.003	7.014	0.285	0.037	0.003	2740	44	1464	18	2113	36	727	60	53
Nkondo	NV3-2	12	0.216	0.005	0.288	0.004	8.799	0.308	0.084	0.006	2949	38	1633	19	2317	32	1629	110	55
Nkondo	NV3-2	13	0.163	0.003	0.256	0.003	6.048	0.180	0.023	0.001	2490	33	1471	17	1983	26	457	25	59
Nkondo	NV3-2	14	0.171	0.003	0.266	0.003	6.431	0.195	0.047	0.003	2564	33	1522	18	2037	27	921	49	59
Nkondo	NV3-2	15	0.077	0.001	0.110	0.001	1.164	0.029	0.033	0.001	1123	35	672	8	784	14	653	23	60
Nkondo	NV3-2	16	0.164	0.003	0.264	0.003	6.088	0.162	0.043	0.002	2494	27	1509	17	1989	23	844	31	61
Nkondo	NV3-2	17	0.210	0.004	0.317	0.004	9.558	0.265	0.029	0.002	2903	30	1773	20	2393	26	580	30	61
Nkondo	NV3-2	18	0.147	0.002	0.251	0.003	5.240	0.132	0.048	0.002	2317	28	1445	17	1859	21	955	38	62
Nkondo	NV3-2	19	0.187	0.003	0.305	0.004	7.830	0.188	0.035	0.001	2714	25	1715	19	2212	22	696	24	63
Nkondo	NV3-2	20	0.182	0.004	0.302	0.004	7.905	0.289	0.090	0.006	2672	36	1701	20	2220	33	1741	105	64
Nkondo	NV3-2	21	0.181	0.004	0.305	0.004	8.126	0.303	0.037	0.003	2665	40	1717	20	2245	34	731	53	64
Nkondo	NV3-2	22	0.074	0.001	0.110	0.001	1.162	0.033	0.045	0.002	1042	39	673	8	783	16	897	43	65
Nkondo	NV3-2	23	0.175	0.003	0.302	0.004	7.294	0.189	0.058	0.002	2606	28	1700	19	2148	23	1141	47	65
Nkondo	NV3-2	24	0.162	0.004	0.293	0.004	6.853	0.360	0.072	0.003	2478	36	1655	21	2093	47	1396	53	67
Nkondo	NV3-2	25	0.212	0.004	0.355	0.005	10.331	0.312	0.092	0.004	2921	28	1957	22	2465	28	1775	74	67
Nkondo	NV3-2	26	0.178	0.003	0.321	0.004	8.085	0.209	0.077	0.003	2634	26	1794	20	2241	23	1492	53	68
Nkondo	NV3-2	27	0.180	0.005	0.333	0.005	8.595	0.350	0.099	0.008	2654	44	1851	22	2296	37	1900	148	70
Nkondo	NV3-2	28	0.177	0.003	0.333	0.004	8.264	0.212	0.062	0.002	2628	25	1851	21	2260	23	1215	42	70
Nkondo	NV3-2	29	0.185	0.003	0.353	0.005	9.049	0.258	0.092	0.005	2696	30	1947	22	2343	26	1770	83	72
Nkondo	NV3-2	30	0.190	0.005	0.381	0.005	10.516	0.495	0.066	0.006	2738	46	2080	25	2481	44	1286	110	76
Nkondo	NV3-2	31	0.180	0.005	0.374	0.005	9.679	0.378	0.061	0.005	2650	44	2048	24	2405	36	1195	96	77
Nkondo	NV3-2	32	0.071	0.002	0.123	0.002	1.263	0.056	0.036	0.002	949	58	748	10	829	25	722	45	79
Nkondo	NV3-2	33	0.177	0.003	0.384	0.005	9.391	0.243	0.079	0.003	2625	27	2096	23	2377	24	1535	59	80
Nkondo	NV3-2	34	0.140	0.003	0.321	0.004	6.663	0.233	0.070	0.004	2226	36	1794	21	2068	31	1371	76	81
Nkondo	NV3-2	35	0.181	0.003	0.395	0.005	10.138	0.282	0.070	0.003	2662	30	2145	23	2448	26	1367	66	81
Nkondo	NV3-2	36	0.070	0.002	0.128	0.002	1.284	0.057	0.037	0.003	931	59	776	10	839	25	739	55	83
Nkondo	NV3-2	37	-0.177	0.005	-0.326	0.005	8.197	0.337	0.075	0.006	0	0	177.821	43	2253	37	1463	120	0
Nkondo	NV3-2	38	0.177	0.003	0.415	0.005	10.419	0.273	0.081	0.003	2626	27	2237	24	2473	24	1570	61	85
Nkondo	NV3-2	39	0.184	0.004	0.434	0.006	11.726	0.388	0.107	0.005	2694	31	2325	25	2583	31	2047	99	86
Nkondo	NV3-2	40	0.179	0.003	0.425	0.005	10.867	0.272	0.101	0.004	2641	26	2283	24	2512	23	1942	69	86

Zircon U-Pb geochronology (Nkondo-Kaiso area) cont.

			Isotope ratios								Age estimates								
Formation	Sample ID	Analysis No.	$^{207}Pb/^{206}Pb$	±1σ	$^{206}Pb/^{238}U$	±1σ	$^{207}Pb/^{235}U$	±1σ	$^{208}Pb/^{232}Th$	±1σ	$^{207}Pb/^{206}Pb$ [Ma]	±1σ [Ma]	$^{206}Pb/^{238}U$ [Ma]	±1σ [Ma]	$^{207}Pb/^{235}U$ [Ma]	±1σ [Ma]	$^{208}Pb/^{232}Th$ [Ma]	±1σ [Ma]	Concordance [%]
Nkondo	NV3-2	41	~~0.184~~	~~0.005~~	~~0.438~~	~~0.006~~	~~11.331~~	~~0.511~~	~~0.110~~	~~0.010~~	~~2692~~	~~47~~	~~2341~~	~~27~~	~~2551~~	~~42~~	~~2116~~	~~178~~	~~87~~
Nkondo	NV3-2	42	~~0.174~~	~~0.004~~	~~0.427~~	~~0.006~~	~~10.835~~	~~0.374~~	~~0.124~~	~~0.008~~	~~2599~~	~~36~~	~~2291~~	~~25~~	~~2509~~	~~32~~	~~2358~~	~~141~~	~~88~~
Nkondo	NV3-2	43	~~0.186~~	~~0.005~~	~~0.448~~	~~0.006~~	~~11.984~~	~~0.455~~	~~0.108~~	~~0.008~~	~~2706~~	~~40~~	~~2388~~	~~27~~	~~2603~~	~~36~~	~~2075~~	~~143~~	~~88~~
Nkondo	NV3-2	44	~~0.175~~	~~0.003~~	~~0.430~~	~~0.006~~	~~10.523~~	~~0.268~~	~~0.092~~	~~0.003~~	~~2602~~	~~25~~	~~2305~~	~~25~~	~~2482~~	~~24~~	~~1780~~	~~58~~	~~89~~
Nkondo	NV3-2	45	0.065	0.002	0.120	0.002	1.122	0.051	0.035	0.003	790	64	732	10	764	24	695	63	93
Nkondo	NV3-2	46	0.138	0.004	0.363	0.005	6.984	0.284	0.095	0.007	2201	44	1998	23	2109	36	1832	135	91
Nkondo	NV3-2	47	0.170	0.005	0.418	0.006	10.002	0.434	0.081	0.008	2558	46	2252	28	2435	40	1576	141	90
Nkondo	NV3-2	48	0.172	0.005	0.441	0.006	10.329	0.454	0.093	0.009	2576	47	2357	29	2465	41	1798	163	92
Nkondo	NV3-2	49	0.177	0.004	0.455	0.006	11.459	0.368	0.107	0.006	2624	33	2417	26	2561	30	2052	109	92
Nkondo	NV3-2	50	0.177	0.004	0.462	0.006	12.114	0.480	0.108	0.007	2629	37	2447	27	2613	37	2071	127	93
Nkondo	NV3-2	51	0.181	0.003	0.462	0.006	11.732	0.287	0.099	0.004	2665	26	2450	26	2583	23	1915	69	92
Nkondo	NV3-2	52	0.181	0.005	0.472	0.007	12.115	0.566	0.117	0.008	2665	41	2492	29	2613	44	2240	153	94
Nkondo	NV3-2	53	0.182	0.004	0.450	0.006	11.632	0.458	0.108	0.006	2668	35	2396	27	2575	37	2072	117	90
Nkondo	NV3-2	54	0.185	0.003	0.495	0.006	12.498	0.344	0.104	0.004	2694	25	2594	27	2643	26	1992	67	96
Nkondo	NV3-2	55	0.186	0.005	0.542	0.008	14.932	0.821	0.129	0.012	2709	47	2792	34	2811	52	2444	218	103
Nkondo	NV3-2	56	0.186	0.005	0.457	0.006	11.737	0.486	0.096	0.007	2709	41	2426	27	2584	39	1857	132	90
Nkondo	NV3-2	57	0.188	0.003	0.511	0.006	13.589	0.360	0.116	0.005	2725	28	2661	28	2722	25	2221	92	98
Nkondo	NV3-2	58	0.190	0.005	0.524	0.008	13.534	0.588	0.123	0.011	2745	45	2717	32	2718	41	2351	205	99
Nkondo	NV3-2	59	0.195	0.005	0.537	0.007	14.724	0.555	0.121	0.010	2789	39	2769	31	2798	36	2318	178	99
Nkondo	NV3-2	60	0.276	0.006	0.619	0.008	24.644	0.949	0.125	0.009	3342	36	3106	33	3294	38	2389	156	93
Warwire	SC1-1m10	1	~~3.863~~	~~0.200~~	~~-0.038~~	~~0.001~~	~~-20.208~~	~~1.494~~	~~0.017~~	~~0.003~~	~~7078~~	~~67~~	~~-251~~	~~6~~	~~177.821~~	~~-79~~	~~338~~	~~63~~	~~-4~~
Warwire	SC1-1m10	2	~~0.197~~	~~0.007~~	~~0.053~~	~~0.001~~	~~1.499~~	~~0.074~~	~~0.001~~	~~0.000~~	~~2804~~	~~54~~	~~336~~	~~5~~	~~930~~	~~30~~	~~30~~	~~3~~	~~12~~
Warwire	SC1-1m10	3	~~0.222~~	~~0.007~~	~~0.098~~	~~0.001~~	~~3.135~~	~~0.137~~	~~0.030~~	~~0.003~~	~~2997~~	~~47~~	~~604~~	~~9~~	~~1441~~	~~34~~	~~597~~	~~58~~	~~20~~
Warwire	SC1-1m10	4	~~0.176~~	~~0.006~~	~~0.093~~	~~0.001~~	~~2.259~~	~~0.121~~	~~0.080~~	~~0.010~~	~~2618~~	~~59~~	~~573~~	~~9~~	~~1200~~	~~38~~	~~1561~~	~~188~~	~~22~~
Warwire	SC1-1m10	5	~~0.299~~	~~0.010~~	~~0.134~~	~~0.002~~	~~5.615~~	~~0.289~~	~~0.027~~	~~0.003~~	~~3467~~	~~50~~	~~808~~	~~12~~	~~1919~~	~~44~~	~~544~~	~~58~~	~~23~~
Warwire	SC1-1m10	6	~~0.206~~	~~0.009~~	~~0.160~~	~~0.003~~	~~4.800~~	~~0.322~~	~~0.066~~	~~0.011~~	~~2878~~	~~72~~	~~955~~	~~16~~	~~1785~~	~~56~~	~~1282~~	~~205~~	~~33~~
Warwire	SC1-1m10	7	~~0.165~~	~~0.006~~	~~0.151~~	~~0.002~~	~~3.513~~	~~0.195~~	~~0.027~~	~~0.004~~	~~2506~~	~~62~~	~~906~~	~~14~~	~~1530~~	~~44~~	~~546~~	~~71~~	~~36~~
Warwire	SC1-1m10	8	~~0.126~~	~~0.004~~	~~0.125~~	~~0.002~~	~~2.233~~	~~0.099~~	~~0.018~~	~~0.002~~	~~2044~~	~~52~~	~~760~~	~~11~~	~~1192~~	~~31~~	~~356~~	~~36~~	~~37~~
Warwire	SC1-1m10	9	~~0.160~~	~~0.006~~	~~0.162~~	~~0.003~~	~~3.618~~	~~0.188~~	~~0.035~~	~~0.004~~	~~2452~~	~~58~~	~~967~~	~~14~~	~~1554~~	~~41~~	~~703~~	~~83~~	~~39~~
Warwire	SC1-1m10	10	~~0.167~~	~~0.007~~	~~0.175~~	~~0.003~~	~~4.062~~	~~0.235~~	~~0.016~~	~~0.002~~	~~2533~~	~~64~~	~~1039~~	~~16~~	~~1647~~	~~47~~	~~314~~	~~43~~	~~41~~
Warwire	SC1-1m10	11	~~0.178~~	~~0.005~~	~~0.184~~	~~0.003~~	~~4.575~~	~~0.182~~	~~0.079~~	~~0.007~~	~~2632~~	~~44~~	~~1091~~	~~14~~	~~1745~~	~~33~~	~~1538~~	~~130~~	~~41~~
Warwire	SC1-1m10	12	~~0.166~~	~~0.008~~	~~0.176~~	~~0.003~~	~~4.053~~	~~0.295~~	~~0.046~~	~~0.009~~	~~2513~~	~~81~~	~~1044~~	~~18~~	~~1645~~	~~59~~	~~917~~	~~166~~	~~42~~
Warwire	SC1-1m10	13	~~0.178~~	~~0.007~~	~~0.186~~	~~0.003~~	~~4.685~~	~~0.262~~	~~0.018~~	~~0.002~~	~~2638~~	~~61~~	~~1099~~	~~16~~	~~1765~~	~~47~~	~~352~~	~~46~~	~~42~~
Warwire	SC1-1m10	14	~~0.282~~	~~0.011~~	~~0.264~~	~~0.004~~	~~10.435~~	~~0.593~~	~~0.041~~	~~0.006~~	~~3374~~	~~59~~	~~1511~~	~~22~~	~~2474~~	~~53~~	~~807~~	~~107~~	~~45~~
Warwire	SC1-1m10	15	~~0.154~~	~~0.005~~	~~0.224~~	~~0.003~~	~~4.907~~	~~0.225~~	~~0.037~~	~~0.004~~	~~2391~~	~~51~~	~~1301~~	~~18~~	~~1803~~	~~39~~	~~727~~	~~74~~	~~54~~
Warwire	SC1-1m10	16	~~0.131~~	~~0.006~~	~~0.201~~	~~0.004~~	~~3.678~~	~~0.240~~	~~0.053~~	~~0.008~~	~~2109~~	~~76~~	~~1181~~	~~19~~	~~1567~~	~~52~~	~~1039~~	~~163~~	~~56~~
Warwire	SC1-1m10	17	~~0.172~~	~~0.005~~	~~0.257~~	~~0.004~~	~~6.294~~	~~0.252~~	~~0.071~~	~~0.006~~	~~2581~~	~~44~~	~~1476~~	~~19~~	~~2018~~	~~35~~	~~1389~~	~~119~~	~~57~~
Warwire	SC1-1m10	18	~~0.074~~	~~0.004~~	~~0.106~~	~~0.002~~	~~1.099~~	~~0.078~~	~~0.027~~	~~0.005~~	~~1050~~	~~94~~	~~647~~	~~11~~	~~753~~	~~38~~	~~541~~	~~90~~	~~62~~
Warwire	SC1-1m10	19	~~0.086~~	~~0.003~~	~~0.147~~	~~0.002~~	~~1.761~~	~~0.081~~	~~0.049~~	~~0.005~~	~~1348~~	~~58~~	~~883~~	~~12~~	~~1031~~	~~30~~	~~968~~	~~93~~	~~65~~
Warwire	SC1-1m10	20	~~0.186~~	~~0.008~~	~~0.319~~	~~0.006~~	~~8.316~~	~~0.526~~	~~0.026~~	~~0.004~~	~~2704~~	~~69~~	~~1783~~	~~27~~	~~2266~~	~~57~~	~~511~~	~~78~~	~~66~~
Warwire	SC1-1m10	21	~~0.082~~	~~0.004~~	~~0.144~~	~~0.003~~	~~1.531~~	~~0.121~~	~~0.046~~	~~0.007~~	~~1236~~	~~96~~	~~867~~	~~16~~	~~943~~	~~48~~	~~910~~	~~142~~	~~70~~
Warwire	SC1-1m10	22	~~0.183~~	~~0.008~~	~~0.364~~	~~0.006~~	~~9.224~~	~~0.614~~	~~0.043~~	~~0.007~~	~~2682~~	~~72~~	~~2001~~	~~31~~	~~2361~~	~~61~~	~~854~~	~~136~~	~~75~~
Warwire	SC1-1m10	23	~~0.169~~	~~0.007~~	~~0.352~~	~~0.006~~	~~8.230~~	~~0.489~~	~~0.073~~	~~0.010~~	~~2547~~	~~65~~	~~1946~~	~~28~~	~~2257~~	~~54~~	~~1424~~	~~193~~	~~76~~
Warwire	SC1-1m10	24	~~0.182~~	~~0.009~~	~~0.377~~	~~0.007~~	~~9.491~~	~~0.689~~	~~0.075~~	~~0.014~~	~~2668~~	~~79~~	~~2061~~	~~33~~	~~2387~~	~~67~~	~~1465~~	~~258~~	~~77~~
Warwire	SC1-1m10	25	~~0.178~~	~~0.005~~	~~0.377~~	~~0.005~~	~~9.595~~	~~0.428~~	~~0.082~~	~~0.007~~	~~2632~~	~~45~~	~~2061~~	~~26~~	~~2397~~	~~41~~	~~1592~~	~~139~~	~~78~~
Warwire	SC1-1m10	26	~~0.174~~	~~0.005~~	~~0.371~~	~~0.006~~	~~8.647~~	~~0.439~~	~~0.097~~	~~0.010~~	~~2595~~	~~50~~	~~2033~~	~~26~~	~~2302~~	~~46~~	~~1872~~	~~180~~	~~78~~
Warwire	SC1-1m10	27	~~0.174~~	~~0.006~~	~~0.374~~	~~0.006~~	~~9.066~~	~~0.512~~	~~0.099~~	~~0.013~~	~~2595~~	~~61~~	~~2047~~	~~28~~	~~2345~~	~~52~~	~~1899~~	~~235~~	~~79~~
Warwire	SC1-1m10	28	~~0.173~~	~~0.007~~	~~0.395~~	~~0.007~~	~~9.409~~	~~0.581~~	~~0.104~~	~~0.015~~	~~2585~~	~~66~~	~~2144~~	~~31~~	~~2379~~	~~57~~	~~1999~~	~~273~~	~~83~~
Warwire	SC1-1m10	29	~~0.179~~	~~0.007~~	~~0.411~~	~~0.007~~	~~10.595~~	~~0.613~~	~~0.062~~	~~0.008~~	~~2646~~	~~63~~	~~2222~~	~~31~~	~~2488~~	~~54~~	~~1212~~	~~161~~	~~84~~
Warwire	SC1-1m10	30	~~0.168~~	~~0.005~~	~~0.393~~	~~0.006~~	~~9.191~~	~~0.386~~	~~0.059~~	~~0.005~~	~~2537~~	~~46~~	~~2135~~	~~26~~	~~2357~~	~~38~~	~~1153~~	~~105~~	~~84~~
Warwire	SC1-1m10	31	~~0.172~~	~~0.006~~	~~0.408~~	~~0.006~~	~~9.667~~	~~0.509~~	~~0.092~~	~~0.011~~	~~2575~~	~~58~~	~~2207~~	~~29~~	~~2404~~	~~48~~	~~1783~~	~~209~~	~~86~~
Warwire	SC1-1m10	32	~~0.173~~	~~0.005~~	~~0.411~~	~~0.006~~	~~10.180~~	~~0.435~~	~~0.111~~	~~0.011~~	~~2585~~	~~47~~	~~2219~~	~~27~~	~~2451~~	~~40~~	~~2133~~	~~196~~	~~86~~
Warwire	SC1-1m10	33	~~0.179~~	~~0.009~~	~~0.430~~	~~0.008~~	~~10.243~~	~~0.824~~	~~0.123~~	~~0.022~~	~~2641~~	~~79~~	~~2304~~	~~37~~	~~2457~~	~~74~~	~~2345~~	~~391~~	~~87~~
Warwire	SC1-1m10	34	~~0.510~~	~~0.057~~	~~1.003~~	~~0.097~~	~~19.461~~	~~14.483~~	~~0.763~~	~~0.149~~	~~4269~~	~~156~~	~~4479~~	~~313~~	~~3065~~	~~719~~	~~177.821~~	~~1704~~	~~105~~
Warwire	SC1-1m10	35	~~0.189~~	~~0.007~~	~~0.453~~	~~0.007~~	~~12.043~~	~~0.662~~	~~0.111~~	~~0.014~~	~~2730~~	~~59~~	~~2407~~	~~32~~	~~2608~~	~~52~~	~~2130~~	~~256~~	~~88~~
Warwire	SC1-1m10	36	~~0.183~~	~~0.007~~	~~0.442~~	~~0.007~~	~~11.004~~	~~0.679~~	~~0.119~~	~~0.017~~	~~2676~~	~~66~~	~~2361~~	~~33~~	~~2524~~	~~57~~	~~2269~~	~~308~~	~~88~~
Warwire	SC1-1m10	38	0.071	0.004	0.159	0.003	1.672	0.129	0.047	0.008	963	100	952	17	998	49	933	158	99
Warwire	SC1-1m10	39	0.072	0.003	0.154	0.003	1.587	0.098	0.045	0.005	985	78	921	14	965	38	895	105	94
Warwire	SC1-1m10	40	0.172	0.005	0.448	0.006	10.719	0.462	0.099	0.009	2576	46	2386	29	2499	40	1908	172	93
Warwire	SC1-1m10	41	0.172	0.007	0.442	0.008	10.453	0.689	0.120	0.018	2577	70	2360	35	2476	61	2296	330	92
Warwire	SC1-1m10	42	0.173	0.005	0.458	0.007	10.499	0.555	0.122	0.013	2587	52	2431	31	2480	49	2333	232	94
Warwire	SC1-1m10	43	0.175	0.006	0.520	0.008	12.327	0.654	0.128	0.015	2602	55	2697	34	2630	50	2429	264	104
Warwire	SC1-1m10	44	0.175	0.005	0.486	0.007	12.440	0.631	0.125	0.013	2605	50	2553	32	2638	48	2384	232	98
Warwire	SC1-1m10	45	0.175	0.008	0.450	0.008	10.933	0.733	0.119	0.020	2608	74	2397	36	2518	62	2274	359	92
Warwire	SC1-1m10	46	0.176	0.005	0.491	0.007	12.170	0.518	0.119	0.011	2611	44	2575	30	2618	40	2271	193	99
Warwire	SC1-1m10	47	0.176	0.008	0.486	0.009	11.866	0.827	0.133	0.023	2614	76	2552	38	2594	65	2527	405	98
Warwire	SC1-1m10	48	0.176	0.006	0.446	0.007	10.795	0.607	0.114	0.015	2617	60	2377	32	2506	52	2189	266	91
Warwire	SC1-1m10	49	0.176	0.007	0.484	0.008	12.228	0.749	0.130	0.018	2617	68	2543	34	2622	57	2470	329	97
Warwire	SC1-1m10	37	0.179	0.010	0.498	0.010	12.109	1.016	0.153	0.030	2640	88	2606	43	2613	79	2876	525	99
Warwire	SC1-1m10	50	0.176	0.006	0.522	0.008	12.460	0.732	0.131	0.016	2619	57	2707	35	2640	55	2490	278	103

Zircon U-Pb geochronology (Nkondo-Kaiso area) cont.

			Isotope ratios								Age estimates								
Formation	Sample ID	Analysis No.	$^{207}Pb/^{206}Pb$	±1σ	$^{206}Pb/^{238}U$	±1σ	$^{207}Pb/^{235}U$	±1σ	$^{208}Pb/^{232}Th$	±1σ	$^{207}Pb/^{206}Pb$ [Ma]	±1σ [Ma]	$^{206}Pb/^{238}U$ [Ma]	±1σ [Ma]	$^{207}Pb/^{235}U$ [Ma]	±1σ [Ma]	$^{208}Pb/^{232}Th$ [Ma]	±1σ [Ma]	Concordance [%]
Warwire	SC1-1m10	51	0.177	0.007	0.442	0.008	12.654	1.043	0.115	0.014	2622	63	2361	35	2654	78	2208	262	90
Warwire	SC1-1m10	52	0.179	0.009	0.499	0.009	12.193	0.890	0.137	0.025	2645	79	2608	40	2619	68	2588	439	99
Warwire	SC1-1m10	53	0.181	0.008	0.505	0.009	12.501	0.808	0.122	0.019	2662	70	2634	38	2643	61	2319	341	99
Warwire	SC1-1m10	54	0.182	0.007	0.526	0.009	12.927	0.777	0.142	0.019	2667	62	2723	37	2674	57	2679	337	102
Warwire	SC1-1m10	55	0.183	0.006	0.490	0.007	12.569	0.615	0.132	0.014	2678	52	2573	32	2648	46	2499	256	96
Warwire	SC1-1m10	56	0.183	0.006	0.455	0.007	11.678	0.565	0.109	0.012	2683	51	2417	30	2579	45	2083	210	90
Warwire	SC1-1m10	57	0.183	0.005	0.456	0.007	11.820	0.525	0.082	0.008	2684	45	2422	29	2590	42	1599	142	90
Warwire	SC1-1m10	58	0.208	0.005	0.479	0.007	13.708	0.569	0.128	0.011	2887	42	2524	30	2730	39	2433	199	90
Warwire	SC1-1m10	59	0.220	0.010	0.496	0.009	15.188	1.060	0.122	0.021	2979	74	2599	39	2827	66	2334	385	90
Kaiso V.	KAI 47-1	60	0.237	0.012	0.534	0.010	17.316	1.290	0.052	0.010	3098	78	2759	43	2953	71	1021	188	90
Kaiso V.	KAI 47-1	1	~~0.173~~	~~0.007~~	~~0.069~~	~~0.001~~	~~1.712~~	~~0.093~~	~~0.029~~	~~0.004~~	~~2584~~	~~62~~	~~430~~	~~6~~	~~1013~~	~~35~~	~~583~~	~~73~~	~~17~~
Kaiso V.	KAI 47-1	2	~~8.995~~	~~0.459~~	~~0.368~~	~~0.007~~	~~490.484~~	~~40.164~~	~~43.123~~	~~7.821~~	~~8000~~	~~0~~	~~2019~~	~~34~~	~~6293~~	~~83~~	~~177.821~~	~~3583~~	~~25~~
Kaiso V.	KAI 47-1	3	~~0.217~~	~~0.008~~	~~0.154~~	~~0.002~~	~~4.889~~	~~0.272~~	~~0.040~~	~~0.004~~	~~2960~~	~~56~~	~~925~~	~~13~~	~~1800~~	~~47~~	~~791~~	~~87~~	~~31~~
Kaiso V.	KAI 47-1	4	~~0.199~~	~~0.007~~	~~0.274~~	~~0.004~~	~~7.699~~	~~0.380~~	~~0.078~~	~~0.008~~	~~2820~~	~~53~~	~~1561~~	~~20~~	~~2197~~	~~44~~	~~1525~~	~~154~~	~~55~~
Kaiso V.	KAI 47-1	5	~~0.168~~	~~0.008~~	~~0.288~~	~~0.005~~	~~6.823~~	~~0.457~~	~~0.074~~	~~0.012~~	~~2538~~	~~76~~	~~1632~~	~~25~~	~~2089~~	~~59~~	~~1442~~	~~225~~	~~64~~
Kaiso V.	KAI 47-1	6	~~0.148~~	~~0.005~~	~~0.279~~	~~0.004~~	~~5.726~~	~~0.306~~	~~0.094~~	~~0.010~~	~~2321~~	~~58~~	~~1585~~	~~21~~	~~1935~~	~~46~~	~~1815~~	~~193~~	~~68~~
Kaiso V.	KAI 47-1	7	~~0.153~~	~~0.005~~	~~0.295~~	~~0.004~~	~~6.686~~	~~0.353~~	~~0.062~~	~~0.007~~	~~2385~~	~~57~~	~~1667~~	~~22~~	~~2071~~	~~47~~	~~1219~~	~~132~~	~~70~~
Kaiso V.	KAI 47-1	8	~~0.172~~	~~0.008~~	~~0.341~~	~~0.006~~	~~8.626~~	~~0.576~~	~~0.114~~	~~0.019~~	~~2574~~	~~76~~	~~1891~~	~~29~~	~~2299~~	~~61~~	~~2187~~	~~338~~	~~73~~
Kaiso V.	KAI 47-1	9	~~0.170~~	~~0.008~~	~~0.355~~	~~0.006~~	~~8.096~~	~~0.560~~	~~0.027~~	~~0.005~~	~~2558~~	~~78~~	~~1960~~	~~30~~	~~2242~~	~~63~~	~~542~~	~~89~~	~~77~~
Kaiso V.	KAI 47-1	10	~~0.170~~	~~0.010~~	~~0.364~~	~~0.008~~	~~8.623~~	~~0.793~~	~~0.096~~	~~0.020~~	~~2554~~	~~94~~	~~2002~~	~~37~~	~~2299~~	~~84~~	~~1844~~	~~363~~	~~78~~
Kaiso V.	KAI 47-1	11	~~0.173~~	~~0.006~~	~~0.389~~	~~0.006~~	~~9.616~~	~~0.506~~	~~0.103~~	~~0.012~~	~~2583~~	~~58~~	~~2120~~	~~27~~	~~2399~~	~~48~~	~~1976~~	~~216~~	~~82~~
Kaiso V.	KAI 47-1	12	~~0.214~~	~~0.012~~	~~0.464~~	~~0.009~~	~~13.406~~	~~1.054~~	~~0.186~~	~~0.037~~	~~2938~~	~~86~~	~~2457~~	~~40~~	~~2709~~	~~74~~	~~3446~~	~~625~~	~~84~~
Kaiso V.	KAI 47-1	13	~~0.120~~	~~0.006~~	~~0.295~~	~~0.006~~	~~4.748~~	~~0.452~~	~~0.080~~	~~0.010~~	~~1959~~	~~82~~	~~1668~~	~~29~~	~~1776~~	~~80~~	~~1549~~	~~193~~	~~85~~
Kaiso V.	KAI 47-1	14	~~0.163~~	~~0.006~~	~~0.391~~	~~0.006~~	~~9.815~~	~~0.640~~	~~0.106~~	~~0.013~~	~~2488~~	~~61~~	~~2127~~	~~29~~	~~2418~~	~~60~~	~~2031~~	~~229~~	~~85~~
Kaiso V.	KAI 47-1	15	~~0.213~~	~~0.009~~	~~0.484~~	~~0.008~~	~~14.886~~	~~1.128~~	~~0.145~~	~~0.021~~	~~2927~~	~~68~~	~~2545~~	~~37~~	~~2808~~	~~72~~	~~2743~~	~~369~~	~~87~~
Kaiso V.	KAI 47-1	16	~~0.179~~	~~0.006~~	~~0.434~~	~~0.006~~	~~10.601~~	~~0.533~~	~~0.091~~	~~0.010~~	~~2644~~	~~54~~	~~2323~~	~~29~~	~~2489~~	~~47~~	~~1769~~	~~183~~	~~88~~
Kaiso V.	KAI 47-1	17	~~0.314~~	~~0.016~~	~~3.547~~	~~0.068~~	~~161.159~~	~~13.344~~	~~7.472~~	~~1.406~~	~~3538~~	~~79~~	~~9762~~	~~97~~	~~5167~~	~~84~~	~~177.821~~	~~3354~~	~~276~~
Kaiso V.	KAI 47-1	18	0.066	0.003	0.139	0.003	1.254	0.087	0.040	0.006	798	95	839	14	825	39	799	125	105
Kaiso V.	KAI 47-1	19	0.071	0.003	0.146	0.002	1.446	0.085	0.043	0.005	971	78	880	13	908	35	843	95	91
Kaiso V.	KAI 47-1	20	0.073	0.004	0.159	0.003	1.585	0.126	0.047	0.008	1017	106	950	17	965	50	928	163	93
Kaiso V.	KAI 47-1	21	0.124	0.005	0.364	0.006	6.493	0.401	0.097	0.013	2018	71	2002	28	2045	54	1864	245	99
Kaiso V.	KAI 47-1	22	0.129	0.006	0.368	0.006	6.558	0.434	0.102	0.016	2078	78	2018	30	2054	58	1962	296	97
Kaiso V.	KAI 47-1	23	0.150	0.007	0.458	0.008	9.370	0.639	0.113	0.018	2343	76	2431	35	2375	63	2159	322	104
Kaiso V.	KAI 47-1	24	0.165	0.010	0.466	0.010	10.560	0.874	0.123	0.026	2508	94	2465	42	2485	77	2349	468	98
Kaiso V.	KAI 47-1	25	0.165	0.007	0.430	0.007	9.775	0.645	0.111	0.017	2509	74	2308	33	2414	61	2129	313	92
Kaiso V.	KAI 47-1	26	0.166	0.009	0.459	0.009	10.044	0.813	0.119	0.024	2519	91	2435	41	2439	75	2281	438	97
Kaiso V.	KAI 47-1	27	0.167	0.009	0.456	0.009	10.560	0.791	0.122	0.023	2526	86	2421	39	2485	70	2330	418	96
Kaiso V.	KAI 47-1	28	0.167	0.006	0.434	0.006	10.024	0.507	0.110	0.012	2528	55	2324	29	2437	47	2109	214	92
Kaiso V.	KAI 47-1	29	0.168	0.010	0.474	0.010	10.819	0.901	0.130	0.028	2537	95	2501	43	2508	77	2462	493	99
Kaiso V.	KAI 47-1	30	0.168	0.010	0.488	0.010	11.180	0.917	0.130	0.027	2540	93	2562	43	2538	76	2469	481	101
Kaiso V.	KAI 47-1	31	0.170	0.009	0.492	0.010	11.340	0.900	0.130	0.026	2554	90	2580	42	2552	74	2478	465	101
Kaiso V.	KAI 47-1	32	0.170	0.009	0.477	0.009	11.596	0.875	0.129	0.024	2560	85	2512	39	2572	71	2459	431	98
Kaiso V.	KAI 47-1	33	0.171	0.010	0.504	0.010	11.284	0.920	0.108	0.022	2563	90	2631	43	2547	76	2067	396	103
Kaiso V.	KAI 47-1	34	0.171	0.009	0.499	0.010	11.445	0.908	0.137	0.027	2567	88	2609	42	2560	74	2598	472	102
Kaiso V.	KAI 47-1	35	0.171	0.009	0.462	0.009	10.871	0.864	0.125	0.024	2571	87	2447	40	2512	74	2390	432	95
Kaiso V.	KAI 47-1	36	0.171	0.006	0.438	0.007	10.728	0.572	0.121	0.014	2572	58	2343	30	2500	50	2304	253	91
Kaiso V.	KAI 47-1	37	0.172	0.009	0.459	0.009	11.060	0.820	0.121	0.022	2574	83	2435	38	2528	69	2317	400	95
Kaiso V.	KAI 47-1	38	0.172	0.009	0.488	0.009	11.456	0.926	0.131	0.024	2577	85	2562	41	2561	75	2496	434	99
Kaiso V.	KAI 47-1	39	0.172	0.008	0.470	0.008	11.323	0.796	0.126	0.019	2577	72	2485	36	2550	66	2400	340	96
Kaiso V.	KAI 47-1	40	0.172	0.008	0.446	0.008	10.587	0.713	0.123	0.020	2578	75	2378	34	2488	62	2336	353	92
Kaiso V.	KAI 47-1	41	0.172	0.008	0.450	0.008	11.093	0.886	0.124	0.018	2578	73	2396	36	2531	74	2363	328	93
Kaiso V.	KAI 47-1	42	0.172	0.008	0.455	0.008	11.078	0.772	0.143	0.024	2578	77	2417	36	2530	65	2706	418	94
Kaiso V.	KAI 47-1	43	0.172	0.007	0.465	0.008	11.479	0.717	0.123	0.017	2580	68	2464	33	2563	58	2348	311	95
Kaiso V.	KAI 47-1	44	0.172	0.007	0.435	0.007	10.310	0.656	0.121	0.018	2581	71	2330	33	2463	59	2314	324	90
Kaiso V.	KAI 47-1	45	0.174	0.007	0.461	0.008	10.657	0.726	0.124	0.017	2593	68	2446	34	2494	63	2366	310	94
Kaiso V.	KAI 47-1	46	0.174	0.007	0.472	0.007	11.739	0.701	0.118	0.014	2598	61	2491	32	2584	56	2257	261	96
Kaiso V.	KAI 47-1	47	0.175	0.006	0.439	0.007	10.981	0.593	0.120	0.014	2602	60	2348	30	2522	50	2296	261	90
Kaiso V.	KAI 47-1	48	0.175	0.009	0.455	0.008	10.898	0.796	0.119	0.021	2603	81	2416	37	2515	68	2274	381	93
Kaiso V.	KAI 47-1	49	0.175	0.007	0.446	0.007	10.875	0.635	0.118	0.015	2606	63	2379	31	2513	54	2249	276	91
Kaiso V.	KAI 47-1	50	0.175	0.007	0.489	0.008	12.205	0.708	0.130	0.016	2608	62	2568	33	2620	54	2469	290	98
Kaiso V.	KAI 47-1	51	0.175	0.008	0.486	0.009	11.800	0.839	0.132	0.022	2609	78	2555	38	2589	67	2508	397	98
Kaiso V.	KAI 47-1	52	0.175	0.008	0.493	0.008	13.022	0.858	0.133	0.019	2610	70	2585	36	2681	62	2521	344	99
Kaiso V.	KAI 47-1	53	0.176	0.007	0.484	0.008	12.228	0.749	0.130	0.018	2617	68	2543	34	2622	57	2470	329	97
Kaiso V.	KAI 47-1	54	0.178	0.006	0.450	0.007	11.279	0.557	0.099	0.010	2631	53	2395	29	2547	46	1901	188	91
Kaiso V.	KAI 47-1	55	0.062	0.003	0.107	0.002	0.928	0.074	0.033	0.006	689	112	653	12	667	39	659	117	95
Kaiso V.	KAI 47-1	56	0.179	0.006	0.477	0.007	12.651	0.624	0.123	0.013	2643	52	2515	30	2654	46	2346	227	95
Kaiso V.	KAI 47-1	57	0.181	0.007	0.494	0.008	12.527	0.767	0.129	0.016	2665	61	2586	34	2645	58	2456	287	97
Kaiso V.	KAI 47-1	58	0.183	0.008	0.470	0.008	11.884	0.851	0.076	0.012	2681	73	2482	36	2595	67	1481	219	93
Kaiso V.	KAI 47-1	59	0.186	0.011	0.544	0.011	14.052	1.145	0.139	0.029	2708	92	2800	46	2753	77	2630	515	103
Kaiso V.	KAI 47-1	60	0.191	0.008	0.502	0.009	13.099	0.913	0.132	0.020	2750	71	2621	37	2687	66	2507	358	95

Zircon U-Pb geochronology (Nkondo-Kaiso area) cont.

			Isotope ratios									Age estimates								
Formation	Sample ID	Analysis No.	$^{207}Pb/^{206}Pb$	±1σ	$^{206}Pb/^{238}U$	±1σ	$^{207}Pb/^{235}U$	±1σ	$^{208}Pb/^{232}Th$	±1σ	$^{207}Pb/^{206}Pb$ [Ma]	±1σ [Ma]	$^{206}Pb/^{238}U$ [Ma]	±1σ [Ma]	$^{207}Pb/^{235}U$ [Ma]	±1σ [Ma]	$^{208}Pb/^{232}Th$ [Ma]	±1σ [Ma]	Concordance [%]
Museta b.	MB-2	1	~~0.179~~	~~0.004~~	~~0.274~~	~~0.004~~	~~6.808~~	~~0.236~~	~~0.056~~	~~0.004~~	~~2641~~	~~39~~	~~1562~~	~~19~~	~~2087~~	~~31~~	~~1098~~	~~79~~	~~59~~
Museta b.	MB-2	2	~~0.077~~	~~0.002~~	~~0.137~~	~~0.002~~	~~1.468~~	~~0.055~~	~~0.047~~	~~0.003~~	~~1118~~	~~48~~	~~830~~	~~11~~	~~918~~	~~23~~	~~925~~	~~53~~	~~74~~
Museta b.	MB-2	3	~~0.082~~	~~0.001~~	~~0.156~~	~~0.002~~	~~1.766~~	~~0.046~~	~~0.053~~	~~0.002~~	~~1249~~	~~32~~	~~933~~	~~11~~	~~1033~~	~~17~~	~~1035~~	~~36~~	~~75~~
Museta b.	MB-2	4	~~0.161~~	~~0.003~~	~~0.340~~	~~0.005~~	~~8.075~~	~~0.300~~	~~0.146~~	~~0.006~~	~~2471~~	~~29~~	~~1888~~	~~22~~	~~2240~~	~~34~~	~~2756~~	~~107~~	~~76~~
Museta b.	MB-2	5	~~0.112~~	~~0.002~~	~~0.254~~	~~0.003~~	~~3.999~~	~~0.103~~	~~0.069~~	~~0.003~~	~~1829~~	~~30~~	~~1460~~	~~17~~	~~1634~~	~~21~~	~~1346~~	~~57~~	~~80~~
Museta b.	MB-2	6	~~0.176~~	~~0.003~~	~~0.400~~	~~0.005~~	~~10.170~~	~~0.261~~	~~0.082~~	~~0.003~~	~~2617~~	~~24~~	~~2171~~	~~23~~	~~2450~~	~~24~~	~~1590~~	~~57~~	~~83~~
Museta b.	MB-2	7	~~0.165~~	~~0.003~~	~~0.383~~	~~0.005~~	~~8.881~~	~~0.264~~	~~0.046~~	~~0.002~~	~~2503~~	~~30~~	~~2091~~	~~23~~	~~2326~~	~~27~~	~~908~~	~~45~~	~~84~~
Museta b.	MB-2	8	~~0.179~~	~~0.004~~	~~0.411~~	~~0.006~~	~~10.369~~	~~0.410~~	~~0.120~~	~~0.008~~	~~2643~~	~~37~~	~~2221~~	~~26~~	~~2468~~	~~37~~	~~2294~~	~~152~~	~~84~~
Museta b.	MB-2	9	~~0.145~~	~~0.002~~	~~0.348~~	~~0.004~~	~~6.945~~	~~0.174~~	~~0.104~~	~~0.004~~	~~2290~~	~~25~~	~~1927~~	~~21~~	~~2104~~	~~22~~	~~2006~~	~~72~~	~~84~~
Museta b.	MB-2	10	~~0.165~~	~~0.003~~	~~0.389~~	~~0.005~~	~~8.907~~	~~0.257~~	~~0.073~~	~~0.004~~	~~2511~~	~~31~~	~~2118~~	~~24~~	~~2329~~	~~26~~	~~1420~~	~~75~~	~~84~~
Museta b.	MB-2	11	~~0.159~~	~~0.003~~	~~0.378~~	~~0.005~~	~~8.088~~	~~0.285~~	~~0.241~~	~~0.013~~	~~2447~~	~~32~~	~~2065~~	~~24~~	~~2241~~	~~32~~	~~4366~~	~~218~~	~~84~~
Museta b.	MB-2	12	~~0.174~~	~~0.004~~	~~0.410~~	~~0.005~~	~~9.731~~	~~0.320~~	~~0.060~~	~~0.004~~	~~2600~~	~~35~~	~~2215~~	~~25~~	~~2410~~	~~30~~	~~1170~~	~~72~~	~~85~~
Museta b.	MB-2	13	~~0.120~~	~~0.002~~	~~0.299~~	~~0.004~~	~~4.879~~	~~0.186~~	~~0.084~~	~~0.003~~	~~1963~~	~~32~~	~~1684~~	~~20~~	~~1799~~	~~32~~	~~1631~~	~~59~~	~~86~~
Museta b.	MB-2	14	~~0.169~~	~~0.003~~	~~0.408~~	~~0.005~~	~~9.673~~	~~0.277~~	~~0.098~~	~~0.005~~	~~2547~~	~~28~~	~~2206~~	~~24~~	~~2404~~	~~26~~	~~1890~~	~~86~~	~~87~~
Museta b.	MB-2	15	~~0.169~~	~~0.004~~	~~0.409~~	~~0.006~~	~~9.738~~	~~0.333~~	~~0.115~~	~~0.007~~	~~2547~~	~~36~~	~~2211~~	~~25~~	~~2410~~	~~32~~	~~2206~~	~~135~~	~~87~~
Museta b.	MB-2	16	~~0.177~~	~~0.004~~	~~0.433~~	~~0.006~~	~~10.745~~	~~0.378~~	~~0.113~~	~~0.008~~	~~2626~~	~~37~~	~~2318~~	~~27~~	~~2501~~	~~33~~	~~2163~~	~~143~~	~~88~~
Museta b.	MB-2	17	~~0.130~~	~~0.003~~	~~0.443~~	~~0.007~~	~~8.440~~	~~0.470~~	~~0.121~~	~~0.008~~	~~2103~~	~~43~~	~~2363~~	~~29~~	~~2279~~	~~51~~	~~2312~~	~~142~~	~~112~~
Museta b.	MB-2	18	~~0.167~~	~~0.003~~	~~0.417~~	~~0.005~~	~~9.769~~	~~0.231~~	~~0.088~~	~~0.004~~	~~2531~~	~~25~~	~~2248~~	~~24~~	~~2413~~	~~22~~	~~1711~~	~~66~~	~~89~~
Museta b.	MB-2	19	~~-0.022~~	~~0.472~~	~~1.805~~	~~0.404~~	~~0.056~~	~~1.215~~	~~-1.164~~	~~2.489~~	~~0~~	~~4085~~	~~6649~~	~~929~~	~~55~~	~~1168~~	~~177.821~~	~~177.821~~	~~177.821~~
Museta b.	MB-2	20	~~-0.095~~	~~0.389~~	~~-22.154~~	~~22.048~~	~~-0.320~~	~~1.372~~	~~0.108~~	~~2.766~~	~~0~~	~~3439~~	~~177.821~~	~~177.821~~	~~-391~~	~~2047~~	~~2067~~	~~177.821~~	~~177.821~~
Museta b.	MB-2	21	0.065	0.002	0.113	0.002	1.015	0.052	0.031	0.002	773	70	692	10	711	26	610	41	90
Museta b.	MB-2	22	0.146	0.004	0.416	0.006	8.779	0.403	0.107	0.008	2300	44	2241	27	2315	42	2053	150	97
Museta b.	MB-2	23	0.155	0.004	0.455	0.006	9.597	0.386	0.117	0.008	2407	38	2418	28	2397	37	2244	142	100
Museta b.	MB-2	24	0.157	0.002	0.441	0.006	9.522	0.298	0.127	0.005	2422	26	2356	26	2390	29	2424	90	97
Museta b.	MB-2	25	0.158	0.003	0.449	0.006	9.773	0.330	0.116	0.007	2433	36	2392	27	2414	31	2214	134	98
Museta b.	MB-2	26	0.158	0.003	0.428	0.005	9.152	0.244	0.115	0.005	2436	28	2295	25	2353	24	2207	96	94
Museta b.	MB-2	27	0.159	0.003	0.413	0.005	8.977	0.233	0.101	0.005	2441	28	2227	24	2336	24	1936	88	91
Museta b.	MB-2	28	0.159	0.003	0.427	0.006	9.687	0.328	0.119	0.005	2446	28	2294	25	2405	31	2274	90	94
Museta b.	MB-2	29	0.159	0.002	0.424	0.005	9.132	0.250	0.114	0.005	2449	26	2281	25	2351	25	2182	85	93
Museta b.	MB-2	30	0.161	0.002	0.415	0.005	9.429	0.254	0.110	0.004	2467	25	2239	24	2381	25	2101	77	91
Museta b.	MB-2	31	0.164	0.002	0.468	0.006	10.569	0.285	0.132	0.005	2500	24	2477	26	2486	25	2500	85	99
Museta b.	MB-2	32	0.165	0.002	0.437	0.005	9.928	0.226	0.076	0.003	2508	23	2338	25	2428	21	1485	49	93
Museta b.	MB-2	33	0.166	0.003	0.467	0.006	11.069	0.470	0.130	0.006	2515	30	2470	28	2529	40	2465	108	98
Museta b.	MB-2	34	0.166	0.004	0.454	0.006	10.787	0.409	0.120	0.008	2516	38	2415	28	2505	35	2294	149	96
Museta b.	MB-2	35	0.166	0.003	0.445	0.006	10.322	0.300	0.111	0.006	2518	30	2371	26	2464	27	2123	103	94
Museta b.	MB-2	36	0.168	0.004	0.483	0.007	11.168	0.414	0.125	0.009	2533	39	2542	29	2537	35	2383	160	100
Museta b.	MB-2	37	0.168	0.003	0.469	0.006	11.101	0.329	0.119	0.006	2537	30	2479	27	2532	28	2272	113	98
Museta b.	MB-2	38	0.168	0.003	0.473	0.006	10.921	0.269	0.124	0.006	2538	27	2495	26	2516	23	2357	103	98
Museta b.	MB-2	39	0.168	0.003	0.482	0.006	11.401	0.328	0.128	0.006	2542	29	2536	27	2557	27	2433	113	100
Museta b.	MB-2	40	0.169	0.003	0.452	0.006	10.532	0.276	0.122	0.005	2545	25	2405	26	2483	24	2325	88	94
Museta b.	MB-2	41	0.169	0.003	0.473	0.006	11.162	0.329	0.120	0.006	2545	31	2499	27	2537	27	2292	117	98
Museta b.	MB-2	42	0.169	0.004	0.524	0.007	12.358	0.490	0.124	0.009	2546	40	2718	31	2632	37	2365	168	107
Museta b.	MB-2	43	0.169	0.003	0.487	0.006	11.593	0.326	0.125	0.006	2548	27	2559	27	2572	26	2384	102	100
Museta b.	MB-2	44	0.169	0.002	0.479	0.006	11.452	0.279	0.149	0.005	2551	24	2523	26	2561	23	2811	95	99
Museta b.	MB-2	45	0.169	0.004	0.425	0.006	9.890	0.366	0.105	0.007	2551	38	2284	26	2425	34	2021	136	90
Museta b.	MB-2	46	0.169	0.004	0.461	0.006	10.812	0.425	0.112	0.009	2551	41	2443	28	2507	37	2154	155	96
Museta b.	MB-2	47	0.169	0.002	0.479	0.006	10.933	0.282	0.134	0.005	2552	23	2524	26	2517	24	2540	84	99
Museta b.	MB-2	48	0.170	0.003	0.469	0.006	11.018	0.365	0.120	0.007	2556	32	2478	27	2525	31	2292	120	97
Museta b.	MB-2	49	0.170	0.004	0.483	0.007	11.487	0.453	0.124	0.008	2558	37	2540	29	2564	37	2356	150	99
Museta b.	MB-2	50	0.170	0.002	0.467	0.006	11.055	0.254	0.098	0.003	2559	23	2469	26	2528	21	1892	63	96
Museta b.	MB-2	51	0.170	0.002	0.435	0.005	10.349	0.240	0.108	0.004	2560	23	2328	25	2467	21	2081	71	91
Museta b.	MB-2	52	0.170	0.003	0.462	0.006	11.285	0.336	0.130	0.005	2560	25	2448	26	2547	28	2471	89	96
Museta b.	MB-2	53	0.171	0.003	0.459	0.006	10.509	0.299	0.097	0.005	2564	28	2436	26	2481	26	1867	86	95
Museta b.	MB-2	54	0.171	0.003	0.492	0.006	11.487	0.374	0.131	0.007	2566	30	2577	28	2564	30	2487	118	100
Museta b.	MB-2	55	0.172	0.003	0.501	0.006	11.952	0.340	0.138	0.005	2573	25	2620	28	2601	27	2609	92	102
Museta b.	MB-2	56	0.173	0.004	0.489	0.007	11.529	0.424	0.126	0.009	2583	39	2567	29	2567	34	2400	165	99
Museta b.	MB-2	57	0.173	0.004	0.457	0.006	11.476	0.381	0.116	0.007	2589	34	2424	27	2563	31	2222	129	94
Museta b.	MB-2	58	0.174	0.003	0.466	0.006	11.430	0.342	0.096	0.006	2594	33	2467	27	2559	28	1847	107	95
Museta b.	MB-2	59	0.189	0.003	0.506	0.006	13.593	0.279	0.130	0.004	2730	22	2641	27	2722	19	2472	80	97
Museta b.	MB-2	60	0.189	0.004	0.489	0.007	12.927	0.481	0.151	0.011	2734	38	2566	29	2674	35	2849	192	94

A6-5 Zircon morphology (Kisegi-Nyabusosi area)

Formation		Kisegi Fm.	Kakara Fm.	Oluka Fm.	Nyaburogo Fm.	Nyabusosi Fm.
Sample ID		SEM 200-2	SEM 92-1	LB-5	GH-10	143-5
Morphology	irregular, patchy, diffuse (auroral-light)	33	41	34	35	17
	homogeneous, locally fractured	3	0	9	3	0
	nearly homogeneous, concentric zoning recognizable	17	16	20	16	17
	irregular oscillatory zoning, locally with zones of recrystallization	5	5	5	4	13
	irregular sector zoning	8	4	1	3	6
	xenocrystic core surrounded by large thick homogenous bands or mantle	33	32	28	37	47
	light core and dark rim	1	3	4	2	0
	regular oscillatory zoning (magmatic zircon)	0	0	0	0	0
Color	pink	5	3	3	4	71
	transparent	70	80	78	80	19
	white/milky	15	9	10	8	4
	yellow/brown	10	8	9	8	6
Length/width ratio	short stubby	7	9	5	13	15
	long stubby	39	34	44	43	30
	short stalky	13	15	34	22	26
	long stalky	11	10	5	8	17
	short prismatic	4	3	0	4	5
	long prismatic	1	1	0	0	0
	needlelike	0	0	0	0	0
	broken	26	29	11	9	8

A6-6 Zircon morphology (Nkondo-Kaiso area)

Formation		Nkondo Fm.	Warwire Fm.	Kaiso Village Fm.	Museta beds Fm.
Sample ID		NV3-2	SC1-1m10	KAI 47-1	MB-2
Morphology	irregular, patchy, diffuse (auroral-light)	28	28	23	41
	homogeneous, locally fractured	6	5	3	1
	nearly homogeneous, concentric zoning recognizable	33	14	18	21
	irregular oscillatory zoning, locally with zones of recrystallization	9	17	3	14
	irregular sector zoning	5	4	3	3
	xenocrystic core surrounded by large thick homogenous bands or mantle	16	33	46	14
	light core and dark rim	4	1	4	5
	regular oscillatory zoning (magmatic zircon)	0	0	0	1
Color	pink	7	7	11	8
	transparent	40	38	66	54
	white/milky	45	30	13	22
	yellow/brown	8	25	10	16
Length/width ratio	short stubby	11	15	12	10
	long stubby	37	34	32	34
	short stalky	27	20	19	16
	long stalky	13	19	7	10
	short prismatic	3	6	2	1
	long prismatic	0	1	0	0
	needlelike	0	0	0	0
	broken	10	5	28	30